Paul A. Iaizzo
Tinen L. Iles
Massimo Griselli
James D. St. Louis *Editors*

# Heart Valves

## From Design to Clinical Implantation

*Second Edition*

Springer

# Heart Valves

Paul A. Iaizzo • Tinen L. Iles
Massimo Griselli • James D. St. Louis
Editors

# Heart Valves

## From Design to Clinical Implantation

Second Edition

Springer

*Editors*
Paul A. Iaizzo
Visible Heart® Laboratories
Department of Surgery Institute
for Engineering in Medicine
University of Minnesota
Minneapolis, MN, USA

Massimo Griselli
Royal Brompton Hospital
Pediatric Cardiac Surgeon at the Newcastle
upon Tyne Hospitals NHS Foundation Trust
Newcastle upon Tyne, London, UK

Formerly at University of Minnesota
Department of Surgery
Minneapolis, MN, USA

Tinen L. Iles
Department of Surgery
University of Minnesota
Minneapolis, MN, USA

James D. St. Louis
Department of Surgery and Pediatrics
Augusta University
Augusta, GA, USA

ISBN 978-3-031-25540-3 ISBN 978-3-031-25541-0 (eBook)
https://doi.org/10.1007/978-3-031-25541-0

© The Editor(s) (if applicable) and The Author(s), under exclusive license to Springer Nature Switzerland AG 2013, 2023
This work is subject to copyright. All rights are solely and exclusively licensed by the Publisher, whether the whole or part of the material is concerned, specifically the rights of translation, reprinting, reuse of illustrations, recitation, broadcasting, reproduction on microfilms or in any other physical way, and transmission or information storage and retrieval, electronic adaptation, computer software, or by similar or dissimilar methodology now known or hereafter developed.
The use of general descriptive names, registered names, trademarks, service marks, etc. in this publication does not imply, even in the absence of a specific statement, that such names are exempt from the relevant protective laws and regulations and therefore free for general use.
The publisher, the authors, and the editors are safe to assume that the advice and information in this book are believed to be true and accurate at the date of publication. Neither the publisher nor the authors or the editors give a warranty, expressed or implied, with respect to the material contained herein or for any errors or omissions that may have been made. The publisher remains neutral with regard to jurisdictional claims in published maps and institutional affiliations.

This Springer imprint is published by the registered company Springer Nature Switzerland AG
The registered company address is: Gewerbestrasse 11, 6330 Cham, Switzerland

# Preface

Cardiovascular disease remains one of the major causes of human morbidity and mortality worldwide. While the past 40 years has brought major progress in cardiac valve repairs and replacements therapies, their still remains large patient populations worldwide that do not receive such procedures. This, in turn, implies a continued need for basic, applied, and clinical research to make available novel therapeutic developments.

Today, it is well recognized that there remains a need, albeit one that poses a great challenge, to provide guidance for all types of researchers in this field, in the form of a practical, state-of-the-art educational textbooks dedicated to cardiac providing insights relative: (1) cardiac valves anatomies and functions; (2) preclinical benchtop and animal models for testing and developing new technologies; (3) the design and execution of clinical trials; and/or (4) defining further clinical needs and potential applications. As such, the presented second edition of this cardiac valve textbooks is a state-of-the-art resource on these aforementioned topics. It should also be noted that this textbook has been written by scientists and clinicians from leading academic and industrial institutions from around the world, whose work has had major impacts on the field of cardiac valve repair and/or replacement. It is hoped that the second edition of this textbook is an insightful reference for patients, educators, students, device designers/developers, clinical study specialists, clinicians, and/or other associated healthcare providers. The editors are grateful to all authors for their excellent contributions, to Merry Stuber for her outstanding support, and to Springer publishers for making this book a reality.

Minneapolis, MN, USA — Paul A. Iaizzo

# Contents

# Part I
# Anatomy, Physiology, Congenital Defects, and Disease

# Chapter 1
# The Anatomy and Function of the Atrioventricular Valves

**Jorge D. Zhingre Sanchez, Michael G. Bateman, Jason L. Quill, Alexander J. Hill, and Paul A. Iaizzo**

## Abbreviations

| | |
|---|---|
| APM | Anterior papillary muscle complex (superoposterior) |
| AV | Atrioventricular |
| PPM | Posterior papillary muscle complex (inferoanterior) |

## 1.1 Introduction

Since the second and third century BC, when Galen used dissections of animals to improve his understanding of cardiac anatomy, great physicians and anatomists such as Vesalius, Leonardo da Vinci, Hunter, and Gray completed postmortem

Michael G. Bateman, Jason L. Quill, and Alexander J. Hill affiliations' at the time of published writing for the first edition of *Heart Valves: From Design to Clinical Implantation (2013)*

J. D. Zhingre Sanchez (✉) · J. L. Quill
Medtronic, Inc., Mounds View, MN, USA
e-mail: jorge.d.zhingresanchez@medtronic.com

M. G. Bateman
Departments of Surgery and Biomedical Engineering, University of Minnesota, Minneapolis, MN, USA

A. J. Hill
Anteris Technologies, Minneapolis, MN, USA

Medtronic, Inc., Minneapolis, MN, USA

P. A. Iaizzo
Visible Heart® Laboratories, Department of Surgery, Institute for Engineering in Medicine, University of Minnesota, Minneapolis, MN, USA

© The Author(s), under exclusive license to Springer Nature Switzerland AG 2023

P. A. Iaizzo et al. (eds.), *Heart Valves*, https://doi.org/10.1007/978-3-031-25541-0_1

examinations on both humans and animals to investigate the frailties of the human body. Their work was often recreated in elegant treatises such as the collection presented in Netter's medical school mainstay, the Atlas of Human Anatomy [1]. More recently, the understanding of the functional internal anatomy of the body has progressed rapidly with the advent of high-resolution non-invasive imaging. The advances in cardiac surgery, and consequently the development and deployment of numerous cardiac devices over the late twentieth century, has continued to reinforce the need to describe areas of the heart as functional complexes, consisting of various anatomical parts, rather than individual anatomical features [2]. Furthermore, with modern cardiac "centers of excellence" routinely collecting detailed images of myocardial contractions, blood movement, and valve function, the present field of cardiac anatomy has undergone a shift to correct the perceived orientation of the heart's anatomical features to align with the overall anatomy of the body; this is known as "attitudinally correct anatomy" [3].

## 1.2 Attitudinally Correct Anatomy

Cardiac anatomy, considered as a relatively young branch of human anatomy, has not adhered to the same fundamental rules of orientation or anatomical position as more generalized gross anatomy. The three define anatomical planes of the body—sagittal, coronal, and transverse (Fig. 1.1)—are used to describe the position

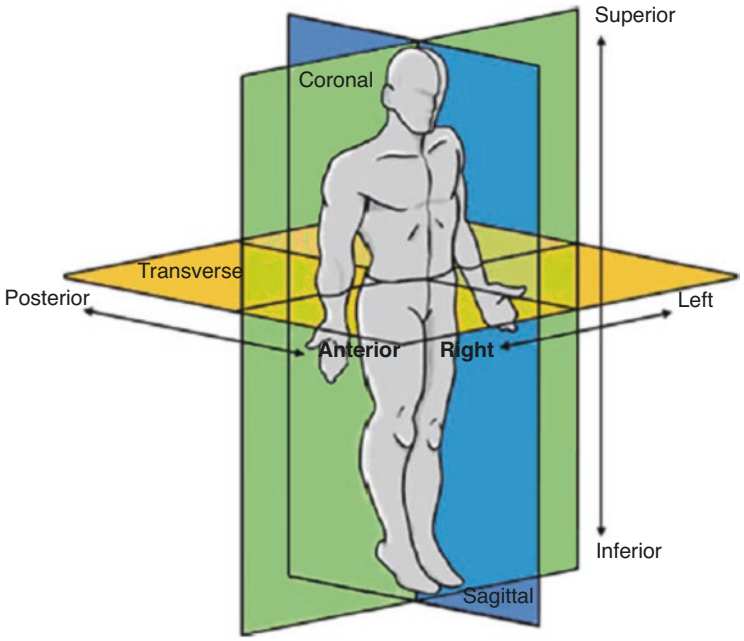


**Fig. 1.1** The anatomical planes of the human body (www.vhlab.umn.edu/atlas [4])

and nature of almost all other aspects of internal anatomy with respect to the patient's own orientation, a convention designed to minimize confusion in determining which of the many structures and organs within the body a particular diagnosis may be referring to. On the other hand, the anatomical features of the heart have commonly been described with the organ removed from the body and held in front of the observer, the right chambers to the patient's right and the apex pointed inferiorly. Only recently have cardiac anatomy specialists pushed to redefine the nomenclature as though the heart was back within the body and described the anatomical features relative to the body's anatomical planes. Thus, structures closest to the spine are described as being posteriorly positioned and those nearest to the diaphragm, inferiorly positioned [3]. A full description of the appropriate nomenclature with respect to the heart and the importance of attitudinally correct anatomical labeling is provided by Anderson et al. [5].

The use of attitudinally correct nomenclature is all the more important with regard to the atrioventricular (AV) valves, as current nomenclatures used to describe the leaflets, still today, are neither standardized nor attitudinally correct [7]. The tricuspid valve is situated between the right atrium and right ventricle, and is so named because, in the majority of cases, there are three major leaflets or cusps. These are currently referred to as the anterior, posterior, and septal leaflets, and are most likely termed in this manner during extra-corporal examinations of the heart. Figure 1.2 shows an anterior view of a human heart in an attitudinally correct orientation, with the tricuspid annulus shown in orange; the theorized locations of the commissures between the leaflets are shown in red. In order for the "anterior" leaflet to be truly anterior, the tricuspid annulus would need to be orthogonal to the image.

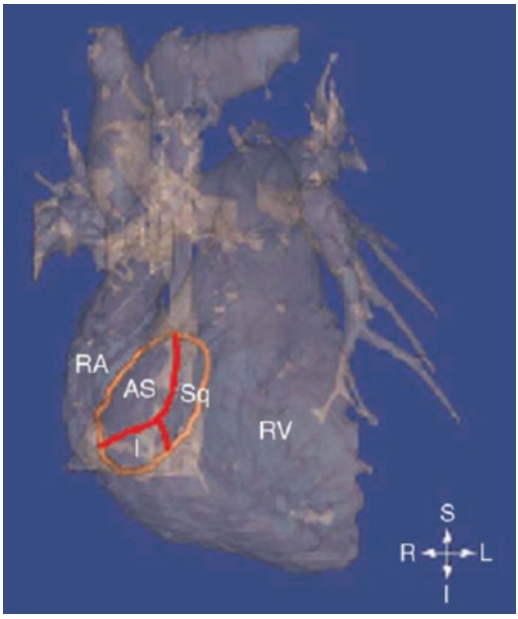


**Fig. 1.2** Volumetric reconstruction of a human heart created from magnetic resonance imaging (MRI). One can observe the anterior surfaces of both the right ventricle and atrium. The tricuspid annulus is highlighted in *orange* and superimposed onto the MRI image. AS antero-superior, I inferior, L left, R right, RA right atrium, RV right ventricle, S superior, Sq septal. (Iaizzo [6])

However, the true location of the annulus is in an oblique plane as shown in the figure, thus the leaflets would be more correctly termed antero-superior, inferior, and septal. Additionally, the mitral valve normally presents with two leaflets commonly referred to as the anterior and posterior. However, the leaflets are not strictly anterior or posterior, and would be better described as antero-superior and postero-inferior or aortic and mural.

Importantly, note that we will use this attitudinally correct anatomical nomenclature for the remainder of the chapter.

## 1.3 The Cardiac Skeleton

Before describing the specific anatomies of the AV valves, it is important to understand the anatomical cardiac framework that holds these valves in position at their respective AV junctions, and thus, consequently, the relationships of each valve to the others [8]. Figure 1.3 shows an anatomical plate of a human heart with the atria and great arteries removed highlighting the close proximity of all four cardiac valves to each other. Traditionally, the four valves of the heart have been described as being supported by a fibrous framework or *cardiac skeleton* made of dense connective tissue passing transversely through the base of the heart between the atria and the ventricles. However, current interpretations of the extent of the skeleton are often greatly exaggerated. As described by Wilcox et al. [8] and by Bateman et al. [9], the strongest part of the skeleton is the area of fibrous continuity between the leaflets of the mitral and aortic valves. This fibrous strap, thickened at both ends by

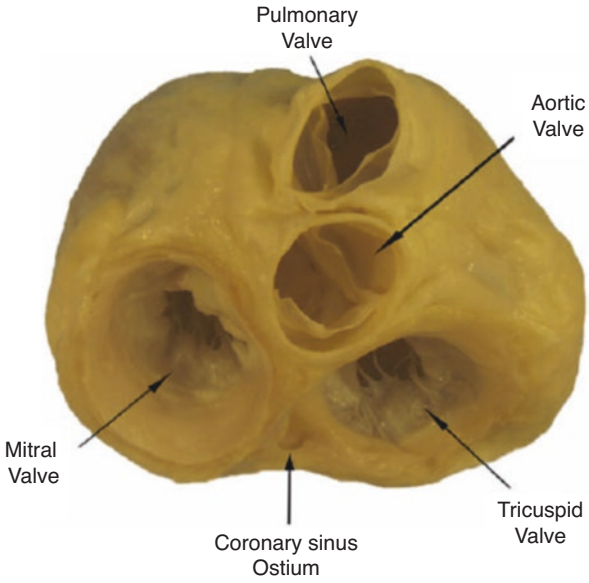


**Fig. 1.3** An anatomical plate of a human heart with the atria and great arteries removed showing the relationship between the four valves at the base of the heart. Note the fibrous connection between the leaflets of the mitral valve creating a double orifice valve

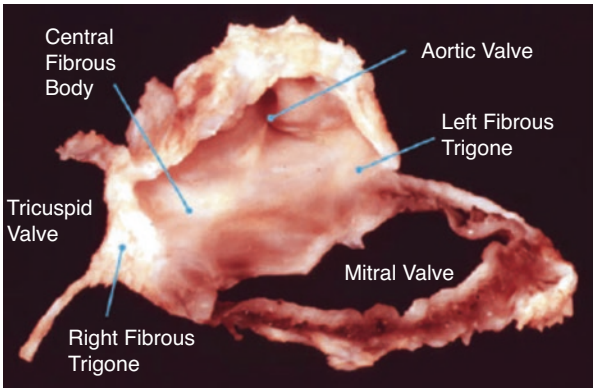


**Fig. 1.4** Dissection of the cardiac skeleton showing the aortic valve (center), the mitral valve annulus (below right), and the fibrous sections of the tricuspid valve (to the left). (The original image for this figure was kindly provided by Professor Robert H. Anderson. It was initially published in "Cardiac Anatomy" [10] and has been modified for this review. Professor Anderson retains the copyright of the initial image)

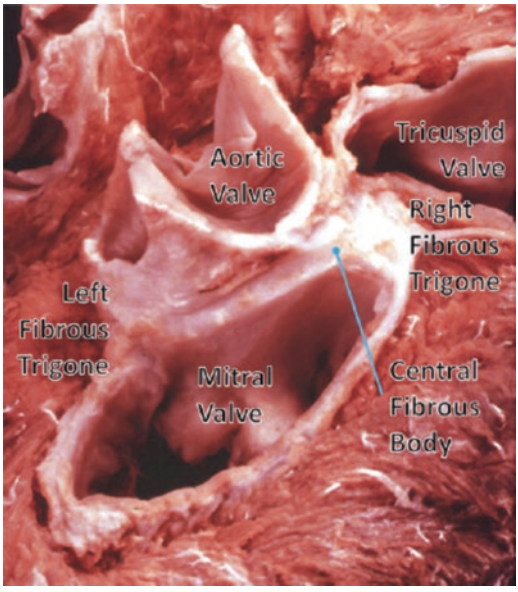


**Fig. 1.5** Dissection of the cardiac skeleton with the atria and great vessels removed showing the coronet shape of the aortic annulus and the mitral valve. (The original image for this figure was kindly provided by Professor Robert H. Anderson. It was initially published in "Cardiac Anatomy" [10] and has been modified for this review. Professor Anderson retains the copyright of the initial image)

the fibrous trigones, anchors the aorticmitral valvar unit within the base of the left ventricle (Fig. 1.4). The coronet-like support of the aortic valvar leaflets extends antero-cranially from the region of fibrous continuity and is often considered to represent an aortic valvar annulus, but there are no anatomical structures supporting the semilunar hinges of the aortic valvar leaflets (Fig. 1.5) [9]. The right fibrous trigone is itself continuous with the membranous part of the ventricular septum and is an integral part of the aortic coronet (Fig. 1.4). The trigone and membranous

septum together are usually described as the central fibrous body. The so-called annular components of the AV valves then extend inferiorly and posteriorly from the central fibrous body and the left fibrous trigone, respectively (Fig. 1.5) [9].

It is the exception rather than the rule, however, for these fibrous cords to extend throughout the full circumferences of the left and right AV junctions. The annulus, as such, is better formed in the mitral as opposed to the tricuspid junction. Even in the mitral junction, nonetheless, it is common to find segments of the valvar leaflets hinged from the fibro-adipose tissue of the AV junction, rather than from a firm fibrous annulus [11]. In the tricuspid junction, the valvar leaflets are normally hinged from fibro-adipose tissue [12]. It is also the fibro-adipose tissues of the junctions that provide the greatest part of the insulation between the atrial and ventricular muscular masses, with the AV bundle of the conduction system being the only structure in the normal heart that crosses the insulating plane. The bundle penetrates through the AV component of the membranous septum. The annuluses, as part of the AV junctions and rarely being complete fibrous rings, are highly dynamic and change dramatically in shape and size throughout the cardiac cycle from systole to diastole [8, 9].

## 1.4 The Atrioventricular Valves

In the most basic anatomical sense, the AV valves are made up of three main components, as seen in Fig. 1.8:

- Valve leaflets attached to the respective annulus,
- Tendinous cords attaching the leaflets to the ventricular myocardium,
- Papillary muscles providing the anchoring points for the tendinous cords to the ventricular wall.

The leaflets of the AV valves can be thought as forming a *skirt* that hangs from the annulus and are divided into a series of sections that constitute the distinct leaflets of each valve. Due to the extent of variations between individuals with regard to leaflet morphologies, there has been much debate relative to nomenclature on the number of leaflets of both the mitral and tricuspid valves [13–15]. Traditionally, the division of the leaflets has been determined by the presence of commissures which can be described as the peripheral attachment of a break in the skirt [8].

The leaflets themselves are attached to the ventricles via the sub-valvar apparatus of each valve. In general, each apparatus consists of both the tendinous cords and the papillary muscle complexes of each valve. The tendinous cords are usually categorized by: (1) those that support the free edges of the valves, (2) those that support the rough zones (the region between the free edge and each annulus), and/or (3) those that attach to the leaflets near to the annulus. Typically, the cords supporting the free edges of the leaflets are known as *fan cords* due to the presence of multiple fenestrations. Those that attach to the rough zone of the leaflets are distinguished by

their larger size and are commonly defined as *strut cords*. Finally, those that attach near the annulus are known as *basal cords*. The strut cords are of specific importance as they bear the highest mechanical loads during systole [16]. Furthermore, the number and distribution of the tendinous cords across a given valve are critical to its function; it is well documented that dysfunction of these structures can lead to prolapse of the valves [2, 17, 18]. In general, the cords attach to the heads of the papillary muscles which themselves play an important role in the function of each valve by contracting during systole to cushion the valve closure.

### *1.4.1 Atrioventricular Valve Function*

During systole, when the ventricles are contracting, the sub-valvar apparatus of each valve prevents the leaflets from prolapsing into the atria and additionally aids in ventricular ejection by effectively drawing the apex of the ventricle toward the basal ring. Additionally, it has also been shown that the sub-valvar apparatus plays a crucial role during diastole, while the ventricle is filling, by moderating wall tensions and improving the efficiencies of the ventricular myocardium [19, 20]. During systole in normal/healthy cardiac function, the valve leaflets, which bulge toward the atrium, can be considered to stay pressed together throughout the contraction and therefore do not prolapse. During diastole, when the ventricles are relaxing and the chambers are filling through the open AV valves, eddy currents that form behind the leaflets and tension in the sub-valvar apparatus keep the leaflets close together.

Figures 1.6 and 1.7 show image sequences obtained employing Visible Heart® methodologies, as described in Chap. 19. These sequences display the normal cardiac function of the mitral and tricuspid valves, respectively [4, 21]; the images were obtained from the atria (above the valve) and from the ventricular apexes (below the valve).

Dysfunction of the AV valves is usually characterized by one of the two following symptoms: (1) failure of a given valve to successfully close or (2) failure of a valve to successfully open. Dysfunction of the valves during systole (i.e., failures of the valve to successfully close) is known as valvar *incompetence* and results in the *regurgitation* of blood back in a retrograde direction though the AV junction. Such dysfunction results in a decrease in cardiac output and also increases the pressure within the atria during systole (potentially causing atrial dilation and/or eventually atrial fibrillation). Dysfunction of the valves in diastole (failures of the valve to fully open and allow blood to fill the expanding ventricles) is termed *stenosis*. This decrease in effective orifice area of the open valve is often due to stiffening or calcification of the valve leaflets. Pathologies of the AV valves are described in detail in Chap. 6.

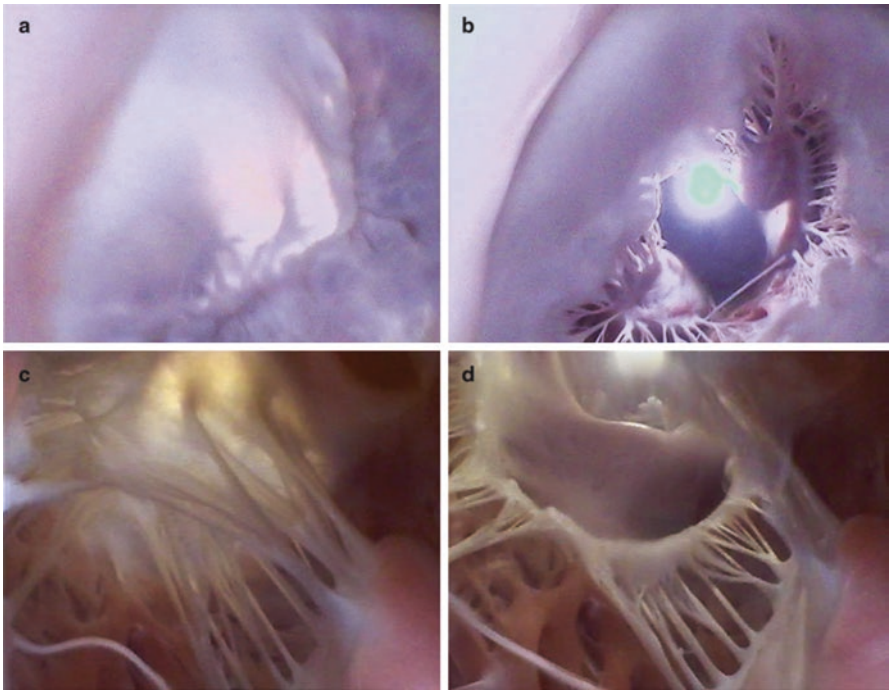


**Fig. 1.6** Internal videoscopic images of the mitral valve from above (**a**, **b**) and below (**c**, **d**) during systole (**a**, **c**) and diastole (**b**, **d**) obtained employing Visible Heart® methodologies

### *1.4.2 Valve Histologies*

Interestingly, the AV valves share very similar leaflet histologies. The atrial sides of the leaflets consist of spongy tissue (lamina spongiosa) comprised of fibrocytes, histiocytes, and collagen fibers [22]. It is these collagen fibers that are considered to supply the mechanical strength required of the AV valves. The ventricular sides consist of fibrous tissue (lamina fibrosa), and both these layers are surrounded by endothelial cells. Additionally, the valve leaflets have been shown to incorporate both primary sensory and autonomic innervation. In general, it is considered that the anterior leaflet of the mitral valve has twice the innervation of the posterior leaflet [23]. These nerves are typically situated in the lamina spongiosa and extend over the proximal and medial portions of the leaflet [22]. Fibroblasts [24], smooth muscle cells [25, 26], and myocardial cells [27] are also commonly located within the leaflet tissue.

Cells within the leaflets have been shown to elicit two types of contractile activities (1) a brief contraction or twitch at the beginning of each heart beat (reflecting contraction of myocytes in the leaflet in communication with and excited by atrial muscle) which has relaxed by mid-systole and whose contractile activity is eliminated with β-receptor blockade, and (2) sustained tonic contractions (or tone) during

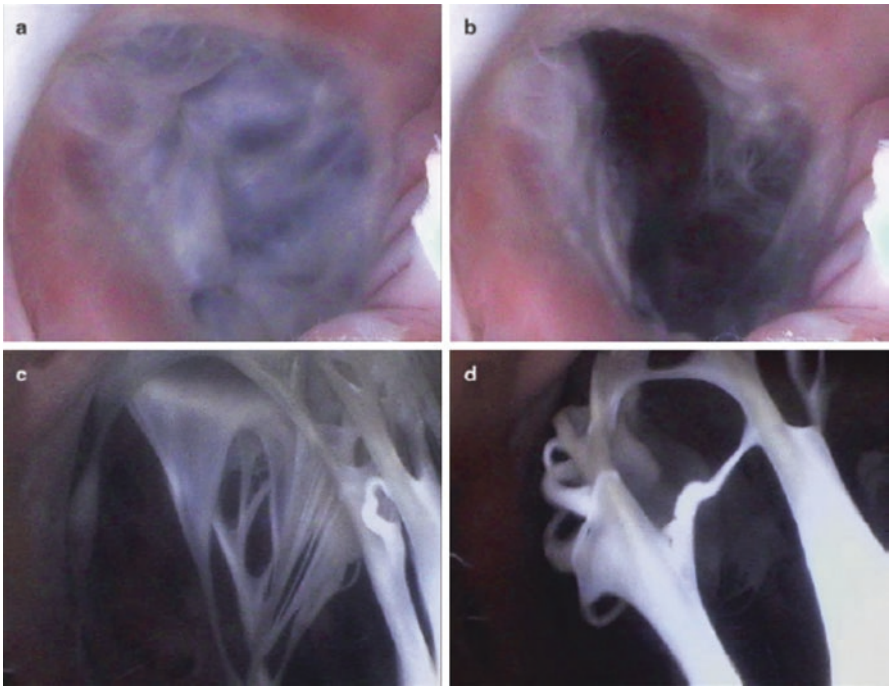


**Fig. 1.7** Internal videoscopic images of the tricuspid valve from above (**a**, **b**) and below (**c**, **d**) during systole (**a**, **c**) and diastole (**b**, **d**) obtained employing Visible Heart® methodologies

isovolumic relaxation, which has been shown to be insensitive to β-blockade, but doubled by stimulation of the neurally rich region of aortic–mitral continuity [28]. These contractile activities within the leaflets are hypothesized to aid in the maintenance of anterior leaflet shape. This, in turn, could help prevent mechanical shock to the leaflets upon valve closure and also aid in optimizing the leaflet shape for funneling blood into the left ventricular outflow tract [28].

The tendinous cords are composed of a collagen core, surrounded by elastin fibers interwoven in layers of loose collagen. Similar to the valve leaflets, they also have an outer layer of endothelial cells, but it is the collagen cores that support the greatest degree of mechanical load during systole and allow for the wavy configuration during diastole. The elastin fibers are normally arranged in parallel fashion relative to the collagen fibers, and as the cords are stretched during systole, the elastin fibers are also stretched, straightening the collagen. It is hypothesized that it is this composite configuration of elastin and collagen that provides a smooth mechanism for the transmission of chordal forces from the leaflets to the papillary muscles. Additionally, during diastole, the stretched elastin fibers likely help to restore the wavy configurations of the primary collagen cores. The relative amount of collagen and elastin within the given tendinous cords varies according to their relative types, as does the relative amount of contained DNA and their degree of vascularization. Normally, the vascularization of the tendinous cords is located between

their collagen cores and the elastin fibers, and is further considered to supply nutrients to the leaflets. It has been reported that a higher DNA content, within both the anterior and posterior marginal tendinous cords, relates to inherently higher rates of collagen syntheses in order to prevent mechanical deterioration compared with other types of tendinous cords [17].

The papillary muscles themselves can be considered part of the ventricular myocardium and hence are composed of aggregated myocytes. The cells exhibit complex junctions, called *intercalated discs*, allowing multiple cells to form long cellular networks. Within the papillary muscles, these muscle fibers run parallel to each other along the length of the muscle to increase contractile force and efficiency. The papillary muscles are extensively innervated and have complex vascular systems in order to maintain coordinated contractions with the continuum of the ventricular myocardium [29].

## 1.5 The Mitral Valve

The left AV valve, or mitral valve, named by Andreas Vesalius due to its structural resemblance to the cardinal's mitre, is situated in the left AV junction and modulates the flow of blood between the left atrium and ventricle. Commonly, the valve consists of an annulus, two leaflets, two papillary muscle complexes, and two sets of tendinous cords, as seen in Fig. 1.8.

In 1976, Carpentier described that the mitral valve consists of two apposing leaflets—a posterior leaflet with three scallops and an anterior leaflet with one scallop. Each region of the leaflets is designated an alphanumeric label to distinguish it from the rest of the valve (Fig. 1.9) [30]. However, when one considers these structures relative to the landmarks of the body (i.e., in an attitudinally correct nomenclature),

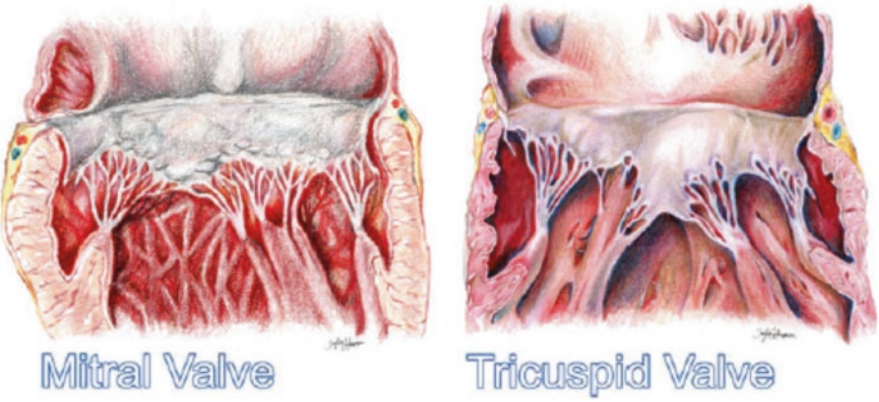


**Fig. 1.8** An artist's rendition of the healthy mitral and tricuspid valves clearly showing the annuluses, leaflets, tendinous cords, and papillary muscles

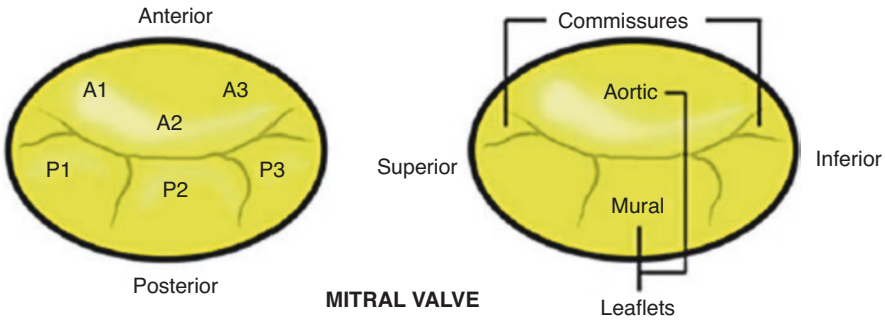


**Fig. 1.9** Nomenclature of the mitral valve leaflets: the left diagram shows Carpentier's 1976 nomenclature; the right depicts the modern attitudinally correct nomenclatures

the leaflets are located in postero-inferior and antero-superior positions. Confusion regarding positional nomenclature can be avoided when adopting the more traditional approach suggested by Vesalius for distinguishing between the leaflets, and recognizing that they are aortic and mural in their locations [31]. The junctions of the two leaflets are commonly referred to as the *anterolateral* and the *posteromedial* commissures; however, these are more accurately described as *superior* and *inferior*. The line of apposition of the leaflets during valve closure is known as the *fibrous ridge*.

The simplicity and practicality of Carpentier's anatomic description of the mitral leaflets led to its widespread use after being introduced in 1976 [30]; yet, while this description defines a majority of mitral valve anatomies, there can be wide variability in both the number of scallops within each leaflet and their relative positions [32].

In general, the aortic leaflet is found to be attached to approximately one-third of the annulus circumference and is supported by the aorto-mitral fibrous continuity, which terminates in the left and right fibrous trigones (Fig. 1.10). The mural leaflet is attached to the remaining two-thirds of the annulus and also to the fibrous extensions that continue from the trigones around the mitral valve. However, the lengths of these extensions can be highly variable. Furthermore, a fibrous-fatty tissue surrounds the valve in areas where the cardiac skeleton is not present. The mitral annulus is a highly dynamic feature of the heart, changing dramatically in shape and size throughout the cardiac cycle. It is often described as being saddle shaped with the highest point of the saddle, the *saddlehorn*, being found at the midpoint of the area of aortic-to-mitral valvar continuity [33] (Figs. 1.6 and 1.11). Both Delgado and Veronisi and their colleagues reported a series of annular dimensions that were recorded using echocardiography in healthy patients; these data are summarized in Table 1.1 [34–36].

In general, the sub-valvar apparatus of the mitral valve consists of two adjacent papillary muscle complexes—the superoposterior (anterior or APM) and the inferoanterior (posterior or PPM)—with their attached tendinous cords which, in turn, insert onto the ventricular surfaces of each of the two valve leaflets [31]. In other words, the superoposterior papillary muscle complex is not solely associated with

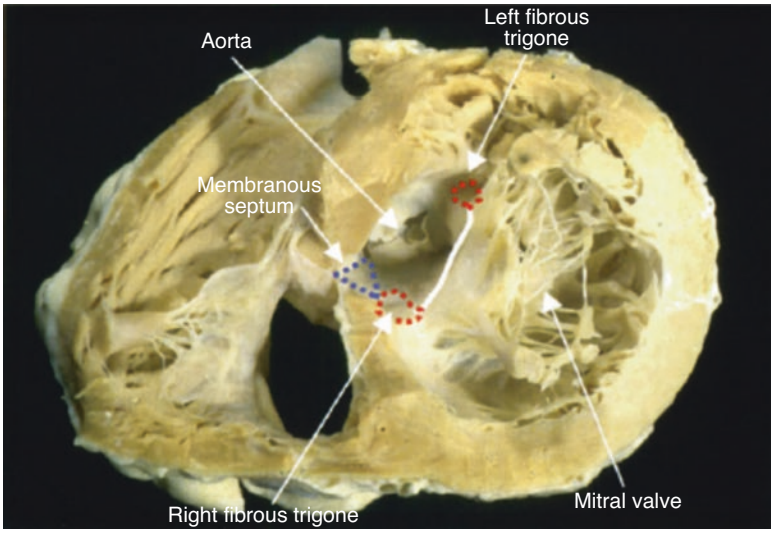


**Fig. 1.10** Trigones and the aorto-mitral fibrous continuity within a sectioned human heart. In this case, the cardiac skeleton is being viewed from the apex of the heart. The anterior cardiac surface appears in the upper part of this image, whereas the posterior surface is below [31]

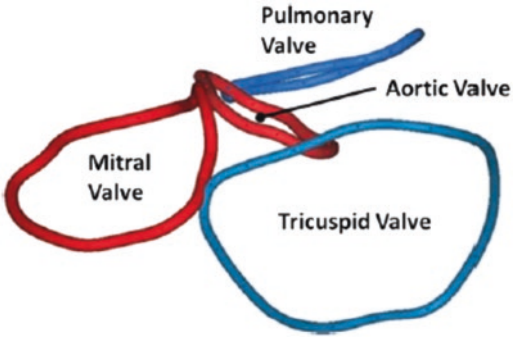


**Fig. 1.11** 3D reconstruction of the annuluses of the mitral (*red*) and tricuspid (*blue*) valves in Mimics® (Materialise, Leuven, Belgium) from CT scans of a human heart in vivo. The image also shows the location of the virtual rings formed by joining together the basal attachments of the leaflets of the aortic and pulmonary valves

the aortic leaflet, but rather both the leaflets; likewise, the inferoanterior papillary muscle complex is not solely associated with the mural leaflet. It is important to note that the morphologies of the papillary muscle are highly variable [34]. Some have proposed a complicated alphanumeric classification to account for the number of heads within each muscle and the number of attachments with the ventricular walls [37]. Even this complex code can be deemed as an oversimplification, as both papillary complexes can exhibit enormous anatomic variation [38]. For example,

**Table 1.1** Data on the mitral valve annulus measured via CT [34] and 3D echocardiography [35, 36]

| Measured anatomical feature | Data | Sample size |
|---|---|---|
| Systolic annular area [34, 35] | 9.12 ± 1.71 $cm^2$<br>9.49 ± 1.25 $cm^2$ | $N = 84$<br>$N = 13$ |
| Septal-lateral (A2–P2) diameter [34, 35] (Considered the short axis of the valve) | 2.38 ± 0.40 cm<br>3.00 ± 0.45 cm | $N = 84$<br>$N = 13$ |
| Commissure–commissure diameter [34, 35] (Considered the long axis of the valve) | 4.10 ± 0.48 cm<br>3.42 ± 0.40 cm | $N = 84$<br>$N = 13$ |
| Annulus height during systole [36] | 8.1 ± 1.7 mm | $N = 24$ |

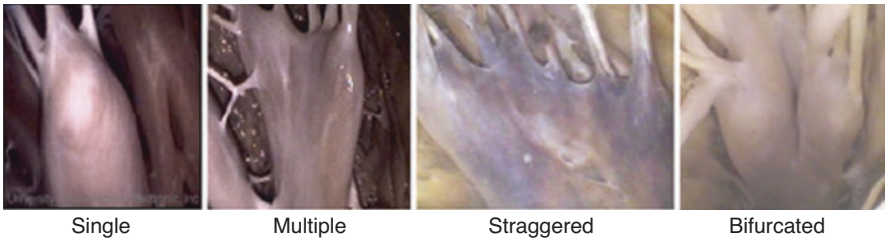


**Fig. 1.12** Several representative examples of the enormous variation in anatomy with regards to the papillary muscle heads associated with the mitral sub-valvar apparatus from four different human hearts taken using Visible Heart® methodologies [38]

Fig. 1.12 displays images of the sub-valvar apparatus of the mitral valve taken from human hearts in the Visible Heart® library [38].

The tendinous cords are typically classified by their number and length, and quantified by one of two measurement techniques—tethering length and insertion length. *Tethering lengths* are defined as the distances from the papillary heads to the saddle horn of the mitral annulus. *Insertion lengths* are defined as the lengths of the cords from their origins at the papillary head to their insertion into the leaflet tissue. Anatomical dimensions obtained from patients with no reported mitral regurgitation or other valvar pathologies as reported by Sonne et al. and Lam et al., and summarized in Table 1.2 [39, 40]. Yet, it should be emphasized that, as with other anatomical studies, these data do not account for all anatomical variations. For example, it has also been reported that the chordal attachments to the mural leaflet may extend simply from the ventricular myocardium to the leaflet without a papillary muscle attachment. Furthermore, it is well known that the tendinous cords themselves may elicit highly variable anatomies, and various subpopulations of chordae have been classified by both the function [41] and type [42]. Figure 1.13 shows examples of these identified variations in the types of chordae, including: posterior marginal chordae, commissural chordae, anterior strut chordae, anterior marginal chordae, basal posterior chordae, and posterior intermediate chordae.

**Table 1.2** Data on the tendinous cord lengths of the mitral sub-valvar apparatus measured in vivo via 3D echocardiography [39] and postmortem [40, 41]

| Measured anatomical feature | Data | Sample size |
|---|---|---|
| APM tethering length in systole [39] | 3.54 ± 0.82 cm | $N = 120$ |
| PPM tethering length in systole [39] | 3.76 ± 0.78 cm | $N = 120$ |
| Anterior leaflet insertion length [40] | 1.81 ± 0.49 cm | $N = 50$ |
| Posterior leaflet insertion length [40] | 1.18 ± 0.26 cm | $N = 50$ |
| Ratio of cord origins to insertions [41] | 1:5 | $N = 18$ |

*APM* superoposterior (anterior) papillary muscle, *PPM* inferoanterior (posterior) papillary muscle

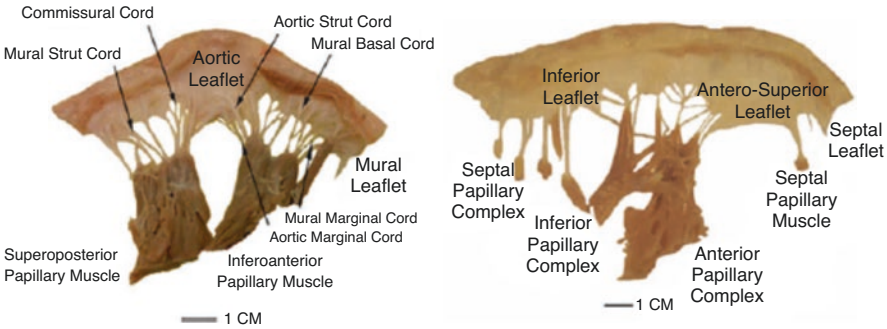


**Fig. 1.13** Dissections of a human mitral valve (*left*) and tricuspid valve (*right*), each labeled with attitudinally correct nomenclature. Note the dramatic differences between the two valves, including their respective sub-valvar apparatuses

## 1.6 The Tricuspid Valve

The right AV valve, or tricuspid valve, is situated within the right AV junction and modulates the flow of blood between the right atrium and right ventricle. This valve is typically defined by three leaflets suspended from the muscular AV junction. When defined using attitudinally correct nomenclature, these leaflets are located in septal, antero-superior (traditionally anterior), and inferior (traditionally posterior) positions (Figs. 1.14 and 1.15) [43].

The antero-superior leaflet is the largest of the three and extends from the medial border of the ventricular septum to the acute margin of the AV junction (Fig. 1.13). The leaflet is hinged from the undersurface of the supraventricular crest and provides a curtain between the inflow and outflow tracts of the right ventricle. The inferior leaflet is hinged from the diaphragmatic aspect of the AV junction. The septal leaflet is then hinged from the ventricular border of the triangle of Koch, with the hinge crossing the right-sided aspect of the membranous septum, dividing it into its AV and ventriculo-arterial components [44]. The septal leaflet is often cleft as it crosses the membranous septum. When viewed in closed position, the trifoliate zones of apposition between the leaflets extend to their peripheral ends. It is these

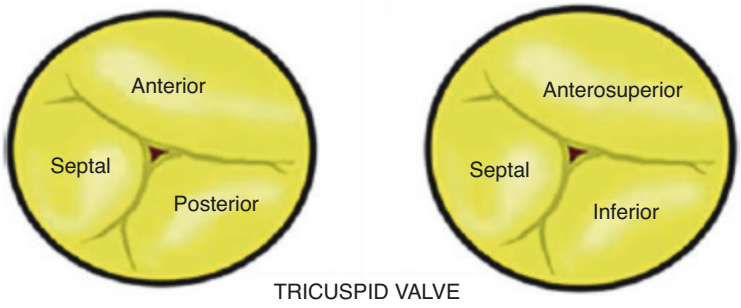


**Fig. 1.14** Nomenclature of the tricuspid valve leaflets: the left diagram shows Carpentier's 1976 nomenclature; the right depicts the modern attitudinally correct nomenclatures

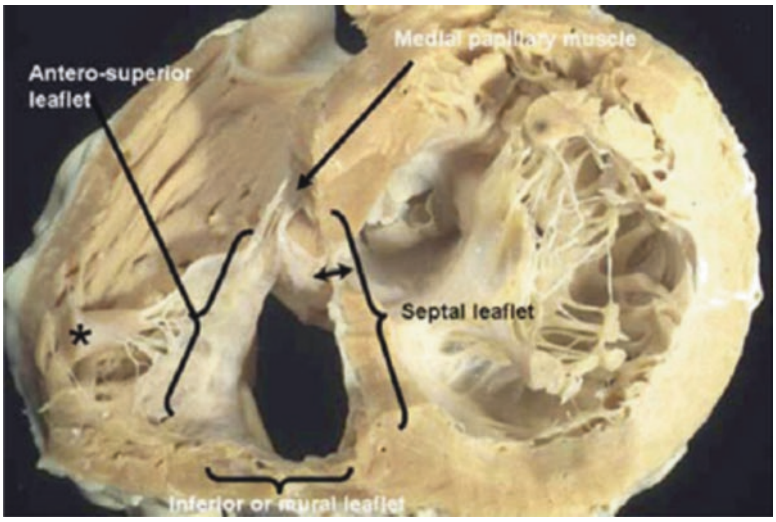


**Fig. 1.15** One can observe here the relative positions of the three leaflets of the tricuspid valve positioned septally, antero-superiorly, and inferior or murally. Note the location of the membranous septum as indicated by the double headed arrow. In this human heart, the anterior papillary muscle (*asterisk*) is attached to the midpoint of the antero-superior leaflet [43]

ends that are typically considered to represent the valvar commissures, which can be named as being antero-septal, antero-inferior, and infero-septal [9].

To date, the morphology of the tricuspid valve has received less attention than the mitral valve, hence thorough anatomical studies are limited. The tricuspid annulus is known to have a non-planar three-dimensional shape, similar to the mitral valve annulus (Fig. 1.11). Further, it has been described as changing its shape dramatically throughout the course of the cardiac cycle. These changes in annular geometries during systole, from a more circular shape to an elliptical shape, result in overall reductions of annular sizes by up to 40% [48]. As the heart contracts, the annulus reaches its minimum size during isovolumetric relaxation and its maximum

during isovolumetric contraction [33]. Data relating to the tricuspid annulus can be seen in Table 1.3 [35, 45–47].

As with the mitral valve, the leaflets of the tricuspid valve are complemented by a sub-valvar apparatus consisting of papillary muscle complexes that work to tether the valve leaflets via tendinous cords to prevent valve prolapse during ventricular contraction (systole). The three main papillary muscle complexes display grossly dissimilar morphology, albeit very characteristic (Fig. 1.16). The zone of apposition between the septal and antero-superior leaflets is supported by the medial papillary muscle complex, also known as the papillary muscle of the conus, or the muscle of Lancisi [43, 49]. It arises from the postero-inferior limb of the septal band, or septomarginal trabeculation, although in some individuals the muscle is replaced by a series of smaller muscles, or even by cords arising directly from the septal band. The largest papillary muscle complex is the anterior, which can support the zone of apposition between the antero-superior and inferior leaflets, but often inserts into the mid-portion of the antero-superior leaflet. The muscle itself is usually in direct continuity with the moderator band [44]. This latter structure is one of a series of septoparietal trabeculations that arise from the anterior margin of the septal band. The smaller inferior muscle complex supports the zone of apposition between the inferior and septal leaflets. The septal leaflet is then supported in addition by multiple cords arising directly from the septum itself. This is a differentiating feature between the tricuspid and mitral valves, the leaflets of the latter valve lacking any septal attachments.

**Table 1.3** Data on the tricuspid valve annulus measured in vivo via 3D echocardiography [35] and postmortem [45–47]

| Measured anatomical feature | Data | Sample size |
|---|---|---|
| Systolic annular area [35] | 10.75 ± 1.81 $cm^2$ | $N = 13$ |
| Postmortem orifice area [45] | 10.60 ± 3.40 cm | $N = 160$ |
| Systolic septo-medial dimension [35] | 3.31 ± 0.32 cm | $N = 13$ |
| Systolic anterior-posterior dimension [35] | 3.79 ± 0.43 cm | $N = 13$ |
| Postmortem annular circumference [46, 47] | 11.10 ± 1.10 cm | $N = 50$ |
| | 11.30 ± 0.50 cm | $N = 24$ |

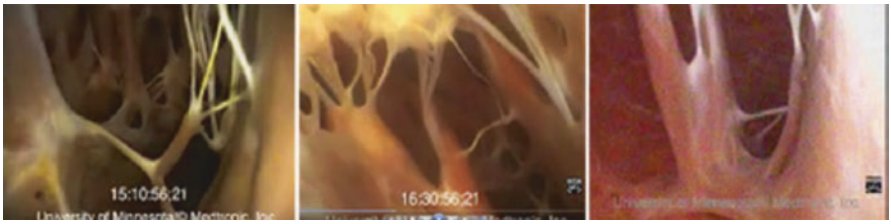


**Fig. 1.16** Several representative examples of the septal (*left*), inferior (*center*), and anterior (*right*) papillary muscle complexes associated with the tricuspid sub-valvar apparatus taken using Visible Heart® methodologies (www.vhlab.umn.edu/atlas [4])

**Table 1.4** Data on the tendinous cord lengths of the tricuspid sub-valvar apparatus measured postmortem [46]

| Measured anatomical feature | Data (cm) | Sample size |
|---|---|---|
| Septal leaflet insertion length [46] | 1.50 ± 0.87 | $N = 50$ |
| Anterior leaflet insertion length [46] | 1.53 ± 0.69 | $N = 50$ |
| Posterior leaflet insertion length [46] | 1.37 ± 0.64 | $N = 50$ |

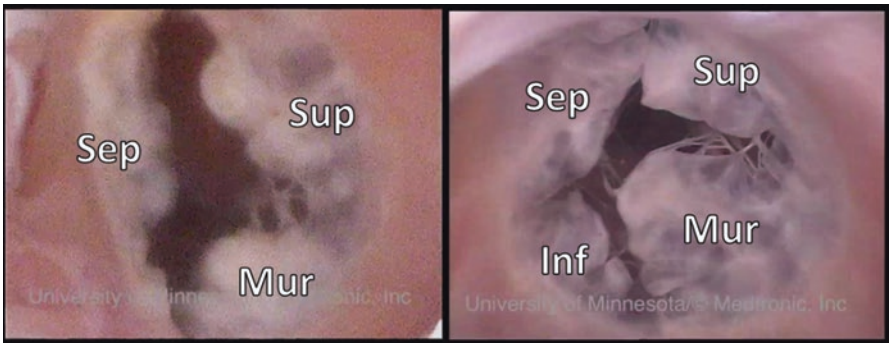


**Fig. 1.17** Endoscopic footage, obtained using Visible Heart®methodologies, of functional heart specimens with a (*left*) "tricuspid" three-leaflet and (*right*) "quadricuspid" four-leaflet right AV valve. These "quadricspid" valves are defined with the precense of a fourth commissure that separates the inferior and mural leaflets. Sep septal, Sup superior, Mur mural, Inf inferior. (Adapted from Refs. [4, 50])

Figure 1.16 displays videoscopic images of the sub-valvar apparatus of the tricuspid valve taken from reanimated human hearts utilizing Visible Heart® methodologies, as described in Chap. 19. Such images emphasize the large anatomical variations that can exist from heart to heart [4].

Previously, Silver et al. reported the common insertion lengths of the tendinous cords of the tricuspid valve for healthy human hearts, which were defined as the distances from the origins of the papillary muscles to their corresponding insertion points on the valve leaflets, (Table 1.4) [46]. These measurements were completed on 50 formalin fixed human hearts; thus, it should be noted that these data may have specific limitations when compared to the modern imaging techniques, e.g., those used to measure the tethering lengths of the mitral cords mentioned earlier in the chapter. As such, we suggest that future detailed assessments of the tricuspid subvalvar apparatus employing modern imaging techniques could greatly benefit the field.

Further classification of the tricuspid leaflets is also of interest due to the extent of leaflet heterogentiy and morphologies. Anatomical case reports have documented that the tricuspid valve can present as either bicuspid [13] or quadricuspid [50] configurations. Figure 1.17 compares the traditional three-leaflet and variant four-leaflet configurations, which were found to be frequently present in over 40% of right AV valves studied by Holda et al. [50] using Visible Heart® methodologies.

## 1.7 Atrioventricular Valve Co-location with Other Cardiac Structures

When performing AV valve surgeries and/or contemplating novel percutaneous approaches to valvar repairs, it is vital to have a strong anatomical appreciation of the AV-associated structures, i.e., those cardiac structures that surround the mitral and tricuspid valves. These anatomical features are displayed in Figs. 1.18 and 1.19. The position and course of the coronary vasculature is key to the clinical anatomy of both the mitral and tricuspid valves. The great coronary vein, continuing as the coronary sinus, circles the mural leaflet of the mitral valve [33, 51]. The circumflex artery, having branched from the main stem of the left coronary artery, courses in concert with the venous channel, usually running much closer to the hinge of the mural leaflet. In the majority of individuals with dominance of the right coronary artery, the circumflex artery does not extend through the full length of the left side of the inferior AV groove [33]. In the minority with left coronary arterial dominance, in contrast, the artery is directly related to the entirety of the mural leaflet, usually continuing into the floor of the triangle of Koch, where it gives rise to the artery supplying the AV node. In many individuals, the circumflex artery crosses underneath the coronary sinus at variable distances [31, 33, 51–53]. An imaging study that assessed the spatial relationship between these vessels and the mitral

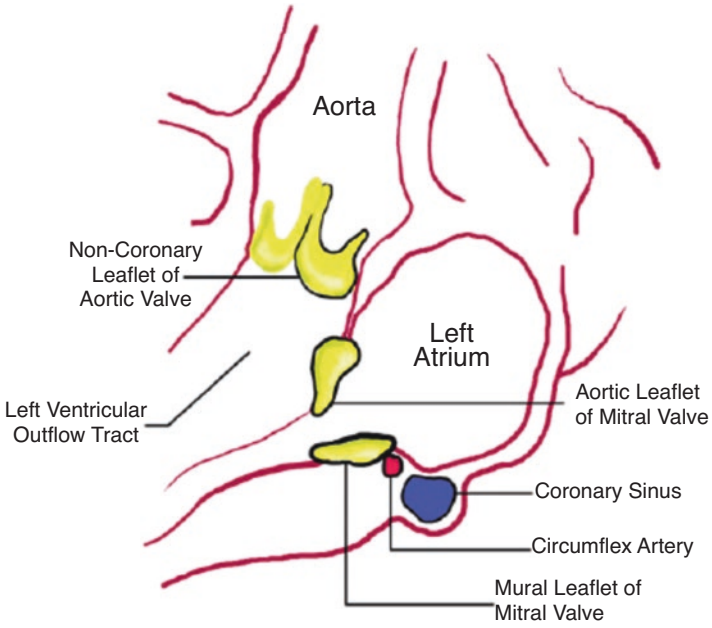


**Fig. 1.18** Graphic representation of the co-location of the mitral valve to the coronary sinus, the left circumflex artery, and the aortic valve

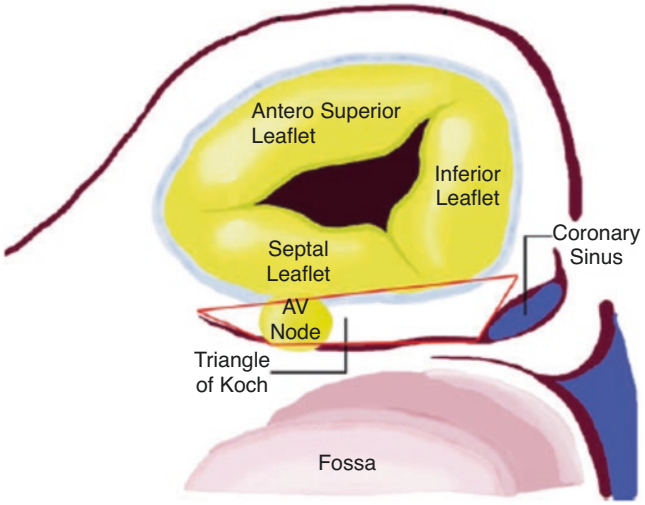


**Fig. 1.19** Graphic representation of the relationship between the cardiac conduction system (i.e., the location of the AV node within the triangle of Koch) and the tricuspid valve when viewed from the right atrium

valve, using MRI scans of perfusion fixed hearts, found that the prevalence of circumflex overlap is common [54]. Both arterial and venous structures, therefore, are at risk when surgical procedures are performed on the mural leaflet of the mitral valve. Such considerations are particularly relevant when employing complex reconstructive techniques [33]. The proximity of the aortic valve is of importance when considering surgical procedures to the aortic leaflet of the mitral valve (Fig. 1.18). The interleaflet triangle between the left coronary and non-coronary (nonadjacent) aortic leaflets is directly related to the saddle horn of the mitral valvar annulus. This feature should be remembered if sutures are to be placed to either side of the saddle horn to prevent damage to the aortic valvar leaflets [33]. The tricuspid valve is bordered within the AV junction by the right coronary artery, but is less related to venous structures, the small cardiac vein being a relatively insignificant structure [3]. However, the 3D spatial assessments between the tricuspid valve and neighboring coronary and conduction system structures may have implications for developing transcatheter tricuspid annuloplasty systems [55, 56].

The AV node and its zones of transitional cells are closely related to the septal hinge of the tricuspid valve, with the slow pathway into the node being a constituent part of the vestibular atrial myocardium in this region. At the apex of the triangle of Koch [3, 33], the specialized cardiomyocytes of the AV node bundle themselves together and pierce the central fibrous body to become the penetrating AV bundle, or the bundle of His (Fig. 1.19). Although closely related again to the hinge of the septal leaflet of the tricuspid valve, and at potential risk whenever surgery is performed within the right atrium or through the tricuspid valve, the AV node should be sufficiently distant not to pose a threat to those operating on the mitral valve. The

bundle of His, having passed through the membranous septum, divides on the crest of the muscular ventricular septum into the left and right bundle branches. These components are at greater risk during procedures on the aortic rather than the AV valves.

## 1.8 Clinical Imaging of the Atrioventricular Valves

Due to its relatively high availability, ease of use, and minimal side effects to the patient, the standard 2D cross-sectional Doppler echocardiogram is considered as the most common imaging modality applied to assess the relative functions and anatomical positions of the AV valves [41, 57]. Clinically, both the mitral and tricuspid valves are commonly imaged via the parasternal long-axis view, allowing the echocardiographer to assess the following valve criteria [57]:

- Size and shape of the annulus
- Mobility of the leaflets, in particular whether they prolapse or show flail or restricted motion (assessment will also include exclusion of thickening calcification, myxomatous degeneration, clefts, fusion along zones of apposition, perforations, vegetations, or abnormal shelves or membranes)
- Length and thickness of the tendinous cords, and whether they are fused or ruptured
- Number, structure, and function of the papillary muscles
- Whether the function of the left ventricle is normal, globally deranged, or shows evidence of regional abnormalities of motion of the walls

Examples of standard 2D cross-sectional Doppler echocardiograms of the mitral and tricuspid valve can be seen in Fig. 1.20. For a comprehensive description of the echocardiographic techniques used to image and assess both healthy and diseased

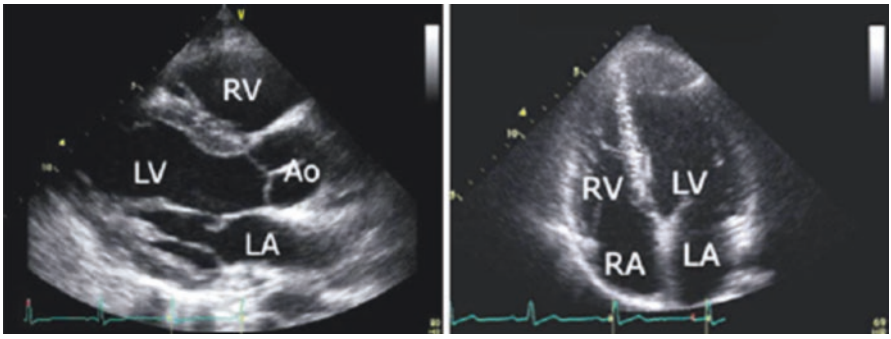


**Fig. 1.20** Common echocardiographic parasternal long-axis and apical sections which show the leaflets of the mitral and tricuspid valves. The sub-valvar apparatus can clearly be seen tethering the leaflets to the ventricular free wall. AO aorta, LA left atrium, LV left ventricle, RA right atrium, RV right ventricle

AV valves the readers are referred to the "*Textbook of Clinical Echocardiography*" by Otto [58] and the recommendations for clinical evaluation of stenosis by Baumgartner et al. [59] and regurgitation by Zoghbi et al. [60]. For more information regarding the echocardiographic imaging of the mitral valve with respect to transcatheter repair procedures, the readers are referred to Chap. 7. In addition to standard echocardiography, enhanced imaging modalities can assess the real-time observation of the valves and interaction with cardiac devices. Multislice computed tomography (CT) is an accurate imaging modality for analyzing valvar dimensions and spatial measurements. The employment of Visible Heart® methodologies, as described in Chap. 19, have been utilized in various experiments to study the detailed anatomy and function of the AV valve leaflets, as illustrated in Figs. 1.6 and 1.7 [61].

## 1.9 Conclusions

The AV (mitral and tricuspid) valves are highly complex anatomical structures composed of annuluses, leaflets, tendinous cords, and associated papillary muscles. Their overall function and/or subsequent dysfunction can be due to abnormalities or failures within any of these components. Thus, it is the detailed understanding of the valve features that will aid in the development and deployment of future clinical therapies, e.g., valvar repairs or replacement via either surgical or minimally invasive (transcatheter) means. Furthermore, the use of common anatomical descriptions of these anatomical structures (defined as attitudinally correct anatomy) by anatomists, clinicians, and medical device designers is recommended for the successful and expedient communication of ideas and information in the modern world of medicine.

## References

1. Netter FH (2006) Atlas of human anatomy, 4th edn. Saunders, Philadelphia
2. Perloff JK, Roberts WC (1972) The mitral apparatus: functional anatomy of mitral regurgitation. Circulation 46:227–239
3. Cook AC, Anderson RH (2002) Attitudinally correct nomenclature. Heart 87:503–506
4. Atlas of Human Cardiac Anatomy website (www.vhlab.umn.edu/atlas). Accessed Mar 2012
5. Anderson RH, Spicer DE, Hlavacek A et al (2013) Describing the cardiac components-attitudinally appropriate nomenclature. J Cardiovasc Transl Res 6(2):118–123
6. Iaizzo PA (ed) The handbook of cardiac anatomy, physiology, and devices, 2nd edn. Humana Press, Totowa
7. Hill AJ (2009) Attitudinally correct cardiac anatomy. In: Iaizzo PA (ed) The handbook of cardiac anatomy, physiology, and devices, 2nd edn. Humana Press, Totowa, pp 15–21
8. Wilcox BR, Cook AC, Anderson RH (2005) Surgical anatomy of the valves of the heart. In: Wilcox BR, Cook AC, Anderson RH (eds) Surgical anatomy of the heart. Cambridge University Press, Cambridge, UK, pp 45–82

9. Bateman MG, Quill JL, Hill AJ et al (2013) The clinical anatomy and pathology of the human atrioventricular valves: implications for repair or replacement. J Cardiovasc Transl Res 6(2):155–165
10. Anderson RH, Becker AE, Allwork SP (1980) Cardiac anatomy: an integrated text and colour atlas. Gower Medical Publishing/Churchill Livingstone, Edinburgh/London
11. Angelini A, Ho SY, Anderson RH et al (1988) A histological study of the atrioventricular junction in hearts with normal and prolapsed leaflets of the mitral valve. Br Heart J 59:712–716
12. Messer S, Moseley E, Marinescu M et al (2012) Histologic analysis of the right atrioventricular junction in the adult human heart. J Heart Valve Dis 21:368–373
13. Victor S, Nayak VM (1994) The tricuspid valve is bicuspid. J Heart Valve Dis 3:27–36
14. Yacoub M (1976) Anatomy of the mitral valve chordae and cusps. In: Kalmason D (ed) The mitral valve. A pluridisciplinary approach. Edward Arnold Publishers, London, pp 15–20
15. Kumar N, Kumar M, Duran CM (1995) A revised terminology for recording surgical findings of the mitral valve. J Heart Valve Dis 4:76–77
16. Ritchie J, Jimenez J, He Z et al (2006) The material properties of the native porcine mitral valve chordae tendineae: an in vitro investigation. J Biomech 39:1129–1135
17. Becker AE, de Wit APM (1979) Mitral valve apparatus. A spectrum of normality relevant to mitral prolapse. Br Heart J 42:680–689
18. Van der Bel-Kahn J, Duren DR, Becker AE (1985) Isolated mitral valve prolapse: chordal architecture as an anatomic basis in older patients. J Am Coll Cardiol 5:1335–1340
19. Gams E, Hagl S, Schad H et al (1992) Importance of the mitral apparatus for left ventricular function: an experimental approach. Eur J Cardiothorac Surg 6(Suppl 1):S17–S23, discussion S24
20. Gams E, Schad H, Heimisch W et al (1993) Importance of the left ventricular subvalvular apparatus for cardiac performance. J Heart Valve Dis 2:642–645
21. Hill AJ, Laske TG, Coles JA Jr et al (2005) In vitro studies of human hearts. Ann Thorac Surg 79:168–177
22. Misfeld M, Sievers HH (2007) Heart valve macro- and microstructure. Philos Trans R Soc Lond Ser B Biol Sci 362:1421–1436
23. Marron K, Yacoub MH, Polak JM et al (1996) Innervation of human atrioventricular and arterial valves. Circulation 94:368–375
24. Filip DA, Radu A, Simionescu M (1986) Interstitial cells of the heart valves possess characteristics similar to smooth muscle cells. Circ Res 59:310–320
25. Icardo JM, Colvee E (1995) Atrioventricular valves of the mouse: III. Collagenous skeleton and myotendinous junction. Anat Rec 243:367–375
26. Icardo JM, Colvee E (1995) Atrioventricular valves of the mouse: II. Light and transmission electron microscopy. Anat Rec 241:391–400
27. Fenoglio JJ Jr, Tuan Duc P, Wit AL et al (1972) Canine mitral complex: ultrastructure and electromechanical properties. Circ Res 31:417–430
28. Itoh A, Krishnamurthy G, Swanson JC et al (2009) Active stiffening of mitral valve leaflets in the beating heart. Am J Physiol Heart Circ Physiol 296:H1766–H1773
29. Laske TG, Shrivastav M, Iaizzo PA (2009) The cardiac conduction system. In: Iaizzo PA (ed) The handbook of cardiac anatomy, physiology, and devices, 2nd edn. Humana Press, Totowa, pp 15–21
30. Carpentier A, Branchini B, Cour JC et al (1976) Congenital malformations of the mitral valve in children: pathology and surgical treatment. J Thorac Cardiovasc Surg 72:854–866
31. Anderson RH, Razavi R, Taylor AM (2004) Cardiac anatomy revisited. J Anat 205:159–177
32. Quill JL, Hill AJ, Laske TG et al (2009) Mitral leaflet anatomy revisited. J Thorac Cardiovasc Surg 137:1077–1081
33. Barker TA, Wilson IC (2011) Surgical anatomy of the mitral and tricuspid valve. In: Bonser RS, Pagano D, Haverich A (eds) Mitral valve surgery. Springer, London, pp 3–19
34. Delgado V, Tops LF, Schuijf JD et al (2009) Assessment of mitral valve anatomy and geometry with multislice computed tomography. JACC Cardiovasc Imaging 2:556–565

35. Kwan J, Kim G, Jeon M et al (2007) 3D geometry of a normal tricuspid annulus during systole: a comparison study with the mitral annulus using real-time 3D echocardiography. Eur J Echocardiogr 8:375–383
36. Veronesi F, Corsi C, Sugeng L et al (2009) A study of functional anatomy of aortic-mitral valve coupling using 3D matrix transesophageal echocardiography. Circ Cardiovasc Imaging 2:24–31
37. Berdajs D, Lajos P, Turina MI (2005) A new classification of the mitral papillary muscle. Med Sci Monit 11:BR18–BR21
38. Bateman MG, Russel C, Chan B et al (2010) A detailed anatomical study of the papillary muscles and chordae tendineae of the left ventricle in perfusion fixed human hearts. FASEB J 24(Meeting Abstract Supplement):446.4
39. Sonne C, Sugeng L, Watanabe N et al (2009) Age and body surface area dependency of mitral valve and papillary apparatus parameters: assessment by real-time three-dimensional echocardiography. Eur J Echocardiogr 10:287–294
40. Lam JH, Ranganathan N, Wigle ED et al (1970) Morphology of the human mitral valve I. Chordae tendineae: a new classification. Circulation 41:449–458
41. Kunzelman KS, Cochran RP, Verrier ED et al (1994) Anatomic basis for mitral valve modelling. J Heart Valve Dis 3:491–496
42. Ritchie J, Warnock JN, Yoganathan AP (2005) Structural characterization of the chordae tendineae in native porcine mitral valves. Ann Thorac Surg 80:189–197
43. Martinez RM, O'Leary PW, Anderson RH (2006) Anatomy and echocardiography of the normal and abnormal tricuspid valve. Cardiol Young 16(Suppl 3):4–11
44. Weinhaus AJ, Roberts KP (2009) Anatomy of the human heart. In: Iaizzo PA (ed) The handbook of cardiac anatomy, physiology, and devices, 2nd edn. Humana Press, Totowa, pp 59–85
45. Westaby S, Karp RB, Blackstone EH et al (1984) Adult human valve dimensions and their surgical significance. Am J Cardiol 53:552–556
46. Silver MD, Lam JH, Ranganathan N et al (1971) Morphology of the human tricuspid valve. Circulation 43:333–348
47. Seccombe JF, Cahill DR, Edwards WD (1993) Quantitative morphology of the normal human tricuspid valve: autopsy study of 24 cases. Clin Anat 6:203–212
48. Tsakiris AG, Mair DD, Seki S et al (1975) Motion of the tricuspid valve annulus in anesthetized intact dogs. Circ Res 36:43–48
49. Wenink AC (1977) The medial papillary complex. Br Heart J 39:1012–1018
50. Hołda MK, Zhingre Sanchez JD, Bateman MG, Iaizzo PA (2019) Right atrioventricular valve leaflet morphology redefined implications for transcatheter repair procedures. JACC Cardiovasc Interv 12(2):169–178
51. Van Miegham NM, Piazza N, Anderson RH et al (2010) Anatomy of the mitral valvular complex and its implications for transcatheter interventions for mitral regurgitation. J Am Coll Cardiol 56:617–626
52. Choure AJ, Garcia MJ, Hesse B et al (2006) In vivo analysis of the anatomical relationship of coronary sinus to mitral annulus and left circumflex coronary artery using cardiac multidetector computed tomography: implications for percutaneous coronary sinus mitral annuloplasty. J Am Coll Cardiol 48:1938–1945
53. Tops LF, Van de Veire NR, Schuijf JD et al (2007) Noninvasive evaluation of coronary sinus anatomy and its relation to the mitral valve annulus: implications for percutaneous mitral annuloplasty. Circulation 115:1426–1432
54. Spencer JH, Prahl G, Iaizzo PA (2014) The prevalence of coronary sinus and left circumflex artery overlap in relation to the mitral valve. J Interv Cardiol 27(3):308–316
55. Zhingre Sanchez JD, Bateman MG, Iaizzo PA (2019) Constructing an anatomical map of the tricuspid valve and adjacent right atrial structures for optimizing the design of transcatheter annuloplasty repair devices: a computational case study of 50 human hearts. Presented at the structural heart disease summit – Transcatheter Valve Therapies (TVT) & LAA/PFO Closure (Meeting Abstract Supplement)

56. Zhingre Sanchez JD, Gaasedelen EN, Bateman MG, Iaizzo PA (2018) Quantifying the proximity of the tricuspid annulus to the right coronary artery and triangle of Koch: implications for transcatheter tricuspid annuloplasty therapies. Presented at the structural heart disease summit – Transcatheter Valve Therapies (TVT) & LAA/PFO Closure (Meeting Abstract Supplement)
57. Asante-Korang A, O'Leary PW, Anderson RH (2006) Anatomy and echocardiography of the normal and abnormal mitral valve. Cardiol Young 16(Suppl 3):27–34
58. Otto CM (2009) Textbook of clinical echocardiography: expert consult, 4th edn. Saunders, Philadelphia
59. Baumgartner H, Hung J, Bermejo J et al (2009) Echocardiographic assessment of valve stenosis: EAE/ASE recommendations for clinical practice. J Am Soc Echocardiogr 22:1–23
60. Zoghbi WA, Enriquez-Sarano M, Foster E et al (2003) Recommendations for evaluation of the severity of native valvar regurgitation with two-dimensional and Doppler echocardiography. J Am Soc Echocardiogr 16:777–802
61. Zhingre Sanchez JD, Bateman MG, Iaizzo PA (2018) Engineering and technologies associated with cardiac valve repair and replacement therapies. In: Engineering in medicine: advances and challenges. Academic Press, London, pp 219–254

# Chapter 2
# The Anatomy and Function of the Semilunar Valves


**Michael G. Bateman, Jason L. Quill, Alexander J. Hill, and Paul A. Iaizzo**

## 2.1 Introduction

### *2.1.1 Historical Perspective*

The advent of high-resolution non-invasive imaging has increased our understanding of the functional internal anatomy of the human body. New insights build on the classic work of anatomists such as Galen, Vesalius, Leonardo da Vinci, and more recently Hunter, Gray, and Netter to provide the detailed description of human anatomy that exists today. This development of the foundational knowledge pertaining to the anatomy and morphology of the cardiac valves is comprehensively reviewed in Chap. 1.

M. G. Bateman (✉)
Cardiovascular Systems Inc., Abbott, Saint Paul, MN, USA
e-mail: MBateman@csi360.com

J. L. Quill
Medtronic, Inc., Minneapolis, MN, USA
e-mail: jquill22@yahoo.com

A. J. Hill
Anteris Technologies, Minneapolis, MN, USA

Medtronic, Inc., Minneapolis, MN, USA

P. A. Iaizzo
Visible Heart® Laboratories, Department of Surgery, Institute for Engineering in Medicine, University of Minnesota, Minneapolis, MN, USA
e-mail: iaizz001@umn.edu

© The Author(s), under exclusive license to Springer Nature Switzerland AG 2023

P. A. Iaizzo et al. (eds.), *Heart Valves*, https://doi.org/10.1007/978-3-031-25541-0_2

### 2.1.2 *Attitudinally Correct Cardiac Anatomy*

As mentioned previously in Chap. 1, published descriptions of human cardiac anatomy have not adhered to the same fundamental rules of orientation and/or anatomical position as overall gross anatomy. Briefly, the three planes of the body, sagittal, coronal, and transverse (Fig. 2.1), are used to describe the position and nature of almost all other aspects of internal anatomy with respect to the patient's own orientation. Only recently have cardiac anatomy specialists moved to redefine the nomenclature of the human heart as situated within the body rather than the traditional practice of labeling the anatomical features with the organ removed and held in the valentine position [1].

The naming of the cardiac semilunar valves, as seen in Fig. 2.2, has not been directly affected by attitudinally correct nomenclature due to the leaflets of each valve being described by their surrounding anatomies, rather than their position within the heart. The three leaflets of the aortic valve are traditionally named after the coronary arteries that branch from the sinus of Valsalva supplying blood to the left and right sides of the heart—the left, right, and non-coronary leaflets (Fig. 2.2). More recently due to repeated reports of coronary arteries arising from the posterior sinus, the non-coronary leaflet is referred to as non-adjacent. Further, due to its oblique positioning in the body, the pulmonary valve leaflets are not named according to the sagittal, coronal, and axial planes, but have rather been described by their

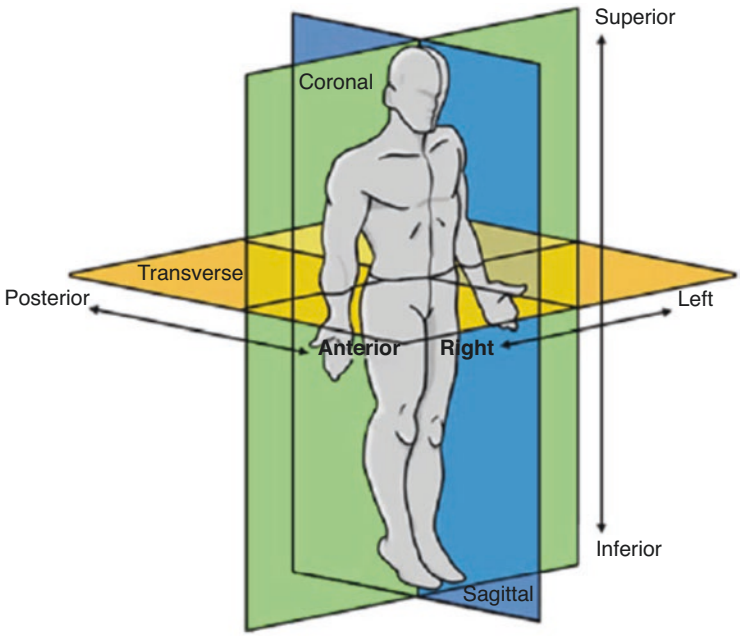


**Fig. 2.1** The anatomical planes of the human body (www.vhlab.umn.edu/atlas)

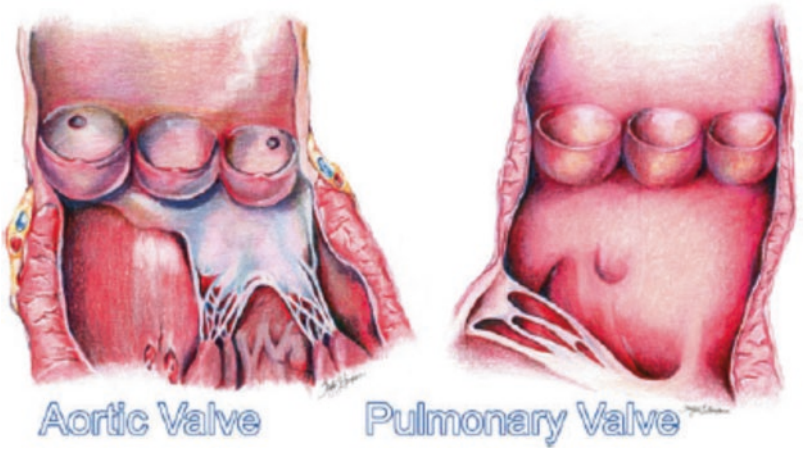


**Fig. 2.2** An artist's rendition of the healthy aortic and pulmonary valves clearly showing the leaflets, sinuses, outflow tracts, and arterial trunks

relationships to the aortic valve [2]. In a normal anatomical orientation, the right and left coronary cusps of the aortic valve face the septum between the right and left chambers. These leaflets are usually opposed by two leaflets of the pulmonary valve; hence, these two leaflets of the pulmonary valve are labeled the "right and left facing leaflets." The third leaflet of the pulmonary valve is consequently labeled as the *non-facing leaflet* to complete the trifecta. The specific anatomies of each semilunar valve will be described in more detail later in this chapter.

## 2.2 The Cardiac Skeleton

The cardiac valves are situated in close proximity to each other, shown in Fig. 2.3, and as with the atrioventricular valves, it is important to carefully describe the anatomical framework that holds these valves in position [2].

The position of the aortic valve within the cardiac base makes it the centerpiece of the organ [3]. However, only part of this support is provided by the so-called fibrous skeleton (Fig. 2.4). In the human heart, the components of the skeleton support the aortic–mitral unit, binding it into the roof of the left ventricle. Inconstant cords of fibrous tissue then extend from the margins of the fibrous continuity between the aortic and mitral valve to support the mural (anterior) leaflet of the mitral valve. The central fibrous body, the strongest portion of the cardiac skeleton, is formed by the union of the right fibrous trigone with the membranous part of the ventricular septum. The right trigone itself is the rightward end of the area of fibrous continuity between the leaflets of the aortic and mitral valves. The smaller left fibrous trigone is formed at the leftward end of this zone of fibrous continuity [3].

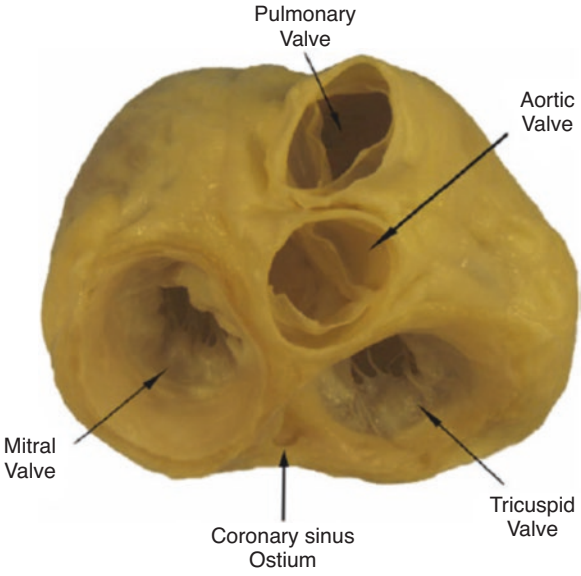


**Fig. 2.3** An anatomical plate of a human heart with the atria and great arteries removed showing the relationship between the four valves at the base of the heart

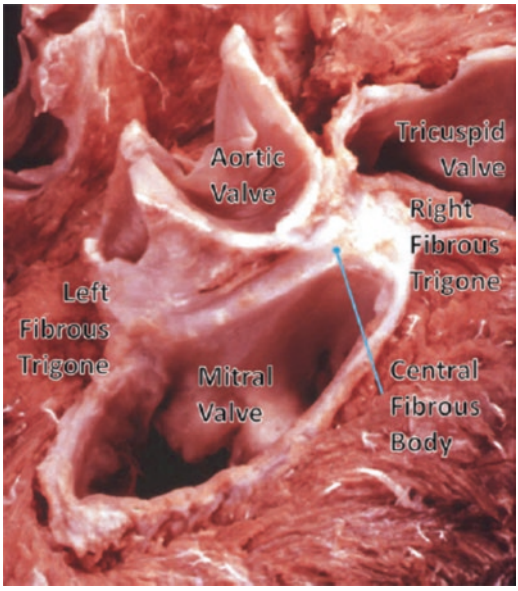


**Fig. 2.4** Dissection of the cardiac base with the atrial walls and great vessels removed. It shows the coronet shape of the aortic root and its relationship with the mitral valve. (The image is reproduced by kind permission of Professor Robert H. Anderson and was published initially in "Cardiac Anatomy" [31]. This figure was published in Cardiac Anatomy: An Integrated Text and Colour Atlas, RH Anderson, AE Becker, and SP Allword, page 239, © Elsevier 1980)

Contrastingly, the pulmonary valve has no direct fibrous support other than that provided by the valvar sinuses. The basal components of each leaflet are supported by the right ventricular infundibulum. It is this unique positioning of the pulmonary root away from the other valvar structures that make possible its surgical removal during the Ross procedure, while the presence of the supporting skirt of infundibular musculature facilitates its use as an autograft to replace the aortic valve [3].

## 2.3 Anatomical Features of the Semilunar Valves

In the most basic anatomical sense, a healthy semilunar valve is composed of three valve leaflets, each attached to its respective sinus, as visualized in Fig. 2.2. These valves lie between the ventricular outflow tracts and the arterial trunks, the main arteries carrying blood away from the heart. This elegant structure is much simpler than that of the atrioventricular valves as described in Chap. 1, in that the semilunar valve leaflets do not require a tension apparatus to maintain competency. When closed, the three leaflets of each valve co-apt along fibrous zones of apposition known as *commissures*.

The valve leaflet margins are attached to the arterial wall in the shape of a half-moon, hence the *semilunar* moniker. Normally, the regions of the valves, where the commissures meet the arterial wall, are considerably higher than the seats of the leaflets, thereby giving the valve a crown-like shape. These three points, particularly in the aortic valve, are used to define the sinutubular junctions (Fig. 2.5). Just distal to the valves are the *arterial sinuses* that are represented by dilations of the artery positioned above each leaflet and additionally house the coronary artery ostia. The sinus also provides a recess for the valve leaflets to retract into, allowing for unrestricted flow from the ventricle to the artery.

Although we have discussed the positioning of the valves in the heart by referring to their respective annuluses, many anatomists contest the idea that there are single-defined annuluses for both the pulmonary and aortic valves [4]. There is a defined annulus at the ventriculoarterial junction, where the respective arteries are attached to the ventricular outflow tract and, due to the crown-like structure of the valve, the hemodynamic junction of the valves spans this annulus. This structural

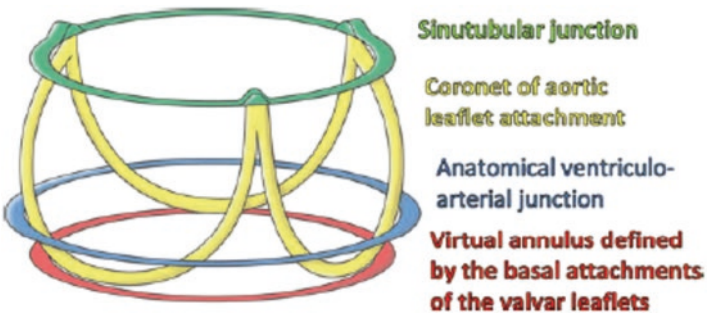


**Fig. 2.5** Idealized three-dimensional arrangement of the semilunar valve (this diagram represents an aortic root). The model contains three circular *rings* with the leaflets suspended within the root in crown-like fashion. (The cartoon is reproduced by kind permission of Professor Robert H. Anderson, who retains the intellectual copyright in the original image [3]. We acknowledge the excellent artwork created by Gemma Price. This same figure is being published in two Springer publications at the same time (Heart Valves: From Design to Clinical Implantation and The Clinical Anatomy and Pathology of the Human Arterial Valves: Implications for Repair or Replacement, J Cardiovasc Transl Res, MG Bateman, AJ Hill, JL Quill, and PA Iaizzo, 2013 Jan 17 [Epub ahead of print], PMID: 23325456))

shape results in part of the arterial wall being considered a ventricular structure (in a hemodynamic sense) and part of the ventricular wall, an arterial structure. Finally, the virtual ring, upon which many annular measurements are based and which defines the basal plane of aortic valve, is defined by the three anatomical anchors at the nadir of each aortic leaflet [5]. These features are illustrated by the diagram in Fig. 2.5.

The position and definition of the valve annulus is often contested by different medical specialists resulting in a current lack of consensus between physicians regarding the optimal means of describing the semilunar valve anatomy [6]. As such, it is important to be precise in the definition of exactly what is being measured when documenting the size and shape of the semilunar valves.

### *2.3.1 The Functioning of the Semilunar Valves*

When a semilunar valve is functioning correctly, the leaflets are pushed into the sinus during myocardial contraction (systole) to allow blood to leave the ventricles. As the myocardium relaxes and the pressure within the ventricle drops below the pressure distal to the valve in the arterial system (the aorta or pulmonary artery), the valve snaps shut. This usually happens soon after ventricular systole but before the heart has completely relaxed, so that during diastole, when the chambers are filling through the atrioventricular valves, the leaflets of the semilunar valves remain tightly closed. A positive pressure difference between the aorta and the coronary sinus, which lies within the right atrium, and the relaxation of the ventricular myocardium during diastole creates the required pressure gradient that drives the flow of blood through the coronary vasculature. Thus, it should be noted that the cardiac muscle, contrary the systemic vasculature is perfused with blood when the semilunar valves are closed.

Figures 2.6 and 2.7 show image sequences of the functional movements of the pulmonary and aortic valves, respectively; these images were obtained from reanimated human hearts employing Visible Heart® methodologies [7, 8]. See Chap. 15 for an in-depth description of this technique. The images include views of semilunar valves from above (i.e., from videoscopes within the pulmonary artery and the aorta) and below (with videoscopes within the right and left ventricular outflow tracts).

In general, dysfunctions of the semilunar valves are usually characterized by one of two symptoms: failure of the valves to successfully close or failure of the valves to successfully open. Such dysfunctions of the valves during systole, i.e., failure of the valve to successfully open, are defined as *stenosis* of the valve. This pathology is characterized by reduction in the effective orifice area of the valve (the size of the opening allowing blood to pass through the valve) increasing the work required by the ventricles to move blood to the body or lungs. Dysfunctions of the semilunar valves during diastole, when the ventricles are relaxing, result in *regurgitation*. The retrograde flow of blood back into the ventricle from the arterial system during

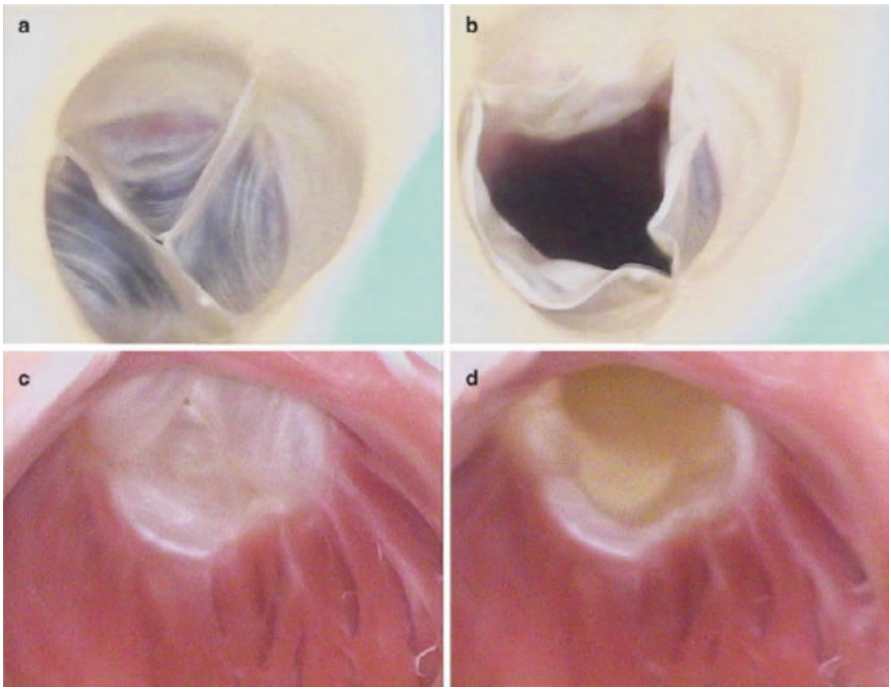


**Fig. 2.6** Internal videoscopic images of the pulmonary valve from above (**a**, **b**) and below (**c**, **d**) during systole (**a**, **c**) and diastole (**b**, **d**) obtained employing Visible Heart® methodologies

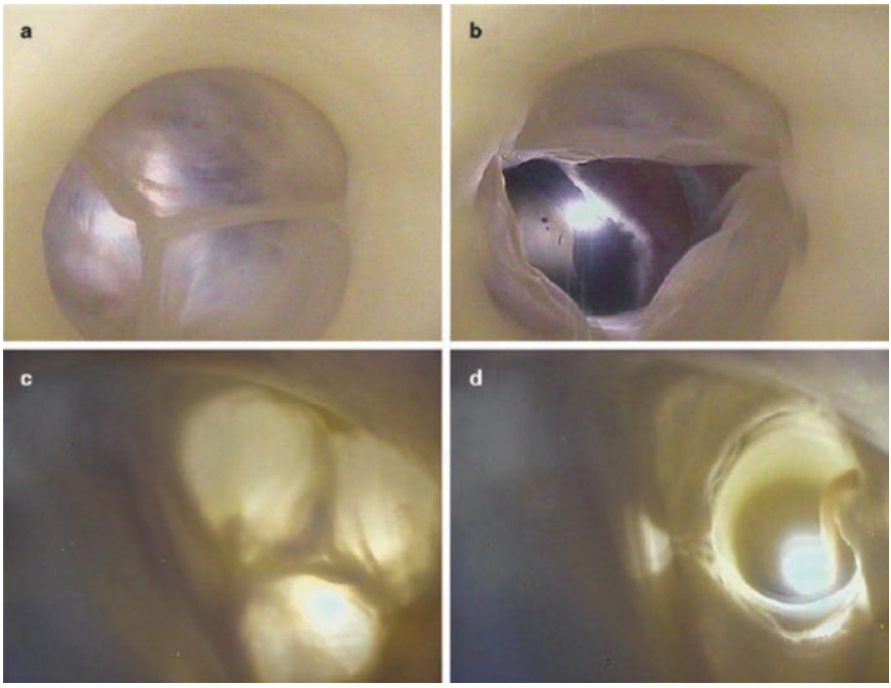


**Fig. 2.7** Internal videoscopic images of the aortic valve from above (**a**, **b**) and below (**c**, **d**) during systole (**a**, **c**) and diastole (**b**, **d**) obtained employing Visible Heart® methodologies

diastole overloads the ventricles and is considered a leading factor in the development of chronic heart failure. These pathologies are described more detail in Chap. 6.

### 2.3.2 *Histologic Features of the Semilunar Valves*

The specific histological structures of the arterial valves were first identified by Gross with his account being later endorsed by others such as Misfeld and colleagues [9, 10]. Each leaflet of the semilunar valve has a fibrous core, or *fibrosa*, with an endothelial lining on the arterial and ventricular aspects. This so-called "fibrous backbone" consists of a dense collagenous layer which transitions to a much looser structure, or *spongiosa*, toward the ventricular aspects of the leaflet cusps. The zone of apposition of the leaflets consists of an abrupt thickening of the fibrous layer made up of closely packed vertically directed fibers building at the central portion of the free edge to create a node termed the *Nodulus Arantii* [9, 10]. Figure 2.8 displays a cross-section of an aortic valve leaflet displaying the varying tissue types [11].

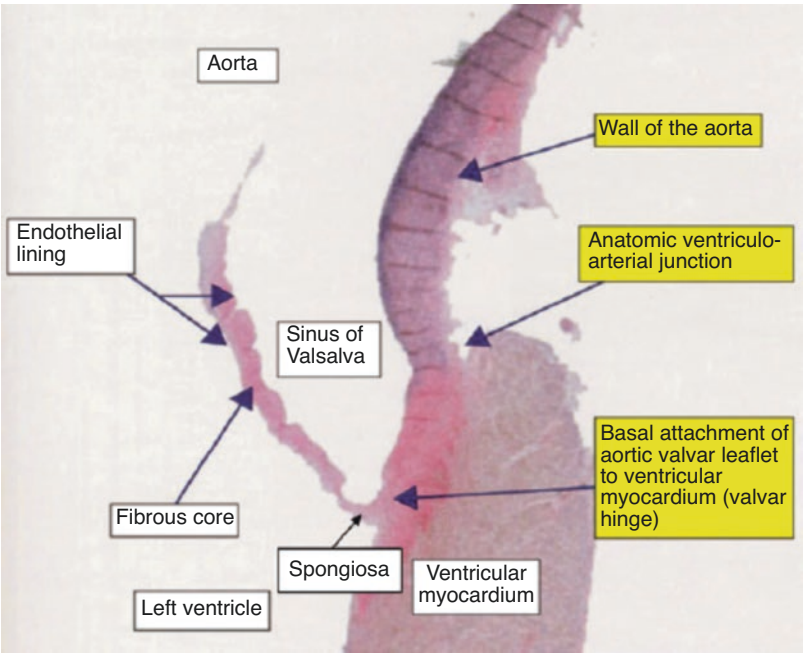


**Fig. 2.8** Histologic features of the aortic valvar complex showing the anatomic ventriculoarterial junction. Also note that the basal attachment of the aortic valvar leaflets to the ventricular myocardium is proximal relative to the anatomic junction [11]

## 2.4 The Aortic Valve

The aortic valve is considered the "centerpiece" of the heart due to its location between the mitral valve and the tricuspid valve, and is often considered the most important cardiac valve with respect to normal cardiac function [11].

### *2.4.1 The Aortic Root*

The aortic root contains three circular rings and one crown-like ring formed by the connection of the leaflets to the arterial wall (Fig. 2.5) [4]. The base of the crown forms a virtual ring known as the basal plane which represents the inlet from the left ventricular outflow tract into the aortic root. The top of the crown can be considered a true ring, the sinutubular junction, defined by the sinus ridge and the related sites of attachment of the peripheral zones of apposition, between the aortic valve leaflets [11]. Hence, the sinutubular junction dictates the transition from the aortic root into the ascending aorta. The semilunar hinges then cross another defined "ring" known as the anatomic *ventriculoarterial* junction. This overall anatomic arrangement is described previously in Fig. 2.5, but can be readily observed when the aortic root is opened linearly as seen in Fig. 2.9.

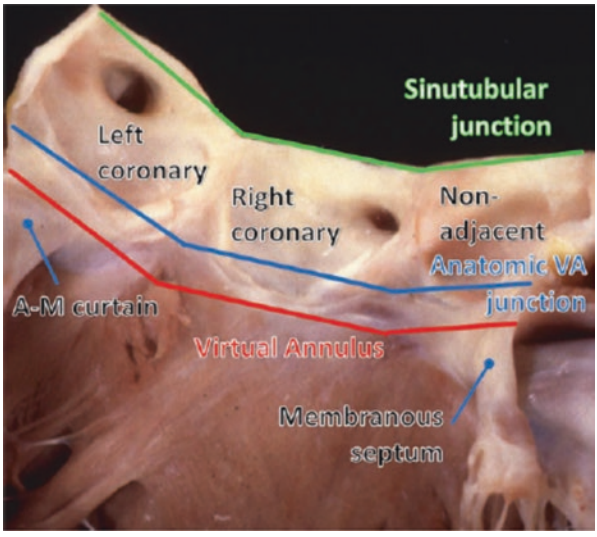


**Fig. 2.9** The aortic leaflets have been removed from this human aortic root specimen; one can then observe the locations of the three defined aortic rings, i.e., relative to the crown-like hinges of the leaflets. A-M aortic–mitral, VA ventriculoarterial [3]. (Image was modified from an original figure provided by Professor Robert H. Anderson; Professor Anderson retains the intellectual copyright of the original image)

The normal aortic root elicits a relatively consistent shape between patients, but can vary dramatically in size (Table 2.1). Kunzelman et al. demonstrated a definable mathematical relationship between root diameter and clinically measurable leaflet dimensions [12]. In general, the diameter at the level of the sinutubular junction typically exceeds that at the level of the basal plane by a factor of 1:1.6 [12, 13]. The valvar complex is a dynamic structure with its geometric parameters changing continuously throughout the phases of the cardiac cycle [14]. For example, the relative changes in diameter at the level of the sinutubular junction and the *ventriculoarterial* junction have been noted to increase by ~12% and decrease by ~16%, respectively, during systole [15–17]. Of particular interest, the ventriculoarterial junction is elliptical in shape with this shape being more pronounced in diastole [17]. This non-circular shape of the aorti annulus is highlighted in the data from patient imaging studies shown in Table 2.1 and must be considered when designing a prosthesis intended for placement in the annulus to replace a diseased valve.

It is important to note that one of the most critical functions of the aortic root is to facilitate coronary artery perfusion during ventricular diastole. This is achieved by directing 3–5% of the circulating blood through both the left and right coronary arteries while the aortic valve itself is closed. In general, the orifices of the coronary arteries arise within the two anterior sinuses of Valsalva, usually positioned just below the sinutubular junctions [13, 19, 20]. Data on the height of the coronary artery ostia above the aortic valve basal plane from both postmortem examinations and patient imaging studies shows the right coronary artery ostium consistently higher than the left (Table 2.2). This difference is significant when considering the potential obstruction of flow to these vessels when the native valve leaflets are forced open in a percutaneous procedure.

**Table 2.1** Data on the aortic valve annulus, sinus of Valsalva, and sinutubular junction measured using multislice computed tomography

| Measured anatomical feature | Data (mm) | Sample size |
|---|---|---|
| Maximum aortic annular diameter [5, 27, 32, 33] | 26.9 ± 2.8<br>26.4 ± 2.8<br>26.2 ± 2.6<br>27.0 ± 3.2 | $N = 25$<br>$N = 150$<br>$N = 177$<br>$N = 506$ |
| Minimum aortic annular diameter [5, 27, 32, 33] | 21.4 ± 2.8<br>24.0 ± 2.6<br>20.5 ± 2.3<br>21.5 ± 2.8 | $N = 25$<br>$N = 150$<br>$N = 177$<br>$N = 506$ |
| Sinus of Valsalva mean diameter [27, 33] | 32.3 ± 3.9<br>34.0 ± 4.6 | $N = 150$<br>$N = 506$ |
| Sinus of Valsalva height above the basal plane [27] | 17.2 ± 2.7 | $N = 150$ |
| Sinutubular junction mean diameter [27, 32, 33] | 28.1 ± 3.1<br>28.1 ± 3.0<br>28.0 ± 4.1 | $N = 150$<br>$N = 177$<br>$N = 506$ |
| Sinutubular junction height above basal plane [27, 32] | 20.3 ± 3.1<br>21.9 ± 3.0 | $N = 150$<br>$N = 177$ |

**Table 2.2** Data on the coronary artery height above the valve basal plane measured postmortem [21] and using multislice computed tomography [32, 33]

| Measured anatomical feature | Data (mm) | Sample size |
|---|---|---|
| Left coronary artery height [21, 32, 33] | 12.6 ± 2.6<br>14.4 ± 3.6<br>13.1 ± 2.8 | $N = 51$<br>$N = 177$<br>$N = 506$ |
| Right coronary artery height [21, 32, 33] | 13.2 ± 2.6<br>16.7 ± 3.6<br>15.8 ± 3.1 | $N = 51$<br>$N = 177$<br>$N = 506$ |

It should be recalled that it is the location of these coronary arteries that dictates the naming of the aortic valve leaflets/cusps—the left coronary, the right coronary, and the non-adjacent (or non-coronary). However, it is not unusual to find these arteries positioned superior to the sinutubular junction and variations in coronary arterial origin such as these can pose as risk factors in sudden cardiac death [22, 23].

### *2.4.2 The Aortic Leaflets*

As noted above, the leaflets of the aortic valve are named for the branching coronary arteries that feed the left and right sides of the heart (Fig. 2.2). More specifically, both the right and left leaflets attach to the aortic root in the predominantly muscular region of the left ventricular outflow tract, whereas the non-adjacent leaflet is chiefly attached to the fibrous region above the membranous septum (Fig. 2.9). This fibrous continuity connects the aortic valve to the anterior (aortic) leaflet of the mitral valve, forming the aortic–mitral curtain. The zone of apposition of the right leaflet to the non-adjacent leaflet is positioned above the membranous part of the ventricular septum. The zone of apposition of the non-adjacent leaflet with the left coronary aortic leaflet is adjacent to the anterior wall of the left atrium. The left leaflet then continues towards the right leaflet, again achieving support from the muscular part of the ventricular septum. As previously mentioned, the zones of apposition themselves extend above the ventriculoarterial junction to be attached peripherally at the sinutubular junction. Below each peripheral attachment, there is a fibrous interleaflet triangle that forms part of the ventricular outflow tract [24].

It should be noted that variations may exist in all aspects of the aforementioned dimensions of individual leaflets, including (1) height; (2) width; (3) surface area; and (4) volume of each of their supporting sinuses of Valsalva [11]. Vollebergh et al. reported that the average widths (measured between the peripheral zones of attachment along the sinus ridge) for the right, the non-adjacent, and the left coronary leaflets were 25.9, 25.5, and 25.0 mm, respectively, in an investigation of 200 normal hearts [25]. It was also described that the average heights (measured from the base of the center of the leaflet to their free edges) for the right coronary, non-adjacent, and left coronary cusps were 14.1, 14.1, and 14.2 mm, respectively. Such

variations in the leaflet dimensions of healthy valves highlight the need to focus on the anatomy and function of each leaflet when developing surgical or transcatheter treatments of aortic valve pathologies.

## 2.5 The Pulmonary Valve

Due to its relative location at the distal portion of the right ventricular outflow tract, the pulmonary valve is considered as a more simple valvar structure than the aortic valve. The left and right leaflets of the aortic valve face lie adjacent to the pulmonary trunk, and this relative anatomic orientation has been used to name the pulmonary valve leaflets: the right and left facing leaflets and the non-facing leaflet (Fig. 2.10) [2]. Anatomically, the commissure of both the right and left leaflets are supported by the supraventricular crest of the right ventricle, which separates the pulmonary valve from the tricuspid valve. Further, the non-facing leaflet is supported by the anterior wall of the right ventricular outflow tract infundibulum and is thereby considered the most anterior part of the heart [2].

Pulmonary valve replacement is recognized as a less challenging procedure than aortic valve replacement due to the relative ease of access to the valve annulus and the lower pressure gradient across the functioning valve. The ease of complete valve removal from the cardiac base has led to its use as an autograft replacement for the aortic valve in some congenital heart patients.

However, information on the valve is less abundant and reports on variations in valve dimensions are less comprehensive. Capps et al. report the mean diameter of

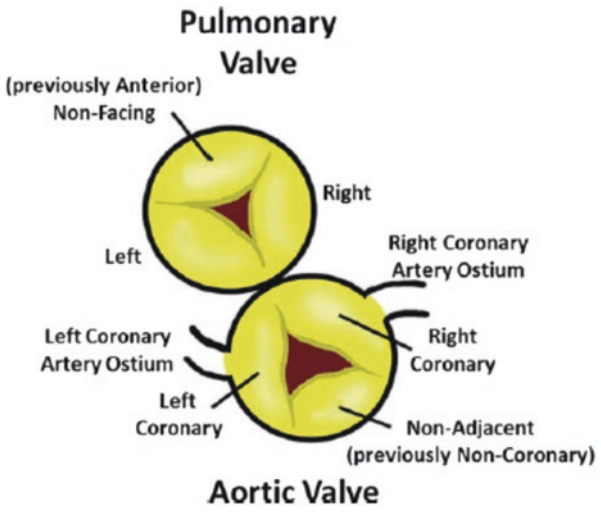


**Fig. 2.10** The nomenclature for the individual leaflets of both the aortic and pulmonary valves

**Table 2.3** Postmortem mean pulmonary and aortic diameters

| Measured anatomical feature | Data (mm) | Sample size |
|---|---|---|
| Mean pulmonary annular diameter [26] | 25.4 ± 3.2 | $N = 3997$ |
| Mean aortic annular diameter [26] | 22.4 ± 2.7 | $N = 3370$ |

the valve as 25.4 ± 3.2 mm in a study comparing the size of the aortic and pulmonary valve to the overall body surface area (Table 2.3). It should be noted that these measurements were taken postmortem using a Hegar dilator with no annular dilation. By the authors' admission. this sizing technique has limitations due to the differing material properties between the pulmonary and aortic annuluses [26]. Additionally, the alternate methodology explains the difference in the measurements reported here from those measured in vivo shown in Table 2.1 [5, 27].

## 2.6 Semilunar Valve Co-location

When one is considering performing semilunar valve surgeries and/or contemplating novel percutaneous approaches to valvar repair or replacement, it is vital to have strong anatomical appreciation of the associated structures surrounding either valve.

The important anatomical structure related to the pulmonary root is the first perforating branch of the anterior interventricular artery which must be avoided during the Ross procedure. Note should also be taken of anomalous coronary arteries either coursing between the arterial roots or extending across the right ventricular infundibulum. Being located in the most anterior aspect of the heart, the pulmonary root is also directly adjacent to the sternum [3]. This location in the thoracic cavity means that any prosthesis placed in the pulmonary annulus may be adversely affected by sternal compressions.

By comparison, the location of the aortic valve and the nature of its surrounding anatomy make procedural planning of aortic interventions much more challenging. One of the most important and complex structures in proximity to the aortic valve is the *cardiac conduction system*. Within the right atrium, the atrioventricular node is located within the *triangle of Koch*, a region demarcated by the tendon of Todaro, the attachment of the septal leaflet of the tricuspid valve, and the orifice of the coronary sinus. Within this region, the atrioventricular node penetrates the central fibrous body just inferior to the apex of the triangle and adjacent to the membranous septum. This situates the atrioventricular node in close proximity to the subaortic region of the left ventricular outflow tract helping to explain why the treatment of pathologies involving the aortic valve can lead to complete heart block or intraventricular conduction abnormalities [11]. Further, as the atrioventricular conduction axis reaches the crest of the muscular ventricular septum it then branches, with the left bundle branch cascading down the left ventricular septal surface, elegantly illustrated by Tawara over a century ago [28] (Fig. 2.11). This anatomical relationship must be considered when planning the repair and/or replacement of the aortic valve

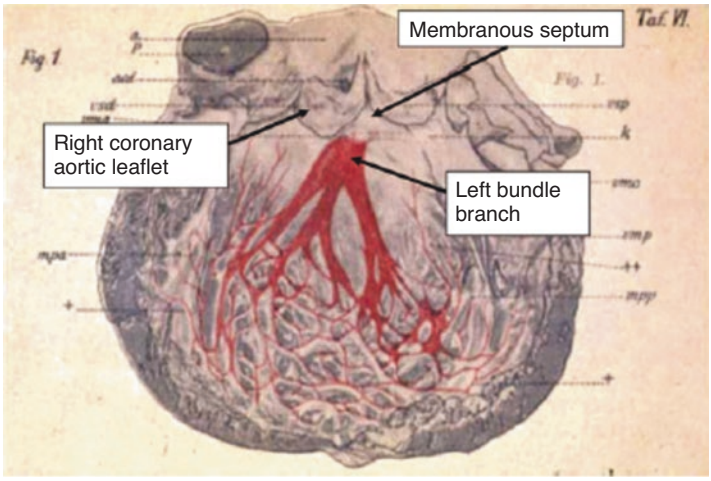


**Fig. 2.11** Tawara's anatomical diagram of the left bundle branch showing the conduction system exiting from the base of the aortic valve between the non-adjacent and right coronary leaflets. It then branches out and descends along the septal, endocardial surfaces of the left ventricular myocardium [11, 23]

as the interaction of a percutaneous prosthesis or the errant placement of sutures during surgical valve implantation can induce conduction abnormalities that lead to chronic cardiac rhythm management.

In addition to the conduction system, knowledge of the aortic valve's proximity to both coronary arteries helps to minimize procedural complications. In particular, the main stem of the left coronary artery can be remarkably short, bifurcating into the left anterior descending and circumflex arteries in close proximity to the root [3]. In the instance of transcatheter valve deployment, the prosthesis typically will crush the leaflets of the native valve against the aortic wall. Consequently, the combination of a relatively low-lying coronary artery ostium and a large, heavily calcified native aortic leaflet can lead to obstruction of the flow into the coronary arteries [11].

Finally, the proximity of the mitral valve to the aortic valve means that care must be taken not to deform the mitral annulus or disrupt of the motion of the mural (anterior) mitral leaflet during a surgical or percutaneous procedure. Either of these outcomes can lead to loss of mitral valve leaflet coaptation and subsequent systolic regurgitation [11], a key factor in the development of congestive heart failure.

## 2.7 Common Clinical Imaging of the Semilunar Valves

Echocardiography quickly provides anatomic information and readily highlights valve function thereby establishing this imaging technique as the modality of choice when first assessing the health of the semilunar valves [29]. An in-depth description

of the use of echocardiography in valvar imaging can be found in Chap. 8. Briefly, the aortic valve can be viewed from the apical, parasternal long-axis, and suprasternal echocardiographic views, whereas the pulmonary valve is usually imaged from the parasternal long-axis view (Fig. 2.12). The following valve criteria are commonly assessed using a bedside transthoracic echocardiographic system [30]:

- Size and shape of the annulus.
- Number and mobility of the leaflets, in particular whether they show restricted motion. This assessment will also include exclusion of thickening calcifications, fusions along zones of apposition, and/or leaflet damage.
- Whether the functioning of the ventricles is normal, globally deranged, or shows evidence of regional abnormalities of motion of the walls.

While echocardiography remains the primary imaging modality in assessing semilunar valve function, computed tomography (CT) and magnetic resonance (MR) imaging play an important role in complete assessment of the valve's anatomy and function. Technological advancements in both modalities have led to higher resolution and shorter image acquisition times making these techniques more accessible to care teams.

Although it often requires contrast enhancement, CT imaging can provide multiphasic imaging of the heart creating high resolution 3D imaging of the valve over the complete cardiac cycle. This imaging modality has become a key tool in the assessment of semilunar valvar disease prior to percutaneous repair and replacement. MR imaging can provide an alternative modality when contrast enhanced imaging is not an option for the patient. The modality can provide accurate 3D imaging and additionally generate data to assess ventricular function and tissue fibrosis. For a complete description of the roles of advanced 3D imaging in cardiac valve assessment refer to Chap. 9.

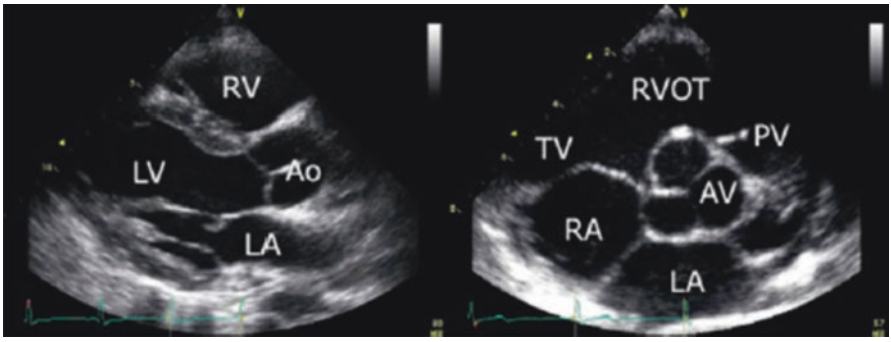


**Fig. 2.12** Parasternal long-axis section through the aortic root (*left panel*) shows the closed aortic valve, while the short-axis section shows all three leaflets of the valve. AO aorta; LA left atrium; LV left ventricle; RA right atrium; RV right ventricle; RVOT right ventricular outflow tract; PV pulmonary valve; TV tricuspid valve

## 2.8 Conclusions

The pulmonary and aortic (semilunar) valves are highly complex anatomical structures that are composed of supporting structures, leaflets, and their associated arterial vessels. The assessment, imaging, and treatment of these structures are considered an important branch of cardiology due to their importance in dictating the supply of blood to the vital organs. Although the anatomies of each semilunar valve are similar, it should be noted that unique pathological changes can affect each valve resulting in differing approaches to disease assessment and treatment. Ultimately, it is a detailed understanding of the semilunar valve anatomy that will aid physicians and engineers alike in the development and deployment of future clinical therapies for the successful treatment of congenital and degenerative diseases affecting these valves.

## References

1. Cook AC, Anderson RH (2002) Attitudinally correct nomenclature. Heart 87:503–506
2. Wilcox BR, Cook AC, Anderson RH (2005) Surgical anatomy of the valves of the heart. In: Wilcox BR, Cook AC, Anderson RH (eds) Surgical anatomy of the heart. Cambridge University Press, Cambridge UK, pp 45–82
3. Bateman MG, Hill AJ, Quill JL, Iaizzo PA (2013) The clinical anatomy and pathology of the human arterial valves: implications for repair or replacement. J Cardiovasc Transl Res. (in press, April 2013). https://doi.org/10.1007/s12265-012-9438-8
4. Anderson RH, Devine WA, Ho SY et al (1991) The myth of the aortic annulus: the anatomy of the subaortic outflow tract. Ann Thorac Surg 52:640–646
5. Schultz CJ, Moelker A, Piazza N et al (2010) Three dimensional evaluation of the aortic annulus using multislice computer tomography: are manufacturer's guidelines for sizing percutaneous aortic valve replacement helpful? Eur Heart J 31:849–856
6. Sievers HH, Hemmer W, Beversdorf F et al (2012) The everyday used nomenclature of the aortic root components: the tower of Babel? Eur J Cardiothorac Surg 41(3):478–482
7. Hill AJ, Laske TG, Coles JA Jr et al (2005) In vitro studies of human hearts. Ann Thorac Surg 79:168–177
8. www.vhlab.umn.edu/atlas/index.
9. Gross L, Kugel MA (1931) Topographic anatomy and histology of the valves in the human heart. Am J Pathol 7:445–473
10. Misfeld M, Sievers HH (2007) Heart valve macro- and microstructure. Philos Trans R Soc Lond Ser B Biol Sci 362:1421–1436
11. Piazza N, de Jaegere P, Schulz C et al (2008) Anatomy of the aortic valvar complex and its implications for transcatheter implantation of the aortic valve. Circ Cardiovasc Intervent 1:74–81
12. Kunzelman KS, Grande KJ, David TE et al (1994) Aortic root and valve relationships: impact on surgical repair. J Thorac Cardiovasc Surg 107:162–170
13. Reid K (1970) The anatomy of the sinus of Valsalva. Thorax 25:79–85
14. Swanson M, Clark RE (1974) Dimensions and geometric relationships of the human aortic valve as a function of pressure. Cir Res 35:871–882
15. Brewer RJ, Deck JD, Capati B et al (1976) The dynamic aortic root: its role in aortic valve function. J Thorac Cardiovasc Surg 72:413–417
16. Thubrikar MPW, Shaner TW, Nolan SP (1981) The design of the normal aortic valve. Am J Phys 10:H795–H801

17. Hamdan A, Guetta V, Konen E et al (2012) Deformation dynamics and mechanical properties of the aortic annulus by 4-dimensional computed tomography: insights into the functional anatomy of the aortic valve complex and implications for transcatheter aortic valve therapy. J Am Coll Cardiol 59(2):119–127
18. Turner K, Navartnam V (1996) The positions of coronary arterial ostia. Clin Anat 9:376–380
19. Muriago M, Sheppard MN, Ho SY et al (1997) Location of the coronary arterial orifices in the normal heart. Clin Anat 10:297–302
20. Cavalcanti JS, de Melo MN, de Vasconcelos RS (2003) Morphometric and topographic study of coronary ostia. Arq Bras Cardiol 81:359–362
21. Jo Y, Uranaka Y, Iwaki H et al (2011) Sudden cardiac arrest: associated with anomalous origin of the right coronary artery from the left main coronary artery. Tex Heart Inst J 38(5):539–543
22. Roynard JL, Cattan S, Artigou JY et al (1994) Anomalous course of the left anterior descending coronary artery between the aorta and pulmonary trunk: a rare cause of myocardial ischaemia at rest. Br Heart J 72(4):397–399
23. Sutton JP, Ho SY, Anderson RH (1995) The forgotten interleaflet triangles: a review of the surgical anatomy of the aortic valve. Ann Thorac Surg 59(2):419–427
24. Vollebergh FE, Becker AE (1977) Minor congenital variations of cusp size in tricuspid aortic valves: possible link with isolated aortic stenosis. Br Heart J 39:1006–1011
25. Capps SB, Elkins RC, Fronk DM (2000) Body surface area as a predictor of aortic and pulmonary valve diameter. J Thorac Cardiovasc Surg 119:975–982
26. Tops LF, Wood DA, Delgado V et al (2008) Noninvasive evaluation of the aortic root with multi-slice computed tomography: implications for transcatheter aortic valve replacement. J Am Coll Cardiol Img 1:321–330
27. Tawara S (1906) Das reizleitungssystem de saugetierherzens: eine anatomichhisologische studie uber das atrioventricularbundel und die Purkinjeschen faden. Verlag von Gustav Fischer, Jena, Germany
28. Skjaerpe T, Hegrenaes L, Hatle L (1985) Noninvasive estimation of valve area in patients with aortic stenosis by Doppler ultrasound and two-dimensional echocardiography. Circulation 72(4):810–818
29. Asante-Korang A, O'Leary PW, Anderson RH (2006) Anatomy and echocardiography of the normal and abnormal mitral valve. Cardiol Young 16(Suppl 3):27–34
30. Anderson RH, Becker AE, Allwork SP (1980) Cardiac anatomy: an integrated text and colour atlas, vol xi. Gower Medical Publishing/Churchill Livingstone, London/Edinburgh, p 239
31. Buellesfeld L, Stortecky S, Kalesan B et al (2013) Aortic root dimensions among patients with severe aortic stenosis undergoing transcatheter aortic valve replacement. JACC Cardiovasc Interv 6(1):72–83
32. Hamdan A, Barbash I, Schwammenthal E et al (2017) Sex differences in aortic root and vascular anatomy in patients undergoing transcatheter aortic valve implantation: a computed-tomographic study. J Cardiovasc Comput Tomogr 11(2):87–96

# Chapter 3
# Congenital Heart Defects Which Include Cardiac Valve Abnormalities


**Massimo Griselli, Rebecca K. Ameduri, and Michael L. Rigby**

## Abbreviations

| | |
|---|---|
| AO | Aorta |
| AS | Atrial septum |
| IBL | Inferior bridging leaflet |
| LA | Left atrium |
| MV | Mitral valve |
| OS | Outlet septum |
| PT | Pulmonary trunk |
| RA | Right atrium |
| RPA | Right pulmonary artery |
| RV | Right ventricle |
| RVOTO | Right ventricular outflow tract obstruction |
| SBE | Superior bridging leaflet |
| TV | Tricuspid valve |
| VSD | Ventricular septal defect |

M. Griselli (✉) · M. L. Rigby
Royal Brompton Hospital, London, UK
e-mail: mgriselli@doctors.org.uk

R. K. Ameduri
Division of Pediatric Cardiology, Mayo Clinic, Rochester, MN, USA

© The Author(s), under exclusive license to Springer Nature Switzerland AG 2023

P. A. Iaizzo et al. (eds.), *Heart Valves*, https://doi.org/10.1007/978-3-031-25541-0_3

## 3.1 Inherited Valve Diseases

| Isolated congenital valve disease | Valve disease with other congenital heart defect |
|---|---|
| Aortic valve stenosis/regurgitation | Atrioventricular septal defect |
| Pulmonary valve stenosis/regurgitation | Tetralogy of Fallot |
| Mitral valve (MV) stenosis/ regurgitation | Truncus arteriosus |
| Ebstein's anomaly | Shone's complex |
| | cc-TGA with Ebstein's anomaly |
| | Complex left ventricular outflow tract obstruction |
| | Pulmonary stenosis with ventricular septal defect (VSD) |
| | Subaortic VSD causing aortic insufficiency |

### *3.1.1 Aortic Valve Stenosis*

Aortic valve stenosis (AS) [1] in children is a congenital heart malformation causing a fixed left ventricular outflow tract obstruction which is found at birth or shortly thereafter. Presentation varies in severity and can be found from minor signs of murmur evaluation to more severe presentation with congestive heart failure with a severe lactic acidosis and cardiovascular collapse requiring emergency treatment. The natural history of mild to moderate stenosis is a gradual increase in severity and patients will often develop aortic regurgitation. Other types of aortic stenosis include discreet fibromuscular and tunnel subaortic stenosis together with supra valve stenosis. The optimal treatment for moderate to severe congenital AS has been debated in the last few decades, either balloon aortic valvuloplasty (BAV) versus surgical aortic valvotomy (SAV). In determining the best treatment, factors that are considered include procedural success, in hospital morality, development of aortic regurgitation, and reintervention rates. There is a strong case for BAV in the neonate or young infant with severe aortic stenosis and resultant severe left ventricular dysfunction. Brown and colleagues stated that overall SAV provides a better gradient reduction, less postoperative aortic regurgitation, and a lower reintervention rate at 10 years compared to BAV without a difference in survival or need for aortic valve replacement. However, a meta-analysis, recently described by Saung and colleagues, showed that although the reintervention rate was higher for BAV compared to SAV, the survival rates, need for aortic valve replacement, and late aortic valve regurgitation are similar.

### 3.1.2 Aortic Valve Regurgitation

Isolated congenital aortic valve regurgitation is extremely rare. Most often, it is associated with congenital AS or occurs following aortic valve procedures. It may arise as a complication of surgical procedures on the left ventricular outflow tract or as a complication of other types of surgery (i.e. VSD closure, subaortic stenosis resection, or other types of interventional cardiology procedure). Beside aortic valve replacement, there are different types of repairs to address these cases.

### 3.1.3 Pulmonary Valve Stenosis

Congenital pulmonary valve stenosis can range in severity from minimal disease to critical disease requiring immediate intervention. Most commonly, if intervention is indicated, this valvular defect is treated with transcatheter balloon valvuloplasty. In the most severe cases, neonates may require prostaglandin infusion before and after intervention in order to augment pulmonary blood flow until the right ventricular compliance improves after relief of the valve obstruction. In rare extreme cases, a pulmonary artery shunt is needed. Percutaneous valvuloplasty remains the treatment of choice with rare complication rates. It can result in excellent intermediate and long-term results, with only 10% restenosis requiring reintervention. More commonly following balloon intervention, patients can develop pulmonary insufficiency, however, this is typically well tolerated for many years. In some cases, if there is severe pulmonary valve insufficiency, patients may require pulmonary valve replacement. A close cousin of severe (critical) pulmonary valve stenosis is pulmonary atresia with intact ventricular septum in which there is an imperforate pulmonary valve. Initial treatment is by percutaneous trans-venous radio-frequency perforation of the atretic valve accompanied by balloon pulmonary valvuloplasty.

### 3.1.4 Pulmonary Valve Regurgitation

Pulmonary valve regurgitation is commonly the acquired outcome of transcatheter intervention for pulmonary stenosis or surgical intervention for tetralogy of Fallot or severe right ventricular outflow tract obstruction (RVOTO). Congenital moderate to severe regurgitation is extremely rare. The only congenital heart defect associated with pulmonary regurgitation as a prominent feature is tetralogy of Fallot with absent pulmonary valve syndrome. This syndrome often requires neonatal intervention due to severe pulmonary valve insufficiency with severe dilation of the

pulmonary artery tree which can compromise the airway anatomy with severe trachea-bronchomalacia. Intervention includes surgical repair of tetralogy of Fallot with pulmonary valve placement with valved conduit and pulmonary arterioplasty.

### *3.1.5 MV Stenosis*

Congenital mitral stenosis can present as an isolated defect or in association with other left heart obstructive lesions [2]. In the latter, patients often need to pursue single ventricle palliation due to hypoplasia of multiple left heart structures. In isolated cases, obstruction around the valve can happen at different levels, either supravalvular, valvular, or subvalvular, or in combination such as in parachute, arcade lesion, or hammock MV. Surgical procedures aim to remove the obstruction and restore leaflet mobility and function. There have been different techniques described to achieve this. The results have improved over the years, although there are several factors that appear to be important for survival and long-term outcomes, including age at presentation, development of pulmonary artery hypertension, and severity of the lesion. In few cases, valve replacement in a supra-annular position can be used. The association of some form of mitral stenosis with left ventricular outflow obstruction and with or without coarctation of the aorta (AO) is sometimes called Shone's complex.

### *3.1.6 MV Regurgitation*

MV regurgitation can result from abnormal development of the MV including MV prolapse, collagen vascular disorders/connective tissue disorders, mucopolysaccharidosis, and papillary muscle dysfunction. In the last 20 years, different surgical techniques have been developed to repair these valves, and in severe cases MV replacement is needed. The technique of percutaneous delivery of a 'Mitra-clip' used in some older adults with severe regurgitation has not been applied to children and younger adults.

## 3.2 Ebstein's Malformation of the Tricuspid Valve (TV)

Ebstein's anomaly is a complex abnormality of the TV and right ventricular myocardium in which the hinged attachments of the septal and inferior leaflets of the TV are displaced away from the atrioventricular junction towards the apex of the right ventricle (RV). The valve leaflets become adherent to right ventricular myocardium giving rise to 'atrialization' of a portion of the RV, right atrial enlargement, and tricuspid regurgitation. Dearani reports the anatomical features of this defect

including failure of the leaflet delamination, apical descent of the functional valvular orifice, right ventricular dilation and atrialization, anterior leaflet abnormal fenestrations and tethering, and right atrioventricular junction dilation. The degree of apical displacement and severity of tricuspid regurgitation remains the most important clinical determinant of the outcome of Ebstein's malformation. Asymptomatic patients can be managed medically for many years, but TV repair using the Cone Operation [3] described by Da Silva, in the correct hands, can produce outstanding results and should be considered if patients start to develop severe tricuspid regurgitation, worsening exercise capacity, cyanosis, and right ventricular dysfunction. Any arrythmias are managed in advance of surgery by radiofrequency ablation techniques. The requirement for TV replacement with a bioprosthetic valve is becoming less frequent.

## 3.3 Atrioventricular Septal Defects ('AV Canal' Defects)

The atrioventricular septum is that part of intracardiac septal structures separating left ventricle from right atrium. The characteristics of an atrioventricular septal defect (AVSD) are complete deficiency of the atrioventricular septum resulting in a common atrioventricular junction, common atrioventricular valve, primum atrial septal defect whose inferior border is the common valve leaflets and interventricular defect whose superior border is the common valve leaflets [4] (Fig. 3.1). AVSD comprises a spectrum of defects ranging from partial to intermediate to complete AVSD. The 'complete' form is characterized by a primum atrial septal defect, inlet VSD, common atrioventricular valve with abnormal leaflet support structures leading to variable degrees of regurgitation. The complete form of AVSD requires surgical repair within

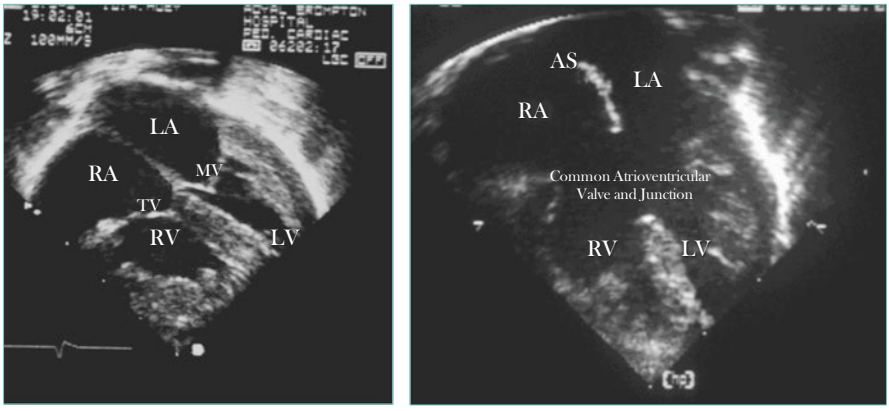


**Fig. 3.1** (**a**) Normal 4 chamber echocardiographic section of the atrioventricular junction with normal tricuspid and MVs. (**b**) By way of contrast this echocardiographic 4 chamber section demonstrates the common atrioventricular junction during diastole in a complete atrioventricular septal defect (AVSD)

the first 6 months of life, either with single or two-patch technique to close the ASD and VSD and repair the commissural 'cleft' between the superior and inferior bridging leaflets of the part of the common valve within the left ventricle. Repair of a so-called 'partial' AVSD is to close the primum ASD and partly to repair the valve leaflets in the same way. The right- and left-sided atrioventricular valves have no similarity to the normal tricuspid and MVs. The results are normally excellent, however, left-sided atrioventricular valve regurgitation is a major cause of morbidity and need for reintervention including re-repair or valve replacement. The outcome of AV canal repair depends on several factors related to the anatomy of the valve leaflets, relative size of the left and right ventricular components of the common valve and ventricular proportions. Association with Down syndrome portends a better prognosis for complete AVSD repair, with non-Down's patients more likely to require more repeat intervention on the left atrioventricular valve.

### *3.3.1 Tetralogy of Fallot*

Tetralogy of Fallot is characterized by constellation of features resulting from anterior and cephalad deviation of the outlet ('infundibular') septum giving rise to a large VSD with overriding of the AO, infundibular pulmonary stenosis and consequently right ventricular hypertrophy (Figs. 3.2, 3.3, and 3.4) [5]. The RVOTO and pulmonary stenosis can occur at multiple levels (infundibular, valve, supra valve, and pulmonary artery bifurcation). The timing of repair is dependent on the severity of the right ventricular outflow obstruction, although in recent years there is a strong tendency for complete repair earlier in life and certainly within 9–12 months of age. Historically, the management of the RVOTO and the rudimentary pulmonary valve was a transannular patch with autologous pericardium, although in recent years there is a tendency for surgeons to reconstruct valve patency in a different way including monocusp valve taken from allograft or re-create valve leaflets from other synthetic materials.

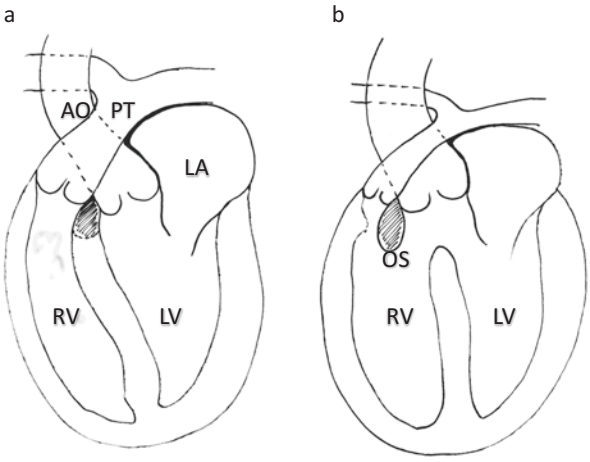


**Fig. 3.2** Line drawing of the essential anatomic features of the normal heart (**a**) compared with tetralogy of Fallot (**b**) illustrating a large VSD, overriding of AO and infundibular pulmonary stenosis

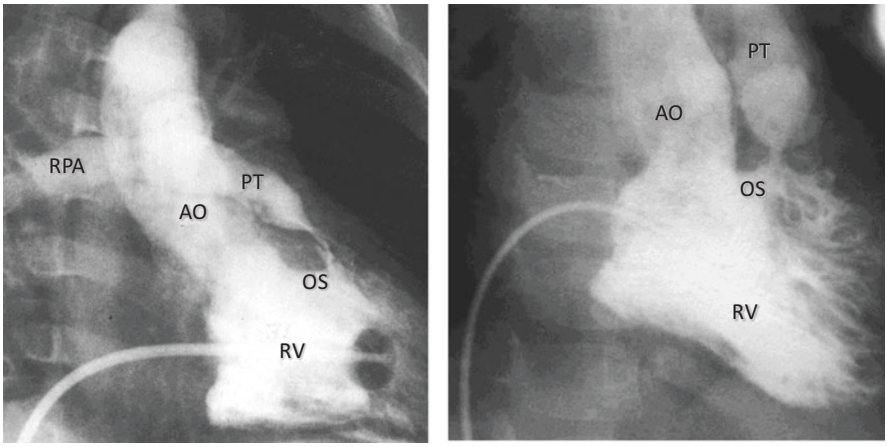


**Fig. 3.3** Right anterior oblique projections of right ventricular angiography in two patients each demonstrating anterior deviation of the outlet (infundibular) septum with severe infundibular pulmonary stenosis. On the right-sided image, there are extensive septo-parietal trabeculations contributing to the stenosis

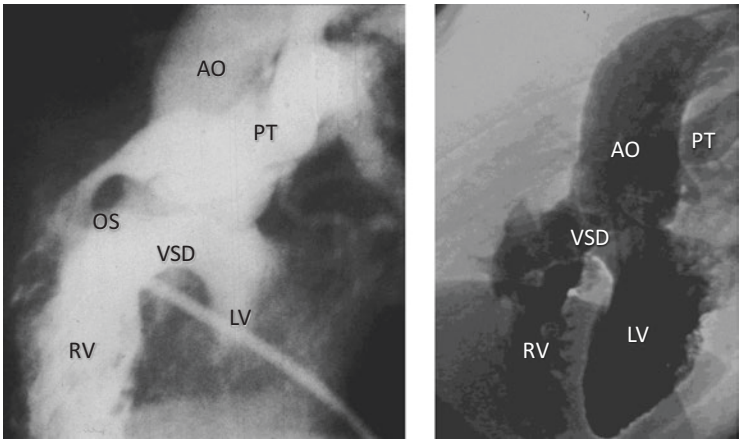


**Fig. 3.4** Right and left ventriculograms in long axis projection from two patients each demonstrating a large VSD, overriding of the AO and infundibular pulmonary stenosis together with the pulmonary trunk and branch pulmonary arteries

### *3.3.2 Truncus Arteriosus*

Truncus arteriosus ('common arterial trunk') is a 'cono-truncal' abnormality in which there is a failure of septation of the AO and main pulmonary artery [6]. A single great artery, the common trunk, overrides a large VSD and arises from the ventricles giving rise to the AO, pulmonary artery, and coronary arteries in its ascending part. The truncal valve usually has three or four leaflets, but can have anything from one to six with resultant stenosis or regurgitation. In 25% of cases,

there is valve insufficiency, and this has been identified as a risk for poor outcome and for subsequent need for truncal valve surgery if not addressed at the primary surgery. However, even after the initial repair, there is a high incidence of reoperation for the truncal valve. It has also been reported that creation of a tricuspid truncal valve confers the best outcome amongst the types of repairs, with the best freedom from truncal valve reoperation. The association with interrupted aortic arch is also a risk factor for poor outcome.

## 3.4 Shone's Complex

This term describes a combination of lesions that lead to multiple levels of left heart obstruction, including any type of mitral stenosis, variable degrees of left ventricular hypoplasia, subaortic or valvular aortic stenosis, hypoplastic aortic arch, and coarctation of the AO. Some of these infants will be palliated with single ventricle pathway, particularly if the MV and left ventricular are too small. If repair is needed, the aforementioned techniques for congenital mitral stenosis are used in association with relief of aortic stenosis and/or coarctation and arch repair. Relief of left ventricular outflow obstruction varies from simple aortic valvotomy to more complex forms of repair including Ross-Konno procedure (described in detail in another chapter).

## 3.5 Congenitally Corrected Transposition of the Great Arteries (CC-TGA) with Ebstein's Anomaly

CC-TGA is characterized by a discordant atrio-ventricular connection (RA to LV and LA to RV) with discordant ventricular-arterial connection. The left-sided TV found in the 'systemic' morphologically RV is often dysplastic in similar fashion to Ebstein's malformation (described by some as 'Ebsteinoid') with varying degrees of regurgitation, although true Ebstein's malformation with significant leaflet displacement occurs in only 5% of hearts with discordant AV connection (Fig. 3.5). The ventriculo-arterial connection may be double outlet RV with subpulmonary VSD in 20% of cases of discordant AV connection but basic surgical management remains the same.

In the anatomical repair of this malformation which includes an atrial switch operation (Senning or Mustard procedure) combined with an arterial switch operation or Rastelli type of intraventricular repair, the TV 'moves' to the sub-pulmonary morphologically RV and rarely requires surgical attention. Following the physiological repair of the malformation, or in previously unoperated cases where the RV remains in the systemic position, progressive tricuspid regurgitation and right ventricular dilation and dysfunction are often the indication for intervention, although

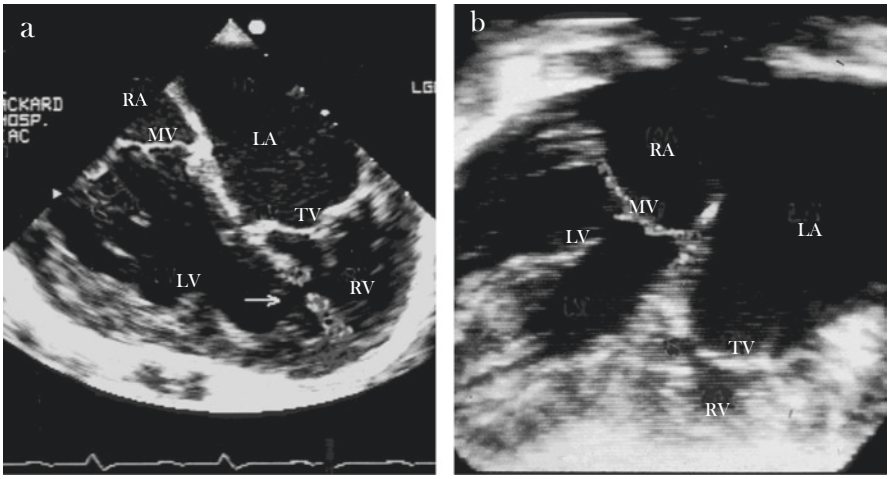


**Fig. 3.5** Four chamber echocardiographic sections from two hearts with discordant atrioventricular connection and Ebstein's malformation of the TV. (**a**) The cardiac apex directed to the right and (**b**) the apex to the left. The arrow highlights a small muscular VSD. In each case, the TV is displaced from the atrioventricular junction into the left sided morphologically RV

in older patients, cardiac transplantation needs to be considered as the preferred option. CC-TGA with moderate pulmonary stenosis with or without VSD carries a good prognosis and surgical intervention may be better avoided is selected cases, delaying any treatment until there is a need for cardiac transplantation in the fourth or fifth decade.

### *3.5.1 Complex Left Ventricular Outflow Tract Obstruction*

Besides the AS which as described previously, left ventricular outflow tract obstruction may occur in subaortic and supravalvular components as well. These areas of obstruction are often amenable to straight forward surgical intervention. However, there are also complex cases with subaortic obstruction with small aortic valve annulus which may require more complicated repair such as the Ross or Ross-Konno procedures, particularly because of the size of the aortic annulus.

### *3.5.2 Pulmonary Stenosis with VSD*

Pulmonary stenosis with VSD is a form of congenital heart disease which differs from tetralogy of Fallot because of the absence of anterior deviation of the infundibular septum and frequently a smaller VSD. However, the treatment remains very

similar to that described above in management of tetralogy. Not infrequently because of the small VSD and gradually increasing severity of muscular subpulmonary stenosis, surgical repair is often later in childhood.

## 3.6 Subaortic VSD and Aortic Insufficiency

Sometimes perimembranous or muscular outlet VSDs in the subaortic or supracristal position, the so-called doubly committed sub-arterial defect, can require surgical intervention due to the development of progressive aortic insufficiency. These are often small to moderate defects that would not require surgery for VSD physiology; however, they can produce a 'venturi effect' on the aortic valve leaflets and lead to progressive aortic insufficiency. Closure of the VSD sometimes is sufficient alone, however, in some cases repair of the aortic valve leaflets or even leaflet resuspension is required.

## 3.7 Valve Disease Late After Repair of Congenital Heart Defects

Following repair of several types of congenital heart defects, valvular disease may develop during follow-up which may necessitate further intervention for repair or replacement. The most common pathology encountered in practice is pulmonary valve regurgitation following tetralogy of Fallot repair which may require treatment in different age groups. Without discussing the indications for treatment which will be addressed in another chapter, historical surgical treatment with valve replacement, with either bioprosthetic or homograft valve or in specific cases with mechanical prosthesis, was the gold standard. As more transcatheter valve options are developed, this has become the preferred choice in cases which are amenable to transcatheter valve placement. Additionally, in tetralogy of Fallot, because of the anatomic nature as part of the conotruncal abnormalities, aortic root enlargement and aortic valve regurgitation may develop particularly in adult congenital age groups and may require surgical intervention with root replacement ± valve repair or replacement. Similarly, in truncus arteriosus, another conotruncal defect, reintervention in the truncal valve for either stenosis or insufficiency may be required particularly in those cases where the valve has previously been addressed during the primary repair.

The other common post-operative valve disease we encounter is mitral regurgitation following AVSD repair. As aforementioned, some of these valves are amenable to further repair or may need replacement with bioprosthesis or mechanical prosthesis depending on the age of the patient. In recent years, techniques have been developed for surgical deployment of Melody Valves, used in percutaneous pulmonary valve replacement, in the mitral position.

Less common malformation in which there is valvular disease include complete transposition of the great arteries ('D-TGA') late following repair with the arterial switch operation. Either the neo-aortic valve (former pulmonary valve) or neo-pulmonary valve can progressively develop regurgitation necessitating repair or replacement.

## 3.8 Valve Disease Related to Inherited Conditions

There are several genetic syndromes that have specific associated valvular disease. Most commonly seen is MV prolapse, whereas MV regurgitation is seen in connective tissue disorders, including Marfan's syndrome, Ehlers-Danlos syndrome, and Loeys-Deitz syndrome. In addition to MV disease, in particular in the Marfan population, they can develop aortic root dilation with subsequent development of aortic valve regurgitation. This is not truly a valvular disease, but is a consequence of the root dilation, therefore in most cases surgical treatment with valve sparing root replacement, as popularized by Magdi Yacoub and Tyrone David, will suffice and rare cases require valve repair or replacement.

Inherited storage disorders, in particular the mucopolysaccharidosis diseases, have progressive multi-valvular disease related to deposition of mucopolysaccharides in the valvular tissue. The most common that requires surgical intervention is development of mitral or aortic stenosis. Due to the nature of the underlying disease, most commonly these require replacement with mechanical valve, as the mucopolysaccharides could be deposited in a bioprosthetic valve.

## References

1. Angelini A, Ho SY, Anderson RH et al (1989) The morphology of the normal aortic valve as compared with the aortic valve having 2 leaflets. J Thorac Cardiovasc Surg 98:362–367
2. Wood AE, Healy DG, Nolke I et al (2005) Mitral valve reconstruction in a Pardoe population: late clinical results and predictors of long-term outcome. J Thorac Cardiovasc Surg 130:66–73
3. Da Silva J, Baumgratz J, da Fonseca I et al (2007) The cone reconstruction of the tricuspid valve in Ebstein's anomaly. The operation: early and mid-term results. J Thorac Cardiovasc Surg 133:215–223
4. Rigby M (2021) Atrioventricular septal defect: what is in a name? J Cardiovasc Dev Dis 8:19. https://doi.org/10.3390/jcdd8020019
5. Anderson RH, Weinberg PM (2005) The clinical anatomy of tetralogy of Fallot. Cardiol Young 15(S1):38–47
6. Konstantinov IE, Karamlou T, Blackstone EH et al (2006) Truncus arteriosus associated with interrupted aortic arch in 50 neonates: a Congenital Heart Surgeons Society study. Ann Thorac Surg 81:214–227

# Part II
# Valve Repair and Replacement

# Chapter 4
# Heart Valve Disease

**Ranjit John and Chesney Siems**

## Abbreviations

| | |
|---|---|
| ACC | American College of Cardiology |
| ACE | Angiotensin Converting Enzyme |
| AHA | American Heart Association |
| PMBC | Percutaneous Mitral Balloon Commissurotomy |
| TAVR | Transcatheter Aortic Valve Replacement |

## 4.1 Introduction

The function of the heart is to circulate blood throughout the body, in closed circuit to the lungs where blood is oxygenated and to the body where oxygen provides fuel for cellular metabolism. Although often described as a single biologic pump, the heart is actually two functional pumps in series, composed of the right and left heart pumps. In the pulmonic circulations, blood is pumped from the body to the lungs by the right heart system. Once oxygenated in the lungs, blood returns to the left heart where it is then pumped out to the body, the systemic circulation. The right and left pumps are composed of atrial and ventricular chambers, whose synchronized contractions result in the forward flow of blood out of the heart. Crucial to the appropriate function of the heart are its four valves: the mitral, aortic, tricuspid, and pulmonic valves. These valves function in concert to maintain and optimize forward flow of blood through the heart (Fig. 4.1). Therefore, diseases affecting the heart valves

R. John (✉) · C. Siems
Division of Cardiovascular and Thoracic Surgery, Department of Surgery, University of Minnesota, Minneapolis, MN, USA
e-mail: johnx008@umn.edu

© The Author(s), under exclusive license to Springer Nature Switzerland AG 2023

P. A. Iaizzo et al. (eds.), *Heart Valves*, https://doi.org/10.1007/978-3-031-25541-0_4

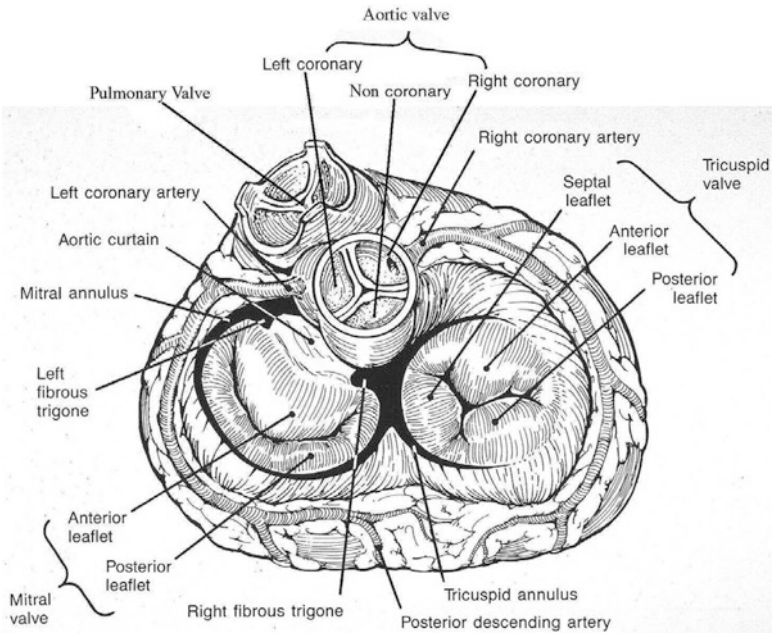


**Fig. 4.1** Apical view of the four heart valves—aortic, mitral, pulmonic, and tricuspid. (Source: Iaizzo [89])

may result in significant morbidity and mortality. These may include obstruction to forward flow (stenosis) or reversal of flow across an incompetent valve (regurgitation). This chapter will cover a brief overview of the current treatment options for heart valve disease. Major topics of discussion include: (1) development of prosthetic valve replacements; (2) current issues with valve replacement; (3) recent advances in and the future of therapeutic options for valvular diseases; and (4) application of prosthetic valves for treatment of major valvular diseases that affect humans in the western World.

## 4.2 A New Frontier—Valve Replacement

Prior to 1950, the ability to safely and effectively operate on the human heart was considered an insurmountable goal or even unethical. Attempts to operate to correct valvular diseases without stopping the heart resulted in severe, often fatal complications including uncontrollable bleeding and the introduction of air emboli [1]. It was not until C. Walton Lillehi, Richard L. Varco, and F. John Lewis at the University of Minnesota perfected the cardiopulmonary bypass procedure in the 1950's that the surgeon was able to stop the heart to access the cardiac valves while maintaining forward flow of blood [2]. With this new technology, a new frontier in surgical interventions for the treatment of heart valve disease began to emerge. During the past

several decades, major advances have occurred in diagnostic techniques (i.e., imaging), therapeutic interventions for valvular diseases, and increased understanding of the natural history of both treated and untreated valvular disease (see Chapters 10-12 on transcatheter delivered valves). Advances in heart valve development continue to evolve, and our knowledge of heart valve functionality has increased continually, so to provide patients with better outcomes after valve surgery and chances for extended life not limited by valve disease. A detailed history outlining the development of currently used valve prostheses is beyond the scope of this text, but the next few sections will review major advances in mechanical and biological prosthetic valves, as well as compare the two technology platforms.

### *4.2.1 Mechanical Prosthetic Valves*

By 1961, Dr. Albert Starr and Lowell Edwards had successfully implanted the world's first mechanical valve into a human to replace a mitral valve that had been deformed by rheumatic fever [3]. Initially, this steel ball and cage design were successful in approximately 50% of implantations; however, major complications were soon recognized, including: (1) clot formation resulting in embolic strokes; (2) significant noise from the valve itself; (3) red blood cell destruction (hemolysis) leading to anemia; and (4) tissue in-growth causing subsequent valve obstruction. Two key aspects of advancing valve design included improved valve hemodynamics and the reduced potential for thrombogenesis (i.e., clot forming). Efforts to optimize valve hemodynamic function date back to the early 1970's with the development of the Lillehei/Kaster tilting disk valve, which allowed blood to flow centrally through the valve. At that time, this new type of device emphasized the necessity for a valve that would reduce turbulent blood flow, reduce cell destruction, and minimize the transvalvular gradient [4]. A transvalvular gradient is defined as the pressure difference across the valve. Despite the advantages of a new steel tilting disk design, careful, strict and long-term anticoagulation therapy was still required to reduce the risk of clot formation [5]. The next advancement in prosthetic valves came with the development of the pyrolytic carbon valve leaflets. The non-thrombogenic weight and strength properties were defined by Drs. Jack Bokros and Vincent Gott in 1964, and subsequently this prosthetic material was applied in the creation of a bileaflet valve, inspired by the earlier work of Dr. Bhagavant Kalke, and first implanted in 1969 [6]. This valve, originally manufactured by St. Jude Medical (St. Paul, MN), provided exceptional performance, and today this design remains as the "gold standard" for mechanical valves [7]. To date, all patients with mechanical valves require anticoagulation (e.g., oral warfarin therapy), which reduces the risk of thromboembolism from 1% to 2% per year (Table 4.1) [8]. It should be noted that numerous studies have demonstrated that the risk of thromboembolism is directly related to the valve implant position. Risks for thromboembolism decreases in the order of tricuspid, mitral, and aortic valve positions. In addition, these risks for emboli appears to be greatest in the early post-implant period and decreases as the valve sewing cuff becomes fully endothelialized over time.

**Table 4.1** Anticoagulation after prosthetic heart valves

| | | Warfarin INR 2–3 | Warfarin INR 2.5–3.5 | Aspirin 80–100 mg |
|---|---|---|---|---|
| Mechanical prosthesis | | | | |
| First 3 months post-implantation | | | + | + |
| After initial 3 months | Aortic valve | + | | |
| | Aortic valve + Risk factor | | + | + |
| | Mitral valve | | + | + |
| | Mitral valve + Risk factor | | + | + |
| Biological prosthesis | | | | |
| First 3 months post-implantation | | | + | + |
| After initial 3 months | Aortic valve | | | + |
| | Aortic valve + Risk factor | + | | + |
| | Mitral valve | | | + |
| | Mitral valve + Risk factor | + | | + |

In general, management of anticoagulation must be individualized, i.e., for a given patient to minimize risks of thromboembolism and, at the same time, prevent bleeding complications.

For example, in situations where a patient with valve prosthesis undergoes non-cardiac surgery, warfarin therapy should be stopped only for procedures where risks for bleeding are substantial. A complete discussion of anticoagulation therapy is beyond the scope of this chapter, but there are several excellent reviews available on this subject [8].

### *4.2.2 Biological Prosthetic Valves*

Given the problems related to anticoagulation with mechanical valves, the majority of subsequent valve research focused on developing a tissue alternative, which avoids the necessity for anticoagulation. Drs. Lower and Shumway performed the first pulmonary valve auto-transplant in an animal model, paving the way for Dr. Donald Ross to complete the first successful replacement in a human in 1967 [9]. Still today, the *Ross Procedure* is a well-established method developed to replace a diseased aortic valve with the patient's own pulmonary valve (Fig. 4.2). A donor tissue valve or homograft (Table 4.2) is then used as a prosthetic pulmonary valve. In general, tissue valves are significantly more biocompatible than their mechanical

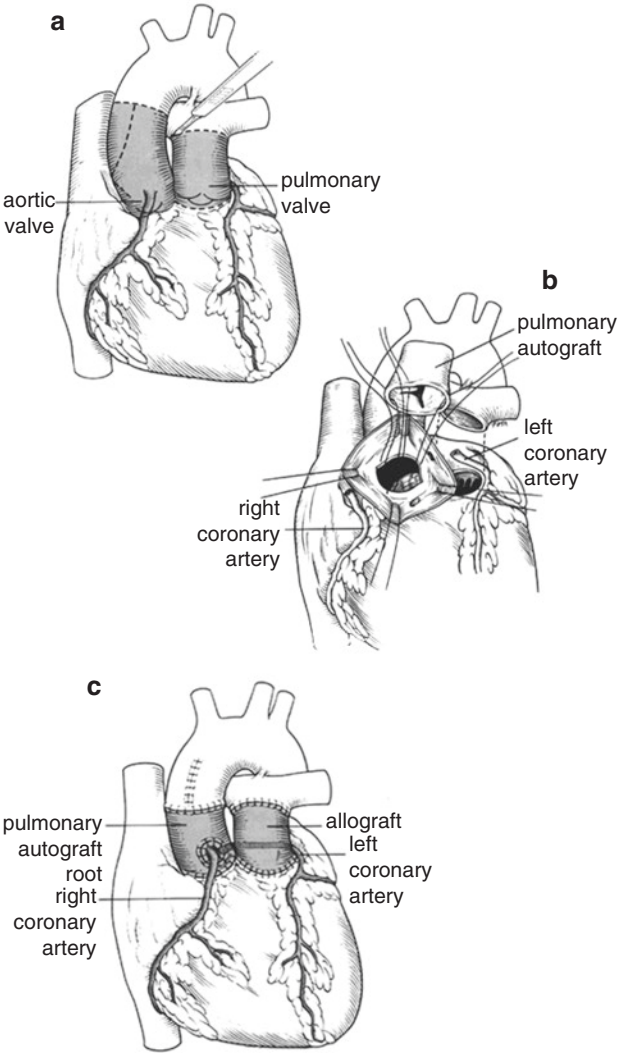


**Fig. 4.2** Schematic drawing of the Ross Procedure. (**a**) Resection of the diseased aortic valve. (**b**) Harvesting of native pulmonary valve. (**c**) Implantation of the native pulmonic valve in the aortic position and reimplantation of coronary arteries. (Source: Iaizzo [89])

counterparts. These valves are naturally less thrombogenic, and thus the patient does not require the same aggressive, lifelong, anticoagulation therapy; as is required with a mechanical valve. Specifically, a risk of <0.7% per year of clinically significant thromboembolism has been reported associated with biological valve replacements in patients eliciting sinus rhythm without warfarin therapy [8]. Thus, this is an advantageous treatment option in clinical situations where the use of anti-coagulation would significantly increase a given patient's morbidity and/or

**Table 4.2** Tissue valve graft options: classification of bioprosthetic valves

| Bioprosthetic valve | Description |
|---|---|
| Stented porcine valve (Xenograft) | A three-leaflet valve supported by three artificial struts or stents to maintain leaflet structure and geometry |
| Stentless porcine valve (Xenograft) | A length of porcine aorta including tissue below (proximal) and above (distal) to the valve, called the *root* |
| Bovine pericardial valve (Xenograft) | A three-leaflet valve created from bovine pericardium attached to a stented frame |
| Homograft | A human aortic valve and root |
| Autograft | A pulmonary valve and root excised from the patient and reimplanted in the same patient |

mortality. On the other hand, a major disadvantage of tissue valve implantation to date is potential for early valvular degeneration as a result of leaflet calcification. As a result, a major focus of research in this field incudes methods for tissue preservation which prevents or minimizes such calcifications.

### *4.2.3 Biological Versus Mechanical Valves*

The choice of a mechanical or biologic valve for implantation depends on a number of factors, including: (1) the patient's disease status and specific native valve involved, (2) the feasibility of anticoagulation and patient preference for long-term anticoagulation, and/or (3) the surgeon's preference and experience. If these factors are not limiting, the choice of valve type should be based on the maximization of benefits over risks for the individual patient. Unfortunately to date, the ideal prosthetic valve that combines excellent hemodynamic performance and long-term durability without increased thromboembolic risk or the need for lifelong anticoagulation remains a bit of an illusion. In general, mechanical valves offer greater durability, but at the cost of requiring lifelong anticoagulation and the given the risks of thromboembolism. In contrast, bioprosthetic valves have a much lower thromboembolic risks negating a need for anticoagulation, but to date they elicit higher risks for structural degenerations requiring a potential need for reoperation or valve-in-valve TAVR procedures. As such, mechanical valves are perhaps most well suited for the younger patient who does not desire future reoperations. Currently in the U.S., mechanical valve replacement has been standardized and is commonplace, yielding satisfactory valve functions that are quite reproducible from patient to patient. Furthermore, the flow gradients with newer bileaflet mechanical valves have dramatically improved from the early ball valve type, relatively reducing the risks of thromboembolism. Preliminary results of a novel trileaflet mechanical aortic valve studied in animal models without anticoagulation is promising [10]. Bioprosthetic or tissue valves offer a safe option for patients with contraindication to anticoagulation or where the risk of anticoagulation is clinically considered to be prohibitively high (e.g., elderly patients >70 years of age or women of child bearing

years desiring pregnancy); yet, acknowledging that the length of durability remains a serious concern for tissue valves. Thus, a patient whose life expectancy is greater than that of the prosthesis can perhaps encounter the risks of requiring another surgery for valve replacement. The option for tissue valve replacement via a transcatheter delivered procedure (discussed later in the chapter) may dramatically change this clinical limitation. There is already evidence that a redo transcatheter procedure is feasible in certain subsets of patients [11, 12].

Two historic randomized clinical trials have compared outcomes between early generation tissue and mechanical valves: the Edinburgh Heart Valve trial and the Veteran Affairs Cooperative Study on Valvular Heart Disease, both published in the early 2000 [9, 13, 14]. Both trials showed increased bleeding associated with mechanical valves and increased numbers of reoperation in patients with tissue valves. While the strengths of these trials include being prospectively randomized, the disadvantages include that the valves used in these trials are now obsolete. Several large studies including meta-analysis comparing mechanical versus bioprosthetic aortic valves found no difference in risk-corrected mortalities, regardless of patient age [15, 16]. Based on this and other studies, the choice of valve should not be based on age alone. There has been a trend towards increasing use of bioprosthetic valves in younger patients based on advances in tissue fixation and improved anti-calcification treatments; these improvements resulting in superior durability of the newer generation bioprosthetic valves. Specifically, third generation bioprosthetic valves have been shown to have a greater than 90% freedom from structural deterioration at 12-year follow-up [17]. Furthermore, continued improvements in cardiac surgery, including better techniques for myocardial preservation, less invasive procedures (i.e., robotic-assisted surgery), as well as improved strategies for cardiac reoperation, have significantly reduced the risks for cardiac reoperation. This has contributed to an increasing application of bioprosthetic valves in patients younger than 55–60 years old. In summary, in the absence of current randomized trials, physicians must make a choice based on existing data and individualize that choice based on patient-related factors such as age, lifestyle, tolerance for anticoagulation, and/or the anatomic position of the replacement valve.

Another important point to make when discussing bioprosthetic valves is the higher risk of infective endocarditis in certain situations, and the need for prophylactic antibiotics, at times. The details of these therapies are beyond the scope of this chapter, but the reader is referred to guidelines published by the joint committee from the American Heart Association (AHA) and American College of Cardiology (ACC) for the applicable protocols [8]. The risks for infective endocarditis are highest within the first 6 months after a valve implantation and sources of transient bacterial seeding, include: (1) poor dental hygiene, (2) various dental procedures, (3) endoscopic procedures, (4) intraabdominal infection, and/or (5) other infections throughout the body. There are established standards for reportable complications after bioprosthetic valve implantation, including infective endocarditis; these are briefly summarized in Table 4.3.

**Table 4.3** Reportable valve prosthesis complications

| Complication | Description |
|---|---|
| Structural valvular deterioration | Any change in function of an operated valve resulting from an intrinsic abnormality, causing stenosis or regurgitation |
| Nonstructural dysfunction | Any stenosis or regurgitation of the operated valve that is not intrinsic to the valve itself, including inappropriate sizing, but excluding thrombosis and infection |
| Valve thrombosis | Any thrombus, in the absence of infection, attached to or near an operated valve that occludes part of the blood flow path or interferes with function of the valve |
| Embolism | Any embolic event that occurs in the absence of infection after the immediate perioperative period (new temporary or permanent, focal or global neurological deficit, and peripheral embolic event) |
| Bleeding event (anticoagulant hemorrhage) | Any episode of major internal or external bleeding that causes death, hospitalization, permanent injury, or requires transfusion |
| Operated valvular endocarditis | Any infection involving an operated valve, resulting in valve thrombosis, thrombotic embolus, bleeding event, or paravalvular leak |

## 4.3 Specific Valvular Diseases: Etiologies and Treatments

We will now start discussing some of the most common valvular diseases affecting patients in the western World. Of the four heart valves, significant primary clinical disease affects all but the pulmonary valve. Although, secondarily compromised functions of a given patient's pulmonary valve have been noted to occur in the adult congenital heart patient, who previously underwent reparative surgeries. Indications for diagnostic, therapeutic, and follow-up interventions will be discussed for each disease. Note that a complete evidenced-based summary of recommendations for intervention and physical activity in individuals with valvular disease is available from several excellent reviews [18, 19].

### *4.3.1 Aortic Valve Disease*

Anatomically, the normal aortic valve is composed of the annulus and the left, right, and non-coronary leaflets (sometimes referred to as *cusps*) (Fig. 4.3). Diseases affecting these structures can be subdivided into aortic stenosis or regurgitation, or some combination thereof. In general, aortic stenosis is considered a surgical disease with aortic valve replacement considered to be the standard of care; especially in younger patients. Treatment of aortic regurgitation is also typically treated surgically, though the exact method chosen will vary widely based on the etiology of the disease. See Chap. 12 on transcatheter aortic valve implantation, for recent advances in this therapy and the new indications for use.

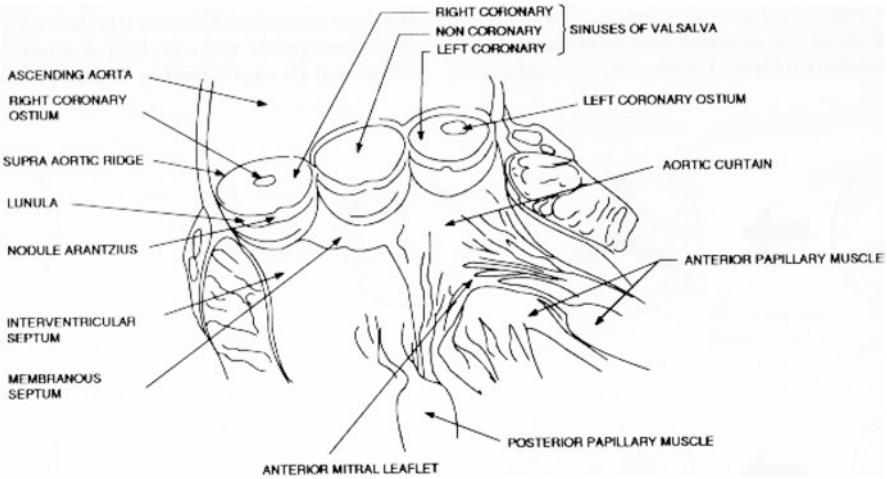


**Fig. 4.3** Anatomy of the aortic valve. (Source: Iaizzo [89])

#### 4.3.1.1 Aortic Stenosis

*Aortic stenosis* causes varying degrees of left ventricular outflow tract obstruction [20, 21]. The various etiologies of aortic stenosis are commonly subdivided into acquired versus congenital. The most common cause of aortic stenosis in adults is calcification of a normal trileaflet or a congenital bicuspid aortic valve. Among individuals under the age of 70, bicuspid aortic valve disease is the most common cause of aortic stenosis. These congenitally abnormal valves typically develop progressive fibrosis and calcification of the leaflets over several decades, and can develop symptoms at any time during an individual's life, depending on the relative degrees of deformity and rates of progression of the narrowing. Patients over the age of 70 more typically elicit what is referred to as *senile aortic stenosis*; these valves originally had normal anatomy, but develop thick calcifications with subsequent stenosis with aging. This progression usually takes longer than in patients with bicuspid valves.

Aortic stenosis may not produce symptoms early in its disease course, but over time with disease, progressive symptoms will develop. Classic symptoms of aortic stenosis include angina, syncope, heart failure, and/or sudden death. Other symptoms include reduced effort tolerance, fatigue, and exertional dyspnea. Once symptoms are present, the average patient survival without intervention is less than 2–3 years [20–27]. Mortalities for untreated aortic stenosis can be broken down by the presence of symptoms such as: (1) angina, 50% within 5 years; (2) syncope, 50% mortality within 3 years; and (3) heart failure, 50% mortality within 2 years. A high degree of suspicion for aortic stenosis is necessary to make the diagnosis prior to the onset of symptoms to maximize patient outcome.

From a physiologic standpoint, progressive outflow tract obstruction subsequently causes an increase in left ventricular pressure. Concentric left ventricular

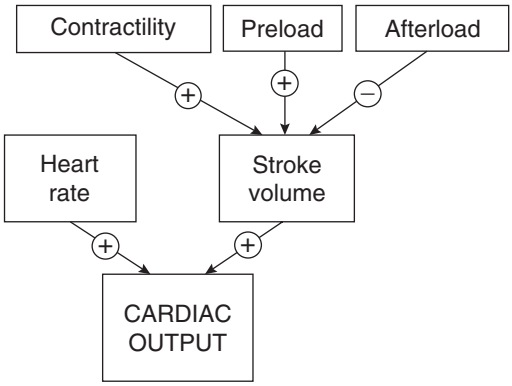


**Fig. 4.4** Determinants of cardiac output include contributions from preload and afterload pressures, contractility, and heart rate. (Source: Iaizzo [89])

hypertrophy is an early response of these elevated pressures; note, which initially assists in maintaining normal left ventricular systolic wall tension and ejection fraction [28]. However, once this response becomes functionally inadequate, afterload tends to increase, resulting in a gradual reduction in overall ejection fractions (Fig. 4.4). In some patients, the initial ventricular hypertrophy itself may also be detrimental, producing subendocardial ischemia even in the absence of coronary artery disease [29, 30]. As such, this results both in further systolic and diastolic left ventricular dysfunctions and may predispose such patients to a potentially larger degree of myocardial ischemia and higher mortality [8, 20, 21, 31].

Early diagnosis of aortic stenosis is based on the presence of a systolic outflow murmur, delayed/diminished carotid upstrokes, sustained left ventricular impulse, reduced intensity of the aortic component of the second heart sound, and/or evidence of left ventricular hypertrophy on exam, chest X-ray, or ECG. Today, echocardiography is both a more reliable tool in diagnosis and is used to provide a detailed assessment of the mean transvalvular pressure gradient (calculated using the Bernoulii equation), valve area (calculated from continuity equation), left ventricle size (i.e., degree of hypertrophy), and systolic function, and/or the presence of concurrent valvular disease (see Chapter by Gorbaty et al., on echocardiography for more details). CT imaging can further be used in detail to quantify the degrees of aortic valve calcification and is especially helpful in planning for transcatheter aortic valve replacement (TAVR) procedures. Note, magnetic resonance imaging (MRI) may also be applied in such patients for diagnosis.

Degrees of mean pressure gradients, peak aortic velocities, and/or valve orifice areas can be taken into account to grade a given aortic stenosis (Table 4.4). The average rates for reductions in valve orifice area have been estimated to be ~0.12 $cm^2$/year [32]. Nevertheless, progression of aortic stenosis varies significantly, and the degree of a patient's symptoms may not correlate well with the objective data. It is difficult to predict an accurate rate of stenotic progression for each individual, so careful and frequent clinical follow-up is mandatory. At the least, patients should have an annual history and physical exam. Furthermore, physicians should urge their patients to promptly report new symptoms as this can indicate disease

**Table 4.4** Degree of aortic stenosis

| | Mean pressure gradient (mmHg) | Valve orifice area ($cm^2$) | Peak aortic velocity (m/s) |
|---|---|---|---|
| Mild | <20 | >1.5 | <3.0 |
| Moderate | 20–29 | >1.0–1.5 | 3.0–3.9 |
| Severe | ≥40 | <1.0 | ≥4.0 |

progression. Any new symptom warrants additional clinical assessment. Annual echocardiography can be used to assess disease progression of ventricular hypertrophy and any functional changes, but note that changes in valve area alone are deemed not predictive. Stress testing is also recommended for patients with equivocal symptoms. Findings suggestive of hemodynamically significant aortic stenosis include limited exercise tolerance and a blunted blood pressure response to exercise. Surgery is typically indicated at the onset of any symptoms given the rapid progression of the disease process once symptoms are present.

Patients being considered for aortic valve replacement should undergo cardiac catheterization if they are over 40 years old to assess for any degree of significant coronary artery disease. Additional indications for preoperative cardiac catheterization include situations where there is a discrepancy between clinical and echocardiographic findings used to assess the hemodynamic severity of the stenosis, and situations where there is evidence of pulmonary hypertension or other valvular or congenital disease. Complete preoperative diagnostic evaluations should include: (1) the measurement of transvalvular flow (liters/min); (2) the determination of the transvalvular pressure gradient (mmHg); and (3) the calculation of the effective valve area ($cm^2$) [33].

Medical therapy for aortic stenosis is primarily relegated to the prevention of endocarditis and the control of arterial hypertension. Asymptomatic patients typically do not warrant medical intervention. Some studies have shown that statin therapy may slow the disease progression, but results have been inconsistent with larger randomized trials [34]. Still today, all patients with known calcific aortic stenosis are recommended statin therapy for atherosclerosis risks, but not necessarily disease progression prevention. There are theoretical benefits for the use of ACE inhibitors in minimizing or improving both left ventricular fibrosis and hypertrophy (and subsequent left ventricular dysfunction and heart failure) in patients with aortic stenosis, but studies have not shown significant benefits relative to disease progression [29, 30]. There are some small clinical studies that suggest benefit of ACE inhibitors on aortic stenosis disease, but larger clinical trials are necessary to further elucidate their potential benefits [35].

Aortic valve replacement is the treatment of choice for aortic stenosis in most adults and can be done at any age [36]. Yet, the degree of stenosis mandating surgery in asymptomatic patients remains an issue of debate. Nevertheless, the degrees of improvement following aortic valve replacements have been directly related to preoperative left ventricular function; patients with depressed ejection fractions caused by excessive afterloads typically demonstrate significant improvements in left ventricular function after aortic valve replacement. Conversely, if a patient's depressed

left ventricular function is caused by myocardial insufficiency, improvement in left ventricular function and resolution of symptoms may not be reversed after valve replacement. In general, survivals are improved for patients undergoing aortic valve replacements, with the possible exceptions of a subset of patients with severe left ventricular dysfunctions caused by coronary artery disease [37, 38]. In summary, in contrast to the dismal survival rates for patients with untreated severe aortic stenosis, the long-term survivals for patients who have undergone aortic valve replacements, approach that in the normal population. Therefore, it is recommended that patients with severe aortic stenosis, with or without symptoms, who are undergoing coronary artery bypass surgery should undergo aortic valve replacement at the time of the revascularization procedure. Similarly, patients with moderate to severe aortic stenosis undergoing surgery for the replacement of other heart valves or an aortic root repair should also undergo aortic valve replacement, as part of their overall surgical procedure. Hence, in the absence of contraindications, aortic valve replacement is indicated in virtually all symptomatic patients with severe aortic stenosis (Table 4.5).

In some patients, percutaneous alternatives to surgical valve replacement include balloon aortic valvulotomy or transcatheter aortic valve replacement (TAVR). Balloon aortic valvulotomy can effectively reduce the transvalvular pressure gradient, but often this is not long term. This procedure uses percutaneously inserted catheters that are advanced into the aortic valve, followed by balloon inflation to fracture calcified deposits and separate fused commissures [39, 40]. Though successful at providing clinical improvements, post-procedure the valve areas rarely exceed 1.0 $cm^2$ and aortic regurgitation can often occur, increasing the burden on the patient's left ventricle. To date, the rate of significant complications (10%) and symptomatic restenosis (within 6–12 months) makes balloon valvotomy a less desirable substitute for aortic valve replacement in adults with aortic stenosis [8].

TAVR is gaining clinical acceptance, an alternative procedure for patients with high-surgical risk and/or severe symptomatic aortic stenosis. This involves percutaneous access and delivery of a bioprosthetic valve to the aortic valve position. This

**Table 4.5** Aortic valve replacement in aortic stenosis

| |
|---|
| Symptomatic patients with severe aortic stenosis alone or: |
| Undergoing coronary artery bypass surgery |
| Undergoing surgery on the aorta or other heart valves |
| Patients with moderate aortic stenosis and: |
| Undergoing coronary artery bypass surgery |
| Undergoing surgery on the aorta |
| Undergoing surgery on other heart valves |
| Asymptomatic patients with severe aortic stenosis and left ventricular systolic dysfunction typified by: |
| Abnormal response to exercise (e.g., hypotension) |
| Ventricular tachycardia |
| Marked or excessive left ventricular hypertrophy (>15 mm) |
| Valve area <0.6 $cm^2$ |
| Prevention of sudden death without the findings listed |

continues to be an evolving procedure since it was first performed for aortic stenosis in 2002. The cardiac care teams' decision making relative to therapeutic approach depends significantly on weighing valve durability with life expectancy. Still today, few studies have compared SAVR to TAVR in patients <65 years of age. Thus, generally adults <65 years old should undergo surgical AVR unless comorbidities preclude them from surgery. Advantages of surgical AVR include lower risk of paravalvular leak, valve intervention, and/or needs for permanent pacemaker. Advantages of TAVR include shorter hospital stays, lower procedure blood losses, less invasive procedure, and slightly lower mortalities in the very sick patients [41]. When considering TAVR, it is important to select patients appropriately and discuss advantages and disadvantages thoroughly (for more information, see Chap. __).

Two areas of controversy in the management of aortic stenosis include: (1) asymptomatic patients with severe aortic stenosis and (2) patients with low-ejection fractions with reduced gradient aortic stenosis [20, 21]. The risks of surgery may outweigh the potential benefits in these two groups of patients. In asymptomatic patients, there is a low (1–2%) risk of sudden death or rapid progression to symptoms. Adverse clinical outcomes related to aortic stenosis in asymptomatic patients are more likely to result seen when there is rapid progression of hemodynamic parameters: e.g., increase in aortic jet velocities greater than 0.3 m/s per year or a decrease in aortic valve area greater than 0.1 $cm^2$ per year. It is important to note that patients with low-ejection fractions and reduced gradient aortic stenoses may present an even more challenging clinically. These complexities partly lie in the difficulties to distinguish this entity from patients with reduced ejection fractions and only mild to moderate aortic stenoses; the latter group will not benefit from aortic valve replacement. These patients with severe aortic stenoses, who present with reduced ejection fractions and reduced gradients, will ultimately face an increased operative mortality. The use of dobutamine stress echocardiography to measure the pressure gradients and the valve areas, both during baseline and at stress, can help determine the true severity of aortic stenosis [42]. In general, patients with reduced ejection fractions, with a low-transvalvar gradients who have no response to stress (e.g., inotropes), elicit poorer outcomes, even with surgery. One recent randomized control trial looked at patients with asymptomatic but severe aortic stenosis and compared early surgical interventions with watchful waiting. Results showed that surgical interventions showed better survivals, at least up to 4 years of follow-up [43]. The EARLY-TAVR Trial is currently ongoing and will look at a similar patient population, but with early TAVR versus watchful waiting.

#### 4.3.1.2 Aortic Sclerosis

*Aortic sclerosis* is a common finding in older patients and is present in approximately 25% of individuals older than 65 years [18, 20]. The classic findings of aortic sclerosis include focal areas of valve thickening with otherwise relatively normal leaflet mobility. It is important to note that, by definition, valvular hemodynamics are within normal limits in those with aortic sclerosis. In other words, other

than the presence of a systolic murmur, there are no clinical signs or associated symptoms, which distinguishes this process from aortic stenosis. Histologic findings in aortic sclerosis include focal subendocardial plaque-like lesions with accumulations of lipoproteins. The similarity of these findings to atherosclerosis suggests that both of these clinical presentations are in some way an age-related process.

Despite the lack of valve-related symptoms with aortic sclerosis, it is generally associated with increased risks of cardiovascular mortality. This may be related to the development of coronary artery disease and, occasionally, to a progression to severe aortic stenosis. Thus, while symptoms in the patient identified with aortic sclerosis may be initially benign, these individuals warrant a careful cardiovascular follow-up.

#### 4.3.1.3 Aortic Regurgitation

Aortic regurgitation typically results from a structural defect within the aortic valve that allows for blood flow to reverse direction across the valve during diastole (i.e., re-enter the ventricle). The etiologies of aortic regurgitation are best discussed by subdividing this disease into acute or chronic regurgitation (Table 4.6). The majority of such lesions result in chronic aortic regurgitations with insidious dilatations of the left ventricle. In contrast, lesions responsible for acute aortic regurgitations may result in sudden catastrophic elevation of left ventricular filling pressures, reduction in cardiac outputs, and/or sudden death.

**Chronic Aortic Regurgitation**
Valve damage that results in progressively larger retrograde flows across the aortic valve and produces the condition of *chronic aortic regurgitation*. These patients'

**Table 4.6** Etiologies of aortic regurgitation (subdivided by presentation time)

| Acute | Chronic |
|---|---|
| Infective endocarditis | Idiopathic aortic root dilatation |
| Aortic dissection | Congenital bicuspid valves |
| Trauma | Calcific degeneration |
| | Rheumatic disease |
| | Infective endocarditis |
| | Systemic hypertension |
| | Myxomatous proliferation |
| | Ascending aortic dissection |
| | Marfan syndrome |
| | Syphilitic aortitis |
| | Rheumatoid arthritis |
| | Osteogenesis imperfecta |
| | Giant cell aortitis |
| | Ehlers-Danlos syndrome |
| | Reiter's syndrome |
| | Discrete subaortic stenosis |
| | Ventricular septal defects with aortic cusp prolapse |

left ventricles respond to the volume load of aortic regurgitation with several compensatory mechanisms, such as an increase in end-diastolic volumes and combinations of eccentric and concentric hypertrophy [44]. An increased diastolic volume allows the ventricle to eject a larger total stroke volume, thereby initially maintaining stroke volumes and cardiac outputs within the normal range. As a result, the majority of such patients remain asymptomatic during prolonged periods of compensation. Yet, after a while, the compensatory mechanisms become inadequate and result in further increases in afterloads and reduced ejection fractions. Once the left ventricle can no longer compensate, patients typically present with symptoms of dyspnea and exertional angina, reflecting declining systolic function, elevated filling pressures, and/or diminished coronary flow reserve of the hypertrophied myocardium [38]. Several natural history studies have identified age and left ventricular end-systolic pressure (or volume) as predictive factors associated with higher risks of mortality in this clinical population (Table 4.7). Although the progression of asymptomatic chronic aortic regurgitation is slow, approximately 25% of such patients will develop systolic dysfunction, or die prior to the onset of warning symptoms [8]. Therefore, quantitative evaluations of left ventricular function with echocardiography are necessary, as a serial history and physical exam alone are generally insufficient.

Clinical diagnosis of chronic severe aortic regurgitation can be made based on the following: (1) the presence of a diastolic murmur (the third heart sound) and/or a rumble (Austin-Flint sign) on auscultation; and/or (2) the detection of a displaced left ventricular impulse and wide pulse pressure [45, 46]. Similar to aortic stenosis, chest X-ray and ECG will typically reflect left ventricular enlargement/hypertrophy and may also elicit evidence of conduction disorders. Further for such a patient, echocardiography is indicated to confirm a diagnosis of aortic regurgitation, assess valve morphology, estimate the degree of severity of regurgitation, and determine aortic root size as well as left ventricular dimensions, relative mass, and systolic function. If the patient has severe aortic regurgitation and is sedentary, or has equivocal symptoms, exercise testing is helpful to assess the following: functional capacity, symptomatic responses, and/or the hemodynamic effects of exercise.

**Table 4.7** Natural history of aortic regurgitation

| | | |
|---|---|---|
| Asymptomatic patients with normal left ventricular systolic function | Progression to symptoms and/or left ventricular dysfunction<br>Progression to asymptomatic left ventricular dysfunction<br>Sudden death | <6%/year<br><3.5%/year<br><0.2%/year |
| Asymptomatic patients with left ventricular systolic dysfunction | Progression to cardiac symptoms | >25%/year |
| Symptomatic patients | Mortality rate | |
| | with angina<br>with heart failure | >10%/year<br>>20%/year |

In patients who are symptomatic on their initial evaluation, cardiac catheterization and angiography are indicated for the subsequent evaluation of coronary artery disease; for possible concurrent revascularization therapy, or if echocardiogram is insufficient for assessment of left ventricular function and determining the severity of aortic regurgitation. The goal of any serial evaluation of an asymptomatic patient with chronic aortic regurgitation is to detect the onset of symptoms and objectively assess changes in left ventricular size and function that may be elicited (Fig. 4.3). Medical therapy for aortic regurgitation is primarily based on the use of vasodilating agents which are believed to improve forward stroke and reduce regurgitant volumes; the use of such agents can often result in regression of left ventricular dilatation and hypertrophy.

Initial left ventricular systolic dysfunction in chronic aortic regurgitation is commonly associated with an increased afterload pressure and is considered to be reversible following aortic valve replacement (i.e., full recovery of left ventricular size and function) [8]. However, depressed myocardial contractility (rather than volume overload) is typically responsible for the systolic dysfunction, as the ventricle becomes more hypertrophic and dilatation progresses the chamber to a more spherical geometry. Importantly at this stage, neither return of normal left ventricular function nor improved long-term survival have been documented even after aortic valve replacement. For patients with chronic aortic regurgitation, their given left ventricular systolic function and end-systolic size have been identified as the most important determinants of postoperative survival and abilities to elicit normalization of left ventricular function following aortic valve replacement [8].

Medical therapy with vasodilating agents is indicated for patients with symptomatic chronic aortic regurgitation, however, it is not an alternative to surgery. Vasodilators used include sodium nitroprusside, hydralazine, and nifedipine to reduce peripheral vascular resistance and augment forward cardiac output with a decrease in regurgitant volume [47]. Medical therapy may also include the administrations of ACE inhibitors, ARBs, and/or sacubitril/valsartan. Both the American College of Cardiology (ACC) and American Heart Association (AHA) recommend medical therapies for chronic aortic regurgitation for the following patients: (1) asymptomatic patients with chronic aortic regurgitation and hypertension and (2) symptomatic patients with severe aortic regurgitation and/or left ventricular dysfunction who are a high-surgical risk. Patients in the latter group often benefit from improved hemodynamic profiles, prior to their aortic valve replacements. Medical therapy also prolongs the compensatory phase of asymptomatic patients who elicit volume overloads, but have normal systolic functions.

**Acute Aortic Regurgitation**

When aortic valve damage is acute and severe, the subsequent and sudden large regurgitant volume that returns into the left ventricle will dramatically decrease the functional forward stroke volume. In contrast to chronic aortic regurgitation, in such acute cases, there is no time for compensatory ventricular hypertrophy and dilatation to develop. As a result, the expected exam findings of ventricular enlargements and diastolic murmurs associated with chronic aortic regurgitation are absent.

Instead, patients with acute aortic regurgitation present with pronounced tachycardias, pulmonary edema, and/or potentially life-threatening cardiogenic shock. Rapid diagnosis and treatment are considered mandatory.

Echocardiography is crucial in the initial workup and diagnosis of acute aortic regurgitation; it will likely demonstrate a rapid equilibration of aortic and left ventricular diastolic pressure and may provide some insights relative to the etiology of aortic regurgitation. Echocardiography also allows for a rapid assessment of the associated valve apparatus, the aorta, and/or the relative degree of pulmonary hypertension (if tricuspid regurgitation is also present). Transesophageal echocardiography is indicated when aortic dissection is suspected [48, 49] (see Chapter by Gorbaty et al., for details on echocardiography). Importantly, acute aortic regurgitation resulting from aortic dissection is a surgical emergency requiring prompt identification and management. Cardiac catheterization, aortography, and coronary angiography are considered as important components of an evaluation of aortic dissection with acute aortic regurgitation and thus should be performed if these procedures do not unduly delay urgent surgery. Additionally, following trauma, computed tomographic imaging can be quite useful in obtaining the appropriate clinical status and underlying diagnoses.

Nevertheless, appropriate treatment of acute aortic regurgitation is dependent on the etiology and severity of the patient's disease. For example, only antibiotic treatment may be required in a hemodynamically stable patient with mild acute aortic regurgitation resulting from infective endocarditis. Conversely, severe acute aortic regurgitation associated with hypotension, pulmonary edema, and/or cardiogenic shock is considered as a surgical emergency. In such cases, temporizing preoperative management may include the use of agents such as nitroprusside (to reduce afterload) and inotropic agents such as dopamine or dobutamine (to augment forward flow and reduce left ventricular end-diastolic pressure). Intra-aortic balloon counter pulsation is contraindicated in such patients, and beta blockers should be used cautiously because of their potential to further reduce cardiac outputs by blocking the compensatory tachycardia. Typically, mortality associated with acute aortic regurgitation is the result of pulmonary edema, ventricular arrhythmias, electromechanical dissociation, and/or circulatory collapse.

In general, aortic valve replacement is the treatment of choice in aortic regurgitation. However, in such cases of aortic disease, additional aneurysm repairs (Fig. 4.5) or aortic root replacements (Figs. 4.6 and 4.7) need to be clinically considered. Aortic root replacement with a homograft or autograft should be offered to patients in whom anticoagulation is contraindicated (e.g., elderly with risk, women of child bearing years); as the tissue valve graft does not require anticoagulation. Similar benefits may be also be observed for patients with endocarditis, as a homograft appears to have a lower risk for recurrent infection. Finally, although the use of mechanical valves is effective, the prosthesis may impose a clinically relevant degree of stenosis in certain patients due to unavoidable size mismatches. Naturally, homografts and autografts are superior as they can be tailored to provide larger outflow tracts. Note in certain situations, required repair of the aorta may involve the use of an artificial conduit using materials such as Dacron.

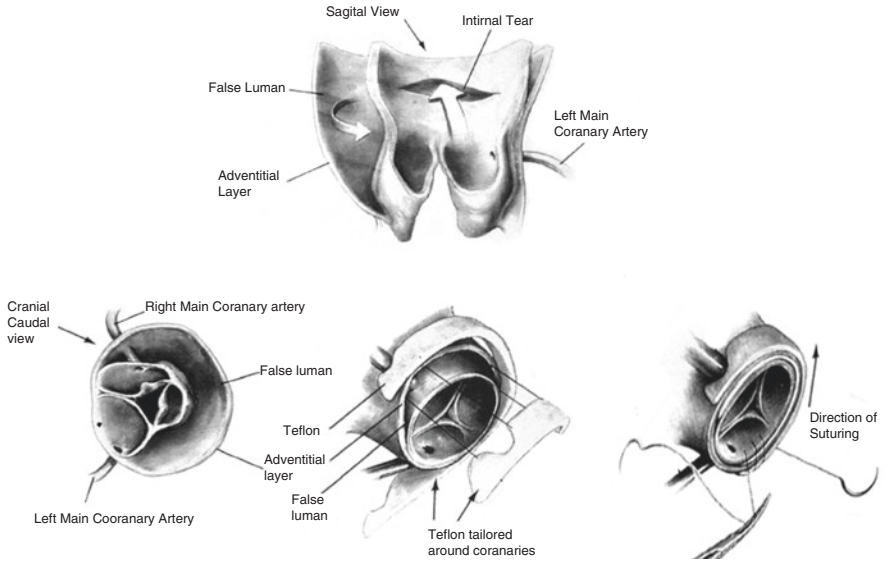


**Fig. 4.5** Aortic aneurysm repair using a Teflon felt reinforcement technique preserving the aortic valve and coronary arteries. (Source: Yun and Miller [90])

To date, the transcatheter approach has been considered to be difficult to apply for patients with aortic regurgitation and thus should be approached cautiously: dilation of the aortic annulus and aortic root, typically prohibits TAVR. Transcatheter valve migration and paravalvular leak are additional risks for employing TAVR therapies. Note, patients who are at a significant surgical risk but have appropriate annular size and valve calcifications are potentially appropriate candidates for TAVR. However, all procedural risks should be thoroughly considered and patient should be medically optimized to improve surgical risk prior to proceeding with a transcatheter approach.

Careful post-aortic valve replacement follow-ups are necessary during both the early and long-term postoperative courses, as means to evaluate both prosthetic valve and left ventricular functions. An excellent predictor of a given long-term success of aortic valve replacement is a reduction in left ventricular end-diastolic volumes occurring within the first 14 days after the operation. It should be emphasized that, in most patients, as much as 80% of the overall reduction in end-diastolic volumes that will occur, happens within this time period. In addition, the degree of regression in left ventricular dilatation typically correlates well with the magnitude of functional increases in ejection fractions [46]. Nevertheless, long-term follow-up should include an exam at 6 months post-aortic valve replacement, and then the yearly examinations are recommended if the clinical course is considered to be uncomplicated. Note that serial postoperative echocardiograms after the initial early postoperative study are usually not indicated. However, repeat echocardiography is warranted at any point when there is evidence of: (1) a new murmur; (2) questions

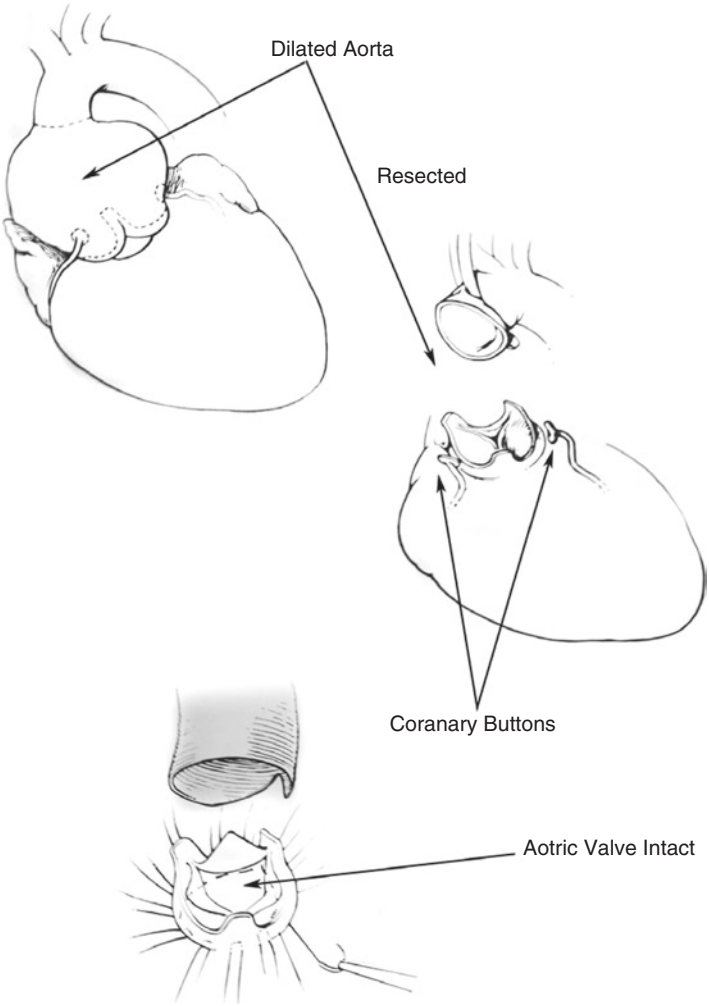


**Fig. 4.6** David Procedure for aortic root replacement. The dilated aorta is resected, sparing the aortic valve and coronary buttons. The repair is then completed with insertion of a graft with reimplantation of the coronary arteries. (Source: Iaizzo [89])

of prosthetic valve integrity; and/or (3) concerns about adequate left ventricular function.

**Aortic Valve Disease Associated with Disease of the Ascending Aorta**

Dilatation of the ascending aorta is a common cause of aortic regurgitation. It is well recognized that patients with bicuspid aortic valves also commonly elicit disorders of the vascular connective tissue system, which can result in dilatation of the ascending aorta and/or aortic root even in the absence of hemodynamically significant valvular disease. The dilatation of the aorta can be progressive over time with

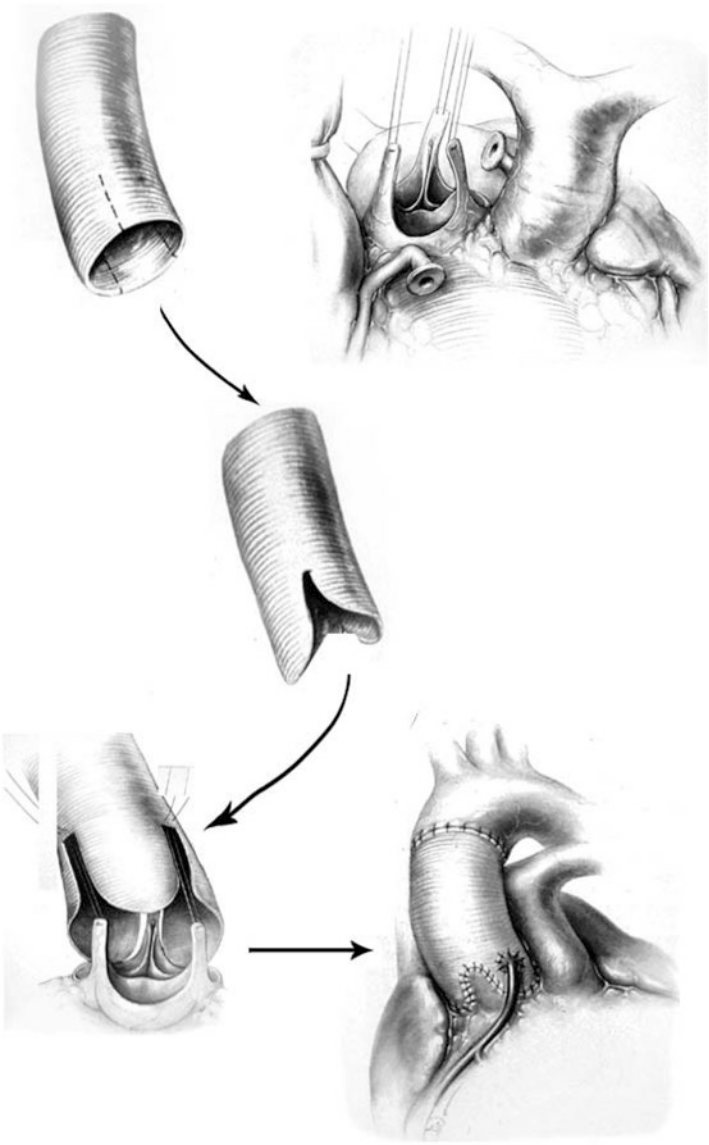

**Fig. 4.7** Aortic root replacement using Dacron graft as the technique used for correct sizing is demonstrated, for suturing in place to yield the final graft implantation along with coronary re-implantation. (Source: Iaizzo [89])

an increased risk for aortic dissection. Currently, echocardiography is the primary diagnostic modality used for these patients. However, a more detailed anatomic study can be obtained with either computerized tomography or cardiac magnetic resonance imaging.

Regardless of the etiology of the dilated ascending aorta, the recommended indications for operative intervention include both an ascending aortic diameter >5.5 cm and growth of the aorta >0.5 cm/year. In patients with bicuspid aortic valves undergoing aortic valve replacement, repair of the aortic root or replacement of the ascending aorta is indicated if the diameter of the aorta is >4.5 cm. Note that aortic valve-sparing operations are feasible in many such patients with dilatation of the aorta, who do not have significant aortic regurgitation or aortic valve calcification. The techniques for aortic valve-sparing surgery have been pioneered by Yacoub and David [50, 51]. In early stages of this disease, the use of beta-adrenergic blocking agents may slow the progression of aortic dilatation.

### *4.3.2 Diseases of the Mitral Valve*

Diseases of the mitral valve can also be subdivided into mitral stenosis and regurgitation. The general anatomy of the mitral valve consists of a pair of leaflets attached to the left ventricle by chordae tendineae. Normal mitral valve area ranges between 4.0 and 5.0 $cm^2$. However, in the case of mitral stenosis, symptoms do not typically develop until the functional valve area is reduced to <2.5 $cm^2$ [52].

#### 4.3.2.1 Mitral Stenosis

Stenosis of the mitral valve orifice typically produces a funnel-shaped mitral apparatus described to resemble a *fish mouth*, which then hinders normal diastolic filling of the left ventricle. In the past, roughly 60% of all patients with mitral stenosis presented with a history of rheumatic fever [53, 54]. However, today the incidence of rheumatic fever is decreasing and is quite rare in well-developed countries. Three typical pathological processes are observed in patients with rheumatic heart disease: (1) leaflet thickening and calcification; (2) commissural and chordal fusions; or (3) a combination of these processes [55, 56]. Congenital malformations of the mitral valve, although rare, are usually responsible for mitral stenosis observed in infants and children [56]. Currently, women (2:1) account for the overall majority of reported cases of mitral stenosis [53, 54, 57]. Other entities can also simulate the clinical features of rheumatic mitral stenosis, such as left atrial myxoma, infective endocarditis, and mitral annulus calcification, i.e., in the elderly.

Mitral stenosis is normally a slowly progressive disease with a typical mean age of presentation of symptoms in the fifth to sixth decade of life [58, 59], with narrowing of the valve to <2.5 $cm^2$ before the development of symptoms. As the severity of stenosis increases, cardiac output becomes reduced even at rest and fails to increase with exercise. The relative degree of pulmonary vascular resistance also influences the development of symptoms. Diagnosis of mitral stenosis may be made solely on the presence of abnormal physical exam findings, or may be suggested by symptoms of fatigue, dyspnea, frank pulmonary edema, atrial fibrillation, and/or embolus

[53]. In the asymptomatic patient, survival is 80% at 10 years, with 60% of these patients eliciting no progression of symptoms. However, once symptoms related to pulmonary hypertension develop, to date, there remains 10-year survival rate of a dismal 0–15% [8]. Common causes of death in the untreated patients with mitral stenosis are due to: (1) progressive heart failure (60–70%); (2) systemic embolism (20–30%); (3) pulmonary embolism (10%); or (4) infection (1–5%) [56, 57].

Shortness of breath (dyspnea) precipitated by exercise, emotional stress, infection, pregnancy, or atrial fibrillation are typically the first symptoms to present in patients with underlying mild mitral stenosis [54]. Yet, as the obstructions across the mitral valve increase, there will typically be progressive symptoms of dyspnea; as the left atrial and pulmonary venous pressures increase [60]. Increased pulmonary artery pressures and distension of the pulmonary capillaries can lead to pulmonary edema, which occurs as pulmonary venous pressures and exceeds that of plasma oncotic pressure. Subsequently, the pulmonary arterioles will elicit vasoconstriction, intimal hyperplasia, and medial hypertrophy, which then further exacerbate pulmonary arterial hypertension.

Commonly, the diagnosis of mitral stenosis can be made based on: (1) the patient's history, (2) physical examination, (3) chest X-ray, and (4) their ECG. Note, a given patient may be asymptomatic but still have abnormal physical findings, including a diastolic murmur [58, 59]. In such patients, diagnostic imaging is recommended using both 2D and Doppler transthoracic echocardiography. Transesophageal echocardiography or cardiac catheterization is not required unless questions concerning overall diagnosis remain [8]. Cardiac catheterization may be indicated to: (1) assess the potential for coronary artery disease or aortic valve disease; (2) assess pulmonary artery pressure; (3) perform balloon valvotomy; and/or (4) evaluate the situation when the clinical status of a symptomatic patient is not consistent with the echocardiography findings.

Typically, echocardiography is capable of providing an appropriate assessment of: (1) the morphological appearance of the mitral valve apparatus; (2) ventricular chamber size/function; (3) the mean transmitral pressure gradient [61, 62]; (4) the relative functional mitral valve area; and (5) the pulmonary artery pressure [58]. In addition, if deemed necessary, non-invasive dobutamine or exercise stress testing can be completed with either the patient supine (using a bicycle) or upright (on a treadmill) to assess relative changes in the patient's heart rate and blood pressure in response to their overall exercise tolerance. Patients who are symptomatic with a significant elevation of pulmonary artery pressure (>60 mmHg), mean transmitral gradient (>15 mmHg), or pulmonary artery wedge pressure (>25 mmHg) on exertion have, by definition, hemodynamically significant mitral stenosis that may require further intervention [8].

In mitral stenosis, medical treatment is typically indicated for the prevention of emboli (10–20%), which is primarily associated with the onset of atrial fibrillation [53, 54, 63–65]. Atrial fibrillation ultimately develops in 30–40% of patients with symptomatic mitral stenosis and, importantly, ~65% of all embolic events occur within the first year after the onset of atrial fibrillation [53, 54]. The etiology behind atrial fibrillation is thought to be disruption of the normal conduction pathways

caused by structural changes in the myocardium resulting from a pressure/volume overloaded atrium; in fewer cases, it may also result from rheumatic fibrosis of the atrium [59]. Development of atrial fibrillation associated with mitral stenosis occurs more commonly in older patients presenting with symptoms and has been associated with a decreased 10-year survival rate (25% versus 46%) [53, 57]. Importantly, in addition to the thromboembolic potential, acute onset of atrial fibrillation can herald sudden deterioration in patients with mitral stenosis. This is considered as secondary to an acute reduction in left ventricular ejection fraction and elevated pulmonary artery pressures, which will result from loss of the atrial contribution (atrial kick) to left ventricular filling. The urgent treatment for an acute episode of atrial fibrillation with an associated rapid rate heart rate typically consists of: (1) drug administrations for heart rate and rhythm control (digoxin, calcium channel blockers, beta blockers, or amiodarone); (2) electrical cardioversion; and/or (3) anticoagulation with heparin. Note, in patients with atrial fibrillation for more than 24–48 h without anticoagulation, cardioversion is associated with an increased risk of embolism. For chronic or recurrent atrial fibrillation that is resistant to prevention or cardioversion, heart rate control and long-term anticoagulation are considered the needed mainstay of therapy [65, 66]. Anticoagulation is recommended for patients with mitral stenosis and atrial fibrillation, prior embolic events, or known left atrial thrombus. Anticoagulation is not recommended for isolated mitral stenosis given the risk of bleeding complications.

The principle behind treating symptomatic mitral stenosis is the alleviation of a fixed left ventricular inflow obstruction, thereby reducing the transvalvular gradients. Methods of disrupting the stenosed valve include surgery (open or closed mitral commissurotomy) or percutaneous mitral balloon commissurotomy (PMBC). Mitral valve replacement is an option for patients who are poor surgical candidates for the aforementioned interventions. The timing of intervention is commonly related to the severity of disease, while the method of intervention is chosen based on: (1) the given morphology of the mitral valve apparatus; (2) presence of other comorbid diseases; and/or (3) expertise at each specific clinical center. Significant calcification, fibrosis, and subvalvular fusions of the valve apparatus can make either commissurotomy or PMBC less likely to be successful. It should also be noted that the presence of mitral regurgitation is a contraindication for valvotomy/commissurotomy and is considered best treated with mitral valve replacement.

Closed commissurotomy is a surgical technique that uses finger fracture of the calcified valve (Fig. 4.8). This procedure has the advantage of not requiring cardiopulmonary bypass; however, the operator is not afforded direct visual examination of the valve apparatus. In contrast, open commissurotomy, which commonly utilizes cardiopulmonary bypass, allows for detailed inspection of the mitral valve apparatus under direct vision. During this procedure, division of the commissures, splitting of fused chordae tendineae/papillary muscles, debridement of calcium deposits [8], and/or mitral valve replacement can be completed to attain optimal results. The 5-year reoperation rate following open commissurotomy has been reported to be between 4% and 7%, and the 5-year complication-free survival rate ranges from 80% to 90%.

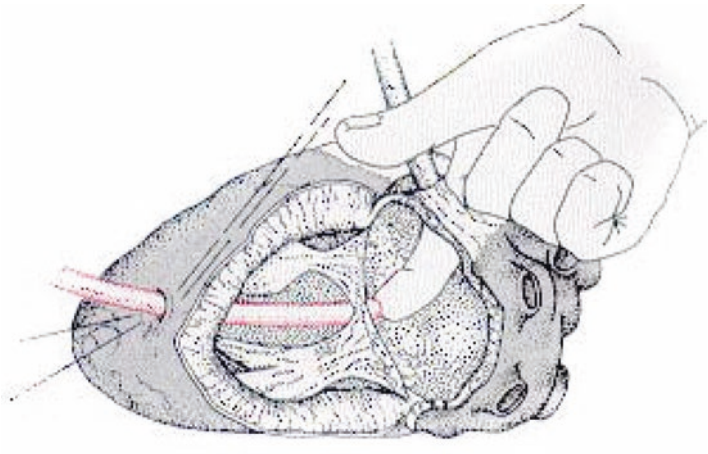

**Fig. 4.8** Treatment of mitral stenosis using the finger fracture closed mitral commissurotomy technique. (Source: Iaizzo [89])

In recent years, these operative techniques have given way to percutaneous mitral balloon commissurotomy (PMBC), which importantly have been shown to be comparable in both safety and efficacy (Fig. 4.9). PMBC is the procedure of choice for most patients with mitral stenosis. Patients with favorable valve morphology, no significant mitral regurgitation, and no left atrial thrombus are candidates for PMBC. Immediate reduction in the transvalvular gradient (by at least 50–60%) is associated with gradual regression of pulmonary hypertension over several months [8]. If selected appropriately, 80–95% of such patients undergoing this procedure will achieve a functional mitral valve area >1.5 $cm^2$ and a resultant decrease in left atrial pressure without complication. Yet, potential acute complications include: mitral regurgitation (10%), atrial septal defect (5%), left ventricle perforations (0.5–4.0%), emboli formation (0.5–3%), myocardial infarctions (0.3–0.5%), and/or increased mortality (<1%) [67]. Currently, echocardiographic assessments of mitral valve morphology are the most important predictor of outcome for percutaneous balloon valvotomy. Note, patients with valvular calcification, thickened fibrotic leaflets with decreased mobilities, and subvalvular fusions elicit higher incidences of acute complications following balloon valvotomy and higher rates of recurrent stenoses on follow-up. Presence of left atrial thrombus, detected by transesophageal echocardiography, is a relative contraindication and, at a minimum, warrants 3 months of oral warfarin anticoagulation in an attempt, to resolve the thrombus prior to the planned procedure. A postprocedural echocardiogram, typically within 72 h after the procedure, is useful to assess postoperative hemodynamics, as well as to exclude significant complications such as mitral regurgitation, left ventricular dysfunction, and/or an atrial septal defect. However, recurrent symptoms have been reported to occur in as many as 60% of patients 9 years post-procedure [68–70]; it should be noted that recurrent stenosis accounts for symptoms in <20% of such patients. In patients with an adequate initial results, progressive mitral

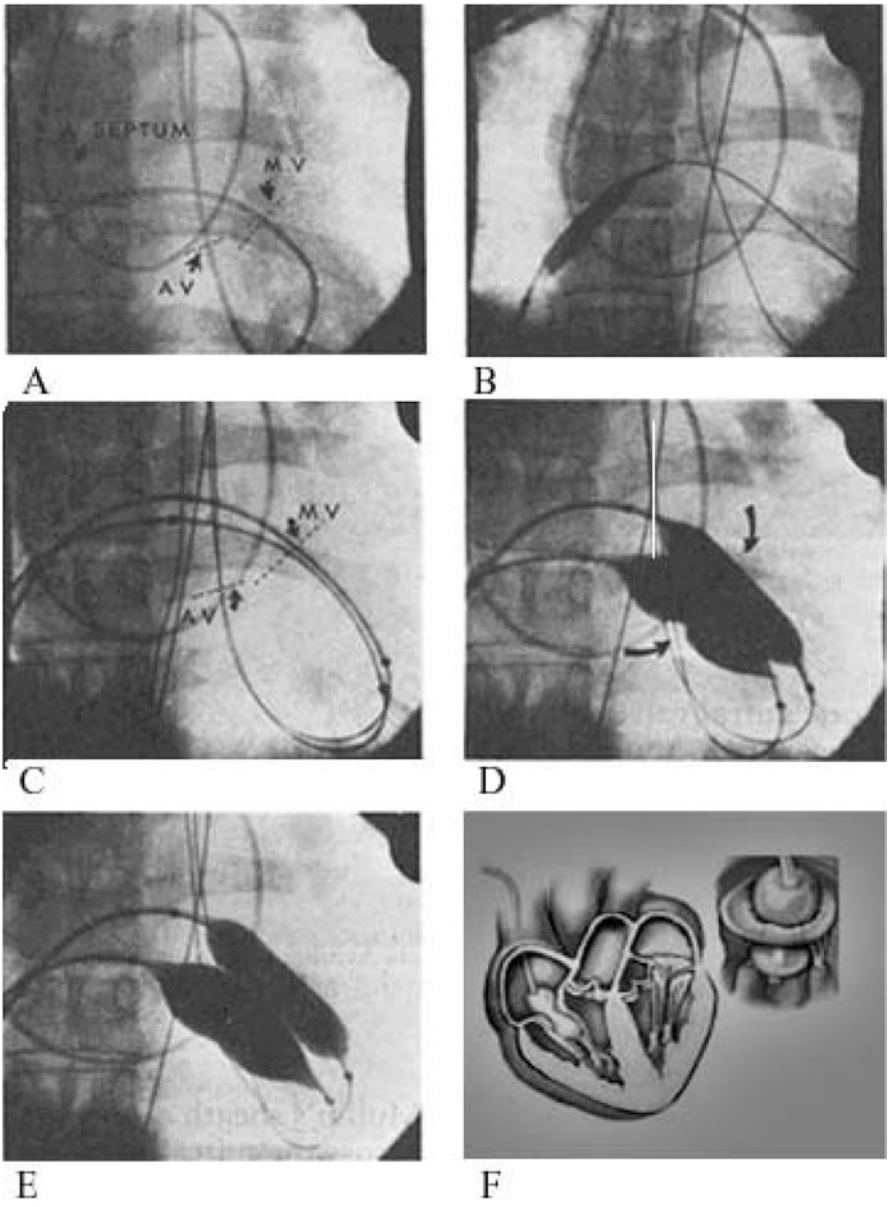


**Fig. 4.9** Treatment of mitral stenosis using balloon valvotomy. Sequence of percutaneous mitral valvotomy: (**a**) floating balloon catheter in position across the atrial septum through the mitral and aortic valves. The tip is in the ascending aorta; (**b**) an 8-mm dilating balloon catheter enlarging the atrial septal puncture site; (**c**) two 20-mm dilating balloon catheters advanced into position across the stenotic mitral valve over two separate 0.038 in transfer guide wires; (**d**) partially inflated dilating balloon catheters across the mitral valve; note the "waist" produced by the stenotic valve (arrows); (**e**) fully inflated dilating balloon catheters in position across the mitral valve; (**f**) illustration of balloon commissurotomy technique. (Source: Iaizzo [89])

regurgitations and developments of other valvular or coronary problems are more frequently responsible for the subsequent presentation of symptoms [68]. Thus, in a given patient presenting with symptoms late after commissurotomy, a comprehensive evaluation is required to look for other causes.

Mitral valve replacement is an accepted surgical procedure for patients with severe mitral stenosis who are not candidates for surgical commissurotomy or percutaneous mitral valvotomy (Table 4.8; Figs. 4.10 and 4.11). In addition, patients with recurrent severe symptoms, severe deformities of the mitral apparatus, severe mitral regurgitation, or a large atrial septal defect should be offered mitral valve replacement. The procedural risks associated with mitral valve replacement are also highly dependent on a given patient's age, left ventricular functional status, the elicitation low-cardiac outputs, presence of comorbid medical problems, and/or concomitant coronary artery disease. More specifically, morbidity and mortality associated with mitral valve replacement is directly correlated with age, with risks in a young healthy person of <5%, but increasing to as high as 10–20% in the older patient with concomitant medical problems or pulmonary hypertension. Mitral valve replacement can be further complicated by: (1) the potential for embolic events; (2) the need for (and risk of) long-term anticoagulation therapy; and/or (3) the potential for valve thrombosis, dehiscence, infection, or malfunction.

#### 4.3.2.2 Mitral Regurgitation

The common etiologies for mitral regurgitation include: (1) mitral valve prolapse secondary to myxomatous degeneration, (2) rheumatic heart disease, (3) coronary artery disease, (4) infective endocarditis, or (5) collagen vascular disease. As with aortic regurgitation, mitral regurgitation can be categorized as both acute and chronic presentations. In some patients, mitral regurgitation due to ruptured chordae tendineae or infective endocarditis may present as both acute and severe. Alternatively, mitral regurgitation may worsen gradually over prolonged periods of time. Yet, these very different presentations of mitral regurgitation can/are both treated with surgical interventions as dictated by the character of the symptoms presented.

**Table 4.8** Mitral valve replacement for mitral stenosis

| |
|---|
| Moderate to severe mitral stenosis (mitral valve area <1.5 $cm^2$): |
| With NYHA functional Class III–IV symptoms |
| Who are not considered candidates for percutaneous balloon valvotomy or mitral valve repair |
| Patients with severe mitral stenosis (mitral valve area <1 $cm^2$): |
| With severe pulmonary hypertension (pulmonary artery systolic pressure >60–80 mmHg) |
| With NYHA functional Class I–II symptoms who are not considered candidates for percutaneous balloon valvotomy or mitral valve repair |

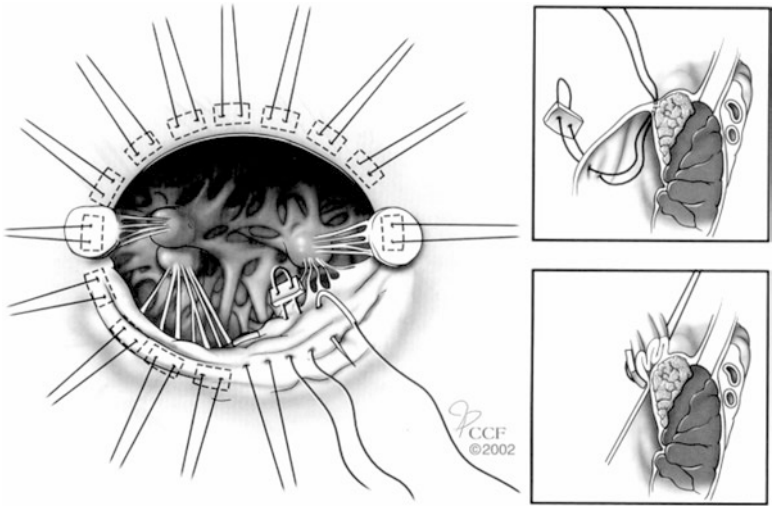


**Fig. 4.10** Placement of circumferential sutures and plication of the anterior leaflet of the mitral valve. (Adapted from Smedira [91])

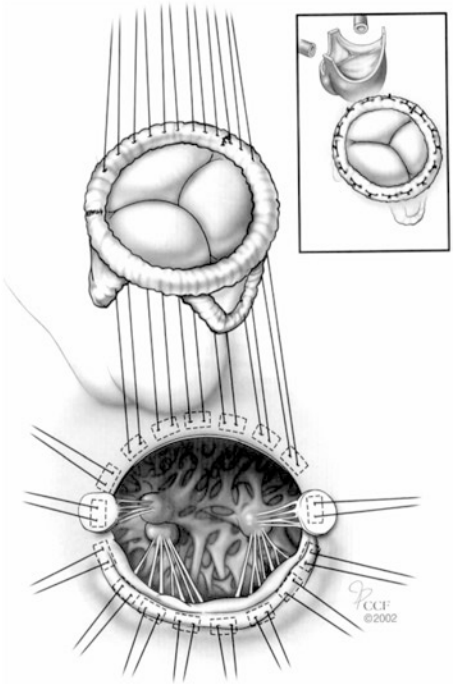


**Fig. 4.11** Mitral valve positioning into the mitral orifice. (Adapted from Smedira [91])

**Acute Severe Mitral Regurgitation**

In the patient presenting with acute severe mitral regurgitation, a sudden volume overload is imposed on the left atrium and the left ventricle is not allow the needed time for typical compensatory hypertrophy. Thus, a sudden drop in forward stroke volumes and cardiac outputs both occur, resulting in cardiogenic shock with simultaneous pulmonary congestion. In severe mitral regurgitation, the hemodynamic overload often cannot be tolerated, and mitral valve repair or replacement must be recommended to be performed urgently.

Patients with acute mitral regurgitation almost always present with signs and symptoms on taken histories and physical exams. Such patients typically elicit a noticeable holosystolic murmur and a third heart sound, on exam. Transthoracic echocardiography is commonly prescribed to confirm the diagnosis and to assess the general degree of disruption within the given patient's the mitral valve apparatus. Additionally, transesophageal echocardiography is warranted if mitral valve morphology and regurgitation are not clearly elucidated following transthoracic echocardiography. Note, it is the high level of detail provided by transesophageal echocardiography that is also helpful in demonstrating the anatomic causes of mitral regurgitation and subsequently directs successful surgical repair. Coronary arteriography is recommended as necessary before surgery in all such patients >40 years of age, unless hemodynamic stability is of concern. Patients with concomitant coronary artery disease should also undergo myocardial revascularization during their mitral valve surgery [71, 72].

If the patient is not a candidate for surgery or if preoperative stabilization is required, medical therapy can help to diminish the relative amount of mitral regurgitation, thus increasing their forward output and reducing pulmonary congestion; yet this therapy should be initiated promptly. However, in acute severe mitral regurgitation, it is considered that medical therapy has a limited role and is primarily used to stabilize such patients prior to surgery. In normotensive patients, nitroprusside has been used to increase the forward output not only by preferentially increasing aortic flow, but also by partially restoring mitral valve competence as the left ventricular size diminishes [73, 74]. In hypotensive patients with severe reduction in forward output, aortic balloon counter pulsation can be employed to increase forward outputs and mean arterial pressures, while simultaneously diminishing mitral valve regurgitant volumes and left ventricular filling pressures. If infective endocarditis is the cause of acute mitral regurgitation, identification and treatments of the infectious organism are important to optimize successful clinical outcomes.

**Chronic Asymptomatic Mitral Regurgitation**

As with other chronic valvular disease, evidence of compensatory mechanisms including hypertrophy and chamber dilatation is typically present in the patient presenting with chronic severe mitral regurgitation [75]. The dilatation, or increase in left ventricular end-diastolic volumes, is a compensatory mechanism which permits increases in total stroke volumes and allows for restoration of forward cardiac outputs [76]. At the same time in such a patient, an increase in left ventricular and left atrial size accommodates the regurgitant volume with a lower filling pressure;

consequentially, symptoms of pulmonary congestion abate. Note, such patients with mild to moderate mitral regurgitations may remain without symptoms for several years with very little hemodynamic compromise. This compensated phase of mitral regurgitation is variable and can last several years. However, the prolonged burden of volume overload may eventually result in left ventricular dysfunction. At this time, contractile dysfunctions impair myocardial ejections and end-systolic volume increases; there may also be further left ventricular dilatations and increased left ventricular filling pressures. Therefore, correction of mitral regurgitation is generally recommended shortly following a patient's diagnosis of severe mitral regurgitation, irrespective of the presence or absence of symptoms.

Initial diagnosis of chronic mitral regurgitation is commonly accomplished by physical exam which may demonstrate findings of left ventricular apical impulse displacement, indicating that mitral regurgitation is severe and chronic and has likely caused cardiac enlargement. Typically, ECG and chest X-ray exams can be useful to evaluate rhythm changes and heart sizes, respectively. Nevertheless, an initial echocardiogram, including Doppler interrogation of the mitral valve, is considered indispensable for the management of the patient identified with mitral regurgitation. This will provide a baseline estimation of left ventricular and left atrial volumes, an estimation of the left ventricular ejection fraction, and an approximation of the severity of regurgitation. Note that any presence of pulmonary hypertension is worrisome because it likely indicates advanced disease with a worsened prognosis [77]. Serial clinical follow-ups are recommended to assess changes in symptomatic status, left ventricular functions, and/or exercise tolerance. Echocardiography is recommended every 6–12 months for asymptomatic patients with known moderate to severe mitral regurgitation. Left ventricular end-systolic functional assessment can typically aid in the timing of mitral valve surgery. For example, an end-systolic dimension, which may be less load-dependent than ejection fraction, should be <45 mm preoperatively to ensure normal postoperative left ventricular function [76, 78]. Note, it is generally considered that if a given patient become symptomatic, they should undergo mitral valve surgery even if left ventricular function is considered appropriately normal. Similar to the patient with acute mitral regurgitation, cardiac catheterization is indicated if: (1) there is discrepancy between clinical and noninvasive findings; (2) there is a need for preoperative coronary assessment for potential revascularization at the time of mitral valve replacement; and/or (3) an absence of chamber enlargement raises the question of the accuracy of the diagnosis, which should then be assessed with ventriculography during cardiac catheterization. Formal exercise testing with hemodynamics is one other test useful in asymptomatic patients with severe mitral regurgitation. In such patients, exercise may worsen mitral regurgitation, causing an otherwise asymptomatic individual to be symptomatic, hence both echocardiography or invasive hemodynamics in a stressed state may provide further information not otherwise elucidated from studies done at rest.

To date, there are no generally accepted therapies for asymptomatic patients with chronic mitral regurgitation. In such patients who develop symptoms but have preserved left ventricular function, surgery is considered as the most appropriate therapy.

Atrial fibrillation is commonly associated with mitral regurgitation, and preoperative atrial fibrillation can be an independent predictor of reduced long-term survival after mitral valve surgery for chronic mitral regurgitation [79]. As noted above, atrial fibrillation should be treated with heart rate control (digoxin, calcium channel blockers, beta blockers, or amiodarone) and anticoagulation to avoid embolism [80, 81]. Common predictors for the persistence of atrial fibrillation after successful valve surgery include: the presence of atrial fibrillation for >1 year and/or a left atrial size >50 mm [82]. Although patients who develop atrial fibrillation also usually manifest other symptomatic or functional changes that would warrant mitral valve repair or replacement, many clinicians would also consider the onset of episodic or chronic atrial fibrillation to be a potential indication for valvular surgery [83, 84].

Three categories of surgical intervention for mitral regurgitation are commonly utilized: (1) mitral valve repair; (2) mitral valve replacement with preservation of part or all of the mitral apparatus; and (3) mitral valve replacement with prior removal of the mitral apparatus. Each procedure has both its advantages and disadvantages, as well as separate indications. Noteworthy in general, with the appropriate valve morphology and sufficient surgical expertise, mitral valve repair is the operation of choice. Yet, valve repair may require longer extracorporeal circulation times and may also occasionally fail, thus in turn requiring mitral valve replacement. Further, valve calcification, rheumatic involvement, and anterior leaflet involvement all decrease the likelihood of an adequate repair, whereas uncalcified posterior leaflet disease is almost always repairable. Primary advantages of mitral valve repair are avoiding long-term anticoagulation and/or avoiding rare prosthetic valve failure. In addition, postoperative left ventricular function and survival are improved with preservation of the mitral apparatus; as the mitral apparatus is considered essential for maintenance of a more normal left ventricular chamber shape, volume, and function [8]. Similar advantages are gleaned with the use of mitral valve replacement with preservation of the mitral chordal apparatus, except that it adds both the risks of deterioration inherent in tissue valves and the need for anticoagulation with mechanical valves. It is generally considered today that mitral valve replacement, in which the mitral valve apparatus is excised, should be performed only in circumstances when the native valve and apparatus are so distorted by the preoperative pathology (e.g., rheumatic disease) that the mitral apparatus cannot be spared.

In an asymptomatic patient with normal left ventricular function, repair of a severely regurgitant valve may be offered as means to: (1) preserve left ventricular sizes and function; and/or (2) prevent the sequela of chronic mitral regurgitation (Fig. 4.12). Similarly, this approach has proven successful in the hemodynamically stable patient with newly acquired severe mitral regurgitation as the result of a ruptured chordae or recent onset of atrial fibrillation. The timing of surgery in asymptomatic patients is indicated by the appearance of echocardiographic indicators of left ventricular dysfunction (i.e., left ventricular ejection fraction <60% or left ventricular end-systolic dimension >45 mm). Mitral valve repair or replacement at this stage will likely prevent further deterioration of a given patient's left ventricular function and thus improve survival [79]. Patients with symptoms of congestive heart

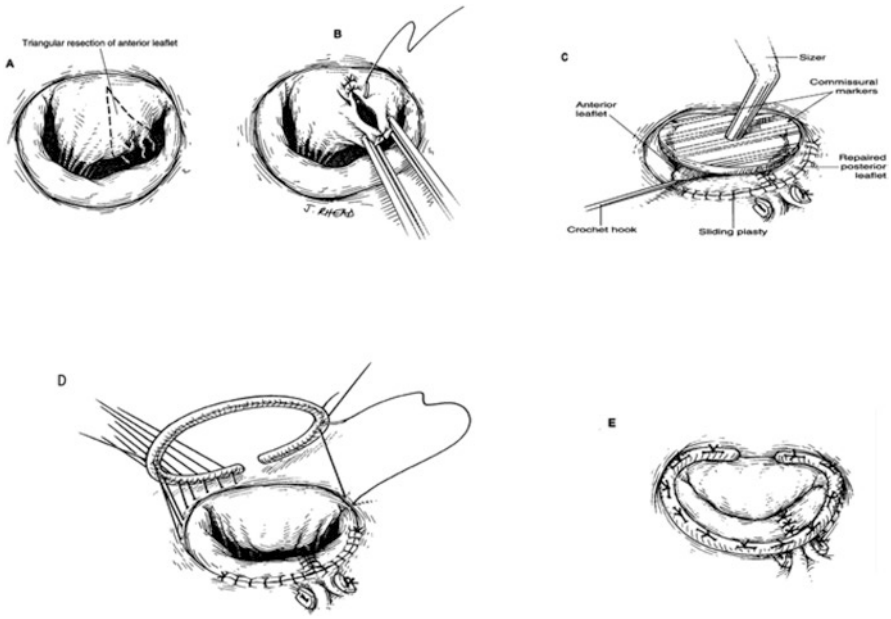


**Fig. 4.12** Operative repair of the mitral valve using a technique developed by Carpentier. (**a**) Triangular resection of anterior leaflet; (**b**) anterior leaflet repair; (**c**) sizing of annulus; (**d**) annuloplasty ring suture technique; and (**e**) completed repair. (Source: Iaizzo [89])

failure, despite normal left ventricular function as determined by echocardiography (ejection fraction >60%, end-systolic dimension <45 mm), will likely require surgery. Again, similar to the above-mentioned situations, mitral repair is preferred when possible. Mitral valve surgery is recommended for severe symptomatic mitral regurgitation with evidence of left ventricular systolic dysfunction; it is likely to both improve symptoms and prevent further deterioration of left ventricular function [85].

Ischemic mitral regurgitation is, by common definition, caused by left ventricular myocardial infarction, hence resulting in an associated papillary muscle dysfunction. Unfortunately, the prognosis for such a patient with ischemic mitral regurgitation is substantially worse when compared with other etiologies [72, 86]. Following an acute infarction with the development of severe mitral regurgitation, hypotension and pulmonary edema often occur. Hemodynamic stabilization, usually with insertion of an intra-aortic balloon pump, is completed preoperatively followed by coronary revascularization which only rarely improves their mitral valve function. Unlike the case with non-ischemic mitral regurgitation, it is more difficult to demonstrate a benefit of repair over replacement with ischemic mitral regurgitation. In general, operative mortality increases and survival is reduced in patients >75 years of age with coronary artery disease, especially if mitral valve replacement must be performed [87]. In these patients, the goal of therapy is typically to improve their quality of life rather than prolong it per se, and medical therapy may be utilized to a greater extent to control cardiac symptoms.

### *4.3.3 Tricuspid Valve Disease*

As with the other cardiac valves, tricuspid valve disease can be subclassified as regurgitation, stenosis, or a combination of both. Disorders of the tricuspid valve may result from a multitude of etiologies, including: (1) rheumatic disease, (2) infective endocarditis, (3) congenital anomalies, (4) papillary muscle dysfunction, (5) myxomatous changes, (6) carcinoid, (7) Fabry's disease, (8) Whipple's disease, (9) methysergide therapy, (10) radiation therapy, and/or (11) trauma [8]. Interestingly, Rheumatic tricuspid disease commonly presents as a combination of tricuspid stenosis and regurgitation. It may also be associated with concomitant mitral or aortic valve disease given the propensity of rheumatic disease to these valves as well. Right atrial myxomas or any type of large vegetation that produces an outflow tract obstruction will mimic stenosis, however, regurgitation may also result as it may cause associated damage to the tricuspid leaflet apparatus. Pressure/volume overload conditions that do not cause direct damage to the leaflets themselves, such as those associated with mitral stenosis and mitral regurgitation, typically cause ventricular enlargement, resultant tricuspid annular dilatation, and thus a sole tricuspid regurgitation [8].

Tricuspid stenosis results in characteristic exam findings, including: (1) a tricuspid opening snap and (2) a holosystolic murmur in the left lower parasternal region that may increase on inspiration. In rare instances, severe tricuspid regurgitation may produce systolic propulsion within the eyeballs, pulsatile varicose veins, or a venous systolic thrill and detectable murmurs in the neck. Echocardiography is commonly used to assess one's tricuspid valve structure and function, measure annular size, evaluate right heart pressures, and rule out other abnormalities influencing tricuspid valve function. Systolic pulmonary artery pressure estimations, combined with information about annular circumference, further improves the accuracy of a given clinical assessment [8].

A patient's clinical condition and the underlying etiology of tricuspid valve disease ultimately dictate the considered therapeutic approach. When pulmonary hypertension is the underlying cause of tricuspid annular dilatation, medical management alone may result in substantial improvement of tricuspid regurgitation, and thus minimize the need for surgical intervention. Medical management in such patients includes: (1) diuretic therapy to treat systemic congestion or (2) pulmonary vasodilators to reduce elevated pulmonary artery pressures. Surgical options for treating tricuspid regurgitation include both valve repair or valve replacement (Fig. 4.13). Today, the vast majority of diseased tricuspid valves are repaired in the U.S. The basic techniques for tricuspid valve repair include bicuspidization, annular placation, and various types of annuloplasty, commonly using artificial rings. Tricuspid regurgitation annuloplasty is effective and can be optimized using intraoperative transesophageal echocardiography. A valve replacement with a low-profile mechanical valve or bioprosthesis is often necessary when the valve leaflets themselves are diseased, abnormal, or totally destroyed [88]. In both such procedures, care must be taken to avoid causing damage to the heart's conduction system.

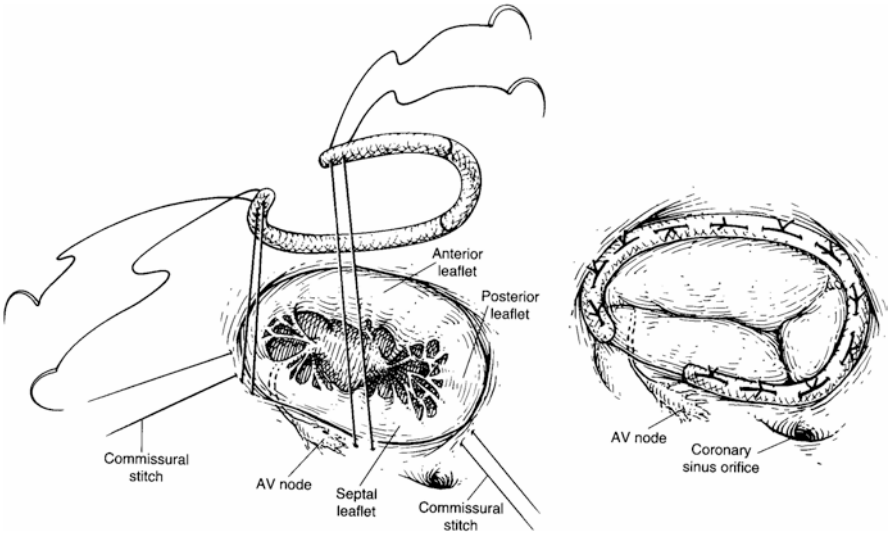


**Fig. 4.13** Tricuspid annuloplasty procedure. (Source: Iaizzo [89])

In such cases, use of biological prostheses is preferred to avoid the high rate of thromboembolic complications known to occur with mechanical prostheses placed in a tricuspid position. Note, combined tricuspid and mitral valve procedures are often completed in the same interventions, as in the setting of rheumatic disease; however, to date, no long-term data regarding the value of such a combined approach exist. Yet, there is increasing awareness of the importance to correct tricuspid valve disease in the setting of associated cardiac diseases, most commonly mitral valve disease. In patients with associated conduction defects, insertion of a permanent epicardial pacing electrode at the time of valve replacement is also suggested. Tricuspid balloon valvotomy is an option for treatment of tricuspid stenosis, understanding the risk of subsequently inducing severe tricuspid regurgitation. It has been documented that a poor long-term outcome is associated with right ventricular dysfunction and/or systemic venous congestion associated with severe tricuspid regurgitation [8].

## 4.4 Summary

The use of cross-circulation followed by the development of the bubble oxygenator for cardiopulmonary bypass is considered as the turning point in the history of cardiac surgery. This allowed for the development of cardiac valvular surgery, which may still be considered in ways to be in its infancy, as the majority of today's employed developments have occurred only in the last 60 years. From the numerous ongoing efforts of researchers and clinicians alike, tremendous advances in the field

of cardiac surgery are inevitable. This chapter was designed to give the reader an introduction to the complex nature of cardiac valve disease. Several excellent textbooks have been written, which provide greater detail for each valve procedure discussed. Such reference texts are valuable for both the clinician and the engineer interested in understanding the etiology and the current treatment techniques for valve disease. Nevertheless, this basis of understanding, along with the use of further animal and clinical research, will allow for the development of the next generation of treatment options for heart valve disease.

## References

1. Miller G (2000) King of hearts. Times Books
2. Bolman IRM, Black SM (2003) Open cardiac repair under direct vision: F. John Lewis and the University of Minnesota. J Card Surg 18:328–332
3. Lewis RP, Herr RH, Starr A, Griswold HE (1966) Aortic valve replacement with the Starr-Edwards ball-valve prosthesis. Indications and results. Am Heart 71:549–563
4. Lillehei C, Kaster R, Coleman M (1974) Heart-valve replacement with Lillehei-Kaster pivoting disk prosthesis. N Y State J Med 74:1426–1438
5. Walton Lillehei C, Kaster RL, Starek PJ, Bloch JH, Rees JR, York N (1972) A new central flow pivoting disc aortic and mitral prosthesis: initial clinical experience. N Y State J Med 72:1738
6. Saxena P, Konstantinov IE (2009) Bhagavant Kalke and his pioneering work on the bileaflet heart valve prosthesis. Ann Thorac Surg 88(1):344–347. https://doi.org/10.1016/j.athoracsur.2009.02.082
7. Emery R, Palmquist W, Mettler E (1978) A new cardiac valve prosthesis: in vitro results. Trans Am Soc Artif Intern Organs 24:550–556
8. Otto CM, Nishimura RA, Bonow RO, Carabello BA, Erwin JP, Gentile F, Jneid H, Krieger E v, Mack M, McLeod C, O'Gara PT, Rigolin VH, Sundt TM, Thompson A, Toly C (2021) 2020 ACC/AHA guideline for the management of patients with valvular heart disease: a report of the American College of Cardiology/American Heart Association Joint Committee on Clinical Practice Guidelines. J Am Coll Cardiol 77(4):e25–e197. https://doi.org/10.1016/j.jacc.2020.11.018
9. el Oakley R, Kleine P, Bach DS (2008) Choice of prosthetic heart valve in today's practice. Circulation 117(2):253–256. https://doi.org/10.1161/CIRCULATIONAHA.107.736819
10. Schaller T, Scharfschwerdt M, Schubert K, Prinz C, Lembke U, Sievers H-H (2021) Aortic valve replacement in sheep with a novel trileaflet mechanical heart valve prosthesis without anticoagulation. JTCVS Open 7:76. https://doi.org/10.1016/j.xjon.2021.05.011
11. Landes U, Webb JG, de Backer O, Sondergaard L, Abdel-Wahab M, Crusius L, Kim WK, Hamm C, Buzzatti N, Montorfano M, Ludwig S, Schofer N, Voigtlaender L, Guerrero M, el Sabbagh A, Rodés-Cabau J, Guimaraes L, Kornowski R, Codner P et al (2020) Repeat transcatheter aortic valve replacement for transcatheter prosthesis dysfunction. J Am Coll Cardiol 75(16):1882–1893. https://doi.org/10.1016/j.jacc.2020.02.051
12. Tang GHL, Zaid S, Gupta E, Ahmad H, Khan A, Kovacic J, Lansman S, Dangas GD, Sharma S, Kini A (2019) Feasibility of repeat TAVR after SAPIEN 3 TAVR: a novel classification scheme and pilot angiographic study. J Am Coll Cardiol Intv 12(13):1288–1292. https://doi.org/10.1016/j.jcin.2019.03.022
13. Oxenham H, Bloomfield P, Wheatley DJ, Lee RJ, Cunningham J, Prescott RJ, Miller HC (2003) Twenty year comparison of a Bjork-Shiley mechanical heart valve with porcine bioprostheses. Heart 89(7):715–721. https://doi.org/10.1136/heart.89.7.715

14. Hammermeister K, Sethi GK, Henderson WG, Grover FL, Oprian C, Rahimtoola SH (2000) Outcomes 15 years after valve replacement with a mechanical versus a bioprosthetic valve: final report of the veterans affairs randomized trial. J Am Coll Cardiol 36(4)
15. Goldstone AB, Chiu P, Baiocchi M, Lingala B, Patrick WL, Fischbein MP, Woo YJ (2017) Mechanical or biologic prostheses for aortic-valve and mitral-valve replacement. N Engl J Med 377(19):1847–1857. https://doi.org/10.1056/nejmoa1613792
16. Lund O, Bland M (2006) Risk-corrected impact of mechanical versus bioprosthetic valves on long-term mortality after aortic valve replacement. J Thorac Cardiovasc Surg 132(1):20. https://doi.org/10.1016/j.jtcvs.2006.01.043
17. Bach D, Metras J, Doty J (2008) Freedom from structural valve deterioration among patients 60 years of age and younger undergoing freestyle aortic valve replacement. J Heart Valve Dis 16:649–655
18. Cheitlin M, Douglas P, Parmley W (1994) 26th Bethesda conference recommendations for determining eligibility for competition in athletes with cardiovascular abnormalities. J Am Coll Cardiol 24(4):874–880
19. Edmunds LH, Clark RE, Cohn LH, Grunkemeier GL, Miller DC, Weisel RD (1996) Guidelines for reporting morbidity and mortality after cardiac valvular operations. Ad hoc liason committee for standardizing definitions of prosthetic heart valve morbidity of the American Association for Thoracic Surgery and the Society of Thoracic Surgeons. J Thorac Cardiovasc Surg 112:708–711
20. Carabello B (2002) Aortic stenosis. N Engl J Med 111:3316–3326
21. Freeman RV, Otto CM (2005) Spectrum of calcific aortic valve disease: pathogenesis, disease progression, and treatment strategies. Circulation 111(24):3316–3326. https://doi.org/10.1161/CIRCULATIONAHA.104.486738
22. Sprigings DC, Forfar JC (1995) How should we manage symptomatic aortic stenosis in the patient who is 80 or older? Heart. BMJ Publishing Group 74(5):481–484. https://doi.org/10.1136/hrt.74.5.481
23. Ross J Jr, Braunwald E (1968) Aortic stenosis. Circulation 38:61–67
24. Schwarz F, Baumann P, Manthey J, Hoffmann M, Schuler G, Mehmel HC, Schmitz W, Kubler W (1982) The effect of aortic valve replacement on survival. Circulation 66:1105–1110. http://ahajournals.org
25. Kelly T, Rothbart R, Cooper C (1988) Comparison of outcome of asymptomatic to symptomatic patients older than 20 years of age with valvular aortic stenosis. Am J Cardiol 61:123–130
26. Livanainen A, Lindroos M, Tilvis R (1996) Natural history of aortic valve stenosis of varying severity in the elderly. Am J Cardiol 78:97–101
27. Horstkotte D, Loogen F (1988) The natural history of aortic valve stenosis. Eur Heart J 9:E57–E64
28. Krayenbuehl HP, Hess OM, Ritter M, Monrad ES, Hoppeler H (1988) Left ventricular systolic function in aortic stenosis. Eur Heart J 9:19
29. Marcus M, Doty D, Hiratzka L (1982) Decreased coronary reserve: a mechanism for angina pectoris in patients with aortic stenosis and normal coronary arteries. N Engl J Med 307:1362–1366
30. Bache RJ, Vrobel TR, Ring WS, Emery RW, Andersen RW (1981) Regional myocardial blood flow during exercise in dogs with chronic left ventricular hypertrophy. Circ Res 48:76. http://ahajournals.org
31. Koyanagi S, Eastham C, Marcus M (1982) Effects of chronic hypertension and left ventricular hypertrophy on the incidence of sudden cardiac death after coronary artery occlusion in conscious dogs. Circulation 65(6):1192–1197. http://ahajournals.org
32. Otto CM, Pearlman AS, Kraft CD, Miyake-Hull CY, Burwash IG, Gardner C, Washington S (1992) Physiologic changes with maximal exercise in asymptomatic valvular aortic stenosis assessed by Doppler echocardiography. JACC 20(5)
33. Cheitlin MD, Armstrong WF, Aurigemma GP, Beller GA, Bierman FZ, Davis JL, Douglas PS, Faxon DP, Gillam LD, Kimball TR, Kussmaul WG, Pearlman AS, Philbrick JT, Rakowski H,

Thys DM, Antman EM, Smith SC, Alpert JS, Gregoratos G et al (2003) ACC/AHA/ASE 2003 guideline update for the clinical application of echocardiography: summary article. Circulation 108(9). https://doi.org/10.1161/01.CIR.0000073597.57414.A9
34. Loomba S, Arora R (2010) Statin therapy and aortic stenosis: a systematic review of the effects of statin therapy on aortic stenosis. Am J Ther 17:e110–e114. www.americantherapeutics.com
35. Bull S, Loudon M, Francis JM, Joseph J, Gerry S, Karamitsos TD, Prendergast BD, Banning AP, Neubauer S, Myerson SG (2015) A prospective, double-blind, randomized controlled trial of the angiotensin-converting enzyme inhibitor Ramipril in Aortic Stenosis (RIAS trial). Eur Heart J Cardiovasc Imaging 16(8):834–841. https://doi.org/10.1093/ehjci/jev043
36. Tsai T, Denton T, Chaux A (1994) Results of coronary artery bypass grafting and/or aortic or mitral valve operation in patients > or = 90 years of age. Am J Cardiol 74:960–962
37. Smith N, McAnulty J, Rahimtoola S (1978) Severe aortic stenosis with impaired left ventricular function and clinical heart failure: results of valve replacement. Circulation 58:255–264
38. Connolly H, Oh J, Orszulak T (1997) Aortic valve replacement for aortic stenosis with severe left ventricular dysfunction. Prognostic indicators. Circulation 95:2395–2400
39. Safian R, Mandell V, Thurer R (1987) Postmortem and intraoperative balloon valvuloplasty of calcific aortic stenosis in elderly patients: mechanisms of successful dilation. J Am Coll Cardiol 9:655–660
40. McKay R, Safian R, Lock J (1986) Balloon dilatation of calcific aortic stenosis in elderly patients: postmortem, intraoperative, and percutaneous valvuloplasty studies. Circulation 74:119–125
41. Spears J, Al-Saiegh Y, Goldberg D, Manthey S, Goldberg S (2020) TAVR: a review of current practices and considerations in low-risk patients. J Interv Cardiol 2020. https://doi.org/10.1155/2020/2582938
42. Monin J, Monchi M, Gest V (2001) Aortic stenosis with severe left ventricular dysfunction and low transvalvular pressure gradients: risk stratification by low-dose dobutamine echocardiography. J Am Coll Cardiol 37:2101–2107
43. Kang D-H, Park S-J, Lee S-A, Lee S, Kim D-H, Kim H-K, Yun S-C, Hong G-R, Song J-M, Chung C-H, Song J-K, Lee J-W, Park S-W (2020) Early surgery or conservative care for asymptomatic aortic stenosis. N Engl J Med 382(2):111. https://doi.org/10.1056/NEJMoa1912846
44. Grossman W, Jones D, McLaurin L (1975) Wall stress and patterns of hypertrophy in the human left ventricle. J Clin Invest 56:56–64
45. Fortuin N, Craige E (1972) On the mechanism of the Austin Flint murmur. Circulation 45:558–570
46. Parker E, Craige E, Hood W Jr (1971) The Austin Flint murmur and the a wave of the apexcardiogram in aortic regurgitation. Circulation 43:349–359
47. Miller R, Vismara L (1976) Afterload reduction therapy with nitroprusside in severe aortic regurgitation: improved cardiac performance and reduced regurgitant volume. Am J Cardiol 38:564–567
48. Cigarroa J, Isselbacher E, DeSanctis R (1993) Diagnostic imaging in the evaluation of suspected aortic dissection. Old standards and new directions. N Engl J Med 328:35–43
49. Smith M, Cassidy J, Souther S (1995) Transesophageal echocardiography in the diagnosis of traumatic rupture of the aorta. N Engl J Med 332:356–362
50. Yacoub M (1983) Results of valve sparing operations for aortic regurgitation. Circulation 68:311–321
51. David T (2001) Aortic valve-sparing operations for aortic root aneurysm. Semin Thorac Cardiovasc Surg 13:291–296
52. Gorlin R, Gorlin S (1951) Hydraulic formula for calculation of the area of stenotic mitral valve, other cardiac valves, and central circulatory shunts. Am Heart J 41:1–29
53. Wood P (1954) An appreciation of mitral stenosis. I. Clinical features. Br Med J 4870:1051–1063
54. Rowe J, Bland E, Sprague H (1960) The course of mitral stenosis without surgery: ten- and twenty-year perspectives. Ann Intern Med 52:741–749

55. Edwards J, Rusted I, Scheifley C (1956) Studies of the mitral valve. II. Certain anatomic features of the mitral valve and associated structures in a mitral stenosis. Circulation 14:398–406
56. Roberts W, Perloff J (1972) A clinicopathologic survey of the conditions causing the mitral valve to function abnormally. Ann Intern Med 77:939–975
57. Olesen K (1962) The natural history of 271 patients with mitral stenosis under medical treatment. Br Heart J 24:349–357
58. Carroll J, Feldman T (1993) Percutaneous mitral balloon valvulotomy and the new demographics of mitral stenosis. J Am Med Assoc 270:1731–1736
59. Selzer A, Cohn K (1972) Natural history of mitral stenosis: a review. Circulation 45:878–890
60. Braunwald E, Moscovitz H, Amram S (1955) The hemodynamics of the left side of the heart as studied by simultaneous left atrial, left ventricular, and aortic pressures; particular reference to mitral stenosis. Circulation 12:69–81
61. Holen J, Aaslid R, Landmark K (1976) Determination of pressure gradient in mitral stenosis with a non-invasive ultrasound Doppler technique. Acta Med Scand 199:455–460
62. Hatle L, Brubakk A, Tromsdal A (1978) Noninvasive assessment of pressure drop in mitral stenosis by Doppler ultrasound. Br Heart J 40:131–140
63. Coulshed N, Epstein E, McKendrick C (1970) Systemic embolism in mitral valve disease. Br Heart J 32:26–34
64. Daley R, Mattingly T, Holt C (1951) Systemic arterial embolism in the rheumatic heart disease. Am Heart J 42:566
65. Abernathy W, Willis P (1973) Thromboembolic complications of rheumatic heart disease. Cardiovasc Clin 5:131–175
66. Adams G, Merrett J, Hutchinson W (1974) Cerebral embolism and mitral stenosis: survival with and without anticoagulants. J Neurol Neurosurg Psychiatry 37:378–383
67. Orrange S, Kawanishi D, Lopez B (1997) Actuarial outcome after catheter balloon commissurotomy in patients with mitral stenosis. Circulation 95:382–389
68. Higgs L, Glancy D, O'Brien K (1970) Mitral restenosis: an uncommon cause of recurrent symptoms following mitral commissurotomy. Am J Cardiol 26:34–37
69. Dahl J, Winchell P, Borden C (1967) Mitral stenosis. A long term postoperative follow-up. Arch Intern Med 119:92–97
70. Currie P, Seward J, Chan K (1985) Continuous wave Doppler determination of right ventricular pressure: a simultaneous Doppler-catheterization study in 127 patients. J Am Coll Cardiol 6:750–756
71. Cohn L, Couper G, Kinchla N (1990) Decreased operative risk of surgical treatment of mitral regurgitation with or without coronary artery disease. J Am Coll Cardiol 16:1575–1578
72. Connolly M, Gelbfish J, Jacobowitz I (1986) Surgical results for mitral regurgitation from coronary artery disease. J Thorac Cardiovasc Surgery 91:379–388
73. Chatterjee K, Parmley W, Swan H (1973) Beneficial effects of vasodilator agents in severe mitral regurgitation due to dysfunction of subvalvar apparatus. Circulation 48:684–690
74. Yoran C, Yellin E, Becker R (1979) Mechanism of reduction of mitral regurgitation with vasodilator therapy. Am J Cardiol 43:773–777
75. Carabello B (1988) Mitral regurgitation: basic pathophysiologic principles. Part 1. Mod Concepts. Cardiovasc Dis 57:53–58
76. Zile M, Gaasch W, Carroll J (1984) Chronic mitral regurgitation: predictive value of preoperative echocardiographic indexes of left ventricular function and wall stress. J Am Coll Cardiol 3:235–242
77. Crawford M, Souchek J, Oprian C (1990) Determinants of survival and left ventricular performance after mitral valve replacement. Department of Veterans Affairs Cooperative Study on Valvular Heart Disease. Circulation 81:1173–1181
78. Wisenbaugh T, Skudicky D, Sareli P (1994) Prediction of outcome after valve replacement for rheumatic mitral regurgitation in the era of chordal preservation. Circulation 89:191–197
79. Enriquez-Sarano M, Tajik A, Schaff H (1994) Echocardiographic prediction of survival after surgical correction of organic mitral regurgitation. Circulation 90:830–837

80. Blackshear J, Pearce L, Asinger R (1993) Mitral regurgitation associated with reduced thromboembolic events in high-risk patients with nonrheumatic atrial fibrillation. Stroke Prevention in Atrial Fibrillation Investigators. Am J Cardiol 72:840–843
81. Beppu S, Nimura Y, Sakakibara H (1985) Smoke-like echo in the left atrial cavity in mitral valve disease: its features and significance. J Am Coll Cardiol 6:744–749
82. Betriu A, Chaitman B (1982) Preoperative determinants of return to sinus rhythm after valve replacement. In: Cardiac bioprosthesis. Yorke Medical Books, pp 184–191
83. Chua Y, Schaff H, Orszulak T (1994) Outcome of mitral valve repair in patients with preoperative atrial fibrillation. Should the maze procedure be combined with mitral valvuloplasty? J Thorac Cardiovasc Surg 107:408–415
84. Horskotte D, Schulte H, Bircks W (1993) The effect of chordal preservation on late outcome after mitral valve replacement: a randomized study. J Heart Valve Dis 2:150–158
85. Bonow R, Nikas D, Elefteriades J (1995) Valve replacement for regurgitant lesions of the aortic or mitral valve in advanced left ventricular dysfunction. Cardiol Clin 13:73–83
86. Akins C, Hilgenberg A, Buckley M (1994) Mitral valve reconstruction versus replacement for degenerative or ischemic mitral regurgitation. Ann Thorac Surg 58:668–675
87. Enriquez-Sarano M, Schaff H, Orszulak T (1995) Valve repair improves the outcome of surgery for mitral regurgitation. A multivariate analysis. Circulation 91:1022–1028
88. Silverman N (1998) Tricuspid valve. In: Mastery of cardiac surgery. Lippincott Williams & Wilkins, Philadelphia, pp 354–360
89. Iaizzo PA (2009) The handbook of cardiac anatomy, physiology, and devices, 2nd edn. Springer, New York, Chapter 31
90. Yun, Miller (1998) Operation for aortic root aneurysm or dissection. In: Operative techniques in cardiac and thoracic surgery. Elsevier, New York, pp 68–81
91. Smedira NG (2003) Mitral valve replacement with a calcified annulus. In: Cox JL (ed) Operative techniques in thoracic and cardiovascular surgery. Saunders, Philadelphia, pp 2–13

# Chapter 5
# History of Heart Valve Repair


**Lauren B. Kwasny, Richard W. Bianco, and Luis H. Toledo-Pereyra**

## Abbreviations

| | |
|---|---|
| AESOP | Automated endoscopic system for optimal positioning |
| ASD | Atrial septal defect |
| ePTFE | Expanded polytetrafluoroethylene |
| LVOTO | Left ventricular outflow tract obstruction |
| NYHAC | New York Heart Association Classification |
| SAM | Systolic anterior motion |

## 5.1 Introduction

At the turn of the twentieth century, numerous hospitals were devoted solely to patients suffering from rheumatic fever; the prevalence of this disease was later compared to the prevalence of AIDS at the turn of the twenty-first century [1]. Yet medical treatments of the day were ineffective, and surgical treatments were stalled by several flawed prevailing theories of the day [2]. First, rheumatic fever was presumed to destroy the myocardium alone rather than the valves; therefore, valvular

L. B. Kwasny
Michigan State University College of Osteopathic Medicine, Western Michigan University, Kalamazoo, MI, USA

R. W. Bianco
Department of Surgery, University of Minnesota, Minneapolis, MN, USA

L. H. Toledo-Pereyra (✉)
Western Michigan University School of Medicine, Michigan State University College of Human Medicine and Osteopathic Medicine, Kalamazoo, MI, USA
e-mail: luis.toledo@med.wmich.edu

© The Author(s), under exclusive license to Springer Nature Switzerland AG 2023

P. A. Iaizzo et al. (eds.), *Heart Valves*, https://doi.org/10.1007/978-3-031-25541-0_5

therapy was considered useless. Second, many still believed any injury to the heart was fatal, including surgical incisions. This belief can be traced from Hippocrates to Galen to Billroth and the physicians of the 1910–1920s [2]. World War I surgeons were consistently successful in suturing the heart, and began the process of dissolving this faulty stance. Third, physicians of the time did not believe that a surgical treatment could permanently cure a disease of medical origin. Thoracic surgeons were hindered by additional conditions, including ineffective resuscitation methods and inadequate diagnostic tools. It must have seemed senseless to broach the inviolable chest cavity to blindly operate on the actively beating heart.

Due to restrictions of time and space, techniques that have been applied clinically will be the focus of study in this chapter. Of the many significant innovators who have contributed to valvular repair techniques, only those who pioneered novel techniques or who managed to bring techniques into worldwide use will be discussed. Whenever possible, the dates of the original operations will be reported; if these dates have not been noted in the literature, the publication dates will be used. Note that many early treatments focused on the mitral valve, as this valve was most frequently involved in rheumatic heart disease. Today, aortic valve disease is much more prevalent in developed nations.

## 5.2 Brunton's Era (1897–1922): Thinking About Valve Repair

Eventually surgeons came to conquer each area of the body. As surgeons gained confidence within the thoracic cavity, some began to dream of applications of surgery to the heart. Herbert Milton published an influential paper in *The Lancet* in 1897 from Cairo, describing a new sternum splitting technique for thoracic surgery [3]. When discussing the implications of his technique, Milton speculated on the application of this surgical approach to valvular surgery. Daniel Samways of Britain and France followed in 1898 with the suggestion of slightly "notching" the orifice of a stenotic mitral valve [4]. Samways was the first surgeon to propose the idea that mitral insufficiency was a lesser evil than stenosis, based on an inaccurate theory of the cardiac cycle. He postulated that the cardiac cycle was peristaltic in nature; if this were true, then the surgical creation of insufficiency in the valve would not result in any regurgitation. However, heart surgery was still in its infancy and only performed in emergency situations. Ludwig Rehn had only just become the first person to successfully suture a heart wound on September 8, 1896 [5]. Naturally, any surgical suggestions for valvular repair were not taken seriously.

Yet it was only a few years later, in 1902, that the London physician Sir Thomas Lauder Brunton (1844–1916) succeeded in inspiring serious debate over the possibility of valvular surgery following a brief publication in *The Lancet* [6]. In his correspondence, Brunton boldly approached the subject of valvular surgery as though it were only a matter of time before surgeons would be completing clinical trials. "The first question that arises is whether the mitral orifice should be enlarged

by elongating the natural opening or whether the valves should be cut through their middle at right angles to the normal opening. I think there can be little doubt that the former would be the better plan, but the latter is the more easily performed, and it might be sufficient to effect the desired purpose of facilitating the flow of blood from the auricle into the ventricle." The response to this *preliminary note* was outrage. As stated in the 1970s by Richardson, "He was a kindly and respected man and a Fellow of the Royal Society—which makes the subsequent vitriolic attack on his integrity all the more surprising" [2]. Even the editors of *The Lancet* at the time expressed their sincere doubt that any surgery of this nature could prove useful: "Should our anticipation of failure prove to be groundless we shall indeed rejoice to witness an extension of surgery which might be attended with great alleviation of human suffering" [7]. Nevertheless, the idea of valvular surgery had been widely disseminated to the scientific community, and professionals were forced to confront the concept.

## 5.3 The First Successful Valve Repairs (1912, 1925): Finger Fracture Valvuloplasty

### *5.3.1 The First Successful Closed Surgery: Aortic Stenosis*

Only a decade after Brunton's disastrous proposal, aortic and mitral stenosis became the first valvular maladies to be successfully treated with surgery. Together, the French surgeons Theodore Tuffier (1857–1929) and Alexis Carrel (1873–1944) comprised a dream team for surgical innovation (Fig. 5.1a, b) [8]. "Carrel was the experimental surgeon, Tuffier was the practical surgeon" [2]. These surgeons continued to collaborate from 1910 to 1914, after Carrel moved to the Rockefeller Institute in New York. They experimented with the simplest techniques to bring

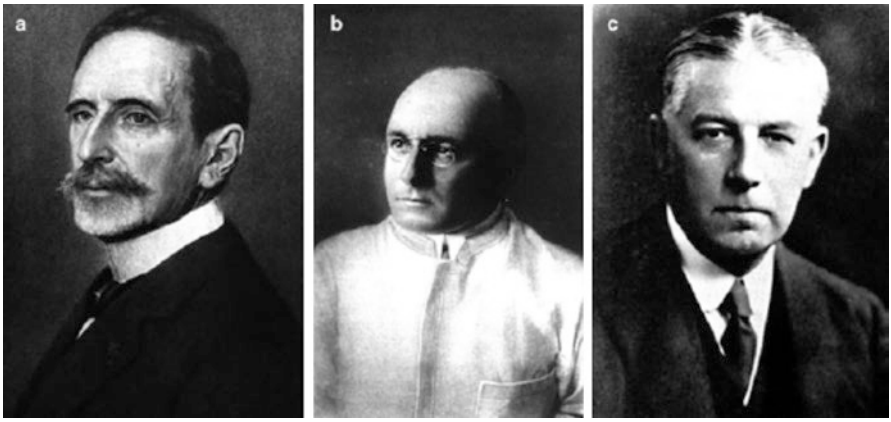


**Fig. 5.1** (**a**) Theodore Tuffier, (**b**) Alexis Carrel, and (**c**) Henry Souttar

**Table 5.1** Summary of operations for valvular disease (1913–1928)

| Author/surgeon | Date | Diagnosis | Method/instrument | Results after operation |
|---|---|---|---|---|
| Doyen | 1913 | Congenital PS; VSD | Tenotome | Died within hours |
| Tuffier | 1914 | AS | Finger dilation | Recovery/improved |
| Cutler, Levine | 5/20/1923 | MS | Tenotome | Died 4 1/2 years |
| Allen, Graham | 8/7/1923 | MS | Cardioscope | Operative death |
| Cutler, Levine, Beck | 10/7/1923 | MS | Tenotome | Died 30 h |
| Cutler, Levine, Beck | 1/12/1924 | MS | Tenotome | Died 20 h |
| Cutler, Levine, Beck | 2/25/1924 | MS | Cardiovalvulotome | Died 6 days |
| Cutler, Levine, Beck | 6/11/1924 | MS | Cardiovalvulotome | Died 3 days |
| Souttar | 5/6/1925 | MS; AI | Finger dilation | Recovery/improved |
| Pribram | 11/14/1925 | MS; Endo | Cardiovalvulotome | Died 6 days |
| Cutler, Beck | 12/8/1926 | MS | Cardiovalvulotome | Died 45 h |
| Cutler, Beck | 6/15/1928 | MS | Cardiovalvulotome | Died 3 h |

*Green* indicates successful surgeries, *yellow* indicates palliative surgeries, and *pink* indicates failed surgeries

*AI* aortic insufficiency, *AS* aortic stenosis, *Endo* endocarditis, *MS* mitral stenosis, *PS* pulmonary stenosis, *VSD* ventricular septal defect

cardiac surgery to the masses using a canine model [9, 10]. In the midst of these experimental trials, a human patient called upon their experience.

A 26-year-old male was prepped for surgery on July 13, 1912 (Table 5.1). "I observed, in a young man, a grave and rapidly progressive aortic stenosis. On the repeated request of his physician I decided to explore it" [11]. After opening the chest of the patient, Tuffier set aside his scalpel, grasped the beating heart, and invaginated the aorta with his little finger. "The vibration was intense: I reached the stenosis and very easily carried out a gradual dilatation by slowly introducing the little finger into the strictured ring, the vibrations under the finger being intense; I abstained from trying to divide the stricture as I did not consider experimental enquiry sufficiently advanced. I did not expect to attain any result. The patient was well in a few days; he improved temporarily and is still alive. I saw him three months ago" (*Fifth Congress of the International Society of Surgery*, Brussels, July 1920). The last report we could find on this patient indicated that he was still alive in 1920 [12].

### *5.3.2 The First Successful Closed Surgery: Mitral Stenosis*

In 1925, the general surgeon Henry Souttar (1875–1964) was asked to consider a 15-year-old girl afflicted with rheumatic mitral valve disease at the London Hospital (Fig. 5.1c) [13, 14]. Lilian Hine was first admitted to the hospital in 1921 with

chorea and mitral stenosis. Her subsequent history was one of many relapses. She was admitted once again in 1925 with heart failure. By this time, Elliot Cutler had already experienced one palliative success and four failures with his technique of incising/resecting portions of the valve through the left ventricle (Table 5.1). However, Souttar's surgery is considered the first successful mitral repair because his approach would eventually prove to be superior to Cutler's.

The auricular appendage was clamped and incised to allow the left forefinger to be inserted, "and the appendage was drawn over the finger like a glove by means of the sutures." Upon entering this appendage, Souttar immediately felt profound regurgitation and concluded that the extent of stenosis was only moderate. To avoid worsening the insufficiency, Souttar dilated the orifice using his finger instead of employing the hernia bistoury which had been set aside to section the valve [13]. While digital dilation succeeded in breaking down the adhesions between the cusps, the patient still suffered from a considerable amount of insufficiency and fought another bout of rheumatic fever only a year later. The patient lived for 7 years total following the operation, eventually passing away from cerebral embolism [7].

Souttar's background in engineering enabled him to make a famous argument against the stance that surgery could not heal medical illnesses. "I felt an appreciation of the mechanical reality of stenosis and regurgitation which I never before possessed… I could not help being impressed by the mechanical nature of these lesions and the practicability of their surgical relief" [13]. He noted that most discussions on valvular surgery focused only on the problems of surgery, and he instead chose to underscore the clinical work of Elliot Cutler and the experimental work of Duff Allen as evidence of the practicality of valvular surgery. Souttar was knighted in 1949 for his daring efforts in surgery, including the introduction of atraumatic sutures [4]. Unfortunately, physicians refused to ever allow this great surgeon to operate on valves again, despite his successes. Souttar later reflected on his experience with valvular surgery in a letter to Dwight Harken: "… it is no use to be ahead of one's time" [7]. Despite Souttar's success, Cutler's approach would dominate and hinder both experimental and clinical studies until after World War II, when Bailey would repopularize finger fracture valvuloplasty.

## 5.4 Cutler's Era (1923–1928): Exchanging Stenosis for Insufficiency

Elliot Cutler (1888–1947) was the first surgeon to repeatedly attempt mitral valve surgery, and his method and theory on the surgical treatment of mitral stenosis would prove extremely influential (Fig. 5.2a) [15, 16]. Of the ten reported surgeries during this time period (1923–1928), seven were completed by Cutler and his assistants Samuel Levin and Claude Beck. Cutler followed the advice of Brunton and Samways and created notches in the valve cusps, approached the heart through the left ventricle with a tenotome in his first three patients, and later created a

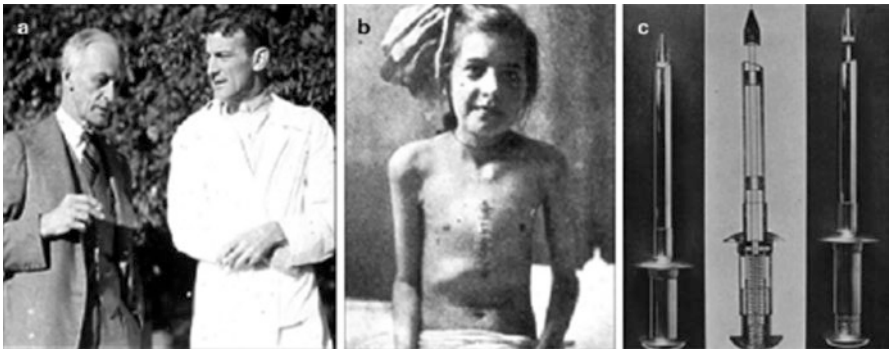


**Fig. 5.2** (**a**) Harvey Cushing (*left*) and Elliot Cutler (*right*), (**b**) Cutler's first and only successful mitral valve surgical patient, and (**c**) tenotome devised by Cutler and Beck to remove and retain large sections of valve tissue

valvulotome for use in the last four patients [17]. Cutler preceded his clinical work with canine experiments in the famous lab of Harvey Cushing (studying stenosis since 1905) (Fig. 5.2a). As a result of his experimentation on the valves of *healthy* animals, Cutler was confident that the only effective treatment would be valvotomy with subsequent production of a degree of insufficiency. In total, they performed operations on 30 dogs, 24 of which survived. Cutler and his associates were ready to take on their first clinical case.

On May 20, 1923 Cutler performed the first operation at the Peter Bent Brigham Hospital in Boston [16]. An 11-year-old girl had experienced dyspnea for 3 years and had been confined to her bed for 8 months, coughing up shocking amounts of blood. A curved tenotomy knife was inserted between control sutures at the apex of the left ventricle, and each valve was incised. After closure, a serious tamponade developed; fortunately, the patient recovered, gained ten pounds, and was relieved of hemoptysis. Her life was prolonged more than 4 years (Fig. 5.2b). However, during that time, she had a restricted level of activity and persistent signs of mitral stenosis. Autopsy would later show a remarkably enlarged heart, particularly on the left side. It is likely that this patient lived because the valvular incision was relatively small; accordingly, the degree of regurgitation was tolerable for a short time.

As Cutler and associates continued with their clinical trials, they experienced difficulties such as tamponade after closure, effectively punching through calcified and fibrosed valves, orienting their instrument blindly, and keeping their decidedly ill patients alive through the significant trauma of sternotomy. Cutler studied each casualty and sought to improve his techniques in the next surgery; still, every patient died. These deaths may have been compounded by the valvulotome, a tool created to punch through the heavily calcified valve tissue and resect a large portion of the leaflet (Fig. 5.2c). In Cutler's final report of all surgeries up to 1929 (Table 5.1) [16], the surgeons expressed their frustration over the lack of a proper animal model for mitral stenosis. Without an animal model and with only one patient surviving after the surgery, it was impossible to tell if valvotomy with a valvulotome produced

satisfactory changes in the mechanical dynamics of the circulatory system. “It may be that the cardiovalvulotome with its actual removal of a piece of valve creates a too sudden change… all the changes created by nature are slow and gradual…” [16].

While disheartened, they called upon others to continue their work. “It is our conclusion that the mortality figures alone should not deter further investigation both clinical and experimental, since they are to be expected in the opening of any new field for surgical endeavor” [16]. It was also clear that thoracic surgical techniques needed desperate attention, as the results of Cutler’s study were marred by death from complications following sternotomy, opening/closure of the pericardial sac, and incision into the heart itself. Respectable surgeons interested in valvular surgery turned to their laboratories to complete these essential experimental tasks.

## 5.5 Bailey, Harken, and Brock (1948–1957): Moving Away from Iatrogenic Insufficiency

The next phase of clinical valvular heart surgery would not begin for another 20 years, when a new generation of war-emboldened surgeons emerged onto the clinical field. Charles Bailey is remembered for performing what he called the first transatrial mitral commissurotomy on June 10, 1948 [18], and Dwight Harken (1910–1992) is noted for performing his mitral valvuloplasty on June 16, 1948 [19] (Fig. 5.3a, b). Russell Brock (1903–1980) performed one of the first successful valvulotomies for pulmonary stenosis on February 16, 1948, and later the first operation for the treatment of infundibular stenosis [20, 21] (Fig. 5.3c). These men, among others, began an era of reliable surgery on all four valves with a steady decrease in mortality and an attempt at objectively measuring patient improvement.

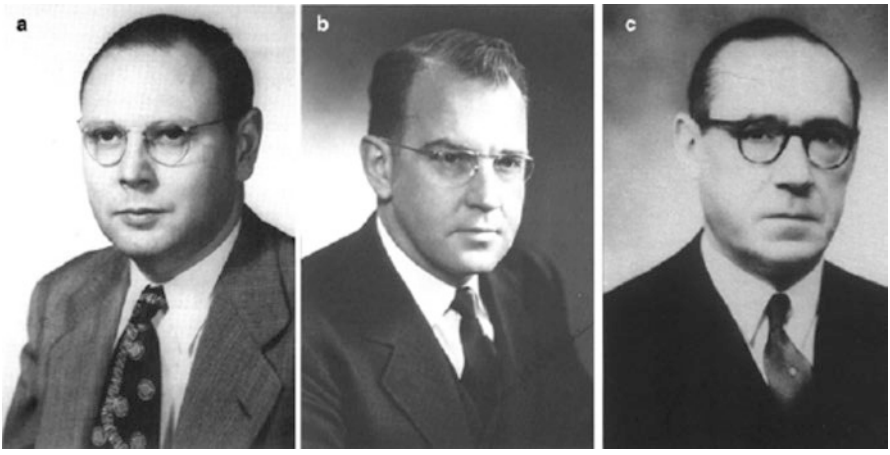


**Fig. 5.3** (**a**) Charles Bailey, (**b**) Dwight Harken, and (**c**) Russell Brock

Note that lesions of the tricuspid valve were comparatively rare; as such, this valve was never specifically targeted by any one surgeon during this time period.

### *5.5.1 A Race to Repair Mitral Stenosis*

An exciting race to successfully repair mitral stenosis occurred between two surgical giants—the talented Dwight Harken in Boston and the colorful Charles Bailey in Philadelphia. While each experienced their first clinical success within days of each other, ultimately Bailey would be considered victorious by many, as he conducted his surgery first and his initial technique would eventually prove more successful.

Dwight Harken (1910–1992) was Elliot Cutler's protégé, inheriting both the title of professor of surgery at the Peter Bent Brigham Hospital in Boston and his laboratory work on mitral stenosis [1]. Harken was well qualified to improve upon Cutler's techniques, as he had been a surgeon at the 160th General Hospital during World War II and had reported a remarkable 139 surgeries in and around the heart without a single death [22, 23]. It was not long before Harken realized that Cutler's technique merely traded one type of cardiac lesion for another. The conclusion was made that if an insufficiency had to be produced, then the posterior leaflet was better able to tolerate defects than the anterior leaflet. They observed that the posterior leaflet was pressed against the ventricle during systole, which would lessen any regurgitation from this portion of the valve. Harken began to advocate for a new technique called *selective insufficiency*, in which the commissures of the mitral valve were resected in thin wedges to treat stenosis and the anterior leaflet was always preserved [19]. This would restore movement to the stenosed valve in exchange for minimal insufficiency, which Harken believed was a necessary byproduct of repair for mitral stenosis due to the influence of Cutler.

They said of their first clinical operation on March 12, 1947: "This case illustrates how completely even a carefully planned procedure can miscarry" [19]. The presence of tachycardia was later blamed for the man's death, but in total six of Harken's first ten patients died [23]. Only the encouragement of his colleague, Dr. Ellis, enabled him to continue operating. Harken then lost just one of the next 15 patients. Over time, Harken would learn that creation of any degree of insufficiency to treat stenosis was unnecessary and would choose to perform the technique presented by Bailey [24].

Charles P. Bailey (1910–1993) avoided Cutler's regurgitant methods from the start [18]. His team was well prepared to begin work on mitral repair, having performed 60 cardiac operations in the canine model over 8 years. Bailey and colleagues demonstrated in the laboratory that (1) sudden creation of mitral regurgitation was tolerated poorly, (2) approach through the left auricular appendage produced fewer complications than a ventricular approach, and (3) several new instruments were useful in operations on stenotic valves.

Their method of commissurotomy was based on the rather simplified understanding of mitral valve anatomy of the day [25]. It was thought that the mitral valve consisted of two distinct leaflets separated by a linear oblique line. When a valve became stenotic, the tissue at the edges of this aperture would become fibrosed and rigid. However, if the stenosis had not progressed too far, a linear oblique incision could be made along the valve opening all the way through to the ring of soft healthy tissue which often surrounded the rigid stenotic portion. The valve would be freely hinged by this soft valvular tissue and would, in theory, return to physiological functioning without creating stenosis.

With this understanding of anatomy and plenty of experience in hand, Bailey operated on his first two patients at Hahnemann Hospital [18]. During the first surgery in 1945, they learned that the human auricular appendage in mitral stenosis can be extremely friable, after the purse string sutures tore through the wall and the bleeding could not be controlled. The second case took place in 1946, this time using digital dilation. Initial improvement was followed by sudden death on the second postoperative day. On autopsy, considerable restoration of the mitral valve orifice was confirmed, but thrombosis along the lines of splitting had greatly reduced the valve opening [23]. The valve had not been torn all the way through to healthy valvular tissue; consequently, fibrin accumulated and sealed the orifice.

Unfortunately, these disastrous surgeries earned Bailey the nickname *butcher of Hahnemann hospital* [26]. As a result of the last surgery, his team conceived the clever idea of commissurotomy using overlapping gloves to slide a small knife safely into a sheath along the dorsum of the palpating finger [18]. Bailey had been threatened with loss of surgical privileges at Hahnemann after the first two surgeries, but was able to try his new instrument at Memorial Hospital in Delaware with his third case, Philadelphia General Hospital for a fourth case, and Episcopal Hospital in Philadelphia for the fifth case [18, 26]. The surgery for the fourth case took place on the morning of June 10, 1948 and ended in mortality due to an extremely irregular and irritable myocardium: “He had a patient with mitral stenosis at the Episcopal Hospital across Philadelphia, and he immediately scheduled that patient for surgery the same afternoon, knowing that when the morning death was publicized his cardiac surgery career was finished. He wanted one more chance; he took it” [27].

This patient was 24-year-old Claire Ward, who had been afflicted with mild mitral stenosis for 2 years [4]. That afternoon, they again employed a hooked knife between gloves to divide the commissures of the thickened noncalcified valve. The operation was completed in 80 min without issue [18]. Even the presystolic murmur disappeared, and a week later she was transported by train some 1000 miles for the American College of Chest Physicians in Chicago. Her life was prolonged for 38 years with marked ballistocardiograph improvements during exercise and no need for digitalis [4]. Bailey suggested reoperation when recurrent stenosis first appeared 36 years later, a suggestion with which the cardiologist remarkably disagreed [4]. This method of splitting the commissures became very popular. The number of successes increased as surgeons developed a better understanding of

valvular anatomy and eventually traded the hooked finger knife for the finger itself, coining the term "finger fracture valvuloplasty."

### 5.5.2 Repairing Aortic Stenosis

The first surgeon to repeatedly attempt surgery for aortic stenosis was Horace Smithy. Smithy from the Medical College of South Carolina operated on seven patients to create insufficiency for the treatment of aortic stenosis (1914–1948) [28]. Smithy was the first to clinically focus on aortic stenosis since Tuffier, but he chose to follow Cutler's techniques [2, 4]. The operations were carried out from January 30, 1948 through June of 1948, with five patients surviving the procedure. Smithy ironically died from aortic stenosis on October 28, 1948, before the long-term results could be determined [28]. Smithy begged his colleague Alfred Blalock to operate on his valve, but Blalock firmly declined. He had some experimental experience with the procedure, but his only clinical attempt had died on the table before any cardiac manipulations. Two of Smithy's five successes were known to be alive in 1955, likely due to advances in medical treatments for heart failure [4]. Smithy's first patient, Betty Woolridge, died just 10 days after Smithy [29].

A reliable surgery for aortic stenosis would prove difficult even for Bailey and Harken to attempt, due to the proximity of the aortic valve to the coronary circulation [30]. Instruments were invented in an attempt to improve results when operating to relieve aortic stenosis. On April 3, 1952, Bailey would apply a new version of his triradiate dilator to correct aortic stenosis. He was able to operate on a series of 29 patients with 20.7% mortality [31]. The transventricular dilator he invented for the initial procedure was later slightly augmented by Andrew Logan in 1954 and again by Tubbs and Brock for commercial use [32]. Despite the use of these elaborate instruments, surgical treatments for aortic stenosis were largely palliative during this time period.

### 5.5.3 Repeated Repair Pulmonary Stenosis

Surgery of the pulmonary valve began with Baron Dr. Russell Brock (1903–1980) of Guy's Hospital, who was the first to consistently attempt surgery on pulmonary stenosis since Doyen's ill-fated attempt in 1913 [20] and Thomas Sellors' single successful case in 1947 [33]. The Blalock–Taussig shunt or *blue baby* operation was typically performed in cases of severe pulmonary stenosis, which resulted from a congenital defect [20]. Many were satisfied with this indirect vascular shunt approach because it allowed excellent palliation of complex congenital cardiac defects (e.g., Tetralogy of Fallot) without having to use cardiopulmonary bypass, which was still experiencing devastating problems. In addition, it was thought that most cases of pulmonary stenosis were infundibular or subvalvular in nature and

thus could not be treated with the new techniques recently developed by Harken and Bailey for mitral stenosis [20].

After a few disastrous clinical cases with the cardioscope invented by Allen and Graham in 1922 to enable direct vision within the closed heart [34], Brock developed his own version of a valvulotome and dilating forceps to incise the valve and enlarge the orifice in a blind procedure [20]. He was successful in correcting the valve of an 18-year-old girl on February 16, 1948; she had been cyanosed since birth, with a history of squatting and clubbing of the fingers characteristic of the *morbus caeruleus* ailment. The patient survived and was known to be doing well 2 months later, after some complications with peripheral emboli.

Even though Thomas Holmes Sellors technically performed the first successful clinical pulmonary valve operation, Brock is typically credited as he more thoroughly explored the subject and published first [33]. Brock's other two cases were also considered to have excellent results; an 11-year-old girl was able to lead a completely normal life, and another patient was able to conceive after her operation [21]. Dr. Brock took treatment of pulmonary stenosis a step further by creating a surgery for resection of infundibular stenosis, by blindly removing the intruding cardiac wall with a punch in 1949 [21]. Of the 11 initial operations performed by Brock for this ailment, eight survivors were known to be alive and improved over a year later [35].

### *5.5.4 After the First Ten Years of Valve Repair*

It was thought that the techniques of Bailey and Brock would essentially cure mitral, aortic, and pulmonary stenosis. However, an extensive summary by Bailey, Zimmerman, and Likoff in 1960 presented the long-term results of closed valvular repair in a less than favorable light [25]. The mortality rate of closed procedures for stenotic valves stabilized at an unsatisfactory 8.5%. "Among surgeons with extensive experience in this field (10,000 cases in aggregate), 50 percent of those who responded expressed dissatisfaction with existing surgical procedures" [25]. Additional problems included the following: (1) cardiologists continued to keep patients with mitral stenosis away from surgeons, (2) only valves with flexible cusps could be palliated for stenosis, and (3) iatrogenic insufficiency continued to be a problem. This was an unfortunate complication as there was no successful surgical treatment for insufficiency at the time. New approaches to palliate stenosis were attempted, including the creation of an atrial septal defect (ASD). Nonetheless, many surgeons sought the open field to improve accuracy via a direct curative approach. Henry Swan summarized this stance nicely: "That the blind but educated finger is capable of accomplishing much within the heart is to be freely admitted, and much admired; that it should be considered as the best method in the long run is absurd" [36].

## 5.6 Lewis, Gibbon, Lillehei, and Kirklin (1953–1955): Development of the Open Field

### *5.6.1 Cold Heart Logic*

While many cardiac surgeons were scrambling to invent complicated pump oxygenator machines, Alfred Bigelow of the University of Toronto took a pure and simple physiological approach—hypothermia [37]. Bigelow had been confronted with the problem of the open field during his surgical training with Alfred Blalock of the University of Toronto, when he realized the inadequacy of the palliative Blalock–Taussig technique [38]. Bigelow discovered a linear relationship between temperature and metabolism while at the University of Toronto. He believed this physiological phenomenon might be utilized to protect vital organs during prolonged periods of cardiac occlusion. Through careful experimentation on dogs and chimpanzees from 1950 to 1953, he estimated that open-cardiac surgery could safely occur for up to 15 minutes at 20 °C. This happened to be enough time to close an ASD, a lesion which could not be treated surgically before this time.

It was F. John Lewis (1916–1993) at the University of Minnesota who would first successfully lay open the heart of a 5-year-old girl with an ASD on September 2, 1952, using hypothermia at 26 °C and inflow occlusion for 6 min [39]. Lewis made numerous improvements to the methods of Bigelow to protect the myocardium and reduce the likelihood of ventricular fibrillation; as a result, the patient was known to be alive 33 years later with two children and a career as a carpenter [39]. Lewis' hypothermic technique was adopted by numerous surgeons across the world to repair simple cardiac lesions, including ASDs. From 1953 to 1960, William Mustard of Toronto reported 95 operations, Bigelow reported 50 operations, and Henry Swan of Denver reported 100 procedures, including the first operation on the aortic valve under direct vision on November 17, 1955 [39, 40]. This was an enormous first step. Progress in the open field was rapid, and surgeons continued to search for other techniques which could prolong the length of time the heart could be opened.

On October 21, 1952, the Dodrill–GMR, the first effective mechanical heart, was used to bypass the left side of the heart of a 16-year-old boy at Harper Hospital in Detroit [41]. The boy's congenital pulmonary stenosis was successfully treated in the open field and the patient was known to be alive and well nearly 50 years after this operation. Even though Forest D. Dodrill (1902–1997) went on to successfully treat numerous other cardiac anomalies with his pump (including the aortic and mitral valves), his success is often overshadowed [42]. The heart had been bypassed but not the lungs, which remained a challenge. Dr. Gibbon's isolated success with the first heart–lung machine would occur just a year later and represented surgery's greatest hope for more complex procedures such as valvular replacement, repair of insufficient valves, or repair of the more extensive congenital abnormalities.

### 5.6.2 The Mechanical Heart and Lungs

As the famous Dr. John H. Gibbon Jr. (1903–1973) recalls from the night of October 3, 1931 [42], during his research fellowship at Harvard, "My job that night was to take the patient's blood pressure and pulse rate every 15 min and plot it on a chart. At 1:00 AM, the patient's condition became worse, manifested by stupor and lowered blood pressure. At 8:05 AM, the blood pressure could not be measured. Churchill immediately opened the chest through an anterolateral incision on the left side… All this took place in the space of 6 min and 30 seconds. Despite the rapidity of the embolectomy, the patient died on the operating table" [42]. This experience lit a fire in Gibbon to prevent future deaths from pulmonary embolism; he imagined a machine which could sustain a patient through such a procedure by oxygenating and pumping the blood. He began to work on this machine in 1934 alongside his wife, Mary, in a surgical research lab at Massachusetts General Hospital (Fig. 5.4a). They used materials found in junk shops to build their small experimental oxygenator on a tiny budget [42]. "The animals used were cats and when our supply ran short, I can recall prowling around Beacon Hill at night with some tuna fish as bait and a gunny sack to catch any of the numerous stray alley cats which swarmed over Boston in those days" [43]. A big break came in 1946 when the Gibbons were introduced to the chairman of IBM, who supplied them with one of his best engineers as well as generous financial backing. The financing and expertise finally enabled the development of a parallel screen oxygenator large enough to support a human patient at the Jefferson Medical College.

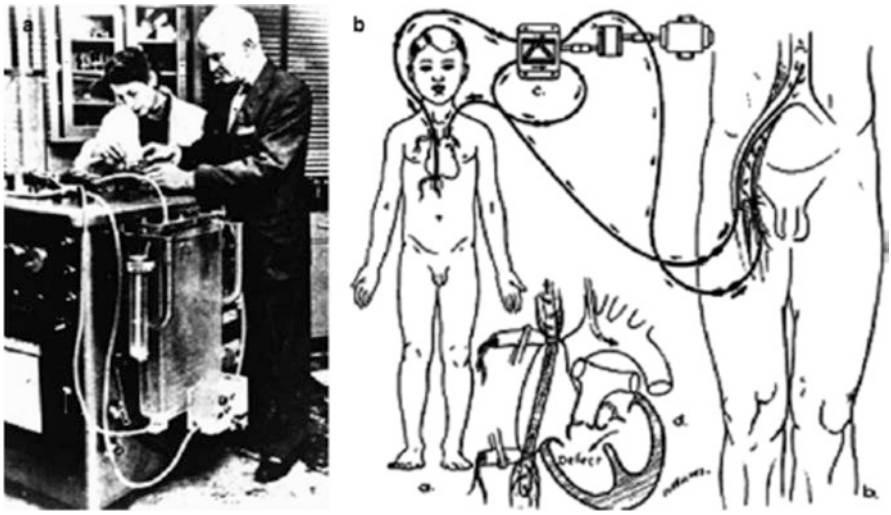


**Fig. 5.4** (**a**) John and Mary Gibbon at the cardiopulmonary bypass machine. (**b**) Diagram of Lillehei's cross circulation

Their first clinical patient died on the table, but on May 6, 1953, Gibbon placed an 18-year-old girl on bypass for 26 min as he mended an ASD [44]; she was known to be alive over 36 years later in 1986 [45]. But after nearly 20 years of working on the pump oxygenator, Gibbon was unable to replicate his success. Brilliant surgeons around the world took up his cross and continued to work on the pump oxygenator, including Clarence Crafoord in Stockholm, Sweden (whom Gibbon called on the night of his success), J. Jongbloed at the University of Utrecht in Holland, and Mario Dogliotti at the University of Torino in Italy (their heart–lung machine was used as early as 1951 to supplement the circulation of sick patients) [46]. Mustard of Toronto even attempted to use a freshly removed monkey lung to oxygenate his patient's blood! Representing the Americans were Clarence Dennis (attempted first heart–lung bypass) from the University of Minnesota and Forest Dodrill (first successful heart bypass) to name a few [46].

### *5.6.3 Controlled Cross Circulation*

C. Walton Lillehei (1918–1999) grew impatient with the progress of cardiopulmonary bypass and desired practice in open-heart repair before this technology was perfected. Lillehei was the second assistant on Lewis' historic ASD procedure and would continue to be on the cutting edge of surgery for the rest of his career [47]. Lillehei set the bar for his academic surgical career at the University of Minnesota, when his team described a procedure called *controlled cross circulation*, in which the heart and lungs of a live donor (typically a parent or family member) were used to oxygenate the blood of a recipient in need of invasive cardiac surgery [48] (Fig. 5.4b). The superficial femoral artery and saphena magna vein of the donor were cannulated as well as the superior/inferior vena cava and aorta of the recipient. The cross circulation was *controlled* by a pump which kept the blood flow between the donor and recipient at a constant low rate. This was a radical idea indeed, although not necessarily original, having been used for end-stage uremia/toxemia [38]. The surgery put an otherwise healthy donor at risk of embolism among other surgical complications, inspiring some to dub this tactic immoral. Nevertheless, after extensive experimentation with dogs, the proposed clinical surgeries received the go-ahead from the adventurous chairman of surgery at the time Owen Wangensteen [49].

On March 26, 1954, Lillehei and his team successfully closed a ventricular septal defect in a 1-year-old boy [50]. This was no isolated success; Lillehei operated on a series of 45 patients from March 1954 to July 1955 using cross circulation (and eventually using other oxygenation techniques developed in the lab) [45]. Twenty-two of these patients were known to be alive and well more than 30 years later. Denton Cooley later said, "C. Walton Lillehei… provided the can opener for the largest picnic thoracic surgeons will ever know." These procedures rocked the surgical world, and countless surgeons flocked to Minnesota to observe the clinical service and laboratory of Walt Lillehei. In the following years, he trained no less than

138 cardiac surgeons from 41 countries, including Christiaan Barnard (performed first heart transplant) and Norman Shumway. While many were satisfied with controlled cross circulation at the time, others such as Dodrill and John Kirklin considered the risk to the donor unnecessary and were determined to succeed in creating a simple and safe mechanical substitute for the heart and lungs.

### *5.6.4 The First Reliable Success with the Pump Oxygenator*

John W. Kirklin (1917–2004) was hard at work at the Mayo Clinic in Rochester, Minnesota, just hours from Lillehei's bustling laboratory. Kirklin began assembling a team for advanced cardiac surgery in 1952 and modifying Gibbon's blueprints in 1953 soon after Gibbon himself had thrown in the towel [51]. The physiologists, cardiologists, and engineers from IBM, along with other skilled people on his team, developed the Mayo-Gibbon pump oxygenator, which featured complex safety mechanisms and a screen oxygenator [52]. They tested their oxygenator in the canine model, of which nine out of ten survived 10–60 min of bypass. By this time, the success of Lillehei was well known, and many were questioning the need for a mechanical pump oxygenator. Nevertheless, on March 22, 1955, Kirklin successfully closed a ventricular septal defect in a 5.5-year-old child with direct suture and reported on his success in four of eight patients only 2 months later [53]. Kirklin and his team reportedly went on to perform cardiopulmonary bypass in a series of 245 patients by 1958 [39], as Lillehei continued to perform cardiac surgery using controlled cross circulation. Kirklin said of his relationship with Lillehei, "…our careers were parallel but intertwined, and it is probably fair to say that although we were 90 miles apart, over about a 12-year period, we constantly scouted each other's programs as intently as does anyone today in the National Football League" [51]. Their friendly rivalry kicked up a notch when in July of 1955, Lillehei switched from human oxygenators to the wonderfully simple and efficient DeWall–Lillehei disposable bubble oxygenator [54], which would take over the market for a number of decades before the disposable membrane oxygenators commonly used today were introduced in the early 1980s [55]. But for a while, it was just Kirklin and Lillehei performing open-heart surgery only 90 miles apart.

One can only imagine the thoughts of the cardiac surgeon during this time period. Suffice it to say, imaginations ran wild and hands itched to begin treatment of cardiac defects which had previously been impossible to approach. The cardiac surgery specialty had certainly existed before this time, but it was like a fish out of water. It struggled for breath and progressed toward the water's edge in desperate leaps and spurts of hopelessness. The development of a reliable pump oxygenator was the push cardiac surgeons needed to finally delve into a vast ocean of surgical possibilities. Naturally inspired and invigorated, the surgeon sought to tackle the most difficult challenge imaginable, and attempted to create artificial versions of the heart and valves.

## 5.7 Attempts to Repair Insufficiency (1956–1965): Before Carpentier

The development of the valvular prosthesis became an obsession in the field, and to many, the mechanical valve represented the perfect solution to all valvular lesions. Although there were many attempts to repair insufficient valves before replacement was possible, they all proved to be palliative, including techniques to occlude the insufficient orifice with foreign material or indirectly/directly altering the size of the valve annulus. As a result, from the advent of the pump oxygenator in the mid 1950s–1970s, the main focus of valvular literature was on mechanical and biological prostheses. However, there were those who doubted that any mechanical or preserved entity could mimic the elegant movements of the innate valve. As the long-term complications of valve replacement began to unfold, surgeons such as Carpentier were hard-pressed for a reparative procedure. Carpentier drew ideas and techniques from many early contributors for the treatment of insufficiency and finally created a set of techniques which enabled the treatment of regurgitation due to nearly any kind of pathology.

### *5.7.1 Earliest Attempts: Before the Open Field*

The primary strategy in the beginning was focused on the creation of biological flaps or slings to be placed below the mitral valve or within the aorta, which in theory would occlude the insufficient areas and could be easily implanted using a closed operation [56]. These slings were explored in the experimental laboratory independently by reputable surgeons such as Murray (1938), Templeton and Gibbon (1949), and used by Bailey (1951) and Logan (1952) in the clinical setting [2]. Despite the efforts of these surgeons and others, all attempts failed in the long-term due to shrinkage/calcification of the tissue or occlusion of the valve orifice. A breakthrough was made in the treatment of insufficiency in 1952 by Charles Hufnagel (1916–1989) of Georgetown University in Washington, D.C., with the first successful ball valve heterotopically placed in the descending aorta [57]. However, this procedure was purely palliative, required great dexterity, and did not correct the original lesion.

Researchers soon realized that many cases of insufficiency could only be corrected if the annulus fibrosus could be prevented from dilating further, which would inevitably occur if any strain on the heart remained. The idea for an *indirect* procedure to address dilation of the valvular orifice was first introduced by Bertrand Bernheim in 1909 while attempting to produce a model for stenosis of the mitral valve in dogs using constricting ligatures or circumferential sutures [58]. Clinical attempts by Glover and Davila (1955) and McCallister (1954) failed in the long-term as these ligatures often cut through the heart (Fig. 5.5a) [59, 60]. Attempts to place a constricting ligature around the aortic valve by Bailey in 1955 and Taylor in

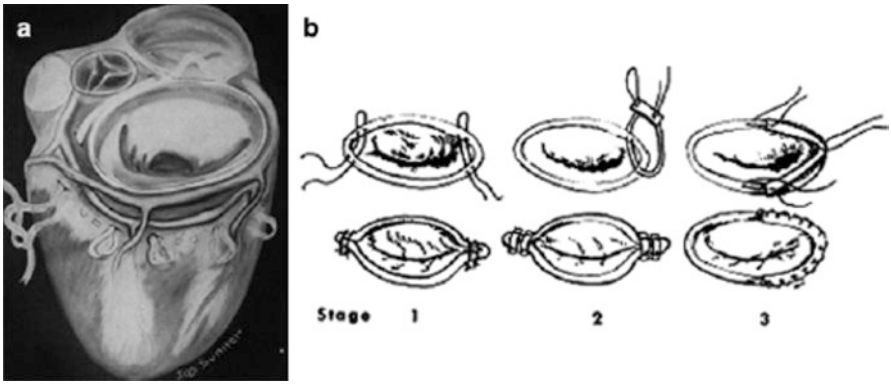


**Fig. 5.5** (**a**) Glover's circumferential purse string suture and (**b**) Kay's review of annuloplasty evolution up to 1960

1958 also failed, as these often slipped out of place [61, 62]. Despite the failure associated with constricting ligatures, these researchers contributed significantly to the literature by recognizing the problem of progressive annular dilation secondary to insufficiency.

The next step toward reliable annuloplasty was to *directly* alter the annulus fibrosus itself. Earle B. Kay (1911–2000) was one of the first to clinically alter the valve annulus of a 26-year-old woman on May 28, 1954, using sutures to reduce the annulus at the posteromedial commissure under guidance of a palpating finger within the valve [63]. Nichols performed a similar technique, in which a portion of the annulus was pinched shut using sutures in a closed technique [64]. This reduced the size of the annulus without altering the leaflets, and it was thought that the annulus was strong enough to prevent the sutures from tearing out. These procedures showed promise but continued to be inconsistent in results due to technical difficulty. "Subsequent clinical application of the previously described technical principle for reducing the size of the dilated mitral annulus at the posteromedial commissure has revealed that it is difficult or impossible in some cases…" [63]. A reliable direct curative technique in the open field was deemed necessary for acquired, congenital, and iatrogenic regurgitation.

### 5.7.2 *First Successful Repair of Mitral Insufficiency: Open Heart*

Fortunately, C.W. Lillehei devoted his brilliant mind toward addressing regurgitation of the mitral valve. In an issue of the *Lancet* in 1957, Lillehei et al. described their extraordinary initial success for treating mitral insufficiency in the open field in four patients with (1) incompetence along the posterior commissure of the valve and/or (2) an enlarged mitral annulus [65]. On August 29, 1956, the initial version

of open annuloplasty was performed at the University of Minnesota on a 15-year-old boy, using heavy silk sutures to close the insufficient portion of the patient's valve. These sutures were anchored in the annulus and tied over "pillows" of polyvinyl sponge to add support to the leaflet and prevent the sutures from cutting through. All four patients were gravely ill, and, despite the creation of a slight stenosis, the patients remarkably improved. Continued improvement was seen in these four patients over the next 14 months [66]. Meredino et al. independently made a similar contribution, with correction of insufficiency via annuloplasty in the open field in October of 1956 [67].

Kay followed Lillehei into the open field in 1958 and would continue to expand upon and pioneer techniques to correct insufficiency of various origins [68]. In one review by Kay and H.A. Zimmerman, the technique for correction of mitral insufficiency in 82 patients under direct vision was summarized up to 1960. Modifications to their technique were necessary during this period as sutures continued to tear out over time in some patients (Fig. 5.5b). Kay eventually implemented a *multipoint fixation* technique, likely inspired by Hufnagel's fixation method for his aortic prosthesis. Kay fashioned a semicircle of Teflon felt to the mitral annulus with a running suture; the sutures were placed farther apart in the annulus than in the felt to reduce the size of the annulus without undue tension on the sutures in any one segment of the valve. Use of the Teflon felt in this way was likely a precursor to the annuloplasty ring that would later be produced by Carpentier and is still in use today. George Reed would also contribute further to this general technique with his asymmetric annuloplasty (asymmetric with respect to the commissures), which reduced the orifice to a precise calculated size [69]; this kept the anterior leaflet full and mobile while ensuring a large enough annulus.

### 5.7.3 *First Successful Repair of Aortic Insufficiency: Open Heart*

Insufficiency of the aortic valve posed a particular challenge as the aortic valve does not possess a rigid annulus fibrosus and has three leaflets which must coapt rather than just two. In 1958, Lillehei's team reported a treatment for insufficiency of the aortic valve, using a novel bicuspidization technique when the leaflets were thickened and/or had curling edges [66]. "Our first patient with aortic stenosis who was operated upon under direct vision 2 years ago had a valve heavily laden with calcium. It was converted into a bicuspid valve of necessity. Not until later experiences did we realize the value and importance of this concept" [66]. The technique required accurate coaptation of only one commissural line instead of three. Production of a bicuspid aortic valve was thus extremely convenient and improved the reliability of other aortic valve surgeries, including correction of aortic stenosis and congenital aortic valve disease. The first surgery took place at the University of Minnesota on May 23, 1956. Two mattress sutures were used to join the thickened

aortic leaflets of a 52-year-old woman to form a bicuspid valve. Lillehei et al. would also use compressed Ivalon sponge to lengthen, shorten, or curl aortic leaflets when necessary. Bailey contributed a similar technique which was successfully performed in the summer of 1957 [70], along with additional methods for creation of a bicuspid valve by resection of one of the cusps or lengthening the leaflets [71].

### *5.7.4 First Successful Repair for Tricuspid and Pulmonary Insufficiency: Open Heart*

Insufficiency of the tricuspid valve was first addressed by Kay from March 1960 to February 1964 after noticing that mitral annuloplasty often resulted in mortality if a secondary tricuspid insufficiency or cardiomegaly existed [72]. He and his team set out to treat a series of 20 patients using a technique similar to their mitral annuloplasty to close the posteromedial commissure with obliteration of the anterior inferior leaflet. This created a bicuspidization effect not unlike that produced by Lillehei with the aortic valve. This technique was used for a number of years. De Vega and Carpentier would also note the development of tricuspid insufficiency after repair of another valve and later came up with their own techniques in the 1970s.

Repair is virtually nonexistent for insufficiency of the pulmonary valve, as some degree of regurgitation is present in most individuals. In cases of pathological regurgitation of the pulmonary valve, replacement was typically preferred.

## 5.8 Carpentier's Era (1968–1983): Development of the Rigid Ring Prosthesis and Techniques to Repair Insufficient Aortic, Mitral, and Tricuspid Valves

Suture-based annuloplasties were the first effective treatment for insufficiency, but major drawbacks to these early procedures included a high rate of recurrence and the production of mild stenosis through the narrowing of the orifice. The next step forward was the development of annuloplasty rings (1969), a functional classification system for different forms of insufficiency, and successful treatments for all the different forms of insufficiency (1983). Carpentier would organize and modify the work of pioneers such as Lillehei, Meredino, Kay, Wooler, and Reed and apply their techniques in the most effective manner while contributing whole new concepts to repair lesions which had never before been addressed.

Alain F. Carpentier (b. 1933) trained in Paris and worked most of his life at Broussais Hospital (Fig. 5.6a) [73]. Carpentier became known as the father of valve repair after establishing a valvular pathology classification system, describing techniques for valve repair still relevant today, assisting with the development of annuloplasty ring bioprostheses, and eventually pioneering robotic valve repair. Like

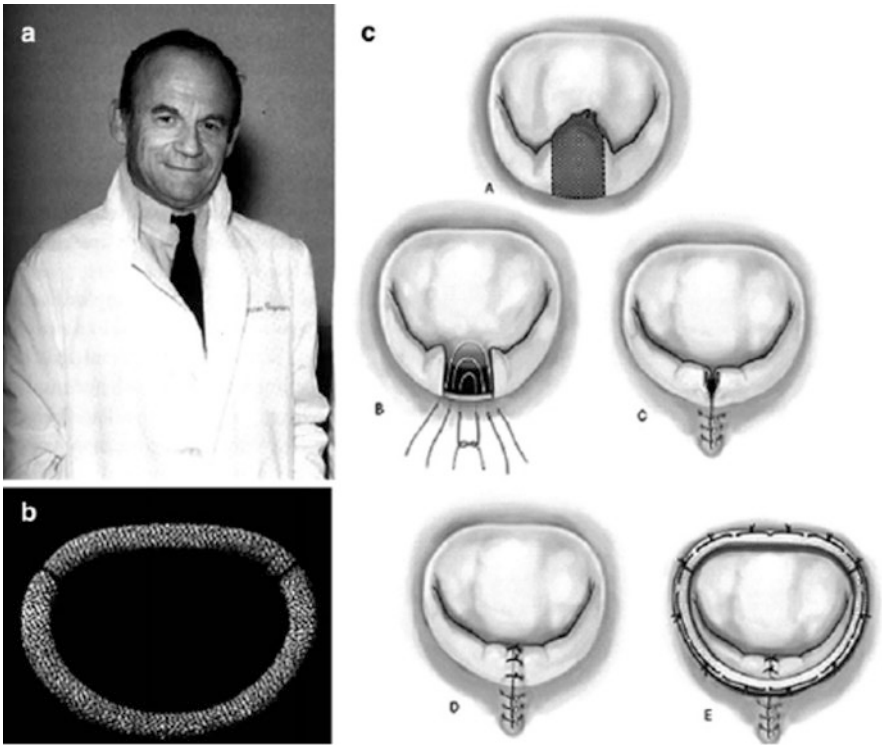


**Fig. 5.6** (**a**) Alain Carpentier, (**b**) Carpentier's Physio-Ring, and (**c**) Carpentier's classic annuloplasty for a flail segment or dilated annulus as reported in 2007, nearly identical to original procedure in 1983

most great innovations, the idea for the ring prosthesis and novel repair techniques came out of urgent necessity. The Clinique Leriche at the Hôpital Broussais performed 2000 cardiovascular operations a year at a rate of 6–7 a day [73]. Forty-six percent of these operations were for valvular lesions, due to the large number of foreign patients from countries still afflicted with rheumatic fever. Furthermore, many of these nations were not capable of administering anticoagulation therapy necessary for valvular replacement. "The broad geographic origin of our patients… the young age of many of them, and the specific risks associated with anticoagulation stimulated our interest in nonthrombogenic techniques, which in turn led us to eclectic use of various types of valve operations" [73].

With this mission in mind, Carpentier introduced a metal ring on October 20, 1968, which allowed remodeling of the mitral and tricuspid valves on a frame sewn to the annulus fibrosus (Fig. 5.6b) [74]. The rigid ring was considered a great advance as it prevented recurrence of insufficiency, prevented sutures from tearing out, and brought dilated valvular annuli back to physiological size without overtly narrowing the orifice. They discovered early on that circular or oval ring shapes were ineffective for the mitral valve and settled on a bean-shaped stainless-steel ring

with a Teflon sewing collar. The steel was grooved, which enabled the knots of 15 mattress sutures to be hidden within the ring and reduced the ring's overall weight (Edwards Laboratories, Santa Ana, CA).

The procedure to implant these rings was simple and readily repeated (Fig. 5.6c). Carpentier reported on 32 operations, with 17 class III patients and 15 class IV patients (NYHAC) [69]. The first five operations were performed using Kay's techniques and Carpentier's new ring annuloplasty was employed for the rest with a 15.5% mortality rate among these grievously ill patients. The 27 patients who survived the operation were known to be alive and improved a year later, although some still possessed some minor regurgitation. By January of 1976, over 500 cases of mitral valve reconstruction were completed at the Broussais Hospital, with a 90% survival rate at 6 years [75]. The ring was altered slightly in subsequent years by removing a portion at the anterior of the ring. Eventually suturing techniques and rings would be designed for specific pathological processes. For instance, if insufficiency was produced due to prolapse of the central portion of the posterior leaflet, then a quadrangular resection was first performed before annuloplasty. If the patient suffered from Barlow's disease, a sliding annuloplasty was used. The importance of proper ring shape/sizing and trimming of excess leaflet material during repair to avoid systolic anterior motion (SAM) also became clear over time [76].

Carpentier was careful to emphasize the role of the subvalvular apparatus in many cases of insufficiency. Others had noted the importance of treating the chordae tendineae and papillary muscles before Carpentier. On April 14, 1959, Kay et al. operated to repair torn chordae by suturing the flail segments to the nearest papillary muscle [77]; this was very similar to operations performed by McGoon in 1958 [78]. Wooler also specifically addressed the subvalvular apparatus in 1962 and described methods of dissecting thickened chordae using a modified suture technique for annuloplasty which elevated and plicated the cusps [79]. These repairs included novel rectangular resection of prolapsed posterior leaflet, repairing anterior chordal rupture by fixation on a secondary chorda or transposition to the posterior leaflet, and shortening elongated chordae by folding them within the papillary muscle, to name a few.

Carpentier's outstanding success in this field opened many doors for him. Carpentier's address as an honored guest at the 63rd Annual Meeting of The American Association for Thoracic Surgery in 1983, entitled *Cardiac Valve Surgery—the* "*French Correction*," is now a classic paper, spotted with humorous anecdotes from the famous surgeons of the day [73]. The paper described a functional classification system for mitral valve insufficiency (type I–III), extraordinarily reliable treatments for each classification, as well as treatments for the tricuspid and aortic valve. Some of these treatments were taken or derived from Kay, Reed, and other early surgeons to provide a choice of treatments for every possible form of insufficiency. In almost all cases, the use of a rigid prosthetic ring was prescribed to reinforce the repair, prevent annular dilation, and reshape the tricuspid annuli.

## 5.9 Improving upon Carpentier (1975–Present): The Evolution of Annuloplasty and Annuloplasty Rings

Carpentier's first ring represented a great advance in the field and was the first technique for the treatment of insufficiency to gain worldwide use. However, many problems were also associated with this early ring design: (1) the shape of the ring did not conform with the saddle shape of the annulus and thus some strain was put on the sutures, (2) the rigid ring did not flex with the natural movement of the ventricles and annulus, (3) the five ring sizes did not perfectly conform to the annulus size of all patients, (4) complications included SAM or left ventricular outflow tract obstruction (LVOTO), (5) the ring was unable to grow with pediatric patients, etc. [76, 80]. The extent of these problems actually proved very difficult to measure, and some debate still exists today about the superiority between the different ring designs. Improper sizing and failure to properly shorten elongated leaflets are factors that are often to blame for the more serious complications, SAM and LVOTO [76]. Nevertheless, inventors went on to create and improve rigid, flexible, semiflexible, incomplete, adjustable, biological, handmade, and biodegradable annuloplasty rings, which could all serve to reinforce the repairs designed by Carpentier [80].

Innovations in annuloplasty suture technique also continued. One of the more important innovations occurred shortly after the introduction of the original annuloplasty ring for mitral and tricuspid valves. Norberto De Vega developed a ringless circular tricuspid annuloplasty technique applied clinically in April 1973 [81]. De Vega used a double row of sutures to plicate the tricuspid annulus; this technique initially was applied to 350 patients, with a 12% mortality and good results in 78% of the patients [81]. De Vega's annuloplasty proved much more reliable than Kay's original technique and represented an alternative to the annuloplasty ring. This technique still proves useful, particularly in pediatric patients [82].

One of the earliest alterations to the annuloplasty ring itself was the Cooley Collar. This was the first incomplete annuloplasty ring described in 1974 [83]; the C-shaped design was thought to improve movement of the left ventricle. Denton Cooley (1920–2016) of the Texas Heart Institute noticed that the Carpentier ring was unnecessarily rigid against the anterior section of the valve and decided to remove this section to improve movement. While early results in 12 patients in the mitral position and two patients in the tricuspid position were favorable, the design was eventually abandoned in the early 1990s after increased fragility was observed from noncircumferential supports. Nonetheless, the logic of this ring design would help inspire future changes to the Carpentier ring. The next generation of Carpentier rings did have a small segment removed from the anterior position to allow the ring to be shaped to the valve annulus.

Carlos G. Duran and Jose Luis M. Ubago of Spain developed the first flexible ring for annuloplasty in 1975 [75]. They hoped that their ring design would move with the actively pumping heart and reduce the risk of the complications experienced with rigid rings. Because this ring was made of Dacron velour, the circular ring was flexible in all planes and could increase in circumference by 10%. These

rings had comparable hemodynamic results to Carpentier's procedure. In fact, over time, the flexible ring took on a conformation similar to Carpentier's rigid ring. Carpentier participated in the discussion of this paper, stating that he too had investigated the possibility of a more flexible ring. Eventually, he would go on to develop a semirigid ring, but did not think that a fully flexible ring could add any long-term benefits [76, 84].

The semiflexible Carpentier–Edwards Physio Annuloplasty Ring, or the Physio-Ring, a saddle-shaped ring with selective flexibility at the posterior and commissural sections, was introduced in October of 1992 (Baxter–Edwards Laboratories, Irvine, CA) [76]. Initially tested in 137 patients, the saddle-shaped ring was thought to fit around the aortic root better, and it was hoped the selective flexibility would produce less strain on the sutures. The ring was made of Elgiloy bands and polyester film strips; whether this ring design improved results over the original is also of some debate [85].

Other ring annuloplasty innovations included the first biodegradable ring by Duran in 1975, which was thought to improve results in pediatric patients and those with infective endocarditis. The first adjustable rings were created by Angell in 1976 [72]. The current trend in annuloplasty ring design is to tailor the ring to specific diseases.

## 5.10 Frater and David (1985–Present): Replacement of Chordae Tendineae with ePTFE

Treatment for mitral insufficiency involving anterior leaflet prolapse has been improved somewhat since Carpentier's original publication in 1983. Chordal transfer from the posterior leaflet to the anterior leaflet can still be used as popularized by Carpentier, as can chordal shortening by creating an incision in the papillary muscle and inserting a loop of the elongated chordae in many cases. But there was a need for chordal replacement in those instances when multiple chordae ruptured, or if there was not enough tissue to perform the traditional elastic procedures. Robert Frater of the Albert Einstein College of Medicine in New York was one of the first to begin work toward this goal [86], only preceded by Rittenhouse et al. who published their 2-year results of replacement with autologous pericardium in 1978. Frater and associates first tried implantation of xenografts and autologous pericardium in 11 patients; however, these grafts only lasted about 3 years before insufficiency developed subsequent to calcification of the grafts. However, they were successful in showing that flail or prolapsing cusps on either anterior or posterior mitral leaflet could be repaired reliably if a more suitable material could be discovered.

A research fellow in Frater's lab by the name of Herbert Vetter would show that expanded polytetrafluoroethylene (ePTFE or Gore-Tex) sutures were durable and became covered in fibrous material when used experimentally to replace the

chordae of sheep [86]. Tirone David of Toronto heard the results of Herbert Vetter's work on sheep and began to use this material clinically in July 1985 to treat mitral and tricuspid insufficiency. His initial publication in 1989 cautiously illustrated results in 22 patients with excellent follow-up up to 48 months after operation [87], 18 of which had complete relief from mitral regurgitation. After 5 years' experience with 43 patients, David used this procedure, not only to replace ruptured chordae in situations where no other plastic procedure was possible, but in lieu of traditional chordal shortening and transfer procedures [86]. They even used chordal replacement over the traditional Carpentier rectangular resection for posterior prolapse, as replacement does not alter the natural annular conformation. Artificial chordae were also used to resuspend papillary muscle after mitral valve replacement to maintain ventricular function. The most difficult aspect of this procedure was ensuring proper length of the artificial chordae; numerous techniques and devices have been developed by a number of different authors over the years, including the use of calipers, transesophageal echocardiography, and manual techniques [88].

## 5.11 Kan, Inoue, and Cribier (1982–Present): Resurgence of Repair with the Advent of Balloon Valvuloplasty and Other Percutaneous Technology

Percutaneous balloon valvuloplasty has been an important innovation which allows repair and even replacement of the valves by an interventional cardiologist in the beating heart, often without general anesthesia. This innovation has been driven by a need for mechanical intervention in the elderly or advanced cardiac patient who would otherwise be unable to withstand surgery. These procedures are considered a modern revitalization of classic finger fracture valvuloplasty.

Jean Kan of John Hopkins University School of Medicine was one of the first to use round balloon pulmonary valvuloplasty for the treatment of a stenotic tricuspid valve of an 8-year-old child in 1982 [89], preceded only by an isolated case by Semb et al. in Norway in 1979 to alleviate a stenotic pulmonary valve of a 2-day-old boy [90]. This technique is still used today with enormous success after some changes to the size and number of balloons [91]. Similarly, Kanji Inoue of Japan was the first to successfully use a balloon catheter for mitral commissurotomy on June 3, 1982 [92]. This balloon catheter was specially reinforced for use on the stenotic mitral valve and delivery through transseptal puncture, and could be inflated into a pillow shape in a series of stages (Fig. 5.7). A stepwise method of commissurotomy was then employed to attain the best results, i.e., the balloon was slowly inflated until insufficiency increased or a minimum pressure gradient was attained [93]. Lock of Delhi would introduce a cylindrical balloon for mitral valvulotomy in 1985, and Zaibag of Saudi Arabia introduced a two-balloon system. Zuhdi Lababidi of the University of Missouri performed the first aortic balloon valvuloplasty in a series of 23 pediatric patients from 1982 to 1983 [94]. Alain Cribier of France was

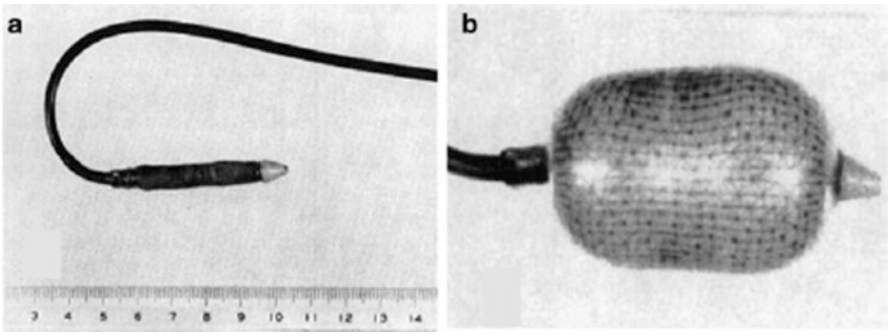


**Fig. 5.7** Example of barrel-shaped balloon used by Inoue in 1984. The balloon is filled with $CO_2$ in stages to inflate: (**a**) before inflation and (**b**) fully inflated

the first to apply a percutaneous balloon technique for dividing the aortic valve of 95 adults as reported in 1986 [95]. These techniques would eventually pave the way for the future of valve replacement using percutaneous methods.

There were many successes for percutaneous treatment of stenosis; however, insufficiency was far more difficult to treat. A method for percutaneous repair of insufficiency resulting from anterior leaflet prolapse has been derived from a procedure called the *edge-to-edge technique*. Originally created by researchers in Italy in June 1991, and sometimes referred to as the Alfieri technique or E-to-E technique, the procedure binds the two leaflets of the mitral valve at the site of prolapse to create a double-barrelled orifice [96]. This procedure was initially performed in the open field using suture and pledgets and represented a simple alternative to leaflet repair with resection or sliding annuloplasty. Midterm results showed that this functional repair had a hospital mortality of 1.6% and 92% of the 121 patients having undergone the procedure were still alive 6 years later, with 95% of patients free from reoperation [97]. Long-term results at 13 years showed survival of up to 100% depending on the location of the original regurgitation [98]. New technology based off this method, the MitraClip system, utilizes a stainless-steel clip to create the double-barrelled orifice or fix together the anterior and posterior leaflets at any point, and can be delivered percutaneously [98]. This was one of the first techniques to treat mitral insufficiency in a percutaneous manner; positive results have been attained in clinical trials (EVEREST I, EVEREST II) despite some concern over the inability to percutaneously implant an annuloplasty ring to prevent recurrent regurgitation.

Long-term results of the early catheter-based procedures have proved very promising. The Inoue balloon catheter would become the most commonly used device for mitral valvuloplasty worldwide and was introduced to the United States in 1994 [99]. It was discovered that children and young adults were nearly cured after balloon aortic valvuloplasty, but geriatric patients nearly always suffered from restenosis within a few years [93]. Many other transcatheter or percutaneous techniques continue to evolve for the treatment of all different kinds of pathological conditions

in the valves of the heart including (1) the use of radiofrequency or heat energy to induce controlled necrosis, followed by fibrosis and shortening in prolapsed leaflets/chordae to reduce the size of the annulus, (2) indirectly altering the mitral annulus through coronary sinus reshaping procedures, and (3) implantation of artificial valves. Many of these technologies are still undergoing trials, and it is likely that some combination will be used in future patients [100].

## 5.12 Minimally Invasive and Robotic Techniques (1996–Present): The *Key* to Reducing Cost and Mortality

Robotic or minimally invasive surgery offers surgical treatment to those who could not withstand a traditional open surgery and/or cannot undergo percutaneous procedures [101]. Minimally invasive thoracic surgery can be defined as any technique that does not require a traditional full sternotomy [101]. The idea of potentially decreasing the visibility of the operative field was met with a considerable degree of criticism. Nonetheless, various thoracotomies, partial sternotomies, video and/or endoscope-assisted port-access techniques, and robot-assisted procedures using the AESOP 3000, Da Vinci system, and/or Zeus system have been developed (Table 5.2). These techniques are evolving concurrently with the evolution of other surgical technologies including aortic occlusion, cardiopulmonary bypass, echocardiography, and cardiac protection. The development of robotic cardiac surgery is typically classified into four logical categories according to Carpentier and Loulment [102, 103]: (1) Level I mini-incisions and direct vision, (2) Level II microincisions and video-assisted, (3) Level III video-directed vision and micro/port incisions, and (4) Level IV video-directed vision and robotic port incisions. For the sake of simplicity, the historically significant landmarks will be clustered into a simpler system of (1) incisions and aortic occlusion, (2) video assistance, and (3) robotic innovations.

**Table 5.2** Table of robotic devices (including robotic arms for light endoscope positioning)

| Name | Function/comments |
|---|---|
| AESOP 2000 (Computer Motion, Santa Barbara, CA) | Robotic arm, enabling voice-activated tremor-free control of endoscopic camera. FDA approved in 1996 |
| AESOP 3000 (Computer Motion, Goleta, CA) | Robotic arm. Voice-activated. Allows in–out, right–left, and up–down movements of camera |
| Da Vinci (Intuitive Surgical, Inc., Sunnyvale, CA) | Three-armed surgical robot. Articulated; offers same movements as human wrist. Filters hand tremor and adds precision. Surgeon operates from a console. FDA approved in 2000 |
| Zeus (Computer Motion, Goleta, CA) | Three-armed surgical robot similar to Da Vinci. Phased out after Computer Motion and Intuitive Surgical merged. FDA approved 2001 |

*AESOP* automated endoscopic system for optimal positioning

### 5.12.1 Cosgrove, Gundry, Falk, and Chitwood: Incisions and Aortic Occlusion

The first minimally invasive surgeries took place under direct vision and utilized 10–12 cm long alternative incisions to the full median sternotomy [104].

Thoracotomies or parasternal incisions have been used for years by surgeons for reoperation on the mitral valve. Shortened parasternal incisions for initial valvular surgery were first introduced by Delos Cosgrove III and associates of the Cleveland Clinic. They were the first to publish on a minimally invasive approach to treat the aortic valve in 25 patients from January to April of 1996 [105] and in 25 patients to repair or replace the mitral valve from April to May of 1996 [106]. This 10-cm incision was possible due to peripheral cardiopulmonary bypass and required ligation of the right internal thoracic artery. Results were excellent with no hospital deaths, reoperations for bleeding, infections, embolisms, or repair failures. In addition, patients were able to leave the hospital earlier, experienced less scarring, and the procedure reduced pain and stress on the ribs.

Others independently showed similar results. Alternative methods for minimally invasive surgery were also developed which avoided peripheral cardiopulmonary bypass, avoided removal of internal thoracic artery, and were easily convertible to full sternotomy in case of complication, etc. Gundry of the Loma Linda University Medical Center utilized a mini-sternotomy (T incision) in 82 patients beginning in January of 1996 for congenital, mitral valve, and aortic valve repairs [107]. Kit Arom of the Minneapolis Heart Institute followed with the use of a 6–7 cm sternal incision in 17 patients in 1997 and specifically noted the potential benefits of this procedure over the Cosgrove approach [108]. Cohn et al. of the Brigham and Women's Hospital at Harvard performed their first surgery in a series of 84 for minimally invasive mitral/aortic valve replacement/repair on July 1, 1996 [109]. They were among the first to retrospectively compare the different available approaches to valvular surgery.

Eventually introduction of the port-access approach allowed a skin incision of less than 4 cm [110]. This procedure is characterized by peripheral cardiopulmonary bypass and the endoaortic clamp balloon occlusion catheter, which occludes the aorta and delivers cardioplegia (Heartport Inc., Redwood, CA). The smaller incision also requires laparoscopic style instruments and surgical techniques, including a *knot pusher* innovated by W. Randolph Chitwood of the East Carolina University School of Medicine, which enables surgeons to tie sutures outside the incision [111]. Port-access cardiac surgery was first proposed by Peters [112] and utilized experimentally by Stevens et al. at Stanford [113]. They performed anastomoses of the internal thoracic artery to the left anterior descending coronary artery successfully in nine out of ten dogs and later applied port-access technology to surgery for coronary artery disease and eventually valvular surgery [113, 114]. Surgeons at New York University also contributed to experimental development of this technique [115].

The first clinical application of this method to cardiac valves occurred at a number of different centers, including Stanford, New York University, University of Leipzig, and East Carolina University. The Stanford group performed their first clinical surgery in May of 1996, involving replacement of the mitral valve [112, 116]. Also in May of 1996, Vassilios Gulielmos et al. at the University Hospital of Dresden successfully operated on 21 patients with mitral valve disease [114]. This was rapidly followed in June of 1996 by Volkmar Falk, Friedrich Mohr, and colleagues at the University of Leipzig in Germany [117, 118] for repair and replacement of the mitral valve (successful in 16 of 24 patients). The Leipzig group performed more clinical valvular surgeries than any previous group and was better able to characterize the difficulties associated with the port-access technique [114, 119]. The Leipzig group reported on 51 patients in 1998, showing significant concern over aortic dissection, aortic balloon migration, the de-airing procedure, mortality rate, length of hospital stay, etc. As a result of these complications, the procedure was viewed with some controversy, as clearly demonstrated at the 11th Annual Meeting of the European Society for Cardiothoracic Surgery [120]. In the discussion of Gulielmos' paper, surgeons debated over the actual cost of the procedure and the risk of aortic dissection. One surgeon stated "I have absolutely no experience of such a system and I must say that I am rather reluctant to use any" [114].

Despite reluctance and debate over complications, over time the port-access technique gained success [112, 119]. The initial report of the Port Access International Registry (PAIR) indicated that 94% of the 1000 port-access procedures at 121 institutions recorded from April 1, 1997 to January 1, 1998 were successful (321 of these procedures involved mitral valve repair or replacement). In the end, aortic dissection had an overall incidence of 0.75% and reflected a significant learning curve [112]. An unexpected benefit was significantly lower incidence of postoperative atrial fibrillation.

Even though aortic dissection was shown to be rare, it is a very serious complication and aortic balloon occlusion is costly. An alternative technique to the port-access/balloon occlusion technique was developed by Chitwood et al. when they invented a transthoracic aortic cross clamp used clinically in one 60-year-old patient on May 28, 1996 [121]. An alternative technique was also described by Angouras and Michler which permitted direct aortic and bicaval cannulation with a 6 cm thoracotomy, anterograde cardioplegia, and a direct aortic cross clamp [122]. Undoubtedly, new techniques will continue to be developed to avoid groin infection, limb ischemia, and aortic dissection, to reduce trauma, and to lower costs associated with endoaortic balloon occlusion.

### *5.12.2 Video Assistance*

Initial success in minimally invasive cardiac surgery encouraged surgeons to continue to minimize the trauma of operations. Microincisions consisted of 4–6 cm skin incisions [102]; in order to obtain adequate visualization of the operative field in

these tiny incisions, new endoscopic and videoscopic tools were necessary. Video assistance indicates an operation performed using a video screen 50–70% of the time [102]. Different kinds of video visualization have developed concurrently, including 2D and 3D video endoscopy. Video-assisted techniques were first introduced to surgery by Dr. Ralph Lewis in 1991 [123]. The first known use of videoscopic assistance for valvular surgery was by Pyng Jing Lin et al. in Taiwan in September 1995 for emergency surgical relief of acute mitral regurgitation and thrombosis of a mitral prosthesis using a minimally invasive thoracotomy of 10 cm [123]. Kaneko also performed surgery under video assistance at this time using traditional sternotomy [124]. This group from Tokyo emphasized the benefits of visualization in teaching residents, illuminating the small left atrium, and accurately recording the operation. Before Kaneko, all video-assisted valvular surgeries called for an assistant to hold the videoscope; in response to this need, Kaneko introduced a stable holder (Flex Arm, Nisco Co. Ltd., Tokyo, Japan) [124].

The first use of video assistance occurred with relatively large incisions. Carpentier performed the first video-assisted minithoracotomy (5 × 4 cm) on February 26, 1996 using a robotic arm to control the videoscope. This complex repair included commissurotomy, repair of torn leaflets, chordal transposition, and ring implantation [125]. Three months later, Chitwood et al. performed the first mitral valve replacement with microincisions, videoscopic vision, and a percutaneous transthoracic aortic clamp. They also reported on using 2D cameras on 31 patients without any major complications. Leipzig used a port-access method and 3D endoscopy in 1998 in 51 patients [118].

While these 2D video techniques greatly enhanced surgery for simple repair, the lack of depth perception prohibited more extensive reparative procedures. As a result, the Leipzig group published results from June 1996 following the use of a 3D videoscope with voice-activated robotic assistance (Aesop 2000, Computer Motion, Goleta, CA) [118, 126]. In June of 1998, the East Carolina University group also used a voice-activated robotically controlled 3D camera and the updated Aesop 3000. The robotic arm for endoscopy enabled "solo" surgery, in which only the surgeon and a scrub nurse were required to perform the procedure [101].

### *5.12.3 Carpentier: Robotic Innovations*

Alain Carpentier was once again responsible for taking a surgical repair approach to the next level. On May 7, 1998, Carpentier et al. performed the first completely robotic cardiac surgery on a 52-year-old patient undergoing open-heart repair of a large ASD, using an instrument developed by Intuitive Surgical, later called the Da Vinci Surgical System [127]. The Da Vinci Surgical System enabled the surgeon to sit at a console two meters away from the patient, and all intracardiac manipulations were done by the robotic arms of the device (Table 5.2). The main difficulty encountered was due to lack of tactile feedback, especially regarding the resistance of the tissue.

In 1998, Carpentier et al. performed the first completely robotic valve repair, followed independently by Falk in December of 1998 [111, 128]. Both groups used the Da Vinci system, which offered up to 7° of freedom at the incision. The instrument filtered the tremors of the surgeon, magnified the 3D image from the endoscope, and reduced fatigue by allowing the surgeon to sit. Grossi of New York University repaired a mitral valve using the Zeus system without an annuloplasty ring after clinical trials in six dogs [129]. This group thought that the size of the port instruments (11 mm in diameter) to achieve 7° of freedom might be unnecessary, and that the 5° of freedom offered by Zeus would likely be sufficient. Four days later, Chitwood et al. performed the first completely robotic repair of mitral valve in North America using Da Vinci. Computer Motion (manufacturer of AESOP and Zeus systems) and Intuitive Surgical (manufacturer of Da Vinci system) merged in 2003, and the Da Vinci system currently dominates market.

These techniques continue to evolve following the work of Mohr in Leipzig, Carpentier in Paris, Reichenspurner in Munich, Cosgrove at the Cleveland Clinic, Stevens at Stanford, Colvin at New York University, Chitwood at East Carolina University, etc. New and simpler mitral valve repair techniques, including *haircut posterior leaflet-plasty* and the *American correction* may enable simple but reliable robotic repair [103]. Improvements continue to be made, such as robotic tactile feedback. "This is an evolutionary process, and even the greatest skeptics must concede that progress has been made toward an endoscopic mitral operation" [102]. This can be evidenced by Mehmanesh et al. in Munich, who performed the first closed-chest endoscopic mitral valve repair on March 17, 2000 [130].

## 5.13 Concluding Remarks

It is clear that each stage in the evolution of valve repair has developed out of a pressing need for some effective treatment for congenital, acquired, and iatrogenic lesions of the mitral, aortic, tricuspid, and pulmonary valves. During the first half of the twentieth century, rheumatic heart disease was the number one cause of death of individuals under the age of 20 [131]. Only the desperate need for some curative procedure for patients with rheumatic heart disease could encourage the respectable cardiologist to relinquish their patients to the daring early cardiac surgeon. Souttar and Cutler did their best to alleviate stenosis of the mitral valve and were followed with some success by Harken, Bailey, and Brock. The percutaneous balloon valvuloplasty techniques used today are a modification of these early procedures in the late 1940s and allow surgery in patients who could not withstand a full sternotomy.

Insufficiency of the mitral valve proved extremely difficult to treat using closed procedures, and even the open procedures were only effective for a handful of years. Many would attempt and fail to treat insufficiency, as it became clear that a regurgitant valve was often a progressive lesion which almost inevitably proved fatal. Most turned to valve replacement as the sole solution to mitral insufficiency; however, once again a pressing need arose for a treatment for those who could not withstand

replacement or the anticoagulation therapy necessary following mechanical replacement. As a result, Carpentier would develop techniques and annuloplasty rings to repair the insufficient mitral valve. Carpentier's original techniques introduced in 1983 continued to be enhanced by surgeons such as David and Alfieri, and the surgical incisions used to administer these repairs continue to decrease in size. The evolution in minimally invasive and robotic procedures pioneered by surgeons such as Cosgrove, Kaneko, Carpentier, and Chitwood enables surgery in patients who could not withstand full sternotomies. These techniques are also driven by the pressing need to reduce the cost of medical care. Percutaneous techniques introduced by Inoue, Kan, and Cribier hope to accomplish similar goals for mitral valve repair.

Reparative techniques of the aortic and pulmonary valves have followed a very similar story—a demonstrated need answered by creative and daring surgeons. Cardiac valve repair continues to evolve today as we attempt to reach the ultimate goal of complete restoration of dysfunctional valves in even the most fragile of patients.

## References

1. Cohn LH (2003) The evolution of mitral valve surgery: 1902-2002. Am Heart Hosp J 1:40–46
2. Richardson RG (1970) The scalpel and the heart. Charles Scribner's Sons, New York
3. Milton H (1897) Mediastinal surgery. Lancet 149:872–875
4. Samways DW (1898) Cardiac peristalsis: its nature and effects. Lancet 151:927
5. Dávila JC (1998) The birth of intracardiac surgery: a semicentennial tribute (June 10, 19481998). Ann Thorac Surg 65:1809–1820
6. Brunton TL (1902) Preliminary note on the possibility of treating mitral stenosis by surgical methods. Lancet 159:352
7. Treasure T, Hollman A (1995) The surgery of mitral stenosis 1898-1948: why did it take 50 years to establish mitral valvotomy? Ann R Coll Surg Engl 77:145–151
8. Jarcho S (1969) Theodore Tuffier on experimental surgery of heart valves. Am J Cardiol 23:73–75
9. Carrel A (1910) On the experimental surgery of the thoracic aorta and the heart. Ann Surg 52:83–85
10. Tuffier T, Carrel A (1914) Patching and section of the pulmonary orifice of the heart. J Exp Med 20:3–8
11. Chisholm H (1922) The Encyclopaedia Britannica, 11th edn. The Encyclopedia Britannica, New York
12. Ravitch MM (1981) A century of surgery 1880–1980, vol 1. Lippincott, Philadelphia
13. Souttar HS (1925) The surgical treatment of mitral stenosis. Br Med J 2:603–607
14. Campbell M (1965) Sir Henry Souttar. Br Heart J 27:453–454
15. Beck C (1925) The application of surgery in the treatment of mitral stenosis. Bull N Y Acad Med 1:104–114
16. Cutler E, Beck C (1929) The present status of the surgical procedures in chronic valvular disease of the heart: final report of all surgical cases. Arch Surg 18:403–416
17. Beck C, Cutler E (1924) A cardiovalvulotome. J Exp Med 40:375–381
18. Bailey CP (1949) The surgical treatment of mitral stenosis (mitral commissurotomy). Dis Chest 15:377–393
19. Harken DE, Ellis LB, Ware PE et al (1948) The surgical treatment of mitral stenosis: I. valvuloplasty. N Engl J Med 239:801–809

20. Brock RC (1948) Pulmonary valvulotomy for the relief of congenital pulmonary stenosis: a report of three cases. Br Med J 1:1121–1126
21. Brock RC (1949) The surgery of pulmonary stenosis. Br Med J 2:399–406
22. Harken DE (1946) Foreign bodies in, and in relation to, the thoracic blood vessels and heart; techniques for approaching and removing foreign bodies from the chambers of the heart. Surg Gyn Obstet 83:117–125
23. Gonzalez-Lavin L, Bailey CP, Harken DE (1992) The dawn of the modern era of mitral valve surgery. Ann Thorac Surg 53:916–919
24. Harken DE, Dexter L, Ellis L et al (1951) The surgery of mitral stenosis: III. finger-fracture valvuloplasty. Ann Surg 134:722–741
25. Bailey CP, Zimmerman J, Likoff W (1960) The complete relief of mitral stenosis: ten years of progress toward this goal. Dis Chest 37:543–560
26. Khan MN (1996) The relief of mitral stenosis: a historic step in cardiac surgery. Tex Heart Inst J 23:258–266
27. Replogle RL (2003) Cardiac surgery in the age of the dinosaurs. Perfusion 18:171–177
28. Smithy HG (1949) Aortic valvulotomy. South Med Surg 111:7–8
29. Crawford FA (2010) Horace Smithy: pioneer heart surgeon. Ann Thorac Surg 89:2067–2071
30. Bailey CP, Glover RP, O'Neill TJ (1951) The surgery of valvular heart disease. Dis Chest 20:453–468
31. Larzelere HB, Bailey CP (1953) Aortic commissurotomy. J Thorac Surg 26:31–66
32. Logan GA, Merendino KA, Bergy GG et al (1956) A preliminary evaluation of transventricular aortic commissurotomy with an improved dilator. N Engl J Med 255:802–809
33. Sellors TH (1948) Surgery of pulmonary stenosis: a case in which the pulmonary valve was successfully divided. Lancet 251:988–989
34. Allen DS, Graham EA (1922) Intracardiac surgery—a new method. JAMA 79:1028–1030
35. Brock RC, Campbell M (1950) Infundibular resection or dilatation for infundibular stenosis. Br Heart J 12:403–424
36. Swan H, Virtue RW, Blount SG et al (1955) Hypothermia in surgery: analysis of 100 clinical cases. Ann Surg 142:382–400
37. Bigelow WG, Linsay WK, Greenwood WF (1950) Hypothermia its possible role in cardiac surgery: an investigation of factors governing survival in dogs at low body temperatures. Ann Surg 132:849–866
38. Fedak PWM (1998) Open hearts: the origins of direct-vision intracardiac surgery. Tex Heart Inst J 25:100–111
39. Lewis FJ, Taufic M (1953) Closure of atrial septal defects with the aid of hypothermia; experimental accomplishments and the report of one successful case. Surgery 33:52–59
40. Swan H, Kortz AB (1956) Direct vision trans-aortic approach to the aortic valve during hypothermia. Experimental observations and report of successful clinical case. Ann Surg 144:205–214
41. Dodrill FD, Hill E, Johnson A (1953) Pulmonary valvuloplasty under direct vision using the mechanical heart for a complete by-pass of the right heart in a patient with congenital pulmonary stenosis. J Thorac Surg 26:584–594
42. Pastuszko P, Edie RN (2004) John H Gibbon, Jr., the inventor of the first successful heartlung machine. J Card Surg 19:65–73
43. Gibbon JH Jr (1963) The gestation and birth of an idea. Phila Med 59:913–916
44. Gibbon JH Jr (1954) Application of a mechanical heart and lung apparatus to cardiac surgery. Minn Med 37:171–185
45. Lillehei CW, Varco RL, Cohen M et al (1986) The first open-heart repairs of ventricular septal defect, atrioventricular communis, and tetralogy of Fallot using extracorporeal circulation by cross-circulation: a 30-year follow-up. Ann Thorac Surg 41:4–21
46. Cohn LH (2011) Cardiac surgery in the adult, 3rd edn. McGraw-Hill, US
47. Bolman RM III, Black SM (2003) Open-cardiac repair under direct vision: F John Lewis and the University of Minnesota. J Card Surg 18:328–332

48. Warden HE, Cohen M, Read RC et al (1954) Controlled cross circulation for open intracardiac surgery: physiologic studies and results of creation and closure of ventricular septal defects. J Thorac Surg 28:331–343
49. Cooley DA (1999) A tribute to C. Walton Lillehei, the "father of open-heart surgery". Tex Heart Inst J 26:165–166
50. Lillehei CW, Cohen M, Warden HE et al (1955) The direct vision intracardiac correction of congenital anomalies by controlled cross circulation: results in thirty-two patients with ventricular septal defects, tetralogy of Fallot, and atrioventricularis communis defects. Surgery 38:11–28
51. Kirklin JW (1989) The middle 1950s and C Walton Lillehei. J Thorac Cardiovasc Surg 98:822–824
52. Daly RC, Dearani JA, McGregor CGA et al (2005) Fifty years of open-heart surgery at the Mayo Clinic. Mayo Clin Proc 80:636–640
53. Kirklin JW, Dushane JW, Patrick RT et al (1955) Intracardiac surgery with the aid of a mechanical pump-oxygenator system (Gibbon type): report of eight cases. Proc Staff Meet Mayo Clin 30:201–206
54. DeWall RA (2003) The evolution of the helical reservoir pump-oxygenator system at the University of Minnesota. Ann Thorac Surg 76:2210–2215
55. Iwahashi H, Yuri K, Nose Y (2004) Development of the oxygenator: past, present, and future. J Artif Organs 7:111–120
56. Brock RC (1954) Mechanical principles in the surgery of aortic and mitral incompetence. Br Heart J 16:317–323
57. Hufnagel CA (1958) Experiences with new types of aortic valvular prostheses. Ann Surg 147:636–644
58. Bernheim BM (1909) Experimental surgery of the mitral valve. Bull Johns Hopkins Hosp 20:107
59. Glover RP, Davila JC (1957) Surgical treatment of mitral insufficiency by total circumferential "purse-string" suture of the mitral ring. Circulation 15:661–681
60. McAllister FF, Fitzpatrick HF (1956) Constriction of the mitral annulus in the correction of certain types of mitral insufficiency and as an aid in by-passing the left ventricle. Surgery 40:54–58
61. Bailey CP, Likoff W (1955) The surgical treatment of aortic insufficiency. Ann Intern Med 42:388–416
62. Taylor WJ, Thrower WB, Black H et al (1958) The surgical correction of aortic insufficiency by circumclusion. J Thorac Surg 35:192–205
63. Kay EB, Cross FS (1955) The surgical treatment of mitral insufficiency. Surgery 37:697–706
64. Nichols HT (1957) Mitral insufficiency; treatment by polar cross-fusion of the mitral annulus fibrosus. J Thorac Surg 33:102–122
65. Lillehei CW, Gott VL, DeWall RA et al (1957) Surgical correction of pure mitral insufficiency by annuloplasty under direct vision. Lancet 77:446–449
66. Lillehei CW, Gott VL, DeWall RA et al (1958) The surgical treatment of stenotic or regurgitant lesions of the mitral and aortic valves by direct vision utilizing a pump-oxygenator. J Thorac Surg 35:154–191
67. Meredino KA, Thomas GI, Jesseph JE et al (1959) The open correction of rheumatic mitral regurgitation and/or stenosis with special reference to regurgitation treated by posteromedial annuloplasty utilizing a pump oxygenator. Ann Surg 150:5–22
68. Kay EB, Nogueira C, Zimmerman HA (1960) Correction of mitral insufficiency under direct vision. Circulation 21:568–577
69. Reed GE, Tice DA (1965) Exaggerated mitral annuloplasty; repair of mitral insufficiency with hemodynamic predictability. J Thorac Cardiovasc Surg 49:752–761
70. Bailey CP, Zimmerman J (1959) The surgical correction of aortic regurgitation bicuspid conversion. Am J Cardiol 3:6–21

71. Bailey CP, Zimmerman J (1959) Advances in the surgical treatment of aortic stenosis and incompetence. Adv Cardiol 2:20–43
72. Kay JH, Maselli-Campagna G, Tsuji H (1965) Surgical treatment of tricuspid insufficiency. Ann Surg 162:53–58
73. Carpentier A (1983) Cardiac valve surgery—the "French correction". J Thorac Cardiovasc Surg 86:323–337
74. Carpentier A (1971) A new reconstructive operation for correction of mitral and tricuspid insufficiency. J Thorac Cardiovasc Surg 61:1–13
75. Duran CG, Ubago JLM (1976) Clinical and hemodynamic performance of a totally flexible prosthetic ring for atrioventricular valve reconstruction. Ann Thorac Surg 22:458–463
76. Carpentier AF, Lessana A, Relland JYM et al (1995) The "physio-ring:" an advanced concept in mitral valve annuloplasty. Ann Thorac Surg 60:1177–1186
77. Kay JH, Tsuji HK, Redington JV (1965) The surgical treatment of mitral insufficiency associated with torn chordae tendineae. Ann Thorac Surg 1:269–276
78. McGoon DC (1989) An early approach to the repair of ruptured mitral chordae. Ann Thorac Surg 47:628–629
79. Wooler GH, Nixon GF, Grimshaw VA et al (1962) Experiences with the repair of the mistral valve in mitral incompetence. Thorax 17:49–57
80. Ghosh PK (1996) Mitral annuloplasty: a ring-side view. J Heart Valve Dis 5:286–293
81. Rabago G, De Vega NG, Castillon L et al (1980) The new De Vega technique in tricuspid annuloplasty: results in 150 patients. J Cardiovasc Surg 21:231–238
82. Kanter KR, Doelling NR, Fyfe DA (2001) De Vega tricuspid annuloplasty for tricuspid regurgitation in children. Ann Thorac Surg 72:1344–1348
83. Cooley DA, Frazier H, Norman JC (1976) Mitral leaflet prolapse: surgical treatment using a posterior annular collar prosthesis. Cardiovasc Dis 3:438–443
84. Carpentier A (1990) Mitral valve annuloplasty. Ann Thorac Surg 49:508
85. Reul RM, Cohn LH (1997) Mitral valve reconstruction for mitral insufficiency. Prog Cardiovasc Dis 39:567–599
86. David TE (2004) Artificial chordae. Sem. Thorac Cardiovasc Surg 16:161–168
87. David TE (1989) Replacement of chordae tendineae with expanded polytetrafluoroethylene sutures. J Card Surg 4:286–290
88. Bizzarri F, Tudisco A, Ricci M et al (2010) Different ways to repair the mitral valve with artificial chordae: a systemic review. J Cardiothorac Surg 5:22–27
89. Kan JS, White RI, Mitchell SE et al (1982) Percutaneous balloon valvuloplasty: a new method for treating congenital pulmonary valve stenosis. N Engl J Med 307:540–542
90. Semb BKH, Tjönneland S, Stake G et al (1979) "Balloon valvulotomy" of congenital pulmonary valve stenosis with tricuspid valve insufficiency. Cardiovasc Radiol 2:239–241
91. McCrindle BW, Kan JS (1991) Long-term results after balloon pulmonary valvuloplasty. Circulation 83:1915–1922
92. Inoue K, Owaki T, Nakamura T et al (1984) Clinical application of transvenous mitral commissurotomy by a new balloon catheter. J Thorac Cardiovasc Surg 87:394–402
93. Feldman T (2003) Core curriculum for interventional cardiology: percutaneous valvuloplasty. Catheter Cardiovasc Interv 60:48–56
94. Lababidi Z, Wu JR, Walls JT (1984) Percutaneous balloon aortic valvuloplasty: results in 23 patients. J Thorac Cardiovasc Surg 88:352–356
95. Cribier A, Savin T, Saoudi N et al (1986) Percutaneous transluminal valvuloplasty of acquired aortic stenosis in elderly patients: an alternative to valve replacement? Lancet 1:63–67
96. Fucci C, Sandrelli L, Pardini A (1995) Improved results with mitral valve repair using new surgical techniques. Eur J Cardiothorac Surg 9:621–627
97. Maisano F, Torracca L, Oppizzi M et al (1998) The edge-to-edge technique: a simplified method to correct mitral valve insufficiency. Eur J Cardiothorac Surg 13:240–246
98. Alfierie O, De Bonis M (2010) The role of the edge-to-edge repair in the surgical treatment of mitral regurgitation. J Card Surg 25:536–541

99. Glazier JJ, Turi ZG (1997) Percutaneous balloon mitral valvuloplasty. Prog Cardiovasc Dis 40:5–26
100. Chiam PTL, Ruiz CE (2011) Percutaneous transcatheter mitral valve repair: a classification of the technology. JACC Cardiovas Interv 4:1–13
101. Schmitto JD, Mokashi SA, Cohn LH (2010) Minimally invasive valve surgery. J Am Coll Cardiol 56:455–462
102. Chitwood WR, Nifong LW (2000) Minimally invasive videoscopic mitral valve surgery: the current role of surgical robotics. J Card Surg 15:61–75
103. Rodriguez E, Chitwood WR (2009) Robotics in cardiac surgery. Scand J Surg 98:120–124
104. Anderson CA, Chitwood WR (2009) Advances in mitral valve repair. Futur Cardiol 5:511–516
105. Cosgrove DM, Sabik JF (1996) Minimally invasive approach for aortic valve operations. Ann Thorac Surg 62:595–597
106. Navia JL, Cosgrove DM (1996) Minimally invasive mitral valve operations. Ann Thorac Surg 62:1542–1544
107. Gundry SR, Shattuck OH, Razzouk AJ et al (1998) Facile minimally invasive cardiac surgery via ministernotomy. Ann Thorac Surg 65:1100–1104
108. Arom KV, Emery RW (1997) Minimally invasive mitral operations. Ann Thorac Surg 63:1219–1220
109. Cohn LH, Adams DH, Couper GS et al (1997) Minimally invasive cardiac valve surgery improves patient satisfaction while reducing costs of cardiac valve replacement and repair. Ann Surg 226:421–428
110. Felger JE, Nifong LW, Chitwood WR (2001) The evolution and early experience with robot-assisted mitral valve surgery. Curr Surg 58:570–575
111. Falk V, Krakor AR, Walther T et al (1999) Computer-enhanced mitral valve surgery: toward a total endoscopic procedure. Semin Thorac Cardiovasc Surg 11:244–249
112. Galloway AC, Shemin RJ, Glower DD et al (1999) First report of the port access international registry. Ann Thorac Surg 67:51–58
113. Stevens JH, Burdon TA, Peters WS et al (1996) Port-access coronary artery bypass grafting: a proposed surgical method. J Thorac Cardiovasc Surg 111:567–573
114. Gulielmos V, Wunderlich J, Dangel M et al (1998) Minimally invasive mitral valve surgery— clinical experiences with a Port Access system. Eur J Cardiothorac Surg 14(Suppl 1):S148–S153
115. Schwartz DS, Ribakove GH, Grossi EA et al (1997) Minimally invasive mitral valve replacement: port-access technique, feasibility, and myocardial functional preservation. J Thorac Cardiovasc Surg 113:1022–1031
116. Pompili MF, Yakub A, Siegel LC et al (1996) Port-access mitral valve replacement: initial clinical experience. Circulation 94(suppl 1):533
117. Falk V, Walther T, Diegeler A et al (1996) Echocardiographic monitoring of minimally invasive mitral valve surgery using an endoaortic clamp. J Heart Valve Dis 5:630–637
118. Mohr FW, Falk V, Diegeler A (1998) Minimally invasive port-access mitral valve surgery. J Thorac Cardiovasc Surg 115:567–576
119. Glower DD, Siegel LC, Frischmeyer KJ (2000) Predictors of outcome in a multicenter portaccess valve registry. Ann Thorac Surg 70:1054–1059
120. Gulielmos V, Dangel M, Solowjowa N et al (1998) Clinical experiences with minimally invasive mitral valve surgery using a simplified port access™ technique. Eur J Cardiothorac Surg 14:141–147
121. Chitwood WR, Elbeery JR, Moran JF (1997) Minimally invasive mitral valve repair using transthoracic aortic occlusion. Ann Thorac Surg 63:1477–1479
122. Angouras DC, Michler RE (2002) An alternative surgical approach to facilitate minimally invasive mitral valve surgery. Ann Thorac Surg 73:673–674
123. Lin PJ, Chang C, Chu J et al (1996) Video-assisted mitral valve operations. Ann Thorac Surg 61:1781–1786

124. Kaneko Y, Kohno T, Ohtsuka T et al (1996) Video-assisted observation in mitral valve surgery. J Thorac Cardiovasc Surg 111:279–280
125. Carpentier A, Loulmet D, Carpentier A et al (1996) First open-heart operation (mitral valvuloplasty) under videosurgery through a minithoracotomy. C R Acad Sci III 319:219–223
126. Falk V, Walther T, Autschbach R et al (1998) Robot-assisted minimally invasive solo mitral valve operation. J Thorac Cardiovasc Surg 115:470–471
127. Carpentier A, Loulmet D, Aupècle B et al (1998) First computer-assisted open-heart operation. C R Acad Sci III 321:437–442
128. Nifong LW, Chu VF, Bailey M et al (2003) Robotic mitral valve repair: experience with the da Vinci system. Ann Thorac Surg 75:438–443
129. LaPietra A, Grossi EA, Erivaux CC (2000) Robotic-assisted instruments enhance minimally invasive mitral valve surgery. Ann Thorac Surg 70:835–838
130. Mehmanesh H, Henze R, Lange R (2002) Totally endoscopic mitral valve repair. J Thorac Cardiovasc Surg 123:96–97
131. Griffith GC (1948) The epidemiology of rheumatic fever, its public health aspects. Am J Public Health Nations Health 38:682–688

# Chapter 6
# The Ross Procedure

**Massimo Griselli, Rebecca K. Ameduri, and Darryl F. Shore**

## 6.1 Introduction

It has been more than 50 years since Donald Ross published the original article in the Lancet regarding his initial experience with this novel procedure and the original vignette describing the operation that is shown in Fig. 6.1 [1].

The Ross Procedure (RP) is a surgical technique that uses healthy pulmonary valve (pulmonary autograft), which is a mirror image of a normal aortic valve, to replace a damaged aortic valve. A donated human pulmonary valve (pulmonary homograft/allograft) is used to replace the pulmonary valve. Donald Ross based his new procedure on the experimental work done by Norman Shumway and his colleagues at the University of Minnesota reported between 1960 and 1961 [2, 3]. Ross published his personal long-term results in 1987 and subsequently in 1997, eliciting an increased interest in the procedure which reached its highest popularity between 1990 and 2000 [4, 5]. However, the interest in the RP declined in the following 20 years reaching only 0.1% of aortic valve replacements (AVR) performed in the United States in 2010. Similarly, between 2007 and 2009 in the UK, only 13 of 653 adult patients aged 18–39 years who underwent elective AVR had a RP [4]. Several reasons were behind this loss of enthusiasm towards the RP, particularly the complexity of the operation with increased operative risk in small volume centers, poor long-term outcomes with progressive failure of the aortic autograft or pulmonary homograft, or both exposing patients to even more complex re-operations [5–7]. Therefore, particularly in United States, very few centers remained interested in the RP with limited opportunities for trainees to learn this operation as an essential

M. Griselli (✉) · D. F. Shore
Royal Brompton Hospital, London, UK
e-mail: mgriselli@doctors.org.uk

R. K. Ameduri
Division of Pediatric Cardiology, Mayo Clinic, Rochester, MN, USA

© The Author(s), under exclusive license to Springer Nature Switzerland AG 2023

P. A. Iaizzo et al. (eds.), *Heart Valves*, https://doi.org/10.1007/978-3-031-25541-0_6

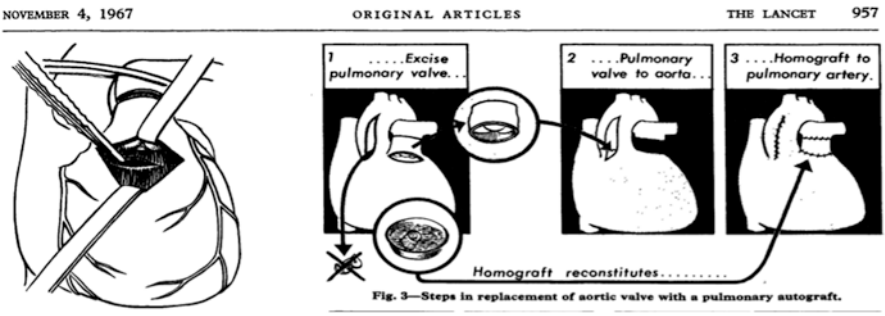


**Fig. 6.1** Original vignette from D.N. Ross describing the surgical procedure

option for replacement of the diseased aortic valve, particularly in young patients. Dr. Bonow in his recent editorial stressed the lack of recognition of RP in multiple societal guidelines for valvular heart disease both in the United States and Europe (American College of Cardiology/American Heart Association/European Society of Cardiology/European Association of Cardio-Thoracic Surgery) [9]. As a result, there are only few centers where cardiologists could send patients they think could benefit from a RP. Yacoub and colleagues considered this a 'loss of opportunity' for several patients who could have better outcomes and quality of life with the RP [10]. However, many groups around the world continued to routinely perform the RP and they focused their efforts in understanding the new 'patho-physiology' created by the pulmonary autograft, its adaptation to systemic conditions, and why and how the pulmonary autograft and the pulmonic homograft replacement may fail. This has led to a steady refinement of surgical techniques which, in turn, resulting in a reduction in the incidence of complications reported in the early series of RP. The outstanding long-term results of RP reported in the last 5 years has stimulated a renewed interest in the RP. The data reported, however, represent the work done in specialized centers dedicated to the RP and in carefully selected patients. These centers are also devoted to the education of cardiologists and junior surgeons in the RP which is paramount in expanding the use whilst continuing to achieve excellent results and provide young physicians with a valuable option for AVR. Appropriate education and proctoring are essential for the RP to be performed in medium- or low-volume centers with comparable results. As an ideal aortic valve prosthesis does not exist at this time and the trans-catheter aortic valve replacement (TAVR), despite the recent expansion in terms of patient eligibility, is commonly not indicated in patients below 60 years, there is a new growing interest in the RP as an excellent option for selected young- and middle-aged adults as confirmed by recent reports in the literature. There are different perspectives in the pediatric population as very small prosthesis are not available, xenografts and homografts degenerate rapidly and there is a wish to avoid anticoagulation. In several notable literature reports, the RP is considered the best surgical option in children with severe anomaly of the aortic valve and, in association with the Konno procedure in cases with left ventricular outflow tract obstruction.

## 6.2 Evolution and Different Techniques for the RP

Since its description more than 50 years ago, the execution of RP has progressively changed due to better understanding of anatomy and post-procedure pathophysiology. In recent years, progressive autograft dilation and/or annular dilation often associated with aortic valve insufficiency has prompted the introduction of techniques to prevent these complications. The RP is a complex operation with several steps which need to be perfectly accomplished to avoid complications, sometimes difficult to address on the operating table. We are describing here the most remarkable changes that happened over the years in performing the RP. The first is the implantation of the pulmonary autograft which moved from its initial scalloped 'sub-coronary' technique described by Donald Ross [1] to the 'root replacement' technique employed by the vast majority of surgeons nowadays (Fig. 6.2). The great advantage of 'sub-coronary' implantation is the support to the autograft provided by the native aortic annulus and aortic wall. However, this technique could be technically very difficult particularly when there is discrepancy between the pulmonary valve and the native ventricular-aortic junction and aortic valve making the re-suspension of commissures very challenging. From this aspect, the 'root' technique is technically easier and more reproducible but leaves the autograft unsupported causing progressive pulmonary autograft dilation.

Therefore, several techniques have been developed to mitigate this complication, including the inclusion technique where the pulmonary autograft is implanted within the native aortic root (Fig. 6.3a) or placing the autograft within a prosthetic material like Dacron tube (Fig. 6.3b). Recently, personalized external aortic root support (PEARS) surgery developed to prevent dilatation of the aortic root in

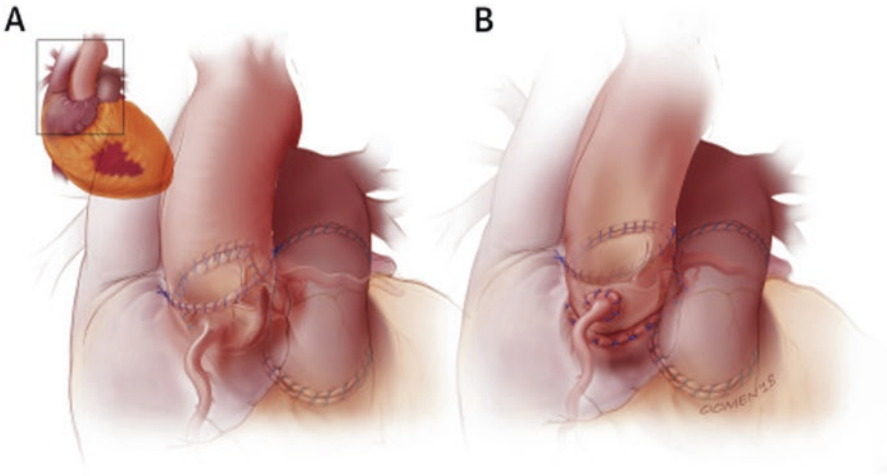


**Fig. 6.2** The scalloped 'sub-coronary' technique described by Donald Ross (**a**) and the 'mini-root replacement' technique (**b**). (Figure from Mazine et al. [8])

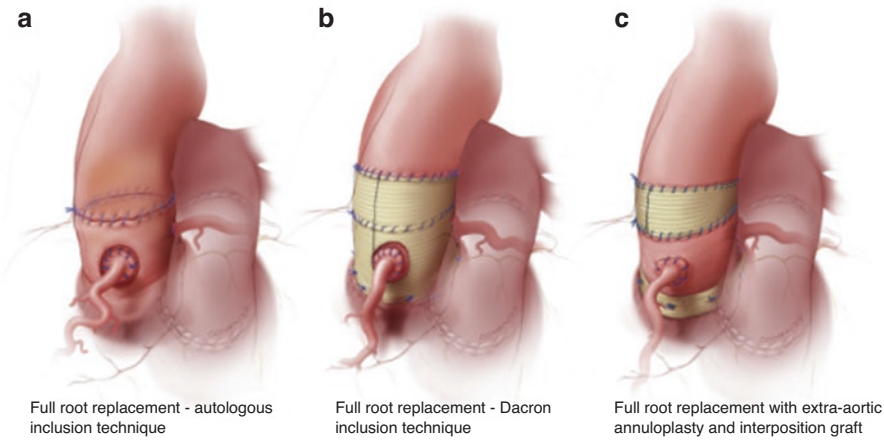


**Fig. 6.3** The root inclusion technique with native aortic root (**a**), the root inclusion technique with Dacron graft (**b**), and the extra-aortic annuloplasty and interposition graft technique (**c**). (Figure from Mazine et al. [8])

Marfan patients and has been employed as an adjunct to the RP. It involves surgical implantation of bispace mesh support around the neo-aortic root and the ascending aorta. As result of the excellent long-term outcome, some groups around the world have extended this novel technique in association to the RP, modeling the PEARS around the pulmonary trunk [11].

Over the years, another two complications became evident and required attention: the annular dilation in patients with already dilated aortic annulus and aortic regurgitation and distal dilation of pulmonary autograft in patient with native dilated ascending aorta. Regarding the first problem, the reduction and fixation of aortic annulus with sutures or annuloplasty reduction with peri-annular external Dacron have been proposed (Fig. 6.3c). However, there is a general consensus regarding the importance to implant the autograft within the native aortic annulus as the pulmonary valve lacks true fibrous support. Interposition graft with prosthetic material-like Dacron have been placed between the pulmonary autograft at the sinu-tubular junction and the ascending aorta to avoid distal dilation of the autograft caused by the progressive dilation of the ascending aorta (Fig. 6.3c). Considering the above possible complications, it is clear that patients, particularly females, below 50 years old with small annulus and underlying aortic stenosis are the best candidates for RP. On the contrary, patients with aortic insufficiency, dilated aortic annulus, and dilated ascending aorta constitute the worst candidates for RP. These statements, however, have been somewhat contradicted by recent large series with outstanding short- and long-term results in patient with aortic regurgitation, making the RP still the best options for these patients [12]. Other less important modifications of RP have been described over the years, including the one proposed by Elkins and colleagues where the left coronary artery button was not detached during the procedure but left in continuity with distal ascending aorta. Authors here argue that this technique may cause distortion of the pulmonary autograft when the distal aortic anastomosis is performed. [13]

## 6.3 Advantages and Disadvantages of RP

One of the major advantages of RP compared with other valve substitutes is the ability to provide excellent hemodynamics with flow patterns similar to normal subjects. Mechanical and bio-prosthetic valves are intrinsically obstructive because of the annular fixation with the sewing ring. However, this is not the case with non-stented valves, such as free-style xenografts and homografts. When the pulmonary autograft performance has been compared with aortic homograft, there was a similar performance data at early stage but in long term the RP maintained the same flow patterns whilst the aortic homograft gradients raised due to progressive calcification/degeneration of the graft. This long-term stability in hemodynamic performance is related to the fact that RP represents the only living substitute to replace the diseased aortic valve, guaranteeing better clinical outcomes. Because of its viability, the pulmonary autograft is sensitive to remodeling causing the leaflets to adapt to the new conditions (systemic pressures, different $\Delta q/\Delta p$) and it has been observed that there are changes in the morphology of the pulmonary valve leaflets to became more similar to those of aortic valve [14].

Although mechanical valves can be a durable option, the usage of life-long anticoagulation poses a substantial risk to patients with several complications including bleeding episodes, thrombo-embolic phenomena, etc. The reported data regarding these life-threatening complications ranges between 1 and 4.5% per patient-year, although the new generations of mechanical valves requiring less anticoagulation may reduce these complications [15, 16]. Therefore, RP offers an excellent possibility to avoid these risks and can be a suitable option for women of child-bearing age and for those individuals with occupations or sporting activities which make avoiding anticoagulation desirable.

However, there are risks related to the RP. It is clear now that RP is a complex surgical procedure and should be performed in centers with high volumes with established surgical expertise and with robust educational and training opportunities for junior surgeons. Such centers have reported early outcomes similar to 'classical' AVR with prosthesis. Traditionally, worse results have been obtained in small centers with up to three times operative mortality compared to classical AVR. When we discussed the surgical techniques, we mentioned the possible complications which may ensue in the pulmonary autograft and the measures developed by surgeons to avoid these complications. Therefore, it is important to identify high-risk patients (dilated aortic annulus, aortic regurgitation, and dilated ascending aorta) in order to implement these technical modifications. Another factor has been identified as important in ameliorating the long-term outcomes: control of systemic and pulmonary artery pressures as systemic or pulmonary hypertension have been correlated with degeneration of both pulmonary autograft and homograft. Patients should be assessed pre-operatively for systemic or pulmonary hypertension and, regardless of the technique employed for implantation, very tight control of blood pressure is required in the post-operative period, mainly with ß-blockers or ACE inhibitors as second line therapy [17] (Fig. 6.4). When the aforementioned complications of RP

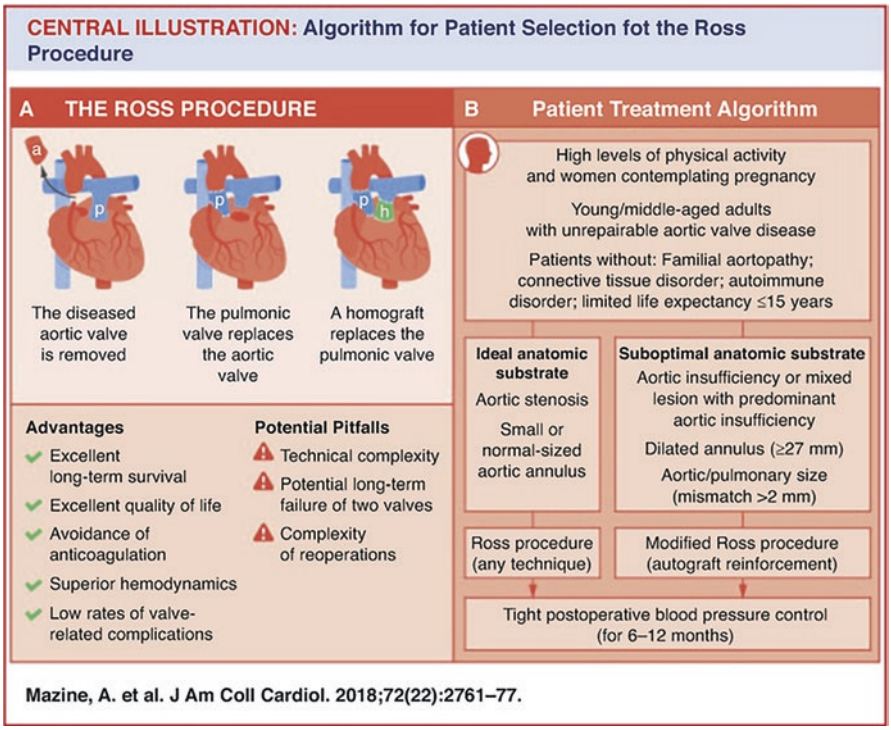


**Fig. 6.4** The advantages and potential disadvantages of Ross Procedure and algorithm for patient selection proposed by the authors. (Figure from Mazine et al. [8])

develop, surgery is required with similar indications as for native aortic regurgitation and ascending aortic dilatation. Dilatation of the aortic root with no aortic valve insufficiency is dealt when it reaches 50 mm or more in size. However, some surgeons have been more aggressive regarding the timing of re-intervention if the aortic valve is competent in an attempt to preserve the pulmonary autograft itself.

Degeneration of the homograft with progressive valvular and supra-valvular pulmonary stenosis occurs in some patients following RP. Some of these mechanical problems remain mild for a long-period, others require intervention because of development of symptoms or right ventricular dilation and dysfunction. Currently, the percutaneous trans-catheter approach with dilation of right ventricular outflow tract and insertion of a valve is increasingly performed [18, 19]. The surgical approach is reserved for those case unsuitable for percutaneous approach because of technical issues (coronary artery compression, distortion of aortic root) or more complex repair is required. Strategies to increase the long-term durability of the homograft have been sought. One is the use of a homograft larger in size than the harvested pulmonary autograft which seems to improve the longevity of the homograft in some literature reports. Another one is the unique use of pulmonary homograft as more durable than aortic homograft in pulmonary position [20]. Other

conduits have been explored as possible alternatives to homograft, but we do not have long-term results in terms of durability. In general, surgical re-interventions after RP are again more complex than other re-operations with increased operative risks and, unsurprisingly, the outcomes are better in high volume centers.

## 6.4 Results of RP

We are aware of high long-term mortality of patients with prosthetic aortic valves compared to matched general population [21–23]. When the same comparison was done with RP, studies showed the superb long-term results in patients who underwent RP with a survival similar to matched general population [24], and these results were not observed with any other type of AVR. When the RP was directly compared with prosthetic AVR or aortic homograft replacement, the benefits of RP became even more evident. RP showed a considerably higher long-term survival compared to aortic homograft (95% vs. 78% at 13 years) [25]. Compared with isolated mechanical prosthesis, RP showed the same early mortality but superior survival at 20 years (94% vs. 84%) and survival after RP was identical to that of age- and sex-matched general population [26]. A study done in United Kingdom looking at isolated AVR between 2000 and 2012 demonstrated that RP was associated with the longest event-free survival, better than mechanical replacement and much better than bioprosthetic valve replacement, and once again resulted in a similar survival to matched general population [27].

## 6.5 RP in Combination with Other Cardiac Surgical Procedures

The Konno procedure (Konno aorto-ventriculoplasty) was introduced to allow AVR with an adequate-sized mechanical valve for young patients with a small aortic annulus in which cases aortic annular enlargement is frequently necessary. The principle of original Konno procedure is an incision into the infundibular septum to enlarge it enough to fit a suitable aortic valve prosthesis and two different patches are used to reconstruct the septum and the aortic wall and the anterior right ventricular outflow tract, respectively [28]. An evolution from the original technique, the so-called modified Konno operation, was developed to treat patients with diffuse subaortic stenosis but with a normal aortic orifice; this includes patients with severe forms of hypertrophic obstructive cardiomyopathy and children with tunnel subaortic stenosis and a normal aortic orifice.

The concept of the original Konno procedure has been applied in conjunction with the RP and has been called the Ross-Konno procedure, becoming the most attractive option for young patients with diffuse LVOT stenosis associated with significant aortic valve stenosis or dysplasia [29] (Fig. 6.5).

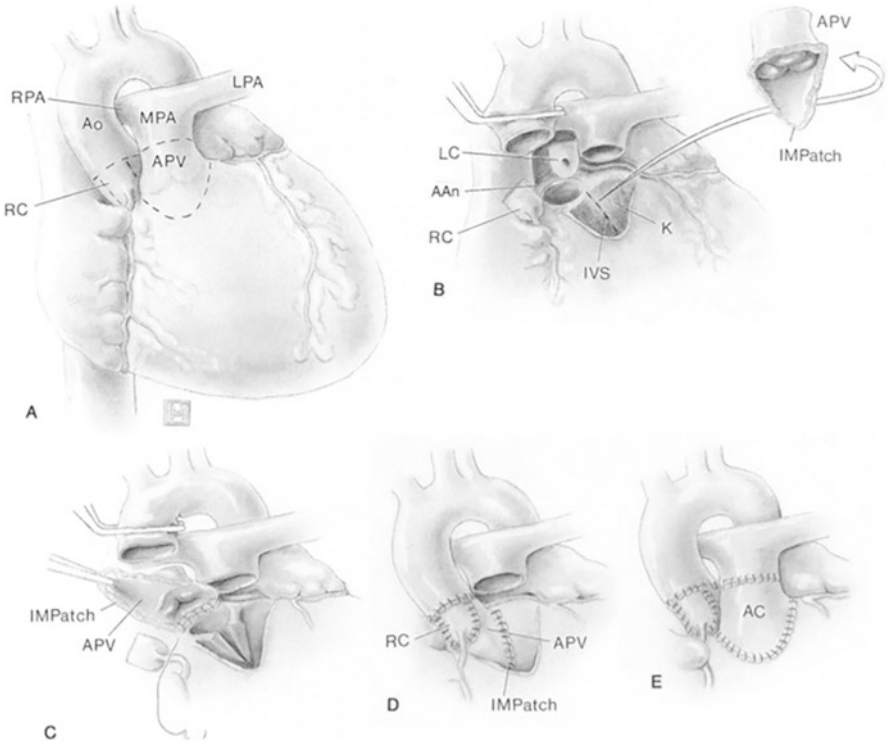


**Fig. 6.5** Technique of Ross-Konno procedure. (**a**) The *dashed lines* indicate the lines of incision along which the autograft pulmonary valve is harvested, the ascending aorta (*Ao*) is transected, and coronary buttons are developed. *RPA* right pulmonary artery, *LPA* left pulmonary artery, *MPA* main pulmonary artery, *APV* pulmonary autograft, *RC* right coronary button. (**b**) The pulmonary autograft is harvested. Large coronary buttons are developed, and diseased aortic valve is excised up to the annulus. The *dashed line* indicates the site of the septal incision for ventriculoplasty. *LC* left coronary button, *IMPatch* infundibular free wall muscle flap used for aortoventriculoplasty, *AAnn* aortic annulus, *IVS* interventricular septum, *K* site of septal incision. (**c**) Pulmonary autograft is seated with the suture line starting posteriorly and continuing along the annulus onto the interventricular septum. (**d**) Pulmonary autograft in place with reimplanted coronary artery buttons. (**e**) Allograft conduit (*AC*) sutured directly to the right ventricle without the use of additional patch material. (Figure and description from Reddy et al. [29])

## 6.6 Surgical Alternatives to the RP

Beside AVR with an aortic homograft or with a mechanical or biological prosthesis, there are not established techniques alternative to RP. In recent years, some attention has been given to the Ozaki procedure, an alternative way of repairing aortic valve, involving the use of autologous pericardium for the aortic leaflet reconstruction. Diseased leaflets are removed, distance between each commissure is measured

with an appropriate sizing apparatus. The new leaflet of the size corresponding to the measured value is trimmed with an original template from glutaraldehyde-treated autologous pericardium. Finally, the annular margin of the pericardial leaflet is running sutured with each annulus and commissural coaptation is secured with additional sutures. The coaptation of three new leaflets was always insured with direct vision. The Ozaki procedure is discussed in another session of this book.

## References

1. Ross DN (1967) Replacement of aortic and mitral valves with a pulmonary autograft. Lancet 2:956–958
2. Lower RR, Stofer RC, Shumway NE (1960) Autotransplantation of the pulmonic valve into the aorta. J Thorax Cardiovasc Surg 39:680–687
3. Lower RR, Stofer RC, Shumway NE (1961) Total excision of the mitral valve and replacement with the autologous pulmonic valve. J Thorac Cardiovasc Surg 42:696–702
4. Matsuki O, Okita Y, Almeida RS, McGoldrick JP, Hooper TL, Robles A, Ross DN (1988 Apr) Two decades' experience with aortic valve replacement with pulmonary autograft. J Thorac Cardiovasc Surg 95(4):705–711
5. Chambers JC, Somerville J, Stone S, Ross DN (1997) Pulmonary autograft procedure for aortic valve disease: long-term results of the pioneer series. Circulation 96(7):2206–2214
6. Klieverik LM, Takkenberg JJ, Bekkers JA, Roos-Hesselink JW, Witsenburg M, Bogers AJ (2014) Rethinking the Ross procedure in adults. Ann Thorac Surg 97:175–181
7. Stulak JM, Burkhart HM, Sundt TM 3rd et al (2007) The Ross operation: a Trojan horse? Eur Heart J 28:1993–2000
8. Mazine A, El-Hamamsy I, Verma S, Peterson MD, Bonow RO, Yacoub MH, David TE, Bhatt DL (2018) Ross procedure in adults for cardiologists and cardiac surgeons: JACC State-of-the-art review. J Am Coll Cardiol 72(22):2761–2777
9. Bonow RO (2021 Jul) Resurgence of the Ross procedure. Ann Cardiothorac Surg 10(4):512–514
10. Yacoub MH, El-Hamamsy I, Sievers HH et al (2014) Under-use of the Ross operation--a lost opportunity. Lancet 384:559–560
11. Pepper J, Golesworthy TJ, Izgi C, Takkenberg JJM, Treasure T (2020) Personalised external aortic root support (PEARS) to stabilise an aortic root aneurysm. Br J Cardiol 27:87–92
12. Poh CL, Buratto E, Larobina M et al (2018) The Ross procedure in adults presenting with bicuspid aortic valve and pure aortic regurgitation: 85% freedom from reoperation at 20 years. Eur J Cardiothorac Surg 54:420–426
13. Elkins RC, Thompson DM, Lane MM, Elkins CC, Peyton MD (2008) Ross operation: 16-year experience. J Thorac Cardiovasc Surg 136(3):623–30, 630.e1-5
14. Gorczynski A, Trenkner M, Anisimowicz L et al (1982) Biomechanics of the pulmonary autograft valve in the aortic position. Thorax 37:535–539
15. Ikonomidis JS, Kratz JM, Crumbley AJ 3rd et al (2003) Twenty-year experience with the St Jude medical mechanical valve prosthesis. J Thorac Cardiovasc Surg 126:2022–2031
16. Van Nooten GJ, Caes F, Francois K et al (2012) Twenty years' single-center experience with mechanical heart valves: a critical review of anticoagulation policy. J Heart Valve Dis 21:88–98
17. Simard L, Perron J, Shen M et al (2017) Vascular burden impact on echocardiographic valvular graft degeneration following a Ross procedure in young adults. J Am Coll Cardiol 70:1099–1105
18. Alassas K, Mohty D, Clavel MA et al (2018) Transcatheter versus surgical valve replacement for a failed pulmonary homograft in the Ross population. J Thorac Cardiovasc Surg 155:1434–1444

19. Gillespie MJ, McElhinney DB, Kreutzer J et al (2015) Transcatheter pulmonary valve replacement for right ventricular outflow tract conduit dysfunction after the Ross procedure. Ann Thorac Surg 100:996–1002
20. Bando K, Danielson GK, Schaff HV, Mair DD, Julsrud PR, Puga FJ (1995) Outcome of pulmonary and aortic homografts for right ventricular outflow tract reconstruction. J Thorac Cardiovasc Surg 109:509–517
21. Bouhout I, Stevens LM, Mazine A et al (2014) Long-term outcomes after elective isolated mechanical aortic valve replacement in young adult. J Thorac Cardiovasc Surg 148:1341–1346.e1
22. Goldstone AB, Chiu P, Baiocchi M et al (2017) Mechanical or biologic prostheses for aortic-valve and mitral-valve replacement. N Engl J Med 377:1847–1857
23. Kvidal P, Bergstrom R, Horte LG, Stahle E (2000) Observed and relative survival after aortic valve replacement. J Am Coll Cardiol 35:747–756
24. Andreas M, Seebacher G, Reida E et al (2014) A single-center experience with the Ross procedure over 20 years. Ann Thorac Surg 97:182–188
25. El-Hamamsy Z, Eryigit LMS et al (2010) Long-term outcomes after autograft versus homograft aortic root replacement in adults with aortic valve disease: a randomised controlled trial. Lancet 376:524–531
26. Buratto E, Shi WY, Wynne R et al (2018) Improved survival after the Ross procedure compared with mechanical aortic valve replacement. J Am Coll Cardiol 71:1337–1344
27. Sharabiani MT, Dorobantu DM, Mahani AS et al (2016) Aortic valve replacement and the Ross operation in children and young adults. J Am Coll Cardiol 67:2858–2870
28. Konno S, Imai Y, Iida Y et al (1975) A new method for prosthetic valve replacement in congenital aortic stenosis associated with hypoplasia of the aortic valve ring. J Thorac Cardiovasc Surg 70:909–917
29. Reddy VM, Rajasinghe HA, Teitel DF et al (1996) Aortoventriculolasty with the pulmonary autograft: the “Ross-Konno” procedure. J Thorac Cardiovasc Surg 111:158–167

# Chapter 7
# Echocardiographic Imaging of Cardiac Valves


**Benjamin Gorbaty, Susana Arango, and Tjorvi E. Perry**

## 7.1 Introduction

Perioperative echocardiography (echo) has become the imaging modality of choice during cardiac valve surgery. By using 2D imaging, spectral Doppler, and color flow Doppler (CFD) in addition to newer 3D imaging, perioperative echo serves as an important tool for assessing valve function before and after replacement or repair. In this chapter, we will discuss the basic principles of ultrasound as well as the specific findings and assessments for each cardiac valve. We will discuss assessments of native valves, valve replacements, and valve repairs.

## 7.2 Basics of Ultrasound

In order to understand how to interpret the images seen on echocardiography, one must have a basic understanding of ultrasound physics and how the echo machine forms the images. In this section, we will discuss how the echo machine creates images in 2D and 3D, as well as color flow Doppler (CFD) and Spectral Doppler. Lastly, we will discuss how to interpret these images correctly and the calculations that can be obtained from these measurements.

B. Gorbaty, MD (✉) · S. Arango, MD · T. E. Perry
University of Minnesota, Minneapolis, MN, USA
e-mail: bgorbaty@umn.edu; arang023@umn.edu; perry655@umn.edu

© The Author(s), under exclusive license to Springer Nature Switzerland AG 2023

P. A. Iaizzo et al. (eds.), *Heart Valves*, https://doi.org/10.1007/978-3-031-25541-0_7

### 7.2.1 Ultrasound Physics

In its most basic form, the ultrasound probe sends out a sound wave of a known frequency into tissue and "listens" for the returning sound frequency. Based on the change in frequency and the time it takes to return to the receiver, the machine determines how dense and how far the object of interest is relative to the probe. Sound propagates through different tissues at different speeds, with air having the slowest propagation (330 m/s) and bone having the greatest (4080 m/s); however, blood and most soft tissue have the same propagation speed of 1540 m/s. For this reason, the ultrasound machine assumes that the sound waves will travel at this speed. By knowing this, and the amount of time it takes for the wave to bounce back to the receiver, the machine can calculate how far an object is located from the probe. It assumes that half of the time travel was toward the object and half was back to the probe; therefore, it can plot the object at that distance from the probe on the display [1].

The strength of the sound wave depends on its amplitude, which can change as the sound wave travels through tissue. Some of the energy is absorbed by the tissue itself and some energy is scattered or reflected from surfaces of differing acoustic impedance. This causes a change in the amplitude of the returning sound wave, which the machine will use to assign a certain amount of brightness to the object [1].

There are two primary modes of producing the echo images used in clinical practice: M-mode and B-mode (Fig. 7.1). M-mode is an older form of ultrasound and will only give a single scan line of the picture being investigated. Using the tracking ball, the cursor should be aligned through the object of interest. The image formed will have time on the *x*-axis and depth on the *y*-axis. The density will appear by the

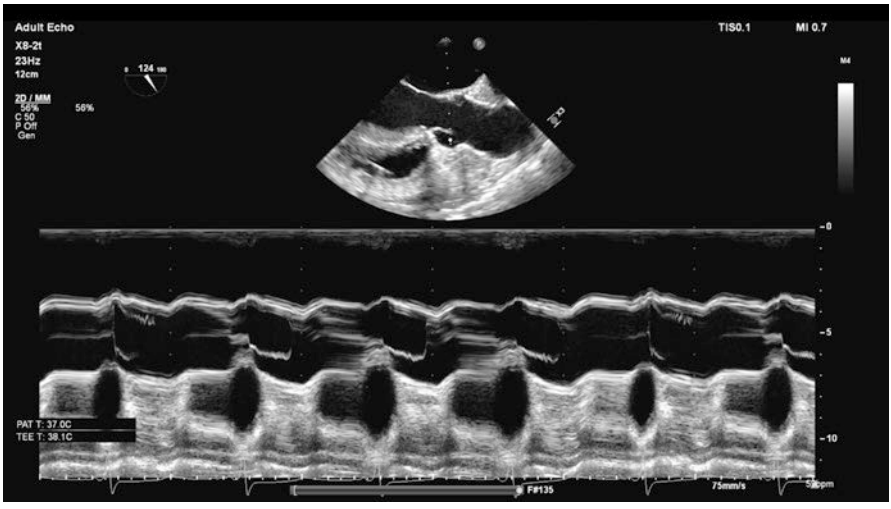


**Fig. 7.1** M-mode and B-mode. At the top of the image is the 2D echo image (B-mode) with the cursor directed across the aortic valve leaflets. Below is the M-mode tracing, demonstrating the density of all the structures through which the ultrasound beam is passing

shades of white and gray on the screen. M-mode has a high frame rate and therefore is useful for fast moving objects valve leaflet motion or the interatrial septum. B-mode, or 2D imaging as it is referred to more commonly, produces an echo image which people are more familiar. With this imaging, the *x*-axis is depth, the *z*-axis is amplitude, and there is no *y*-axis. A line of B-mode data is transmitted in an arc back and forth through the tissue. The images are generated very quickly to give the appearance of a continuous moving picture. As frequency of the sound waves increases, the resolution increases at the expense of decreased tissue penetration. However, if imaging deeper structures, the frequency can be reduced to improve tissue penetration at the expense of the image resolution [1].

3D echo uses the same principles as 2D echo adding an extra plane (Fig. 7.2). While a 2D echo probe crystal contains around 64–128 elements per row, a 3D probe has 3000 elements per row. Instead of a triangular dataset that is then converted to a 2D image, a pyramidal dataset is created and converted to a 3D image. Shading is then used to convey depth on 3D echo. Color flow Doppler can also be added to the image to demonstrate flow dynamics in the 3D dataset [2].

### *7.2.2 Doppler Physics*

The Doppler effect is the change in frequency that occurs when a sound wave bounces off a moving object. The Doppler shift is the *amount* of change in frequency that occurs when the sound wave bounces off the moving object. For the purposes of understanding clinical echocardiography, there are two types of relevant Doppler: Spectral Doppler and color flow Doppler (CFD). Calculating the Doppler

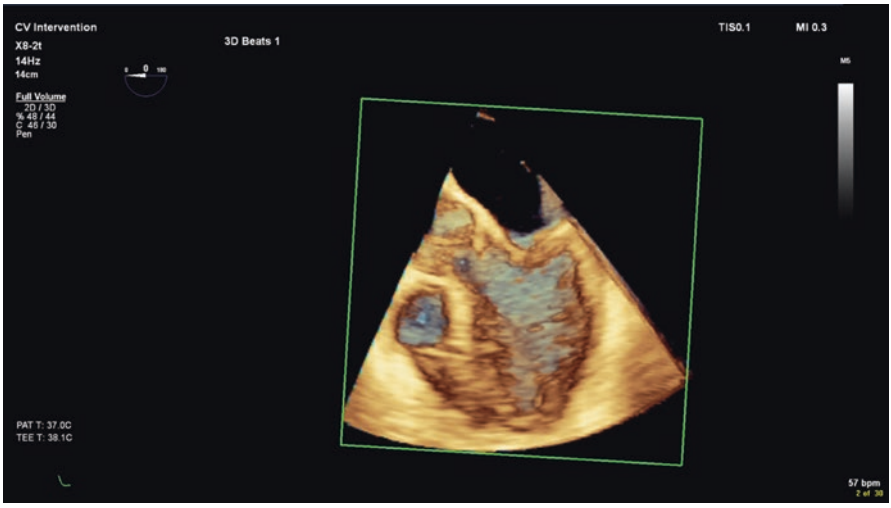


**Fig. 7.2** 3D Full Volume Image. This is a 3D image of the left ventricle from the mid-esophageal 5-chamber view. This data set can be manipulated and cropped to focus on the valves of interest

Shift allows us to determine the speed and direction of a moving object, such as blood flow or valve leaflets [1].

The major forms of spectral Doppler are continuous wave Doppler (CWD) and pulse wave Doppler (PWD) (Fig. 7.3). For CWD, the echo probe uses two different crystals to continuously send and receive sound waves. By continuously sending and receiving sound waves, all velocities can be measured through the cursor line but location of the highest velocity cannot be determined. This is known as range ambiguity. CWD is used for stenotic lesions because we assume that the highest velocity will be in the narrowest location in the line of the cursor. PWD uses only a single crystal which sends out a sound wave and waits for it to return before sending out the next pulse of sound. By placing the cursor at a known location, velocities can be determined at that one spot. This is known as range resolution. PWD is not ideal for measuring higher velocities and is subject to aliasing, a phenomenon whereby the velocity of an object is greater than the rate that the PWD can record, resulting in the tracing to appear on the opposite side of the baseline. Aliasing is also known as the wagon wheel effect—when a wagon wheel in old Westerns moved faster than the framerate of the camera and therefore appeared to be rotating in the opposite direction. For both CWD and PWD, the cursor must be appropriately alignment with the direction of flow. If the angle is off by more than 20°, it will create significant underestimation in measurement [1].

CFD is PWD that utilizes multigated acquisition to measure Doppler shifts by assigning color to the direction of flow, transposing a semi-quantitative measure of flow velocities onto a 2D echo image (Fig. 7.4). The standard format is to assign blue color to blood flowing away from the probe and red to blood flowing toward the probe (BART = Blue Away, Red Towards). Since this is a form of PWD, it is also subject to aliasing, which can be seen at high velocities. Aliasing on CFD will appear as blue flow toward the probe and red flow away from the probe. The amount of aliasing can be adjusted by changing the color scale, also known as the Nyquist limit. The Nyquist limit is typically set between 60 and 70 cm/s—decreasing this value will permit more aliasing to occur at lower blood flow velocities while increasing the Nyquist limit will allow less aliasing [1]. These concepts are important for recognizing laminar and turbulent flow, and calculation of PISA.

### *7.2.3 Quantitative Echocardiography*

The simplest way to conceptualize quantitative echocardiography is to address the following questions: What is amount of blood flowing through the lesion of interest, what is the velocity and calculated pressure gradient across the lesion of interest, and what is the calculated the cross-sectional area of the lesion of interest? Answering these questions is the basis for understanding the concept of continuity of flow. The principle of continuity of flow holds that the velocity through a small orifice must increase in order to maintain the same amount of flow through a larger

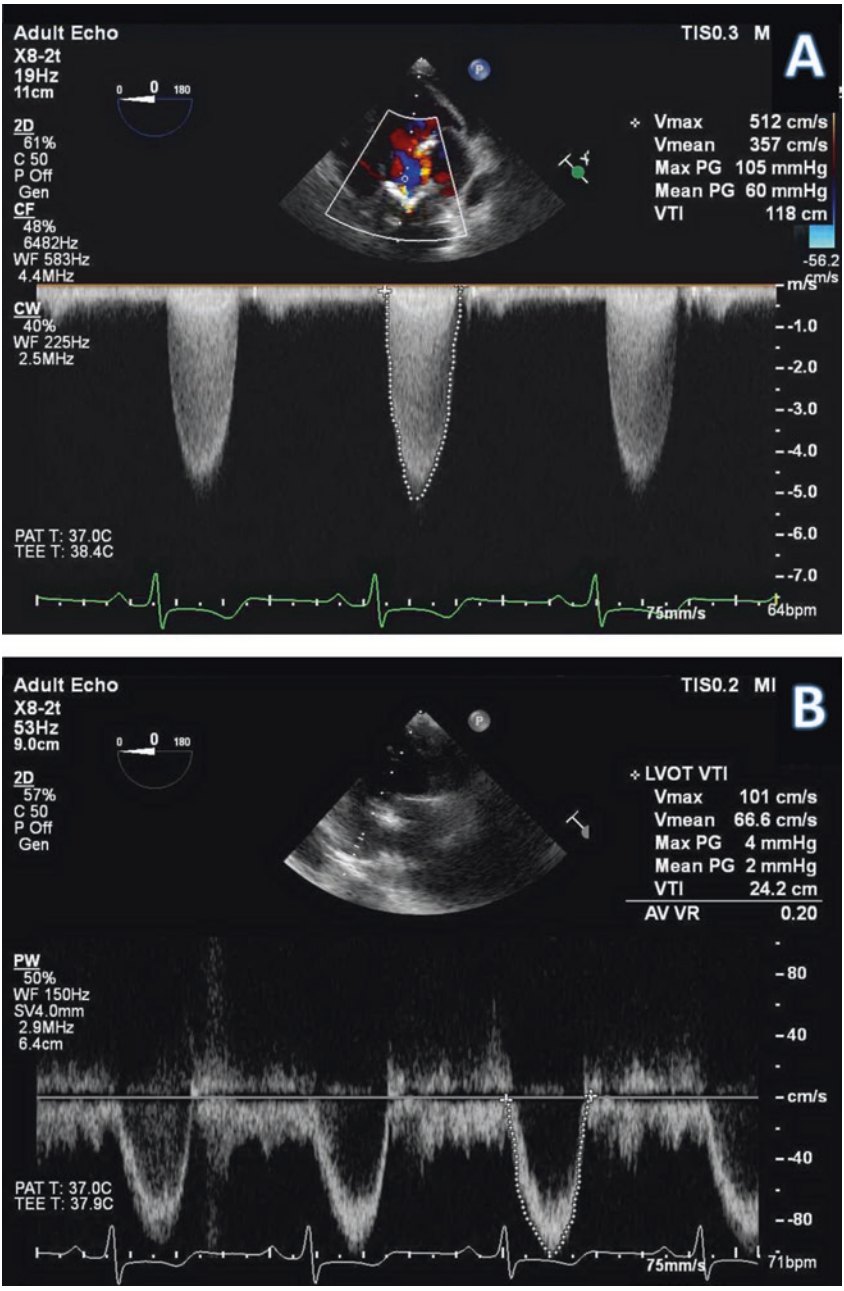


**Fig. 7.3** (**a**, **b**) (**a**) Continuous wave Doppler (CWD) though the aortic valve (AV). Note how the tracing is filled in. (**b**) Pulse wave Doppler (PWD) through the AV but has an "empty" tracing

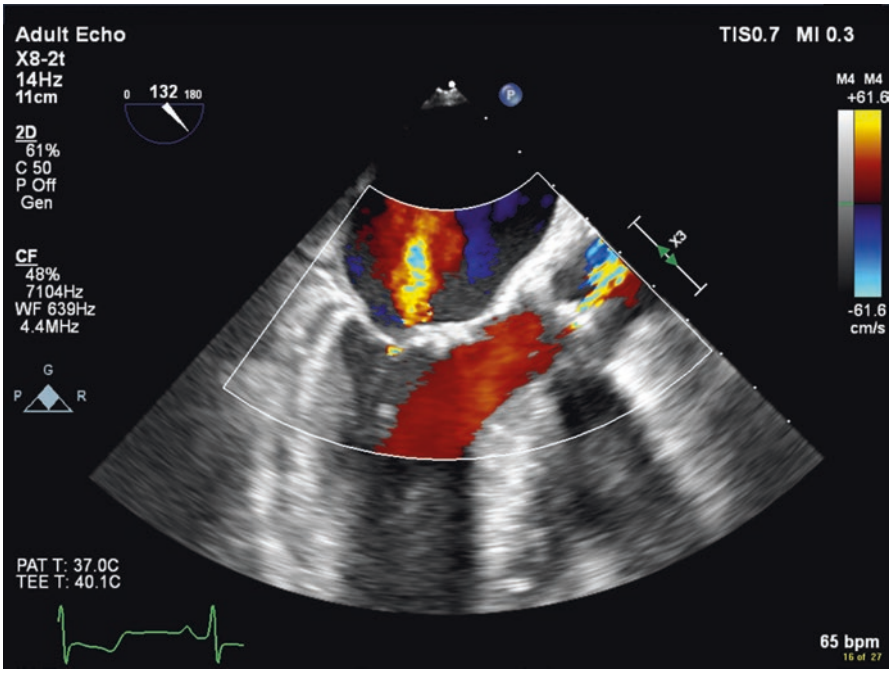


**Fig. 7.4** Color Flow Doppler. The Nyquist limit scale can be seen at the top right corner of the image. By convention, blue color represents blood flow away from the probe while red signifies flow toward from the probe (BART = Blue Away, Red Toward). Note in this image that blood in the LVOT is red because it is flowing toward the probe. Similarly, flow in the aortic root has blue mixed in, signifying turbulent flow and aliasing. In this patient, the aortic valve is stenotic and the velocity through the valve exceeded the Nyquist limit, resulting in aliasing

orifice. This is why fluid traveling across a bottleneck will increase in velocity to maintain the same volume.

Flow (or stroke volume) is directly proportional to the cross-sectional area (CSA) and stroke distance. The stroke distance is the distance that a given volume of blood will travel over time during a single cardiac ejection. For instance, if one heartbeat ejected blood 20 cm, then the stroke distance through the aortic valve would be 20 cm. The stroke distance can be determined from the velocity time integral (VTI) by tracing the spectral Doppler (Fig. 7.5). This takes the spectral tracing and integrates the curve to determine the stroke distance. After tracing the outer portion of the Doppler envelope, the echo machine will calculate the VTI. This can be used to calculate the flow through a lesion by multiplying by the CSA. Conversely, the CSA can be determined by dividing the stroke volume by the VTI [1].

The area of the aortic and pulmonic valves can be estimated by assuming that the valves are true circles. Though this is rarely the case, it does allow for simple calculation for the area of a circle as $\pi r^2$. By measuring the diameter ($D$) of the valve, one can rearrange this equation to be CSA = $\pi$ $(D/2)^2$. This same technique is used for

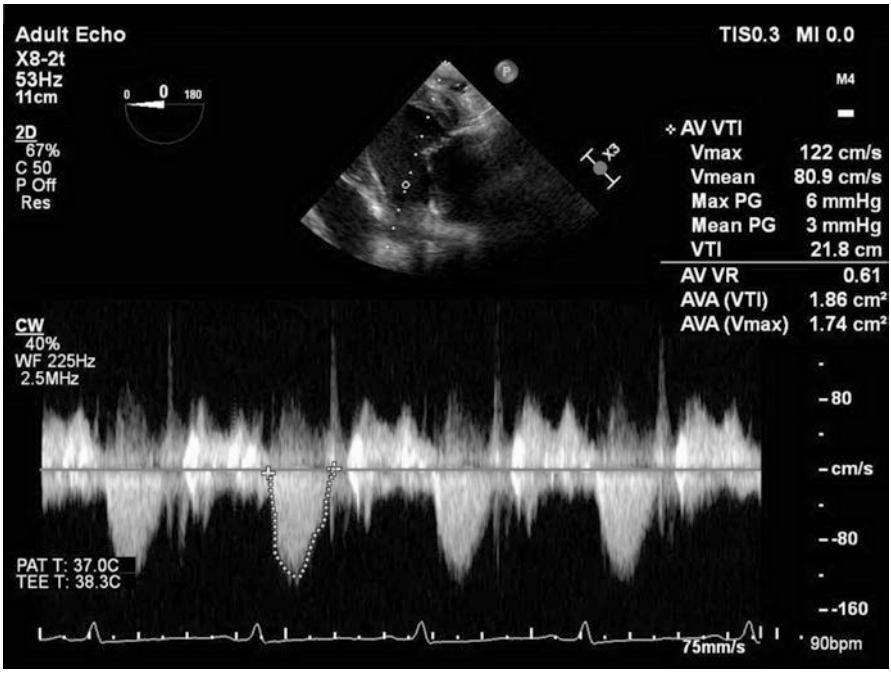


**Fig. 7.5** Velocity time integral (VTI) through the aortic valve. The CWD waveform has been traced and the echo machine will automatically integrate the tracing to calculate the VTI (or stroke distance). In this case, the VTI was measured as 21.8 cm

calculating the left ventricular outflow tract (LVOT) CSA; however, it should be noted that the greatest source of error is inaccurate measurement of the diameter, as this error will be squared [1]. Of note, this calculation assumes that the annuli and outflow tracts are circular, which we know from various imaging studies not to be the case. Further discussion of this is beyond the scope of this chapter.

If we assume that the flow through a small orifice will be the same flow as that through an in-line larger orifice, then, based on the principle of the continuity of flow, the CSA of one orifice can be calculated by knowing the CSA of another. This is the basis of the continuity equation, which is $CSA_{stenosis} \times VTI_{stenosis} = CSA_{conduit} \times VTI_{conduit}$. This can be rearranged as $CSA_{stenosis} = (CSA_{conduit} \times VTI_{conduit})/VTI_{stenosis}$. The continuity equation is regularly used in clinical echocardiography to calculate the area of a stenotic valvular lesion including aortic or mitral stenosis (see Eqs. 7.1 and 7.2). Keep in mind that one should use PWD to measure the VTI of the known entity and CWD for the unknown entity. One should assume that the highest velocity measured with CWD is through the narrowest lesion, which in this case should be the stenotic valve [1].

***Equations 7.1 and 7.2*** *Calculation of aortic valve area and mitral valve area by the continuity equation.*

$$\text{Aortic Valve Area}\left(\text{AVA}\right)\left(\text{cm}^2\right)=\frac{\text{CSA}_{\text{LVOT}}\times\text{VTI}_{\text{LVOT}}}{\text{VTI}_{\text{AV}}} \tag{7.1}$$

$$\text{Mitral Valve Area}\left(\text{MVA}\right)\left(\text{cm}^2\right)=\frac{\text{CSA}_{\text{LVOT}}\times\text{VTI}_{\text{LVOT}}}{\text{VTI}_{\text{MV}}} \tag{7.2}$$

The continuity equation can also be rearranged to evaluate regurgitant valvular lesions via the regurgitant volume (RegV) and regurgitant fraction (RegF). By knowing the CSA and VTI of the LVOT and the mitral valve, respectively, the regurgitant volume can be determined. By assuming that the blood flow through the mitral valve in diastole is the same as through the LVOT in systole, the difference is the regurgitant fraction. Similarly, the aortic regurgitant volume in the setting of aortic insufficiency can be calculated (see Eqs. 7.3 and 7.4). The RegF is the RegV divided by the stroke volume (SV) (see Eq. 7.5). Both the RegF and RegV are important for grading the severity of regurgitant valvular lesions. Lastly, this equation can be rearranged to calculate the effective regurgitant orifice area (EROA) by using the RegV and VTI of the regurgitant jet (see Eq. 7.6) [1].

***Equations 7.3 and 7.4*** *Calculation of aortic valve and mitral valve regurgitant volumes by the continuity equation.*

$$\text{RegV}_{\text{AV}}\left(\text{mL}\right)=\left(\text{CSA}_{\text{LVOT}}\times\text{VTI}_{\text{LVOT}}\right)\ \left(\text{CSA}_{\text{MV}}\times\text{VTI}_{\text{MV}}\right)=\text{SV}_{\text{LVOT}}\ \ \text{SV}_{\text{MV}} \tag{7.3}$$

$$\text{RegV}_{\text{MV}}\left(\text{mL}\right)=\left(\text{CSA}_{\text{MV}}\times\text{VTI}_{\text{MV}}\right)\ \left(\text{CSA}_{\text{LVOT}}\times\text{VTI}_{\text{LVOT}}\right)=\text{SV}_{\text{MV}}\ \ \text{SV}_{\text{LVOT}} \tag{7.4}$$

***Equation 7.5*** *Calculation of regurgitant fraction.*

$$\text{RegF}\ \left(\%\right)=\frac{\text{RegV}_{\text{valve}}}{\left(\text{CSA}_{\text{valve}}\times\text{VTI}_{\text{valve}}\right)}=\frac{\text{RegV}_{\text{valve}}}{\text{SV}} \tag{7.5}$$

***Equation 7.6*** *Calculating effective regurgitant orifice Area by the continuity equation.*

$$\text{EROA}\ \left(\text{cm}^2\right)=\frac{\text{RegV}_{\text{valve}}}{\text{VTI}_{\text{regurg jet}}} \tag{7.6}$$

The concept of continuity of flow is also important for understanding how to calculate valvular areas using proximal isovelocity surface area (PISA). As blood flow accelerates through a narrowing like a valvular orifice for example, a “shell” of

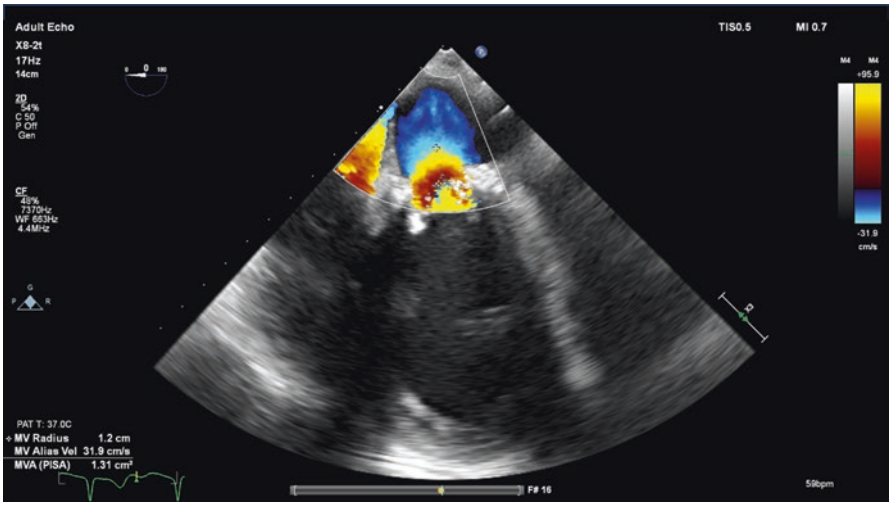


**Fig. 7.6** Proximal isovelocity surface area (PISA) through the mitral valve. The semicircle of color represents the hemispheric shell of velocity approaching the valve orifice. In this case, the patient had a MV area of 1.31 $cm^2$, graded as moderate mitral stenosis. Note that the Nyquist limit baseline has been shifted downward to accentuate the PISA shell

surface area of increasing velocities can be visualized using CFD (Fig. 7.6). Assuming that the flow velocities of the surface of each shell or hemisphere is equivalent, or having "isovelocity," then flow through a given shell can be calculated by knowing the velocity at that shell (see Eq. 7.7) [1].

***Equation 7.7*** *Calculation of flow through a PISA shell.*

$$\text{Flow}\ \left(\text{mL}/\text{s}\right) = \text{PISA} \times \text{Velocity}_{\text{hemispheric surface}} \tag{7.7}$$

By shifting the baseline of the Nyquist limit in the direction of flow, typically to 30–40 cm/s (away from the probe for mitral stenosis, for example), the PISA shell can be made more prominent. Although CFD is semi-quantitative, the site of aliasing is known. By assuming that the distance from the orifice to the site of the most prominent aliasing velocity is the PISA shell radius, the surface area of the hemisphere can be calculated using $2\pi r^2$ (see Eq. 7.8) [1].

***Equation 7.8*** *Calculation of orifice area by the PISA Method.*

$$\text{CSA} = \frac{\text{PISA} \times \text{Velocity}_{\text{aliasing}}}{\text{Peak Velocity}} \tag{7.8}$$

When applying the PISA method to calculate stenotic mitral valve lesions, an alpha ($\alpha$) angle correction must be applied to account for the saddle-shaped leaflets (see

Eq. 7.9). For mitral regurgitation, this is not necessary because the calculation assumes that the site of regurgitation is the same as the vena contracta (see Eq. 7.10) [1].

***Equation 7.9*** *Calculation of MVA by the PISA method.*

$$\text{MVA} = \frac{2\pi r^2 \times (\alpha / 180) \times \text{Velocity}_{\text{aliasing}}}{\text{Peak Velocity}_{\text{MV inflow}}} \tag{7.9}$$

***Equation 7.10*** *Calculation of MV EROA by the PISA method.*

$$\text{EROA}_{\text{MV}} = \frac{2\pi r^2 \times (\alpha / 180) \times \text{Velocity}_{\text{aliasing}}}{\text{Peak Velocity}_{\text{MV regurgitation}}} \tag{7.10}$$

In addition to calculating areas, determining blood flow velocities and pressure gradients across valves is important. The Bernoulli equation can be applied to convert blood flow velocities to pressure gradients. The true Bernoulli equation is complicated and beyond the scope of this text. For clinical echocardiography, either the modified or simplified Bernoulli equation can be applied to convert blood flow velocities to pressure gradients (see Eqs. 7.11 and 7.12). Blood flow velocity across a valve can be measured using spectral Doppler. Specifically, the peak blood flow velocity can be assessed distal to the valve using CWD and the blood flow velocity proximal to the valve can be assessed with PWD. The simplified Bernoulli equation is the default setting on most echo machines and in the majority of instances is used to convert the proximal and distal blood flow velocities to pressure gradient. Because the simplified Bernoulli equation will overestimate the pressure gradient when proximal velocity exceeds 1.5 m/s, the modified Bernoulli equation should be used. Examples include severe aortic insufficiency, intracardiac shunts, excessive cardiac output, subaortic stenosis, or LVOT obstruction. It should also be noted that the modified equation may be more appropriate for prosthetic valves [1].

***Equation 7.11*** *The Simplified Bernoulli Equation.*

$$\text{Pressure Gradient} = 4 \times \text{Velocity}_{\text{distal}}{}^2 \tag{7.11}$$

***Equation 7.12*** *The Modified Bernoulli Equation.*

$$\text{Pressure Gradient} = 4\left(\text{Velocity}_{\text{distal}}{}^2 - \text{Velocity}_{\text{proximal}}{}^2\right) \tag{7.12}$$

### 7.2.4 *Other Echocardiographic Calculations to Evaluate Heart Valves*

In addition to the continuity and PISA methods, areas within the heart can be calculated using planimetry. This is simple, fast, and easy to perform with relative accuracy (Fig. 7.7). From a 2D short-axis cross section of the valve of interest, the orifice area of valve is manually traced at the moment at which the valve is completely open. Due to its symmetrical nature of the aortic valve annulus, using the planimetry technique is more accurate when compared with non-symmetric valves like the mitral or tricuspid [1]. By tracing the regurgitant orifice when the valve is closed, planimetry can also be used to measure EROA [3]; however, this is not accurate and not recommended due to the often dynamic nature of regurgitant lesions.

Pressure half-time (PHT) and deceleration time (DT) can be used to evaluate both stenotic and regurgitant lesions. PHT is the time it takes for the pressure gradient across an orifice to decrease by 50%, a reflection of velocity decline and pressure equilibration between two chambers, and can be calculated as PHT = 0.7 × peak velocity. Similarly, the DT is the amount of time it takes for peak velocity to completely fall to zero. PHT and DT are related to one another by Eq. 7.13 [3].

***Equation 7.13*** *Relationship between pressure half-time and deceleration time.*

$$\mathrm{PHT} = 0.29 \times \mathrm{DT} \tag{7.13}$$

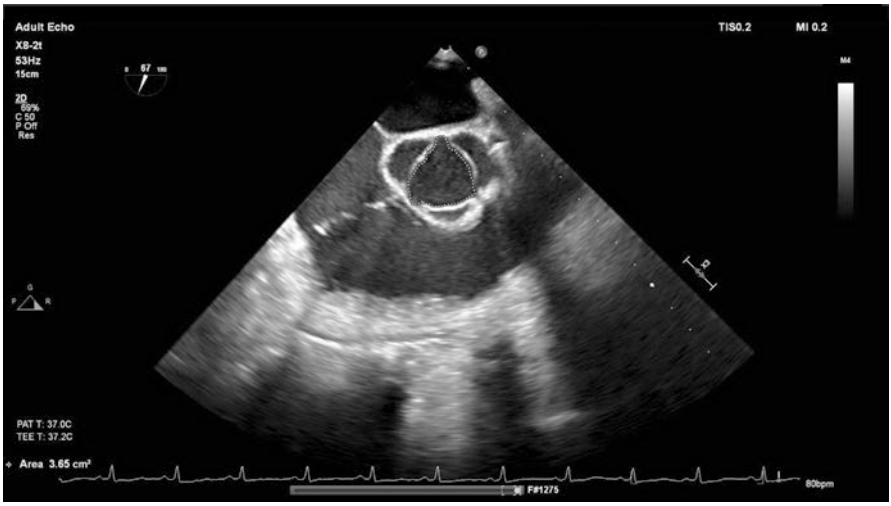


**Fig. 7.7** Planimetry measurement of aortic valve area in the AV SAX view. In this image, the measured area appears in the lower left-hand corner

Clinically, PHT is used to determine mitral valve area (MVA) and to grade aortic insufficiency. Using CWD through the MV during diastole, the distance from the peak velocity to the baseline, both PHT and DT can be calculated (see Fig. 7.8 and Eqs. 7.14 and 7.15). Similarly, using CWD through the AV during diastole, the deceleration slope is manually traced to calculate the PHT. Based on the rate of pressure decline through the AV, the rate of chamber pressure equilibration across the valve, a reflection of severity of insufficiency, is calculated [3] (see the Aortic Valve Insufficiency section for more details about grading aortic insufficiency).

***Equations 7.14 and 7.15*** *Calculating mitral valve area with pressure half-time and deceleration time.*

$$\text{MVA} = 220 / \text{PHT} \tag{7.14}$$

$$\text{MVA} = 759 / \text{DT} \tag{7.15}$$

Finally, the vena contracta (VC) is important for grading aortic and mitral valvulopathies and represents the area of greatest blood flow velocity across a stenotic or regurgitant valvular lesion can be determined using CFD with 2D echo (Fig. 7.9). Typically, for stenotic valvular lesions, the VC is slightly distal to the actual stenotic lesion so should not be measured at the site of the valve lesion. For regurgitant lesions, the VC should be measured at the site of the lesion as the narrowest portion of the lesion represents the highest blood flow velocity [1]. The use of VC for grading aortic and mitral valvulopathies is discussed in more detail later in this chapter.

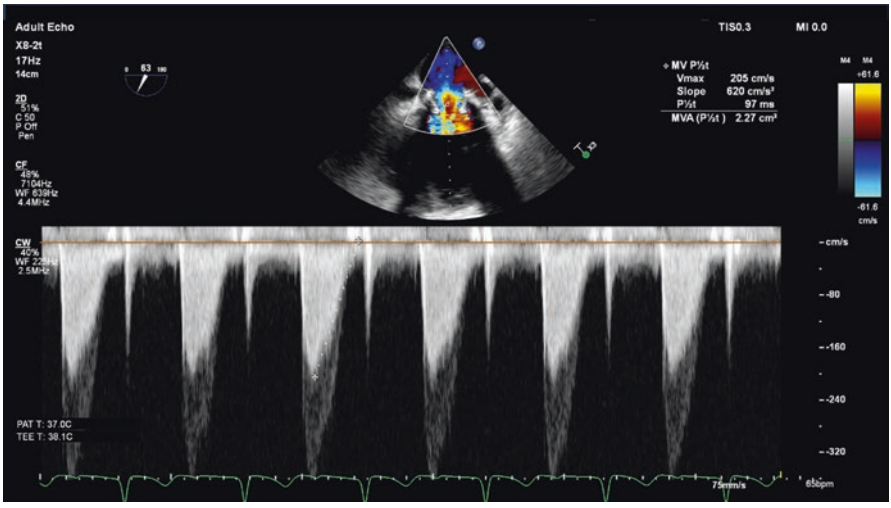


**Fig. 7.8** Pressure half-time (PHT) through a prosthetic mitral valve. Notice that the denser CWD wave through is used for measurement of the PHT

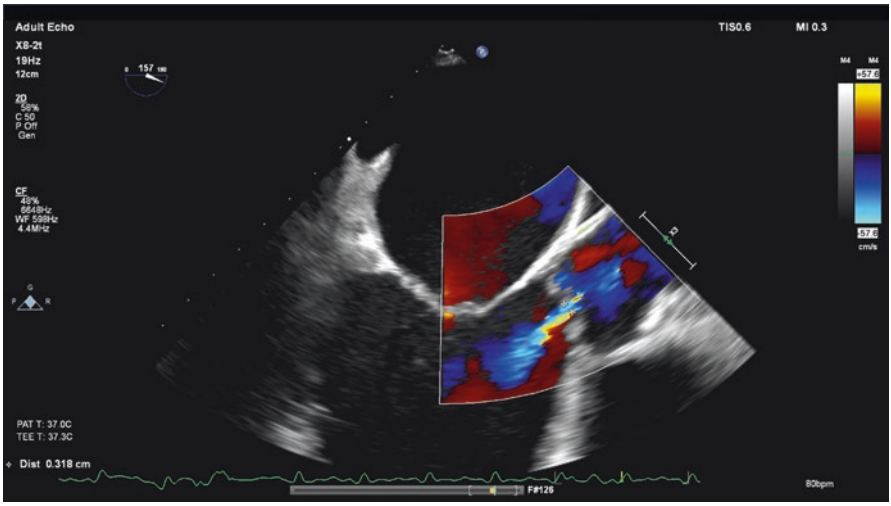


**Fig. 7.9** Vena contracta for aortic valve insufficiency. In this patient, the vena contracta is consistent with mild–moderate aortic insufficiency

## 7.3 Basic Transesophageal Echocardiographic Exam

In 2013, the American Society of Echocardiography (ASE) and Society of Cardiovascular Anesthesiologists (SCA) released their most recent guidelines for performing a comprehensive TEE exam in which they defined 28 standard views (Fig. 7.10) [4]. In this section, we will focus on views X, Y, and Z as we specifically review how to assess each cardiac valve.

## 7.4 Aortic Valve

The standard exam of the aortic valves includes views from both esophagus also referred to as mid-esophageal (ME) and the stomach, referred to as transgastric (TG) views. Assessment should allow for visualization of all three cusps as well as the measurement of gradients across the aortic valve and LVOT. The standard ME views include the 5-chamber (5C), LV long axis (LAX), AV LAX, AV short axis (SAX), TG LAX, and the deep TG 5C (dTG 5C) views (Fig. 7.10). These views should be acquired both with and without CFD to assess for turbulence, blood flow acceleration through the valve in the setting of a stenotic lesion or reverse flow through the valve in the setting of regurgitant lesions. In addition, the AV can be assessed with 3D echo via the ME SAX or ME LAX by acquiring a narrow angle or wide angle with either single beat or multibeat modes (Fig. 7.11) [4].

A comprehensive echocardiographic exam of the aortic valve includes the components of the aortic valve itself and the surrounding structures. The components of

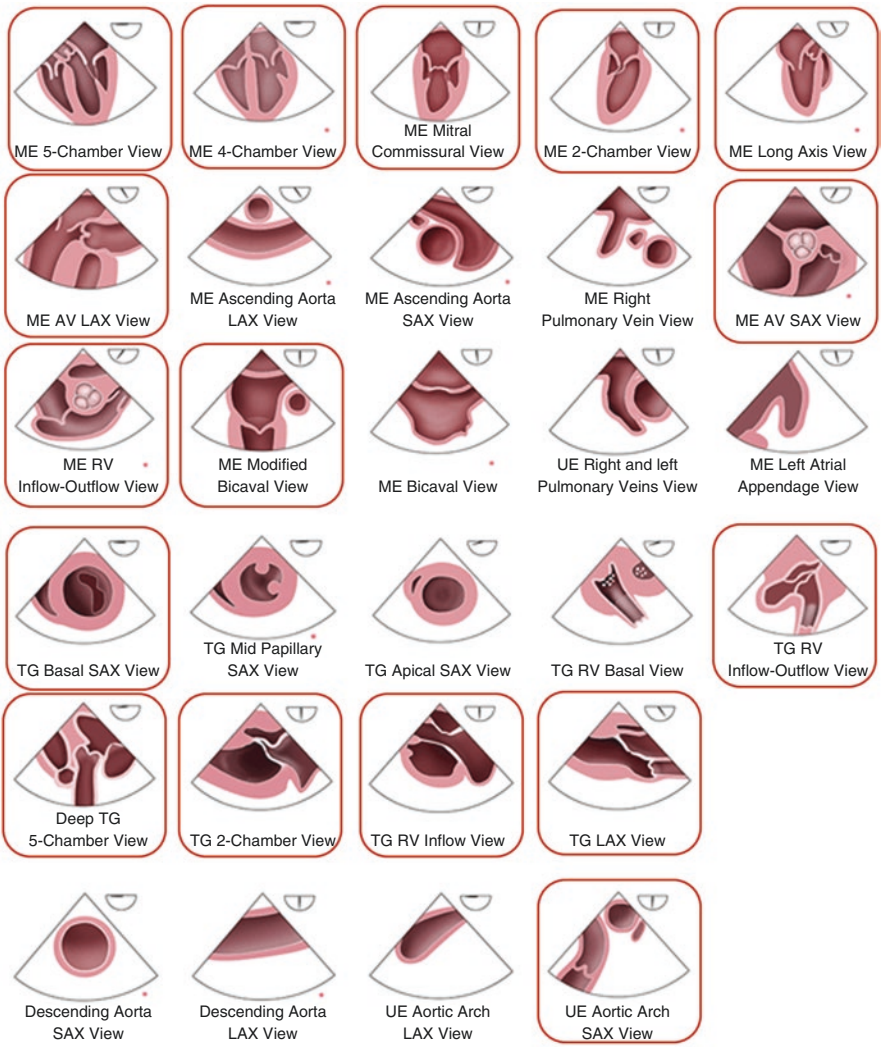


**Fig. 7.10** The 28 recommended views for a comprehensive perioperative echo exam. The boxed views are the ones to which we will refer when interrogating the heart valves. (Source: Mathew et al. [1])

a normal aortic valve and surrounding structures include three aortic cusps, the left and right coronary artery ostia, the shape and diameters of the LVOT, the aortic annulus, the sinus of Valsalva, the sinotubular junction (STJ), and the proximal ascending aorta [4]. The three aortic cusps should be assessed for proper excursion during systole and closure with good coaptation during diastole, and the presence and extent of calcifications that might impede this movement. The LVOT diameter should be measured 1 cm proximal to the AV annulus, inner edge to inner edge. The

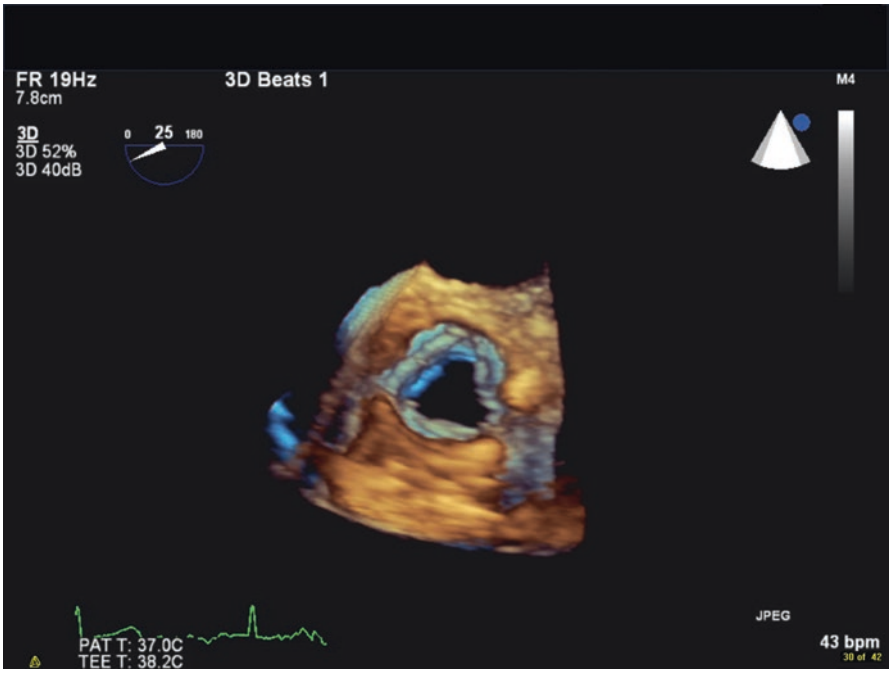


**Fig. 7.11** 3D aortic valve. For orientation, in this view, we are looking from the aortic root into the LVOT. The right coronary cusp is toward the bottom of the annulus, the left coronary cusp is toward the right of the image, and the non-coronary cusp is toward the left of the image

AV annulus should also be measured inner edge to inner edge; however, the sinus of Valsalva, STJ, and ascending aorta should be measured from leading edge to leading edge [5]. These can best be assessed in the ME AV LAX view (Fig. 7.12). For normal values, see Table 7.1 [6]. Newer technologies now allow for more accurate 3D modeling of the aortic root, which can relate the AV, MV, and aortomitral curtain more precisely than 2D echo [7].

In addition to the 2D imaging with and without CFD, Doppler assessment is part of any comprehensive evaluation of the aortic valve. Spectral Doppler should also be used to evaluate velocities and gradients across the valve and LVOT using continuous wave Doppler and pulse wave Doppler, respectively. The CWD through the AV and the PWD through the LVOT can be acquired in the transgastric long-axis view but more commonly in the deep transgastric 5 chamber view (Fig. 7.13) [5]. These images allow for the best Doppler alignment and, therefore, the lowest likelihood of error during calculation. See the Aortic Stenosis and Aortic Regurgitation sections for a more complete discussion of Doppler for diagnosis in those pathologies.

Although a normal AV has three cusps, a significant portion of the population has two. A bicuspid aortic valve is the most common congenital heart defect and is often found incidentally (Fig. 7.14). A bicuspid aortic valve generally has aberrant flow

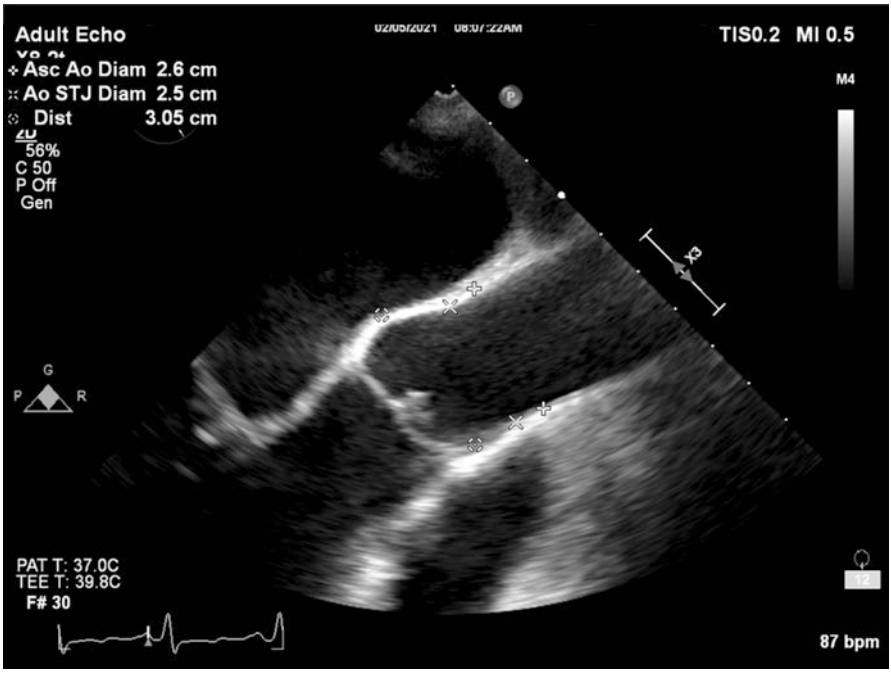


**Fig. 7.12** Measurements of the aortic root. Note that these measurements should be made during diastole (AV is closed) and are measured leading edge-to-leading edge. The aortic root measurements appear in the top left-hand corner of the image

**Table 7.1** Basic measurements for assessing the aortic valve [6, 8]

| Structure | When to measure | How to measure | Normal Value (cm) |
|---|---|---|---|
| Left Ventricular Outflow Tract [8] | Systole | Inner edge to inner edge | Male: 2.2 ± 0.2<br>Female: 2 ± 0.2 |
| Aortic annulus | Systole | Inner edge to inner edge | Male: 2.6 ± 0.3<br>Female: 2.3 ± 0.2 |
| Sinus of Valsalva | Diastole | Leading edge to leading edge | Male: 3.4 ± 0.3<br>Female: 3 ± 0.3 |
| Sinotubular Junction | Diastole | Leading edge to leading edge | Male: 2.9 ± 0.3<br>Female: 2.6 ± 0.3 |
| Ascending Aorta | Diastole | Leading edge to leading edge | Male: 3 ± 0.4<br>Female: 2.7 ± 0.4 |

dynamics in and around the valve, making the valve more prone to calcification and subsequent dysfunction, often resulting in either valve stenosis or regurgitation. Not uncommonly, bicuspid aortic valves are associated with post-valvular aortic root or ascending aortic dilatation [9]. A bicuspid AV has a higher prevalence in patients with Turner's syndrome and is associated with coarctation of the aorta. Both unicuspid and quadracuspid aortic valves have been documented [3] but further discussion on these pathologies is beyond the scope of this chapter.

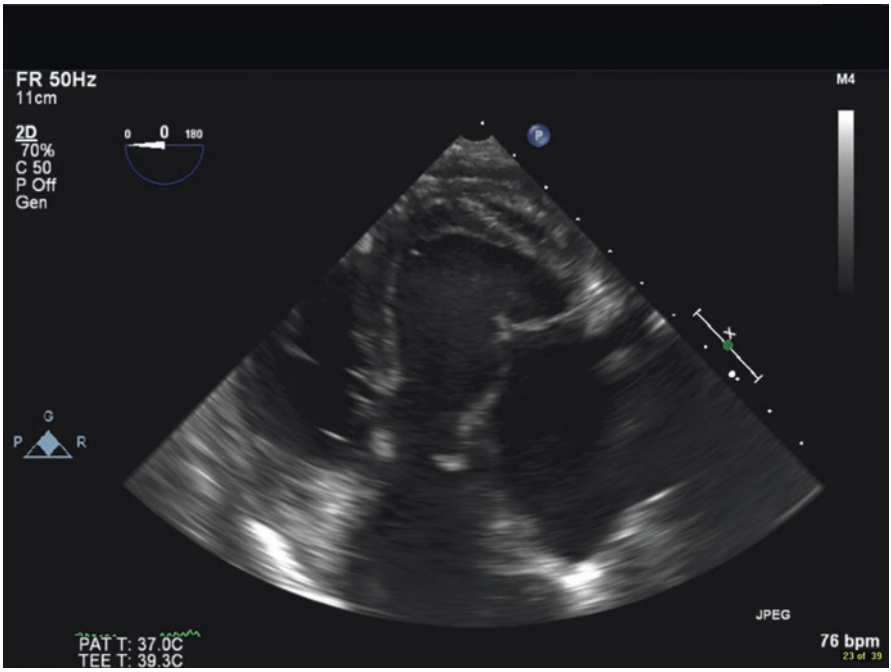


**Fig. 7.13** Deep transgastric 5-chamber view. In this view, one can assess the aortic valve and LVOT with CFD, CWD, and PWD

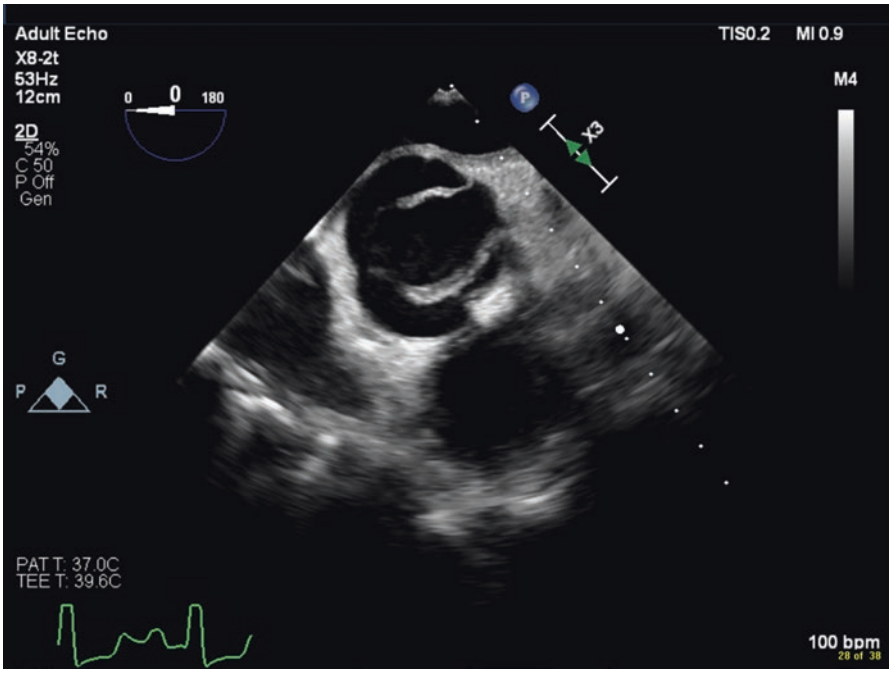


**Fig. 7.14** Bicuspid aortic valve. The most common type of BAV is fusion of the right and left coronary cusps, creating a raphe

### 7.4.1 Aortic Valve Stenosis

Aortic valve stenosis is a common indication for either surgical or transcatheter aortic valve replacement. While the AV area is normally 3–4 $cm^2$ [1], this area can decrease significantly in the setting of increased valvular calcification, rheumatic, or bicuspid valvular disease. A calcific AV typically has calcium deposits on the cusp body with an irregular orifice opening without commissural fusion while a rheumatic AV will have commissural fusion with a calcified cusp free edge [5]. A BAV often has a raphe where two cusps have been fused with an elliptical orifice, the so-called "fish mouth opening." Most commonly, there is congenital fusion of the right and left coronary cusps [9]. Less common forms of AV stenosis may be due to subvalvular and supravalvular causes. Subvalvular causes include systolic anterior motion of the mitral valve (SAM), idiopathic hypertrophic subaortic stenosis (IHSS), and a subvalvular membrane, while supravalvular stenosis may be from narrowing of the ascending aorta, typically due to a congenital anomaly [5].

A stenotic aortic valve should be evaluated using 2D imaging, spectral Doppler, and CFD. It is important to keep in mind that CWD velocities and gradients will vary with flow; therefore, the true severity of stenosis may be under or overestimated depending on the circumstances. Severity will be underestimated in the setting of poor LV systolic function, significant mitral regurgitation, poor Doppler alignment, and left-to-right shunting. The severity of stenosis will be overestimated in the setting of aortic insufficiency and a hyperdynamic left ventricle [5]. For severity grading, see Table 7.2. Other commonly associated echocardiographic findings include LV hypertrophy, inferior basal LV hypokinesis, post-stenotic aortic root or ascending aortic dilatation, mitral regurgitation, and mitral annular calcification [3].

Quantification of AV stenosis can be performed in a number of ways, the simplest being by tracing the AV orifice during systole in the AV SAX view, referred to as planimetry. Using the planimetry technique is acceptable according to ASE guidelines, but is prone to inaccuracy due to inter- and intra-user variability in tracing the plane of interest [10]. A more commonly used way of quantifying the AV area is by using the simplified continuity equation (see discussion above about the Continuity Equation). By measuring the diameter of the LVOT from the AV LAX view and the VTI through both the AV and LVOT from either the dTG 5C view or the TG LAX view [5], the diameter of the AV can be calculated using the simplified

**Table 7.2** EACVI/ASE Guidelines for Aortic Stenosis Severity [5]

| Parameter | Sclerosis | Mild | Moderate | Severe |
|---|---|---|---|---|
| Vmax (m/s) | ≤2.5 | 2.6–2.9 | 3–4 | ≥4 |
| Mean PG (mmHg) | | <20 | 20–40 | ≥40 |
| AVA ($cm^2$) | | >1.5 | 1–1.5 | <1 |
| Indexed AVA ($cm^2/m^2$) | | >0.85 | 0.6–0.85 | <0.6 |
| Velocity Ratio (Dimensionless Index) | | >0.5 | 0.5–0.25 | <0.25 |

*Vmax* peak velocity, *mean PG* mean pressure gradient, *AVA* aortic valve area

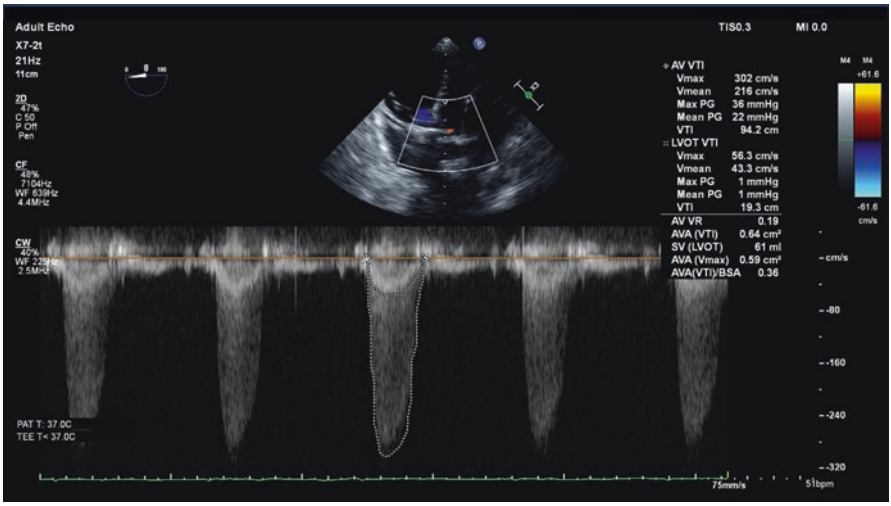


**Fig. 7.15** CWD through the aortic valve with a double-envelope tracing. Here, the LVOT and AV VTIs can be compared on the same cardiac ejection with the same Doppler alignment

continuity equation. Alternatively, the "double envelope" technique can be used whereby two envelopes of flow velocities are seen as superimposed by aiming a CWD vector through the AV and LVOT from the dTG 5C view (Fig. 7.15). The inner tracing (tracing with slower blood flow velocities) represents the LVOT flow while the outer tracing (tracing with higher blood flow velocities) represents the AV flow. Unlike the continuity equation in which area and velocities are assessed over several cardiac cycles, the advantage of using the "double envelope" technique is that flow velocities through the AV and LVOT can be assessed during a single cardiac beat [11].

Because the most common source of error in the continuity equation is the LVOT diameter measurement, the ratio of the $VTI_{LVOT}$:$VTI_{AV}$ without the LVOT diameter also referred to as the dimensionless index (DI) or velocity ratio (VR) can be used to assess severity of the aortic valve stenosis [5]. By measuring CWD through the AV, most echo machines will automatically display the velocities and gradients across the valve, which is calculated via the simplified Bernoulli equation. In cases of subaortic stenosis, such as in IHSS, the modified Bernoulli is more appropriate for accurate calculation (see discussion above about the Bernoulli equation) [3]. Another way to improve the evaluation of the AV is to compare the AVA to the patient's body surface area (BSA) known as the indexed AVA. This can give a better picture of true aortic stenosis in children and other patients who may have a low AVA but physiologically do not have AV stenosis [12].

**Aortic Stenosis Variants**

There are situations when assessing the severity of aortic valve stenosis can become complicated. These include classic low flow–low gradient AS (classic LFLG AS), pseudosevere AS, and paradoxical low flow–low gradient AS

**Table 7.3** Comparison of the aortic stenosis variants [5]

| Aortic Stenosis Type | AVA ($cm^2$) | Mean Pressure Gradient (mmHg) | Ejection Fraction (%) | AVA after Dobutamine ($cm^2$) | Typical Patient |
|---|---|---|---|---|---|
| Typical AS | <1 | >40 | Normal | <1 | Severe AS |
| Classic LFLG AS | <1 | <40 | Reduced | <1 | Severe AS + Reduced LV systolic function |
| Paradoxical LFLG AS | <1 | <40 | Normal | <1 | Severe AS + Reduced LV diastolic function |
| Pseudosevere AS | <1 | <40 | Reduced | >1 | Reduced LV systolic function |

(paradoxical LFLG AS) (see Table 7.3). These conditions all have in common a reduced aortic valve areas but pressure gradients due to poor left ventricular function that do not qualify these lesions as stenotic. In Classic LFLG AS, the AV is calcified with a low AVA in the setting of reduced LV systolic function. Despite a truly stenotic lesion, the left ventricle is unable to generate transvalvular gradients necessary to qualify the lesion as stenotic according to the traditional definition (see Table 7.2 for typical AS and Table 7.3 for variants). Similarly, in paradoxical LFLG AS, the AV is calcified with a low AVA in the setting of reduced LV diastolic function resulting in low stroke volume. Lastly, in pseudosevere AS the AVA is normal, but in the setting of reduced LV systolic function whereby the left ventricle cannot generate enough blood flow through the aortic valve to cause excursion of the AV leaflets, resulting in a low AVA calculation. A dobutamine stress test can differentiate pseudosevere from classic LFLG AS if during the stress test, the AVA increases more than 1 $cm^2$ [5].

### *7.4.2 Aortic Insufficiency*

Aortic insufficiency (AI) may be due to pathology of the AV specifically or secondary to aortic pathology. AV pathology is often acquired (calcifications, rheumatic disease, or endocarditis) or congenital (bicuspid AV). Similarly, aortic pathology resulting in AI may be acquired (aortic aneurysm or dissections or infectious causes, such as syphilitic aortitis) or congenital (connective tissue diseases, such as Ehlers-Danlos or Marfan's syndrome) [13]. El Khoury et al. developed a classification for differentiating between the mechanisms of AI and whether or not each mechanism is amenable to surgical intervention (see Table 7.4) [14].

Similar to AS, the aortic valve in the setting of AI should be examined with 2D echo as well as with Doppler modes. As described for stenotic aortic valve lesions, the ME AV SAX and ME AV LAX views should be acquired with and without CFD to assess AV cusp functioning and severity of calcification [13]. In addition, the

**Table 7.4** El Khoury Classification of Aortic Insufficiency [14]

| Type | Subtype | Description |
|---|---|---|
| Type I | | Normal cusps + functional aortic annulus dilation |
| | Ia | STJ dilation |
| | Ib | Sinus of Valsalva dilation + STJ dilation |
| | Ic | Isolated functional aortic annulus dilation |
| | Id | Cusp perforation + functional aortic annulus dilation |
| Type II | | Cusp prolapse: excess cusp tissue or commissural disruption |
| Type III | | Cusp retraction and thickening |

*STJ* sinotubular junction

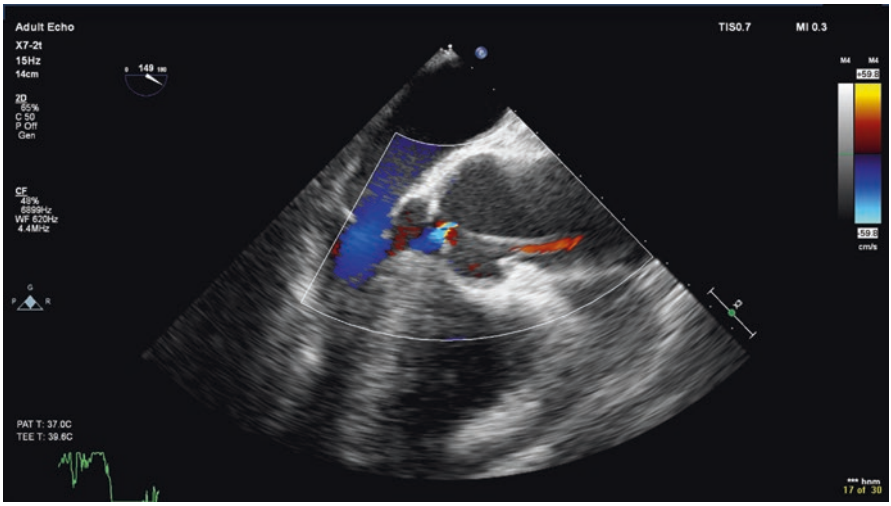


**Fig. 7.16** Aortic insufficiency in the setting of an acute Type A aortic dissection. In this image, one can see an AI jet in addition to the CFD in the dissection flap and an aortic root hematoma

ascending aorta can be assessed from the upper esophageal (UE) ascending aorta LAX and SAX views to rule out aortic dissection, dilation, or aneurysm, all three of which may be secondarily causing or contributing to AI (Fig. 7.16). From the ME and transgastric views, the LV cavity should be inspected for eccentric hypertrophy or dilation, an indication of long-standing or chronic AI. If the dimensions of the LV cavity are normal, then the AI is more likely to be acute in nature, as seen in Type A dissections [13].

The ME AV SAX and LAX views with CFD can help determine the location, number, and direction of the regurgitant jet(s) through the aortic valve. When AI is due to pathology of the AV itself, including vegetation, perforations, or calcifications of the aortic valve cusps, regurgitant jets are often asymmetric or multiple. When AI is due to dilation of the aortic annulus, sinuses of Valsalva, STJ, and/or ascending aorta, the cusps often poorly coapt resulting in a single, central

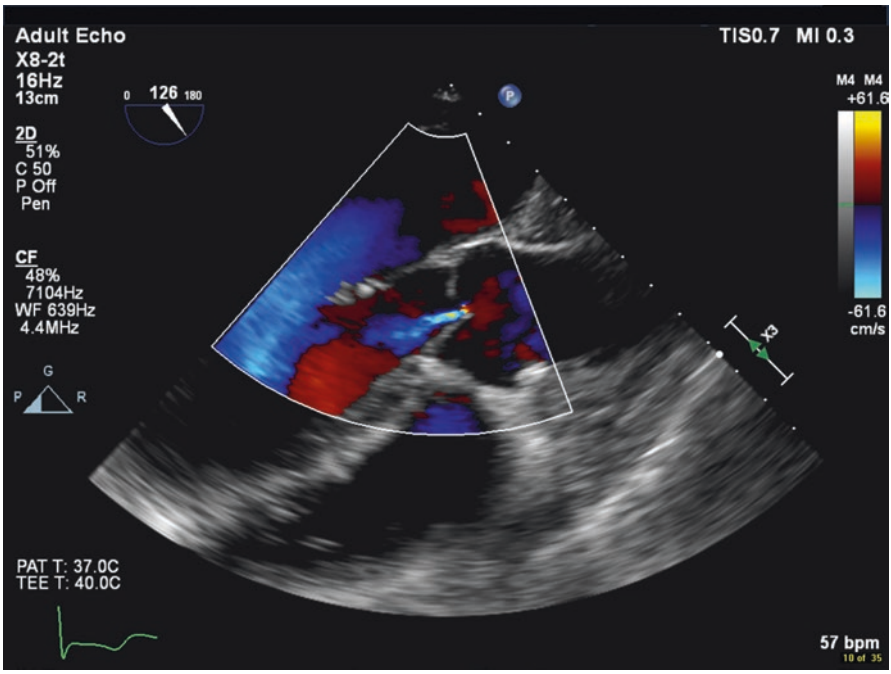


**Fig. 7.17** Central AI jet due to poor AV leaflet coaptation

regurgitant jet (Fig. 7.17). As the AI worsens, the CFD jet becomes wider, reaches deeper into the LV cavity, and displays more aliasing and turbulence. The narrowest portion of the AI jet, known as the vena contracta, is very useful for grading AI severity (see Table 7.5) [13].

Spectral Doppler exam can also be used to assess and grade the severity of AI, not only through the valve. CWD should be acquired in either the TG LAX or the dTG 5C view. By adding CFD to the 2D image and then directly overlay the CWD beam over the area of the most turbulent regurgitant flow, clearly defined flow velocities can be traced. In this view, the regurgitant jet is above the baseline, as it is directed toward the echo probe [3]. The rate of decline of the blood flow velocity is used to calculate the pressure half-time (PHT) (see above discussion of hemodynamic calculations), a measure to grade the severity of AI (see Table 7.5). A steeper PHT slope indicates a shorter time for the pressure in the left ventricle to equalize the pressure in the aortic root (Fig. 7.18).

It stands to reason that the faster these pressures equalize, the more severe the aortic valvular insufficiency [13]. The effective regurgitant orifice area (EROA) can be assessed by determining the peak regurgitant velocity across the aortic valve using either the PISA method or the volumetric method (see above discussion of hemodynamic calculations). Lastly, diastolic flow reversal in the descending aorta as measured using PWD from the transgastric view is an indicator of severe AI (see

**Table 7.5** ASE Guidelines for Grading Aortic Insufficiency Severity [13]

| | Measurement | Mild | Moderate | Severe |
|---|---|---|---|---|
| Structural Findings | Aortic Leaflets | Variable | Variable | Visible coaptation defect |
| | LV Size | Normal | Variable | Dilated |
| Qualitative | CFD LVOT jet width | Small | Intermediate | Large |
| | Flow convergence | Small | Intermediate | Large |
| | CWD density | Faint | Dense | Dense |
| | PHT (ms) | >500 | 200–500 | <200<br>*Decel slope > 3 m/s* |
| | Descending Ao reversal | Early and brief | Intermediate | Holodiastolic |
| Semi-Quantitative | VC width (mm) | <3 | 3–6 | >6 |
| | Jet/LVOT CSA (%) | <5 | 5–59 | ≥60 |
| | Jet/LVOT width (%) | <25 | 25–64 | ≥65 |
| Quantitative | RegVol (mL) | <30 | 30–59 | ≥60 |
| | RegF (%) | 20–30 | 30–49 | ≥50 |
| | EROA ($cm^2$) | <0.1 | 0.1–0.29 | ≥0.3 |

*LV* left ventricle, *CFD* color flow Doppler, *LVOT* left ventricular outflow tract, *CWD* continuous wave Doppler, *PHT* pressure half-time, *VC* vena contracta, *CSA* cross-sectional area, *RegV* regurgitant volume, *RegF* regurgitant fraction, *EROA* effective regurgitant orifice area

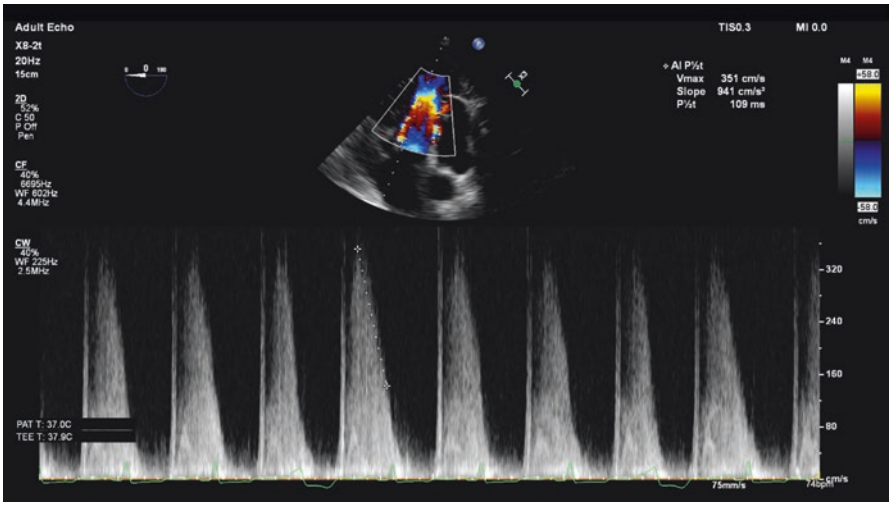


**Fig. 7.18** Pressure half-time through the aortic valve. In this patient, the steep curve indicates rapid equalization of chamber pressures suggesting severe AI. Also note that CFD was used to guide proper spectral Doppler alignment

Fig. 7.10). The peak blood flow velocity in the descending aorta is not as important as the direction of flow and the more distal in the aorta that flow reversal is observed, the more likely the AI is severe [13].

## 7.5 Mitral Valve

The mitral valve (MV) is the atrioventricular valve separating the left atrium (LA) and the left ventricle (LV). The MV complex consists of the mitral annulus, the anterior leaflet (AMVL), and posterior leaflet (PMVL) and the sub-mitral apparatus including the anterolateral and posteromedial papillary muscles with corresponding chordae tendineae that can be divided into primary, secondary, and tertiary chords, depending on their attachment patterns. The mitral annulus is in fibrous continuity with the aortic valve via the aortomitral curtain or aortomitral fibrosa located between the right and left fibrous trigones within the fibrous skeleton of the heart valve system [4]. Primary mitral valve chordae attach to the anterior and posterior MV leaflet free margin while secondary chordae attach to the ventricular side of each leaflet. The "stay chordae" are secondary chordae that helps prevent leaflet prolapse and maintain valve geometry by inserting into the ventricular side of the leaflet body. Lastly, tertiary chordae are only found on the PMVL and attach to the ventricular wall [3]. A properly functioning MV has a large area of leaflet coaptation with minimal regurgitation.

The mitral valve complex as described above is complex, multidimensional structure that is difficult to image using 2D echocardiography. Unlike the mostly one-dimensional tricuspid valve, the MV is saddle-shaped with its peaks at the center points of the AMVL and PMVL and its troughs at the anterior and posterior commissures. The AMVL makes up approximately 2/3 of the area of the mitral valve while the PMVL makes up approximately 2/3 of the annulus circumference [15]. The normal valve area is 4–5 $cm^2$, which is smaller than that of the TV [1].

Due to the complex nature of the mitral valve and surrounding structures, two systems of nomenclature were developed to describe the MV and associated pathology: the Duran Classification and the Carpentier Classification. The Duran Classification is not as widely used in the United States and is therefore beyond the scope of this chapter [16]. The Carpentier Classification divides the AMVL and PMVL into three portions based on the normal embryological development of each of the three PMVL scallops. From lateral to medial, starting from the anterior commissure, the PMVL is divided into P1, P2, and P3 portions. The corresponding AMVL is then divided into A1, A2, and A3 counterparts (Fig. 7.19). The American Society of Echocardiography (ASE) and Society of Cardiovascular Anesthesiologists recommend using the Carpentier system for describing the MV and associated pathology to ensure clear and accurate communication within and between specialties [13].

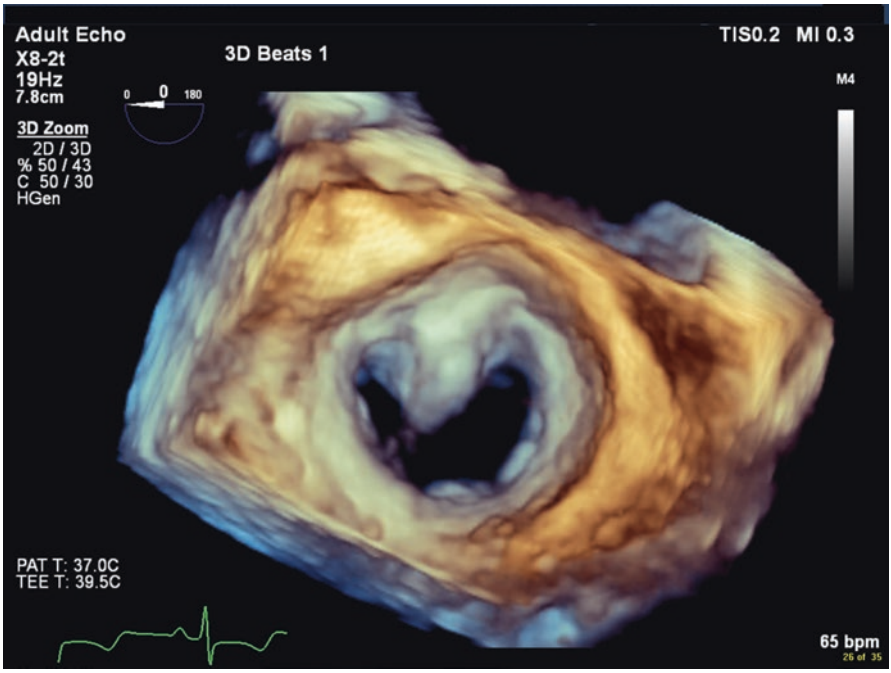


**Fig. 7.19** 3D Mitral valve. This is the Surgeon's view, with the AV at the top of the screen. The anterior commissure is to the left of the image while the posterior commissure is to the right of the image. The anterior leaflet is toward the AV and the posterior leaflet is toward the bottom of the annulus. Moving from left to right, the segments are A1/P1, A2/P2, and A3/P3, respectively

### *7.5.1 Mitral Valve Echocardiography Exam*

The mitral valve and surrounding structures are positioned immediately anterior to the esophagus and using transesophageal echocardiography lends itself well to excellent 2D and 3D image quality as well as Doppler alignment to assess blood velocities across the mitral annulus. A comprehensive examination of the mitral complex includes 2D imaging in the ME 5C, 4C, MC, 2C, and LAX views with and without CFD [4]. As previously highlighted, the complex nature of the mitral valve makes a complete and comprehensive examination imperative. In some views, the valve may look normal while in others, significant pathology may be revealed. In the 5C view, the mitral leaflet juxtaposed to the aortic valve is A1 while the mitral leaflet closer to the lateral wall of the left ventricle is P1 (see Fig. 7.10) [4]. In the 4C view, what used to be the A1 portion of the AML in the 5C view becomes A2 portion and the P1 portion of the PML becomes P2 [3]. In the ME MC view, sometimes referred to as the "seagull view," P1, A2, and P3 are seen moving from right to left on the screen. Both papillary muscles should be visible, with the posteromedial on the left side of the screen and anterolateral on the right (Fig. 7.20). If the probe is rotated clockwise and then counter-clockwise, the entire MV can be

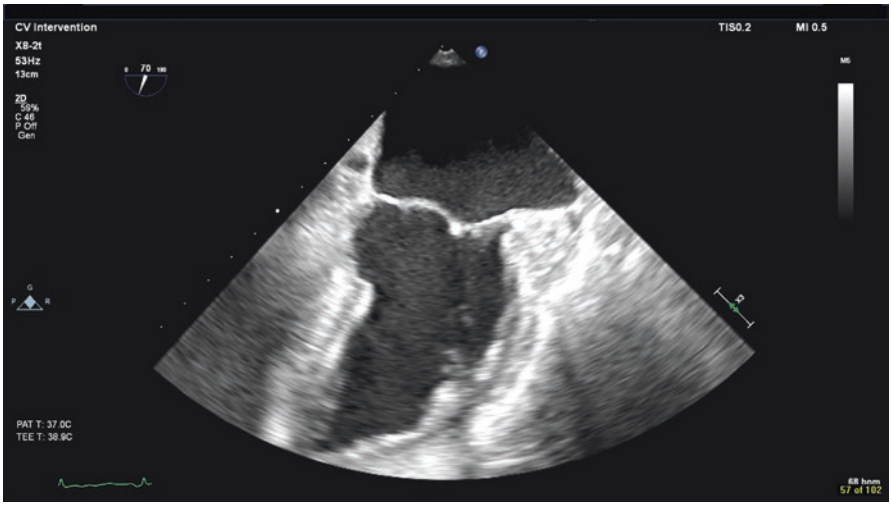


**Fig. 7.20** Mid-esophageal midcommissural view. In this image, one can appreciate the "seagull" view of the mitral valve, with P1, A2, and P3 segments visible when going right to left

examined. By rotating the probe to the clockwise, P3 is still on the left of the screen but now A3, A2, and A1 will make up the leaflet on the right. Similarly, if the probe is rotated to the counter-clockwise, all of the PMVL is seen, with P3, P2, and P1 seen moving from left to right [4]. In the ME 2C view, the P2 portion of the PML is visualized on the left side of the screen and the A2-A1 portions of the AML are on the right with the posteromedial papillary muscle on the left [4]. In the ME LAX view, the P2 portion of the PML is visualized on the left side of the screen and A2 portions of the AML on the right in addition to the aortomitral fibrosa [4].

PWD or CWD in the ME 4C or LAX views can be used assess blood flow velocities though the MV. PWD is typically used when assessing diastolic function with the cursor placed at the tips of the mitral leaflet. In the setting of mitral valve stenosis and potentially elevated blood flow velocities through the mitral annulus, CWD should be used to assess the mean and peak pressure gradients (Fig. 7.21) [12].

A complete examination of the mitral valve also includes the TG views. The TG views allow for evaluation of the sub-mitral apparatus, not easily visualized in the mid-esophageal views [4]. The entire mitral valve can be visualized in the TG basal SAX with the posterior mitral commissure in the near field and anterior commissure in the far field. Moving from near to far field, the PMVL is on right of the screen displays P3, P2, and P1. On the left part of the screen, the AMVL displays A3, A2, and A1 [3] (Fig. 7.22). The TG 2C view is similar to the ME counterpart except rotated 90°. In this view, P2 is in the near field and A2-A1 is in the far field. The posteromedial papillary muscle is in the near field and the mitral chordae can be well characterized in this view [3]. Finally, while the mitral valve should be evaluated in the TG LAX and dTG 5C views with and without CFD, these views are of limited diagnostic utility for this valve.

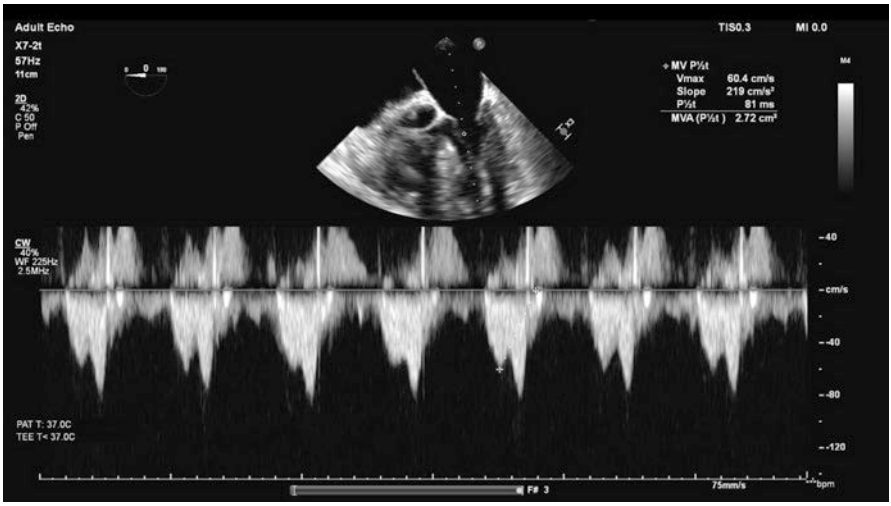


**Fig. 7.21** Continuous wave Doppler through the mitral valve to measure MVA by pressure half-time. Note that the E-wave is traced to estimate the MVA, and the A-wave is excluded from this measurement

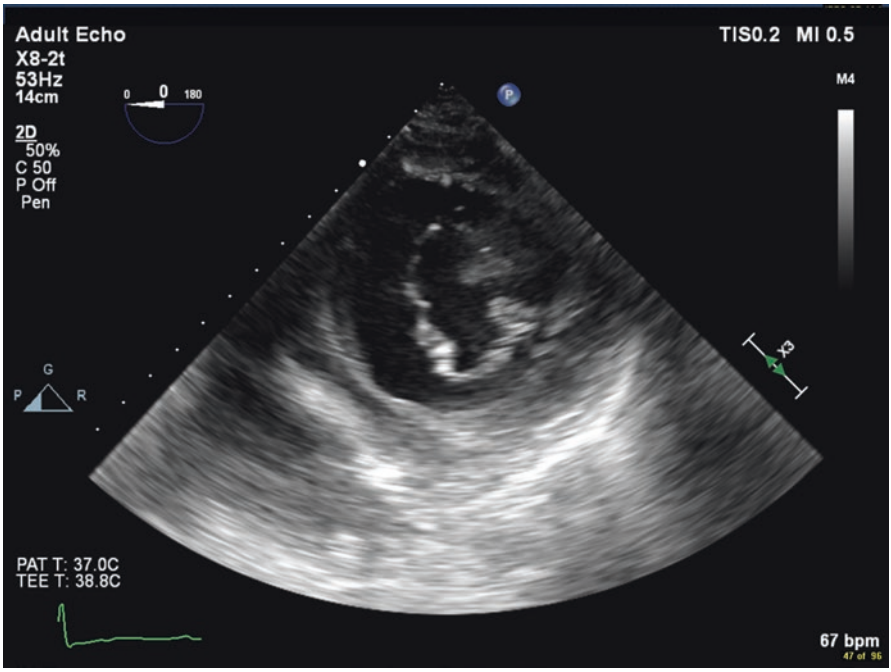


**Fig. 7.22** Transgastric basal LV short-axis view. The AMVL is to the left of the screen and the PMVL is to the right of the screen. The posterior commissure is toward the top and the anterior commissure is toward the bottom of the screen. Going from top to bottom, the leaflet segments go A3/P3, A2/P2, and A1/P1 respectively

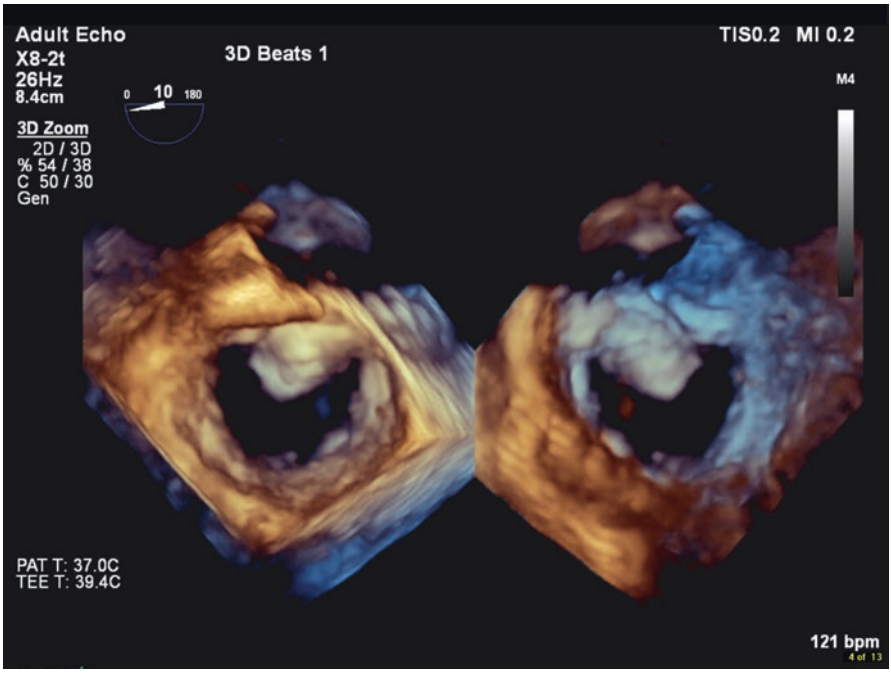


**Fig. 7.23** 3D MV Dual-Volume Layout. From this image, one can see the surgeon's view on the left and a view from the LV looking into the LA and LVOT on the right. This allows for evaluation of flow through the LVOT and for estimating the potential for systolic anterior motion SAM of the anterior mitral valve leaflet

Due to its proximity to the esophagus, the MV is very clearly visualized in 3D. From a 2D ME 4C view or the ME LAX view, a narrow-angle multibeat acquisition should be used to image the mitral valve and surrounding structures in 3D [4]. After acquiring a 3D image, the gain should be adjusted, usually decreased, to better visualize the valve. The image can be rotated along the *z*-axis to approximate what the surgeon sees in the surgical field; looking at the MV from the LA into the LV with the AV at the top of the screen. In this view, the AMLV is on top and the PMVL below. The posterior commissure is on the left side of the screen and anterior commissure is on the right [4] (Fig. 7.18). Adding CFD to a 3D image of the mitral valve can help characterize severity and direction of mitral regurgitation in 3D. Lastly, the entire 3D image can be rotated 180° to visualize the mitral valve from below, looking from the LV into the LA (Fig. 7.23). This maneuver can be useful for visualizing the LVOT and AV especially in the setting of systolic anterior motion (SAM) of the AMVL.

### 7.5.2 *Mitral Stenosis*

Although the incidence of rheumatic heart disease is diminishing in the developed world, it remains the most common cause of mitral valve stenosis with calcific mitral disease being the second most common [17]. Less common causes include carcinoid, lupus, and congenital defects. Left atrial masses, particularly thrombi and myxomas, may cause mechanical obstruction of the MV, resulting in a functional stenosis; however, in this case, the valve itself does not usually require intervention [3]. A comprehensive 2D exam of the mitral valve and surrounding structures as described in the preceding section can reliably delineate the etiology of mitral stenosis and associated defects of surrounding structures including chordae and aortomitral fibrosa.

Rheumatic mitral disease is characterized by leaflet thickening and restricted mitral leaflet motion with diastolic bowing of the leaflet body. Bowing can be particularly pronounced on the AMVL in the ME LAX and is often likened to the shape of a hockey stick [17] (Fig. 7.24). Rheumatic mitral disease is also associated with commissural fusion and sub-mitral involvement. Calcific MS typically

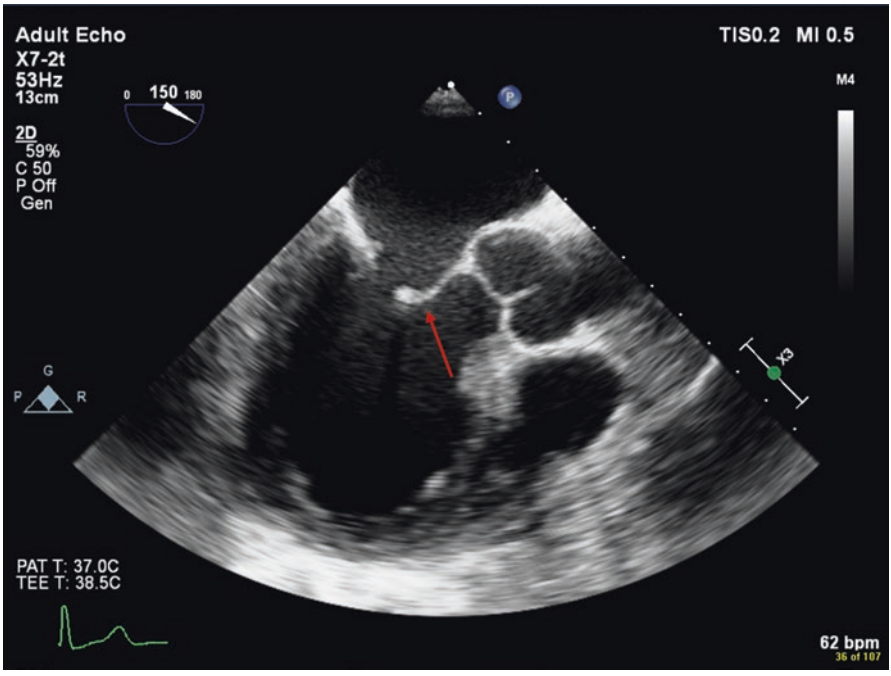


**Fig. 7.24** "Hockey stick" sign (red arrow) of the anterior mitral valve leaflet. This is characteristic of rheumatic mitral valve stenosis, indicating restriction of leaflet excursion during diastole

is due to extensive MAC that extends from the mitral annulus onto the mitral leaflets. Calcific MS is not typically associated with mitral commissural fusion and the leaflet tips are freely mobile; however, the sub-mitral apparatus may be calcified [17]. While rheumatic mitral disease is commonly associated with MR, calcific MS is less likely to be.

A comprehensive 2D examination of the mitral valve with and without CFD should be used to characterize MS. The ME views allow for assessment of the MV annulus, leaflet morphology, and function and are particularly helpful in grading the severity and extent of MAC. Using M-mode to characterize leaflet thickness and mobility is helpful when considering the etiology of MS, rheumatic, or calcific. Left atrial (LA) dilation should be noted and the left atrial appendage (LAA) should be interrogated, as patients with MS often have atrial fibrillation and are at elevated risk for developing LA or LAA thrombus. LAA blood flow velocity assessed using PWD less than 20 cm/s greatly increase the risk of thrombus formation and may require surgical or procedural LAA obliteration [18]. The transgastric views should be used to evaluate the sub-mitral apparatus, including any calcifications or restrictions of the chordae [3]. The orifice area of the mitral valve can be assessed using planimetry, PHT, the continuity equation, or PISA. Each has its limitations; 2D planimetry in the setting of MAC and/or leaflet calcification can overestimate the MVA, PHT is not reliable in the setting of severe AI or a dilated LV, and continuity equation is not reliable in situations with LVOT obstruction, severe MR, or atrial fibrillation, PISA is not reliable in the setting of atrial fibrillation, severe MR or AI, or in patients with prosthetic valves [3]. While the PHT has traditionally been favored as the most accurate in most settings, 3D planimetry is becoming popular as accuracy increases [17].

2D imaging of the mitral valve in the ME 4C view with CFD will reveal blood flow acceleration in the left atrium proximal to the valve and turbulent flow distally to the valve in the left ventricle. By adjusting the baseline velocity of the Nyquist limit in the same direction as the blood flow, PISA can be used to calculate the MV area (MVA) (Fig. 7.25). Spectral Doppler can be used to measure the mean and peak pressure gradients across the mitral valve from either the ME 4C or ME LAX view. CWD is typically used due to high blood flow velocity through stenotic lesion. To calculate the MVA, PHT can be measured from the associated CWD profile (Fig. 7.21) [12] (see Table 7.6).

When the 2D exam of the mitral valve is technically difficult, a 3D exam can bring clarity to the etiology and impact of a stenotic lesion. Restricted leaflets motion and leaflet and/or annular calcification can be visualized and more easily be communicated to the surgeon. From this same view, the LAA can also be assessed for thrombus. Adding CFD will reveal 3D flow acceleration in the left atrium proximal to the mitral valve and depending on the software package may allow for MVA measurements with 3D planimetry, which should be measured in mid-diastole [17] (Fig. 7.26).

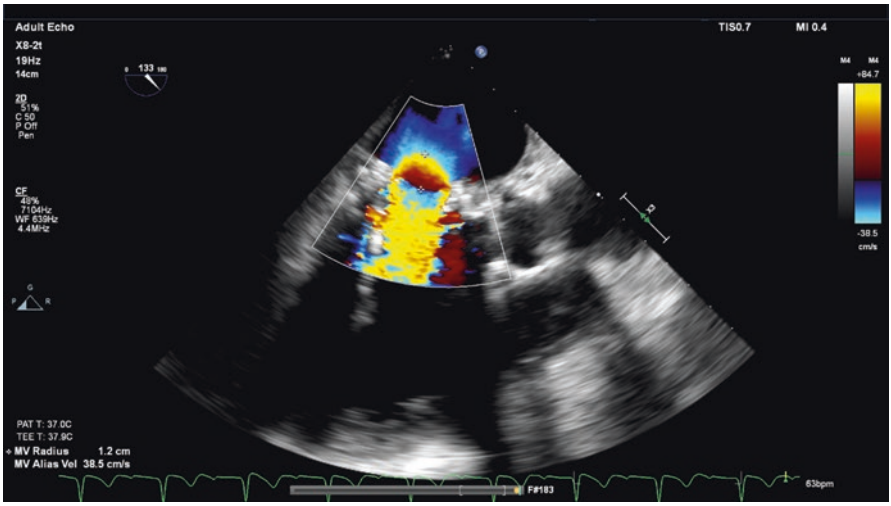


**Fig. 7.25** PISA to evaluate mitral stenosis. By using the PISA radius, MV aliasing velocity, and peak regurgitant jet velocity, one can calculate the MVA

**Table 7.6** EAE/ASE Guidelines for Grading Mitral Stenosis Severity [3, 12]

| Parameter | Normal | Mild | Moderate | Severe |
|---|---|---|---|---|
| Area ($cm^2$) | 4–6 | 1.5–2 | 1–1.5 | <1 |
| Mean PG (mmHg) | 0–5 | 5 | 5–10 | >10 |
| PHT (ms) | 40–70 | 70–150 | 150–200 | >220 |
| Systolic PAP (mmHg) | <30 | <30 | 30–50 | >50 |

*Mean PG* mean pressure gradient, *PHT* pressure half-time, *PAP* pulmonary artery pressure

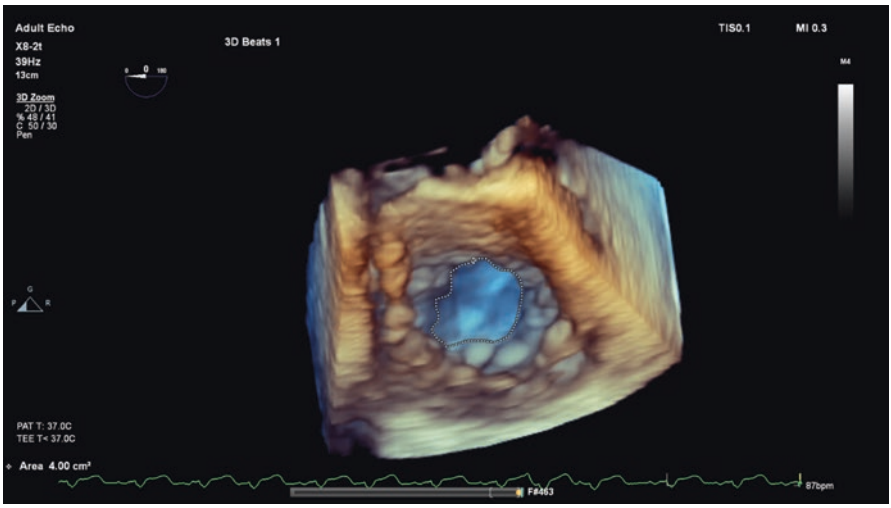


**Fig. 7.26** 3D Planimetry of the mitral valve. In this example, the patient has a normal MVA of 4 $cm^2$

### 7.5.3 *Mitral Regurgitation*

Nearly 40% of all adults have a trace amount of mitral regurgitation (MR) that does not require intervention [3]. MR is usually divided into structural/primary type and functional/secondary type. Primary MR is due to an abnormal mitral complex as the result of degenerative or rheumatic mitral valve disease or endocarditis, mitral annular dilation or MAC, chordae rupture or elongation or rupture of a papillary muscle. Secondary MR is associated with normal mitral complex anatomy and is most commonly due to LV dilation that results in mitral annular dilation, restricted systolic leaflet motion, and reduced or nonexistent coaptation of the anterior and posterior mitral leaflets [13]. A less common form of secondary MR is due to aortic stenosis and/or systolic anterior motion (SAM) of the AMVL leaflet and will be discussed later in this chapter.

MR is typically classified using the Carpentier Classification System (Fig. 7.27) and based on the MV leaflet motion [19]. Type I MR has *normal* mitral leaflet motion and is due primarily to annular dilation, leaflet vegetation or leaflet clefts. Type II MR has *excessive* leaflet motion and is typically due to leaflet prolapse. Type III MR is divided into two subtypes, Type IIIa and Type IIIb, both of which have *restricted* leaflet motion. Type IIIa has restricted leaflet motion throughout the cardiac cycle and often associated with MS. Type IIIb has restricted leaflet motion

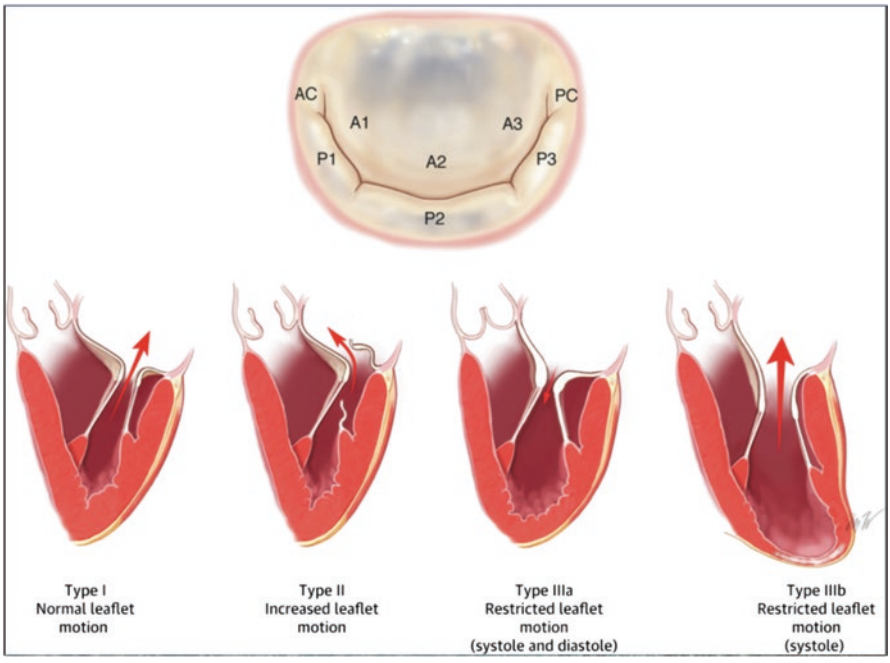


**Fig. 7.27** The Carpentier Classification System for describing mitral regurgitation [20]

during systole only and generally associated with secondary MR during LV remodeling and/or dilation [19].

The excessive mitral leaflet motion seen in Type ll MR can be divided into three types: billowing, prolapse, and flail (Fig. 7.28). Using this nomenclature when describing the various portions of the MV allows for more accurate description of the pathology. Billowing refers to when the leaflet body is above the plane of the mitral annulus but the coaptation point of the leaflet tips is below the annulus. Prolapse refers to when not only the body but also the leaflet tips are above the mitral annular plane. In this situation, the chordae are still stabilizing the leaflet tip to the point where they appear to be pointing toward the LV. Lastly, flail refers to when the leaflet body and tip are both above the annular plane but the leaflet tip is pointing toward the LA. This usually occurs with chordal or papillary muscle rupture [3].

Knowing the MR type (primary vs. secondary) and the Carpentier classification may help predict the direction and severity of the MR jet. In most cases, the jet will move toward a restricted leaflet and away from a leaflet with excessive motion. The exception to this heuristic is in the situation of SAM, in which the jet will course in the same direction as the leaflet with excessive motion [15]. As such, an anteriorly directed MR jet is most commonly associated with a prolapsed PMVL or a restricted AMVL. In this situation, the jet stays close to the atrial side of the AMVL and wraps around the LA. Depending on the severity of the lesion, the MR may result in blunting of systolic blood flow or even reversal in the right pulmonary vein (Fig. 7.29) [13].

Similarly, posteriorly directed jets are due to a prolapsed AMVL or a restricted PMVL. Under these circumstances, the jet will travel along the atrial side of the PMVL, wrap around the LA, and may result in blunting of systolic blood flow or reversal in the left pulmonary veins. On CFD, these atrial "wall hugging" jets occur as a result of the Coanda effect (Fig. 7.30), and most often appear to be high velocity jets, low area jets. Despite having a similar regurgitant volume and fraction as central MR jets, the Coanda effect traditionally underestimates the severity of eccentric MR jets because they have a smaller area on CFD [3]. Lastly, central MR jets are most commonly seen with secondary MR due to annular dilation or LV dilatation, but may also be seen with bileaflet prolapse [3]. Typically, the pulmonary venous flow pattern will be the same in all four pulmonary veins.

A comprehensive exam of mitral regurgitation includes 2D imaging with and without CFD. Ideally, the location and severity of all mitral regurgitant lesions are described using the Carpentier classification (see Table 7.7). The area of MR jet on CFD is directly correlated to the severity of the MR and can also be used to measure the vena contracta and to calculate the EROA using PISA (Fig. 7.31). PWD through the MV annulus can reveal a distinct blood flow velocity profile associated with either mild or severe MR. The E-wave represents early diastolic filling and generally is more pronounced in normal a MV inflow pattern. The A-wave follows the E-wave and represents atrial contraction. In the setting of severe MR, the E-wave is more pronounced, while in milder forms of MR, the A-wave is more pronounced [3].

Practically, this is not often done, as MR with significant LA dilation can lead to atrial fibrillation and loss of the A-wave. Additionally, the LA diameter should be

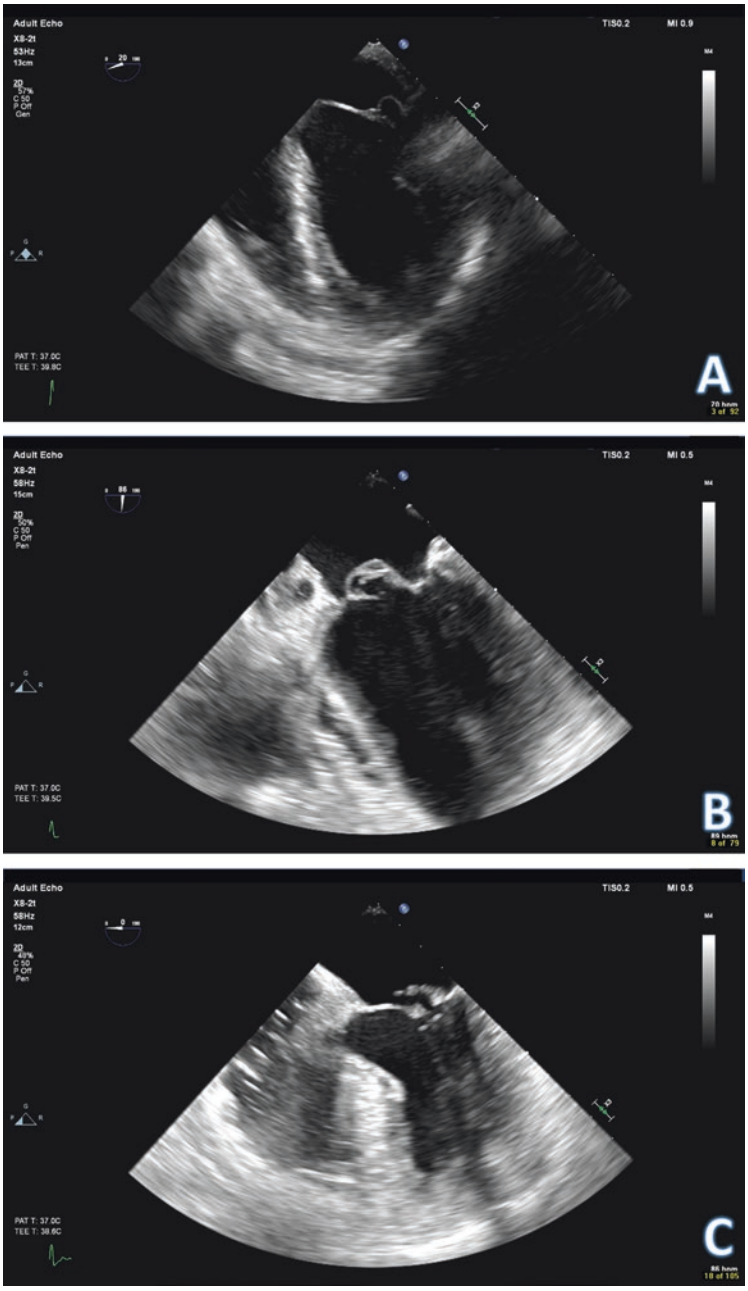


**Fig. 7.28** (**a–c**) (**a**) Billowing anterior mitral leaflet. (**b**) A prolapsing posterior mitral leaflet. (**c**) A flail posterior mitral leaflet

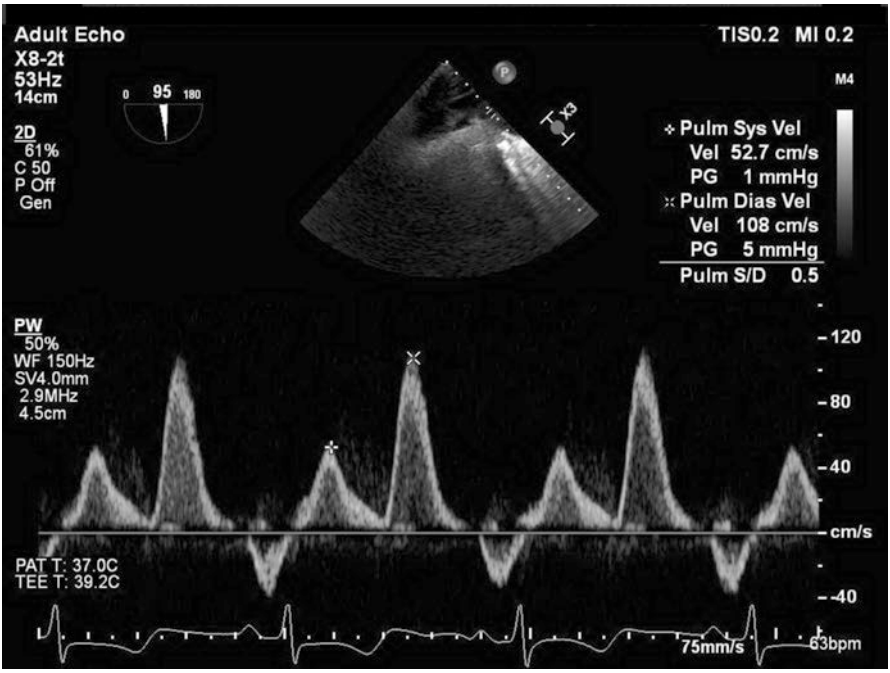


**Fig. 7.29** Pulmonary Venous Flow blunting. In a normal PVF tracing, the S-wave will be larger than the D-wave. Here, the S-wave is blunted, suggesting moderate MR

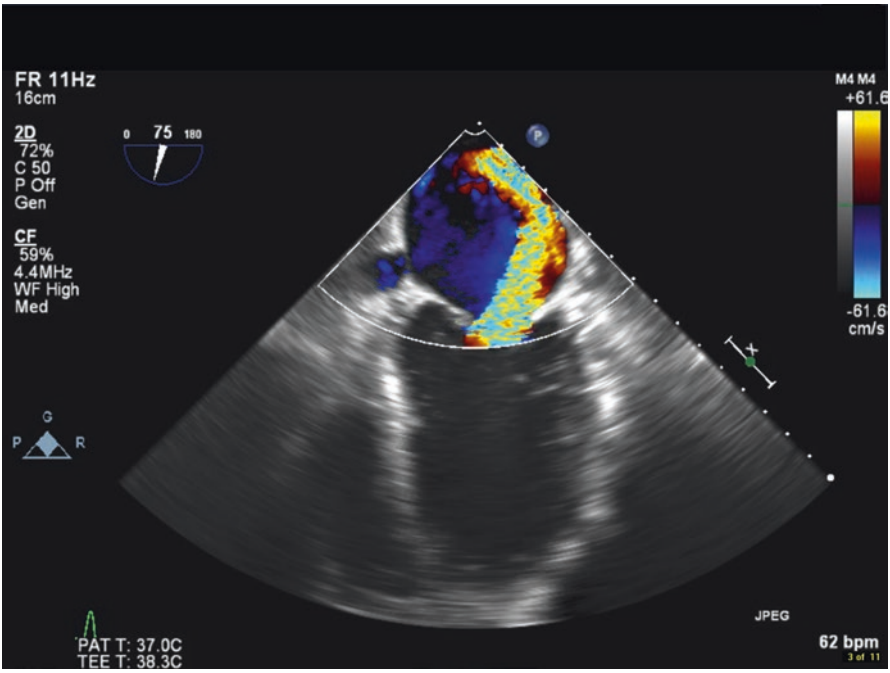


**Fig. 7.30** Severe MR. From this image, one can appreciate how the MR jet is hugging the wall of the left atrium, referred to as the Coanda Effect

**Table 7.7** AHA/ASE Guidelines for Grading Mitral Regurgitation Severity [3, 13]

| | Parameter | Mild | Moderate | Severe |
|---|---|---|---|---|
| Structural findings | *Leaflets* | Mild abnormality | Moderate abnormality or tenting | Severe valve lesion |
| | *LA size* | Normal | Mild dilation | Significant dilation |
| Qualitative | *CFD area* | Small | Intermediate | Large (>50% LA) or eccentric |
| | *Flow Convergence (cm)* (PISA radius, Nyquist 40 cm/s) | <0.3 | 0.3–1 | ≥1 |
| | *CWD Signal Strength* | Faint and parabolic | Partial and parabolic | Holodiastolic and triangular |
| Semi-qualitative | *VC (cm)* | <0.3 | 0.3–0.7 | ≥0.7 |
| | *PVF* | Normal S-wave | S-wave blunting | S-wave reversal |
| | *Mitral Inflow* | A-wave dominant | Variable | E-wave dominant *(>120 cm/s)* |
| Quantitative | *2D EROA (cm²)* | <0.2 | 0.2–0.39 | ≥0.4 |
| | *RegV (mL)* | <30 | 30–59 | ≥60 |
| | *RegF (%)* | <30 | 30–49 | ≥50 |

*LA* left atrium, *CFD* color flow Doppler, *PISA* proximal isovelocity surface area, *CWD* continuous wave Doppler, *VC* vena contracta, *PVF* pulmonary venous flow, *EROA* effective regurgitant orifice area, *RegV* regurgitant volume, *RegF* regurgitant fraction

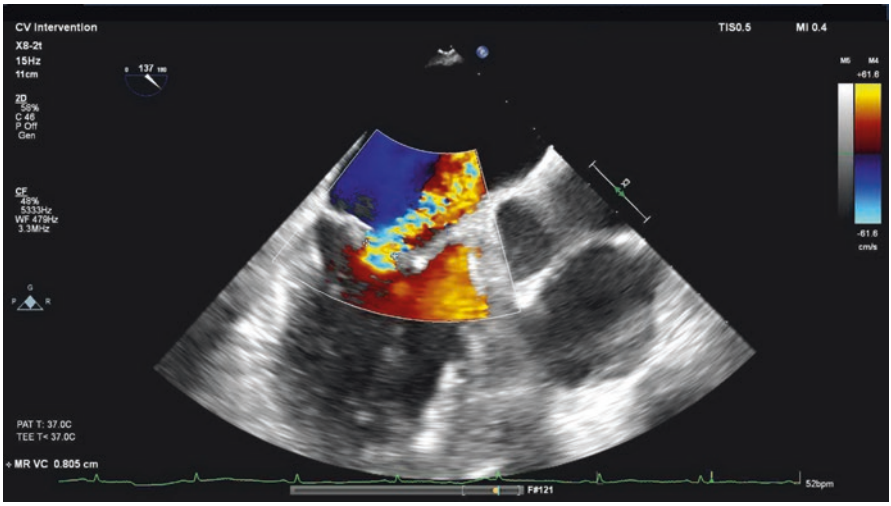


**Fig. 7.31** Mitral regurgitation vena contracta. This patient has a vena contracta width of 0.805 cm displayed in the bottom left-hand corner of the screen, consistent with severe MR

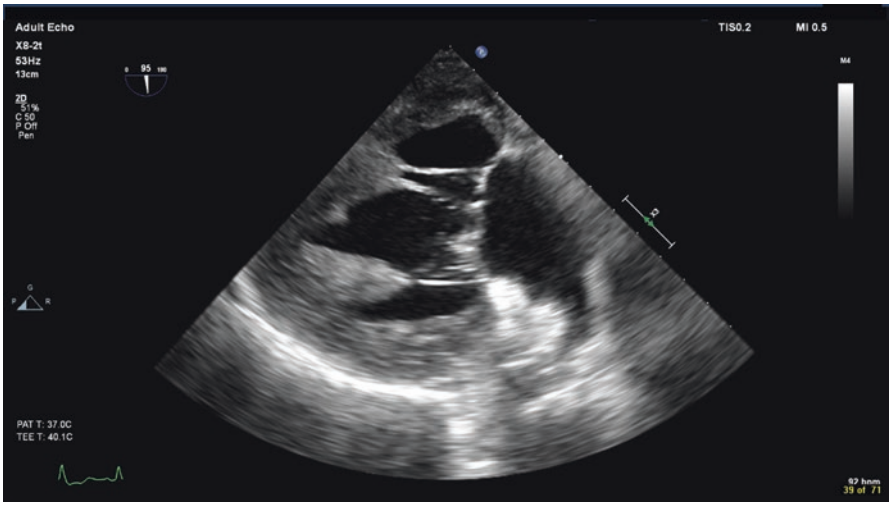


**Fig. 7.32** Transgastric 2 chamber view. One can appreciate in this image how the sub-mitral apparatus can be well-visualized and evaluated

noted as this may indicate chronicity of the disease [13]. The sub-mitral apparatus should be examined in the transgastric views to identify chordal or papillary muscle pathology (Fig. 7.32). Annular size and extent of MAC should also be evaluated, as this may impact the type of repair or replacement [15]. All four pulmonary veins should be examined with PWD to determine if there is systolic flow blunting or reversal, which helps grade severity. All of the leaflet segments should be identified and examined individually to determine the location of pathology [13]. The measures with the highest predictive value for MR severity are vena contracta, pulmonary vein systolic flow reversal, and any visualized structural defect in the valve [3].

The most common etiology of MR is a prolapsing P2 portion of the PML [21]. As the precise location and mechanism of P2 prolapse can be challenging to identify using 2D echo, 3D is now commonly used to characterize exact leaflet pathology including clefts, flail and prolapse, extent and severity of MAC or vegetation [22]. Additionally, CFD can be added to the 3D image to better characterize the number and direction of the MR jet(s). If the MR is severe or complex (multiple jets), consider rotating the 3D image so that one of the mitral commissures is in the near field and the other is in the far field. We prefer to have the posterior commissure (A3/P3) in the near field and anterior commissure (A1/P1) in the far field (Fig. 7.33). After using the plane crop feature to identify the location of the MR jet, the entire image can be rotated back to the surgeon's view to confirm what sections of the valve are the source of MR.

More recently, multiplanar reconstruction (MPR) is being utilized to determine 3D EROA and 3D vena contracta [15]. After acquiring a 3D dataset of the mitral valve with CFD, three orthogonal planes are aligned across the MR jet using MPR software when available (Fig. 7.34).

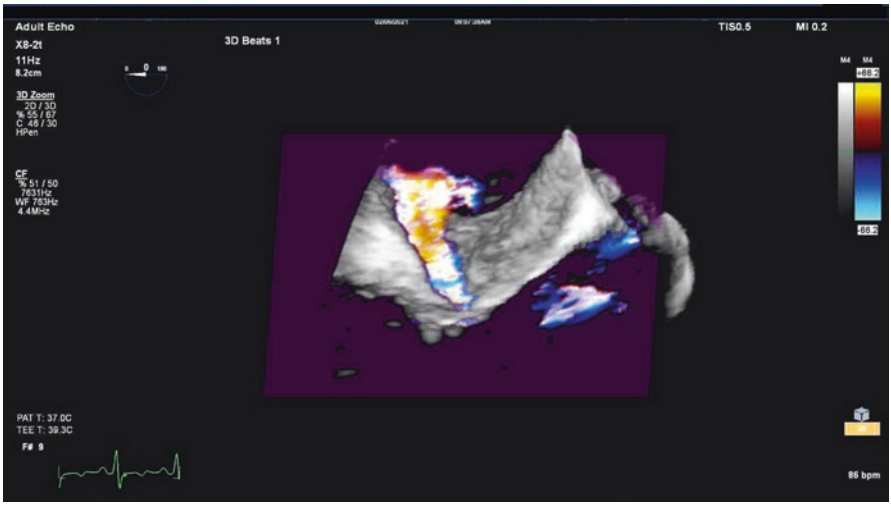


**Fig. 7.33** 3D MR assessment. The 3D MV with CFD can be cropped and manipulated to characterize the exact location of the MR jet. This is also useful for characterizing multiple jets and determining which jet is the most significant

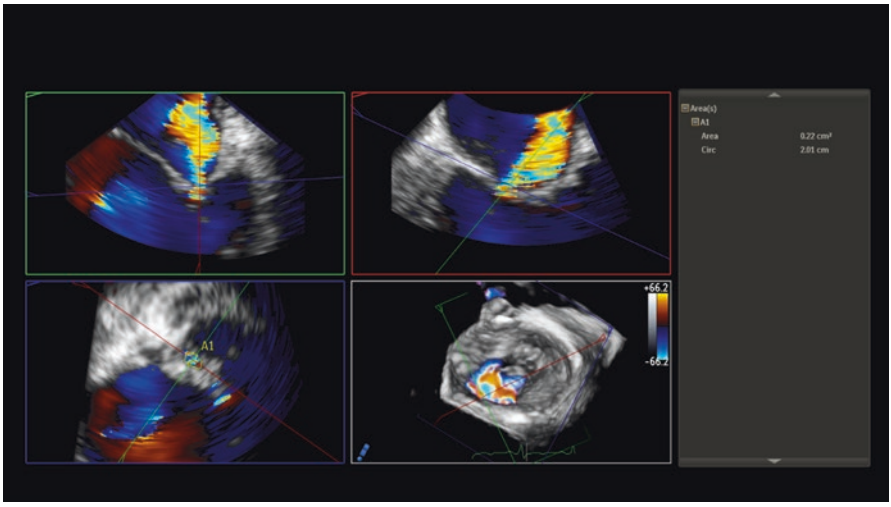


**Fig. 7.34** 3D MR EROA by multiplanar reconstruction. In this patient, the 3D EROA is 0.22 $cm^2$, which is consistent with mild-moderate MR

The most common MV disorders are fibroelastic mitral disease and Barlow's disease [15] (Table 7.8). Fibroelastic disease is a degenerative disease of aging that results in segmental mitral valve prolapse or flail and an associated eccentric MR jet. Unlike Barlow's disease, the mitral leaflets in fibroelastic disease are normal thickness. Barlow's disease secondary to mucopolysaccharide deposits associated

**Table 7.8** Fibroelastic disease vs. Barlow's disease [3]

| | Fibroelastic Disease | Barlow's Disease |
|---|---|---|
| Leaflets | Normal thickness | Thickened leaflets >4 mm |
| Segments | Isolated prolapse/*flail* segment | Prolapse of BOTH leaflets |
| MR jet | Eccentric | Central > eccentric |
| Annular dilation | +/− dilation | Dilation > 36 mm |
| Annular displacement | No displacement | Atrialization of leaflets (displacement into atrium) |
| Chordae | Rupture is common | Elongated and thickened but NOT ruptured |
| Repair | Simple repair | Complex |
| Associations | Aging | Secundum ASD |

with bileaflet mitral prolapse with central MR and is more common in younger individuals [3]. The chordae in patients with Barlow's disease are often elongated the extent that the mitral annulus is actually displaced toward LA [15].

## 7.6 Tricuspid Valve

The tricuspid valve (TV) is the atrioventricular valve between the right atrium and right ventricle with a normal area of 5–8 $cm^2$. Similar to the MV, the TV has an incomplete fibrous annulus, leaflets attached to chordae, and papillary muscles. The TV has ventricularly displaced annulus and three asymmetric leaflets (septal, anterior, and posterior). Unlike the MV, the TV annulus is not in fibrous continuity with its ventricular outflow valve (the pulmonic valve in this case) [3]. Due to its anterior location and orientation in the chest, the TV is not easily imaged or assessed by Doppler using transesophageal echocardiography.

A comprehensive TEE examination of the TV includes the ME 4C, ME 5C, ME coronary sinus, ME RV inflow-outflow, and ME-modified bicaval 2D views with and without CFD (Fig. 7.10) [4]. When assessing flow velocities and gradients across the TV, the modified bicaval view provides the most reliable Doppler alignment. The TG RV inflow and TG RV inflow-outflow views can be used to assess the sub-tricuspid apparatus [4]. Hepatic venous flow and flow reversal from TV regurgitation can be assessed using the TG hepatic vein view [13].

Correctly identifying the three TV leaflets can be challenging primarily due to their asymmetric nature. In the ME 4C, 5C, and coronary sinus views, the leaflet on the right side of the screen is the septal leaflet while the other leaflet is either the anterior or posterior leaflet depending on the position of the probe; if the probe is anteflexed in the 4C view, it is more likely the anterior leaflet; if the probe is retroflexed, it is more likely the posterior leaflet [3]. In the 5C view, the leaflet on the left side of the screen is the anterior leaflet while in the coronary sinus view, this leaflet on the left side of the screen is the posterior leaflet. In the ME RV inflow-outflow view, the leaflet on the left side of the screen is the posterior leaflet and the leaflet

**Table 7.9** Severity Grading of Tricuspid Stenosis [3, 12]

| Parameter | Mild | Moderate | Severe |
|---|---|---|---|
| Mean PG (mmHg) | ≤2 | 2–5 | ≥5 |
| EOA (Continuity) ($cm^2$) | >1.5 | 1–1.5 | ≤1 |
| Vmax (m/s) | | | >1.5 m/s |
| VTI (cm) | | | >60 cm |
| PHT (ms) | | | ≥190 |

*Mean PG* mean pressure gradient, *EOA* effective orifice area, *Vmax* peak velocity, *VTI* velocity time integral, *PHT* pressure half-time

on the right side of the screen is anterior leaflet, though it might be septal. If one turns the probe to the clockwise in this view, it is even more likely the anterior leaflet. In the modified bicaval view, the leaflet on the left side of the screen is usually the posterior leaflet and the leaflet on the right side of the screen is the anterior leaflet. If the probe is anteflexed, the left leaflet becomes septal. Finally, in the TG RV inflow view, the left leaflet is the anterior leaflet and the right leaflet is the posterior leaflet (Fig. 7.10) [3].

### *7.6.1 Tricuspid Stenosis*

Although isolated tricuspid valve stenosis is not a common valvulopathy in adults, the etiology is typically due to rheumatic disease, carcinoid disease, or an obstructing vegetation or tumor [12]. Tricuspid valve stenosis can be seen iatrogenically after TV annuloplasty and will be discussed later in this chapter. A comprehensive echocardiographic examination of rheumatic tricuspid valve disease should include a thorough assessment of the MV. Similarly, the pulmonic valve should be interrogated in the setting of carcinoid disease of the tricuspid valve [12].

Patients with TV stenosis will have turbulent blood flow through the valve best seen with CFD. The stenotic TV area can be calculated using the PISA method and the continuity equation (see Hemodynamic Calculations above) with similar cutoffs to the MV [12] (see Table 7.9). While appropriate Doppler alignment may be challenging, the modified bicaval view is often the ideal view for assessing blood flow velocities and calculating pressure gradients and VTIs across the TV (Fig. 7.35). According to the most recent ASE guidelines, PHT derived from the trans-TV VTI will not be accurate and should not be used in the setting of TV stenosis [12].

### *7.6.2 Tricuspid Regurgitation*

Tricuspid regurgitation (TR) is common in otherwise healthy adults; an estimated 85–90% of adults have trivial or physiologic TR [3]. Similar to the primary and secondary MR, primary TR is due to a structural abnormality of the TV annulus and

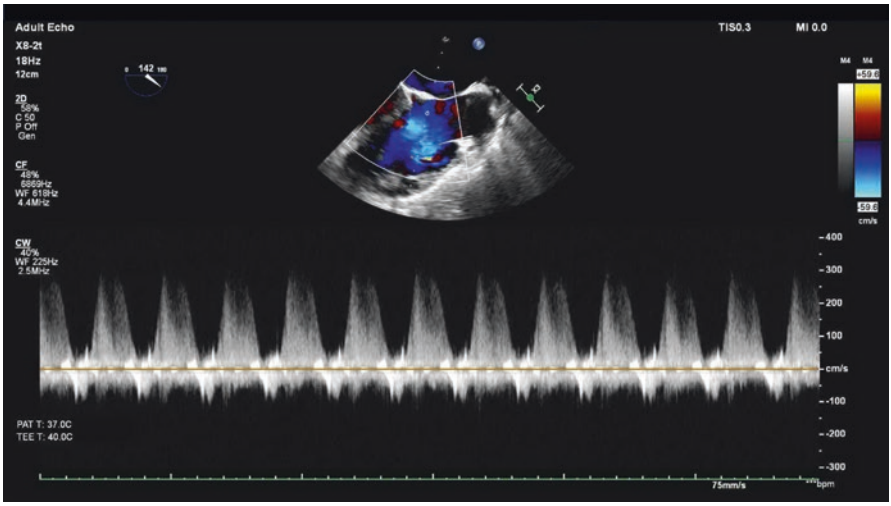


**Fig. 7.35** Continuous wave Doppler through the tricuspid valve from the modified bicaval view. This the tracing, one can measure the pressure gradient across the TV

leaflets while secondary TR is due to an abnormality of the sub-TV apparatus and surrounding structures. Primary TR may be the result of myxomatous or degenerative changes to the TV, rheumatic or carcinoid disease, or iatrogenic injury to the valve from pacing wires or pulmonary artery catheters [13]. TR secondary to repeated right ventricular post-transplant myocardial biopsies is not uncommon in heart transplant recipients. Secondary or functional TR is commonly due to dilatation of the TV annulus from RV distention and dysfunction. This may be secondary to pulmonary hypertension, LV dysfunction, or isolated RV failure [3].

The TV annulus diameter should be measured in the ME 4C view during diastole (Fig. 7.36). A normal diameter in this view is ≤3.5 cm. A diameter ≥4 cm usually warrants intervention [13]. There is a direct correlation between regurgitant blood flow on CFD and severity of TR (Fig. 7.37). Similarly, a more dense and triangular tracing using CWD across the TV is consistent with worsening TR severity. As part of a comprehensive exam of the TV, the number of regurgitant jets, their direction, and severity should be noted [3].

Severity of TR can be graded using the regurgitant jet area, vena contracta width, the EROA, and regurgitant volume [13] (see Table 7.10) PWD across the valve can also be useful for grading TR; mild TR is A-wave dominant while severe TR is E-wave dominant, with an E velocity > 1 cm/s [13]. Finally, hepatic venous flow pattern with S-wave reversal is indicative of severe TR. Lastly, though not part of the official grading system for TR, one can obtain PWD in the coronary sinus via the ME coronary sinus view. Significant systolic reversal of flow is suggestive of severe TR [13].

3D imaging of the TV, while sometimes challenging due to the distance of the valve from the TEE probe, can help elucidate leaflet pathology in the setting of TR [14]. Ideally, multibeat images with and without CFD are acquired during

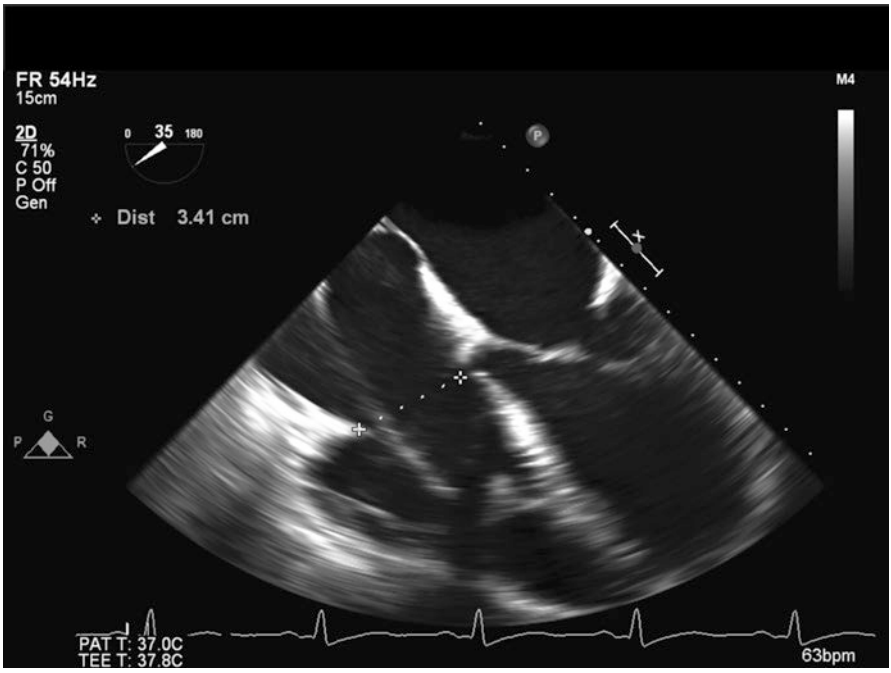


**Fig. 7.36** TV annulus measured during diastole. A normal diameter is ≤3.5 cm and a diameter >4 cm usually needs intervention. In this patient, the TV annulus diameter is 3.41 cm, which is in the normal range

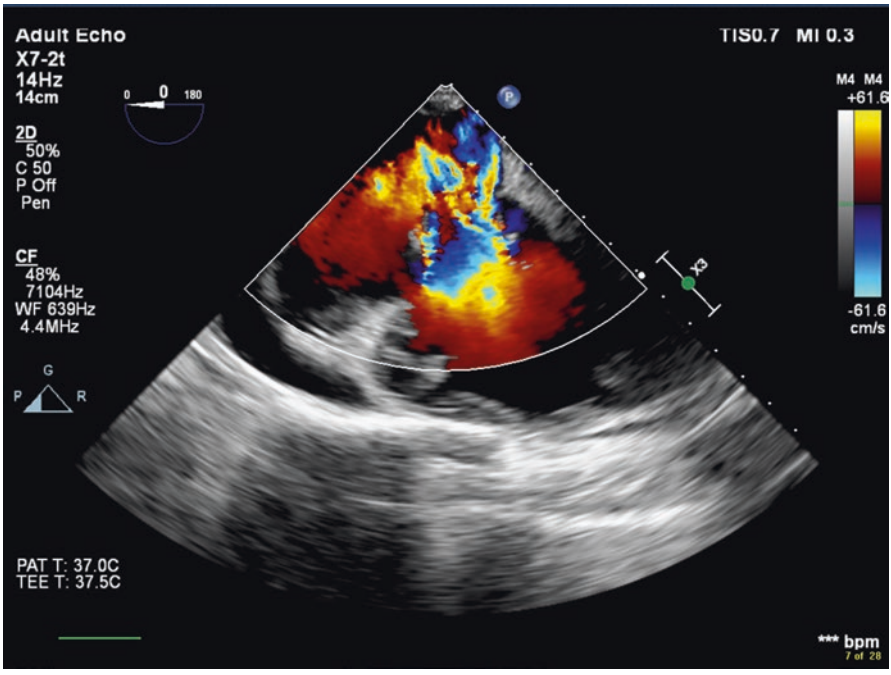


**Fig. 7.37** Severe TR with multiple jets and turbulence on CFD

**Table 7.10** ASE Guidelines for Tricuspid Regurgitation Severity [3, 13, 24]

| | Measurement | Mild | Moderate | Severe |
|---|---|---|---|---|
| Structural findings | Valve morphology | Normal or mildly abnormal | Moderately abnormal | Severe valve lesions |
| | Chamber size | Normal | Mild dilation | Severe dilation |
| | IVC diameter (cm) | <2 | 2.1–2.5 | >2.5 |
| Qualitative Doppler | Jet Area ($cm^2$) | <5 | 5–10 | >10 |
| | Flow Convergence | Small | Moderate | Large |
| | CWD | Soft, parabolic | Dense, variable | Dense, early peaking triangle |
| Semi-quantitative | CFD jet area ($cm^2$) | | | >10 |
| | VC width (mm) | <3 | 3–6.9 | ≥7 |
| | PISA Radius (cm) | ≤0.5 | 0.6–0.9 | >0.9 |
| | HVF | Normal | Systolic blunting | Systolic reversal |
| | TVI | A-wave dominant | Variable | E-wave dominant |
| | EROA ($cm^2$) | <0.2 | 0.2–0.4 | ≥0.4 |
| | RegV (mL) | <30 | 30–44 | ≥45 |
| | 3D VC Area ($cm^2$) | | | >0.61 |

*IVC* inferior vena cava, *CWD* continuous wave Doppler, *CFD* color flow Doppler, *VC* vena contracta, *HVF* hepatic venous flow, *TVI* tricuspid valve inflow, *EROA* effective regurgitant orifice area, *RegV* regurgitant volume

breath-holding after the patient is prepped and before surgical incision is made to avoid stitch artifact (Fig. 7.38) [4]. Depending on the software package, a 3D vena contracta can be measured and used for grading TR severity [23]. A 3D vena contracta area is >0.61 $cm^2$ which is consistent with severe TR [24].

### *7.6.3 Carcinoid Disease*

Carcinoid disease is typically due to serotonin deposits on the right-sided heart valves. The primary tumor is from gastrointestinal tumors that secrete serotonin; however, this is usually metabolized by the liver before it can reach the heart [25]. The typical patient who presents with carcinoid heart disease has had liver metastasis and therefore the serotonin is circulating outside the portal venous system. Serotonin is also metabolized in the lungs, which is why the left sided heart valves are not involved unless there is a connection between the chambers, such as a PFO, ASD, or VSD [25]. Carcinoid disease on the TV will present with not only TR but also TS, though the TR is typically graded worse than the TS. On echo, the leaflets are thickened and immobile due to endocardial plaques that form on the valve. These plaques can also be found on the pulmonic valve and within the RV chamber [25].

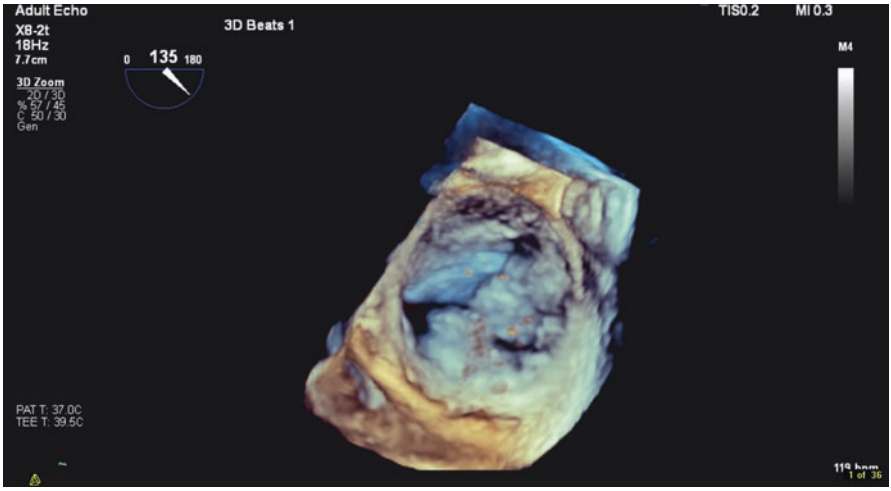


**Fig. 7.38** 3D acquisition of the tricuspid valve

## 7.7 Pulmonic Valve

The pulmonic valve (PV) is the right heart equivalent of the aortic valve; however, there are several key structural differences between the two. The pulmonary root includes the RV outflow tract (RVOT), pulmonary annulus, pulmonary valve, and the main pulmonary artery (MPA). Unlike the aortic valve, which is in fibrous continuity with the mitral valve, the PV and the tricuspid valve are not an intricately related complex as the RVOT occupies the infundibulum of the RV [13]. The PV tends to be slightly larger in area than the AV (3.5–4.5 $cm^2$ versus 3–4 $cm^2$) [1]. Additionally, the PV is positioned more anteriorly than the AV with thinner cusps. The PV has three semi-lunar cusps, known as the anterior, left, and right pulmonic cusps [13]. The pulmonic root also has a sinotubular junction, though it is not as pronounced as its aortic counterpart and does not have coronary sinus [3].

Due to the anterior position of the PV and its thin cusps, TEE imaging of the PV is not always easy (Fig. 7.39). The main views for 2D echo evaluation are the RV inflow-outflow view, in which the left cusp is visualized in the near field and the anterior cusps in the far field [3]. From the UE ascending aorta SAX view, the diameter of the MPA and right PA can be measured, as can blood flow velocities through the MPA using spectral Doppler [4]; however, due to the curving nature of the MPA, Doppler alignment is not always ideal from this view and the PV cusps are not always visible. Alternatively, the UE aortic arch SAX and the TG RV modified view may offer better alignment. In the UE aortic arch SAX view, one can visualize the left cusp on the left and the anterior cusp on the right [3]. Similar to the 2D view of the PV, 3D evaluation is not always obtainable. For the 3D acquisition, we the UE aortic arch SAX view with a narrow-angle acquisition or the ME 5C view with a wide-angle acquisition and crop the image to focus on the PV (Fig. 7.40) [4].

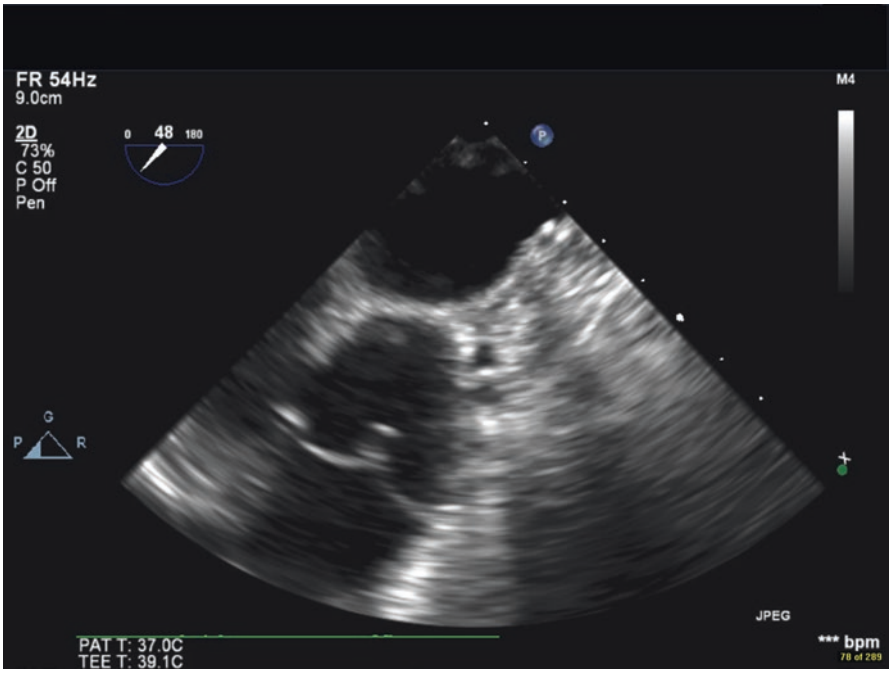


**Fig. 7.39** Pulmonic valve visualized from the UE aortic arch SAX view. From here, one can measure velocities and gradients across the PV due to excellent Doppler alignment

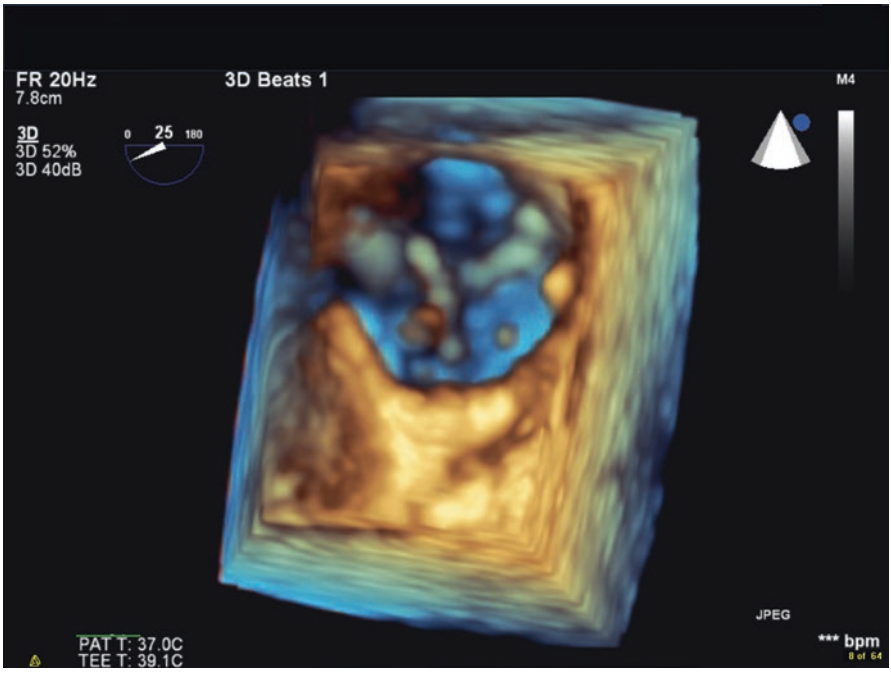


**Fig. 7.40** 3D view of the pulmonic valve. This image was acquired from the UE aortic arch SAX view and is the perspective from inside the main pulmonary artery looking through the valve into the RV infundibulum.

**Table 7.11** ASE Guidelines for Grading Pulmonic Stenosis Severity [3, 12].

| Parameter | Mild | Moderate | Severe |
|---|---|---|---|
| Vmax (m/s) | <3 | 3–4 | >4 |
| Peak PG (mmHg) | <46 | 36–64 | >64 |
| EOA (by Continuity) ($cm^2$) | | | <0.5 |

*Vmax* peak velocity, *Peak PG* peak pressure gradient, *EOA* effective orifice area

### *7.7.1 Pulmonic Stenosis*

Although uncommon, pulmonic stenosis (PS) can be caused by acquired such as rheumatic disease, carcinoid syndrome, calcifications, endocarditis, and restenosis of prosthetic pulmonic valves. Congenital heart disease presents earlier in life and these patients should be carefully examined for other concomitant congenital heart lesions [12].

On 2D echo evaluation, each view should be obtained with and without CFD. In addition, the RV, RVOT, and MPA should all be examined for changes related to the PS, namely concentric hypertrophy of the RV or eccentric hypertrophy in the setting of pulmonary insufficiency and RV volume overload [12]. The RVOT should be measured, with special note of the moderator band, as this can also become hypertrophied, resulting in a dynamic RVOT obstruction [3]. Post-stenotic dilation of the MPA > 2 cm is common in long-standing PS [3]. On CFD, the post-stenotic turbulence can be seen within the PA with elevated PA gradients. Grading of PS is primarily based on peak gradients and velocities [12] (see Table 7.11). The RV should be evaluated in the ME 4C view while RVOT obstruction is best viewed in the RV inflow-outflow view. The MPA diameter should be measured in the UE ascending aorta SAX or the aortic arch SAX view, while the aortic arch SAX view or TG modified RV view is ideal for the spectral Doppler exam (Fig. 7.41).

### *7.7.2 Pulmonic Insufficiency*

Unlike PS but similar to TR, pulmonic regurgitation (PI) is very common, seen in up to 75% of patients [13]. Most of this PI is physiologic and does not require intervention. Pathologic PI is divided into primary and secondary causes. The main primary causes include congenital lesions, rheumatic disease, carcinoid disease, and endocarditis. The secondary causes are usually due to pulmonary arterial pathology such as pulmonary hypertension or dilated pulmonary root complex resulting in distorted PV anatomy [3]. Correctly identifying the cause of the PI is crucial as this may impact surgical planning.

The same views used to assess PS apply when assessing PI with and without CFD (Fig. 7.10). The regurgitant jet should be noted for turbulence, direction, and number of jets. The proportion of the jet area compared to the RVOT area is important for grading the severity of PI (see Table 7.12). Acute PI can be distinguished

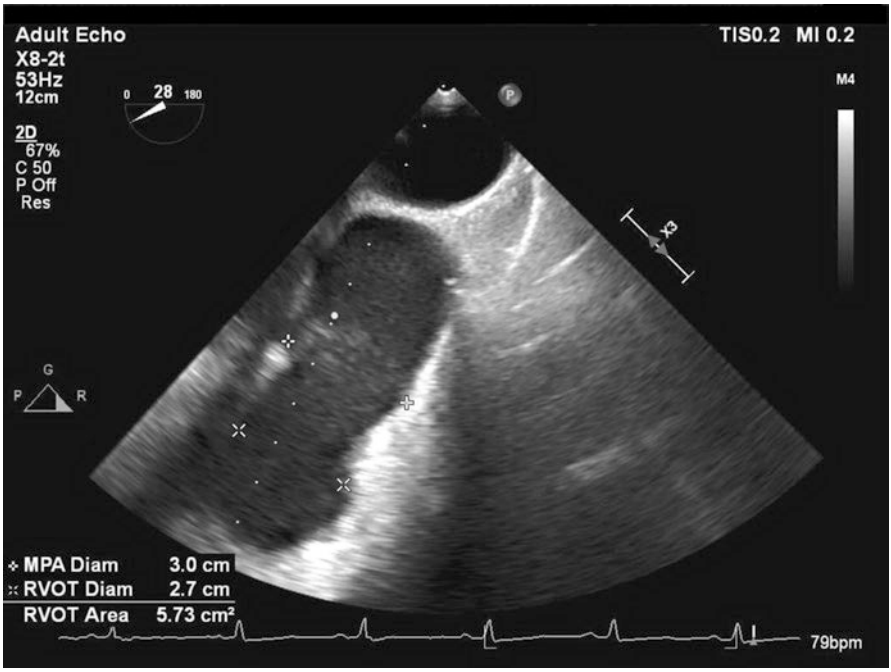


**Fig. 7.41** Measurements of the PA and RVOT from the UE aortic arch SAX view. In this patient, the RVOT and main PA measurements are in the normal range

**Table 7.12** ASE Guidelines for Grading Pulmonic Insufficiency Severity [3, 13]

| Parameter | Mild | Moderate | Severe |
|---|---|---|---|
| Pulmonic valve | Normal | Normal or abnormal | Abnormal or not visible |
| RV size | Normal | Variable | Dilated |
| CFD Jet Size (mm) | <10 | >10 | Broad origin |
| PR Jet:PV Annulus | | | >0.7 |
| DT (ms) | | | <260 |
| PHT (ms) | | | <100 |
| PR Index | | <0.77 | <0.77 |
| PA Diastolic Flow Reversal (PWD) | + | ++ | +++ |
| Qp:Qs | Slight increase | Intermediate | Greatly increased |
| RegF (%) | <20% | 20–40% | >40% |

*RV* right ventricle, *CFD* color flow Doppler, *PR* pulmonic regurgitation, *PV* pulmonic valve, *DT* deceleration time, *PHT* pressure half-time, *PR index* pulmonic regurgitation index, defined as PR signal duration divided by diastolic time, *PWD* pulsed wave Doppler, *Qp:Qs* ratio of pulmonary flow to systemic flow, measured as the ratio of pulmonary artery VTI:LVOT VTI, *RegF* regurgitant fraction

from chronic PI by the size of the RV; chronic PI is often associated with RV dilation due to volume overload [13]. The RVOT diameter should be measured in the ME RV inflow-outflow view and the MPA should be measured in the UE aortic SAX views. Spectral Doppler will have blood flow velocities moving away from the probe (under the baseline) and PHT or DT can be used to grade the severity of regurgitation similar to other valves [13]. Due to the anterior position of the PV in the chest and the difficulty in obtaining ideal Doppler alignment, grading the severity of PI may be difficult in some patients. For this reason, comparing the PA flow and the systemic flow via the ratio of the $VTI_{PV}$:$VTI_{AV}$ is a viable alternative [13].

## 7.8 Endocarditis

Endocarditis is technically an infection of the endocardium; however, its most common presentation is due to dysfunctional valves. The valves themselves are made of endocardium and are avascular, therefore, unable to mount an appropriate immune response to seeded bacteria. Conditions that make valves prone to infection include low-flow states and turbulent flow. Additionally, congenital valve disease and prosthetic valves are more prone to infection [26].

Diagnosis of endocarditis follows the Duke criteria, which consists of two major and six minor criteria. In order to make a diagnosis of endocarditis, either both major criteria, one major and three minor criteria, or five minor criteria must be met. The major criteria are positive blood cultures with endocarditis-causing microorganisms (*S. aureus*, *Candida*, HACEK group) and major echo findings consistent with endocarditis, which will be discussed. The minor criteria include a high-risk patient, fever over 38 °C, vascular complications, immunologic complications, microbiologic complications, and minor echo findings [27].

The major echocardiographic findings consistent with endocarditis include identification of vegetations on or around any one of the four valves, ranging in appearance from freely mobile echogenic masses to leaflet thickening and resulting in valve regurgitation and valve dehiscence [28]. The minor findings may be nodular thickening, non-mobile masses, or valve perforations [3]. It is important to note that non-surgical management of endocarditis is a common treatment plan for many patients. This can eradicate the infection and, if the valve lesions are minimal, may have no lasting effect on valve function; however, once a valve is infected, it is prone to re-infection in the future [3]. Furthermore, the valve itself becomes weakened and, therefore, may be more prone to perforations or dehiscence in the future without the presence of infection.

When evaluating the heart for endocarditis, a comprehensive examination of all valves is warranted, noting the size, location and number of vegetations, any pre-existing valvulopathies, the leaflet function, annular pathology, and any extra-valvular anomalies such as abscesses, fistulae, or pseudoaneurysms. Additionally, extrinsic devices, such as pacing leads and catheters, should also be interrogated for vegetations as these may need to be removed or replaced [3].

Vegetations are the most commonly associated complication of valvular endocarditis and consist of platelets, fibrin, and microbes [3]. On echo, vegetations will appear as a soft tissue density that are often hypermobile compared to the surrounding structures (Fig. 7.42). They move independently of the valve and surrounding myocardium and may result in obstruction of the valve. Most commonly, vegetations result in valvular insufficiency but if obstructive, it may cause stenotic effects [28].

The most commonly infected valve is the aortic valve, followed by the mitral, tricuspid, and pulmonic; however, a mitral valve vegetation is most likely to embolize. The most common risk factors for embolization are vegetation size >10 mm and attachment to the AMVL [10]. Another complication of vegetation is the seeding of bacteria on a downstream valve, known as a jet lesion. The most common jet lesion is from the aortic valve to the underside of the AMVL or the sub-mitral apparatus. Essentially, the regurgitant AV jet carries microbes and fibrin into the LVOT and seeds in these locations [28]. These lesions can harbor microbes if not removed but do not require a full valve replacement or repair—just clipping off the lesion is sufficient treatment. This should not be confused with a Node of Arantius or Lambl's excrescences, which are normal findings and do not require intervention [3] (Fig. 7.43).

Other major complications of endocarditis include valve dehiscence, abscess, fistula, and pseudoaneurysm formation. Valve dehiscence is more common with prosthetic valves but can be seen in native valves as well [28]. In the setting of a prosthetic valve, endocarditis can weaken the cartilaginous annulus in which the prosthetic valve sits resulting in the sutures securing the valve ring to fail. On echo, turbulent regurgitant flow is seen around the sewing ring and back through the annulus. The valve itself is described as having a "rocking motion" independent of the

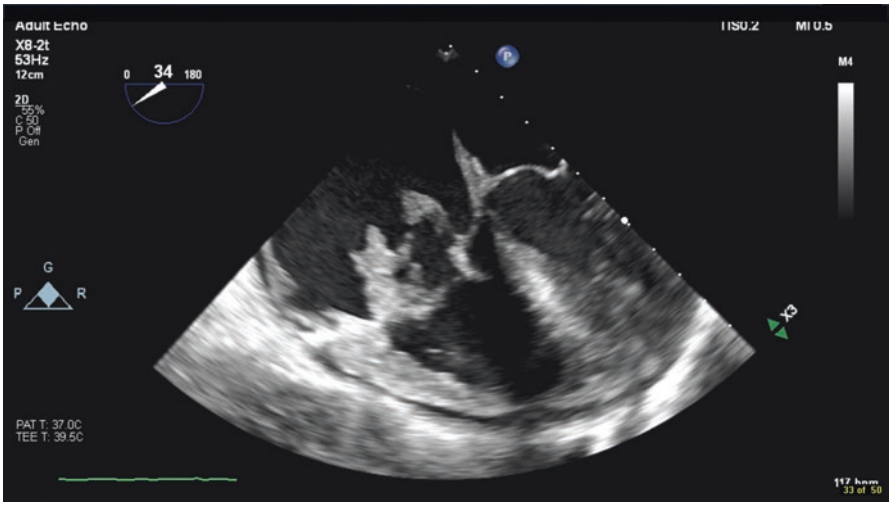


**Fig. 7.42** Tricuspid valve endocarditis with large, mobile vegetation. This valve lesion was complicated by severe TR in the setting of IV drug use

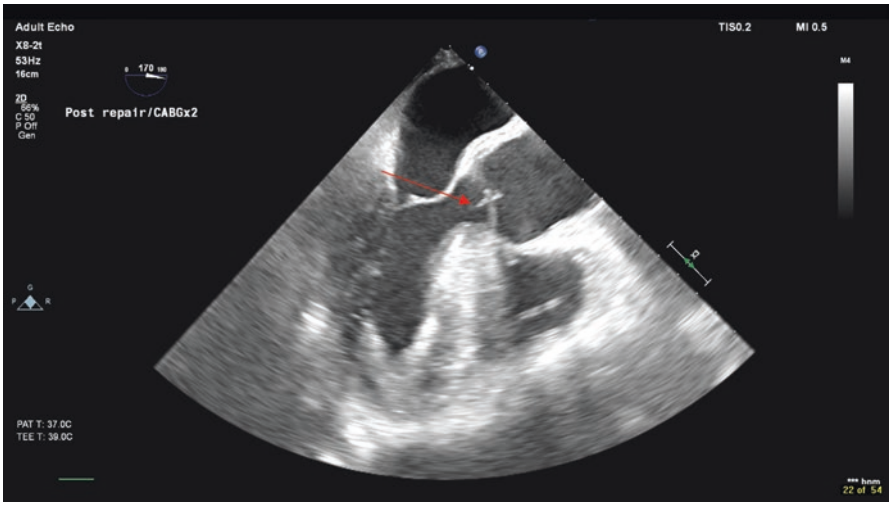


**Fig. 7.43** Lambl's excrescence (arrow) seen on the aortic valve. This is a normal finding and should not be confused for a vegetation. It often does not require surgical intervention

surrounding myocardium [28]. In some cases, failed sutures can be seen around the sewing ring and may be confused for mobile vegetations. An abscess is a cavity adjacent to the infected valve that may appear echo-dense or lucent but will not have flow on CFD because it does not communicate with the cardiac chambers. Unlike abscesses, a fistula connects two cardiac chambers and will have flow with CFD. Fistulas are often due to rupture of an abscess into a cardiac chamber [28]. Finally, pseudoaneurysms are an outpouching of the aortomitral fibrosa and are associated with AV or MV endocarditis. Similar to fistulas, pseudoaneurysms will contain blood flow by CFD [28]. During systole, pseudoaneurysms will expand while contracting during diastole [3]. Pseudoaneurysms are at risk for rupture and very poor outcomes.

## 7.9 Surgical Treatment of Valvular Disease

Once the valvular pathology has been identified, the decision to repair or replace a valve is made by a team of cardiologists and cardiac surgeons. The decision-making process for repairing or replacing a valve from the surgeon's perspective is discussed in other chapters of this text. For completeness, this section will discuss the echocardiographic findings and goals after a valve repair or replacement has been performed. This section will not discuss transvascular valve interventions, as these are discussed at length in other chapters of this text. The following includes a discussion of the similarities and differences between the surgical valve replacement options: mechanical valves vs. bioprosthetic valves.

### 7.9.1 Mechanical Valves

There are three major mechanical valve types: the ball-in-cage valve, the tilting disc valve, and the bileaflet valve. The ball-in-cage valve, also known as the Starr-Edwards, was discontinued in 2007 due to high transvalvular gradients and higher thromboembolic risk [3, 29]. It is included in this text because it is very durable, and some patients may still present with a ball-in-cage valve in place. A ball-in-cage valve consists of an occluder ball that is confined to a cage and its function depends on the pressure gradient between the two chambers it sits. It opens when the proximal pressure is greater than the distal pressure and closes when the distal pressure equilibrates or exceeds the proximal pressure [3]. It is characterized on echo with turbulent flow on CFD and a high profile, projecting above the true aortic annulus. Due to the high profile, imaging may be difficult in the mid-esophageal views, as it has significant acoustic shadowing [3]. Unlike the other mechanical valves, the ball-in-cage does not have washing jets, which are important for preventing valve thrombosis [29].

The tilting disc mechanical valve has a single disc that opens based on the pressure gradient between chambers. The most commonly used tilting disc valve are the Medtronic-Hall and the Sorin Allcarbon valves. This type of valve can be identified on echo with CFD by having a major and minor orifice of antegrade flow and three retrograde washing jets [29]. The Medtronic-Hall has a unique large central washing jet with smaller jets at the occluding disc periphery. These washing jets help prevent static flow near the valve surface to mitigate the risk of thrombus formation [29]. The tilting disc mechanical valve is approved in the United States for the mitral position only but approved in Europe for the mitral and aortic position.

The mechanical bileaflet valve is produced by St. Judes, Carbomedics, and On-X. Though they use the same mechanism, they have different flow patterns to be recognized on echo. The bileaflet valve has the most regurgitation of all mechanical valves, though anything greater than mild is abnormal [3]. Additionally, it requires the lowest pressure gradient among the mechanical valves to open. The mechanical bileaflet has two major orifices and one minor orifice and will typically have four washing jets seen on CFD (Fig. 7.44). The St. Jude valve is characterized by divergent washing jets while the On-X valve has convergent washing jets [29]. Bileaflet mechanical valves are approved for both the mitral and aortic position.

A comprehensive echocardiographic evaluation of mechanical valves should include 2D exam with and without CFD, assessing for a well-seated valve with symmetric leaflet excursion and normal washing jet patterns [3]. CFD is used to evaluate for laminar antegrade flow and to measure the peak and mean pressure gradients across the mechanical valve (see Table 7.13). A mechanical valve should have characteristic washing jets inside the sewing ring; if regurgitant flow is seen outside the sewing ring, a paravalvular leak (PVL) should be suspected [3]. Though PVLs may be traced to mild in nature, these can result in hemolysis over time. Of note, very small PVLs that may be visible immediately after separating from cardiopulmonary bypass often resolve after administration of protamine. The use of 3D

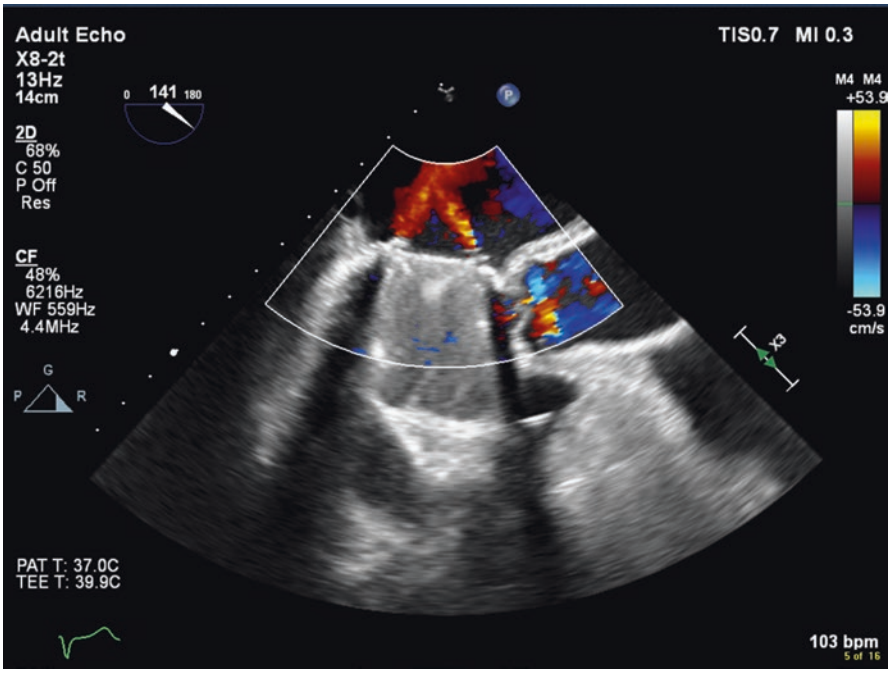


**Fig. 7.44** Mechanical bileaflet prosthetic valve in the mitral position. Normal washing jets can be seen at the periphery within the sewing ring. These washing jets are important for preventing thrombus formation on the leaflets

**Table 7.13** Normal range of mean pressure gradients across prosthetic heart valves [3]

| | Mitral Position | | | Aortic Position | | |
|---|---|---|---|---|---|---|
| Valve Type | Vmax (m/s) | Pmax (mmHg) | Pmean (mmHg) | Vmax (m/s) | Pmax (mmHg) | Pmean (mmHg) |
| Ball-cage | 1.9 ± 0.4 | 14 ± 5 | 5 ± 2 | 3.2 ± 0.6 | 38 ± 11 | 23 ± 8 |
| Bileaflet | 1.6 ± 0.3 | 10 ± 3 | 4 ± 1 | 2.4 ± 0.3 | 25 ± 5 | 12 ± 6 |
| Tilting disc | 1.6 ± 0.3 | 10 ± 2 | 3 ± 2 | 2.5 ± 0.6 | 23 ± 8 | 14 ± 5 |
| Bovine pericardium | 1.8 ± 0.2 | 12 ± 3 | 6 ± 2 | 2.5 ± 0.5 | 23 ± 8 | 14 ± 5 |
| Porcine heterograft | 1.5 ± 0.3 | 9 ± 3 | 4 ± 2 | 2.4 ± 0.4 | 23 ± 7 | 11 ± 2 |
| Stentless bioprosthetic | | | | 2.2 | 19 | 3 ± 1 |

*Vmax* peak velocity, *Pmax* peak pressure gradient, *Pmean* mean pressure gradient

echo with CFD can facilitate further evaluation and localization of PVL (Fig. 7.45) [30].

The EOA and dimensionless index should be evaluated for mechanical valves in the aortic position [29]. Additionally, the mitral valve and LVOT should be evaluated for SAM, an indication that an aortic mechanical valve is an undersized [3].

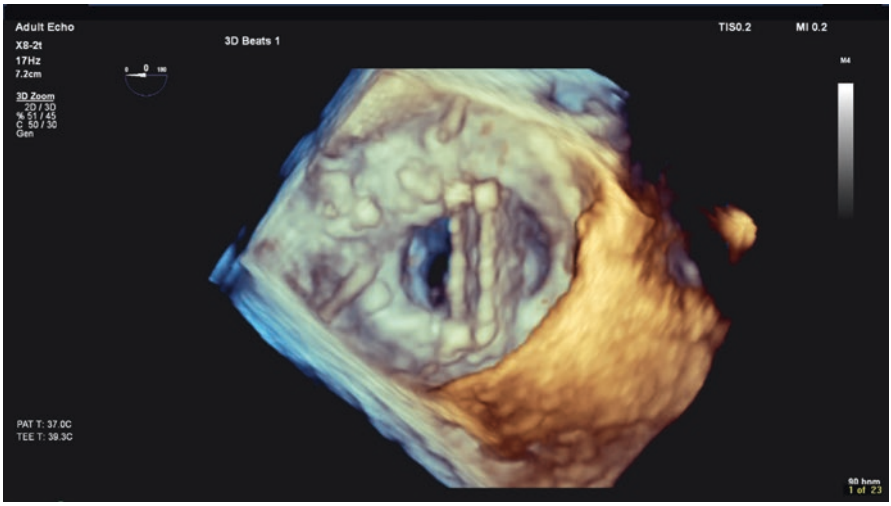


**Fig. 7.45** 3D view of bileaflet St. Jude mechanical valve in the mitral position. Notice how both leaflets are opening appropriately during diastole in the anti-anatomic position

Due to significant acoustic shadowing, a mechanical valve in the AV position would be best evaluated from the transgastric view. On the other hand, a mechanical valve in the mitral position is well visualized in the mid-esophageal view. For prosthetic mitral valves, the LVOT should be evaluated for obstruction due to a misplaced stitch or malpositioned valve strut. Lastly, for any mitral procedure, LV regional wall motion should be assessed prior to placement and after, as the left circumflex artery travels close to the mitral annulus and can be damaged by an anchoring stitch [3].

### *7.9.2 Bioprosthetic Valves*

Bioprosthetic valves are usually made of porcine valves or bovine pericardium and come in three varieties: stented, stentless, and homograft. Stented bioprosthetic valves are the most common and can be used for any of the four heart valves [29], unlike mechanical valves, which are not typically used on the right heart valves, due to low-pressure gradients and increased risk of thrombosis [3]. Similarly, the stentless bioprosthetic valve and a homograft can only be implanted in the aortic position. The advantage of a stentless valves or homografts is their larger effective orifice when compared with a stented valve [3]. All bioprosthetic valves have three symmetric leaflets with a small central gap at the coaptation point. This gap is more prominent in bovine pericardial valves, resulting in mild valvular regurgitation following implantation; however, the leaflets eventually soften and this regurgitation may resolve over time.

As with mechanical valves, a comprehensive echocardiographic evaluation of bioprosthetic valves should include 2D echo with and without CFD. Bioprosthetic valves should be well-seated and all three leaflets assessed for proper motion. No washing jets are expected in or around bioprosthetic valves, so any regurgitation within the sewing ring outside of trace to mild should be investigated further. Bioprosthetic valves have much less acoustic shadowing compared with mechanical valves, making them easier to evaluate in the mid-esophageal view (Fig. 7.46) [30]. With CFD, the valve should be evaluated for laminar antegrade flow and the absence of PVLs. CWD should be obtained across the valve to measure the mean and peak pressure gradients (see Table 7.13). The gradient across a bioprosthetic valve is expected to be lower than a corresponding mechanical valve. Again, for valves in the aortic position, the LVOT and MV should be evaluated for SAM in addition to calculating the EOA and dimensionless index. Similarly, evaluation of valves in the mitral position should also examine the LVOT for any struts and the LV wall motion in for left circumflex artery injury [3].

### *7.9.3 Aortic Valve Replacement and Repair*

A comprehensive assessment similar to that described for the native aortic valve is warranted following an aortic valve replacement or repair. The gradient across a newly replaced aortic valve is often significant in the immediate post-bypass period and normalizes with time. Regardless, all replaced or repaired valves should be

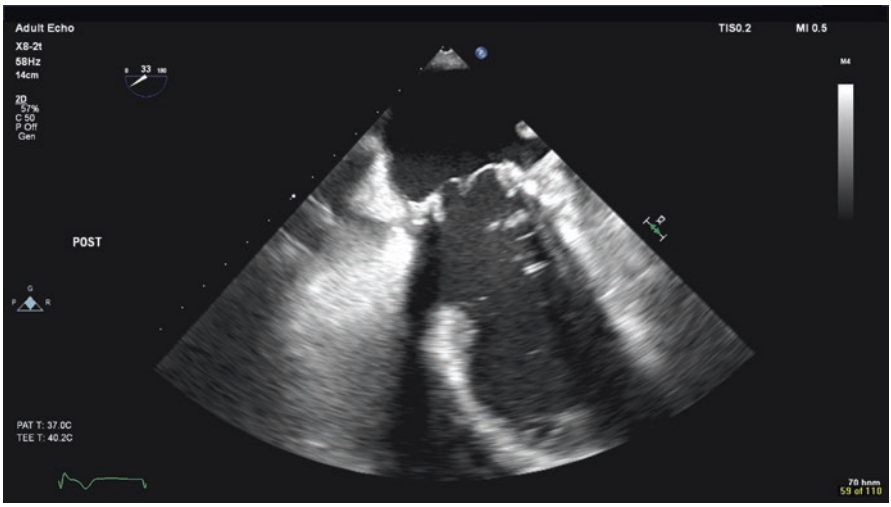


**Fig. 7.46** Bioprosthetic valve in the mitral position. Compared to mechanical valves, much less acoustic shadowing is seen and the LV can be assessed more easily from the mid-esophageal views

assessed for mean pressure gradient, peak velocity, dimensionless index, effective orifice area (EOA), and acceleration time [29]. See Table 7.14 for normal values.

Replaced aortic valves should be assessed for regurgitation. As previously mentioned, mechanical valves should have normal washing jets and bioprosthetic valves may have trace to mild insufficiency [29]. These are normal findings and do not require intervention. Regurgitation beyond these normal phenomena or regurgitant jets outside the sewing ring are concerning for dysfunctional leaflets and PVL, respectively, and must be communicated with the surgeon [30]. See Table 7.15 for grading of prosthetic AV regurgitation.

Patient-Prosthetic Mismatch (PPM) is a serious complication of aortic valve replacement. PPM occurs when the effective orifical area of a given aortic valve replacement is not adequate to cover the body surface area, resulting in high a transvalvular gradient [29]. PPM more common in smaller patients undergoing AV replacement, but can be seen with the mitral valve as well. PPM can be avoided by performing a root enlargement procedure and placing a larger valve, but untreated PPM is associated with decreased survival. A normal EOA:BSA ratio is > 0.85 but < 0.65 is considered severe PPM [29] (see Table 7.16).

**Table 7.14** Prosthetic Aortic Valve Stenosis [29]

| Parameter | Normal | Possible Stenosis | Significant Stenosis |
|---|---|---|---|
| CWD | Triangular | Intermediate | Parabolic |
| Vmax (m/s) | <3 | 3–4 | >4 |
| Mean PG (mmHg) | <20 | 20–35 | >35 |
| Dimensionless Index | ≥0.3 | 0.25–0.29 | <0.25 |
| EOA ($cm^2$) | >1.2 | 0.8–1.2 | <0.8 |
| Acceleration Time (ms) | <80 | 80–100 | >100 |

*CWD* continuous wave Doppler, *Vmax* peak velocity, *mean PG* mean pressure gradient, *EOA* effective orifice area

**Table 7.15** Prosthetic Aortic Valve Insufficiency [29]

| | Mild | Moderate | Severe |
|---|---|---|---|
| Valve appearance | Normal | Abnormal | Abnormal |
| LV size | Normal | Mild dilation | Severe dilation |
| Vena contracta (cm) | <0.3 | 0.3–0.6 | >0.6 |
| Jet:LVOT ratio | <0.25 | 0.26–0.64 | ≥0.65 |
| CWD density | Faint | Dense | Dense |
| PHT (ms) | >500 | 200–500 | <200 |
| LVOT flow vs. PA flow | Slight increase | Intermediate | Large increase |
| Descending aorta diastolic flow reversal | Brief | Intermediate | Holodiastolic |
| RegV (mL) | <30 | 30–59 | ≥60 |
| RegF (%) | <30 | 30–49 | ≥50 |

*LV* left ventricle, *LVOT* left ventricular outflow tract, *CWD* continuous wave Doppler, *PHT* pressure half-time, *PA* pulmonary artery, *RegV* regurgitant volume, *RegF* regurgitant fraction

**Table 7.16** Diagnosis of Patient-Prosthetic Mismatch [28, 30]

| | | Normal | Mild-moderate PPM | Severe PPM |
|---|---|---|---|---|
| EOA/BSA ($cm^2/m^2$) | AVP | >0.85 | 0.65–0.86 | <0.65 |
| | MVP | | | <1.2 |

*EOA* effective orifice area, *BSA* body surface area, *PPM* patient-prosthetic mismatch, *AVP* aortic valve prosthesis, *MVR* mitral valve prosthesis

**Table 7.17** Prosthetic mitral valve stenosis [28, 30]

| Parameter | Normal | Possible Stenosis | Significant Stenosis |
|---|---|---|---|
| Vmax (m/s) | <1.9 | 1.9–2.5 | ≥2.5 |
| Mean PG (mmHg) | ≤5 | 6–10 | >10 |
| $VTI_{MV}/VTI_{LVOT}$ | <2.2 | 2.2–2.5 | >2.5 |
| EOA ($cm^2$) | ≥2 | 1–2 | <1 |
| PHT (ms) | <130 | 130–200 | >200 |

*Vmax* peak velocity, *mean PG* mean pressure gradient, $VTI_{MV}$ velocity time integral through the mitral valve, $VTI_{LVOT}$ velocity time integral through the left ventricular outflow tract, *EOA* effective orifice area, *PHT* pressure half-time

In some patients, AV repair is a viable alternative to replacement. The benefits of AV repair when compared with replacement include better durability, flow mechanics as well as the avoidance of anticoagulation. For a discussion of the various types of AV repair procedures, please see the corresponding chapters in this text.

Echo evaluation for AV repair should include aortic root measurements found in the ME LAX view. These include assessment of aortic leaflet morphology, motion and calcification, ascending aortic anatomy and size as well as extent of calcium or plaque [3]. 2D with CFD should be used to assess for AI. After the repair, the AV should be closely scrutinized for the coaptation length and height. The cusps should remain above the annular plane and minimal AI should be present. Of course, all other measures with spectral Doppler should also be utilized to rule out any stenosis [3].

### *7.9.4 Mitral Valve Replacement and Repair*

Similar to AV replacement, the echo exam of a prosthetic MV should be the same as the native MV. Though significant shadowing from the prosthetic valve can make LV assessment difficult from the ME views, the echo probe should have good alignment to evaluate the MV. The 2D and 3D exam should be performed to evaluate for stenosis or regurgitation (see Tables 7.17 and 7.18) [30].

Any regurgitation outside the sewing ring should raise suspicion for a PVL and can be accurately localized using 3D echo with CFD. With the AV positioned at 12 o'clock, the location of the PVL should be described using a clockface descriptor [30].

Repair of the MV is becoming more common as surgical techniques become more specialized. The most common repair is placement of a MV annuloplasty ring

**Table 7.18** Prosthetic mitral valve regurgitation [28, 30]

| | Measurement | Mild | Moderate | Severe |
|---|---|---|---|---|
| Structural findings | LV size | Normal | Variable | Dilated |
| | Prosthetic valve | Normal | Abnormal | Abnormal |
| Doppler parameters | CFD Jet Area | <4 $cm^2$<br><20% LA area | 4–8 $cm^2$<br>20–40% LA area | >8 $cm^2$<br>>40% LA area |
| | Flow convergence | Minimal | Intermediate | Large |
| | CWD | Faint, parabolic | Dense, parabolic | Dense, triangular, early peaking |
| | PVF | Normal | Systolic blunting | Systolic reversal |
| Quantitative parameters | VC (cm) | <0.3 | 0.3–0.6 | ≥0.6 |
| | RegV (mL) | <30 | 30–59 | ≥60 |
| | RegF (%) | <30 | 30–49 | ≥50 |
| | EROA ($cm^2$) | <0.2 | 0.2–0.49 | ≥0.5 |

*LV* left ventricle, *CFD* color flow Doppler, *LA* left atrium, *CWD* continuous wave Doppler, *PVF* pulmonary venous flow, *VC* vena contracta, *RegV* regurgitant volume, *RegF* regurgitant fraction, *EROA* effective regurgitant orifice area

with a quadrangular resection and sliding plasty of the defected posterior mitral leaflet. For a more detailed discussion of MV replacement surgical techniques, please refer to the corresponding chapter in this text.

The risk of systolic anterior motion (SAM) of the anterior mitral leaflet into the LVOT is important to predict prior to any MV repair. SAM occurs when blood flow velocity increases in the LVOT during systole and the pressure on the LVOT side of the AMVL is less than the pressure on the LA side of the leaflet, also known as the Venturi effect. This pressure differential causes the AMVL to be "pulled" into the LVOT, leading to a dynamic LVOT obstruction. As the pressure differential becomes more severe and the AMVL is pulled further into the LVOT during the systolic phase of the cardiac cycle, MR will correspondingly worsen. MR due to excessive leaflet motion is Type II MR however, unlike MR due to prolapse or flail, the MR jet is in the opposite direction of the leaflet of excessive motion.

The most predictive measurements to forecast SAM after MV repair are the AMVL leaflet length, PMVL length, septal leaflet contact length (C-Sept), and the aortomitral angle [3, 31] (see Table 7.19 for values) (Fig. 7.47). An AMVL:PMVL ratio > 3 and a C-Sept distance > 3 cm are considered low risk for SAM post-bypass [3]. SAM after MV repair can be treated by increasing afterload and/or preload and increasing LV filling time. If these maneuvers are not successful, a modification of the repair or an edge-to-edge repair (Alfieri stich) should be considered.

Other complications of MV repair or replacement include new regional wall motion abnormalities and atrioventricular groove disruption. As previously mentioned, the left circumflex artery traverses in close proximity to the MV annulus and

**Table 7.19** Risk Factors for Post-MV Repair SAM

| Patient Factors | | Procedure Factors |
|---|---|---|
| *Parameter* | *Measurement* | Small MV replacement or annuloplasty<br>PMVL length remains > 15 mm |
| Aortomitral angle | <120° | |
| C-sept (mm) | <25 mm | |
| PMVL length | >15 mm | |
| Basal IVS diameter | >15 mm | |
| AMVL/PMVL length ratio | ≤1.3 | |
| LV hyperkinesis | | |
| Anterior displaced papillary muscles | | |

*C-sept* distance between the interventricular septum and mitral leaflet coaptation point, *MV* mitral valve, *AMVL* anterior mitral valve leaflet, *PMVL* posterior mitral valve leaflet, *IVS* interventricular septum, *LV* left ventricle

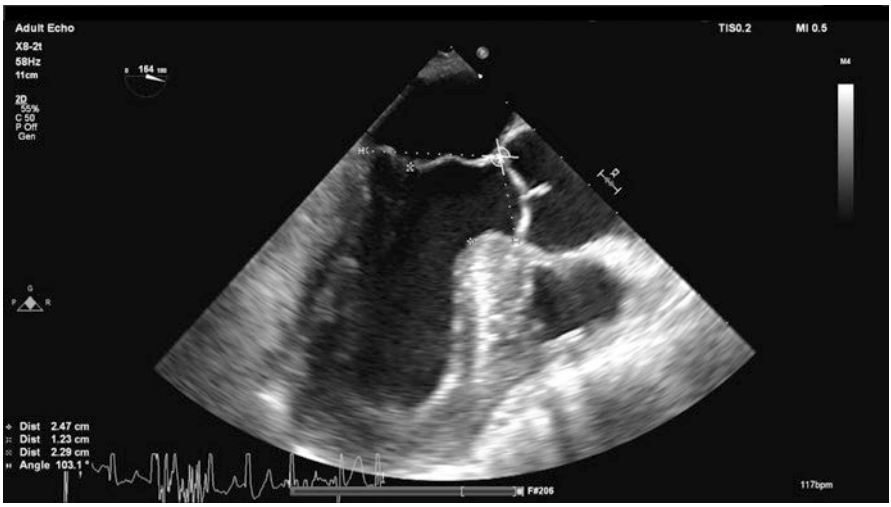


**Fig. 7.47** Measurements for SAM risk prior to MV repair. In this image, the C-sept is 2.49 cm, the AMVL and PMVL lengths are 2.29 cm and 1.23 cm (which is an AMVL:PMVL ratio of 1.86), and the aortomitral angle is 96.8°. This patient has two risk factors (C-sept and aortomitral angle) for post-MV repair SAM

can be damaged or occluded by an annular stitch. For this reason, a comprehensive assessment of LV performance is imperative following any MV repair or replacement [32]. Damage to the circumflex artery may necessitate a coronary artery bypass graft, PCI, or return to bypass to remove the stitch. An atrioventricular groove disruption is a serious complication associated with significant intraoperative mortality. In the event of an AV groove disruption, the LV separates from the MV annulus resulting in massive and difficult-to-control bleeding. On echo, extracardiac flow will be seen with CFD. Treatment requires return to bypass, removal of the prosthetic ring or valve, and patch repair of the AV groove [3].

### 7.9.5 Tricuspid Valve Replacement

A prosthetic TV in nearly all cases will be bioprosthetic and is unlikely to cause acoustic shadowing that prevents the assessment of adjacent structures. Due to the proximity of the AV node and the Triangle of Koch (Tendon of Todoro, the Thebesian valve, and the septal leaflet of the TV) to the site where anchoring sutures are placed during TV repair or replacement, the risk of heart block is relatively high. Typically, a TV annuloplasty ring is placed when the diastolic TV annulus diameter in the ME 4C view is >4 cm [3]. The normal values and cutoffs for TV prosthetic stenosis can be found in Table 7.20 [29]. Importantly, due to significant respiratory variation, these measurements should be averaged over 5 beats [29]. Prosthetic TV regurgitation is evaluated and graded the same as native TV regurgitation (see Table 7.21).

### 7.9.6 Pulmonic Valve Replacement

Pulmonic valve replacement, similar to TV replacement, is almost exclusively performed with bioprosthetic valves. On 2D echo with CFD and Spectral Doppler, the prosthetic valve should be evaluated for proper leaflet motion, signs of stenosis, and regurgitation [3] (See Table 7.22). Although a bioprosthetic PV will have a higher mean pressure gradient and peak velocity when compared to a homograft, a

**Table 7.20** Prosthetic tricuspid valve stenosis [29]

| Parameter | Normal | Stenosis |
|---|---|---|
| Vmax (m/s) | <1.7 | >1.7 |
| Mean PG (mmHg) | <6 | ≥6 |
| PHT (ms) | <230 | ≥230 |

*Vmax* peak velocity, *mean PG* mean pressure gradient, *PHT* pressure half-time

**Table 7.21** Prosthetic tricuspid valve regurgitation [29]

| Parameter | Mild | Moderate | Severe |
|---|---|---|---|
| Valve structure | Normal | Abnormal | Abnormal |
| Jet area by CFD (central jets only) ($cm^2$) | <5 | 5–10 | >10 |
| VC width (cm) | | <0.7 | >0.7 |
| CWD | Faint, parabolic | Dense, variable | Dense, early peaking |
| HVF | Normal | Systolic blunting | Systolic reversal |
| Chamber size | Normal | Dilated | Markedly dilated |

*CFD* color flow Doppler, *VC* vena contracta, *CWD* continuous wave Doppler, *HVF* hepatic venous flow

**Table 7.22** Prosthetic Pulmonic Valve Stenosis [3]

| Valve Type | Parameter | Normal | Stenosis |
|---|---|---|---|
| Homograft | Vmax (m/s) | <2.5 | >2.5 |
| | Mean PG (mmHg) | <15 | >15 |
| Bioprosthetic | Vmax (m/s) | <3.2 | >3.2 |
| | Mean PG (mmHg) | <20 | >20 |

*Vmax* peak velocity, *mean PG* mean pressure gradient

**Table 7.23** Prosthetic pulmonic valve regurgitation [29]

| Parameter | Mild | Moderate | Severe |
|---|---|---|---|
| Valve structure | Normal | Abnormal | Abnormal |
| RV size | Normal | Variable | Dilated |
| Jet size by CFD (% of PV annulus) | ≤25% | 26–50% | >50% |
| CWD | Faint, slow deceleration | Dense, variable deceleration | Dense, steep deceleration |
| Qp:Qs by PWD | Slightly increased | Intermediate | Greatly increased |
| PA diastolic flow reversal | None | Present | Present |

*RV* right ventricle, *CFD* color flow Doppler, *PV* pulmonic valve, *CWD* continuous wave Doppler, *PWD* pulsed wave Doppler, *Qp:Qs* ratio of pulmonary flow to systemic flow, measured as the ratio of pulmonary artery VTI:LVOT VTI, *PA* pulmonary artery

clinically meaningful stenosis will have significant turbulent flow on CFD [29]. Prosthetic PV regurgitation is evaluated and graded the same way as native PV regurgitation (see Table 7.23) [29].

## 7.10 Conclusion

Transesophageal echo is a very useful tool not only for diagnosis of valvular disease but also for intraoperative monitoring of repair or replacement success. Being able to recognize potential issues with native and newly replaced or repaired valves is crucial for good surgical planning, especially in the immediate post-bypass period. By understanding how the ultrasound technology works as well as how to interpret echo image and measurements can aid intraoperative decision-making and lead to successful patient outcomes.

## References

1. Mathew JP, Nicoara A, Ayoub CM, Swaminathan M (2019) Clinical manual and review of transesophageal echocardiography, 3rd edn. McGraw-Hill, New York
2. Salgo IS (2007) Three-dimensional echocardiographic technology. Cardiol Clin 25(2):231–239

3. Vegas A (2018) Perioperative two-dimensional transesophageal echocardiography: a practical handbook, 2nd edn. Springer, Cham
4. Hahn R, Abraham T, Adams MS et al (2013) Guidelines for performing a comprehensive transesophageal echocardiographic examination: recommendations from the ASE and the SCA. J Am Soc Echocardiogr 26:921–964
5. Baumgartner H, Hung J, Bermejo J et al (2017) Recommendations on the echocardiographic assessment of aortic valve stenosis: a focused update from the European Association of Cardiovascular Imaging and the American Society of Echocardiography. J Am Soc Echocardiogr 30:372–392
6. Lang R, Badano LP, Mor-Avi V et al (2015) Recommendations for cardiac chamber quantification by echocardiography in adults: an update from the American Society of Echocardiography and the European Association of Cardiovascular Imaging. J Am Soc Echocardiogr 28(1):1–39.e14
7. Calleja A, Thavendiranathan P, Ionasec RI et al (2013) Automated quantitative 3-dimensional modeling of the aortic valve and root by 3-dimensional transesophageal echocardiography in normals, aortic regurgitation, and aortic stenosis: comparison to computed tomography in normals and clinical implications. Circ Cardiovasc Imaging 6:99–108
8. Kou S, Caballero L, Dulgheru R et al (2014) Echocardiographic reference ranges for normal cardiac chamber size: results from the NORRE study. Eur Heart J Cardiovasc Imaging 15(6):680–690
9. Gilmanov A, Sotiropoulos F (2016) Comparative hemodynamics in an aorta with bicuspid and trileaflet valves. Theor Comput Fluid Dyn 30:67–85
10. Berard Y, Meneveau N, Vuillemonet A et al (1997) Planimetry of aortic valve area using multiplane transesophageal echocardiography is not a reliable method for assessing severity of aortic stenosis. Heart 78:68–73
11. Maslow A, Mashikian J, Haering HM et al (2001) Transesophageal echocardiographic evaluation of native aortic valve area: utility of the double-envelope technique. J Cardiothorac Vasc Anesth 15:293–299
12. Baumgartner H, Hung J, Bermejo J et al (2009) Echocardiographic assessment of valve stenosis: EAE/ASE recommendations for clinical practice. J Am Soc Echocardiogr 22:1–23
13. Zoghbi WA et al (2017) Recommendations for the noninvasive evaluation of native valve regurgitation: a report from the American Society of Echocardiography Developed in Collaboration with the Society of Cardiovascular Magnetic Resonance. J Am Soc Echocardiogr 30:303–371
14. Khoury GE, Glineur D, Rubay J et al (2005) Functional classification of aortic root/valve abnormalities and their correlation with etiologies and surgical procedures. Curr Opin Cardiol 20(2):115–121
15. Mahmood F, Maytal R (2015) A quantitative approach to the intraoperative echocardiographic assessment of the mitral valve for repair. Anesth Analg 121:34–58
16. Kumar N, Kumar M, Duran CMG (1995) A revised terminology for recording surgical findings of the mitral valve. J Heart Valve Dis 4:70–75
17. Cherry AD, Maxwell CD, Nicoara A (2016) Intraoperative evaluation of mitral stenosis by transesophageal echocardiography. Anesth Analg 123:14–20
18. Gorbaty BJ, Perelman S, Applebaum RM (2020) Left atrial appendage thrombus formation after perioperative cardioversion in the setting of severe rheumatic mitral stenosis. J Cardiothorac Vasc Anesth 35:589–592
19. Carpentier A (1983) Cardiac valve surgery—the "French Correction". J Thorac Cardiovasc Surg 86:323–337
20. Stone GW, Vahanian AS, Adams DH, Mitral Valve Academic Research Consortium (MVARC) et al (2015) Clinical trial design principles and endpoint definitions for transcatheter mitral valve repair and replacement: part 1: clinical trial design principles: a consensus document from the Mitral Valve Academic Research Consortium. J Am Coll Cardiol 66(3):278–307
21. Delling FN, Vasan RS (2014) Epidemiology and pathophysiology of mitral valve prolapse: new insights into disease progression, genetics, and molecular basis. Circulation 129(21):2158–2170

22. Faletra FF, Demertzis S, Pedrazzini G et al (2015) Three-dimensional transesophageal echocardiography in degenerative mitral regurgitation. J Am Soc Echocardiogr 28(4):437–448
23. Muraru D, Hahn RT, Soliman OI et al (2019) 3-Dimensional echocardiography in imaging the tricuspid valve. J Am Coll Cardiol 12(3):500–515
24. Utsunomiya H, Harada Y, Susawa H et al (2019) Comprehensive evaluation of tricuspid regurgitation location and severity using vena contracta analysis: a color Doppler three-dimensional transesophageal echocardiographic study. J Am Soc Echocardiogr 32(12):1526–1537
25. Smith SA, Waggoner AD, de las Fuentes L et al (2009) Role of serotoninergic pathways in drug-induced valvular heart disease and diagnostic features by echocardiography. J Am Soc Echocardiogr 22:883–889
26. McDonald JR (2009) Acute infectious endocarditis. Infect Dis Clin N Am 23(3):643–664
27. Durak DT, Lukes AS, Bright DK et al (1994) New criteria for diagnosis of infective endocarditis: utilization of specific echocardiographic findings. Am J Med 96:200–209
28. Habib G, Babano L, Tribouilloy C et al (2010) Recommendations for the practice of echocardiography in infective endocarditis. Eur Heart J 11:203–219
29. Zoghbi WA, Chambers JB, Dumesnil JG et al (2009) Recommendations for evaluation of prosthetic valves with echocardiography and Doppler ultrasound: a report from the American Society of Echocardiography's Guidelines and Standards Committee and the Task Force on Prosthetic Valves, Developed in Conjunction With the American College of Cardiology Cardiovascular Imaging Committee, Cardiac Imaging Committee of the American Heart Association, the European Association of Echocardiography, a registered branch of the European Society of Cardiology, the Japanese Society of Echocardiography and the Canadian Society of Echocardiography, Endorsed by the American College of Cardiology Foundation, American Heart Association, European Association of Echocardiography, a registered branch of the European Society of Cardiology, the Japanese Society of Echocardiography, and the Canadian Society of Echocardiography. J Am Soc Echocardiogr 22(9):975–1014
30. Sordelli C, Severino S, Ascione L et al (2014) Echocardiographic assessment of heart valve prostheses. J Cardiovasc Echogr 24(4):103–113
31. Alfieri O, Lapenna E (2015) Systolic anterior motion after mitral repair: where do we stand in 2015? Eur J Cardiothorac Surg 48(3):344–346
32. Poelaert JI, Bouchez S (2016) Perioperative echocardiographic assessment of mitral regurgitation: a comprehensive review. Eur J Cardiothorac Surg 50(5):801–812

# Chapter 8
# Advanced 3D Imaging and Transcatheter Valve Repair/Implantation

**Derek Phan, Santanu Biswas, and Sameer Gafoor**

## Abbreviations

| | |
|---|---|
| 2D | Two-dimensional |
| 3D | Three-dimensional |
| 4D | Four-dimensional |
| AV | Atrioventricular |
| CS | Coronary sinus |
| CT | Computed tomography |
| ECG | Electrocardiogram |
| IVC | Inferior vena cava |
| LCX | Left circumflex artery |
| LVOT | Left ventricular outflow tract |
| MA | Mitral annulus |
| MRI | Magnetic resonance imaging |
| RA | Right atrium |
| RCA | Right coronary artery |
| RV | Right ventricle |
| SVC | Superior vena cava |
| TAVI | Transcatheter aortic valve implantation |
| TEE | Transesophageal echocardiography |
| TMVr | Transcatheter mitral valve repair |

D. Phan · S. Biswas
Swedish Heart and Vascular, Seattle, WA, USA

S. Gafoor (✉)
Swedish Heart and Vascular, Seattle, WA, USA

Cardiovascular Center Frankfurt, Frankfurt, Germany

© The Author(s), under exclusive license to Springer Nature Switzerland AG 2023

P. A. Iaizzo et al. (eds.), *Heart Valves*, https://doi.org/10.1007/978-3-031-25541-0_8

TMVR Transcatheter mitral valve replacement
TV Tricuspid valve

## 8.1 Introduction

Valvular heart disease is a major cause of morbidity and mortality in developing and industrialized countries. While rheumatic and infectious causes are more common in developing countries, degenerative valvular disease is the predominant etiology in the aging population of the industrialized world. For patients with advanced, symptomatic disease, surgical open-heart valve replacement or repair remains the standard treatment with excellent short- and long-term outcomes. However, there is a significant percentage of typically older patients that are not considered surgical candidates. For example, in Europe and the United States surveys, about 30% of patients with severe symptomatic aortic stenosis are not considered surgical candidates secondary to advanced age and comorbidities [1]. Because these patients have a poor outcome with medical management [2–5], less-invasive transcatheter approaches for valve repair/implantation appear promising for subgroups of these high-risk patients.

Transcatheter aortic valve implantation (TAVI) for symptomatic patients with severe aortic stenosis utilizes stent systems, in which a bioprosthetic valve is mounted. The procedure can be performed using a transfemoral, transcaval, transcarotid, transaxillary, transaortic, or transapical approach [6–11]. The stent/valve systems are anchored at the annulus and extend into the root or proximal ascending aorta. Since the initial successful human implantation in 2002, different generations of balloon-expandable or self-expandable valve prostheses have been implanted in several thousand patients with severe symptomatic aortic stenosis. The results in experienced centers are good, with high implantation success rate, significant hemodynamic and clinical improvements, and improved survival rates [11–13]. TAVI was associated with improved outcomes compared to medical therapy, and comparable outcomes to open-heart surgery [14]. See chapter on TAVI devices for more information.

There are several percutaneous approaches for the treatment of mitral regurgitation, including both transcatheter mitral valve repair (TMVr) and replacement (TMVR). The most common percutaneous mitral valve repair procedure is derived from the Alfieri edge-to-edge repair, which consists of suturing the free edges of the anterior and posterior mitral leaflets [15, 16]. The transcatheter procedure deploys a clip to join the free edges of the opposing leaflets, thus creating a double-orifice valve [17–20]. Alternative percutaneous procedures include coronary sinus (CS) annuloplasty with placement of devices in the CS. The goal is to displace the posterior portion of mitral annulus (MA), in order to improve the coaptation of the leaflets [21–24]. One study [24] showed the feasibility of percutaneous reduction in functional mitral regurgitation with a CS-based mitral annuloplasty device in patients with heart failure and was associated with an improvement in quality of life

and exercise tolerance. For prosthetic mitral valve paravalvular regurgitation, percutaneous device closure has been successful. Several TMVR devices are currently under clinical investigation, and mitral valve-in-valve implantation with an aortic transcatheter valve has been performed with much success. See chapter on transcatheter mitral valve repair and replacement devices for more information.

Transcatheter pulmonic valve replacement has also been established in patients with dysfunctional right ventricular outflow tract conduits and pulmonary regurgitation [25, 26]. More information on transcatheter pulmonic valve replacement is in future chapters.

Recent studies also describe transcatheter tricuspid valve implantation [27] and valve-in-valve implantation [28, 29]. Transcatheter tricuspid valve repair or replacement is a rapidly advancing field. Several therapies are currently under investigation, including suture or ring annuloplasty devices, coaptation devices (edge-to-edge repair), direct valve replacement, and caval (superior or inferior vena cava) implantation devices. Tricuspid valve edge-to-edge repair is currently the most commonly used method and heavily relies on two-dimensional (2D) and three-dimensional (3D) transesophageal echocardiography for technical success.

As described in more detail in other chapters of the book, transcatheter valvular procedures are becoming an alternative to open surgical approaches in selected patient populations. Low frequency of procedural-related complications and good long-term outcomes depend on careful selection of potential candidates, with an important role for imaging [30].

## 8.2 Imaging in the Context of Transcatheter Valve Procedures

Due to the lack of direct visualization of the operative field during transcatheter procedures, imaging for preoperative planning and intraoperative guidance is an integral component of transcatheter procedures [31, 32].

Standard 2D imaging is performed with conventional X-ray angiography and echocardiography before and during the procedure. Since angiography and echocardiography create 2D projections or acquire 2D planes, understanding of 3D relationships requires viewing and mentally reconstructing the object from multiple different projections or planes. In contrast, 3D imaging provides 3D visualization and is increasingly used for pre- and intraoperative visualization [33–37]. Three-dimensional imaging modalities include 3D echocardiography, computed tomography (CT), C-arm CT, and magnetic resonance imaging (MRI).

Three-dimensional echocardiography [38, 39] is used for real-time procedural image guidance during catheter-based therapies. Three-dimensional transthoracic and transesophageal echocardiography (TEE) is performed with rectangular (or matrix) array transducers, which acquire a 3D pyramidal data volume [39–42]. With a full-volume acquisition, commonly acquired over several cardiac cycles, a full 3D data set with high temporal and spatial resolution can be obtained. Similar to CT,

offline reconstruction generates multiple 2D cut planes that can be applied to display structures of interest from different perspectives. This approach allows reconstruction of images orthogonal to the vessel's centerline for measurement, e.g., of the aortic annulus. Alternatively, 3D data acquisition can be real time, with a slightly lower temporal resolution compared to full 3D data sets obtained over several cardiac cycles. Real-time 3D echocardiography is especially useful in the guidance of mitral valve procedures, as it provides the unique enface viewing perspective of the mitral valve from the left atrium (often termed the "surgeon's view"). Further, the 3D matrix probe also allows the simultaneous real-time display of two adjustable image planes at high temporal and spatial quality, in both 2D and color Doppler modes. This is especially important for color Doppler imaging where low temporal resolution often significantly limits the use of true 3D techniques such as real-time and full-volume acquisitions. Biplane imaging is particularly useful in assessing mitral, aortic, and tricuspid valve pathologies where high spatial and temporal resolutions similar to 2D echocardiography are often needed, but simultaneous imaging of two planes helps to assess the 3D structure. Initial experience with 3D TEE demonstrates its value in the clinical evaluation of structural heart disease, intraoperative assessment, and guidance of interventional procedures [43–49].

C-arm CT describes the use of CT-like acquisition and reconstruction techniques to obtain 3D data with C-arm-based X-ray angiography systems. The C-arm is rotated over a wide arc (>180°) around the patient typically during continuous contrast injection, acquiring multiple views of the cardiovascular structure in order to reconstruct a 3D image [50, 51]. For electrocardiogram (ECG)-referenced cardiac imaging, alternating forward and backward rotations are triggered by the ECG signal to acquire projections covering the entire acquisition range at a similar cardiac phase. C-arm CT has shown potential for use during various cardiovascular interventional procedures including coronary angiography and percutaneous coronary interventions [52, 53], pulmonary vein isolation [54], and endovascular stent repair of aortic disease [55].

The use of CT for cardiovascular indications has become possible due to improvements of spatial and temporal resolution and an increased number of detector systems [56–58]. Using dual-tube technology, temporal resolution of 75 ms can be achieved with a spatial resolution of about 0.5 mm and slice thickness of about 0.5–0.75 mm. With 320-slice systems, 16 cm can be covered in one rotation. These isotropic data sets allow oblique reconstruction without degradation of spatial resolution. Most imaging experience in the context of transcatheter valve procedures is based on retrospectively ECG-gated helical acquisitions (typically with use of tube current modulation, but a wide dose modulation window). The ECG-synchronized image acquisition throughout the cardiac cycle allows reconstruction at any point throughout the R-R interval, and cine display of multiple phases throughout the cardiac cycle permits dynamic display of cardiac and valvular motion, as well as reconstruction at specific positions in the R-R interval. For example, visualization of a plane at the tip of the leaflets at different times during the cardiac cycle allows determination of the maximal opening of the aortic valve during the cardiac cycle by planimetry (typically mid-late systole). However, the temporal resolution of CT is lower than that of echocardiography and MRI.

These CT protocols are usually associated with increased radiation exposure [59–61]. Careful individual planning of the imaging protocol and consideration of potential alternative imaging modalities are important to control radiation exposure [62]. Strategies associated with lower doses for cardiovascular CT imaging include tube current modulation with retrospective ECG-gated helical imaging, prospectively ECG-triggered imaging techniques, and use of low X-ray tube voltage (e.g., 100 kVp) [63–67]. If four-dimensional (4D) imaging is not necessary, prospective ECG-triggered axial acquisitions focused on a specific phase in the cardiac cycle should be preferred in patients with stable heart rate, because of the significantly lower radiation exposure. Most protocols are performed after intravenous contrast administration. If contrast administration is not feasible, non-contrast images can be useful to visualize calcification of the valve and/or aortic root and remaining segments of the vasculature, although precise measurements may be difficult.

Interventional cardiovascular MR techniques have been developed to guide transcatheter procedures [68–72]. The advantage of these approaches is that they provide good soft tissue visualization and functional assessment, including blood flow without radiation exposure. However, they add significant complexity to the procedure and require special compatible instruments and considerable capital investment [73]. An important concept is the development of MR road maps, which are combined with live X-ray fluoroscopy using a conventional clinical environment and conventional catheter equipment (Fig. 8.1). Such data provide additional anatomic landmarks and functional information to guide procedures [74, 75]. Magnetic resonance might aid in positioning nonsurgical replacement of heart valves, relative to vital structures such as coronary artery ostia [69]. A limitation of MRI in the context of TAVI is the signal void caused by calcium and metal, which precludes precise assessment of densely calcified valves and after stent-valve placement.

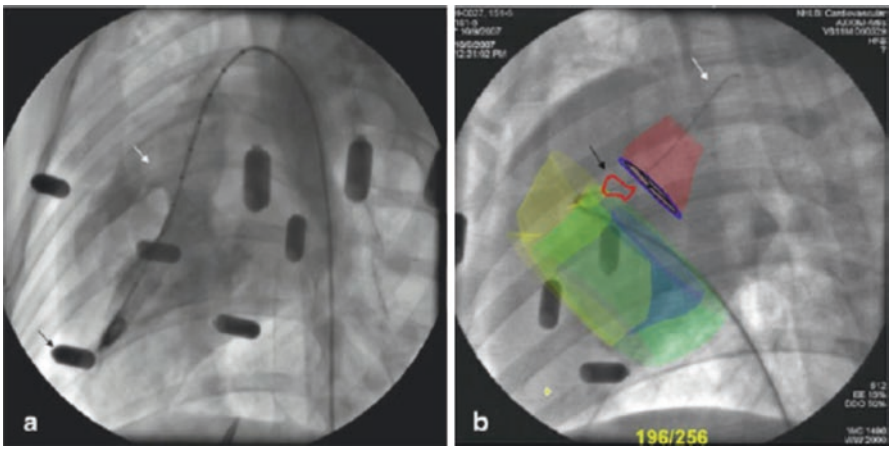


**Fig. 8.1** Interventional MRI and angiographic fusion. Interventional applications of MRI allow real-time fusion of angiographic and MRI images in hybrid MRI/angiosuites for direct procedural guidance. (Image courtesy of Dr. Lederman; adapted with permission from Ratnayaka et al. [74])

## *8.2.1 Transcatheter Aortic Valve Implantation*

### 8.2.1.1 Anatomy

Aortic root anatomy, including the aortic valve and coronary artery ostia, is complex [76–78]. The geometry and relationship of the aortic root structures change throughout the cardiac cycle [79–82]. Implantation of a stent/valve is incompletely understood, including the consequences of these structures and their relationships.

The aortic annulus describes the interface between the left ventricular outflow tract and the aortic root at the commissures of the aortic valve leaflets (Fig. 8.2). The three commissures extend upward into the aortic root similar to the shape of a crown or the struts of a bioprosthetic valve. The "annular" level at the lowest point of the valve hinge point ("inferior virtual basal ring") defines the level where valve prostheses are sutured or secured. During valve surgery, the annulus is fitted to the valve. On the other hand, when the transcatheter valve is deployed, the stent/valve must adjust to the "aortic root." Therefore, in addition to size and shape, the composition and material properties of the surrounding structures have important implications for the interaction between device and root. Approximately two-third are in contact

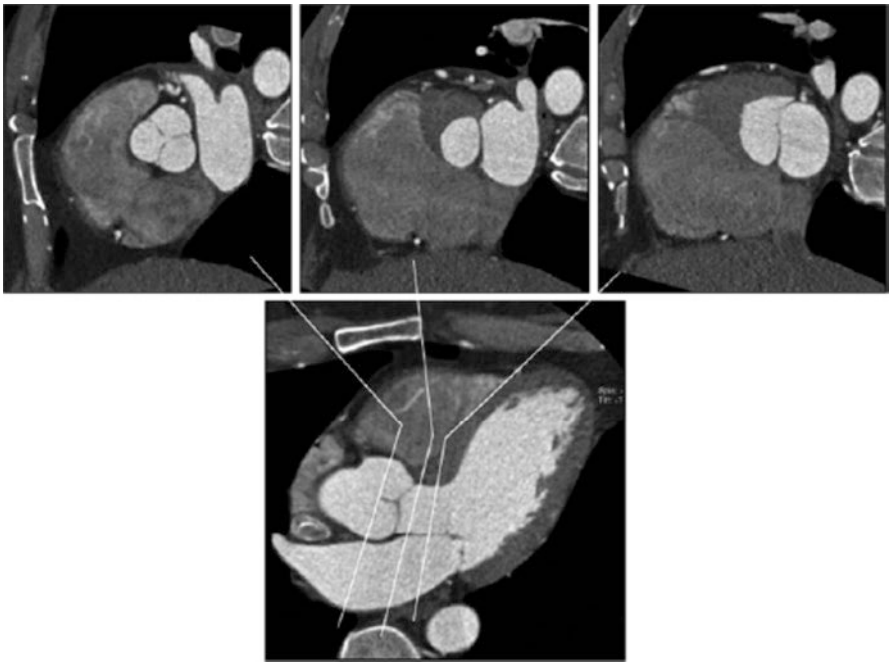

**Fig. 8.2** Relationship between aortic valve, left ventricular outflow tract (LVOT), and anterior mitral leaflet. The upper panels show (*left* to *right*) cross sections through aortic valve, LVOT, and anterior mitral leaflet. The close relationship between these structures is demonstrated

with ventricular myocardium, and the remaining one-third are composed of the aortic leaflet of the mitral valve [31].

The three individual cusps of the aortic valve are attached to the aortic wall along the commissures in a crescentic fashion (Fig. 8.3). Behind the cusps are the outward bulging sinuses of Valsalva, with the origins of the coronary arteries at the superior aspect of the left and right aortic sinuses. There is a wide variation in distance between the leaflet tips and the coronary ostia, and in about 50% of patients, the length of the left coronary leaflet exceeds the distance between the annulus and the ostium of the left coronary artery. This has important implications during preprocedural planning for TAVI, especially when evaluating risk of coronary obstruction with valve implantation.

The sinotubular junction describes the margin between the aortic root and tubular ascending aorta and has an important role in maintaining valve competence (Fig. 8.4) [83]. During the TAVI procedures, the sinotubular junction provides support for the deployment balloon; depending on valve design (short vs. long), the sinotubular junction and proximal ascending aorta are important for proper implantation (distal anchor zone). Please see Chap. 2 for more information on the anatomy of the semilunar valves.

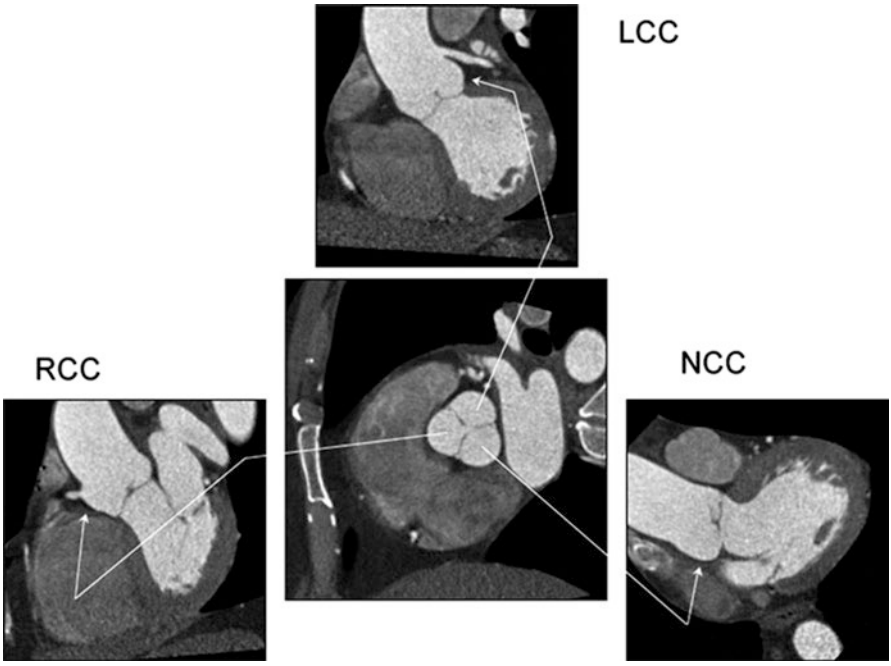


**Fig. 8.3** Relationship between aortic valve cusps and coronary ostia. The central panels show a cross section through the aortic root with the three aortic valve cusps. The three surrounding panels show oblique sagittal images of each cusp. *LCC,* left coronary cusp; *RCC,* right coronary cusp; *NCC,* non-coronary cusp

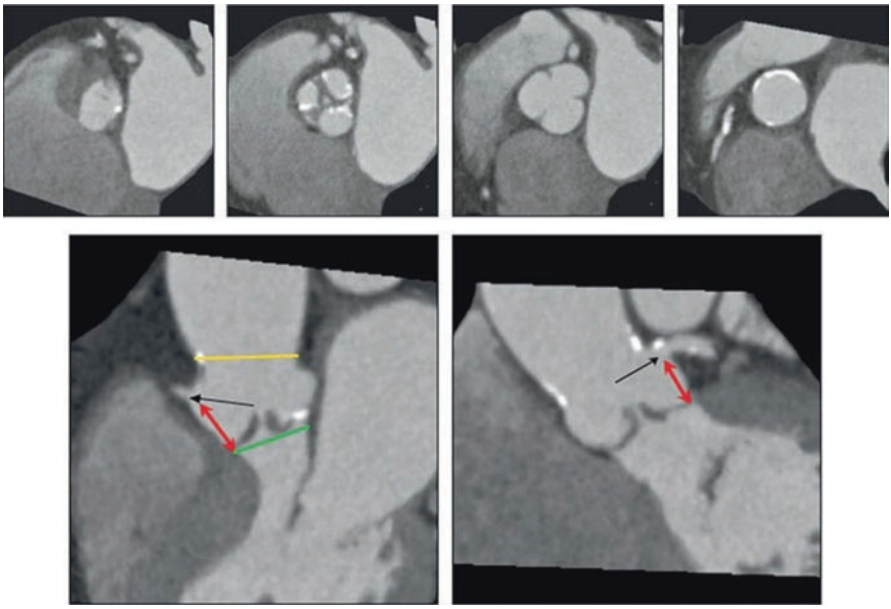

**Fig. 8.4** Aortic root, aortic valve, and coronary ostia. The upper panels show (*left* to *right*) cross sections at the "aortic annulus," aortic valve, sinuses of Valsalva, and sinotubular junction. There is moderate thickening and calcification of the aortic valve leaflets

#### 8.2.1.2 Imaging

The position of the aortic root relative to the body axis and corresponding alignment of the X-ray plane are critically important for precise placement of the valve. With angiography, overlap-free visualization of the three coronary cusps, which are oriented along the aortic valve plane, typically requires caudal angulation in the RAO projection and cranial angulation in the LAO projection. The current standard approach is based on the identification of X-ray root angiograms (using a pigtail catheter in either the non-coronary cusp or right coronary cusp depending on the type of valve being used) in one or preferably two orthogonal planes prior to the procedure after repeated root injections. Pre-procedural multi-detector CT data of the aortic root allow prediction of the optimal angulation of the root angiogram, which facilitates the angiographic procedure and reduces the number of root injections (Fig. 8.5) [84, 85]. In cases of TAVI within a prior surgical or transcatheter bioprosthetic aortic valve (i.e., "valve-in-valve"), X-ray fluoroscopy alone can be used to identify the bottom aortic annulus (coplanar view), obviating the need for aortic root angiograms during positioning and deployment of the transcatheter heart valve [86].

As described above, using imaging modalities, the annulus plane is defined as the plane created by the lowest hinge point of the three leaflets of the aortic valve ("inferior virtual basal ring") (Figs. 8.2 and 8.4). Detailed 3D analysis demonstrates

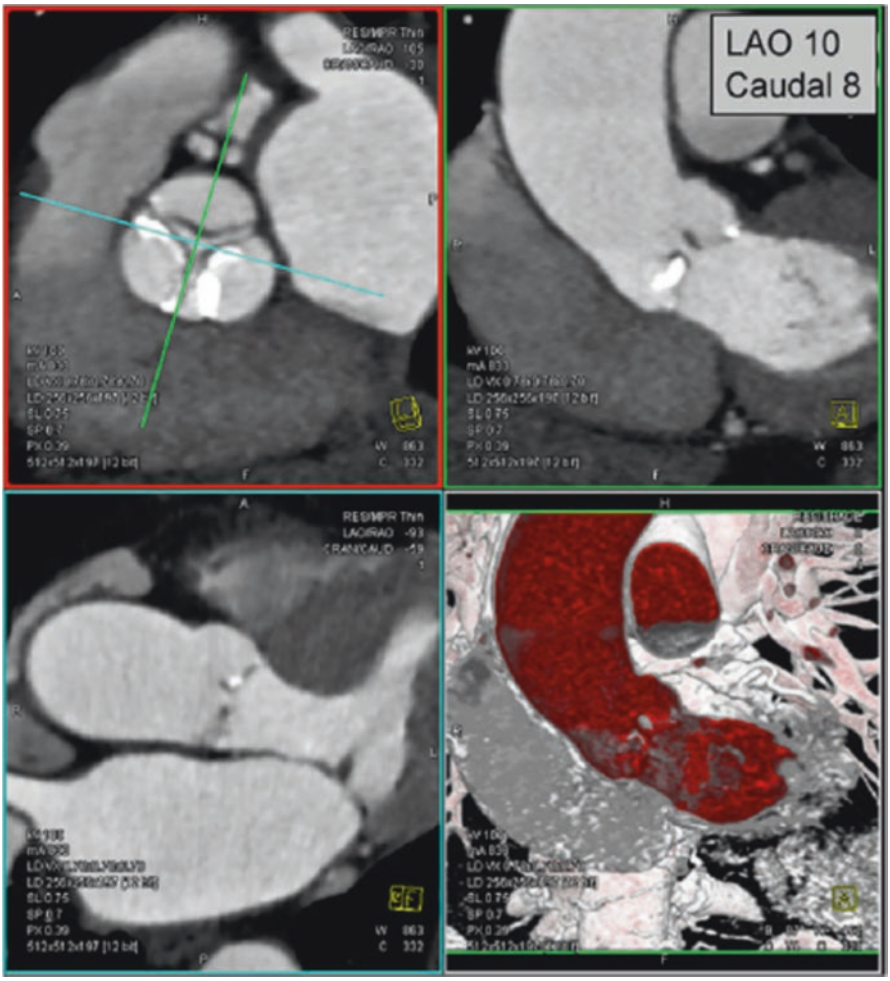


**Fig. 8.5** Prediction of angiographic planes for transcatheter aortic valve implantation. In a double-oblique reconstructed image, the crosshair of the cut planes is centered on the aortic valve (*left upper panel*) and rotated to obtain images of the aortic root, described in angiographic coordinates/planes (*right upper panel*)

that this clinically defined annulus is typically elliptical [87–97], and therefore, maximal and minimal annular diameters are reported with CT. Mean annular diameter by CT correlates best but is typically slightly larger than that obtained with TEE. Despite this, CT is now the most commonly used method for valve sizing/selection (based on the aortic annulus area or perimeter) given its superiority in clinical outcomes compared to echocardiography [98]. Measurement of the distance between the coronary arteries, artery ostia, and distal tip of the aortic valve leaflets is important and can be derived from angiography, CT, and TEE (Fig. 8.4). In the case of a low ostium or a long leaflet, there is increased risk of coronary (particular

left main) occlusion [87, 89, 90, 94]. This information is vital intra-procedurally such that operators can prepare for coronary protection in advanced. Coronary re-access can be challenging due to a multitude of reasons, including native leaflet obstruction, stent frame position, and mal-aligned commissures [99]. Studies have shown this to be particularly more challenging in self-expanding valves compared to balloon-expandable valves [100]. Due to this, special device advancement techniques have been utilized and validated to significantly reduce the occurrence of commissural overlap with the coronary ostium and thereby theoretically increase success of coronary re-access if needed [101]. A special leaflet laceration technique called BASILICA (Bioprosthetic or native Aortic Scallop Intentional Laceration to prevent Iatrogenic Coronary Artery obstruction during TAVR) has been shown to be feasible and safe to prevent coronary artery obstruction from TAVR in high-risk patient subsets [102].

Imaging allows detailed description of the presence and distribution of valve and root calcification (Fig. 8.6) [103–109]. For example, calcification frequently extends from the aortic valve commissures to the base of the anterior mitral leaflets and sinotubular junction. The amount and distribution of calcification in the proximal device landing zone at the annulus can affect sealing of the prosthesis, leading to paravalvular regurgitation post-valve deployment. Aortic calcification of the sinotubular junction can influence precise placement of the valve during TAVI by restricting balloon expansion and potentially leading to the ventricular displacement of

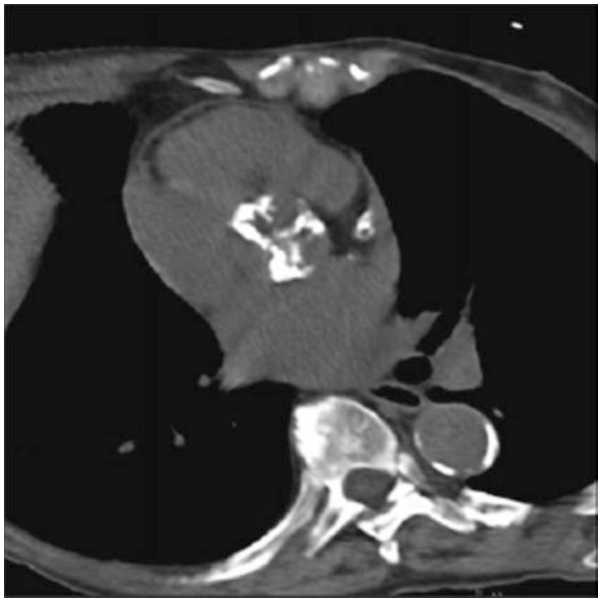

**Fig. 8.6** Dense calcification of aortic valve. In this image of a non-contrast-enhanced scan, dense calcification is seen along all three aortic valve cusps. This pattern suggests a tricuspid valve. Using calcium scoring software, the extent of calcification can be quantified

device at the time of deployment. Presence of eccentric or calcified nodules can also increase the risk of rare, but catastrophic peri-procedural complications such as aortic annular rupture or ventricular septal defects. Lastly, the extent and quantification of aortic calcification using calcium scoring software (and using sex-specific thresholds of the Agatston score) can assist clinically with the diagnosis of severe aortic stenosis in difficult or ambiguous cases.

Direct observation of the aortic valve opening area allows for correlation of the pattern of valve opening with leaflet anatomy and leaflet calcification. Direct planimetry of the aortic valve opening area with CT has been shown to provide reproducible results in comparison with TEE and MRI (Fig. 8.7) [110–117].

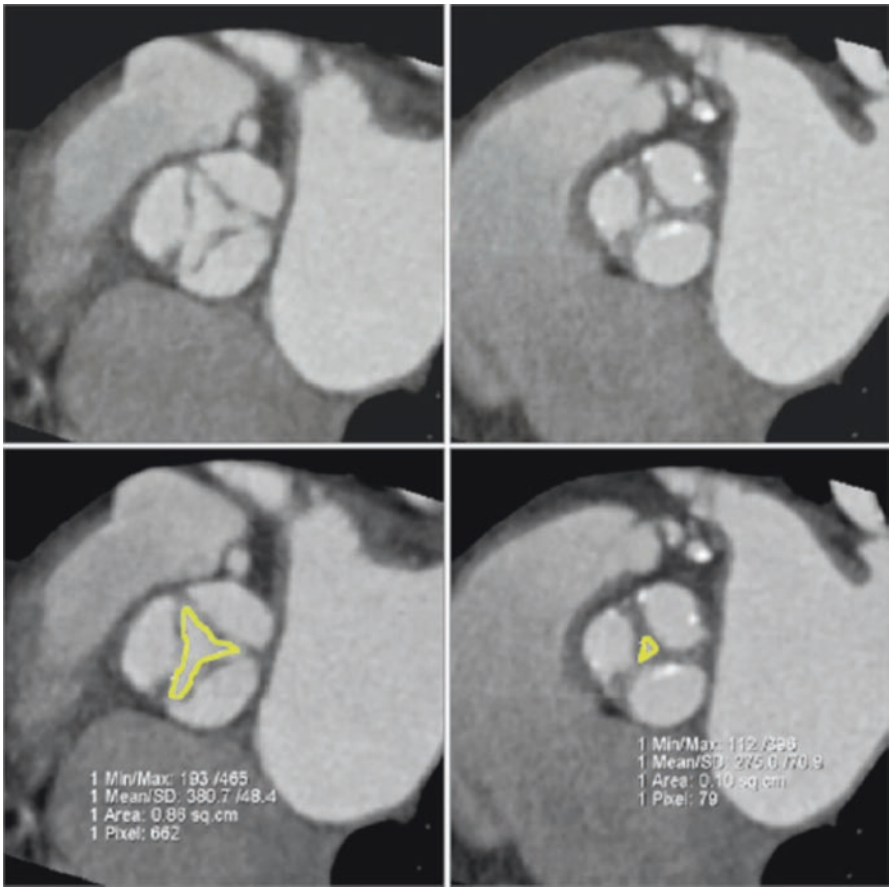


**Fig. 8.7** Image reconstruction in systolic and diastolic phase of the cardiac cycle. Image reconstruction in systolic (*left*) and diastolic (*right*) phase of the cardiac cycle demonstrates restricted systolic opening and incomplete diastolic coaptation, consistent with moderate aortic stenosis and mild insufficiency, respectively

During periprocedural 3D TEE, the biplane imaging mode is valuable in simultaneously imaging the aortic valve in both the short- and long-axis views, both in 2D and in color Doppler (Fig. 8.8). This allows the accurate positioning of the prosthetic device in the center of the stenotic valve in both orientations, as well as rapidly localizing post-implantation paravalvular regurgitation. However, the trend has been moving away from general anesthesia, and more toward conscious sedation, hence decreasing the usage of intra-procedural TEE. Transthoracic echocardiogram, aortic root angiography, and/or hemodynamics are now the most commonly used assessments for post-implantation paravalvular regurgitation.

## *8.2.2 Transcatheter Mitral Valve Procedures*

### 8.2.2.1 Anatomy

The annulus of the mitral valve is an oval, saddle-shaped structure which is formed by continuity of the left atrial tissue with the left ventricular tissue, as well as the base of the mitral valve leaflets (Figs. 8.9 and 8.10) [118, 119]. The mitral valve apparatus consists of the annulus, leaflet, chordae, and the papillary muscles (the anteromedial and posterolateral papillary muscles). The annulus is divided into anterior and posterior parts by the commissures.

The anterior leaflet is larger in length but covers only about one-third of the circumference of the annulus. The posterior leaflet is shorter in length but covers approximately two-third of the annulus. The chordae arise from the papillary muscle tips and then span to the leaflets in a fan-shaped manner (Fig. 8.11). There are two main chordae arising from each head of the papillary muscle, reaching each of the leaflets. However, there is a considerable variation in the origin and distribution of the chordae.

The coronary sinus (CS) extends along the left atrioventricular groove close to the mitral annulus and drains into the right atrium. In the context of sinus annuloplasty procedures, a major concern is the close proximity of the CS to the left circumflex artery (LCX) and the potential risk of CS-based devices potentially impinging on the LCX [120]. See Chap. 1 for more information on the anatomy of the atrioventricular valves.

### 8.2.2.2 Imaging

Three-dimensional imaging allows a detailed understanding of the mitral valve apparatus including the mitral annulus and leaflets and has been extensively described with echocardiography [121–126]. Description of mitral valvular anatomy is critical for procedures involving the mitral leaflets, including mitral valve repair/replacement procedures and percutaneous closure of paravalvular regurgitation. Real-time 3D and full-volume acquisition with TEE allows imaging of the

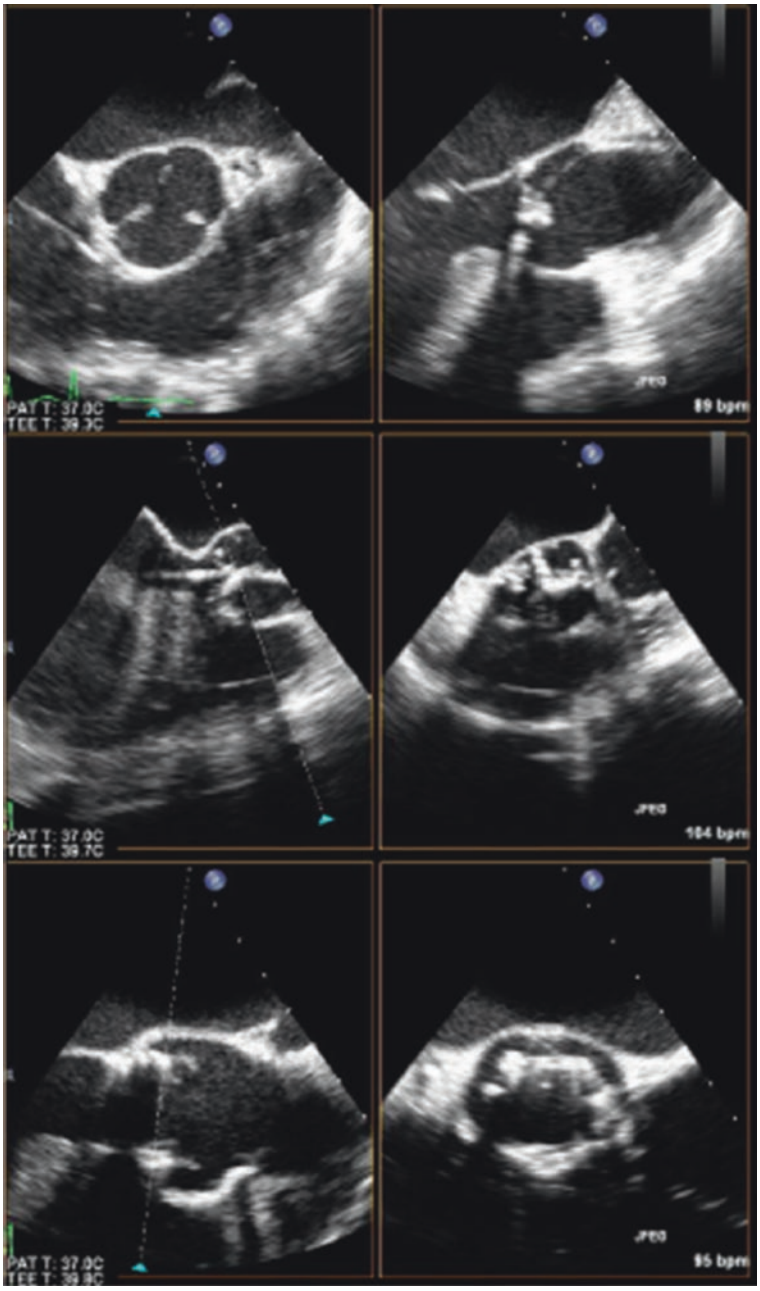

**Fig. 8.8** Biplane real-time three-dimensional (3D) echocardiography. Biplane real-time imaging of a patient with severe aortic stenosis undergoing transcatheter aortic valve implantation (TAVI), in both short and long axis, before (*top panel*), during (*middle panel*), and after (*bottom panel*) device deployment. Simultaneous imaging of the aortic valve in two planes in high spatial and temporal resolution is crucial for the precise positioning of the prosthetic device in TAVI

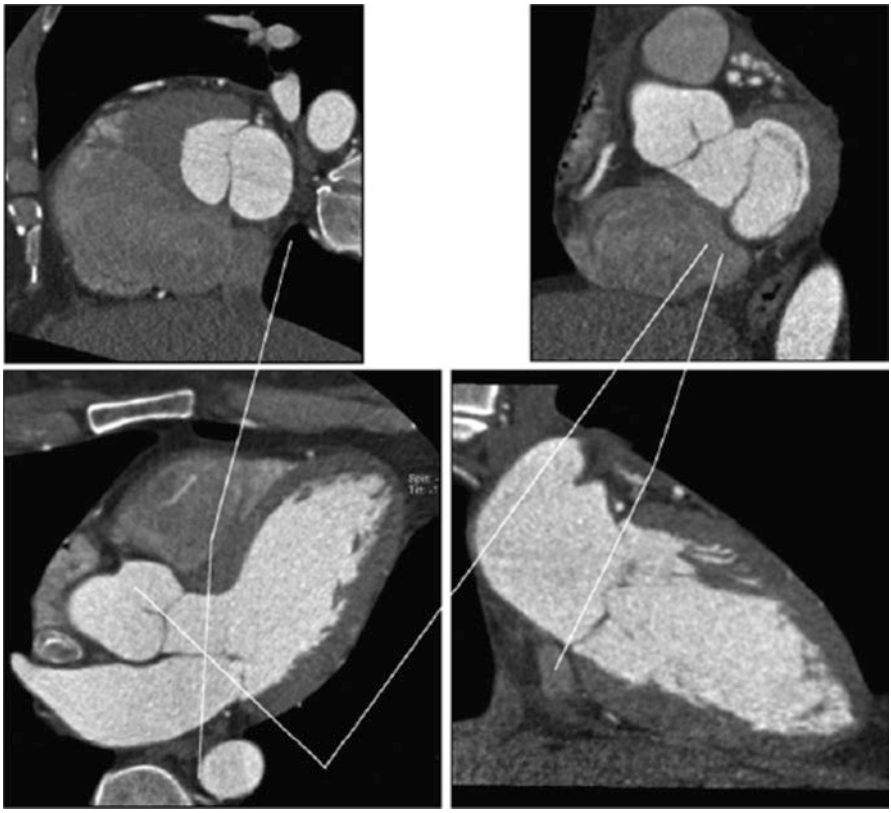

**Fig. 8.9** Relationship between LVOT, anterior mitral leaflet, and mitral annulus. The upper panels show (*left* to *right*) cross sections of the LVOT/anterior mitral leaflet and mitral annulus. The close relationship of the structures is demonstrated

entire mitral valve and annulus over full cardiac cycles [47, 127–130]. Therefore, 3D echocardiography is a critical part of the pre-procedural assessment of patients with mitral regurgitation and allows clarification of etiology (i.e., degenerative versus functional mitral regurgitation), determination of severity, and assessment of amenability of the mitral valve to percutaneous procedures and pre-procedural planning (Fig. 8.12). For periprocedural guidance, full-volume 3D echocardiography data acquisition is less useful because of the need for offline analysis. However, real-time 3D echocardiography with its enface mitral valve view from the left atrium similar to the surgeon's view, as well as simultaneous biplane imaging with its high temporal and spatial resolutions both in 2D and in color Doppler modes, is invaluable for procedures such as mitral valve clip (Fig. 8.13) and percutaneous closure of paravalvular regurgitation (Fig. 8.14). Specifically, the 3D enface mitral valve view is particularly useful for orientation of the mitral valve clip device. Biplane imaging in the 2D echocardiography mode is particularly useful for medial/lateral and anterior/posterior orientation and is the key view for leaflet grasping. In addition, 2D

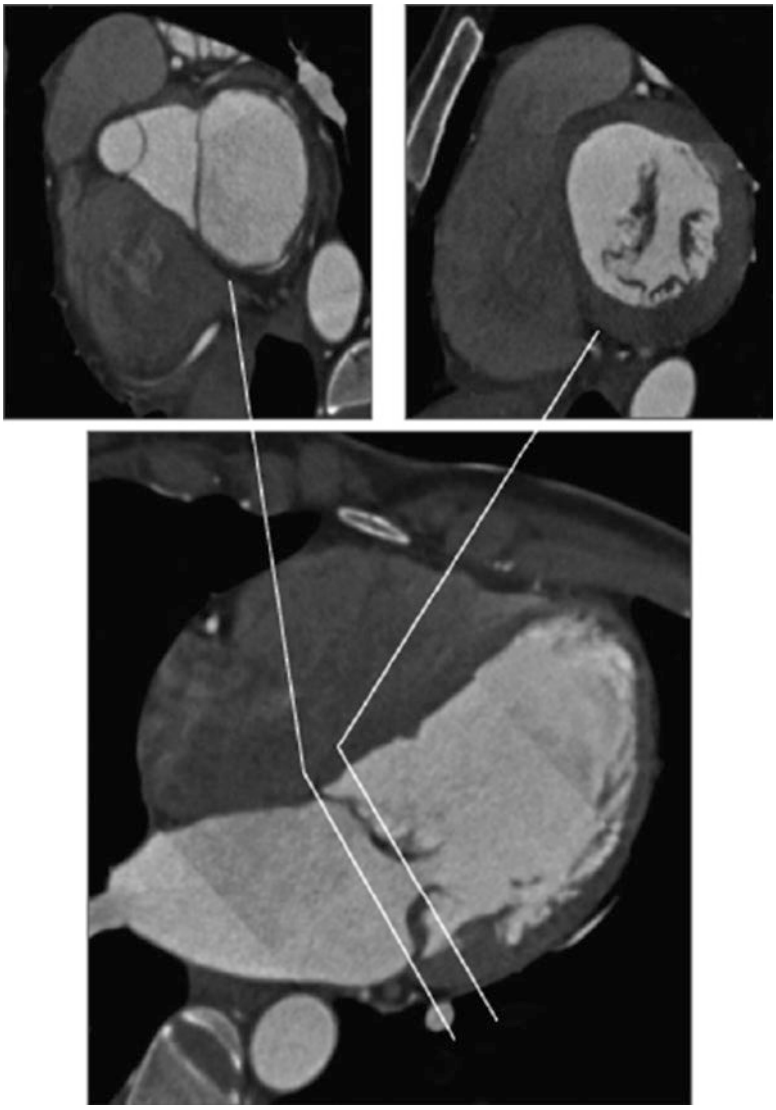

**Fig. 8.10** Mitral annulus and mitral valve leaflets. The upper panels show a cross section through the mitral annulus (*left*) and mitral leaflets close to the tips

biplane imaging is crucial for the trans-septal puncture (crossing from the right atrium into the left atrium), which is a crucial procedural step to the mitral valve clip device and other transcatheter mitral valve replacement (TMVR) procedures.

Similar to TAVI, CT is essential for annular sizing in TMVR. The typical measurements obtained from CT include the annular: projected area, perimeter, intercommissural, septal-lateral, and trigone-trigone distances [131]. Depending on the

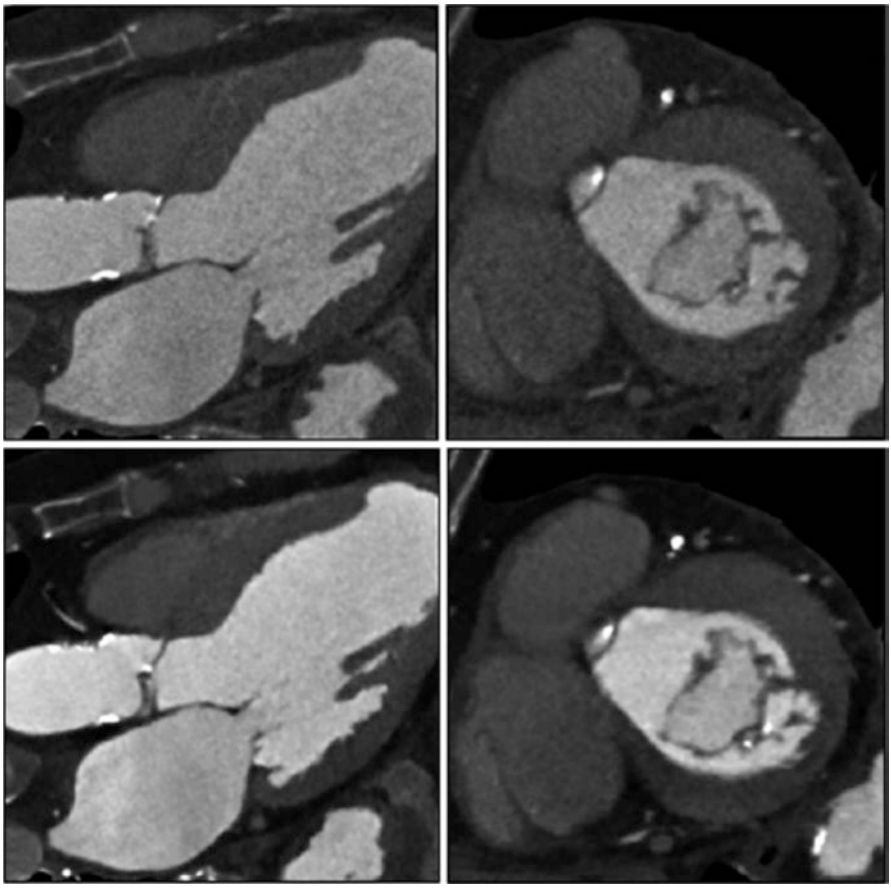

**Fig. 8.11** Mitral leaflets, mild mitral annular calcification, and papillary muscles. In this image, mild mitral annular calcification is seen in the infero-lateral aspect of the annulus. The images also show the posterior papillary muscles and chordae tendineae. The images are reconstructed with standard "filtered back projection" (*upper panels*) and "iterative reconstruction" (*lower panels*). Iterative reconstruction is associated with significantly decreased image noise

device selected for use, different variables/parameters are used for sizing. Three-dimensional TEE sizing of the mitral annulus can also be used as well, with the added benefit of the high temporal resolution providing information on the dynamics and function of the mitral annulus. CT and echocardiography are also helpful in evaluating the transapical access point, ideal intercostal access site, annular landing zone, presence of calcification (i.e., mitral annular calcification), fluoroscopic coplanar angles, and prediction of left ventricular outflow tract (LVOT) obstruction post-procedure [132]. This is helpful in cases of transcatheter valve-in-valve, valve-in-ring, valve-in-mitral annular calcification, or TMVR. For any type of implantation in the mitral position, post-procedural LVOT obstruction is a concern and CT simulations (along with aortomitral angulation, left ventricular cavity size,

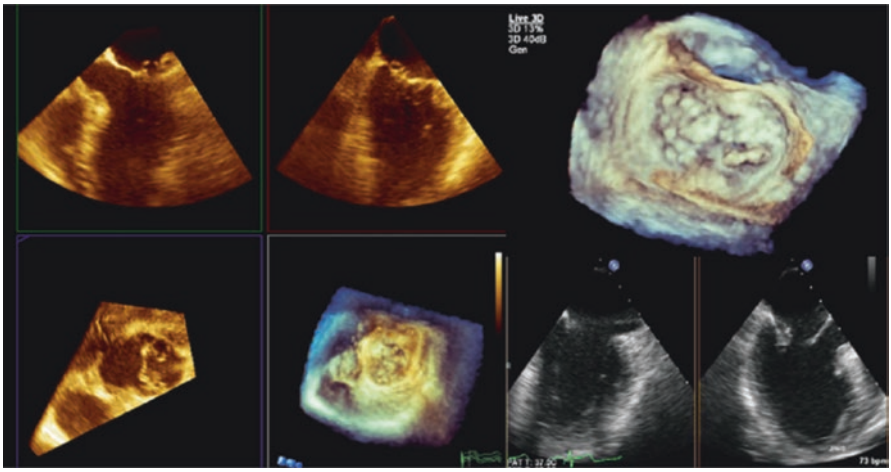

**Fig. 8.12** Three-dimensional echocardiography assessment of a patient with severe mitral regurgitation. With the full-volume 3D acquisition, offline analysis of the data set accurately identifies the posterior mitral leaflet medial flail segment (*left panel*). Real-time 3D acquisitions also visualize the posterior medial flail segment with an enface view of the mitral valve from the left atrium, similar to the surgeon's view of the mitral valve (*top right panel*). Simultaneous biplane imaging of the mitral valve allows the assessment of the flail segment in high temporal and spatial resolution, both in two-dimensional (2D) and in color Doppler modes (*bottom right panel*). The medial location of the flail segment near the commissure makes it challenging for percutaneous treatment

interventricular septal size) can be used to predict the risk in patients being evaluated for TMVR. A technique similar to BASILICA for prevention of coronary obstruction in TAVR has been developed for TMVR called LAMPOON (Laceration of the Anterior Mitral leaflet to Prevent Outflow Obstruction) technique and has been shown to be effective in preventing and treating LVOT obstruction [133]. Two-dimensional and three-dimensional echocardiography are vital intra-procedurally to assist with trans-septal puncture, trans-apical cannulation, guidewire and device positioning/functioning, assessment of paravalvular leak, device seating and stability, and LVOT obstruction [132]. Figure 8.15 depicts fluoroscopic images of mitral valve-in-valve, valve-in-ring- and valve-in-mitral annular calcification, respectively.

For CS-related procedures, fluoroscopy, CT, and TEE are helpful for proper positioning of the device and evaluating the effectiveness of the intervention. Several studies have used angiography and CT to describe the in vivo anatomical relationships between mitral annulus and CS as well as CS and LCX [134–137]. These studies observed significant variance of CS to mitral annulus separation. The LCX crossed between the CS and mitral annulus in 74–97% of patients at a variable distance from the ostium of CS, depending on coronary dominance. In addition, obtuse marginal branches and posterolateral branches were also in a position to potentially be compressed by a device placed within the CS. Therefore, evaluation of the relationship between the CS/great cardiac vein and the LCX is an important factor in determining the safety of CS-based devices.

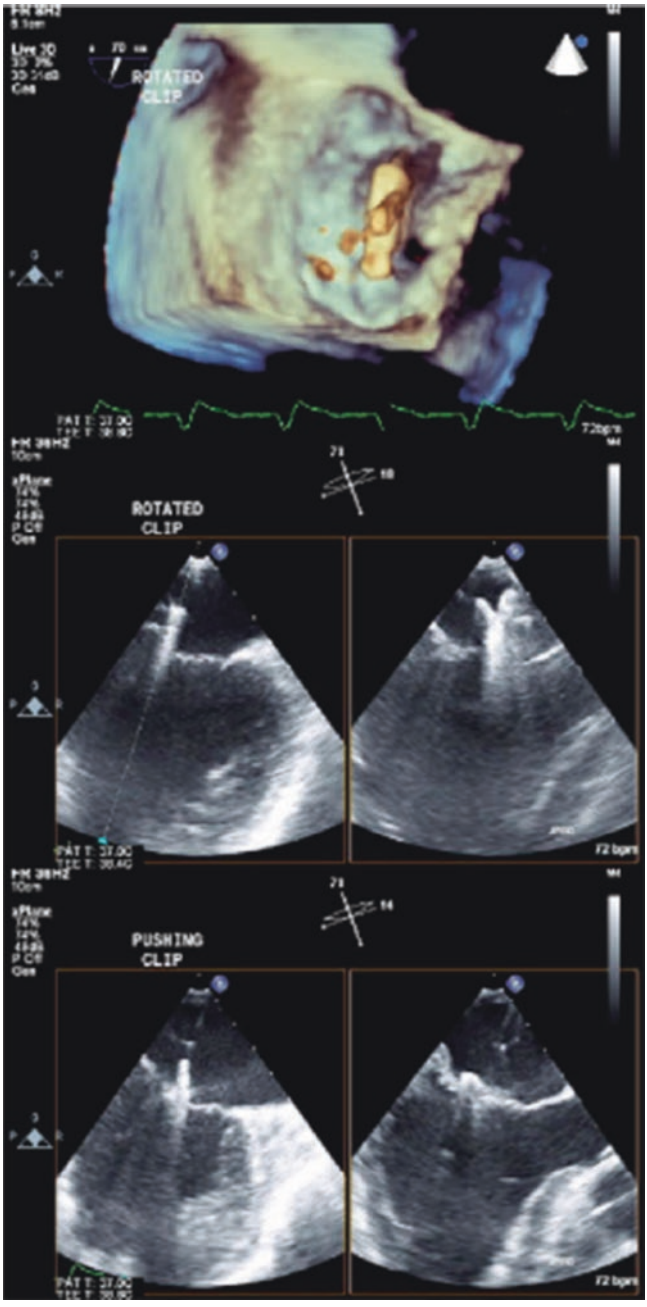


**Fig. 8.13** Three-dimensional echocardiography and mitral valve clip. In the mitral valve clip procedure, real-time 3D echocardiography identifies the position of the clip with respective to the mitral valve, in the enface perspective (*top panel*). The accurate positioning of the mitral clip often relies on simultaneous biplane imaging that more precisely defines the relationship between the arms of the clip with the valve leaflets (*bottom panel*)

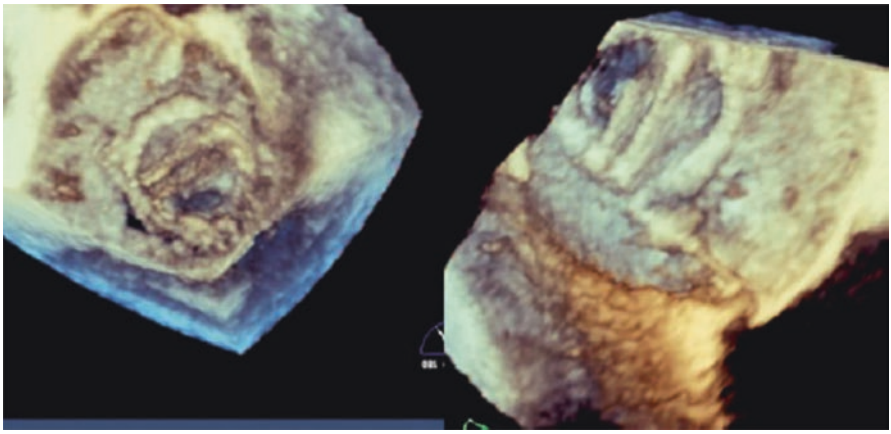

**Fig. 8.14** Three-dimensional echocardiography and percutaneous closure of paravalvular leaks. The enface view of the mitral valve obtained by real-time 3D echocardiography is especially important in the percutaneous closure of prosthetic paravalvular mitral regurgitation, as it provides the interventionist an anatomical orientation of the paravalvular regurgitation and the valve leaflets and surrounding structure. In this example, the defect is identified in the posterior aspect of the mitral prosthesis (*left panel*). In combination with other 2D and color Doppler views, a guidewire is successfully passed through the defect with subsequent successful deployment of the closure device (*right panel*)

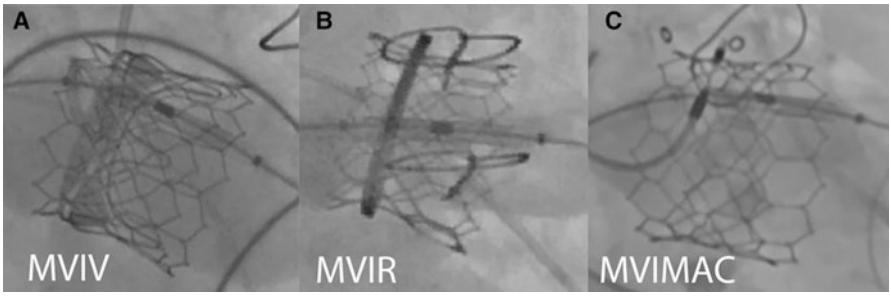


**Fig. 8.15** Fluoroscopic Images of mitral: (**a**) valve-in-valve, (**b**) valve-in-ring, and (**c**) valve-in-mitral annular calcification

For all transcatheter valvular procedures, assessment of vascular access is important and relies on different imaging modality (Fig. 8.16). Absolute size, amount, and extent of calcification, as well as tortuosity of iliac and femoral artery determine suitability for the procedure [138, 139]. Vascular complications are the major cause of morbidity and mortality in patients undergoing TAVI, and this should therefore be considered as transcatheter valve procedures increase in number with an expansion toward lower-risk, younger patients.

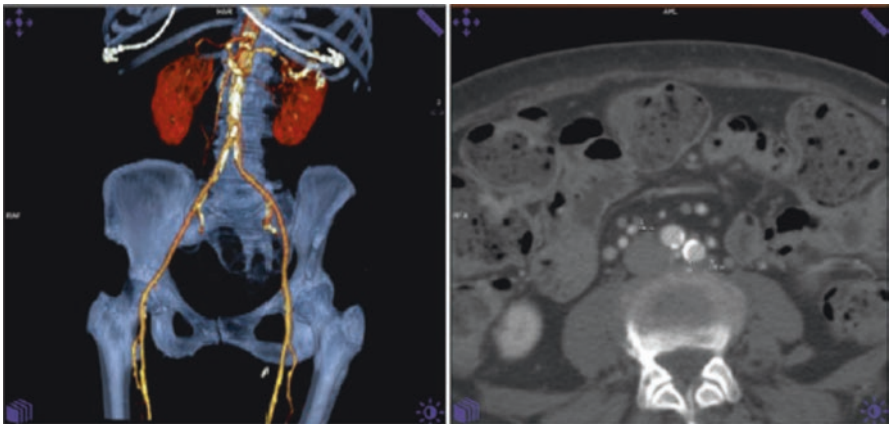

**Fig. 8.16** Assessment of vascular access. Computed tomography allows assessment of the iliac anatomy including vessel diameter, calcification, and tortuosity

## *8.2.3 Transcatheter Tricuspid Valve Procedures*

### 8.2.3.1 Anatomy

The tricuspid valve (TV) is the most anterior and apical of the four cardiac valves, and its apparatus is composed of leaflets, chordae and papillary muscles, annulus, and surrounding structures [140–142]. The valve leaflet orifice area is typically large at 7–9 $cm^2$ and with a low diastolic pressure gradient across the valve between the right atrium (RA) and right ventricle (RV) (mean gradient < 2 mmHg). The number of tricuspid leaflets is variable, but most commonly consists of an anterior, posterior, and septal leaflet; usually of unequal size, with anatomical variations of > 3 leaflets being present not being uncommon. The anterior leaflet is usually the largest, longest, and the most mobile of the three leaflets while the septal leaflet is the shortest in the radial direction and the least mobile. The posterior leaflet may have multiple scallops depending on anatomic variations. Overall, the leaflets are very thin and translucent which may be less ideal for anchoring interventional devices.

There are typically two papillary muscles with an occasional variant third. The anterior papillary muscle is the largest, located along the anterolateral RV wall, and provides chordae support to the anterior and posterior leaflets. The posterior papillary muscle provides chordae to the posterior and septal leaflets. The third variable septal papillary muscle may be present, absent, or even multiple. Chordae may even arise directly from the interventricular septum attaching to the anterior and septal leaflets, as well as other locations such as the RV free wall or moderator band.

The tricuspid annulus lacks a robust fibrous structure, is D-shaped (flat along the septum), and nonplanar. Due to this, annular dilation typically occurs laterally and posteriorly where there is lack of fibrous tissue. Coaptation of the TV leaflets occurs at the level or just below the annulus. The tricuspid annulus is dynamic, with

significant changes in area size depending on phase in the cardiac cycle and volume loading conditions.

Surrounding structures to the TV include the non-coronary sinus of Valsalva near the anteroseptal commissure, atrioventricular (AV) node and Bundle of His near the septal leaflet attachment, right coronary artery (RCA) which courses in the AV groove, and the superior vena cava (SVC) and inferior vena cava (IVC) which are potential therapeutic targets. Awareness of these structures is important as they can be inadvertently damaged during transcatheter tricuspid valve interventions leading to significant complications, morbidity, and mortality.

#### 8.2.3.2 Imaging

Pre-procedural and intra-procedural imaging are vital to transcatheter TV interventions. Two-dimensional and three-dimensional imaging is useful in pre-procedural planning using various modalities (i.e., echocardiography, computed tomography, and cardiac magnetic resonance imaging) [143]. Imaging is imperative to evaluate severity of pathology, tricuspid annulus size, leaflet coaptation/tethering, and etiology. Pre-procedural echocardiography is essential to assess amenability and feasibility. Sometimes the tricuspid valve may be difficult to image from an echocardiographic standpoint due to the anterior location of the valve; hence, feasibility is partially based on image quality suitable for intra-procedural guidance. Important measurements include RA & RV dimensions/areas and function, tricuspid annulus dimensions (i.e., antero-posterior/septal-lateral diameter, perimeter, area, RV apex-annulus distance), calcification, relationship and distance of the RCA to the tricuspid annulus, leaflet tethering height, coaptation gap, distance, tenting area and volume, subvalvular apparatus, and IVC/SVC dimensions [144, 145]. Similar to TAVI and TMVR, pre-procedural CT is essential in obtaining measurements to choose the optimal tricuspid intervention device.

TV edge-to-edge repair is currently the most commonly used and shown to be an effective method for transcatheter-based treatment of severe tricuspid regurgitation [140, 146, 147]. TV edge-to-edge repair cannot be possible without TEE guidance intra-procedurally. Both 2D (with biplane imaging) and 3D echocardiography are essential intra-procedurally to guide the clip device to the TV (making sure to avoid puncture of the inter-atrial septum), clip positioning and grasping of leaflets, evaluate for device stability and efficacy after clip deployment, and assess for any adverse complications during and post-procedure (i.e., pericardial effusion). Specifically, 3D TEE enface view in the deep transgastric position is used for clip orientation, and 2D TEE biplane imaging in the mid or deep esophageal position is often used for leaflet grasping. Other views are used to verify or confirm adequate tissue grasp before full deployment of the clips. Typically, approximation of the edges of the anterior and septal leaflets together has been associated with the best outcomes; however, each case is tailored based on the etiology of pathology.

There are several other transcatheter tricuspid interventional devices (annular reduction devices, heterotopic caval valve implantation, valve-in-valve

transcatheter valve replacement, and total tricuspid valve replacement) that are still under clinical investigation. Similar to the edge-to-edge repair device, intra-procedural 2D & 3D TEE guidance is imperative to device implantation and success. Given the rapid advancement of these technologies and current clinical investigation, the optimal techniques and intra-procedural imaging protocols are yet to be determined.

## 8.3 From Bench to Bedside: Imaging and Device Design/ Development

Beyond its value for clinical decision-making in the individual patient, 3D data are increasingly used for device design [148, 149]. Advances in medical imaging and computational modeling allow simulation of physiological conditions in patient-specific 3D vascular models. Such models can account for the unique features of the human circulation with appropriate 3D anatomical and physiological input data. This approach will allow prospective design of devices. Computed tomography is particularly attractive, because it acquires high-resolution volumetric data sets with sufficient temporal resolution for multiphasic analysis [150]. Along with high spatial resolution, newer state-of-the-art multi-detector CT systems have improved temporal resolutions and allow for quantification of the anatomy at multiple points in the cardiac cycle and subsequent mathematical modeling [151].

Finite element analysis is widely used in clinical research and device development. Finite element models quantitate the effects of changes in one or more of the parameters characterizing the system, including geometrical dimensions, mechanical properties, and fluid dynamics. The reliability of the results obtained through finite element modeling depends on the degree of realism achieved in modeling the physical characteristics that affect valvular biomechanics, including geometry, tissue mechanical properties, and boundary conditions due to the interaction with the surrounding tissues.

Models derived from in vivo 3D imaging provide realistic data. For example, finite element analysis using real-time 3D echocardiography examined regional mitral annular geometry and demonstrated that the nonplanar shape of the mitral annulus diminishes mitral leaflet stress [152]. Three-dimensional finite element models were also developed based on MRI of normal human aortic valve and root [153].

Computational methodology simulating valve systems is an integral part of valve design. The Food and Drug Administration in the United States and similar regulatory bodies in the European Community have established detailed guidelines for in vitro and in vivo preclinical testing of heart valve prostheses, with standardized methods and equipment in assessing fatigue, flow dynamics, and hydrodynamics of valve implants [154–156].

Direct clinical application has been described in the context of implantation of a new percutaneous pulmonary valve into a dilated pulmonary trunk, using patient-specific data to influence the design of the device and ensure patient safety [157–160].

## 8.4 Conclusion

Transcatheter procedures for valvular and structural heart disease require multimodality imaging both for preoperative planning and direct guidance. Imaging modalities include 2D modalities, such as fluoroscopy and 2D echocardiography, as well as 3D imaging modalities, including CT, MRI, C-arm CT, and 3D echocardiography, which acquire volumetric data sets and allow subsequent 3D display and visualization in unlimited planes. The data described above suggest an emerging role of 3D imaging for novel surgical and transcatheter approaches including device design.

## References

1. Iung B, Baron G, Butchart EG et al (2003) A prospective survey of patients with valvular heart disease in Europe: the Euro heart survey on valvular heart disease. Eur Heart J 24:1231–1243
2. Mihaljevic T, Nowicki ER, Rajeswaran J et al (2008) Survival after valve replacement for aortic stenosis: implications for decision making. J Thorac Cardiovasc Surg 135:1270–1278
3. Varadarajan P, Kapoor N, Bansal RC et al (2006) Clinical profile and natural history of 453 nonsurgically managed patients with severe aortic stenosis. Ann Thorac Surg 82:2111–2115
4. Pai RG, Kapoor N, Bansal RC et al (2006) Malignant natural history of asymptomatic severe aortic stenosis: benefit of aortic valve replacement. Ann Thorac Surg 82:2116–2122
5. Kapadia SR, Goel SS, Svensson L et al (2009) Characterization and outcome of patients with severe symptomatic aortic stenosis referred for percutaneous aortic valve replacement. J Thorac Cardiovasc Surg 137:1430–1435
6. Cribier A, Eltchaninoff H, Tron C et al (2004) Early experience with percutaneous transcatheter implantation of heart valve prosthesis for the treatment of end-stage inoperable patients with calcific aortic stenosis. J Am Coll Cardiol 43:698–703
7. Grube E, Schuler G, Buellesfeld L et al (2007) Percutaneous aortic valve replacement for severe aortic stenosis in high-risk patients using the second and current third-generation self-expanding CoreValve prosthesis: device success and 30-day clinical outcome. J Am Coll Cardiol 50:69–76
8. Lichtenstein SV, Cheung A, Ye J et al (2006) Transapical transcatheter aortic valve implantation in humans: initial clinical experience. Circulation 114:591–596
9. Webb JG, Pasupati S, Humphries K et al (2007) Percutaneous transarterial aortic valve replacement in selected high-risk patients with aortic stenosis. Circulation 116:755–763
10. Petronio AS, De Carlo M, Bedogni F et al (2010) Safety and efficacy of the subclavian approach for transcatheter aortic valve implantation with the CoreValve revalving system. Circ Cardiovasc Interv 3:359–366
11. Krishnaswamy A, Tuzcu EM, Kapadia SR (2010) Update on transcatheter aortic valve implantation. Curr Cardiol Rep 12:393–403

12. Gurvitch R, Wood DA, Tay EL et al (2010) Transcatheter aortic valve implantation: durability of clinical and hemodynamic outcomes beyond 3 years in a large patient cohort. Circulation 122:1319–1327
13. Eltchaninoff H, Prat A, Gilard M et al (2010) Transcatheter aortic valve implantation: early results of the FRANCE (FRench Aortic National CoreValve and Edwards) registry. Eur Heart J 32:191–197
14. Leon MB, Smith CR, Mack M et al (2010) Transcatheter aortic-valve implantation for aortic stenosis in patients who cannot undergo surgery. N Engl J Med 363:1012–1015
15. Alfieri O, Maisano F, De Bonis M et al (2001) The double-orifice technique in mitral valve repair: a simple solution for complex problems. J Thorac Cardiovasc Surg 122:674–681
16. Maisano F, Torracca L, Oppizzi M et al (1998) The edge-to-edge technique: a simplified method to correct mitral insufficiency. Eur J Cardiothorac Surg 13:240–245
17. St Goar FG, Fann JI, Komtebedde J et al (2003) Endovascular edge-to-edge mitral valve repair: short-term results in a porcine model. Circulation 108:1990–1993
18. Silvestry FE, Rodriguez LL, Herrmann HC et al (2007) Echocardiographic guidance and assessment of percutaneous repair for mitral regurgitation with the Evalve MitraClip: lessons learned from EVEREST I. J Am Soc Echocardiogr 20:1131–1140
19. Feldman T, Wasserman HS, Herrmann HC et al (2005) Percutaneous mitral valve repair using the edge-to-edge technique: six-month results of the EVEREST phase I clinical trial. J Am Coll Cardiol 46:2134–2140
20. Feldman T, Kar S, Rinaldi M et al (2009) Percutaneous mitral repair with the MitraClip system: safety and midterm durability in the initial EVEREST (Endovascular Valve Edge-to-Edge REpair Study) cohort. J Am Coll Cardiol 54:686–694
21. Webb JG, Harnek J, Munt BI et al (2006) Percutaneous transvenous mitral annuloplasty: initial human experience with device implantation in the coronary sinus. Circulation 113:851–855
22. Maniu CV, Patel JB, Reuter DG (2004) Acute and chronic reduction of functional mitral regurgitation in experimental heart failure by percutaneous mitral annuloplasty. J Am Coll Cardiol 44:1652–1661
23. Kaye DM, Byrne M, Alferness C et al (2003) Feasibility and short-term efficacy of percutaneous mitral annular reduction for the therapy of heart failure-induced mitral regurgitation. Circulation 108:1795–1797
24. Schofer J, Siminiak T, Haude M et al (2009) Percutaneous mitral annuloplasty for functional mitral regurgitation: results of the CARILLON Mitral Annuloplasty Device European Union Study. Circulation 120:326–333
25. Eicken A, Ewert P, Hager A et al (2011) Percutaneous pulmonary valve implantation: two centre experience with more than 100 patients. Eur Heart J 32:1260–1265
26. Zahn EM, Hellenbrand WE, Lock JE et al (2009) Implantation of the melody transcatheter pulmonary valve in patients with a dysfunctional right ventricular outflow tract conduit early results from the US Clinical trial. J Am Coll Cardiol 54:1722–1729
27. Lauten A, Ferrari M, Hekmat K et al (2011) Heterotopic transcatheter tricuspid valve implantation: first-in-man application of a novel approach to tricuspid regurgitation. Eur Heart J 32:1207–1213
28. Webb JG, Wood DA, Ye J et al (2010) Transcatheter valve-in-valve implantation for failed bioprosthetic heart valves. Circulation 121:1634–1636
29. Nunez-Gil IJ, Goncalves A, Rodriguez E et al (2011) Transapical mitral valve-in-valve implantation: a novel approach guided by three-dimensional transesophageal echocardiography. Eur J Echocardiogr 12:335–337
30. Vahanian A, Alfieri O, Al-Attar N et al (2008) Transcatheter valve implantation for patients with aortic stenosis: a position statement from the European Association of Cardio-Thoracic Surgery (EACTS) and the European Society of Cardiology (ESC), in collaboration with the European Association of Percutaneous Cardiovascular Interventions (EAPCI). Eur Heart J 29:1463–1470

31. Kapadia SR, Schoenhagen P, Stewart W et al (2010) Imaging for transcatheter valve procedures. Curr Probl Cardiol 35:228–276
32. Laissy JP, Messika-Zeitoun D, Serfaty JM et al (2007) Comprehensive evaluation of preoperative patients with aortic valve stenosis: usefulness of cardiac multidetector computed tomography. Heart 93:1121–1125
33. Ewe SH, Klautz RJ, Schalij MJ et al (2011) Role of computed tomography imaging for transcatheter valvular repair/insertion. Int J Cardiovasc Imaging 27:1179–1193
34. Schoenhagen P, Numburi U, Halliburton SS et al (2010) Three-dimensional imaging in the context of minimally invasive and transcatheter cardiovascular interventions using multidetector computed tomography: from pre-operative planning to intra-operative guidance. Eur Heart J 31:2727–2740
35. Saeed M, Hetts SW, English J et al (2011) MR fluoroscopy in vascular and cardiac interventions (review). Int J Cardiovasc Imaging 28:117–137
36. Siegel RJ, Luo H, Biner S (2011) Transcatheter valve repair/implantation. Int J Cardiovasc Imaging 27:1165–1177
37. Schoenhagen P, Tuzcu EM, Kapadia SR et al (2009) Three-dimensional imaging of the aortic valve and aortic root with computed tomography: new standards in an era of transcatheter valve repair/implantation. Eur Heart J 30:2079–2086
38. Johri AM, Passeri JJ, Picard MH (2010) Three dimensional echocardiography: approaches and clinical utility. Heart 96:390–397
39. Hung J, Lang R, Flachskampf F et al (2007) 3D echocardiography: a review of the current status and future directions. J Am Soc Echocardiogr 20:213–233
40. Handke M, Heinrichs G, Moser U et al (2006) Transesophageal real-time three-dimensional echocardiography methods and initial in vitro and human in vivo studies. J Am Coll Cardiol 48:2070–2076
41. Pothineni KR, Inamdar V, Miller AP et al (2007) Initial experience with live/real time three dimensional transesophageal echocardiography. Echocardiography 24:1099–1104
42. Sugeng L, Shernan SK, Salgo IS et al (2008) Live 3-dimensional transesophageal echocardiography initial experience using the fully-sampled matrix array probe. J Am Coll Cardiol 52:446–449
43. Balzer J, Kelm M, Kühl HP (2009) Real-time three-dimensional transoesophageal echocardiography for guidance of non-coronary interventions in the catheter laboratory. Eur J Echocardiogr 10:341–349
44. Balzer J, Kuhl H, Rassaf T et al (2008) Real-time transesophageal three-dimensional echocardiography for guidance of percutaneous cardiac interventions: first experience. Clin Res Cardiol 97:565–574
45. Scohy TV, Ten Cate FJ, Lecomte PV et al (2008) Usefulness of intraoperative real-time 3D transesophageal echocardiography in cardiac surgery. J Card Surg 23:784–786
46. Sugeng L, Shernan SK, Weinert L et al (2008) Real-time three-dimensional transesophageal echocardiography in valve disease: comparison with surgical findings and evaluation of prosthetic valves. J Am Soc Echocardiogr 21:1347–1354
47. Grewal J, Mankad S, Freeman WK et al (2009) Real-time three-dimensional transesophageal echocardiography in the intraoperative assessment of mitral valve disease. J Am Soc Echocardiogr 22:34–41
48. Iwakura K, Ito H, Kawano S et al (2006) Comparison of orifice area by transthoracic three-dimensional Doppler echocardiography versus proximal isovelocity surface area (PISA) method for assessment of mitral regurgitation. Am J Cardiol 97:1630–1637
49. Sharma R, Mann J, Drummond L et al (2007) The evaluation of real-time 3-dimensional transthoracic echocardiography for the preoperative functional assessment of patients with mitral valve prolapse: a comparison with 2-dimensional transesophageal echocardiography. J Am Soc Echocardiogr 20:934–940
50. Tommasini G, Camerini A, Gatti A et al (1998) Panoramic coronary angiography. J Am Coll Cardiol 31:871–877

51. Schwartz JG, Neubauer AM, Fagan TE et al (2011) Potential role of three-dimensional rotational angiography and C-arm CT for valvular repair and implantation. Int J Cardiovasc Imaging 27:543–546
52. Garcia JA, Chen SY, Messenger JC et al (2007) Initial clinical experience of selective coronary angiography using one prolonged injection and a 180 degrees rotational trajectory. Catheter Cardiovasc Interv 70:190–196
53. Neubauer AM, Garcia JA, Messenger JC et al (2010) Clinical feasibility of a fully automated 3D reconstruction of rotational coronary X-ray angiograms. Circ Cardiovasc Interv 3:71–79
54. Nölker G, Gutleben KJ, Marschang H et al (2008) Three-dimensional left atrial and esophagus reconstruction using cardiac C-arm computed tomography with image integration into fluoroscopic views for ablation of atrial fibrillation: accuracy of a novel modality in comparison with multislice computed tomography. Heart Rhythm 5:1651–1657
55. Biasi L, Ali T, Thompson M (2008) Intra-operative dynaCT in visceral-hybrid repair of an extensive thoracoabdominal aortic aneurysm. Eur J Cardiothorac Surg 34:1251–1252
56. Petersilka M, Bruder H, Krauss B et al (2008) Technical principles of dual source CT. Eur J Radiol 68:362–368
57. Rybicki FJ, Otero HJ, Steigner ML et al (2008) Initial evaluation of coronary images from 320-detector row computed tomography. Int J Cardiovasc Imaging 24:535–546
58. Achenbach S, Marwan M, Ropers D et al (2010) Coronary computed tomography angiography with a consistent dose below 1 mSv using prospectively electrocardiogram-triggered high-pitch spiral acquisition. Eur Heart J 31:340–346
59. Einstein AJ, Henzlova MJ, Rajagopalan S (2007) Estimating risk of cancer associated with radiation exposure from 64-slice computed tomography coronary angiography. JAMA 298:317–323
60. Brenner DJ, Hall EJ (2007) Computed tomography—an increasing source of radiation exposure. N Engl J Med 357:2277–2284
61. Morin RL, Gerber TC, McCollough CH (2003) Radiation dose in computed tomography of the heart. Circulation 107:917–922
62. Halliburton SS, Schoenhagen P (2010) Cardiovascular imaging with computed tomography: responsible steps to balancing diagnostic yield and radiation exposure. JACC Cardiovasc Imaging 3:536–540
63. Hausleiter J, Meyer T, Hermann F et al (2009) Estimated radiation dose associated with cardiac CT angiography. JAMA 301:500–507
64. Hausleiter J, Meyer T, Hadamitzky M et al (2006) Radiation dose estimates from cardiac multislice computed tomography in daily practice: impact of different scanning protocols on effective dose estimates. Circulation 113:1305–1310
65. Bischoff B, Hein F, Meyer T et al (2009) Impact of a reduced tube voltage on CT angiography and radiation dose: results of the PROTECTION I study. JACC Cardiovasc Imaging 2:940–946
66. Herzog BA, Husmann L, Burkhard N et al (2008) Accuracy of low-dose computed tomography coronary angiography using prospective electrocardiogram-triggering: first clinical experience. Eur Heart J 29:3037–3042
67. Husmann L, Valenta I, Gaemperli O et al (2007) Feasibility of low-dose coronary CT angiography: first experience with prospective ECG-gating. Eur Heart J 29:191–197
68. Eggebrecht H, Kuhl H, Kaiser GM (2006) Feasibility of real-time magnetic resonance-guided stent-graft placement in a swine model of descending aortic dissection. Eur Heart J 27:613–620
69. Kuehne T, Yilmaz S, Meinus C (2004) Magnetic resonance imaging-guided transcatheter implantation of a prosthetic valve in aortic valve position: feasibility study in swine. J Am Coll Cardiol 44:2247–2249
70. Kim JH, Kocaturk O, Ozturk C et al (2009) Mitral cerclage annuloplasty, a novel transcatheter treatment for secondary mitral valve regurgitation: initial results in swine. J Am Coll Cardiol 54:638–651

71. Guttman MA, Ozturk C, Raval AN et al (2007) Interventional cardiovascular procedures guided by real-time MR imaging: an interactive interface using multiple slices, adaptive projection modes and live 3D renderings. J Magn Reson Imaging 26:1429–1435
72. Elgort DR, Wong EY, Hillenbrand CM et al (2003) Real-time catheter tracking and adaptive imaging. J Magn Reson Imaging 18:621–626
73. Ratnayaka K, Faranesh AZ, Guttman MA et al (2008) Interventional cardiovascular magnetic resonance: still tantalizing. J Cardiovasc Magn Reson 10:62
74. Ratnayaka K, Raman VK, Faranesh AZ et al (2009) Antegrade percutaneous closure of membranous ventricular septal defect using X-ray fused with MRI (XFM). JACC Cardiovasc Interv 2:224–230
75. Rhode KS, Sermesant M, Brogan D et al (2005) A system for real-time XMR guided cardiovascular intervention. IEEE Trans Med Imaging 24:1428–1440
76. Lam CS, Xanthakis V, Sullivan LM et al (2010) Aortic root remodeling over the adult life course: longitudinal data from the Framingham Heart Study. Circulation 122:884–890
77. Choo SJ, McRae G, Olomon JP et al (1999) Aortic root geometry: pattern of differences between leaflets and sinuses of Valsalva. J Heart Valve Dis 8:407–415
78. Rankin JS, Dalley AF, Crooke PS et al (2008) A 'hemispherical' model of aortic valvar geometry. J Heart Valve Dis 17:179–186
79. Lansac E, Lim HS, Shomura Y et al (2005) Aortic root dynamics are asymmetric. J Heart Valve Dis 14:400–407
80. Lansac E, Lim HS, Shomura Y et al (2002) A four-dimensional study of the aortic root dynamics. Eur J Cardiothorac Surg 22:497–503
81. Kazui T, Izumoto H, Yoshioka K et al (2006) Dynamic morphologic changes in the normal aortic annulus during systole and diastole. J Heart Valve Dis 15:617–621
82. Kazui T, Kin H, Tsuboi J et al (2008) Perioperative dynamic morphological changes of the aortic annulus during aortic root remodeling with aortic annuloplasty at systolic and diastolic phases. J Heart Valve Dis 17:366–370
83. Maselli D, De Paulis R, Scaffa R et al (2007) Sinotubular junction size affects aortic root geometry and aortic valve function in the aortic valve reimplantation procedure: an in vitro study using the Valsalva graft. Ann Thorac Surg 84:1214–1218
84. Kurra V, Kapadia SR, Tuzcu EM et al (2010) Pre-procedural imaging of aortic root orientation and dimensions: comparison between X-ray angiographic planar imaging and 3-dimensional multidetector row computed tomography. JACC Cardiovasc Interv 3:105–513
85. Gurvitch R, Wood DA, Leipsic J et al (2010) Multislice computed tomography for prediction of optimal angiographic deployment projections during transcatheter aortic valve implantation. JACC Cardiovasc Interv 3:1157–1165
86. Tarantini G, Dvir D, Tang GHL (2021) Transcatheter aortic valve implantation in degenerated surgical aortic valves. EuroIntervention 17(9):709–719. https://doi.org/10.4244/EIJ-D-21-00157. PMID: 34665140
87. Tops LF, Wood DA, Delgado V et al (2008) Noninvasive evaluation of the aortic root with multislice computed tomography: implications for transcatheter aortic valve replacement. J Am Coll Cardiol Img 1:321–330
88. Ng ACT, Delgado V, van der Kley F et al (2010) Comparison of aortic root dimensions and geometries before and after transcatheter aortic valve implantation by 2 and 3-dimensional transesophageal echocardiography and multislice computed tomography. Circ Cardiovasc Imaging 3:94–102
89. Akhtar M, Tuzcu EM, Kapadia SR et al (2009) Aortic root morphology in patients undergoing percutaneous aortic valve replacement: evidence of aortic root remodeling. J Thorac Cardiovasc Surg 137:950–956
90. Stolzmann P, Knight J, Desbiolles L et al (2009) Remodelling of the aortic root in severe tricuspid aortic stenosis: implications for transcatheter aortic valve implantation. Eur Radiol 19:1316–1323

91. Schultz CJ, Moelker A, Piazza N et al (2010) Three dimensional evaluation of the aortic annulus using multislice computer tomography: are manufacturer's guidelines for sizing for percutaneous aortic valve replacement helpful? Eur Heart J 31:849–856
92. Doddamani S, Grushko MJ, Makaryus AN et al (2008) Demonstration of left ventricular outflow tract eccentricity by 64-slice multi-detector CT. Int J Cardiovasc Imaging 25:175–181
93. Hutter A, Opitz A, Bleiziffer S et al (2010) Aortic annulus evaluation in transcatheter aortic valve implantation. Catheter Cardiovasc Interv 76:1009–1019
94. Tuzcu EM, Kapadia SR, Schoenhagen P (2010) Multimodality quantitative imaging of aortic root for transcatheter aortic valve implantation: more complex than it appears. J Am Coll Cardiol 55:195–197
95. Messika-Zeitoun D, Serfaty JM, Brochet E et al (2010) Multimodal assessment of the aortic annulus diameter: implications for transcatheter aortic valve implantation. J Am Coll Cardiol 55:186–194
96. Bouzas-Mosquera A, Alvarez-Garcia N, Ortiz-Vazquez E et al (2009) Role of real-time 3-dimensional transesophageal echocardiography in transcatheter aortic valve implantation. Eur J Cardiothorac Surg 35:909
97. Détaint D, Lepage L, Himbert D et al (2009) Determinants of significant paravalvular regurgitation after transcatheter aortic valve: implantation impact of device and annulus discongruence. JACC Cardiovasc Interv 2:821–827
98. Binder RK, Webb JG, Willson AB, Urena M, Hansson NC, Norgaard BL, Pibarot P, Barbanti M, Larose E, Freeman M, Dumont E, Thompson C, Wheeler M, Moss RR, Yang TH, Pasian S, Hague CJ, Nguyen G, Raju R, Toggweiler S, Min JK, Wood DA, Rodés-Cabau J, Leipsic J (2013) The impact of integration of a multidetector computed tomography annulus area sizing algorithm on outcomes of transcatheter aortic valve replacement: a prospective, multicenter, controlled trial. J Am Coll Cardiol 62(5):431–438. https://doi.org/10.1016/j.jacc.2013.04.036. Epub 2013 May 15. PMID: 23684679
99. Tang GHL, Kaneko T, Cavalcante JL (2020) Predicting the feasibility of post-TAVR coronary access and redo TAVR: more unknowns than knowns. JACC Cardiovasc Interv 13(6):736–738. https://doi.org/10.1016/j.jcin.2020.01.222. PMID: 32192694
100. Barbanti M, Costa G, Picci A, Criscione E, Reddavid C, Valvo R, Todaro D, Deste W, Condorelli A, Scalia M, Licciardello A, Politi G, De Luca G, Strazzieri O, Motta S, Garretto V, Veroux P, Giaquinta A, Giuffrida A, Sgroi C, Leon MB, Webb JG, Tamburino C (2020) Coronary cannulation after transcatheter aortic valve replacement: the RE-ACCESS study. JACC Cardiovasc Interv 13(21):2542–2555. https://doi.org/10.1016/j.jcin.2020.07.006. Epub 2020 Oct 14. PMID: 33069648
101. Tang GHL, Zaid S, Fuchs A, Yamabe T, Yazdchi F, Gupta E, Ahmad H, Kofoed KF, Goldberg JB, Undemir C, Kaple RK, Shah PB, Kaneko T, Lansman SL, Khera S, Kovacic JC, Dangas GD, Lerakis S, Sharma SK, Kini A, Adams DH, Khalique OK, Hahn RT, Søndergaard L, George I, Kodali SK, De Backer O, Leon MB, Bapat VN (2020) Alignment of transcatheter aortic-valve neo-commissures (ALIGN TAVR): impact on final valve orientation and coronary artery overlap. JACC Cardiovasc Interv 13(9):1030–1042. https://doi.org/10.1016/j.jcin.2020.02.005. Epub 2020 Mar 16. PMID: 32192985
102. Khan JM, Greenbaum AB, Babaliaros VC, Rogers T, Eng MH, Paone G, Leshnower BG, Reisman M, Satler L, Waksman R, Chen MY, Stine AM, Tian X, Dvir D, Lederman RJ (2019) The BASILICA Trial: prospective multicenter investigation of intentional leaflet laceration to prevent TAVR coronary obstruction. JACC Cardiovasc Interv 12(13):1240–1252. https://doi.org/10.1016/j.jcin.2019.03.035. Epub 2019 Jun 12. PMID: 31202947; PMCID: PMC6669893
103. Latsios G, Gerckens U, Buellesfeld L et al (2010) "Device landing zone" calcification, assessed by MSCT, as a predictive factor for pacemaker implantation after TAVI. Catheter Cardiovasc Interv 76:431–439

104. John D, Buellesfeld L, Yuecel S et al (2010) Correlation of device landing zone calcification and acute procedural success in patients undergoing transcatheter aortic valve implantations with the self-expanding CoreValve prosthesis. J Am Coll Cardiol Intv 3:233–243
105. Zegdi R, Ciobotaru V, Noghin M et al (2008) Is it reasonable to treat all calcified stenotic aortic valves with a valved stent? Results from a human anatomic study in adults. J Am Coll Cardiol 51:579–584
106. Morgan-Hughes GJ, Roobottom CA (2004) Aortic valve calcification on computed tomography predicts the severity of aortic stenosis. Clin Radiol 59:208
107. Willmann JK, Weishaupt D, Lachat M et al (2002) Electrocardiographically gated multidetector row CT for assessment of valvular morphology and calcification in aortic stenosis. Radiology 225:120–128
108. Morgan-Hughes GJ, Owens PE, Roobottom CA et al (2003) Three dimensional volume quantification of aortic valve calcification using multislice computed tomography. Heart 89:1191–1194
109. Cueff C, Serfaty JM, Cimadevilla C et al (2010) Measurement of aortic valve calcification using multislice computed tomography: correlation with haemodynamic severity of aortic stenosis and clinical implication for patients with low ejection fraction. Heart 97:721–726
110. Okura H, Yoshida K, Hozumi T et al (1997) Planimetry and transthoracic two-dimensional echocardiography in noninvasive assessment of aortic valve area in patients with valvular aortic stenosis. J Am Coll Cardiol 30:753–759
111. Poh KK, Levine RA, Solis J et al (2008) Assessing aortic valve area in aortic stenosis by continuity equation: a novel approach using real-time three-dimensional echocardiography. Eur Heart J 29:2526–2535
112. John AS, Dill T, Brandt RR et al (2003) Magnetic resonance to assess the aortic valve area in aortic stenosis: how does it compare to current diagnostic standard. J Am Coll Cardiol 42:519–526
113. Burgstahler C, Kunze M, Loffler C et al (2006) Assessment of left ventricular outflow tract geometry in non-stenotic and stenotic aortic valves by cardiovascular magnetic resonance. J Cardiovasc Magn Reson 8:825–829
114. Del Valle-Fernández R, Jelnin V, Panagopoulos G et al (2010) A method for standardized computed tomography angiography-based measurement of aortic valvar structures. Eur Heart J 31:2170–2178
115. Delgado V, Ng ACT, van de Veire NR et al (2010) Transcatheter aortic valve implantation: role of multi-detector row computed tomography to evaluate prosthesis positioning and deployment in relation to valve function. Eur Heart J 8:113–123
116. Feuchtner GM, Dichtl W, Friedrich GJ et al (2006) Multislice computed tomography for detection of patients with aortic valve stenosis and quantification of severity. J Am Coll Cardiol 47:1410–1417
117. Janosi RA, Kahlert P, Plicht B et al (2009) Guidance of percutaneous transcatheter aortic valve implantation by real-time three-dimensional transesophageal echocardiography—a single-center experience. Minim Invasive Ther Allied Technol 18:142–148
118. Quill JL, Hill AJ, Laske TG et al (2009) Mitral leaflet anatomy revisited. J Thorac Cardiovasc Surg 137:1077–1081
119. Van Mieghem NM, Piazza N, Anderson RH et al (2010) Anatomy of the mitral valvular complex and its implications for transcatheter interventions for mitral regurgitation. J Am Coll Cardiol 56:617–626
120. Maselli D, Guarracino F, Chiaramonti F et al (2006) Percutaneous mitral annuloplasty: an anatomic study of human coronary sinus and its relation with mitral valve annulus and coronary arteries. Circulation 114:377–380
121. Ormiston JA, Shah PM, Tei C et al (1981) Size and motion of the mitral valve annulus in man. I. A two-dimensional echocardiographic method and findings in normal subjects. Circulation 64:113–120

122. Ormiston JA, Shah PM, Tei C et al (1982) Size and motion of the mitral valve annulus in man. II. Abnormalities in mitral valve prolapse. Circulation 65:713–719
123. Pai RG, Tanimoto M, Jintapakorn W et al (1995) Volume-rendered three-dimensional dynamic anatomy of the mitral annulus using a transesophageal echocardiographic technique. J Heart Valve Dis 4:623–627
124. Kaplan SR, Bashein G, Sheehan FH et al (2000) Three dimensional echocardiographic assessment of annular shape changes in the normal and regurgitant mitral valve. Am Heart J 139:378–387
125. Komoda T, Hetzer R, Uyama C et al (1994) Mitral annular function assessed by 3D imaging for mitral valve surgery. J Heart Valve Dis 3:483–490
126. Levine RA, Handschumacher MD, Sanfilippo AJ et al (1989) Three-dimensional echocardiographic reconstruction of the mitral valve, with implications for the diagnosis of mitral valve prolapse. Circulation 80:589–598
127. Faletra F, Grimaldi A, Pasotti E et al (2009) Real-time 3-dimensional transesophageal echocardiography during double percutaneous mitral edge-to-edge procedure. JACC Cardiovasc Imaging 2:1031–1033
128. Swaans MJ, Van den Branden BJ, Van der Heyden JA et al (2009) Three-dimensional transoesophageal echocardiography in a patient undergoing percutaneous mitral valve repair using the edge-to-edge clip technique. Eur J Echocardiogr 10:982–983
129. Daimon M, Shiota T, Gillinov AM et al (2005) Percutaneous mitral valve repair for chronic ischemic mitral regurgitation: a real-time three-dimensional echocardiographic study in an ovine model. Circulation 111:2183–2189
130. Feuchtner GM, Alkadhi H, Karlo C et al (2010) Cardiac CT angiography for the diagnosis of mitral valve prolapse: comparison with echocardiography. Radiology 254:374–383
131. Weir-McCall JR, Blanke P, Naoum C, Delgado V, Bax JJ, Leipsic J (2018) Mitral valve imaging with CT: relationship with transcatheter mitral valve interventions. Radiology 288(3):638–655. https://doi.org/10.1148/radiol.2018172758. Epub 2018 Jul 31. PMID: 30063194
132. Blanke P, Naoum C, Webb J, Dvir D, Hahn RT, Grayburn P, Moss RR, Reisman M, Piazza N, Leipsic J (2015) Multimodality imaging in the context of transcatheter mitral valve replacement: establishing consensus among modalities and disciplines. JACC Cardiovasc Imaging 8(10):1191–1208. https://doi.org/10.1016/j.jcmg.2015.08.004. PMID: 26481845
133. Case BC, Lisko JC, Babaliaros VC, Greenbaum AB, Satler L, Ben-Dor I, Forrestal BJ, Yerasi C, Kamioka N, Rogers T, Waksman R, Lederman RJ, Khan JM (2021) LAMPOON techniques to prevent or manage left ventricular outflow tract obstruction in transcatheter mitral valve replacement. Ann Cardiothorac Surg 10(1):172–179. https://doi.org/10.21037/acs-2020-mv-25. PMID: 33575191; PMCID: PMC7867420
134. Alkadhi H, Desbiolles L, Stolzmann P et al (2009) Mitral annular shape, size, and motion in normals and in patients with cardiomyopathy: evaluation with computed tomography. Investig Radiol 44:218–225
135. Choure AJ, Garcia MJ, Hesse B et al (2006) In vivo analysis of the anatomical relationship of coronary sinus to mitral annulus and left circumflex coronary artery using cardiac multidetector computed tomography: implications for percutaneous coronary sinus mitral annuloplasty. J Am Coll Cardiol 48:1938–1945
136. Gopal A, Shah A, Shareghi S et al (2010) The role of cardiovascular computed tomographic angiography for coronary sinus mitral annuloplasty. J Invasive Cardiol 22:67–73
137. Tops LF, Van de Veire NR, Schuijf JD et al (2007) Noninvasive evaluation of coronary sinus anatomy and its relation to the mitral valve annulus: implications for percutaneous mitral annuloplasty. Circulation 115:1426–1432
138. Kurra V, Schoenhagen P, Roselli EE et al (2009) Prevalence of significant peripheral artery disease in patients evaluated for percutaneous aortic valve insertion: preprocedural assessment with multidetector computed tomography. J Thorac Cardiovasc Surg 137:1258–1264
139. Joshi SB, Mendoza DD, Steinberg DH et al (2009) Ultra-low-dose intra-arterial contrast injection for iliofemoral computed tomographic angiography. JACC Cardiovasc Imaging 2:1404–1411

140. Hahn RT, Nabauer M, Zuber M, Nazif TM, Hausleiter J, Taramasso M, Pozzoli A, George I, Kodali S, Bapat V, Maisano F (2019) Intraprocedural imaging of transcatheter tricuspid valve interventions. JACC Cardiovasc Imaging 12(3):532–553. https://doi.org/10.1016/j.jcmg.2018.07.034. PMID: 30846126
141. Rodés-Cabau J, Hahn RT, Latib A, Laule M, Lauten A, Maisano F, Schofer J, Campelo-Parada F, Puri R, Vahanian A (2016) Transcatheter therapies for treating tricuspid regurgitation. J Am Coll Cardiol 67(15):1829–1845. https://doi.org/10.1016/j.jacc.2016.01.063. PMID: 27081024
142. Dahou A, Levin D, Reisman M, Hahn RT (2019) Anatomy and physiology of the tricuspid valve. JACC Cardiovasc Imaging 12(3):458–468. https://doi.org/10.1016/j.jcmg.2018.07.032. PMID: 30846121
143. Khalique OK, Cavalcante JL, Shah D, Guta AC, Zhan Y, Piazza N, Muraru D (2019) Multimodality imaging of the tricuspid valve and right heart anatomy. JACC Cardiovasc Imaging 12(3):516–531. https://doi.org/10.1016/j.jcmg.2019.01.006. Erratum in: JACC Cardiovasc Imaging. 2019 Dec;12(12):2611–2612. PMID: 30846125
144. van Rosendael PJ, Kamperidis V, Kong WK, van Rosendael AR, van der Kley F, Ajmone Marsan N, Delgado V, Bax JJ (2017) Computed tomography for planning transcatheter tricuspid valve therapy. Eur Heart J 38(9):665–674. https://doi.org/10.1093/eurheartj/ehw499. PMID: 27807057
145. Muraru D, Hahn RT, Soliman OI, Faletra FF, Basso C, Badano LP (2019) 3-dimensional echocardiography in imaging the tricuspid valve. JACC Cardiovasc Imaging 12(3):500–515. https://doi.org/10.1016/j.jcmg.2018.10.035. PMID: 30846124
146. Nickenig G, Weber M, Lurz P, von Bardeleben RS, Sitges M, Sorajja P, Hausleiter J, Denti P, Trochu JN, Näbauer M, Dahou A, Hahn RT (2019) Transcatheter edge-to-edge repair for reduction of tricuspid regurgitation: 6-month outcomes of the TRILUMINATE single-arm study. Lancet 394(10213):2002–2011. https://doi.org/10.1016/S0140-6736(19)32600-5. Epub 2019 Nov 7. Erratum in: Lancet. 2020 Mar 14;395(10227):870. PMID: 31708188
147. Nickenig G, Kowalski M, Hausleiter J et al (2017) Transcatheter treatment of severe tricuspid regurgitation with the edge-to-edge mitraclip technique. Circulation 135:1802–1814
148. Schoenhagen P, Hill A (2009) Transcatheter aortic valve implantation and potential role of 3D imaging. Expert Rev Med Devices 6:411–421
149. Abel DB, Dehdashtian MM, Rodger ST et al (2006) Evolution and future of preclinical testing for endovascular grafts. J Endovasc Ther 13:649–659
150. Zarins CK, Taylor CA (2009) Endovascular device design in the future: transformation from trial and error to computational design. J Endovasc Ther 16(Suppl 1):I12–I21
151. Grbi S, Ionasec R, Vitanovski D et al (2010) Complete valvular heart apparatus model from 4D cardiac CT. Med Image Comput Comput Assist Interv 13:218–226
152. Verhey JF, Nathan NS, Rienhoff O et al (2006) Finite-element-method (FEM) model generation of time-resolved 3D echocardiographic geometry data for mitral-valve volumetry. Biomed Eng Online 3:5–17
153. Conti CA, Votta E, Della Corte A et al (2010) Dynamic finite element analysis of the aortic root from MRI-derived parameters. Med Eng Phys 32:212–221
154. Kaplan AV, Baim DS, Smith JJ et al (2004) Medical device development: from prototype to regulatory approval. Circulation 109:3068–3072
155. Baim DS, Donovan A, Smith JJ et al (2007) Medical device development: managing conflicts of interest encountered by physicians. Catheter Cardiovasc Interv 69:655–664
156. Vassiliades TA Jr, Block PC, Cohn LH et al (2005) The clinical development of percutaneous heart valve technology: a position statement of the Society of Thoracic Surgeons (STS), the American Association for Thoracic Surgery (AATS), and the Society for Cardiovascular Angiography and Interventions (SCAI) Endorsed by the American College of Cardiology Foundation (ACCF) and the American Heart Association (AHA). J Am Coll Cardiol 45:1554–1560

157. Schievano S, Taylor AM, Capelli C et al (2010) First-in-man implantation of a novel percutaneous valve: a new approach to medical device development. EuroIntervention 5:745–750
158. Schievano S, Taylor AM, Capelli C et al (2010) Patient specific finite element analysis results in more accurate prediction of stent fractures: application to percutaneous pulmonary valve implantation. J Biomech 43:687–693
159. Capelli C, Taylor AM, Migliavacca F et al (2010) Patient-specific reconstructed anatomies and computer simulations are fundamental for selecting medical device treatment: application to a new percutaneous pulmonary valve. Philos Transact A Math Phys Eng Sci 368:3027–3038
160. Lurz P, Nordmeyer J, Giardini A et al (2011) Early versus late functional outcome after successful percutaneous pulmonary valve implantation are the acute effects of altered right ventricular loading all we can expect? J Am Coll Cardiol 57:724–731

# Chapter 9
# Transcatheter Mitral Repair and Replacement


**Jason L. Quill, Ana R. Menk, Gilbert H. L. Tang, and Jorge D. Zhingre Sanchez**

## Abbreviations

| | |
|---|---|
| DMR | Degenerative mitral regurgitation |
| FMR | Functional mitral regurgitation |
| LV | Left ventricular/ventricle |
| LVOT | Left ventricular outflow tract |
| MR | Mitral regurgitation |
| TAVI | Transcatheter aortic valve implantation |
| TEER | Transcatheter edge-to-edge repair |

## 9.1 Introduction

The anatomy and function of the atrioventricular valves have been described in detail (Chap. 1). In this chapter, a brief review of functional mitral regurgitation (FMR) and degenerative mitral regurgitation (DMR) will be described due to their clinical importance in a large number of transcatheter mitral repair and replacement devices. FMR is considered to be a disease of the left ventricle (LV). An enlarging

Jason L. Quill and Gilbert H. L. Tang affiliations' at the time of published writing for the first edition of *Heart Valves: From Design to Clinical Implantation (2013)*

J. L. Quill · A. R. Menk · J. D. Zhingre Sanchez (✉)
Medtronic, Inc., Mounds View, MN, USA
e-mail: jorge.d.zhingresanchez@medtronic.com

G. H. L. Tang
Mount Sinai Medical Center, New York, NY, USA

© The Author(s), under exclusive license to Springer Nature Switzerland AG 2023

P. A. Iaizzo et al. (eds.), *Heart Valves*, https://doi.org/10.1007/978-3-031-25541-0_9

LV, typically due to a myocardial infarction (resulting in ischemic MR) or dilated cardiomyopathy (resulting in idiopathic FMR), causes annular dilatation, papillary translocation, and chordal tethering. About 2.5 hospital admissions out of every 1000 included a diagnostic code for heart failure in the USA, and 25% of these patients were shown to have moderate or severe MR [1]. Furthermore, there is growing recognition of FMR, isolated from LV enlargement or annular dilation, in the presence of atrial fibrillation and atrial remodeling patients [68, 69].

Progression to severe heart failure significantly increases the risk of surgical mitral repair or replacement among these patients. Improvements in MR, heart failure symptoms, survival rates, and quality of life in this population may benefit from transcatheter treatment. Compared to treatment with medical therapy alone, transcatheter mitral valve repair resulted in lower rate of hospitalization and mortalities within 2-year clinical follow-up [2, 70].

DMR is considered a disease of the mitral valve. Leaflet perforation, elongation or rupture of chordae, and the rupture of papillary muscles are all causes of DMR. Mitral valve prolapse, a form of DMR, has been found to have a 2.4% prevalence in the US population [3], and more than 60% of surgical repair patients have DMR [4]. Surgical repair of DMR has been shown to improve survival compared to medical therapy alone [5], but there is still a bias against surgical intervention due to the invasive nature of open-heart surgery. Transcatheter mitral devices are therefore conceived to address this clinical gap by attempting to offer patients a less invasive approach to the treatment of both FMR and DMR.

Due to the complex anatomy and the various etiologies associated with mitral valve disease, several devices may be required to meet the clinical needs among this heterogeneous patient population. In absence of a single transcatheter mitral repair or replacement device that is suitable to use in all cases, a combination of device therapies will likely be necessary to correct the underlying pathology of the diseased mitral valve in each patient. Different categories of transcatheter mitral repair and replacement devices will now be described, with design features and design criteria discussed as well.

## 9.2 Design Criteria for Transcatheter Repair and Replacement

While many devices are in continued development, the design criteria and design features of these products can be understood from surgical mitral and transcatheter aortic experiences. For this chapter, a combination of direct references and coauthor experiences were provided for discussions of design criterion. Additionally, we will assume that these devices will be used primarily in patients unfit for surgery. The field of transcatheter mitral therapies appears to follow this similar path. While some of these devices may aim for or achieve equivalent safety and efficacy to surgical devices, it is outside the scope of this chapter to compare transcatheter mitral repair and replacement devices directly to surgical outcomes.

### 9.2.1 General Design Requirements

An ideal transcatheter mitral repair or replacement device would have several characteristics in common (Table 9.1). The delivery system would be of a minimal diameter with one of the preferred access routes: transseptal, transapical, transatrial, or retrograde aortic approach (Fig. 9.1). It would be able to accurately, reliably, and quickly reach the implant site. At the delivery site, the device would need to be deployed in a controlled and predictable manner. In the event of an improper device placement, the ideal device would be capable of being repositioned without damage to the mitral valve apparatus. Additionally, the device would be able to be recaptured back into the delivery system and withdrawn from the body should the need arise. Once the device is implanted, it would show acute success and exhibit durability for as many years as possible. The ideal device would also not prevent subsequent transcatheter or surgical interventions.

Clinical testing and evaluation for these different approaches for device delivery to the mitral valve are continuing and can benefit from the experiences of TAVI procedures. Early TAVI registry studies that evaluated device delivery reported high rates of access site complications [6, 7]. Major vasculature complications were defined as (1) any thoracic aortic dissection, (2) access site or access-related vascular injury, (3) distal embolization (noncerebral) from a vascular source requiring surgery or resulting in amputation or irreversible end-organ damage, or (4) LV perforation. Major bleeding following TAVI procedures was defined as (1) bleeding that caused death, (2) bleeding that caused hospitalization, (3) required pericardiocentesis or open and/or endovascular procedure for repair or hemostasis, (4) caused permanent disability (e.g., blindness, paralysis, hearing loss), or (5) required

**Table 9.1** Generalized characteristics of an ideal transcatheter mitral repair or replacement device

| Ideal mitral characteristics | Description |
|---|---|
| Ease of delivery | Accurate and reliable delivery via a transseptal, transapical, transatrial, or retrograde aortic approach through the smallest diameter delivery system possible |
| Ease of deployment | Controlled and predictable deployment with intraoperative imaging modalities, including echocardiography and fluoroscopy. |
| Ability to accurately position device | Allow for reliable positioning and potential correction of improper device placement |
| Ability to retrieve device | Allow for removal of device without surgical intervention |
| Ability to assess functionality intraoperatively | Able to assess quality of repair or replacement during the procedure |
| Preservation of future reintervention options | Device would be easily removed and/or not interfere with future surgical or transcatheter procedures required |
| Adjustability | Related more to repair procedures, this would allow for the device to be modified intraoperatively to optimize the performance of the device |
| Durability | Devices must maintain clinical benefits over time |

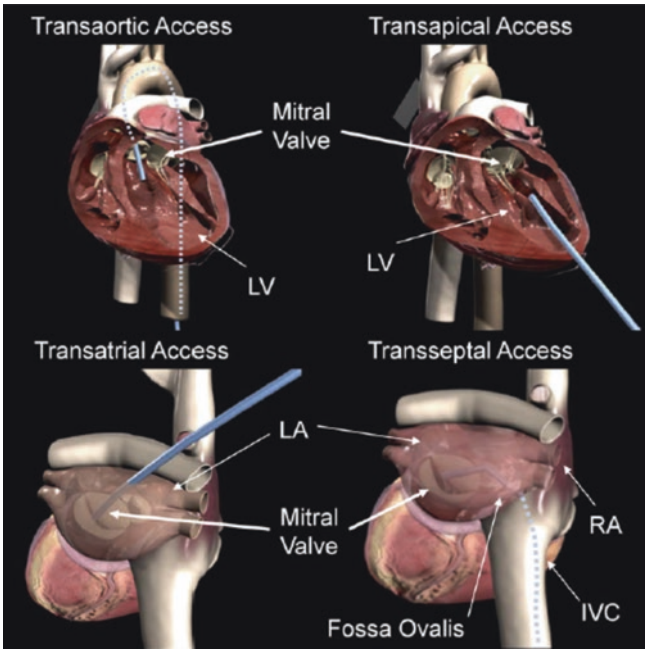


**Fig. 9.1** Transaortic access, transapical access, transatrial access, and transseptal access are depicted using a generic blue delivery system for illustrative purposes. A transfemoral approach is depicted in the transaortic access image, but other retrograde access sites are possible. Similarly, the transatrial access image shows an angulation of the catheter representative of a right thoracotomy, but the surgical approach could vary. *IVC*, inferior vena cava; *LA*, left atrium; *LV*, left ventricle

transfusion of >3 units of blood within 24-h period). However, these vascular complications and bleeding rates have significantly decreased in recent TAVI clinical cohort populations across the USA [71]. Further innovation to device delivery, including reducing sheath sizes, optimizing catheter designs, and procedural training, is necessary to reduce the incidence of these TAVI access complications, which may be translated to the mitral side.

Several publications have extensively studied and reported transcatheter access experiences with a percutaneous mitral repair device/procedure that utilizes the TEER technique (see Sect. 9.2.5). Initial TEER clinical trials had reported the use of transfemoral/transseptal venous route with minimal access site complications that included crossing the fossa ovalis [8–10]. Today, the clinical outcomes of transcatheter valve therapy registries with larger patient cohorts [67, 72] report that the transseptal route is used in majority of TEER cases [67].

In the transapical approach, a left anterior mini-thoracotomy is made to access the LV apex. Using this approach for TAVI procedures, Walther et al. reported access site complications requiring cardiopulmonary bypass in only 2 of 97 patients undergoing transapical TAVI [11]. Reported limitations of the transapical access that could pertain to transcatheter mitral cases include (1) calcifications of the apex,

(2) previous thoracotomies, (3) risk of myocardial perforation, (4) mitral or aortic valve trauma from misdirected stiff catheters, and (5) disruption of the LV or formation of a false aneurysm in the apical LV cannulation site [12, 13], leading some investigators to propose alternative surgical approaches for TAVI [13]. Due to these complications, there is favorable support and shift toward the transfemoral procedures [77]. However, there is ongoing clinical evidence and outcomes for using the transapical route to access the mitral valve. Recent analyses of patients treated with a specific transcatheter mitral valve replacement prosthesis, that is delivered using the transapical approach, reported few cases of LV apical and chest wall bleeding complications [73, 78].

Transatrial approaches have been used for minimally invasive mitral repair and surgical repair through a right thoracotomy. However, these procedures are performed on an arrested or fibrillating heart with open atriotomies, making the complication rates associated with the surgical approaches not representative of the expected complication rates in a percutaneous beating heart procedure. Nonetheless, percutaneous transatrial access from the left atrium is a potential option to directly intervene on the mitral valve and may be feasible with an appropriate atrial closure device. Transseptal access via femoral, internal jugular, or subclavian vein is familiar to cardiologists and surgeons as well as user-friendly. Access to the mitral valve does require an acute bend involving the use of stiff, large-bore delivery systems. After the procedure, the septal puncture site may need to be closed with a percutaneous device to avoid the risk of the development of an iatrogenic atrial septal defect.

Recent data suggest that the transfemoral/transseptal approach is the preferred delivery system approach for devices targeting the mitral valve. There are certain transcatheter mitral repair and replacement techniques that lend themselves to a particular approach, and when applicable, they will be discussed in subsequent sections of the chapter.

Once implanted, transcatheter mitral repair and replacement devices will be subjected to a highly dynamic environment. The mitral annulus is a three-dimensional structure that changes in both diameter and height throughout the cardiac cycle. The aortic valve is only separated from the mitral valve by a fibrous structure called the aorto-mitral fibrous continuity. Additionally, surrounding anatomical structures such as the left atrial appendage, pulmonary vein ostium, the coronary sinus, and the circumflex artery must be taken into consideration when evaluating device designs. Devices implanted in this complex environment need to pay special attention to defining the specifications of their device within the intended patient population to ensure safety. Please refer to Chap. 1 for a more detailed description of mitral and surrounding anatomy.

### *9.2.2 Mitral Replacement*

Transcatheter mitral valve replacement includes delivering a prosthetic valve to displace the native valve and function in its place (Fig. 9.2). Most commonly, this would consist of a bioprosthetic valve mounted on a self-expanding or balloon-expandable

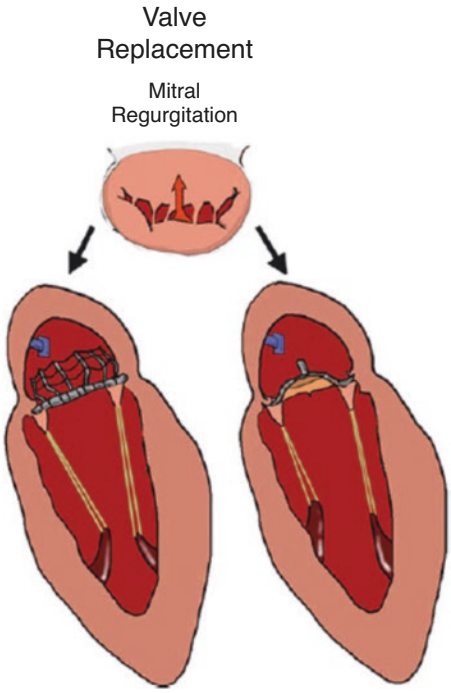


**Fig. 9.2** Transcatheter valve mitral replacement devices are implanted in the native annulus and take the place of the unhealthy, regurgitant valve

frame. It would undergo a crimping process in order to be loaded into a delivery system, and the native valve and subvalvular apparatus would not be removed. In addition to a degenerate native valve, transcatheter mitral valve replacement has been implemented in patients with previously implanted failed prostheses (valve-in-valve and valve-in-ring) or severe mitral calcification (valve-in-mitral annular calcification) [74]. The following sections will discuss the general characteristics and function of these transcatheter mitral valve replacement devices. Current comprehensive reviews of these replacement systems detail the early clinical experience and future directions for these technologies [59, 60, 76].

#### 9.2.2.1 Accurate Positioning and Migration Resistance

The ability to deliver the valve to the target location in order for the prosthetic valve to reliably remain in place is of critical importance. For accurate positioning, the system should have adequate visibility with available imaging techniques such as fluoroscopy and echocardiography. The mechanism for valve expansion (see Sect. 9.2.2.3) should allow for controlled, predictable deployment. Rapid ventricular pacing may be required during valve deployment to ensure secure anchorage to the mitral annulus and prevent acute embolization.

Once deployed, the valve must maintain a therapeutic position when exposed to pressure changes across the functioning valve, as well as external loading from the

beating heart. In the case of FMR patients, the valve would also need to stay in place with the potential for continued dilation of the mitral annulus. Migration resistance is especially challenging in the mitral position, because the pressure gradient across the closed valve is higher than any other cardiac valve [14]. Mechanisms for migration resistance may include radial interference with surrounding structures, physical anchors that engage the tissue, and axial anchoring created by the expanded shape of the frame or interaction with surrounding anatomical structures.

#### 9.2.2.2 Access

Due to the relatively large amount of material needed to fabricate a prosthetic mitral valve, the delivery system size is expected to be larger than that of percutaneous repair devices. Transcatheter aortic valve delivery systems can range from 16 to 30 Fr for transfemoral and transapical approaches [15, 16]. Since transcatheter mitral valves will need to be larger than transcatheter aortic valves because of larger native annular size, delivery system profiles may be slightly larger, ranging between 20- to 35-Fr [76]. For larger introduction sizes, it may be necessary to use a transapical or transatrial approach. These approaches have the potential advantage of more direct alignment of the prosthesis with the native valve, but the disadvantage of added invasiveness. If the introduction size is sufficiently small, a transarterial (retrograde aortic) or transseptal approach is possible. Delivery systems accessed via transseptal and transapical approaches have been designed and tested in animal models [14, 17] during early development. Since then, these systems have been implemented in selected patient studies [59, 60, 63, 67, 72, 73]. Both are feasible options and although the transseptal access is considered more technically challenging, it presents with fewer complications compared to the more invasive transapical or transatrial routes [64, 67].

#### 9.2.2.3 Mechanism for Valve Expansion

In transcatheter aortic valve design, two primary mechanisms for valve expansion have emerged: balloon-expandable frames and self-expanding frames. Both methods have been clinically acceptable in the aortic position [18]. These mechanisms have unique implications when applied to the mitral position.

For valves utilizing balloon-expandable frames, the device is compressed onto the balloon catheter using a crimper or it is crimped manually by the physician. Balloon-expandable frame materials include stainless-steel alloys, platinum-iridium alloys, and cobalt chromium alloys. These materials generally have higher stiffness than materials used in self-expanding frames, potentially maintaining a more consistent prosthetic valve geometry once deployed. Balloon-expandable frames may require rapid pacing during implantation, to prevent large shifts in position resulting from changes in chamber pressure when the valve orifice is occluded. These frames would be deployed to a diameter (perimeter) that is larger than the native annulus

diameter (perimeter) in order to create an interference fit with the annulus and surrounding anatomy. This serves to firmly affix the device in place, maximizing valve orifice area and mitigating against both paravalvular leakage and device migration. After expansion, these frame materials experience some elastic recoil or reduction in the frame diameter upon balloon deflation; the recoil characteristics must be considered for proper sizing and function of the device.

Self-expanding frames are made of a material called Nitinol. Nitinol is a nickel titanium alloy frame material which exhibits superelastic and shape-memory properties, allowing it to be compressed to a small diameter and then re-expanded to a preset shape when deployed within the body at the target implant location. For Nitinol frames, loading the device onto the delivery system is typically conducted with the device immersed in a cold saline bath such that the frame material is in its low-temperature martensitic phase. This facilitates loading of the device onto the delivery system in a controllable manner. Upon deployment, the frame attempts to expand to its preformed geometry via the shape-memory effect. The frame expands until it apposes the valve annulus creating an interference fit with the surrounding anatomy, maximizing valve orifice area and mitigating against both paravalvular leakage and device migration. Nitinol structures tend to be more flexible than balloon-expandable frames, allowing them to conform to the surrounding structures and accommodate imposed deformations. They generate outward radial force, which contributes to anchoring, and may continue to expand over time as annular dilation progresses. Alternative frame geometries may also be created from Nitinol, which may allow the frame to uniquely conform to the surrounding anatomy.

#### 9.2.2.4 Valve Performance

The hemodynamic performance of a prosthetic mitral valve should fully correct the patient's pathologic condition by providing freedom from stenosis or regurgitation. Ideally, a transcatheter prosthetic valve would provide hemodynamic performance comparable with surgical prosthetic valves.

One aspect of valve performance that will be particularly challenging in the mitral position is paravalvular leakage, the shunting of blood around the outside of the prosthetic valve. The valve replacement must create a reliable seal with the complex mitral valve structure and surrounding anatomy. As discussed in Chap. 1, the mitral annulus is generally saddle-shaped and elliptical, with complex dynamics throughout the cardiac cycle. With surgical valve replacement, paravalvular leakage can be largely prevented by the multitude of sutures used to secure the valve in place. For transcatheter valves, which are not sewn into place, this will be challenging in the mitral position due to the irregular shape of the annulus, as well as the potential for annular dilation to progress over time if not anchored by the frame.

#### 9.2.2.5 Anatomic Interactions

The profile of the mitral valve replacement must allow for normal function of the surrounding anatomic structures. One notable interaction is between the mitral valve and the left ventricular outflow tract (LVOT). The mitral valve and LVOT are located in close proximity to one another (Fig. 9.3). If the subvalvular apparatus is preserved during mitral replacement, the presence of the prosthesis could result in systolic anterior motion of the anterior mitral valve leaflet toward the LVOT, leading to obstruction of blood flow through the LVOT [19–21].

The valve must also allow adequate drainage of blood from the left atrium, thereby avoiding areas of stasis. On the atrial side, the prosthetic valve must also avoid disruption of the pulmonary veins and left atrial appendage. In general, any contact between the device and tissue must be atraumatic.

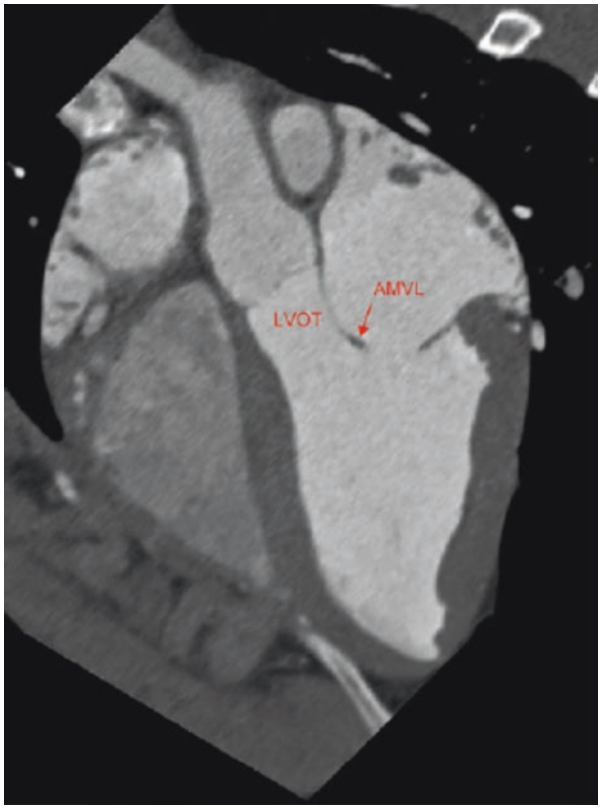


**Fig. 9.3** Aortic and mitral valve anatomy, as shown by computed tomography imaging in swine. The mitral valve can be seen in close proximity to the aortic valve and left ventricular outflow tract. *AMVL*, anterior mitral valve leaflet; *LVOT*, left ventricular outflow tract

#### 9.2.2.6 Preservation of Native Valve Structures

In surgical mitral valve replacement, there is evidence suggesting that it is critical to preserve at least the posterior subvalvular apparatus [22–24]. Studies comparing partial (posterior only) and complete (anterior and posterior) sparing of the chordae tendineae conclude that complete preservation of the subvalvular structure contributes to superior LV function following surgery [23, 24]. These findings suggest that percutaneous mitral valve replacement would be similarly effective by not removing the existing valve structures. The impact of the transcatheter bioprosthesis on the orientation and tension of the native valve structure should be studied. Specifically, appropriate tension on the chordae should be maintained [23], and the anterior mitral leaflet may need to be restricted from interference with flow through the LVOT. Another technique to partially preserve and restore native valve competence is mitral leaflet augmentation. This repair involves patching the leaflets with an autologous pericardium tissue to extend the leaflet surface area and improve coaptation. Leaflet augmentation can be implemented on the anterior or posterior leaflets and in conjunction with annuloplasty (see Sect. 9.2.4) [75].

In addition to preservation of the subvalvular apparatus, a prosthetic valve designer must determine if it is appropriate to mimic other structural elements of a mitral valve. For example, the shape of the native annulus is generally saddle-shaped and elliptical, with complex dynamics throughout the cardiac cycle. Surgical valve replacement involves sewing the annulus to a rigid sewing ring, so the anatomy conforms to the planar, circular structure of the bioprosthesis. With transcatheter valves, however, the valve may need to conform to the complex mitral anatomy. Also, the native mitral valve structure is a bileaflet configuration. Again, there is precedent with bioprosthetic surgical valves, which replace the bicuspid valve with a tricuspid valve. However, a bileaflet valve design may more closely mimic the flow dynamics of the native valve [25].

#### 9.2.2.7 Applicability for Various Sizes and Conditions

Transcatheter mitral valve replacement therapy may present a distinct advantage over repair techniques if they are applicable to a variety of underlying disease states. Since the existing valve would be fully replaced, the same therapy could apply to a broad range of severities and etiologies of both MR and stenosis. Transcatheter replacement valves could even be made compatible with failed surgical bioprostheses or annuloplasty devices [26–29, 74]. In addition to treating a variety of underlying conditions, a prosthetic mitral valve should accommodate a wide range of mitral annulus sizes (Chap. 1, Table 1.1).

### 9.2.3 *Indirect Annuloplasty*

Transcatheter indirect annuloplasty devices aim to mimic surgical annuloplasty devices by reducing the mitral annulus in order to achieve better apposition of the native mitral leaflets (Fig. 9.4). This technique specifically targets patients with FMR [30–32]. Indirect annuloplasty utilizes the close proximity of the coronary sinus to the mitral annulus. By implanting a device into the coronary sinus, which is easily accessible, a change can be made to the morphology of the mitral valve.

The relationship between the coronary sinus and the mitral annulus is highly variable, and the coronary sinus is most often aligned with left atrial wall rather than directly behind the mitral annulus (Fig. 9.5) [33, 34]. For such a treatment to be effective, it must accommodate variable anatomies to produce a sufficient change to the mitral annulus.

The variability between patients, including the coronary sinus and mitral annuli dimensions, has been reported in several anatomical studies. Maselli et al. reported measurements ranging from 1 to 15 mm (mean = 5.7 mm) at the P2 region of the mitral annulus, and from 5 to 19 mm (mean = 9.7 mm) at the P3 region in human cadaveric hearts [33]. Other anatomic studies with multi-slice computed tomography report similar ranges for the distance between the coronary sinus and mitral annulus [30, 34, 35]. Plass et al. noted that in 12% of the patients studied, the coronary sinus ran oblique to the mitral valve annulus, resulting in especially variable distances along the length of the coronary sinus in these patients [35]. Tops et al.

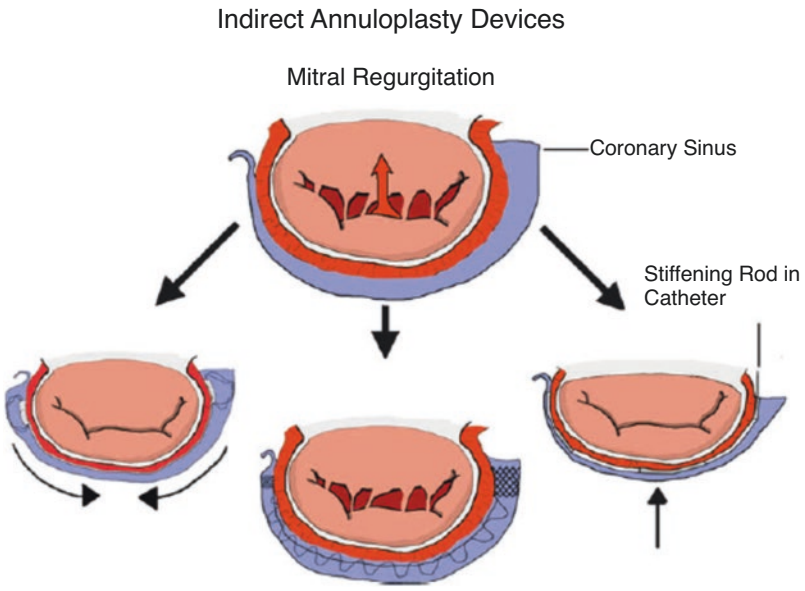


**Fig. 9.4** Indirect annuloplasty devices are implanted within the coronary sinus. The goal of these devices is to reduce the septal-lateral diameter of the mitral valve to increase coaptation

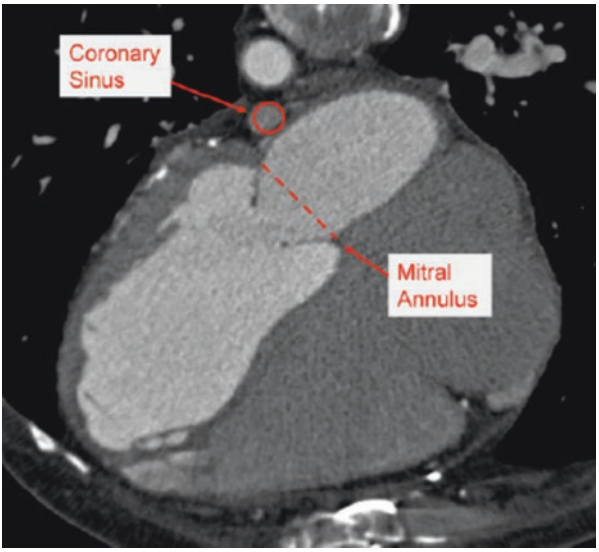


**Fig. 9.5** Anatomic relationship between coronary sinus and mitral valve annulus, as shown by computed tomography imaging in human

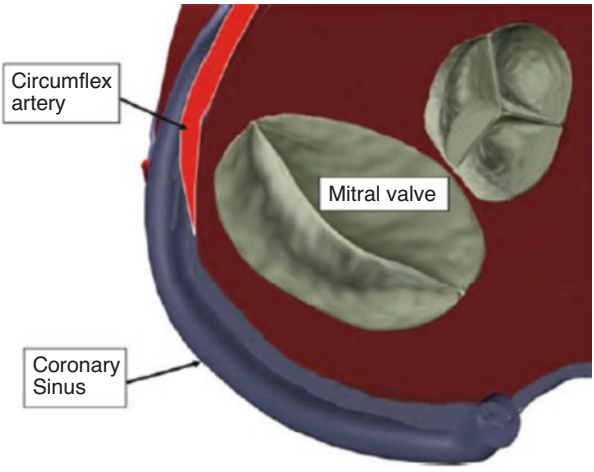


**Fig. 9.6** Anatomic relationship between coronary sinus, circumflex artery, and mitral valve. In this example, the circumflex artery is shown crossing under the coronary sinus. In such cases, the circumflex artery can be compressed when a device in the coronary sinus is tensioned toward the mitral valve

showed that patients with severe MR had a significantly higher minimum distance between the coronary sinus and mitral annulus, as compared to patients without severe MR [34].

Another critical anatomic feature for indirect annuloplasty is the relationship between the coronary sinus and the circumflex coronary artery (Fig. 9.6). Several anatomic studies have reported the varying relationship between the coronary sinus and the circumflex artery. The percentage of patients in which the circumflex crosses between the coronary sinus and the mitral annulus has been reported within the

range of 68% and 88% [34, 36, 61]. It is critical for preoperative imaging to reveal this relationship, and the indirect annuloplasty device must avoid prolonged impingement of the circumflex artery.

An indirect annuloplasty device should either provide a predictable and reproducible amount of annular reduction or provide real-time adjustability. Real-time adjustability is preferred for indirect annuloplasty devices, providing functional assessment of the valve while cinching is taking place. In addition to evaluating acute efficacy intraoperatively, the flow to the coronary circulation should also be confirmed before final device deployment.

In addition to adjustability during implant, the devices would ideally allow reintervention as needed at a later date. The device should not interfere with a surgical mitral repair or replacement, if required in the future. In the event of a device failure, the device would ideally be fully retrievable with minimal intervention required. Additionally, the profile of the device in the coronary sinus should also allow other future procedures such as retrograde cardioplegia cannulation for cardiac arrest, biventricular cardiac pacing, or radio-frequency ablation procedures.

### *9.2.4 Direct Annuloplasty*

Direct annuloplasty devices are transcatheter repair devices that mimic a surgical annuloplasty ring (Fig. 9.7). The purpose of a surgical annuloplasty ring is twofold. In patients with a dilated annulus, such as FMR patients, an undersized

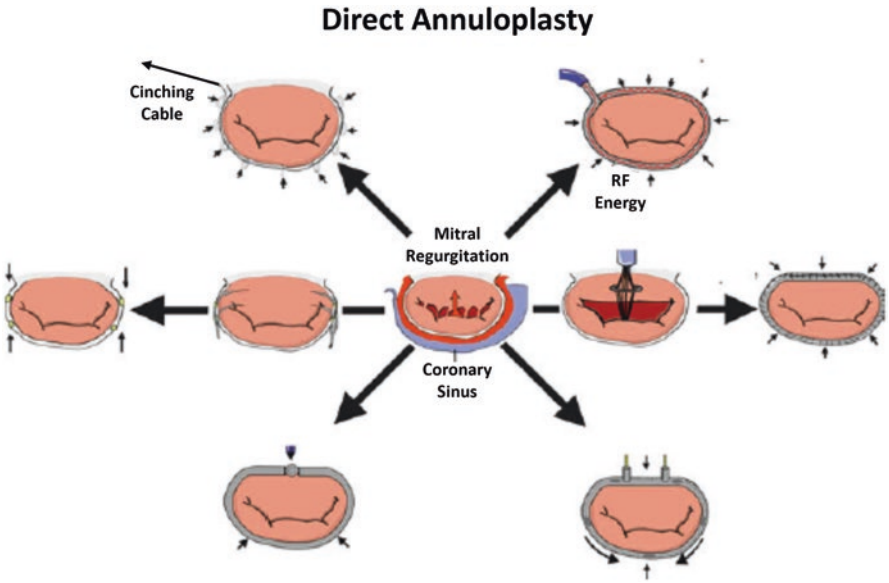


**Fig. 9.7** Direct annuloplasty devices act upon the mitral annulus to improve coaptation of the mitral leaflets

annuloplasty ring can increase the coaptation surface of the mitral leaflets, and surgical annuloplasty is the predominant approach [37]. Despite the widespread use of annuloplasty for this purpose, the clinical benefit has been difficult to demonstrate within the heart failure population [38, 39]. The second reason for using an annuloplasty ring is to maintain the durability of a surgical repair in DMR patients. In this setting, the annuloplasty ring does not reduce the orifice area of the valve, but rather prevents long-term dilatation of the annulus and maintains the durability of the surgical repair. Transcatheter repair devices in the category of direct annuloplasty typically seek to mimic the reduction in annulus area achieved with surgical annuloplasty rings in patients with a dilated mitral annulus.

Surgical experience from valve repair can offer insight on different techniques to reduce the annulus area that could be used by percutaneous devices (Table 9.2). Continuous radial force techniques draw the annulus inward toward the center of the mitral valve, similar to annuloplasty rings. Another technique to reduce the annulus area is to provide circumferential force around the entire circumference of the annulus. There is surgical precedence for this type of repair; thus, some of the suture techniques will be described. Early suture techniques such as the De Vega have proved to be less effective than current annuloplasty techniques in functional tricuspid regurgitation patients [40–43]. The De Vega technique has been criticized for being unpredictable and unreliable, perhaps owing to the long suture line or the use of polypropylene suture material, which may break and slide through the tissue as the annulus dilates [44]. However, the De Vega technique has shown long-term durability out to 6.8 years in 232 patients with 86% of patients having zero to moderate regurgitation [45], and posterior suture bicuspidization has shown long-term durability out to 3 years with no significant difference in regurgitation severity compared to surgical annuloplasty [46]. A segmented circumferential force can reduce the annulus area, but there is no surgical precedence for this type of repair. Areas of the annulus tissue located between the repaired segments of the annulus would not be constrained and could potentially continue to dilate over time. Devices that use septal-lateral reduction of the mitral annulus reduce the distance between A2 and P2 scallops on the mitral valve. By reducing the A2–P2 distance, the anterior and posterior leaflets would be brought in closer proximity and be capable of coaptation again. This surgical technique has demonstrated its effectiveness in the acute reduction of regurgitation in an FMR animal model [47]. Finally, the tissue properties of the annulus can be modified as a means of therapy for DMR patients. Radiofrequency energy can cause structural changes to the annulus by creating fibrotic tissue which, in turn, decreases the motion of the annulus as well [48].

Surgical annuloplasty rings are sewn to the endocardial surface of the annulus and have a long history of success and durability. Endocardial placement of the ring allows for access to the device during subsequent procedures, should the need arise. Transcatheter direct annuloplasty devices that are also placed on the endocardium are the closest to mimicking a surgical annuloplasty ring procedure [63–65]. Transcatheter direct annuloplasty devices that are placed on the ventricular side of the mitral valve or traverse from the LV to the left atrium could still potentially provide reduction in perimeter and area similar to an annuloplasty ring.

**Table 9.2** Different mechanisms that are utilized by transcatheter valve mitral annuloplasty devices to reduce the annulus dimensions and increase leaflet coaptation

| Categories of percutaneous device repair | Description |
|---|---|
| Continuous radial force  | Devices create a reduction in annulus area by providing radial force toward the center of the mitral valve, as surgical annuloplasty rings do |
| Continuous circumferential force  | Devices reduce annulus area by cinching along the perimeter of the annulus; cinching could be complete or partial |
| Segmented circumferential force  | Devices reduce annulus area by cinching portions of tissue along the perimeter of the annulus |
| Septal-lateral reduction 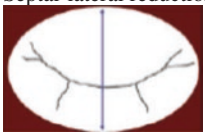 | Devices aim to reduce the septal-lateral dimension of the mitral valve; reduction in septal-lateral diameter allows for greater coaptation of the native leaflets |
| Alteration of tissue properties  | Devices alter tissue properties of the annulus and cause fibrotic tissue to form |

A direct annuloplasty device must either be able to provide a predictable amount of cinching based upon preoperative or intraoperative imaging measurements or provide real-time adjustability. Real-time adjustability is a preferred characteristic for direct annuloplasty devices; it provides functional assessment of the valve while cinching is taking place, allowing the implanting physician to “dial-in” the optimal amount of cinching to reduce regurgitation.

### 9.2.5 *Transcatheter Edge-to-Edge Repair (TEER)*

Transcatheter edge-to-edge mitral valve repair (TEER, also known as the Alfieri stitch) is a repair technique in which the free edge of the anterior leaflet is sewn to the free edge of the posterior leaflet at the area of regurgitation, creating a double orifice mitral valve (Fig. 9.8) [49–51]. The main indications for surgical repair using the edge-to-edge technique are bileaflet prolapse, anterior leaflet prolapse, commissural prolapse, or FMR [52]. However, the procedure has been shown to be effective in a variety of clinical settings, with a low risk for creating mitral stenosis [53].

Due to the simplicity of the surgical edge-to-edge technique, percutaneous valve repair has been explored [8–10] and established in clinical studies [70, 79]. The preferred delivery method for TEER devices is transseptal; since the device is small compared to other repair and replacement devices, the delivery system can navigate the additional tortuosity of the transseptal approach.

Early studies regarding edge-to-edge aimed to evaluate the durability of the repair. In surgical repair, annuloplasty rings were used concomitantly with the edge-to-edge technique in 83% of cases, using almost exclusively a partial flexible band [53]. Additionally, not including an annuloplasty band was determined to be one of the risk factors for a return of high-grade MR, suggesting that a complete, rigid annuloplasty ring would maintain the repair better than the partial, flexible band [53]. However, recent clinical data are promising and have resulted in the TEER repair technique having the most experience and system(s) with or approaching FDA approval and/or CE mark [59, 63, 64, 67, 72]. Finally, the ability to assess the quality of the TEER repair intraoperatively is preferable to devices that can only be assessed post-deployment. This, of course, is only useful if the device is able to be repositioned and/or recaptured.

### 9.2.6 *Chordal Replacement*

Surgical chordal replacement has proven to be highly reproducible with excellent long-term outcomes for posterior leaflet prolapse, resulting in freedom from valve-related reoperation of >95% [54, 55]. Chordal replacement is also an attractive

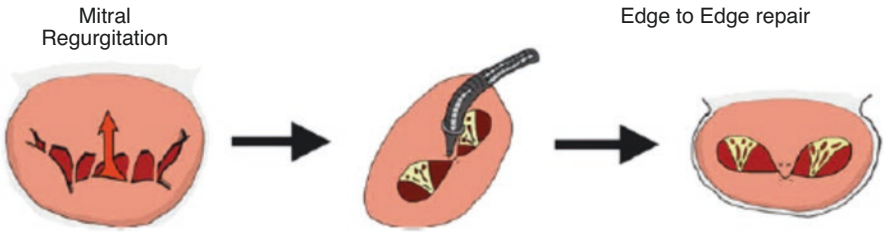


**Fig. 9.8** Transcatheter edge-to-edge repair (TEER) devices [8–10] reduce regurgitation by attaching the anterior leaflet to the posterior leaflet, creating a double orifice valve

surgical option for anterior and bileaflet prolapse. Motivation for percutaneous chordal replacement is based upon the desire for less invasive therapy [56]. A percutaneous chordal replacement device must be capable of attaching suture or a chordal equivalent to the leaflets of the mitral valve in an off-pump procedure (Fig. 9.9). Once attached to the leaflet, the replacement chordae must be attached to the papillary muscles, the endocardial surface of the LV, or externalized through the ventricular wall and anchored on the epicardial surface. The length of the chordal replacement would then be capable of being adjusted based upon intraoperative assessment of the mitral valve. Variations of these chordal replacement percutaneous systems are in continued development [63–65].

### *9.2.7 LV Repair*

Other devices have targeted changes in the LV geometry for repair of dilated or ischemic cardiomyopathy and type I MR, since it is considered to be a disease of the LV rather than the valve itself (Fig. 9.10). Animal studies have shown that dilation of the LV due to an ischemic event result in a relative translocation of the papillary muscles with respect to the annulus [57, 58]. The goal of these transcatheter versions of LV repair devices is to reshape the LV so that the papillary muscles are brought back into the correct relative position with respect to the annulus [63–65].

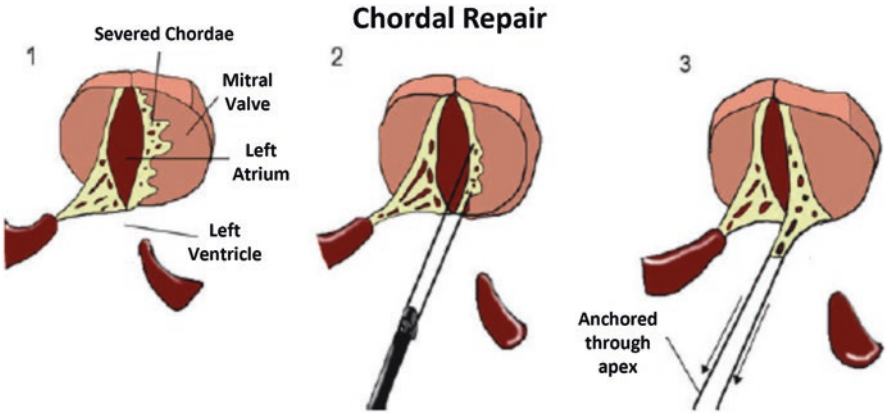


**Fig. 9.9** Chordal replacement devices attach artificial chords to the anterior and/or posterior leaflet, externalize the sutures through the left ventricular apex, and affix at an appropriate tethering length to achieve leaflet coaptation

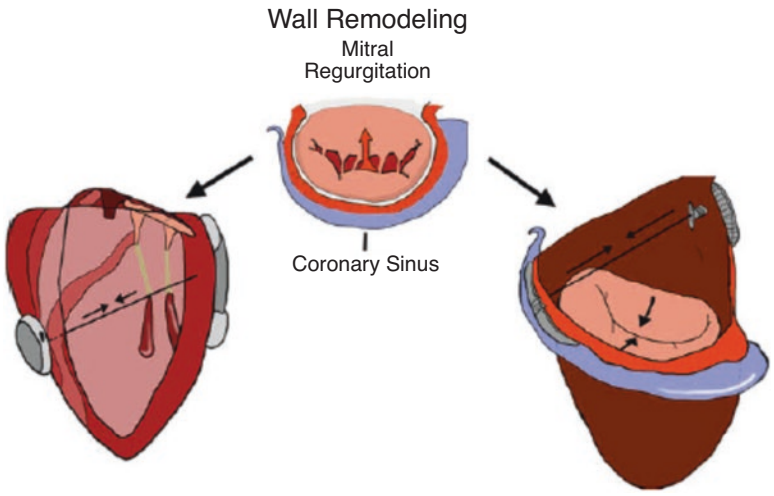


**Fig. 9.10** Wall remodeling devices aim to either reshape the LV in functional mitral regurgitation patients, thereby reducing the annulus dimensions and translocating papillary muscles, or create a tether in the left atrium capable of reducing the septal-lateral diameter of the mitral annulus

## 9.3 Transcatheter Mitral Replacement Versus Transcatheter Mitral Repair

There have been evolving discussions on the role of transcatheter mitral repair vs. replacement in patients with mitral valve disease. Currently, surgical therapy remains the gold standard in the treatment of both mitral stenosis and MR secondary to organic disease (e.g., DMR). Approved transcatheter devices for clinical use need to demonstrate noninferior outcomes. However, there will be situations where patients assessed for surgery are deemed inoperable or at extreme risk, as determined by the logistic EuroScore or Society of Thoracic Surgeons (STS) risk score. Other factors such as high-risk reoperations, multiple comorbidities, and frailty should be considered. In these cases, transcatheter mitral therapy may be an alternative option to conservative management, which would carry an inferior prognosis or surgery which may carry significant operative risks.

Although surgeons have advocated for mitral repair over replacement based on historical data, comparison studies between transcatheter repair and replacement are ongoing [59, 76]. Both techniques have shown promising clinical outcomes with respective advantages and limitations. However, more clinical evidence regarding efficacy and long-term results needs to be established. Most surgeons and the STS database acknowledge that the operative mortality of mitral repair is lower than mitral replacement, although the precise cause remains uncertain. Assuming the design hurdles of transcatheter mitral repair and replacement can be overcome, it is conceivable that for the same patient population, the procedural mortalities of replacement and repair may be equivalent.

The potential cannibalization of rising transcatheter mitral therapy cases against open surgery, as seen in percutaneous coronary intervention vs. coronary artery bypass graft and in the future TAVI vs. aortic valve replacement, is an issue to consider as well. We have seen the similar favorable outcomes of TAVI vs. surgical aortic valve replacement in the PARTNER and EVOLUT trials, and we have observed increasing adoption of TAVI in lower-risk populations. Assuming the early challenges in clinical implantation have been overcome, there is no reason to suspect that transcatheter mitral valve replacement will have a higher procedural mortality than surgical replacement. Similarly, transcatheter mitral repair should have the same low operative mortality as surgical repair. The fundamental question is one of long-term durability, since transcatheter mitral repair, if failed, may preclude surgical re-repair and the patient will be committed to a surgical mitral replacement, which has been shown to have a higher operative mortality than repair. A multidisciplinary team should be created to evaluate and manage these patients to determine which therapy is best for the patient with the lowest procedural risk and most durable results.

Transcatheter mitral therapy will continue to have an increasing complimentary role to surgery in the treatment of high-risk or inoperable patients with mitral valve disease. These patients may (1) have end-stage mitral stenosis too sick to undergo surgery, (2) have had multiple mitral valve surgeries making re-repair or surgical replacement too high risk, (3) be candidates for valve-in-valve applications as seen demonstrated in several clinical series, or (4) have too many comorbidities for conventional surgery.

For both transcatheter mitral repair and replacement therapies, imaging will likely play a critical role to expand the utility of these devices. Ultimately, the indirect impact of expansion of transcatheter mitral therapy will be one of increasing patient referral for intervention. Careful patient selection, education, and a team approach in management will ensure therapy success.

## 9.4 Conclusions/Summary

Percutaneous mitral valve technologies are at the current frontier of device development and continue to gain momentum. According to recent reviews, which highlighted transcatheter mitral technologies in active development, there are approximately 15 repair and 13 replacement systems [62–66]. Majority of these technologies are currently CE approved, in clinical trials, or in advanced stages of development [63, 76]. The success of the transcatheter mitral valve repair and replacement market will rely on demonstrating safety and efficacy compared to surgical intervention. In addition to maximizing patient clinical outcomes, training and imaging of these technologies will also be vital for the field. It will be essential to continually revisit these therapies to reassess the technological development of the devices and their impact on clinical practice.

## References


1. Martinez-Selles M, Garcia Robles JA, Prieto L et al (2002) Annual rates of admission and seasonal variations in hospitalizations for heart failure. Eur J Heart Fail 4:779–786
2. Gillinov AM, Wierup PN, Blackstone EH et al (2001) Is repair preferable to replacement for ischemic mitral regurgitation? J Thorac Cardiovasc Surg 122:1125–1141
3. Freed LA, Levy D, Levine RA et al (1999) Prevalence and clinical outcome of mitral-valve prolapse. N Engl J Med 341:1–7
4. Monin JL, Dehant P, Roiron C et al (2005) Functional assessment of mitral regurgitation by transthoracic echocardiography using standardized imaging planes diagnostic accuracy and outcome implications. J Am Coll Cardiol 46:302–309
5. Montant P, Chenot F, Robert A et al (2009) Long-term survival in asymptomatic patients with severe degenerative mitral regurgitation: a propensity score-based comparison between an early surgical strategy and a conservative treatment approach. J Thorac Cardiovasc Surg 138:1339–1348
6. Zahn R, Gerckens U, Grube E et al (2011) Transcatheter aortic valve implantation: first results from a multi-centre real-world registry. Eur Heart J 32:198–204
7. Leon MB, Smith CR, Mack M et al (2010) Transcatheter aortic-valve implantation for aortic stenosis in patients who cannot undergo surgery. N Engl J Med 363:1597–1607
8. Feldman T, Kar S, Rinaldi M et al (2009) Percutaneous mitral repair with the MitraClip system: safety and midterm durability in the initial EVEREST (Endovascular Valve Edge-to-Edge REpair Study) cohort. J Am Coll Cardiol 54:686–694
9. Feldman T, Wasserman HS, Herrmann HC et al (2005) Percutaneous mitral valve repair using the edge-to-edge technique: six-month results of the EVEREST Phase I Clinical Trial. J Am Coll Cardiol 46:2134–2140
10. Tamburino C, Ussia GP, Maisano F et al (2010) Percutaneous mitral valve repair with the MitraClip system: acute results from a real world setting. Eur Heart J 31:1382–1389
11. Walther T, Schuler G, Borger MA et al (2010) Transapical aortic valve implantation in 100 consecutive patients: comparison to propensity-matched conventional aortic valve replacement. Eur Heart J 31:1398–1403
12. Bleiziffer S, Ruge H, Mazzitelli D et al (2009) Survival after transapical and transfemoral aortic valve implantation: talking about two different patient populations. J Thorac Cardiovasc Surg 138:1073–1080
13. Bruschi G, De Marco F, Fratto P et al (2010) Direct aortic access through right minithoracotomy for implantation of self-expanding aortic bioprosthetic valves. J Thorac Cardiovasc Surg 140:715–717
14. Lozonschi L, Bombien R, Osaki S et al (2010) Transapical mitral valved stent implantation: a survival series in swine. J Thorac Cardiovasc Surg 140(2):422–426.e1
15. Wendling P (2011) PARTNER puts TAVR in reach of older, high-risk patients. MedConnect Cardiology, Elsevier Global Medical News, 4 April 2011
16. Falk V, Walther T, Schwammenthal E et al (2011) Transapical aortic valve implantation with a self-expanding anatomically oriented valve. Eur Heart J 32:878–887
17. Mack M (2011) Progress with transcatheter mitral valve replacement I: CardiAQ. Paper presented at transcatheter valve technologies, Vancouver, Canada, 6 June 2011
18. Krishnaswamy A, Tuzcu EM, Kapadia SR (2010) Update on transcatheter aortic valve implantation. Curr Cardiol Rep 12:393–403
19. De Canniere D, Jansens JL, Unger P et al (1997) Left ventricular outflow tract obstruction after mitral valve replacement. Ann Thorac Surg 64:1805–1806
20. Okamoto K, Kiso I, Inoue Y et al (2006) Left ventricular outflow obstruction after mitral valve replacement preserving native anterior leaflet. Ann Thorac Surg 82:735–737
21. Said SM, Schaff HV, Suri RM et al (2011) Bulging subaortic septum: an important risk factor for systolic anterior motion after mitral valve repair. Ann Thorac Surg 91:1427–1432

22. Gams E, Schad H, Heimisch W et al (1990) Preservation versus severance of the subvalvular apparatus in mitral valve replacement: an experimental study. Eur J Cardiothorac Surg 4:250–255; discussion 255–256
23. Natsuaki M, Itoh T, Tomita S et al (1996) Importance of preserving the mitral subvalvular apparatus in mitral valve replacement. Ann Thorac Surg 61:585–590
24. Tsuneyoshi H, Komeda M (2005) Update on mitral valve surgery. J Artif Organs 8:222–227
25. Faludi R, Szulik M, D'Hooge J et al (2010) Left ventricular flow patterns in healthy subjects and patients with prosthetic mitral valves: an in vivo study using echocardiographic particle image velocimetry. J Thorac Cardiovasc Surg 139:1501–1510
26. Webb JG, Wood DA, Ye J et al (2010) Transcatheter valve-in-valve implantation for failed bioprosthetic heart valves. Circulation 121:1848–1857
27. Kempfert J, Blumenstein J, Chu MW et al (2009) Minimally invasive off-pump valve-in-a-ring implantation: the atrial transcatheter approach for re-operative mitral valve replacement after failed repair. Eur J Cardiothorac Surg 35:965–969; discussion 969
28. Kempfert J, Blumenstein JM, Borger MA et al (2008) Minimally invasive off-pump valve-in-a-valve implantation: the atrial transcatheter approach for re-operative mitral valve replacement. Eur Heart J 29:2382–2387
29. Boudjemline Y, Pineau E, Borenstein N et al (2005) New insights in minimally invasive valve replacement: description of a cooperative approach for the off-pump replacement of mitral valves. Eur Heart J 26:2013–2017
30. Siminiak T, Hoppe UC, Schofer J et al (2009) Effectiveness and safety of percutaneous coronary sinus-based mitral valve repair in patients with dilated cardiomyopathy (from the AMADEUS trial). Am J Cardiol 104:565–570
31. Dubreuil O, Basmadjian A, Ducharme A et al (2007) Percutaneous mitral valve annuloplasty for ischemic mitral regurgitation: first in man experience with a temporary implant. Catheter Cardiovasc Interv 69:1053–1061
32. Sack S, Kahlert P, Bilodeau L et al (2009) Percutaneous transvenous mitral annuloplasty: initial human experience with a novel coronary sinus implant device. Circ Cardiovasc Interv 2:277–284
33. Maselli D, Guarracino F, Chiaramonti F et al (2006) Percutaneous mitral annuloplasty: an anatomic study of human coronary sinus and its relation with mitral valve annulus and coronary arteries. Circulation 114:377–380
34. Tops LF, Van de Veire NR, Schuijf JD et al (2007) Noninvasive evaluation of coronary sinus anatomy and its relation to the mitral valve annulus: implications for percutaneous mitral annuloplasty. Circulation 115:1426–1432
35. Plass A, Valenta I, Gaemperli O, Kaufmann P et al (2008) Assessment of coronary sinus anatomy between normal and insufficient mitral valves by multi-slice computer tomography for mitral annuloplasty device implantation. Eur J Cardiothorac Surg 33:583–589
36. Mao S, Shinbane JS, Girsky MJ et al (2005) Coronary venous imaging with electron beam computed tomographic angiography: three-dimensional mapping and relationship with coronary arteries. Am Heart J 150:315–322
37. Feldman T, Cilingiroglu M (2011) Percutaneous leaflet repair and annuloplasty for mitral regurgitation. J Am Coll Cardiol 57:529–537
38. Wu AH, Aaronson KD, Bolling SF et al (2005) Impact of mitral valve annuloplasty on mortality risk in patients with mitral regurgitation and left ventricular systolic dysfunction. J Am Coll Cardiol 45:381–387
39. Mihaljevic T, Lam BK, Rajeswaran J et al (2007) Impact of mitral valve annuloplasty combined with revascularization in patients with functional ischemic mitral regurgitation. J Am Coll Cardiol 49:2191–2201
40. McCarthy PM, Bhudia SK, Rajeswaran J et al (2004) Tricuspid valve repair: durability and risk factors for failure. J Thorac Cardiovasc Surg 127:674–685
41. Matsuyama K, Matsumoto M, Sugita T et al (2001) De Vega annuloplasty and Carpentier Edwards ring annuloplasty for secondary tricuspid regurgitation. J Heart Valve Dis 10:520–524

42. Rivera R, Duran E, Ajuria M (1985) Carpentier's flexible ring versus De Vega's annuloplasty. A prospective randomized study. J Thorac Cardiovasc Surg 89:196–203
43. Yada I, Tani K, Shimono T et al (1990) Preoperative diagnosis and surgical treatment of tricuspid regurgitation (TR) in patients with acquired valvular heart disease—comparison of Kay's annuloplasty and Carpentier's ring annuloplasty for tricuspid valve surgery. Nippon Kyobu Geka Gakkai Zasshi 38:421–428
44. Holper K, Haehnel JC, Augustin N et al (1993) Surgery for tricuspid insufficiency: long-term follow-up after De Vega annuloplasty. Thorac Cardiovasc Surg 41:1–8
45. Bernal JM, Gutierrez-Morlote J, Llorca J et al (2004) Tricuspid valve repair: an old disease, a modern experience. Ann Thorac Surg 78:2069–2074; discussion 2074–2075
46. Ghanta RK, Chen R, Narayanasamy N et al (2007) Suture bicuspidization of the tricuspid valve versus ring annuloplasty for repair of functional tricuspid regurgitation: midterm results of 237 consecutive patients. J Thorac Cardiovasc Surg 133:117–126
47. Tibayan FA, Rodriguez F, Langer F et al (2004) Does septal-lateral annular cinching work for chronic ischemic mitral regurgitation? J Thorac Cardiovasc Surg 127:654–663
48. Chiam PT, Ruiz CE (2011) Percutaneous transcatheter mitral valve repair: a classification of the technology. JACC Cardiovasc Interv 4:1–13
49. Nakanishi K, Raman J, Hata M et al (2001) Early outcome with the Alfieri mitral valve repair. J Cardiol 37:263–266
50. Alfieri O, Maisano F, De Bonis M et al (2001) The double-orifice technique in mitral valve repair: a simple solution for complex problems. J Thorac Cardiovasc Surg 122:674–681
51. Alfieri O, Maisano F (1999) An effective technique to correct anterior mitral leaflet prolapse. J Card Surg 14:468–470
52. Alfieri OM, Maisano F, De Bonis M (2005) The edge-to-edge repair. Multimed Man Cardiothorac Surg. https://doi.org/10.1510/mmcts.2004.000869
53. Bhudia SK, McCarthy PM, Smedira NG et al (2004) Edge-to-edge (Alfieri) mitral repair: results in diverse clinical settings. Ann Thorac Surg 77:1598–1606
54. David TE, Bos J, Rakowski H (1991) Mitral valve repair by replacement of chordae tendineae with polytetrafluoroethylene sutures. J Thorac Cardiovasc Surg 101:495–501
55. Seeburger J, Falk V, Borger MA et al (2009) Chordae replacement versus resection for repair of isolated posterior mitral leaflet prolapse: a egalite. Ann Thorac Surg 87:1715–1720
56. Seeburger J, Borger MA, Tschernich H et al (2010) Transapical beating heart mitral valve repair. Circ Cardiovasc Interv 3:611–612
57. Tibayan FA, Rodriguez F, Langer F et al (2005) Annular or subvalvular approach to chronic ischemic mitral regurgitation? J Thorac Cardiovasc Surg 129:1266–1275
58. Tibayan FA, Rodriguez F, Zasio MK et al (2003) Geometric distortions of the mitral valvular-ventricular complex in chronic ischemic mitral regurgitation. Circulation 108(suppl 1):II116–II121
59. del Val D, Ferreira-Neto NA, Wintzer-Wehekind J et al (2019) Early experience with transcatheter mitral valve replacement: a systematic review. J Am Heart Assoc 8(17):e013332
60. Hensey M, Brown RA, Lal S et al (2021) Transcatheter mitral valve replacement: an update on current techniques, technologies, and future directions. JACC Cardiovasc Interv 14(5):489–500
61. Spencer JH, Prahl G, Iaizzo PA (2014) The prevalence of coronary sinus and left circumflex artery overlap in relation to the mitral valve. J Interv Cardiol 27(3):308–316
62. Zhingre Sanchez JD, Bateman MG, Iaizzo PA (2018) Engineering and technologies associated with cardiac valve repair and replacement therapies. In: Engineering in medicine: advances and challenges. Elsevier, pp 219–254
63. Badhwar V, Thourani VH, Ailawadi G et al (2016) Transcatheter mitral valve therapy: the event horizon. J Thorac Cardiovasc Surg 152(2):330–336
64. Testa L, Latib A, Montone RA et al (2016) Transcatheter mitral valve regurgitation treatment: state of the art and a glimpse to the future. J Thorac Cardiovasc Surg 152(2):319–327
65. Mangieri A, Laricchia A, Giannini F et al (2019) Emerging technologies for percutaneous mitral valve repair. Front Cardiovasc Med 6:161

66. Testa L, Popolo Rubbio A, Casenghi M et al (2019) Transcatheter mitral valve replacement in the transcatheter aortic valve replacement era. J Am Heart Assoc 8(22):e013352
67. Mack M, Carroll JD, Thourani V, Vemulapalli S, Squiers J et al (2021) Transcatheter mitral valve therapy in the United States: a report from the STS-ACC TVT Registry. J Am Coll Cardiol 78(23):2326–2353. https://doi.org/10.1016/j.jacc.2021.07.058
68. Dziadzko V, Dziadzko M, Medina-Inojosa JR, Benfari G, Michelena HI et al (2019) Causes and mechanisms of isolated mitral regurgitation in the community: clinical context and outcome. Eur Heart J 40(27):2194–2202. https://doi.org/10.1093/eurheartj/ehz314
69. Deferm S, Bertrand PB, Verbrugge FH, Verhaert D, Rega F et al (2019) Atrial functional mitral regurgitation: JACC review topic of the week. J Am Coll Cardiol 73(19):2465–2476. https://doi.org/10.1016/j.jacc.2019.02.061
70. Stone GW, Lindenfeld J, Abraham WT, Kar S, Lim DS et al (2018) Transcatheter mitral-valve repair in patients with heart failure. N Engl J Med 379(24):2307–2318. https://doi.org/10.1056/NEJMoa1806640
71. Sherwood MW, Xiang K, Matsouaka R, Li Z, Vemulapalli S et al (2020) Incidence, temporal trends, and associated outcomes of vascular and bleeding complications in patients undergoing transfemoral transcatheter aortic valve replacement: insights from the Society of Thoracic Surgeons/American College of Cardiology Transcatheter Valve Therapies Registry. Circ Cardiovasc Interv 13(1):e008227. https://doi.org/10.1161/CIRCINTERVENTIONS.119.008227
72. von Bardeleben RS, Hobohm L, Kreidel F, Ostad MA, Schulz E et al (2019) Incidence and in-hospital safety outcomes of patients undergoing percutaneous mitral valve edge-to-edge repair using MitraClip: five-year German national patient sample including 13,575 implants. EuroIntervention 14(17):1725–1732. https://doi.org/10.4244/EIJ-D-18-00961
73. Muller D, Sorajja P, Duncan A, Bethea B, Dahle G et al (2021) 2-year outcomes of transcatheter mitral valve replacement in patients with severe symptomatic mitral regurgitation. J Am Coll Cardiol 78(19):1847–1859., ISSN 0735-1097. https://doi.org/10.1016/j.jacc.2021.08.060
74. Yoon SH, Whisenant BK, Bleiziffer S, Delgado V, Dhoble A et al (2019) Outcomes of transcatheter mitral valve replacement for degenerated bioprostheses, failed annuloplasty rings, and mitral annular calcification. Eur Heart J 40(5):441–451. https://doi.org/10.1093/eurheartj/ehy590
75. Mihos CG, Pineda AM, Capoulade R, Santana O (2016) A systematic review of mitral valve repair with autologous pericardial leaflet augmentation for rheumatic mitral regurgitation. Ann Thorac Surg 102(4):1400–1405. https://doi.org/10.1016/j.athoracsur.2016.04.009. Epub 2016 Jun 17
76. Alperi A, Granada JF, Bernier M, Dagenais F, Rodés-Cabau J (2021) Current status and future prospects of transcatheter mitral valve replacement: JACC state-of-the-art review. J Am Coll Cardiol 77(24):3058–3078. https://doi.org/10.1016/j.jacc.2021.04.051
77. Blackstone EH, Suri RM, Rajeswaran J, Babaliaros V, Douglas PS et al (2015) Propensity-matched comparisons of clinical outcomes after transapical or transfemoral transcatheter aortic valve replacement: a placement of aortic transcatheter valves (PARTNER)-I trial substudy. Circulation 131(22):1989–2000. https://doi.org/10.1161/CIRCULATIONAHA.114.012525
78. Bapat V, Rajagopal V, Meduri C, Farivar RS, Walton A, Intrepid Global Pilot Study Investigators et al (2018) Early experience with new transcatheter mitral valve replacement. J Am Coll Cardiol 71(1):12–21. https://doi.org/10.1016/j.jacc.2017.10.061
79. Feldman T, Foster E, Glower DD, Kar S, Rinaldi MJ, EVEREST II Investigators et al (2011) Percutaneous repair or surgery for mitral regurgitation. N Engl J Med 364(15):1395–1406

# Chapter 10
# Percutaneous Pulmonary Valve Implantation: 20 Years of Development


**Liam Swanson, Claudio Capelli, Andrew M. Taylor, Philipp Bonhoeffer, Matthew J. Gillespie, and Silvia Schievano**

## 10.1 Introduction

Patients born with congenital heart disease (CHD) have benefitted from immense advances in cardiothoracic intervention, surgery, intensive care, as well as non-invasive imaging since the mid-twentieth century. Whereas survival in the 1950s used to be a mere 15%, today, 90% of CHD patients live well into adulthood, albeit with 'adult congenital heart disease' (ACHD) [1]. Indeed, in high-income countries, the burgeoning ACHD population has exceeded the paediatric population and continues to grow as more and more paediatric patients transition into adult care [1–3]. Morbidity in children and ACHD patients late after neonatal repairs of complex CHD is most commonly a consequence of right ventricular outflow tract (RVOT), pulmonary trunk or surgical conduit dysfunction which manifests in pulmonary stenosis and or pulmonary regurgitation. These dysfunctions have been treated for decades via surgical pulmonary valve replacement (PVR) using valved conduits, a well-developed and safe procedure, associated with low levels of morbidity and mortality. However, still today, these implanted valves have a limited lifespan of approximately 10 years [4]. Thus, surgery is commonly delayed for as long as possible resulting in progressive right ventricular (RV) remodelling and dysfunction, in

L. Swanson · C. Capelli · A. M. Taylor · S. Schievano (✉)
UCL Institute of Cardiovascular Science & Great Ormond Street Hospital for Children, London, UK
e-mail: s.schievano@ucl.ac.uk

P. Bonhoeffer
Fondazione Toscana Gabriele Monasterio, Pisa, Italy

M. J. Gillespie
Children's Hospital of Philadelphia & Perelman School of Medicine, University of Pennsylvania, Philadelphia, PA, USA

© The Author(s), under exclusive license to Springer Nature Switzerland AG 2023

P. A. Iaizzo et al. (eds.), *Heart Valves*, https://doi.org/10.1007/978-3-031-25541-0_10

some cases to the point of no return, where RV dysfunction, exercise capacity and risk of sudden death may be irreversible [5].

One of the greatest leaps forward in modern cardiology – percutaneous pulmonary valve implantation (PPVI) – was pioneered by Phillip Bonhoeffer et al. in the late 1990s [6]. An existing bovine xenograft with a native valve was sutured onto an existing stent (Cheatham Platinum, NuMED Inc., Hopkinton, NY, USA), crimped onto a balloon catheter and delivered through the inferior vena cava, the right atrium and finally the right ventricle (RV). By doing so, it was possible to deploy the valved stent into the dysfunctional surgical conduit and the valve function through intervention, rather than reoperation. Following this successful first-in-human trial implantation in 2000 [6, 7], the first PPVI device - Melody®, Medtronic, Minneapolis, MN, USA - paved the way for the development of transcatheter valves by several manufacturers, not just for PVR but also to include transcatheter aortic valve implantation (TAVI) - by Alain Cribier with Sapien, Edwards Lifesciences, Irvine, CA, USA since 2002 [8] - and, more recently, the delivery of mitral and tricuspid valves. Additionally, the introduction of these innovative technologies in clinical practice has driven the development of advanced engineering methods, which have improved the device design process and the regulatory approval pathways towards greater patient safety and benefits [11–15]. In the past decade, the limitations and risks associated with the first devices - freedom from Melody® stent-fracture 68 ± 5% at 2-years after implantation [9] and >85% of patients who needed PVR presented with unsuitable anatomies for the Melody® stent [10] - prompted a resurgence of innovation in PPVI. Today a wave of new devices is currently under regulatory review or have been recently commercialised: Harmony (Medtronic), Alterra Adaptive Prestent (Edwards Lifesciences), Venus P-Valve (Venus Medtech, Shanghai, China) and Pulsta (TaeWoong Medical Company, Gyeonggi-do, South Korea), to name a few.

In this chapter, we review current PPVI device designs and their on-going clinical experiences. In addition, we describe how novel computational methods have contributed to the optimisation of device design in the past: specifically studying stent fracture in Melody®, pre-stenting and patient selection for PPVI candidacy screening and regulatory processes.

## 10.2 Balloon Expandable Devices

### *10.2.1 Medtronic Melody® Valve*

Melody® is used in dysfunctional surgical PVR conduits. The Melody® PPVI system (Fig. 10.1) comprises a balloon-expandable stent, which houses a bovine jugular vein conduit with a contained native venous valve, and is deployed via the Ensemble® system – a balloon-in-balloon catheter device.

**Fig. 10.1** Medtronic's PPVI Melody Valve shown in a valve open (top left), closed (top right), and deployed state (bottom). The blue stitching evident in the top views is aligned with the blue carrot-tipped catheter to ensure correct orientation of the valve. The inner and outer balloons of the balloon-in-balloon system can be seen in the lower image. (Images reproduced with permission from Medtronic, Inc.)

The stent is constructed from six platinum-10% iridium wires which are formed into a zig-zag pattern with 8 'crowns' and laser-welded together. During early clinical experiences, the initial brittle laser welds were found to elicit high rates of fracture; necessitating a gold-braising process to increase the durability of the stent. The stent can be expanded up to a maximum diameter of 24 mm. Due to foreshortening, the length of the stent at 18, 20 and 22 mm deployment diameter is 26, 24 and 21 mm, respectively. The stent material makes it possible to manually crimp the device onto the delivery system, yet one can treat irregular conduit anatomies while avoiding valve distortions [11] and also re-dilate the device through balloon angioplasty should there be subsequent RVOT obstruction.

Formerly known as the Contegra conduit, a segment of bovine jugular vein with a native valve of 16–18 mm is sutured into the stent frame, suitable for deployment up to 24 mm [12]. The valves found in the bovine jugular veins can have various bicuspid or tricuspid arrangements with thin leaflets that have deep commissures to provide competent coaptation at all recommended deployment diameters [11]. Furthermore, the valve can fully recover from the compression caused by the crimping onto the delivery catheter, making it ideal for implementation in PPVI. Early clinical experiences showed that the initial method of suturing the conduit to the stent at only the proximal and distal rings made the conduit susceptible to a 'hammock' effect [13], prompting subsequent suturing along the full length of the stent [11]. Once assembled, the device is sterilised, packaged and transported using a proprietary sterilant, containing glutaraldehyde and isopropyl alcohol. Prior to intervention, the device needs to be washed in a series of saline baths before being crimped onto the Ensemble® delivery system – a bespoke balloon-in-balloon catheter comprising of a higher pressure inner balloon and lower pressure outer balloon, both constructed of nylon; this allows the stent to be inflated in two separate steps. Currently, the outer balloons are available in 18, 20 and 22 mm sizes, and at full inflation, the inner balloon has half the diameter of the outer balloon and is slightly

shorter. Note, the tip of the catheter is blue for correct orientation of the valve, which has blue stitching on the distal side (Fig. 10.1) as opposed to white for the rest. The device mounted on the catheter is covered by a protective polytetrafluoroethylene (PTFE) sheath to allow navigation through the vasculature. Two radiopaque marker bands on the inner shaft of the catheter aid positioning within the patient's RVOT under fluoroscopy, together with contrast agent that can be delivered through a side port (green, in Fig. 10.2) to confirm positioning before deployment. The catheter shaft is 16 Fr, but once assembled, the deployment system is 22 Fr and has a length of 100 cm [14]. Once the device has been advanced to the deployment location, the inner balloon is inflated first through the blue port to position the device, followed by the outer balloon inflation through the orange port for final deployment (Fig. 10.2).

#### 10.2.1.1 Clinical Experience

In September 2000, the first PPVI device was successfully implanted at Hôpital Necker Enfants Malades (Paris, France) in a 12-year-old boy who had developed dysfunction of his RVOT conduit [6]. In the following decade, the Melody® device

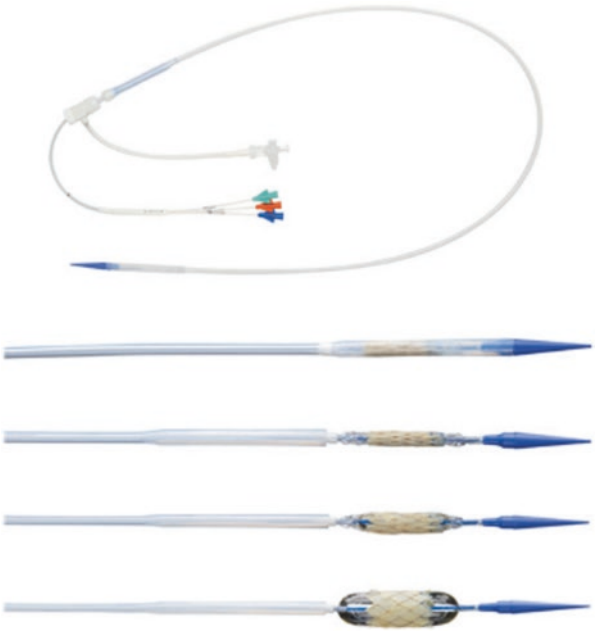

**Fig. 10.2** Three ports are used to control the inflation of the inner balloon (blue), outer balloon (orange and includes a label of the balloon size) and the indigo port for the guide wire. The process of inflating the balloon is shown in four steps below, from top to bottom. Once at the correct location (1), the sheath is retracted (2), the inner balloon inflated (3) followed by the outer balloon (4). (Image from McElhinney and Hennesen [11])

design was improved towards better safety and efficacy. It received the CE mark in 2006 and USA Food and Drug Administration (FDA) approval in 2010.

The transcatheter Melody® valve offered a minimally invasive alternative to open heart surgery for treatment of RVOT conduit dysfunction [11] and, being the first device to market, has had the longest running post-implant safety and efficacy studies [15–17]. Results of a 10-year follow-up of the cohort involved in the investigational device exemption (IDE) study upheld initial findings of good long-term performance. Importantly, freedom from mortality was 90%, which is similar to surgical valve replacement for a comparable patient population [16]. Endocarditis remains the highest cause of post-procedural mortality, whilst conduit rupture and coronary artery compression are the highest procedural risks [16, 18, 19]. Freedom from dysfunction was 53%, with patients treated younger presenting higher likelihoods of dysfunction and therefore requiring closer follow-up [16]. Stent fracture (Fig. 10.9), at its varying degrees of severity, is one of the commonest adverse events linked to Melody®, where freedom from stent fracture was found to be 68 ± 5% of implanted devices within 2 years [9], although more than half maintain stent integrity [9]. Currently, pre-stenting is used to reduce the risk of stent fracture, as implanting one or more stents creates a more rigid and cylindrical scaffold at the site of deployment [9, 20, 21]. Furthermore, Melody valve-in-valve procedures have been carried out in patients where valve dysfunction requires reintervention [22].

### *10.2.2 Edwards Lifesciences Sapien (XT, S3, Ultra)*

The Sapien (Edwards Lifesciences, Irvine, CA, USA) valve was initially designed for TAVI and later translated to PPVI. Since its inception, it has undergone three primary design iterations (Fig. 10.3), from Sapien (A) to Sapien XT (B), Sapien 3 (C) and finally Sapien 3 Ultra (D), which spans a device diameter range of 20–29 mm. The Sapien devices are comprised of a tricuspid, bovine pericardial tissue valve, housed within a balloon expandable stent which is wrapped with a

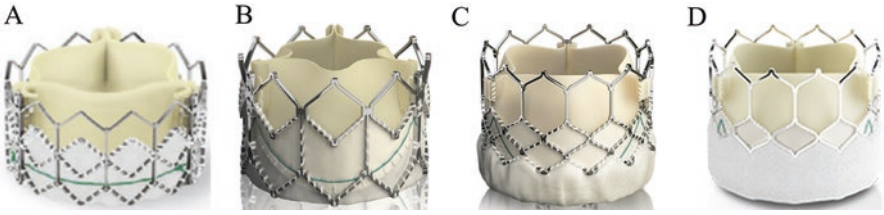


**Fig. 10.3** Evolution of the Sapien family of devices for transcatheter valve replacements starting with the Sapien valve (**A**), Sapien XT (**B**), Sapien 3 (**C**), Sapien 3 Ultra (**D**). (**C**, **D**) highlight the introduction of the 'cuff' of PET fabric on the proximal end. (Images from various sources)

polyethylene terephthalate (PET) fabric skirt on the proximal end and folded into a cuffed end from the Sapien 3 iteration onwards. This later device is delivered through a unique Edwards' deployment system.

The original Sapien stent used laser cut stainless steel to fabricate an open cell design which, although not applicable in PPVI, allowed coronary flow and coronary ostia access in TAVI. Since the transition to the larger diameter Sapien XT model, a laser cut cobalt-chromium frame is now used instead, so to reduce the profile of the crimped device and lower the risk of vascular complications during delivery, yet while maintaining enough radial strength to guarantee stability. Also, these redesigns allowed the 23 mm and 26 mm diameter Sapien XT devices to be accommodated in 18 and 19 Fr sheaths, respectively, as opposed to its predecessors who required 22 and 24 Fr sheaths [23]. The increased upper range of stent diameters of the Sapien family, summarised in Table 10.1, has made this device suitable for treating a broader patient population which includes both dysfunctional conduits and smaller native/patched RVOTs [24–29].

The PET stent skirt design, which initially covered only the internal surface of the stent, was updated in the Sapien 3 redesign and extended to wrap around the proximal edge. This created a sealing cuff to minimise paravalvular leak – an identified post-TAVI complication. The update to the Sapien 3 Ultra has extended the cuff higher on the outer stent surface and used a rougher material surface to further improve sealing and reduce valve migration.

The Sapien family of valves are comprised of three bovine pericardium leaflets mounted to the PET skirt to form a tricuspid arrangement. The use of pericardium tissue instead of harvested valved conduits has the benefit of providing more controls over the valve design for replicable fabrications and shape optimisations at different sizes. However, these handmade valves can be susceptible to calcification, thus requiring a fixation process (Carpentier-Edwards ThermaFix™) to reduce binding sites and elongate their functional lifespan. These valves are sterilised and stored in a glutaraldehyde-based sterilant, which requires thorough rinsing prior to implantation.

**Table 10.1** Summary of dimensions and recommended sizing for Sapien XT, Sapien 3 and Sapien 3 Ultra based on either Transoesophageal Echocardiography diameter measurements or diameters derived from the orifice area based on CT imaging

| | Height [mm] | | TEE derived diameter [mm] | | CT area derived diameter [mm] | |
|---|---|---|---|---|---|---|
| Diameter [mm] | XT | 3/Ultra | XT | 3/Ultra | XT | 3/Ultra |
| 20 | – | 15.5 | – | 16–19 | – | 18.6–21 |
| 23 | 14.3 | 18 | 18–22 | 18–22 | 20–23 | 20.7–23.4 |
| 26 | 17.2 | 20 | 21–25 | 21–25 | 23–26 | 23.4–26.4 |
| 29 | 19.1 | 22.5 | 24–27 | 24–28 | 26–29 | 26.2–29.5 |

The Sapien XT and Sapien 3 are delivered using a specialised system: a single balloon catheter with a rated burst pressure of 7 atm. Each device is crimped onto the delivery system, just proximal to the balloon, using Edwards' specifically designed crimping tool. The system has a controlled 'pushing action' which uncovers and advances the stent onto the balloon, once in the inferior vena cava [28]. The catheter includes radiopaque markers for device positioning under fluoroscopy. The recent introduction of an expandable sheath (eSheath) that expands while the device is passed through it and contracts when the device is deployed reduces the chances of vessel injury.

#### 10.2.2.1 Clinical Experience

After being successfully used for TAVI for several years, the Sapien was first used for PPVI on compassionate grounds in 2006 [30] and the COngenital Multicenter trial of Pulmonic vAlve regurgitation Studying the Sapien InterventiONal (COMPASSION) phase I USA FDA trial was initiated in 2008. FDA approval for use of the Sapien XT device in the pulmonic position was received in 2016 [31].

Primary endpoints of the COMPASSION trial comprised device failure or procedure-related death and/or reoperation at 1 year. Secondary endpoints included freedom from major adverse cardiac and cerebral events and functional improvement at 6 months. Subsequent end of phase 1 [32] and 3-year [33] interim reports of the COMPASSION trial, centre-specific studies [34] and national registry studies [35, 36] spanning 1–5 years follow-up showed consistently positive implantation success rates of up to 97.4% [26]. There was an emergence of a minor incidence of infective endocarditis, albeit lower than that reported for Melody® implantations [37–39]. Incidence of valve migration and valve retrieval was reported [26, 32], but otherwise good durability was demonstrated with no reported occurrence of stent fractures. Differently from the early Melody® trials, pre-stenting was approved a priori and conducted in all patients enrolled in COMPASSION, due to its recognised benefits during Melody® investigations. The phase-1 follow-up report on the COMPASSION trial highlighted that pre-stenting related free regurgitation may create a challenge for accurate placement of the valve due to its single balloon inflation method [32]. In those patients who required reintervention, the majority were a result of re-obstruction of the RVOT, treatable via either surgical valve replacement or valve-in-valve procedures [33, 39]. Yet, the uncovered configuration of the device before positioning in the RVOT may present risks of the Sapien valve being captured in the tricuspid valve apparatus, but this was reported as a low frequency complication [26, 28, 40].

Long-term trials of the Sapien 3 valve in PPVI are expected to conclude in 2027. Interim results, however, have shown it to be an efficacious PPVI device, albeit not without risks and limitations.

## 10.3 Self-Expanding Devices

### *10.3.1 Medtronic Harmony® Valve*

The Harmony™ device was designed for a wide range of anatomies, sizes, and dynamics to overcome the noted limitations of Melody®, and also to treat native and patched RVOTs [41]. Indeed, in 2021, Harmony™ TPV 22 and TPV 25 became the first PPVI devices to be approved by the FDA for patients with native or patched RVOTs [42]. Development of the Harmony™ device began in 2007 with the first-in-human implantation taking place in 2009 on compassionate grounds [43, 44]. This device comprises a non-symmetrical hourglass-shaped, self-expanding nitinol stent, covered by a knitted PET cloth, with a tricuspid porcine pericardial valve sutured into the central portion (Fig. 10.4). It is delivered through a specialised deployment system.

The stent is made of six nitinol wires formed in zig-zag patterns. A knitted PET cloth is sewn onto the wires covering the entire length. The stent is available in two designs: TPV22 and TPV25 with inner valve diameter, inflow diameter, outflow diameter and nominal length dimensions of 22, 42, 34 and 55 mm, and 25, 54, 43 and 51 mm, respectively. These allow for the treatment of patients with a perimeter-derived diameter of 22–38 mm and of 23–39 mm at the distal and proximal RVOT, respectively. The crowns on the inflow circumference of the stent have sutured loops which are used to thread it onto the deployment system coils to control the final release of the device. A loading funnel collapses the valve onto the shaft before being covered by the outer, protective and restraining capsule.

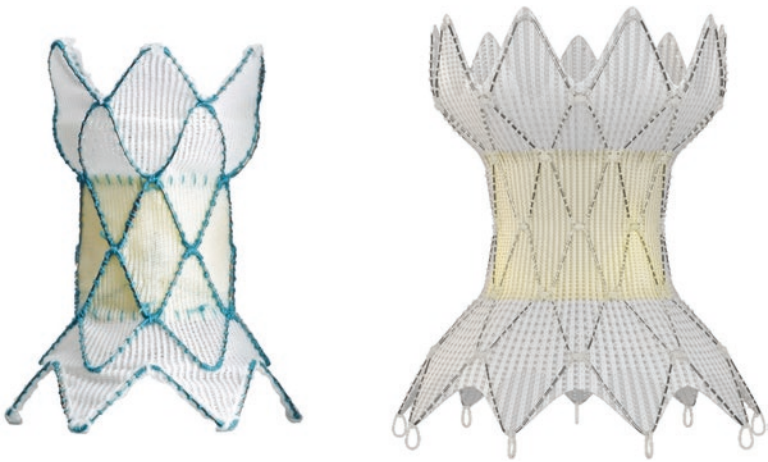

**Fig. 10.4** Renderings of the Medtronic Harmony TPV22 (left) and Harmony TPV25 (right). The key differences in shape can be seen in the proximal (marked by the sutured loops on the crowns) and distal edges of the valve, where there are larger diameters in the TPV25. (Reproduced with permission from Medtronic, Inc.)

The incorporated Harmony valve is comprised of three leaflets crafted from porcine pericardium and sutured to the central region of the stent, thus enabling controlled optimisation of sizing and shape for optimal haemodynamic performances and coaptations. These valves are treated with an $\alpha$-amino oleic acid antimineralisation process, so to mitigate leaflet calcification and also sterilised with 0.2% glutaraldehyde. Prior to device loading, several saline rinsing phases are carried on the given device to clear the sterilant.

The Harmony TPV is delivered through a specialised catheter deployment system (Fig. 10.5) with an outer diameter of 25 Fr and effective length of 101 cm. During delivery, the soft distal tip aids navigation and, once in place, the outer shaft is pulled back to retreat the outer capsule and jointly exposes the device to allow its progressive self-expansion into the main pulmonary artery. Once fully exposed, the proximal coil is rotated, freeing the distal ring loops for final device release [41].

#### 10.3.1.1 Clinical Experience

Following successful first-in-human implantation [43], the acute and short-term results of the early feasibility study (EFS) aimed to confirm implanted device loading conditions as well as assess feasibility, safety and valve performance [41]. Bergersen et al. highlight that only 8% of those indicated for RVOT repair were suitable, given the sizing of the Harmony TPV 22 design [41, 45]. Subsequently, the available range of sizes was expanded, leading to the TPV25 device; this improved Harmony screening pass rate to 70–80% [46].

As a result of the FDA regulatory approval process, three studies – the EFS, pivotal trial and continued access study (CAS) – have been carried out and are producing acute, mid- and long-term outcome studies [41, 46–48]. The EFS implanted 20 TPV22 devices, whilst the Pivotal and CAS study implanted 31 ($N_{TPV22}$ = 21, $N_{TPV25}$ = 10) and 37 ($N_{TPV22}$ = 1, $N_{TPV25}$ = 36) devices, respectively. As of 2021, the EFS offers 5-year follow-up, the Pivotal trial covers a mean of 27.2 months and CAS a mean 6.9 months. Of all these studies, only one unsuccessful implant occurred from the CAS cohort. One EFS device migrated during deployment system removal but remained functional. Considering all studies, only several patients required re-intervention within 24 hours of implantation. These were related to one device migration, which was surgically explanted, wire repositioning, balloon

**Fig. 10.5** Medtronic Melody's specialised deployment system (https://www.medtronic.com/us-en/healthcare-professionals/products/cardiovascular/transcatheter-pulmonary-valve/harmony/pr-toolkit.html)

angioplasty to improve stent apposition and a Melody® valve-in-valve procedure; due to the TPV25 device being too big for the anatomy and not expanding completely. Freedom from reintervention through various time frames remained good across the studies, although valve-in-valve procedures to address pulmonary regurgitation and valve stenosis were necessary in one patient from the Pivotal trial and two from the EFS. Also, 1 surgical explant occurred within 1 month in the EFS trial due to frame fracture [41].

Furthermore, it was observed that there has been freedom from moderate to severe paravalvular leakage. Two patients were found with mild and moderate paravalvular leak, not originally recorded on discharge examination in the EFS. In the pooled data from the Pivotal and CAS trials, freedom from any trace of paravalvular leak remained >93% across all follow-up time frames, with <2% at each time point experiencing moderate to severe leakage. Improvements of pulmonary regurgitation were excellent in all studies. After 1 year follow-up, all Pivotal trial patients were free of regurgitation and across all follow-up periods, <2% presented with moderate or severe regurgitation. The EFS showed freedom from moderate to severe pulmonary regurgitation through 5 years of follow-up. In contrast to Melody, there were no reported cases of endocarditis. Thrombosis was observed in one patient and successfully treated medically, and any periprocedural arrhythmias were self-limiting and had no hemodynamic instability.

Although limited to clinical trials, the current record of clinical outcomes in the cohort of patients with reasonable follow-up records indicates an efficacious device. Yet, follow-up is set to continue to complete a 10-year assessment, and it is noteworthy that with the recent FDA approval, further clinical reporting should ensue.

### *10.3.2 Alterra Adaptive Prestent*

To extend PPVI indications without redesigning the device itself, Edwards Lifesciences developed the Edwards Alterra Adaptive Prestent reducer that creates a stable and appropriately sized landing zone for the 29 mm Sapien 3 in native and patched RVOTs [49]. Following its first-in-human implantation in 2018 [49], the Alterra device, in combination with the 29 mm Sapien 3 valve, received approval by the FDA in December 2021. This device is comprised of a self-expanding, nitinol frame with a partial PET fabric covering (Fig. 10.6).

The stent is made of a radiopaque, laser cut nitinol frame, with a symmetrical, hour-glass shape. The central portion has a 27 mm diameter with strong sutures stitched circumferentially at the waist to support against the radial forces induced by the deployed Sapien 3 device. The inflow and outflow sealing rings, with diameters of 39 and 41 mm, respectively, are flexible, allowing the stent to conform to several different anatomies [46]. The unconstrained device length is 49 mm, and the proximal and central portions are covered by the sutured PET fabric for 30 mm [49]. This creates a seal against para-Alterra leakage at the inflow region, but also does not obstruct flow if the outflow struts encroach on the lumen of the branch PAs after

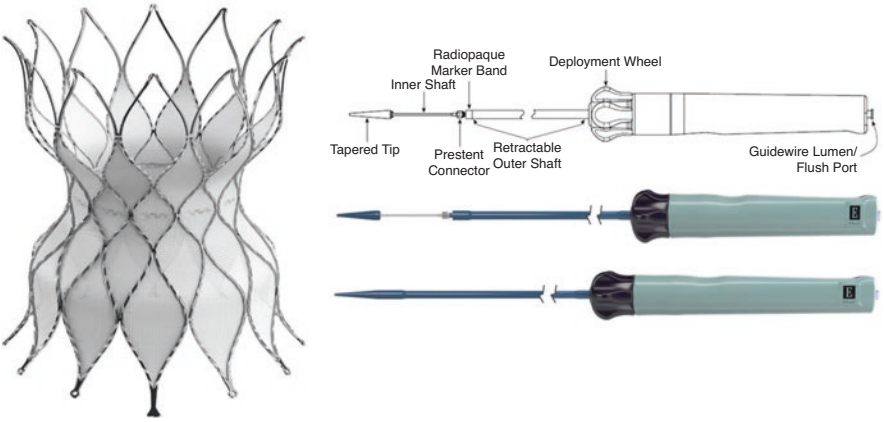


**Fig. 10.6** Alterra Adaptive Prestent (left) and the bespoke delivery system and schematic (right)

deployment. Radiopaque markers are distributed around the waist to aid procedural positioning.

The Alterra Adaptive Prestent is deployed using a custom deployment device; one different from that of the Sapien valve. The Alterra is mounted onto an inner delivery shaft and covered by a retractable outer shaft, which allows the frame to expand incrementally as it is uncovered. The inflow section of the device is identifiable by two triangular tabs which attach the device to the delivery system connector. The deployment system fits through Edwards' 16 Fr eSheath and can be controlled using one hand through a single knob that allows for both deployment and recapturing, if necessary. The tapered tip aids tracking through the vasculature and a port exists to flush the guidewire lumen [46].

#### 10.3.2.1 Clinical Experience

The first human implantation was reported in February 2018, in a 48-year-old, born with valve and subvalvular pulmonary stenosis, and who underwent surgical valvotomy and resection of the sub-pulmonic obstruction as a child. Gated CT images of the RVOT and pulmonary arteries allowed analysis of the stent wall apposition, and 3D-printing of both systolic and diastolic geometries enabled in-vivo testing of stent deployment [43, 44, 49]. The patient procedure was successful, and the 4-month follow-up echocardiography showed excellent pulmonary valve function.

The Sapien 3 with Alterra Adaptive Prestent was approved by the FDA for use in severe pulmonary regurgitation, in native and patched RVOTs, and the clinical study is likely to be completed in 2026. However, early experience ($n = 15$ patients) shows procedural success based on successful deployment of Alterra and Sapien devices following strict selection protocols [45], low RV-PA peak-to-peak pressure gradients, low pulmonary regurgitation and no reported explants to date. Furthermore, in

early assessments, no para-Alterra leaks were found. After 6 months, there were no reports of major adverse cardiac and cerebrovascular events, deaths or reinterventions. One patient presented with worsening pressure gradient in the pulmonic region at 6 months after implantation. Investigation showed that the patient's native valve leaflet was not fully captured behind the Alterra device, which resulted in a sub-valvular obstruction [50]. One further case was reported to have tricuspid valve regurgitation relating to valve apparatus damage; however, this was deemed a result of the Sapien device delivery instead of Alterra deployment [50]. Upon follow-up, one patient was found to have a single, type I fracture of the Alterra stent, but with no loss of integrity [50].

Long-term efficacy and freedom from adverse events are still to be demonstrated by longer follow-ups and larger, more heterogeneous sample sizes.

### *10.3.3 Venus P-Valve*

The Venus P-Valve (Venus Medtech, Shanghai, China) was developed for PPVI in native or patched RVOTs and differentiates itself from the other designs by offering a wider spectrum of device sizes with a larger upper limit diameter; i.e., to offer an accurate fit for each patient including larger RVOTs. The Venus P-Valve comprises a nitinol stent with a porcine pericardial covering and tricuspid porcine pericardial valve leaflets as shown in Fig. 10.7. Early results of Venus P-Valve implantation were first reported in 2014 [51].

The Venus P-Valve consists of a laser-cut, self-expanding, stiff nitinol frame with all except the distal cells covered by porcine pericardium sutured along the entire length of the frame. The frame is manufactured in several combinations of diameters and lengths. The central portion of the stent housing the valve is available in lengths from 20 to 35 mm, in 5 mm increments, and each available length comes in diameters from 16 to 36 mm, in 2 mm increments [53]. The flared inlet and outlet

**Fig. 10.7** Venus P-Valve demonstrating its unloaded configuration and open distal cells (right) which aim to prevent occlusion of the branch pulmonary arteries [52]

portions are wider than the central portion by 7 and 10 mm, respectively, and are both 10–14 mm in length, depending on the valve size [12]. Three radiopaque markers are dotted onto the stent to show the distal, valvular and proximal portion of the stent under fluoroscopy.

The incorporated three valve leaflets are manufactured from porcine pericardium and preserved in a low concentration solution of buffered glutaraldehyde to maintain the pericardium flexibility and strength. The device is crimped in ice cold water to reduce its stiffness, placed over a 16 Fr shaft and covered with an outer capsule, resulting in a 20–22 Fr deployment system; depending on the chosen device [54]. A given device is attached to the delivery system via two proximal 'ears' to control final deployment and device positioning [46]. The length of the deployment system is 100 cm. Typically, one selects a device diameter to be 2–4 mm larger than the minimum diameter of the MPA while the length is matched to the distance from the RVOT to PA bifurcation [55].

#### 10.3.3.1 Clinical Experience

The Venus P-Valve received CE mark certification in 2021, but to date, being developed outside European and American jurisdictions, only multiple small scale trials, on compassionate grounds [54–56], were allowed in these areas and elsewhere in the world. Yet, together these studies showed sufficient evidence to embark directly on a CE mark trial without further stringent patient selection criteria [46].

In 2014, results became available of the first cohort ($N$ = 5, mean age = 33 ± 9.5 years) with follow-up data of 3.4 ± 2.5 months. This initial study showed successful implantation in each patient with a physical improvement by at least one New York Heart Association (NYHA) class; RV volumes normalised and no paravalvular leaks or device migrations were described [51].

Furthermore, a small trial of five patients in the United Kingdom was conducted and early results published in 2016 [55], reporting no or only trivial pulmonary regurgitation, as well as improved RV volumes and no stent fractures. However, an experience in one patient highlighted the importance of pre-procedural consideration of the morphology of the PA branching which should ideally be symmetrical due to the distal flair of the stent. In this patient, one of the PA branches was smaller and had a high branching angle, resulting in the covered portion of the stent occluding this branch and requiring subsequent stenting of the branch vessel. This points to certain branching morphology being a possible contraindication to Venus P-Valve PPVI [55].

In general, the clinical experience, albeit small and short, has shown good outcomes. In a review of 38 patients enrolled across compassionate clinical studies conducted outside China, between 2013 and 2017, only one patient did not have a successful implantation [57]. The diameters of the implanted devices ranged from 24 to 26 mm and lengths were 30 ($N$ = 32) and 35 mm ($N$ = 5). The single procedural failure was related to the outer sheath tearing due to the presence of a previously implanted LPA stent. Branch stenting was retrospectively identified as a relative

contraindication. Stent fractures in the proximal flare were encountered in 27% of patients within 3 months. Although additional fractures were found in one patient over the course of the first year, none had resulted in loss of integrity. Although endocarditis and coronary compression did not occur in any of these patients, neither are ruled out and should be considered during patient preparation and management.

### *10.3.4 Pulsta Valve*

The Pulsta Valve (TaeWoong Medical Company, Gyeonggi-do, South Korea) is one of the latest PPVI devices developed for treating native and patched RVOTs. The Pulsta Valve's first animal implantation was reported in 2014 [58] and first human implantation was done in 2017 [59]. Market approval in South Korea was granted in 2019 after successful mid-term results for a trial involving 25 patients. A CE approval study begun in December 2019 with 11 cardiac centres enrolling patients across Europe and South Korea. The device comprises a knitted Nitinol wire frame with porcine pericardium cover and porcine pericardium valves in a tricuspid arrangement as shown in Fig. 10.8.

This device's frame is made from 0.0115 inch diameter, double strand, knitted nitinol wires [60]. The knitted fabrication removes welds and regions of high bending where stresses would become elevated; this aims to reduce the likelihood of stent fracture and allows the crimped device to reach a relatively low profile [61]. The hyperboloid shape of the stent is symmetric with each flare being 4 mm wider than the valve diameter [59]. The valve diameters range from 18 to 32 mm in 2 mm increments, and each diameter has an associated length between 28 and 38 mm [61]. The central portions of the given frame is covered by a porcine pericardium layer whose position is biased proximally, to leave a larger area of the

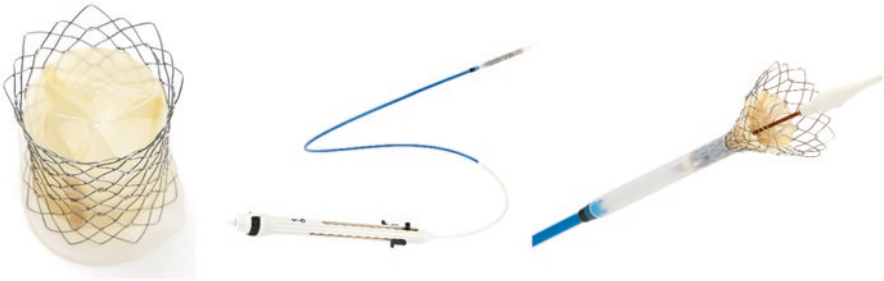

**Fig. 10.8** Pulsta valve demonstrating the knitted structure and porcine pericardial cover and valves along with its delivery system where the knob and slider deployment controls can be seen in black on the handle. The device in a mid-deployment state is additionally shown. (Reproduced with permission from Taewoong Medical Company)

distal stent uncovered and prevent PA branch occlusion. Radiopaque markers on each stent mark the positions of the valve. Valve sizing for each patient is based on all available image modalities (echocardiography, CT and MR) and the use of a sizing balloon during the procedure, with ultimate selection depending on the largest diameter for the proximal, mid (or narrowest-mid) and distal main pulmonary artery.

Today, the valve is manufactured from three equal porcine pericardium pieces, specifically designed for each valve diameter to maintain adequate coaptation and are hand-sewn onto the stent wall using a 5-0 braided polyester. The tissue undergoes multiple types of treatment including decellularisation, $\alpha$-galactosidase to reduce immunogenicity, space filling, glutaraldehyde fixation and detoxification.

The valved stent can be crimped over a 12 Fr cable shaft, and the proximal end is attached to a hook block to control final deployment of the device and any repositioning. This system results in either an 18 Fr (for device diameters up to 28 mm) or 20 Fr (for 30 and 32 mm valves) devices. The deployment system has a conical tapered tip which is 17 mm in length with two main controllers: a knob and a slider. The stent can be half uncovered through clockwise rotation of the knob, and final retraction of the stent cover is done by pulling back the slider. The useable length of the delivery system is 110 cm.

#### 10.3.4.1 Clinical Experience

Mid-term results of a multicentre trial of the Pulsta valve in South Korea became available in 2021 [61]. All 25 enrolled patients in this study had patched RVOTs after total repair of ToF, Fallot-type double outlet RV or pulmonary atresia. Implanted valve sizes were 26 mm ($n$ = 11), 28 mm ($n$ = 12) and 32 mm ($n$ = 2). The mean follow-up was 33.1 ± 14.2 months (range 12.0–50.6 months). All patients had a successful procedure and were transferred directly to a general ward with no complications in the first 24 hours. At discharge, trivial to mild pulmonary regurgitation ($n$ = 18) and trivial paravalvular leak ($n$ = 6) were detected. The improvement seen in mean pressure gradient at discharge was sustained across all follow-up data, indicating good resilience to device stenosis. At 6 months, it was reported that there was significant improvement in RV end-diastolic and end-systolic volumes. At 1 year follow-up, pulmonary regurgitation remained non-existent ($n$ = 4), trivial ($n$ = 16) or mild ($n$ = 5). No endocarditis or stent-fractures were reported. Although in this study all patients had procedural success, a subsequently published case scenario highlighted possible procedural complications where the deployed device accidently migrated into the RV during the withdrawal of the deployment system. Emergency transfer to surgery led to a successful removal of the device and the patient had a surgical valve implanted successfully [62] (Table 10.2).

**Table 10.2** Table summary of PPVI devices for surgical PVR and native RVOT repair

| Device | Melody | Sapien XT/S3/S3 Ultra | Harmony | Alterra Adaptive Prestent | Venus P-Valve | Pulsta |
|---|---|---|---|---|---|---|
| |  | 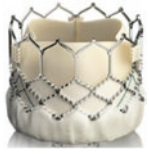 | 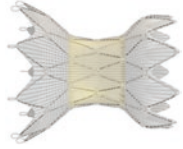 | 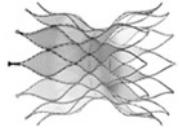 |  | 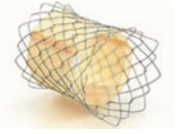 |
| Deployment method | Balloon expandable | Balloon expandable | Self-expandable | Self-expandable | Self-expandable | Self-expandable |
| Dimensions (diameter × length) [mm] | Max<br>22 × 21 | 20 × 15.5<br>23 × 18<br>26 × 20<br>29 × 22.5 | (22 × 55<br>25 × 51 | 27 × 49 | 16 × 20<br>36 × 35 | 18 × 28<br>32 × 38 |
| Stent Material | Platinum-10%Iridium | Chromium-cobalt | Nitinol | Nitinol | Nitinol | Nitinol |
| Stent Fabrication | Welded wires with gold brazing | Laser cut | Wire | Laser cut | Laser cut | Double thread, knitted wires |
| Valve | Bovine jugular vein bicuspid/tricuspid valve | Bovine pericardial tricuspid valve | Porcine pericardial tricuspid valve | – | Porcine pericardial tricuspid valve | Porcine Pericardial tricuspid valve |
| Stent Cover | Bovine Xenograft Conduit | PET Skirt covering 30% with (S3/Ultra) or without (XT) cuff | PET fabric covering total frame | PET fabric covering ~75% | Porcine pericardium | Porcine pericardium |

## 10.4 Engineering Studies in PPVI

During the development of Melody® technologies, stent fractures did not occur in the standardised bench testing in a distensible tube with dynamic conditions mimicking 2 years of cardiac cycles. However, a review of the US Melody Valve trial data found freedom from stent fracture to be 68 ± 5% within 2 years [9]. This prompted the development and introduction of new engineering methodologies to expand, not only our knowledge with regard to stent fracture [44, 63, 64] but also stent fabrication [65], RVOT population anatomies, [66] RVOT dynamics [10], patient selection, bench testing methodologies [67] and the inclusions of innovative computational methods in the design and regulatory processes [43, 44].

For example, finite element (FE) modelling is an engineering method that can be used to simulate the deployment and interaction of devices with the RVOT implantation site, to analyse: (1) the resulting material stresses in patient-specific and/or (2) anatomically representative RVOT geometries of varied population [63, 64, 68–70]. These new methodologies have guided the design improvements of the next generation of self-expanding PPVI devices to address native RVOTs, and regulatory bodies are accepting that modern computational and imaging analysis methods have a role to play, particularly where the limitations of bench and animal testing are exceeded [68].

### *10.4.1 Stent Fracture*

Our group adopted FE modelling to study stent fracture in a patient-specific RVOT anatomy of a 25-year-old who underwent PPVI and experienced stent fractures with loss of stent integrity within 6 months (Fig. 10.9). Geometric properties and device stresses and fatigue in the patient-specific geometry were compared to simulations of uniformly deployed stents in tubes mimicking bench-testing at 20 and 22 mm deployment [64].

To do so, the patient pre-procedural MR images were segmented to create a 3D, rigid-shell model of the patient's RVOT, pulmonary trunk and branches to guide the realistic geometrical FE expansion of the stent [65]. Post-PPVI bi-plane fluoroscopy images were used to extract the stent configurations in the patient's anatomy and validate the FE simulations. Once deployed, systolic and diastolic stent loading were replicated.

As seen in Fig. 10.10, the stent remained cylindrical throughout systole and diastole phases in both bench testing simulations (PL and $PL_{22}$), whereas a notable elliptical cross-section and curvature formed in the patient-specific case ($PL_{RVOT}$), where ~20 stent cells were overexpanded. Furthermore, the majority of these cells lay at the proximal end of the stent and corresponded to those which eventually failed in situ. Indeed, the geometrical differences between the bench testing and in situ configuration translated in higher stress distributions for the latter (Fig. 10.10), with

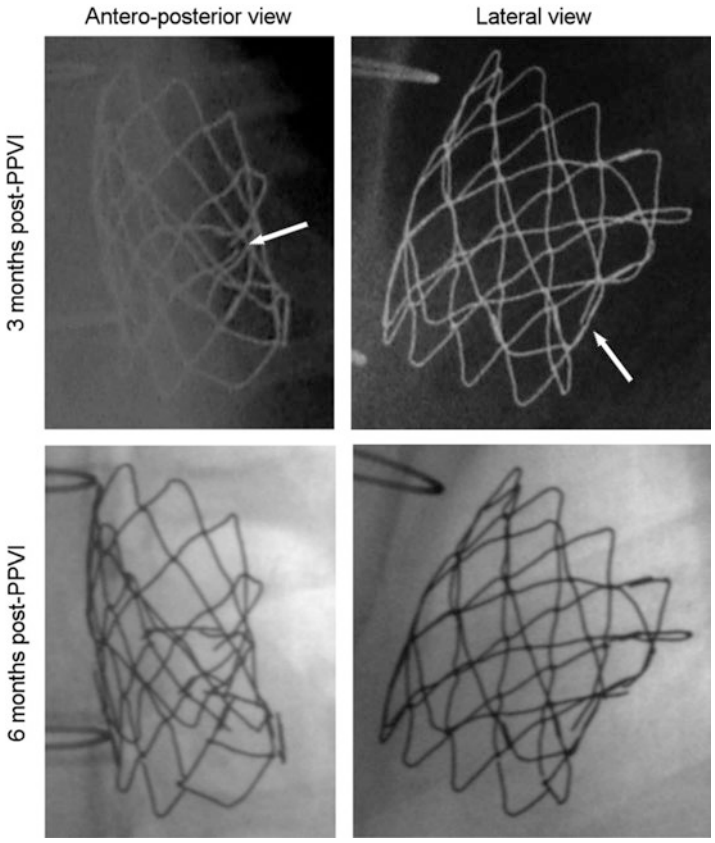


**Fig. 10.9** Fluoroscopy images of an implanted PPVI device in a 25-year-old woman at 3- and 6-months after implantation. The white arrows show minor stent fractures at 3 month after implantation. Further fracturing is seen at 6 months after implantation which led to loss of stent integrity, followed by a second PPVI device being fitted. (Images from Schievano [64])

fatigue stress distribution closer to the limit (Fig. 10.11) and inherently lower fatigue safety factor [71, 72].

Albeit limited to a single case, this novel study by Schievano et al. demonstrated the need for more representative anatomies and loading conditions to be included in pre-clinical testing and how computational methods could be used to compensate for the lack of relevant animal models or limited bench testing. Cosentino et al. further expanded this understanding of the impact of varied RVOT anatomies on the risk of stent fracture, using post-PPVI fluoroscopy images of 42 patients who received Melody® [63]. The patient-specific displacements of each stent between inflation, early systole and diastole phases were simulated to identify stresses and geometric parameters which were linked to stent fracture.

All deployed stents had elliptical and asymmetrical cross-sections with non-cylindrical configurations which directly contrasted the imposed conditions applied

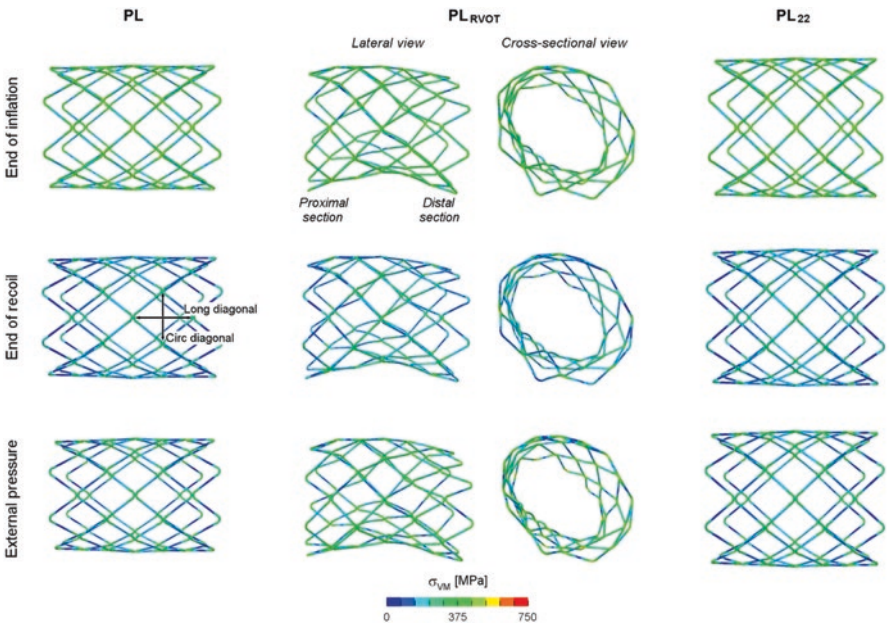


**Fig. 10.10** Von Mises stress map in the stent after each phase is simulated. Noting the qualitatively higher stress in the patient-specific simulation ($PL_{RVOT}$) results as the uniformly expanded stent [64]

during bench testing in tubes. Described good risk identifiers for stent fracture were the extent to which the cross-section became elliptical and how much the cross-section changed configurations throughout the cardiac cycle. Overall, the statistical analyses stratified 42 patients into high and low risk with 93% accuracy.

Pre-stenting was introduced in PPVI to prevent Melody® stent fractures, as one or multiple pre-stents can enhance the strength of the system and thus decrease the stresses experienced by the PPVI stent and ultimately leading to fracture [9, 28, 73, 74]. The premise of pre-stenting was computationally tested by simulating the expansion of two PPVI stents, one inside the other [65]. The mechanical performance of the coupled device was compared with that of a single stent, expanded and cyclically loaded at the same conditions. The stresses in the outer stent of the coupled devices were similar to those of the single-valved stent. However, the stresses in the inner stent, which holds the valve, were lower when compared to the stresses in the single-valved stent. Therefore, the implantation of a stent prior to the PPVI device acts functionally to bolster the vessel and reduce the stresses on the valved stent, thus decreasing the risks of PPVI fractures. Furthermore, the use of multiple stents could allow for thinner wires to be employed in manufacturing devices that, therefore, ultimately would require smaller delivery systems thus allowing treatment of younger patients in need of a new valve.

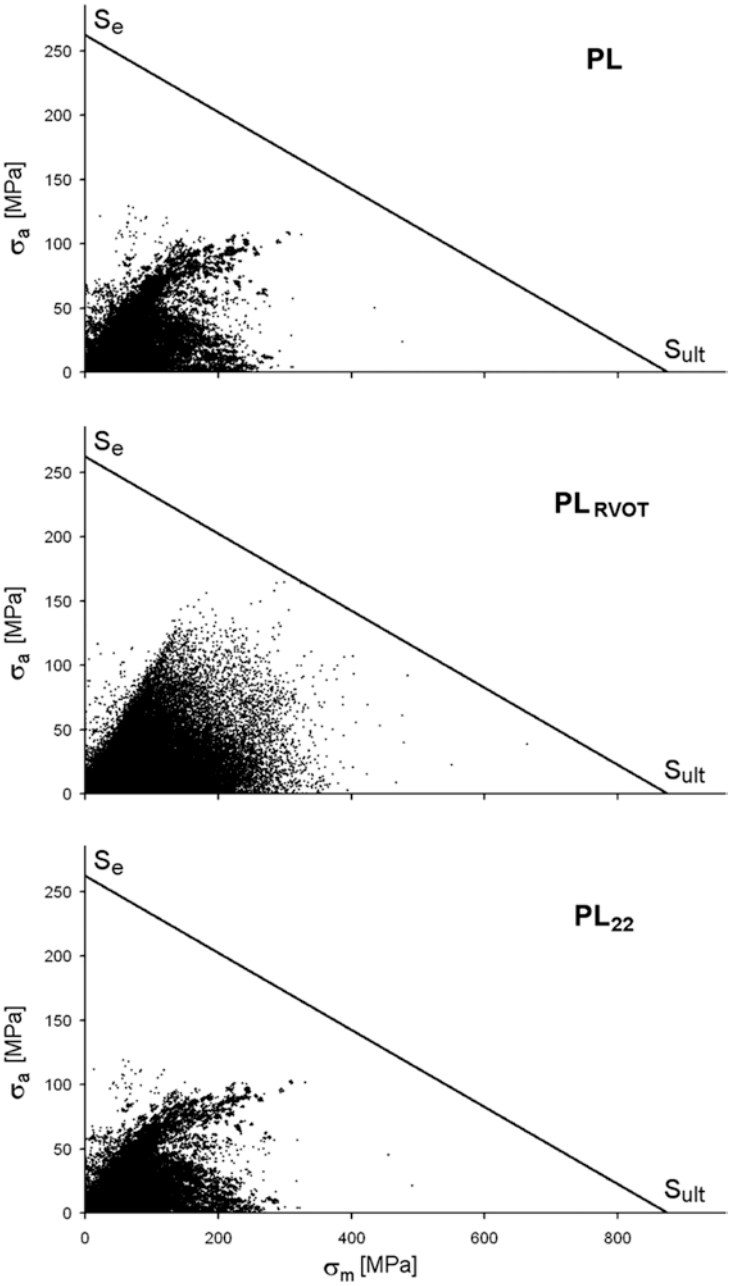


**Fig. 10.11** Goodman diagrams of the PL, $PL_{22}$ and $PL_{RVOT}$ simulations showing how the distribution of points skews towards the fatigue limit in the patient-specific geometry ($PL_{RVOT}$) as compared to the 20 and 22 mm expanded, cylindrical test [64]

### *10.4.2 Patient Selection*

The 3D anatomical variations of PPVI candidates were first investigated by our group in 2007 to identify classes of RVOT morphologies most suitable for the percutaneous approach and to document their prevalence in a population of patients with RVOT dysfunction, following CHD repair [66]. A morphological classification was created according to visual assessment of 3D MR reconstructions and detailed measurement, showing heterogeneous characteristics. Nevertheless, five patterns were identified with a pyramidal morphology being the most prevalent (49%), related to the presence of a transannular patch and deemed at the time unsuitable for PPVI with Melody.

Caimi et al. proposed a workflow for predicting case-specific periprocedural risks by comprehensively simulating stent expansions in patient-specific FE models [70]. This methodology was tested on three cases, retrospectively. The RVOT, conduit, calcific conduit deposits, aortic root and coronary arteries were segmented from CT imaging and realistic balloon-in-balloon, stent and implantation site FE models were recreated. The transient simulation modelled the phases of RVOT pre-PPVI balloon angioplasty and device implantation, including delivery system inflation and stent recoil. Of the three cases simulated, the FE model detected obstructions to coronary flow in one patient, consistent with the results of the in vivo balloon angioplasty investigation. Each simulation found evidence of aortic root compression to varying degrees. The stress analyses of the deployed stents were consistent with the findings by Cosentino et al. [63], indicating again the elevated stresses at the welds of a given stent. Caimi et al. importantly highlighted the effects of the pattern of calcific deposits on the resultant irregularities of the stent configurations, which further increased stresses in regions where a given stent was forced to conform to the calcification deposits.

Furthermore, in FDA EFS trials, both the Harmony – and later the Alterra Adaptive Prestent – were introduced to patients in small cohorts. In this framework, medical image analyses, computational assessments and rapid prototyping played a pivotal role in patient selection; i.e. to enroll patients with higher chances of successful and safe implantations, consequently reflected in the procedural success rates of both devices [45, 50].

It should be noted, that Gillespie et al. published the patient selection protocol for the Harmony EFS in 2017 [45] which was later closely followed for the Alterra Adaptive Prestent EFS [50]. In the Harmony trial, 270 patients indicated for pulmonary valve replacements were clinically screened across three sites. A pre-screening phase studied the implantation sites, anatomical dimensions using MR and echocardiography, thus identifying 66 eligible patients. These, after consenting, underwent cardiac gated CT angiography, focusing on RV, RVOT, MPA and proximal branch PAs. The CT images were segmented to extract 3D reconstructions of the right-side cardiac anatomies in both end at systole and diastole. From these, a perimeter plot (PP) of the RVOT from the levels of the valve annulus to the branching point of the proximal PAs were generated. By superimposing the PP of the detailed anatomies

at both end systole and diastole onto the PP of the Harmony device, the interference fits of the devices along the entire implantations site could be assessed. This method, although different and more simplified compared to a full FE approach [43, 44], is faster, saving in labour and computational time with the data gleaned from the analyses considered to outweigh the losses of accuracies. Each patient's reconstruction at end systole and diastole were also 3D printed to physically test the deployment of a given Harmony device. The deployed devices in the 3D printed vessel models were subsequently CT scanned to allow for analyses of potential wall interferences. The PP analyses and rapid prototyping results were submitted to the patient's assessment package for analyses by the screening committee. Twenty-one patients were approved for Harmony and, after a similar screening process of 29 patients, 15 were approved for the Alterra Adaptive Prestent EFS [50]. The results of each study were discussed previously above in each devices detailed overview.

### *10.4.3 Device Design*

Computational simulations [43, 44, 67, 75] and image analyses [10, 76] have also been employed as traditional engineering tools in the product development process to support designs of the second-generation PPVI devices (Harmony, Alterra) and in silico clinical trials [43]. For example, Capelli et al. used FE modelling in 62 patients who underwent surgical PVR to compare outcomes between the initial designs of the Harmony TPV22 and a proposed dimension modification, with TPV25 [44]. Capelli et al. showed marked improvements in patient applicabilities of the TPV25 devices, which were subsequently manufactured. This demonstrated one important role that computational modelling can provide in device design optimisations; which will be further expanded upon with the introduction of rapid computational testing in populations of relevant anatomies, and this should allow for the reduction of manufactured prototypes.

Computational and rapid prototyping methodologies showed clear utilities in expediting the product development process as well as allowing for safer first approximations for the patients for whom such device should benefit; also showing the potential uses for regulatory approval processes. This was highlighted in the first-in-human implantation of Harmony, which, although having passed bench and animal testing in sheep [77], required design adaptations. In 2008, a 42-year-old patient with CHD and four previous open-heart procedures, presented with severe pulmonary valve insufficiency. Surgical repair was deemed too risky and PPVI with Melody not suitable due to the size of the patient's native RVOT. Harmony, at the time at the end of preclinical trials, was offered to the patient on compassionate grounds, following MHRA approval. The patient-specific assessment protocol combined medical image analysis of the RVOT anatomy following ECG gated CT with analyses of 10 frames over the cardiac cycle, patient-specific FE modelling of deployment and 3D printing to test device deployment in vivo [43]. Measurements of the 3D anatomic diameters and lengths over the cardiac cycle were gathered,

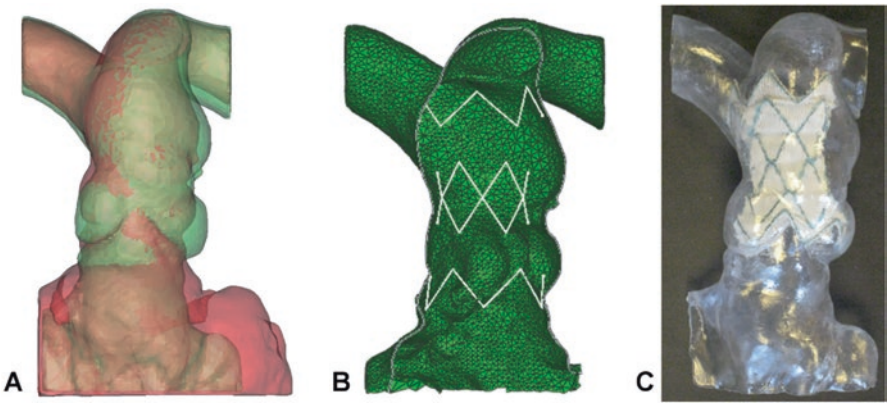


**Fig. 10.12** Imaging segmentation (**a**) of systolic and diastolic geometries, in silico FE analysis of deployment (**b**) and physical deployment of the stent in a 3D printed model of the patient's specific geometry (**c**)

showing the native dynamic environment with large variations from end systole to end diastole. These measurements provided a physical band of sizing for the proximal, central and distal portions of the stent, from which the ring size could be optimised.

The final sizing and delivery of a customised device were trialled in in silico deployments in rigid-wall FE models of the systolic and diastolic anatomies, and also in vitro within the equivalent 3D printed models. The FE model was able to confirm definitive and adequate interferences between the struts and the implantation site which was confirmed by the deployment into the 3D printed prototype of the patient's vessels (Fig. 10.12).

The approach developed and described in this first-in-human case was a precursor of the route to FDA regulatory approval through the innovative Early Feasibility Trial (EFS): Harmony was the first device to go through EFS.

## 10.5 Conclusion

It has been over 20 years since the first-in-human PPVI procedure by Phillip Bonhoeffer et al., and the possibilities for transcatheter heart valve replacement have boomed and many lives have been enhanced. The therapeutic market has been expanded by dozens of solutions which are collectively able to treat any heart valve, using different materials, designs and deployment methods to innovate around well-recognised limitations in all applications.

In the context of PPVI, enlarged patient eligibility criteria, reduced intra-procedural complications, like coronary compression, and progress towards greater device durabilities remain top priorities for next-generation devices. Importantly,

the story of PPVI device development has benefitted from the pivotal role of interdisciplinary research: i.e., in uncovering key design aspects, treatable anatomies and thus better patient selection understandings, novel device design developments and advances in regulatory processes. Melody and Harmony developed therapies were pioneers within surgical PVR and native RVOT PPVI devices, respectively, and were made possible through close partnerships between clinical, engineering and medical imaging experts. There remain still many open questions for this interdisciplinary community to solve to further improve clinical outcomes. For example, assessments of in-vivo boundary conditions and predictions of implantation site compliances when overstretched (as is the case of stenting) remain challenging, especially in highly dynamic RVOTs as presented by Bosi et al. [75]. For this same group of patients, long-term results may be impacted by the abilities of the deployed devices to replicate the natural RVOT dynamics and the subsequent closer-to-physiological haemodynamics. Furthermore, selection of optimal timing for administering such interventions still requires full knowledge of the population longitudinal growth characteristics, so that clinicians can elect to delay or expedite PPVI accordingly.

After its revolutionary introduction over 20 years ago, PPVI has seen a continued march of both progress and innovation. Through continued inter-disciplinary partnerships between engineers, clinicians and industry, further developments will make it possible to improve overall clinical outcomes and benefit all patients requiring a new pulmonary valve.

## References

1. Brida M, Gatzoulis MA (2019) Adult congenital heart disease: past, present and future. Acta Paediatr Int J Paediatr 108(10):1757–1764. https://doi.org/10.1111/apa.14921
2. Marelli AJ, Mackie AS, Ionescu-Ittu R, Rahme E, Pilote L (2007) Congenital heart disease in the general population: changing prevalence and age distribution. Circulation 115(2):163–172. https://doi.org/10.1161/CIRCULATIONAHA.106.627224
3. Zühlke L et al (2019) Congenital heart disease in low- and lower-middle–income countries: current status and new opportunities. Curr Cardiol Rep 21(12). https://doi.org/10.1007/s11886-019-1248-z
4. Oosterhof T et al (2006) Long-term follow-up of homograft function after pulmonary valve replacement in patients with tetralogy of Fallot. Eur Heart J 27(12):1478–1484. https://doi.org/10.1093/eurheartj/ehl033
5. Gatzoulis MA et al (2000) Risk factors for arrhythmia and sudden cardiac death late after repair of tetralogy of Fallot: a multicentre study. Lancet 356(9234):975–981. https://doi.org/10.1016/S0140-6736(00)02714-8
6. Bonhoeffer P et al (2000) Percutaneous replacement of pulmonary valve in a right-ventricle to pulmonary-artery prosthetic conduit with valve dysfunction. Lancet 356(9239):1403–1405. https://doi.org/10.1016/S0140-6736(00)02844-0
7. Bonhoeffer P et al (2000) Transcatheter implantation of a Bovine valve in pulmonary position. Circulation 102:813–816

8. Boone RH et al (2010) Transcatheter pulmonary valve implantation using the Edwards SAPIEN™ transcatheter heart valve. Catheter Cardiovasc Interv 75(2):286–294. https://doi.org/10.1002/ccd.22250
9. McElhinney DB et al (2011) Stent fracture, valve dysfunction, and right ventricular outflow tract reintervention after transcatheter pulmonary valve implantation: patient-related and procedural risk factors in the US melody valve trial. Circ Cardiovasc Interv 4(6):602–614. https://doi.org/10.1161/CIRCINTERVENTIONS.111.965616
10. Schievano S et al (2011) Four-dimensional computed tomography: a method of assessing right ventricular outflow tract and pulmonary artery deformations throughout the cardiac cycle. Eur Radiol 21(1):36–45. https://doi.org/10.1007/s00330-010-1913-5
11. Mcelhinney DB, Hennesen JT (2013) The Melody® valve and Ensemble® delivery system for transcatheter pulmonary valve replacement. Ann N Y Acad Sci 1291(1):77–85. https://doi.org/10.1111/nyas.12194
12. Mcelhinney DB (2021) Transcatheter valve devices in congenital heart disease. In: Butera G, Chessa M, Eicken A, Thomson J (eds) Cardiac catheterization for congenital heart disease: from fetal life to adulthood, vol 01, no. 02, 2nd edn. Springer Nature Switzerland AG, pp 125–136
13. Khambadkone S et al (2005) Percutaneous pulmonary valve implantation in humans: results in 59 consecutive patients. Circulation 112(8):1189–1197. https://doi.org/10.1161/CIRCULATIONAHA.104.523266
14. Alkashkari W, Albugami S, Abbadi M, Niyazi A, Alsubei A, Hijazi ZM (2020) Transcatheter pulmonary valve replacement in pediatric patients. Expert Rev Med Devices 17(6):541–554. https://doi.org/10.1080/17434440.2020.1775578
15. Armstrong AK et al (2014) One-year follow-up of the melody transcatheter pulmonary valve multicenter post-approval study. JACC Cardiovasc Interv 7(11):1254–1262. https://doi.org/10.1016/j.jcin.2014.08.002
16. Jones TK et al (2021) Long-term outcomes after Melody Transcatheter pulmonary valve replacement in the US Investigational Device exemption trial. Circ Cardiovasc Interv (January):22–32. https://doi.org/10.1161/circinterventions.121.010852
17. Cheatham JP et al (2015) Clinical and hemodynamic outcomes up to 7 years after transcatheter pulmonary valve replacement in the US melody valve investigational device exemption trial. Circulation 131(22):1960–1970. https://doi.org/10.1161/CIRCULATIONAHA.114.013588
18. McElhinney DB et al (2010) Short-and medium-term outcomes after transcatheter pulmonary valve placement in the expanded multicenter US melody valve trial. Circulation 122(5):507–516. https://doi.org/10.1161/CIRCULATIONAHA.109.921692
19. McElhinney DB et al (2018) Endocarditis after Transcatheter pulmonary valve replacement. J Am Coll Cardiol 72(22):2717–2728. https://doi.org/10.1016/j.jacc.2018.09.039
20. Cabalka AK et al (2017) Relationships among conduit type, pre-stenting, and outcomes in patients undergoing Transcatheter pulmonary valve replacement in the prospective North American and European Melody valve trials. JACC Cardiovasc Interv 10(17):1746–1759. https://doi.org/10.1016/j.jcin.2017.05.022
21. Shahanavaz S et al (2020) Outcomes after Transcatheter reintervention for dysfunction of a previously implanted Transcatheter pulmonary valve. JACC Cardiovasc Interv 13(13):1529–1540. https://doi.org/10.1016/j.jcin.2020.03.035
22. Butera G, Mac Donald S, Chessa M, Bonhoeffer P (2021) Melody valve implantation in pulmonary position. In: Butera G, Chessa M, Eicken A, Thomson J (eds) Cardiac catheterization for congenital heart disease: from fetal life to adulthood, 2nd edn. Springer Nature Switzerland AG, Cham, pp 729–748
23. Binder RK, Rodés-Cabau J, Wood DA, Webb JG (2012) Edwards SAPIEN 3 valve. EuroIntervention 8:83–87
24. Guccione P, Milanesi O, Hijazi ZM, Pongiglione G (2012) Transcatheter pulmonary valve implantation in native pulmonary outflow tract using the Edwards SAPIEN™ transcatheter heart valve. Eur J Cardio-Thoracic Surg 41(5):1192–1194. https://doi.org/10.1093/ejcts/ezr130

25. Suntharos P, Prieto LR (2017) Percutaneous pulmonary valve implantation in the native right ventricular outflow tract using a 29-mm Edwards SAPIEN 3 valve. World J Pediatr Congenit Heart Surg 8(5):639–642. https://doi.org/10.1177/2150135116655125
26. Shahanavaz S et al (2020) Transcatheter pulmonary valve replacement with the Sapien prosthesis. J Am Coll Cardiol 76(24):2847–2858. https://doi.org/10.1016/j.jacc.2020.10.041
27. Haas NA et al (2018) Early outcomes of percutaneous pulmonary valve implantation using the Edwards SAPIEN XT transcatheter heart valve system. Int J Cardiol 250:86–91. https://doi.org/10.1016/j.ijcard.2017.10.015
28. Lehner A et al (2019) Intermediate outcomes of transcatheter pulmonary valve replacement with the Edwards Sapien 3 valve–German experience. Expert Rev Med Devices 16(9):829–834. https://doi.org/10.1080/17434440.2019.1653180
29. Tannous P, Nugent A (2021) Transcatheter pulmonary valve replacement in native and non-conduit right ventricle outflow tracts. J Thorac Cardiovasc Surg 162(3):967–970. https://doi.org/10.1016/j.jtcvs.2020.07.126
30. Garay F, Webb J, Hijazi ZM (2006) Percutaneous replacement of pulmonary valve using the Edwards-Cribier percutaneous heart valve: first report in a human patient. Catheter Cardiovasc Interv 67(5):659–662. https://doi.org/10.1002/ccd.20753
31. Edwards Lifesciences (2016, March 2) Edwards SAPIEN XT valve receives FDA approval for pulmonic procedures, Irvine, California
32. Kenny D et al (2011) Percutaneous implantation of the Edwards SAPIEN transcatheter heart valve for conduit failure in the pulmonary position: early phase 1 results from an international multicenter clinical trial. J Am Coll Cardiol 58(21):2248–2256. https://doi.org/10.1016/j.jacc.2011.07.040
33. Kenny D et al (2018) 3-year outcomes of the Edwards SAPIEN Transcatheter heart valve for conduit failure in the pulmonary position from the COMPASSION multicenter clinical trial. JACC Cardiovasc Interv 11(19):1920–1929. https://doi.org/10.1016/j.jcin.2018.06.001
34. Wilson WM, Benson LN, Osten MD, Shah A, Horlick EM (2015) Transcatheter pulmonary valve replacement with the Edwards Sapien system: the Toronto experience. JACC Cardiovasc Interv 8(14):1819–1827. https://doi.org/10.1016/j.jcin.2015.08.016
35. Plessis J et al (2018) Edwards SAPIEN Transcatheter pulmonary valve implantation: results from a French registry. JACC Cardiovasc Interv 11(19):1909–1916. https://doi.org/10.1016/j.jcin.2018.05.050
36. Lehner A et al (2019) Expert review of medical devices intermediate outcomes of transcatheter pulmonary valve replacement with the Edwards Sapien 3 valve – German experience. Expert Rev Med Devices 16(9):829–834. https://doi.org/10.1080/17434440.2019.1653180
37. Haas NA et al (2018) The risk of bacterial endocarditis after percutaneous and surgical biological pulmonary valve implantation. Int J Cardiol 268:55–60. https://doi.org/10.1016/j.ijcard.2018.04.138
38. Hascoet S et al (2017) Infective endocarditis risk after percutaneous pulmonary valve implantation with the Melody and Sapien valves. JACC Cardiovasc Interv 10(5):510–517. https://doi.org/10.1016/j.jcin.2016.12.012
39. Le Ruz R et al (2021) Edwards SAPIEN XT transcatheter pulmonary valve implantation: 5-year follow-up in a French registry. Catheter Cardiovasc Interv 98(5):990–999. https://doi.org/10.1002/ccd.29862
40. Butera G, Hansen JH, Jones MI (2019) Tricuspid regurgitation complicating SAPIEN 3 valve implantation in pulmonary position. Catheter Cardiovasc Interv 94(6):894. https://doi.org/10.1002/ccd.28083
41. Bergersen L et al (2017) Harmony feasibility trial: acute and short-term outcomes with a self-expanding Transcatheter pulmonary valve. JACC Cardiovasc Interv 10(17):1763–1773. https://doi.org/10.1016/j.jcin.2017.05.034
42. Food and Drug Administration of the United States of America (2021) FDA approves first in the world device to treat patients with congenital heart disease. https://www.fda.gov/news-events/press-announcements/fda-approves-first-world-device-treat-patients-congenital-heart-disease. Accessed 10 Feb 2022

43. Schievano S et al (2010) First-in-man implantation of a novel percutaneous valve: a new approach to medical device development. EuroIntervention 5(6):745–750. https://doi.org/10.4244/EIJV5I6A122
44. Capelli C, Taylor AM, Migliavacca F, Bonhoeffer P, Schievano S (2010) Patient-specific reconstructed anatomies and computer simulations are fundamental for selecting medical device treatment: application to a new percutaneous pulmonary valve. Philos Trans R Soc A Math Phys Eng Sci 368(1921):3027–3038. https://doi.org/10.1098/rsta.2010.0088
45. Gillespie MJ et al (2017) Patient selection process for the Harmony Transcatheter pulmonary valve early feasibility study. Am J Cardiol 120(8):1387–1392. https://doi.org/10.1016/j.amjcard.2017.07.034
46. Shahanavaz S, Tang J, Gillespie MJ, Morgan GJ (2021) Emerging solutions for the dilated native right ventricular outflow tract. Prog Pediatr Cardiol 61(January):101369. https://doi.org/10.1016/j.ppedcard.2021.101369
47. Gillespie MJ, Bergersen L, Benson LN, Weng S, Cheatham JP (2021) 5-year outcomes from the harmony native outflow tract early feasibility study. JACC Cardiovasc Interv 14(7):816–817. https://doi.org/10.1016/j.jcin.2021.01.046
48. Benson LN et al (2020) Three-year outcomes from the harmony native outflow tract early feasibility study. Circ Cardiovasc Interv (January):1–10. https://doi.org/10.1161/CIRCINTERVENTIONS.119.008320
49. Zahn EM, Chang JC, Armer D, Garg R (2018) First human implant of the Alterra Adaptive Prestent TM : a new self-expanding device designed to remodel the right ventricular outflow tract. Catheter Cardiovasc Interv 91(6):1125–1129. https://doi.org/10.1002/ccd.27581
50. Shahanavaz S et al (2020) Alterra Adaptive Prestent and SAPIEN 3 THV for congenital pulmonic valve dysfunction: an early feasibility study. JACC Cardiovasc Interv 13(21):2510–2524. https://doi.org/10.1016/j.jcin.2020.06.039
51. Cao QL et al (2014) Early clinical experience with a novel self-expanding percutaneous stent-valve in the native right ventricular outflow tract. Catheter Cardiovasc Interv 84(7):1131–1137. https://doi.org/10.1002/ccd.25544
52. Qureshi SA, Jones MI (2018) Recent advances in transcatheter management of pulmonary regurgitation after surgical repair of tetralogy of Fallot. F1000Research 7(May):1–6. https://doi.org/10.12688/f1000research.14301.1
53. Kogure T, Qureshi SA (2020) The future of paediatric heart interventions: where will we be in 2030? Curr Cardiol Rep 22(12). https://doi.org/10.1007/s11886-020-01404-z
54. Garay F, Pan X, Zhang YJ, Wang C, Springmuller D (2017) Early experience with the Venus p-valve for percutaneous pulmonary valve implantation in native outflow tract. Netherlands Hear J 25(2):76–81. https://doi.org/10.1007/s12471-016-0932-5
55. Husain J, Praichasilchai P, Gilbert Y, Qureshi SA, Morgan GJ (2016) Early european experience with the venus p-valve®: filling the gap in percutaneous pulmonary valve implantation. EuroIntervention 12(5):e643–e651. https://doi.org/10.4244/EIJV12I5A105
56. Promphan W, Prachasilchai P, Siripornpitak S, Qureshi SA, Layangool T (2016) Percutaneous pulmonary valve implantation with the Venus P-valve: clinical experience and early results. Cardiol Young 26(4):698–710. https://doi.org/10.1017/S1047951115001067
57. Morgan G et al (2019) Medium-term results of percutaneous pulmonary valve implantation using the Venus P-valve: international experience. EuroIntervention 14(13):1363–1370. https://doi.org/10.4244/EIJ-D-18-00299
58. Kim GB, Lim HG, Kim YJ, Choi EY, Kwon BS, Jeong S (2014) Novel self-expandable, stent-based transcatheter pulmonic valve: a preclinical animal study. Int J Cardiol 173(1):74–79. https://doi.org/10.1016/j.ijcard.2014.02.005
59. Kim GB, Kwon BS, Lim HG (2017) First in human experience of a new self-expandable percutaneous pulmonary valve implantation using knitted nitinol-wire and tri-leaflet porcine pericardial valve in the native right ventricular outflow tract. Catheter Cardiovasc Interv 89(5):906–909. https://doi.org/10.1002/ccd.26910

60. Kim GB et al (2018) Successful feasibility human trial of a new self-expandable percutaneous pulmonary valve (Pulsta valve) implantation using Knitted Nitinol wire backbone and Trileaflet-Gal-Free Porcine Pericardial valve in the native right ventricular outflow tract. Circ Cardiovasc Interv 11(6):1–7. https://doi.org/10.1161/CIRCINTERVENTIONS.118.006494
61. Lee SY et al (2021) Mid-term outcomes of the Pulsta transcatheter pulmonary valve for the native right ventricular outflow tract. Catheter Cardiovasc Interv 98(5):E724–E732. https://doi.org/10.1002/ccd.29865
62. Cho SA et al (2021) Catastrophic case scenario during percutaneous pulmonary valve replacement. J Cardiothorac Vasc Anesth 35(5):1466–1468. https://doi.org/10.1053/j.jvca.2020.05.019
63. Cosentino D et al (2014) Geometrical and stress analysis of factors associated with stent fracture after melody percutaneous pulmonary valve implantation. Circ Cardiovasc Interv 7(4):510–517. https://doi.org/10.1161/CIRCINTERVENTIONS.113.000631
64. Schievano S et al (2009) Patient specific finite element analysis results in more accurate prediction of stent fractures: application to percutaneous pulmonary valve implantation. J Biomech 43(4):687–693. https://doi.org/10.1016/j.jbiomech.2009.10.024
65. Schievano S et al (2007) Finite element analysis of stent deployment: understanding stent fracture in percutaneous pulmonary valve implantation. J Interv Cardiol 20(6):546–554. https://doi.org/10.1111/j.1540-8183.2007.00294.x
66. Schievano S et al (2007) Variations in right ventricular outflow tract morphology following repair of congenital heart disease: implications for percutaneous pulmonary valve implantation. J Cardiovasc Magn Reson 9(4):687–695. https://doi.org/10.1080/10976640601187596
67. Biglino G et al (2012) Virtual and real bench testing of a new percutaneous valve device: a case study. EuroIntervention 8(1):121–128. https://doi.org/10.4244/EIJV8I1A19
68. Biglino G, Capelli C, Bruse J, Bosi GM, Taylor AM, Schievano S (2017) Computational modelling for congenital heart disease: how far are we from clinical translation? Heart 103(2):98–103. https://doi.org/10.1136/heartjnl-2016-310423
69. Bosi GM et al (2018) Population-specific material properties of the implantation site for transcatheter aortic valve replacement finite element simulations. J Biomech 71:236–244. https://doi.org/10.1016/j.jbiomech.2018.02.017
70. Caimi A et al (2018) Prediction of stenting related adverse events through patient-specific finite element modelling. J Biomech 79:135–146. https://doi.org/10.1016/j.jbiomech.2018.08.006
71. Marrey RV, Burgermeister R, Grishaber RB, Ritchie RO (2006) Fatigue and life prediction for cobalt-chromium stents: a fracture mechanics analysis. Biomaterials 27(9):1988–2000. https://doi.org/10.1016/j.biomaterials.2005.10.012
72. Beden SM, Abdullah S, Ariffin AK, Al-Asady NA, Rahman MM (2009) Fatigue life assessment of different steel-based shell materials under variable amplitude loading. Eur J Sci Res 29(2):157–169
73. Boudjemline Y (2018) A new one-step procedure for pulmonary valve implantation of the melody valve: simultaneous prestenting and valve implantation. Catheter Cardiovasc Interv 91:64–70. https://doi.org/10.1002/ccd.27332
74. Eicken A et al (2011) Percutaneous pulmonary valve implantation: two-Centre experience with more than 100 patients. Eur Heart J 32(10):1260–1265. https://doi.org/10.1093/eurheartj/ehq520
75. Bosi GM, Capelli C, Khambadkone S, Taylor A, Schievano S (2015) Patient-specific finite element models to support clinical decisions: a lesson learnt from a case study ofPercutaneous pulmonary valve implantation. Catheter Cardiovasc Interv 86:1120–1130. https://doi.org/10.1002/ccd.25944
76. Chung R, Taylor AM (2014) Imaging for preintervention planning transcatheter pulmonary valve therapy. Circ Cardiovasc Imaging 7(1):182–189. https://doi.org/10.1161/CIRCIMAGING.113.000826
77. Bonhoeffer P et al (2008) Transcatheter pulmonic valve replacement in sheep using a grafted self-expanding stent with tissue valve. Circulation 118(S_812) [Online]. Available: https://doi.org/10.1161/circ.118.suppl_18.S_812-a

# Chapter 11
# Transcatheter Aortic Valve Implantation

**Horacio A. Medina de Chazal, Ali Zgheib, Abdullah Al Ismaili, Ali Abualsaud, Marco Spaziano, Giuseppe Martucci, and Nicolo Piazza**

## 11.1 Introduction

In 2002, Cribier and colleagues described the implantation of the first-in-human balloon expandable transcatheter heart valve (THV) in the aortic position [1]. This ground-breaking procedure was successfully performed on a patient suffering from refractory cardiogenic shock secondary to severe aortic stenosis (AS); this valve was a 23 mm bovine pericardial stent valve developed by Percutaneous Valve Technologies (New Jersey, USA). The device required a 24 French (Fr) catheter delivery system advanced through transvenous approach and transeptal puncture.

In July 2004, the CoreValve ReValving system was first implanted via a 25Fr delivery system [2]. Initially, these transcatheter procedures were complex and time consuming, requiring general anesthesia, cardiopulmonary bypass, and surgical cut-down of the femoral artery.

Since the first procedures, the transcatheter aortic valve implantation (TAVI or TAVR replacement) procedure has experienced a long journey with a tremendous improvement both in devices, implantation technique and operator experience, post-procedure care, as well as generation of robust clinical evidence derived from several randomized controlled trials [3–10] (Table 11.1). These refinements have improved patient safety and procedural intermediate-term outcomes leading toward a progressive expansion of TAVI candidates. Currently, TAVI has been approved for use across a broad risk spectrum. In addition, there has been an increase in off-label indications such as valve-in-valve procedures, bicuspid aortic valve (BAV) anatomy

H. A. Medina de Chazal · A. Zgheib · A. Al Ismaili · M. Spaziano
G. Martucci · N. Piazza (✉)
McGill University Health Center, Glen Hospital, Department of Medicine, Division of Cardiology, QC, Canada

A. Abualsaud
Department of Cardiology, Jewish General Hospital, McGill University, QC, Canada

© The Author(s), under exclusive license to Springer Nature Switzerland AG 2023

P. A. Iaizzo et al. (eds.), *Heart Valves*, https://doi.org/10.1007/978-3-031-25541-0_11

**Table 11.1** Major TAVI randomized clinical trials

| Study/year | Device | Population and design | | | Outcomes | | | | | | | | | | | | | | | | | |
|---|---|---|---|---|---|---|---|---|---|---|---|---|---|---|---|---|---|---|---|---|---|---|
| | | n TAVR (Total) | Risk | Age/STS mean | F/U | All-cause mortality | | Major stroke | | Major vascular complications | | ≥Moderate PVL | | NPMI | | Rehospitalization | | Myocardial infarction | | Hemodynamics MG EOA ($cm^2$) (mmHg) | | | |
| | | | | | | TAVI | SAVR | TAVI | SAVR | TAVI | SAVR | TAVI | SAVR | TAVI | SAVR | TAVI | SAVR | TAVI | SAVR | TAVI | SAVR | TAVR | SAVR |
| PARTNER 1A (2011 and 2015) | SAPIEN | 348 (699) | HR | 83.6/11.8 | 30 days | 3.4 | 6.5 | 3.8 | 2.1 | 9.3 | 19.5 | 12.2 | 0.9 | 3.8 | 3.6 | – | – | – | – | 9.9 | 10.8 | 1.7 | 1.5 |
| | | | | | | $p = 0.07$ | | $p = 0.20$ | | $p = 0.001$ | | $p = 0.001$ | | $p = 0.89$ | | – | | – | | $p = 0.004$ | | $p = 0.001$ | |
| | | | | | 1 year | 24.2 | 26.8 | 5.1 | 2.4 | – | – | – | – | | | 18.2 | 15.5 | 0.4 | 0.6 | – | – | – | – |
| | | | | | | $p = 0.44$ | | $p = 0.38$ | | – | | – | | – | | $p = 0.38$ | | $p = 0.69$ | | – | | – | |
| | | | | | 5 years | 67.8 | 62.4 | 10.4 | 11.3 | – | – | 14 | 1 | | | 42.3 | 34.2 | 2.9 | 5.9 | | | | |
| | | | | | | $p = 0.76$ | | $p = 0.61$ | | – | | $p = <0.0001$ | | – | | $p = 0.17$ | | $p = 0.15$ | | – | | – | |
| PARTNER 1B[#1] (2010 and 2015) | SAPIEN | 179 (358) | HR | 83.1/11.2 | 30 days | 5 | 2.8 | 5 | 1.1 | 16.8 | 3.9 | 12 | 0 | 3.4 | 5.0 | – | – | – | – | 1.5 | 0.8 | 11.4 | 33.1 |
| | | | | | | $p = 0.41$ | | $p = 0.06$ | | $p = <0.001$ | | NA | | $p = 0.6$ | | | | | | NA | | NA | |
| | | | | | 1 year | 30.7 | 50.7 | 7.8 | 3.9 | – | – | – | – | – | – | 22.3 | 44.1 | 0.6 | 0.6 | – | – | – | – |
| | | | | | | $p = <0.001$ | | $p = 0.18$ | | – | | – | | – | | $p = <0.001$ | | $p = 1.00$ | | – | | – | |
| | | | | | 5 years | 71.8 | 93.6 | 16 (any | 18.2 (any) | – | – | – | – | – | – | 47.6 | 87.3 | – | – | – | – | – | – |
| | | | | | | $p = <0.0001$ | | $p = 0.555$ | | – | | – | | – | | $p = <0.0001$ | | – | | – | | – | |
| CoreValve High Risk (2014–2016–2018) | Core Valve | 394 (795) | HR | 83.2 /7.3 | 30 days | 3.3 | 4.5 | 3.9 | 3.1 | 28.1 | 34.5 | 9.0 | 1.0 | 19.8 | 7.1 | – | – | – | – | 8.8 | 11.7 | 1.95 | 1.6 |
| | | | | | | $p = 0.43$ | | $p = 0.55$ | | $p = 0.05$ | | $p = <0.001$ | | $p = <0.001$ | | – | | – | | $p = <0.001$ | | $p = <0.001$ | |
| | | | | | 1 year | 14.2 | 19.1 | 5.8 | 7.0 | – | – | 15 | 2.5 | 22.4 | 11.9 | 16.5 | 13.9 | 1.9 | 1.5 | 8.9 | 12.2 | 1.7 | 1.5 |
| | | | | | | $p = 0.04$ non inf | | $p = 0.59$ | | – | | – | | – | | NA | | $p = 0.70$ | | – | | – | |
| | | | | | 3 years | 32.9 | 39.1 | 8.1 | 11.8 | – | – | 11.7 | 0 | 28 | 14.5 | – | – | 2.7 | 2.7 | 7.6 | 11.4 | 1.7 | 1.5 |
| | | | | | | $p = 0.068$ | | $p = 0.18$ | | – | | – | | $p = <0.001$ | | – | | $p = 0.96$ | | – | | $p = <0.0001$ | |
| | | | | | 5 years | 55.3 | 55.4 | 12.3 | 13.2 | – | – | 3.6 | 0 | 33 | 19.8 | 37.5 | 31.5 | 3.1 | 3.3 | 7.1 | 10.9 | – | – |
| | | | | | | $p = 0.50$ | | $p = 0.49$ | | – | | – | | – | | $p = 0.08$ | | $p = 0.93$ | | – | | – | |

| | | | | | | | | | | | | | | | | | | | | | | | |
|---|---|---|---|---|---|---|---|---|---|---|---|---|---|---|---|---|---|---|---|---|---|---|---|
| PARTNER 2A (2016 and 2019) | SAPIEN XT | 1011 (2032) | IR | 81.5/5.8 | 30 days | 6.1[a] | 8[a] | – | – | 7.9 | 5 | 3.7 | 0.6 | 8.5 | 6.9 | 6.5 | 6.5 | 1.2 | 1.9 | 9.7 | 10.9 | 1.7 | 1.5 |
| | | | | | | 011 | | – | | $p = 0.008$ | | | | 0.17 | | 0.99 | | 0.22 | | $p = 0.001$ | | $p = 0.001$ | |
| | | | | | 2 years | 19.3[a] | 21.1[a] | – | – | 8.6 | 5.5 | 8 | 0.6 | 11.8 | 10.3 | 19.6 | 17.3 | 3.6 | 4.1 | 10.8 | 11.7 | 1.5 | 1.4 |
| | | | | | | 0.33 | | – | | $p = 0.006$ | | | | 0.29 | | 0.22 | | 0.56 | | $p = 0.001$ | | $p = 0.001$ | |
| | | | | | 5 years | 47.9[a] | 43.4[a] | | | | | 4.1 | 0 | 15.5 | 13 | 33.3 | 25.2 | 11.1 | 8.2 | 11.4 | 10.8 | 1.5 | 1.3 |
| | | | | | | 1.09 [0.9–1.2] | | | | | | | | | | 1.28 [1.07–1.5] | | 1.26 [0.9–1.7] | | | | | |
| SURTAVI[##2] (2017 – TCT2021) | EVOLUT R | 864 (1660) | IR | 79.9/4.4 | 30 days | 2.2 | 1.7 | 1.2 | 2.5 | 12.1 | 9.3 | 3.4 | 0.3 | 25.9 | 6.6 | | | | | 8.9 | 12.4 | 2.1 | 1.8 |
| | | | | | | 0.5 [−0.9,1.8] | | −2.3 [−2.6,0.6] | | 2.8 [−0.1,5.9] | | | | 19.3 [15.9,22.7] | | 0.99 | | 0.22 | | NA | | NA | |
| | | | | | 2 years | 12.6 | 14 | 2.6 | 4.5 | | | 4.9 | 0 | | | 13.2 | 9.7 | 2.2 | 2.2 | 7.8 | 11.8 | 2.2 | 1.7 |
| | | | | | | (−1.4[−5.2–2.3]) | | −4.0 to 0.1 | | $p = 0.006$ | | 2.8 to 6.8 | | | | 0.1 to 7.0 | | −1.1 to 2.4 | | | | | |
| | | | | | 5 years | 31.3 | 30.8 | 4.1 | 5.8 | | | | | 35.8 | 14.5 | 12.8 | 9.5 | | | 8.6 | 11.2 | 2.2 | 1.8 |
| | | | | | | 1.02 CI 0.8–1.2 | | 0.6 CI 0.4–1.1 | | | | | | $p = 0.001$ | | $p = 0.06$ | | | | $p = 0.001$ | | $p = 0.001$ | |
| NOTION (2015–1019–2021) | Core Valve | 145 (280) | LR | 79.2 /4.4 | 30 days | 2.1 | 3.7 | 1.4 | 3.0 | 11.3 | 20.9 | 15.7 | 0.9 | 34.1 | 1.6 | – | – | 2.8 | 6.0 | 8.9 | 12.4 | 2.1 | 1.8 |
| | | | | | | $p = 0.43$ | | $p = 0.37$ | | $p = 0.03$ | | $p = 0.001$ | | $p = 0.001$ | | – | | 0.2 | | NA | | NA | |
| | | | | | 1 year | 13.1[b] | 16.3[b] | 2.9 (any) | 4.6 (any) | – | – | 15.7 | 0.9 | 38 | 2.4 | | | 3.5 | 6.0 | 8.6 | 12.5 | 1.7 | 1.3 |
| | | | | | | $p = 0.43$ | | $p = 0.44$ | | – | | $p = 0.001$ | | $p = 0.001$ | | | | $p = 0.33$ | | $p = 0.001$ | | $p = 0.001$ | |
| | | | | | 5 years | 38.0[b] | 36.3[b] | 9.0 | 7.4 | – | – | 8.2 | 0 | 41.7 | 7.8 | – | – | 7.7 | 7.4 | 8.2 | 13.7 | 1.6 | 1.2 |
| | | | | | | $p = 0.86$ | | $p = 0.65$ | | – | | $p = 0.001$ | | $p = 0.001$ | | – | | $p = 0.96$ | | $p = 0.001$ | | $p = 0.001$ | |
| | | | | | 8 years | 54.5 | 54.8 | 8.3 | 9.1 | – | – | 21.6 | 1.5 | 11 | 1.9 | | | 6.2 | 3.8 | 10 | 15 | 1.6 | 1.3 |
| | | | | | | $p = 0.94$ | | $p = 0.9$ | | – | | $p = 0.0001$ | | $p = 0.001$ | | | | $p = 0.33$ | | $p = 0.05$ | | $p = 0.05$ | |

(continued)

**Table 11.1** (continued)

| Study/year | Device | Population and design | | | Outcomes | | | | | | | | | | | | | | | | | |
|---|---|---|---|---|---|---|---|---|---|---|---|---|---|---|---|---|---|---|---|---|---|---|
| | | n TAVR (Total) | Risk | Age/STS mean | F/U | All-cause mortality | | Major stroke | | Major vascular complications | | ≥Moderate PVL | | NPMI | | Rehospitalization | | Myocardial infarction | | Hemodynamics MG EOA ($cm^2$) (mmHg) | | | |
| | | | | | | TAVI | SAVR | TAVI | SAVR | TAVI | SAVR | TAVI | SAVR | TAVI | SAVR | TAVI | SAVR | TAVI | SAVR | TAVI | SAVR | TAVR | SAVR |
| PARTNER 3[#3] (2019 and 2020) | SAPIEN 3 | 496 (1000) | LR | 73.3/5.8 | 30 days | 0.4 | 1.1 | 0 | 0.4 | 3.6 | 24.5 | 0.8 | 0 | 6.5 | 4.0 | | | | | 12.8 | 11.2 | 1.7 | 1.8 |
| | | | | | | 0.37 [0.07,1.8] | | NA | | 0.12 [0.07,0.21] | | NA | | 1.66 [0.9,2.96] | | | | | | 1.5 [0.9,2.0] | | −0.1 [−0.1,−0.0] | |
| | | | | | 1 year | 8.5[c] | 15.1[c] | 0.2 | 0.9 | 2.8 | 1.5 | 0.8 | 0.5 | 7.3 | 5.4 | 7.3 | 11 | 1.2 | 2.2 | 13.7 | 11.6 | 1.7 | 1.8 |
| | | | | | | $p = 0.001$ non inf | | 0.22 [0.03,2.0] | | 1.8 [0.7,4.5] | | 0.1 [−0.9,1.1] | | 1.38 [0.8,2.3] | | 0.65 [0.4,1.0] | | 0.5 [0.2,7.9] | | 2.0 [1.3,2.7] | | −0.1 [−0.1,0.0] | |
| | | | | | 2 years | 11.5[c] | 17.4[c] | 0.8 | 1.1 | | | 0.5 | 0 | 9.1 | 7 | 8.5 | 12.5 | 1.8 | 2.7 | 13.6 | 11.8 | 1.7 | 1.7 |
| | | | | | | $p = 0.007$ | | $p = 0.6$ | | | | – | | $p = 0.21$ | | $p = 0.04$ | | $p = 0.36$ | | $p = 0.06$ | | $p = 0.34$ | |
| EVOLUT Low Risk [#2](2019) | Core Valve EVOLUT R/ PRO | 734 (1468) | LR | 74/1.9 | 30 days | 0.8 | 2.6 | 0.5 | 1.7 | 3.8 | 3.2 | 3.4 | 0.4 | 17.4 | 6.1 | 1.2 | 2.5 | | | 8.4 | 10.5 | 2.2 | 2.0 |
| | | | | | | −1.8 [−3.2,−0.5] | | −1.2 [−2.4,−0.2] | | 0.6 [−1.4,2.5] | | NA | | 11.3 [8.0,14.7] | | −1.3 [−2.8,0.1] | | | | NA | | NA | |
| | | | | | 1 year | 2.9 | 4.6 | 0.8 | 2.4 | 3.8 | 3.5 | | | 19.4 | 6.7 | 3.2 | 6.5 | 1.7 | 1.6 | 8.4 | 10.5 | 2.2 | 2.0 |
| | | | | | | −1.8 [−4.0,−0.4] | | −1.6 [−3.1,−0.3] | | 0.3 [−1.7,2.3] | | | | 12.6 [9.2,16.2] | | −3.4 [−5.9,−1.0] | | 0.0 [−1.0,0.9] | | | | | |
| | | | | | 2 years | 5.0 | 6.6 | 1.1 | 3.5 | | | | | | | | | | | 12.3 | 9.0 | 2.2 | 2.0 |
| | | | | | | −1.5 [−4.9,1.8][d] | | −2.3 [−4.8,−0.4] | | | | | | | | | | | | | | | |

*HR* high risk; *IR* intermediate risk; *LR* low risk; *STS* society of thoracic surgeons; *PVL* Paravalvular leak; *NPMI* new permanent pacemaker implantation; *MG* mean gradient; *EOA* effective orifice area; *TAVI* transcatheter aortic valve implantation; *SAVR* surgical aortic valve replacement

#1 Results are provided with differences between TAVI and SAVR

#2 Results are provided with differences [TAVI-SAVR] and 95% Bayesian credible interval [BCI]

#3 Results are provided with hazard ratios and 95% confidence intervals [CI]

[a]All-cause death or disabling stroke

[b]All-cause death, stroke and myocardial infarction

[c]All-cause death, stroke and rehospitalization

[d]Posterior probability of noninferiority >0.999

and patients with pure aortic regurgitation (AR) although these challenging scenarios are still on the periphery of the evidence base for TAVI.

Despite these procedures' "maturity," TAVI still faces many challenges especially surrounding durability when implanted in low-risk patients. The potential impact of permanent pacemaker implantation (PMI), the potential long-term impact of mild peri-valvular leak, coronary access for treatment of future coronary artery disease (CAD), and bioprosthetic valve failure (BVF) with the need for a second valve (with subsequent issues such as coronary obstruction/access and residual gradient that may arise from patient/prosthesis mismatch [PPM]) are part of the clinical unmet aspects that need to be optimized.

## 11.2 Patient Selection

Indications for TAVI were initially limited to high to prohibitive surgical risk patients with symptomatic severe AS [11]. Following several iterative randomized clinical trials demonstrating superiority or non-inferiority of TAVI compared with surgical aortic valve replacement (SAVR), the most recent, 2020, ACC/AHA and 2021, ESC/EACTS, valvular heart disease guidelines recommended TAVI as alternative to SAVR in patients >65 and >75 years of age, respectively, who are candidates for bioprostheses across the entire spectrum of surgical risk as assessed by the heart team [12, 13]. As both replacement therapies have their own strengths and limitations, the decision making for TAVI versus SAVR should be made individually, considering patient's age, clinical and anatomical factors, and their preferences.

## 11.3 Clinical Criteria

### *11.3.1 Surgical Risk*

Surgical risk is usually assessed by risk scores such as STS-PROM (Society of thoracic surgeons predicted risk of mortality), EUROSCORE, and EUROSCORE II [14–16]. According to these scores, patients have been stratified into three categories: high (>8%), intermediate (4–8%), and low (<4%) surgical risk. These classifications have directed enrollment into TAVI trials although several limitations regarding accuracy or the exclusion of critical clinical factors such as frailty have been described [17, 18]. Recently, a new surgical risk stratification taking into account all these factors have been proposed (Table 11.2). Nevertheless, clinical judgment should always supersede surgical risk algorithms.

**Table 11.2** Risk assessment for surgical aortic valve procedures. (2020 AHA/ACC valvular heart disease guideline)

| Criteria | Low-risk SAVR (must meet ALL criteria in this column) | Low-risk surgical mitral valve repair for primary MR (must meet ALL criteria in this column) | High surgical risk (Any 1 criterion in this column) | Prohibitive surgical risk (Any 1 criterion in this column) |
|---|---|---|---|---|
| STS-predicted risk of death* | <3%<br>AND | <1%<br>AND | >8%<br>OR | Predicted risk of death or major morbidity (all-cause) >50% at 1y<br>OR |
| Frailty[a] | None<br>AND | None<br>AND | ≥2 indices (moderate to severe)<br>OR | ≥2 indices (moderate to severe)<br>OR |
| Cardiac or other major organ system compromise not to be improved postoperatively[b] | None<br>AND | None<br>AND | 1 to 2 Organ systems<br>OR | ≥3 Organ systems<br>OR |
| Procedure-specific impediment[c] | None | None | Possible procedure-specific impediment | Severe procedure-specific impediment |

[a]Seven frailty indices: Katz Activities of Daily Living (independence in feeding, bathing, dressing, transferring, toileting, and urinary continence) plus independence in ambulation (no walking aid or assistance required, or completion of a 5-m walk in <6 s). Other scoring can be applied to calculate no, mild, or moderate to severe frailty

[b]Examples of major organ system compromise include cardiac dysfunction; kidney dysfunction (chronic kidney disease, stage 3 or worse); pulmonary dysfunction (FAV1 < 50% or DLCO2 < 50% of predicted; central nervous system dysfunction (dementia, Alzheimer's disease, Parkinson's disease, cerebrovascular accident with persistent physical limitation); gastrointestinal dysfunction (Crohn's disease, ulcerative colitis, nutritional impairment, or serum albumin <3.0; cancer (active malignancy); and liver dysfunction (any history of cirrhosis, variceal bleeding, or elevated INR in the absence of VKA therapy)

[c]Examples of procedure-specific impediments include presence of tracheostomy, heavily calcified (porcelain) ascending aorta, chest malformation, arterial coronary graft adherent to posterior chest wall, and radiation damage

### *11.3.2 Age*

To date, the given patient's age remains one of the most important variable for decision-making [12]. Due to the lack of evidence in younger populations, mainly in terms of durability, the most recent ACC/AHA valvular heart disease guidelines [12] provide recommendation for TAVI in patients aged >65 years, whereas SAVR with either mechanical or bioprosthetic valves is still recommended for patients

<65 years. For patients who are >80 years of age or for younger patients with a life expectancy <10 years without anatomical contraindications, transfemoral TAVI is recommended in preference to SAVR. In patients who are aged 65 to 80 years, both TAVI and SAVR should be considered according to these guidelines, taking into account other clinical and anatomical factors, as well as patient preferences. Regarding 2021 ESC/EACTS guidelines [13], transfemoral TAVI is recommended as the preferred treatment for patients >75 years or those who are high-risk (STS-PROM/EuroSCORE II >8%) or unsuitable for surgery. SAVR is recommended in patients who are low-risk for surgery (<75 years and STS-PROM/EuroSCORE II <4%) or those with unsuitable transfemoral access. Non-transfemoral TAVI can be considered for inoperable patients.

### *11.3.3 Frailty*

Frailty, a state of increased vulnerability resulting from aging-associated decline in reserve and function across multiple physiologic system, is another important clinical factor that must be considered in the patient selection process [12]. Despite variations in the assessment, frailty has been consistently associated with increases in morbidity, mortality, and functional decline after TAVI or SAVR [19–24].

To date, there are several tools prescribed for assessing frailty [19–21, 23], although the Essential Frailty Toolset integrating lower-extremity weakness, cognitive impairment, anemia and hypoalbuminemia, outperformed the other scales and was recommended for use [22]. While the presence of frailty supports selection of TAVI in preference of SAVR, severely advanced frailty may suggest futility of the intervention and favor conservative management rather than TAVI [12].

Psoas muscle area (PMA) is a biological marker for sarcopenia and frailty, readily measurable from clinical multidetector computer tomography (MDCT) that is routinely ordered prior to a given planned TAVI procedure. A low PMA has been associated with increased mortalities after TAVI, particularly in females, and thus is used as a prognostic risk factor [25].

### *11.3.4 Coronary Artery Disease*

Coronary artery disease is a comorbidity frequently found in TAVI recipients. Its prevalence ranges between 15 and 80% depending on the clinical definition of CAD used by a given institution and the population studied [26]. Severe CAD has been associated with impaired mid- and long-term outcomes after TAVI [27]. Thus, prior screening for CAD using contrast-enhanced MDCT or invasive angiography [28] is the proposed strategy in the latest guidelines [12, 13]. However, the central question of whether PCI before TAVI is beneficial was recently addressed in a randomized trial [29]. Among patients whom underwent PCI before TAVI, the endpoint of

mortality and re-hospitalizations did not meet the non-inferiority margin compared with those patients with CAD treated medically. Moreover, patients treated with PCI had more bleeding events. However, this initial trial did not include myocardial infarction and/or urgent revascularization as a primary endpoint, thus outcomes could be more relevant in this group of patients than mortality. In the presence of complex left main and/or complex multiple vessel disease, SAVR with concomitant coronary artery bypass grafting (CABG) should be favored [30, 31]. Otherwise to date, in patients with one or two vessels disease, the best strategy remains unanswered. In the presence of significant angina, LV dysfunction as well as treating younger patients, proceeding with PCI might be reasonable.

### *11.3.5 Mixed Valve Disease*

The presence of other associated valve lesions is an important consideration in the treatment decision for TAVI and should be carefully evaluated before such an intervention [32]. Treatment of multivalvular disease is associated with an increased risk of adverse outcomes.

In the presence of associated severe mitral regurgitation (MR), among low to intermediate risk SAVR candidates, surgically mitral valve repair/replacement should be favored [12]. Conversely, those patients considered primarily TAVI recipients with associated severe secondary or repairable primary MR, a staged approach of TAVI plus transcatheter edge-to-edge mitral valve repair may be considered as the best option if symptoms and severe MR persist after treatment of the severe AS [12].

In patients with severe AS and severe mitral stenosis (MS) (mitral valve area $\leq$1.5 $cm^2$), SAVR and combined mitral valve surgery should be considered, unless the surgical risk is too high or prohibitive [12]. In the latter case, if the given patient's mitral valve morphology is suitable for percutaneous mitral balloon commissurotomy (PMBC), TAVI combined with PMBC may be a reasonable option. In cases with unfavorable mitral valve morphology for PMBC, decision-making is more challenging. Although transcatheter mitral valve replacement has recently evolved and may be an option, still today, the data are limited at this moment and may require transapical access [33–35].

There is currently no data or consensus recommendation in the management of tricuspid regurgitation (TR) for TAVI patients. Interestingly, clinically relevant TR has been shown to improve to 15–60% after TAVI [32]. Today, as both prospective and retrospective studies in high or prohibitive surgical risk provide promising results of transcatheter devices for the treatment of secondary TR [36, 37], transcatheter tricuspid valve intervention (particularly transcatheter tricuspid edge-to-edge repair) after TAVI may be a reasonable option if symptoms and severe TR persist after treatment of the severe AS.

## 11.4 Anatomical Criteria

### *11.4.1 Valve Anatomy*

In order for TAVI procedure to be successful, it is critical that pre-procedural imaging-based screening of the aortic valve complex and peripheral arterial vasculature be performed. The following measurements should be measured before implantation: (1) diameter/perimeter/area of the annulus, (2) diameter/perimeter of the left ventricular outflow tract (LVOT), (3) the height and width (intercommissural distance) of the sinus of Valsalva (SOV), (4) the height of takeoff of the coronary artery ostia, (5) diameter and height of the sinotubular junction, and (6) diameter of the ascending aorta (Fig. 11.1). This is commonly achieved using a multi-modality imaging approach: i.e., a combination of transthoracic and transesophageal echocardiography (TTE, TEE), MDCT, and fluoroscopy/angiography [38]. This extensive screening aids one to determine the feasibility of the given procedure, THV size, as well as the most appropriate access route. The preferred and most widely utilized modality for this purpose is MDCT [39] due to its 3D nature and high spatial resolution. Additionally, MDCT allows for multiplanar reconstructions of the original images, which can provide reformatted coronal, sagittal, and axial images of the aortic root/vascular access [40]. Depending on the orientation, 2D echocardiography appreciates only one view of the aortic annulus and usually underestimates the annulus diameter with respect to MDCT. However,

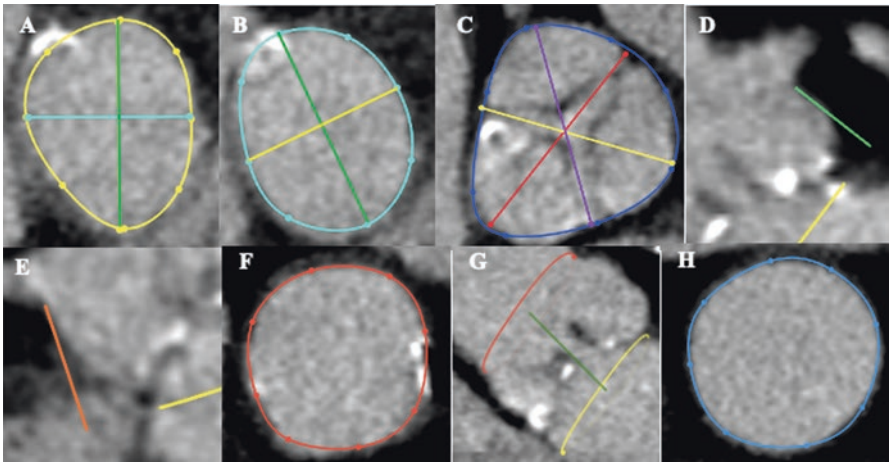


**Fig. 11.1** MDCT TAVI protocol. (**a**) Aortic annulus perimeter, minor and major diameter, area. (**b**) LVOT perimeter, minor and major diameter, area. (**c**) SOV perimeter, intercommissural distance. (**d**) LM height. (**e**) RCA height. (**f**) STJ perimeter. (**g**) STJ height. (**h**) Ascending aorta perimeter. MDCT Multidetector computer tomography; TAVI transcatheter aortic valve implantation; LVOT left ventricular outflow tract; SOV sinus of Valsalva; LM left main; RCA right coronary artery; STJ sinutubular junction

a good measurement correlation by 3D-echocardiography has been described [41]. Thus, this imaging modality may benefit certain group of patients such as those with chronic kidney disease.

### *11.4.2 Assessment of the Aortic Valve Complex*

Assessment of the aortic valve complex remains as one of the most important aspects in order to determine the feasibility and the risk of performing a TAVI procedure.

The aortic valve annulus corresponds to a virtual plane defined by the basal attachment points of the three leaflets [42] (Fig. 11.2) and typically represents the tightest part of the aortic root. The aortic annular size during systole is used as a standard measurement for quantitative assessment of the site of implantation. Furthermore, the relation of the annulus dimensions with the LVOT and SOV dimensions (both in anatomical continuity) usually is the first step in the selection of prosthesis size. The correct measurement of the aortic valve annulus is essential to avoid undersizing or oversizing of the THV. Specifically, undersizing of the annulus, could lead to the selection and deployment of a smaller THV, resulting in increased risk of PVL and/or THV embolization [43]. In contrast, oversizing can lead to underestimation of the prosthesis, with possible reduced valve durabilities, conduction disturbances, coronary obstructions, and/or annular ruptures [44].

A severely calcified aortic valve complex is an important anatomical feature that requires particular attention related to PVL and aortic root injury after TAVI [45]. In particular, LVOT calcification has been singled out as the most important hostile anatomy for TAVI. In a retrospective analysis of a prospective TAVI registry including 1635 patients, moderate or severe LVOT calcification conferred an increased risk of annular rupture when treated with balloon-expandable valves (BEV) and a higher incidence of PVL irrespective of valve type or generation [46]. When LVOT calcification is recognized on pre-procedural MDCT, its volume, extension and distribution, as well as shape should be carefully evaluated. If the relevant risk for adverse events related to TAVI is deemed high, SAVR may be preferred if the surgical risk is acceptable.

Conversely, non-calcified aortic valves have been considered also as risk factors for valve dislocation or embolization after TAVI, due to lack of calcification anchoring the prosthesis [47]. Although it should be noted that observational studies suggest that both BEV and self-expanding (SEV) can be safely implanted in patients with non-calcified aortic valves [48, 49].

The evaluation of the aortic valve at the leaflets level allows for the assessment of the number of leaflets, the amount of calcium, and its distribution. Of note, a symmetrical calcium distribution along the leaflets predicts better anchoring of the valve. The presence of a BAV defines a different clinical scenario that will be discussed separately.

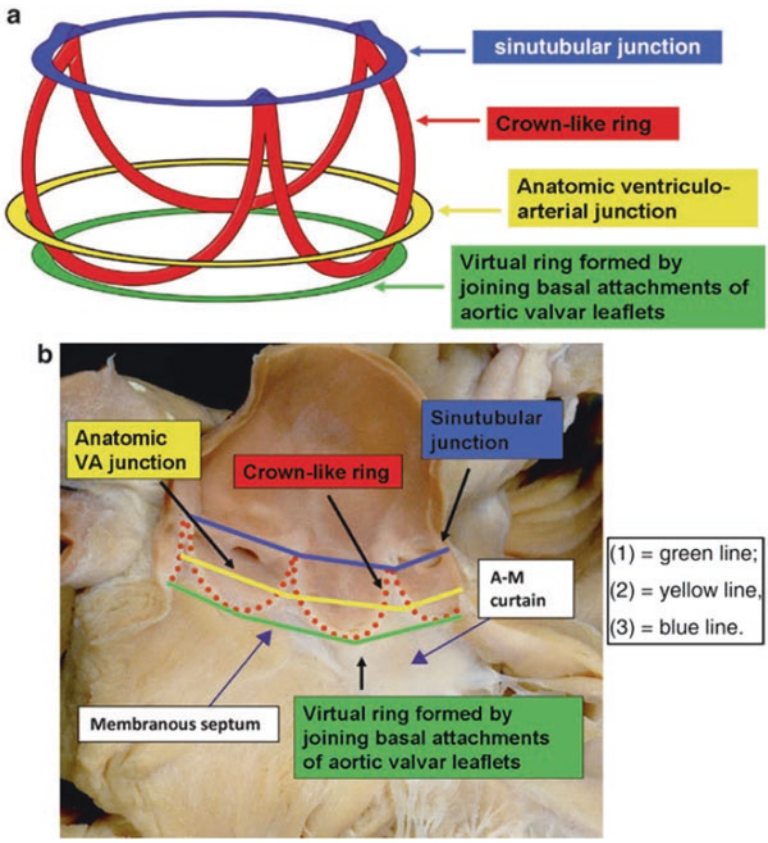


**Fig. 11.2** *Aortic root.* The aortic root extends from the basal attachment point of the aortic valve leaflets (aortic annular plane) to their superior attachment points at the level of the sinotubular junction. There are three circular rings within the aortic root: (1) a virtual ring (i.e., without histological demarcation) formed by joining the basal attachments of the aortic valvar leaflets; (2) a ring at the anatomic ventriculo-arterial junction identified histologically as the transformation zone between aortic wall tissue and ventricular myocardium; and (3) a ring at the sinotubular junction found at the apical attachment points of the aortic valvar leaflets. The crown-like ring is formed by the curtain-like attachment line of the aortic valvar leaflets. For purposes of transcatheter aortic valve sizing, it is the diameter of the virtual basal ring that is taken into consideration

Knowledge of the location of the coronary arteries is essential for appropriate TAVI. THVs are designed such that a skirt of fabric or tissue is sewn within the stent or frames to help to create a seal and prevent PVL. In situations in which the coronary arteries take their origin low within the SOV and/or the prosthesis is placed too high, the skirt may obstruct their orifices, and thus ultimately impede coronary arterial flow. Furthermore, when the TAVI is deployed, it crushes the leaflets of the native valve against the aortic wall. The combination of a relatively low-lying coronary artery ostia and a large native aortic valvar leaflet, therefore, can obstruct the flow into the coronary ostia during valvar deployment [50] and/or result in difficulty

of coronary reaccess. Thus, measuring the height of the coronary ostia takeoff is crucial to assess the risk of coronary obstruction and the feasibility of coronary access post THV implantation [51, 52]. Furthermore, the width of the SOV also needs to meet minimum requirement if the THV is to be properly accommodated without impinging on the orifices of the coronary arteries. Device sizing for a given patient should be discussed based on the manufacturer's recommendations and MDCT-derived SOV size.

Precise coaxial alignment of the stent valve along the centerline of the aortic valve and aortic root (root angulation) is important during THV positioning. Inappropriate alignment of the implanted device is associated with increased risk of procedural complications such as valve embolization and/or conduction disturbances [53, 54]. During a given procedure, defining an optimal projection view, meaning the one which allows the perpendicular visualization of both the THV and the prosthetic delivery catheter, is of upmost importance in order both to define the optimal implantation depth and reduce the risks of the aforementioned complications. BEV are commonly centered and deployed in the so-called coplanar view, with the right coronary cusp projected between the non and left coronaries cusps [55]. Self-expandable valves are deployed in "cusp-overlap" view [56] or with "double S-curve" [57] approach typically displaying the left and right coronaries cusp overlapped, while the non-coronary cusp is isolated inferiorly and to the left of the screen. Both techniques eliminate or reduce the aortic annulus and delivery system parallax, while depicting maximal elongation of the aortic root, LVOT, as well as the delivery catheter providing a realistic perception of THV implant depth. The utilization of these techniques has shown to reduce the rate of both LBBB and PPI compared with the classical implantation technique [58, 59].

### *11.4.3 Vascular Access (Transfemoral and Alternative Access Sites)*

Vascular access must be carefully evaluated on pre-procedural MDCT (Fig. 11.3). Currently available THV sheaths and delivery systems have minimal luminal diameters depending on the platform ranging as low as 14Fr requiring a minimal vessel diameter of 5.5 mm. An area-derived vessel dimensions measurement may and in many cases should be performed for determining the feasibility of a specific access route. A minimal vessel area of 20, 25, and 30 $mm^2$ is required for a 14, 16, and 18Fr introducer sheath, respectively. In non-calcified vessels, a 5–15% oversize may be achieved while in the presence of calcium device oversizing should not exceed 5%.

In general, transfemoral access is considered the least invasive and the default strategy when performing TAVI [12]. However, it has been reported that 10–15% of TAVI candidates do not have favorable iliofemoral anatomies (small vessel calibers, calcifications, tortuosity, or a combinations of these factors) for safe transfemoral access [60]. In this group of patients, several alternatives access routes have been

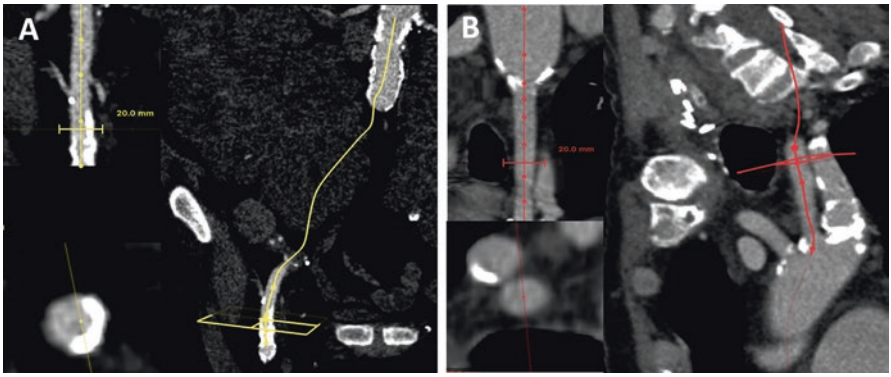


**Fig. 11.3** Vascular access assessment. MDCT can provide the ability of multiplanar reconstruction and therefore can provide information about minimum vessel diameter, area, tortuosity, and degree of calcification. (**a**) Multiplanar reconstruction of the right common iliac/external iliac and common femoral arteries. (**b**) Multiplanar reconstruction of the left internal carotid artery as alternative access

used [61]. For such, transthoracic (transapical and transaortic) constitute the alternative approaches for TAVI that are best documented with respect to evidence. Transapical access is performed via left anterolateral intercostal incision followed by needle puncture of the apex through a pledged purse-string suture. A dedicated sheath is placed and the THV deployed in a similar fashion to the transfemoral approach thereafter. Of note, this procedure is still a type of thoracotomy and is associated with delayed recovery due to its invasiveness. In the PARTNER IA trial, the risk of all-cause mortality at 5 years was 79% in the transapical TAVI group versus 60% in the SAVR group ($p = 0.067$) [62]. More recently, in the PARTNER II trial, transthoracic TAVI (including both transapical and transaortic) was associated with a higher rate of death or disabling stroke at 5 years compared with SAVR [63].

Transaortic access is performed through the ascending aorta via a right anterior mini-thoracotomy in the second intercostal space. The aorta is inspected to avoid areas of calcification. Using a purse-string suture, needle puncture and access with a dedicated sheath is obtained. The puncture is made with a minimum of 6 cm above the aortic annulus for the CoreValve platform and 8 cm for the SAPIEN platform. The valve is then deployed in the same way as via the transfemoral approach.

Alternative transarterial approaches (including transaxillary, transubclavian, and transcarotid) have demonstrated high technical success rates and favorable safety profiles in selected patients and are particularly valuable in the presence of poor respiratory function or previous cardiothoracic surgery, i.e., compared to the transthoracic approaches. Trans-subclavian access is typically performed via surgical cut-down, while transaxillary may be performed percutaneously with pre-closure sutures most frequently into the proximal third of the axillary artery. There is no dedicated sheath available. A left-sided approach is selected in >95% of cases as a more favorable alignment of the THV when the native valve is commonly achieved. In a recent retrospective analysis of the STS/ACC TVT registry, trans-subclavian/

axillary approaches were used in 1249 (34,4%) of the 3628 patients undergoing alternative access. After propensity matching, trans-subclavian/axillary approaches were shown to elicit a lower 30-days mortality (5.3% vs. 8.4% $p = <0.001$), shorter lengths of intensive care unit and hospital stays, but higher stroke rates (6.3% vs. 3.1%, $p = <0.05$) compared with transthoracic approach [64].

Transcarotid access is commonly performed percutaneously or via surgical cut-down under local or general anesthesia; while employing cerebral oximetry monitoring. Left internal carotid is typically the preferred access. In a propensity-matched study of the national French TAVI registry (FRANCE TAVI) access, non-femoral peripheral TAVI, including transcarotid ($n = 914$) and trans-subclavian ($n = 702$) accesses, were associated with similar outcomes compared with transfemoral TAVI ($n = 19{,}995$), except for a two-fold lower rate of major vascular complications (OR 0.41, 95% CI 0.29 to 0.59, $p < 0.001$). Note, the authors concluded that non-femoral peripheral TAVI may be favored over SAVR in patients who are deemed ineligible for transfemoral TAVI [65].

In a given patient, if there is lack of alternatives access sites, transcaval access constitutes an innovative approach performed completely percutaneously and allowing the introduction of a large-bore sheath despite the presence of severe peripheral artery disease. To do so, at the level of the inferior vena cava, an arteriovenous fistula is created by the application of electrocautery over a coronary wire. The TAVI is then carried out in a standard fashion, and the fistula is closed with a nitinol occluder device. Today, there remains limited outcome data, but with major vascular complications ranging between 11% and 28% and major life-threatening bleeding rated between 13% and 28%, a significant learning curve must be considered as well as operator experience [66].

Due to the unavailability of comparative data, the choice of alternative access should be made by the given institution's Heart Team, on a case-by-case basis, determined by patient's anatomic features and comorbidities as well as local experience.

## 11.5 TAVI Procedure

### *11.5.1 Pre-procedural Planning*

Pre-procedural planning is of critical importance when considering TAVI for a given patient. Thus, the multidisciplinary heart team plays a pivotal role in integrating the clinical factors and anatomical factors obtained by MDCT, echocardiography, and cardiac catheterization to determine the best procedural strategy. As there are multiple device options in this field (Table 11.3 and Fig. 11.4), the Heart team needs to be familiar with the strengths and limitations of each device that is available [67]. Device sizing should be discussed based on the manufacturers' sizing

**Table 11.3** Main characteristics of newer generation devices and prostheses

| Company | Deployment mechanism | Valve | Access | Position of the valve | Valve size | Annular range | Delivery system diameter Retrograde TA | | Valve leaflets | Reference vessel diameter | Frame | Sealing skirt | Advantages |
|---|---|---|---|---|---|---|---|---|---|---|---|---|---|
| MEDTRONIC | Self-expandable | EVOLUT R | Retrograde | Supra-annular | 23–26–29–34 mm | 18–30 mm | 14F (23–26–29 mm)<br>16F (34 mm) | | Porcine | >5 mm (23,26,29 mm)<br>>5,5 mm (34 mm) | Nitinol | Pericardial skirt | Low profile system (for 23–26 and 29)<br>Repositionable<br>Retrievable<br>Large range sizes<br>Anticalcification leaflet technology |
| | | EVOLUT PRO | Retrograde | Supra-annular | 23–26–29 | 18–26 mm | 16F | | Porcine | >5,5 mm (23,26,29 mm) | Nitinol | Pericardial skirt and external pericardial wrap | Retrievable<br>Repositionable<br>Additional skirt to minimize PVL<br>Anticalcification leaflet technology |
| | | EVOLUT PRO+ | Retrograde | Supra-annular | 23–26–29–34 mm | 18–30 mm | 14F (23–26–29 mm)<br>18F (34 mm) | | Porcine | >5 mm (23,26,29 mm)<br>>6 mm (34 mm) | Nitinol | Pericardial skirt and external pericardial wrap | In addition to Evolut PRO advantages:<br>Reduced capsule diameter for 23–36–39 mm valves<br>Pericardial wrap on the 34 mm valve |

(continued)

**Table 11.3** (continued)

| Company | Deployment mechanism | Valve | Access | Position of the valve | Valve size | Annular range | Delivery system diameter Retrograde TA | | Valve leaflets | Reference vessel diameter | Frame | Sealing skirt | Advantages |
|---|---|---|---|---|---|---|---|---|---|---|---|---|---|
| | | EVOLUT FX | Retrograde | Supra-annular | 23–26–29–34 mm | 18–30 mm | 14F (23–26–29 mm) 18F (34 mm) | | Porcine | >5 mm (23,26,29 mm) >6 mm (34 mm) | Nitinol | Pericardial skirt and external pericardial wrap | In addition to Evolut PRO+ advantages: enhanced visualization Smoother catheter tip More flexible delivery catheter, 360-degree motion, enhanced trackability Simplified coronary access |
| EDWARDS | Ballon expandable | SAPIEN 3 | Transapical Retrograde | Intra-annular | 20–23–26–29 mm | 16–28 mm | Sheath 14F (20–23–26 mm) 16F (29 mm) Axella 14F | 18–21 F | Bovine | >5,5 mm (20,23,26 mm) >6 mm (29 mm) | Cobalt chromium | Inner and outer fabric skirt | Low profile system Positioning marker for precise deployment Taller skirt to minimize PVL |
| | | SAPIEN ULTRA | Retrograde | Intra-annular | 20–23–26 mm | | Axella 14F | | Bovine | >5,5 mm | Cobalt chromium | PET skirt | Low profile system Taller (40%) skirt than SAPIEN3 On balloon delivery system-easy to use Pusher eliminated Short, tapered distal tip with a smooth tip to valve transition |

| | | | | | | | | | | | | | |
|---|---|---|---|---|---|---|---|---|---|---|---|---|---|
| BOSTON SCIENTIFIC | Self-expandable | ACURATE NEO | Transapical Retrograde | Supra-annular | 23–25–27 mm | 21–27 mm | Regular sheath 18F<br>iSleeve 14F | 22F | Porcine | >5,5 mm (with iSleeve) | Nitinol | Outer and Inner porcine pericardium skirt | Two steps, top-down deployment provide a stable positioning and predictable valve release<br>Biofix anticalcification process |
| | | ACURATE NEO2 | Retrograde | Supra-annular | 23–25–27 mm | 21–27 mm | iSleeve 14F | | Porcine | >5,5 mm | Nitinol | Outer and Inner porcine pericardium | Radiopaque marker<br>Taller (60%) outer skirt than Neo |
| ABBOTT | Self-expandable | PORTICO | Transapical Retrograde | Intra-annular | 23–25–27–29 mm | 19–27 mm | Regular sheath 18F<br>FlexNav system 14F (23–25)-15F (27–29 mm) | | Bovine | >5 mm (23,25)<br>>5,5 mm (27,29) | Nitinol | Pericardial sealing cuff | Repositionable and retrievable<br>Linx anticalcification technology |
| | Self-expandable | NAVITOR | Retrograde | Intra-annular | 23–25–27–29 mm | 19–27 mm | FlexNav system 14F (23–25) 15F (27–29 mm) | | Bovine | >5 mm | Nitinol | Inner and outer skirt | Recapturable, repositionable and retrievable<br>Active outer cuff (NaviSeal Cuff) |

(continued)

**Table 11.3** (continued)

| Company | Deployment mechanism | Valve | Access | Position of the valve | Valve size | Annular range | Delivery system diameter Retrograde TA | | Valve leaflets | Reference vessel diameter | Frame | Sealing skirt | Advantages |
|---|---|---|---|---|---|---|---|---|---|---|---|---|---|
| JENAVALVE TECHNOLOGY | Self-expandable | JENAVALVE PERICARDIAL TAVI SYSTEM | Transapical Retrograde | Intra-annular | 23–25–27 mm | 21–27 mm | 18F | 22F | Porcine | | Nitinol | | Repositionable Clipping mechanism for valve fixation Suitable for non-calcific valve and aortic regurgitation |
| JIECHENG MEDICAL | Self-expandable | J-VALVE | Transapical | Intra-annular | 21–23–25–27 mm | 10–27 mm | 18F | | Porcine | | Nitinol | | U-shape anatomically oriented anchor rings encircling the stent. Suitable for aortic regurgitation Partially retrievable and repositionable |
| MICROPORT MEDICAL | Self-expandable | VITAFLOW | Retrograde | Intra-annular | 21–24–27–30 mm | 19–29 mm | 16F (21–14)18F (27–30 mm) | | Bovine | | Nitinol | Inner and outer skirts | Monitorized handle Increased radial force for bicuspid valve |

| | | | | | | | | | | | | | |
|---|---|---|---|---|---|---|---|---|---|---|---|---|---|
| | Self-expandable | VITAFLOW Second Generation | Retrograde | Intra-annular | 21–24–27–30 mm | | 16F (21 mm) 18F (24–27–30 mm) | | Bovine | | Nitinol | Inner and outer skirts | Monitorized handle<br>Increased radial force for bicuspid valve<br>Repositionable and retrievable<br>Radiopaque marker<br>Anticalcification leaflet technology |
| VENUS MEDTECH | Self-expandable | VENUS A-VALVE | Retrograde | Supra-annular | 23–26–29–32 mm | | 19F 15F Sheathless | | Porcine | | Nitinol | | Higher radial force, ideal for bicuspid valve<br>Positioning marker |
| | | VENUS A- PLUS | Retrograde | Supra-annular | 23–26–29–32 mm | | 19F 15F Sheathless | | Porcine | | Nitinol | | Higher radial force, ideal for bicuspid valve<br>Positioning marker<br>Repositionable |
| | | VENIBRI | Retrograde | Supra-annular | 26–29–32 mm | | 18F | | Porcine | | Nitinol | | Higher radial force, ideal for bicuspid valve<br>Positioning marker<br>Dry tissue technology |

(continued)

**Table 11.3** (continued)

| Company | Deployment mechanism | Valve | Access | Position of the valve | Valve size | Annular range | Delivery system diameter Retrograde TA | | Valve leaflets | Reference vessel diameter | Frame | Sealing skirt | Advantages |
|---|---|---|---|---|---|---|---|---|---|---|---|---|---|
| MERIL LIFE SCIENCES | Balloon-expandable | MYVAL | Retrograde | Intra-annular | Conventional (20–23–26–29) Medium (21,5–24,5–27,5) Extra-large (30,5–32 mm) | 16–31 mm | Phyton 14F | | Bovine | >5,5 (20–21,5–23–24,5) >6 (26–27,5–29) >6,5 (30,5–32 mm) | Nickel-cobalt | Inner and outer PET skirts | Medium sizes limit the extent of annulus overexpansion Wider range of sizes On balloon delivery system |
| BIOTRONIC | Self-expandable | BIOVALVE | Retrograde | Supra-annular | 26–29 mm | 20–26 mm | 18F | | Porcine | | Nitinol | Porcine pericardial skirt | Repositionable Retrievable Early function during deployment |
| NEW VALVE TECHNOLOGY | Self-expandable | ALLEGRA | Retrograde | Supra-annular | 23–27–31 mm | 19–18 mm | 18F | | Bovine | >6 mm | Nitinol | Bovine pericardial skirt | Repositionable Retrievable Positioning marker Early function during deployment |
| VASCULAR INNOVATIONS | Self-expandable | HYDRA | Retrograde | Supra-annular | 22–26–30 mm | 18–28 mm | 18F | | Bovine | | Nitinol | Bovine pericardial skirt | Recapturable Repositionable Retrievable |

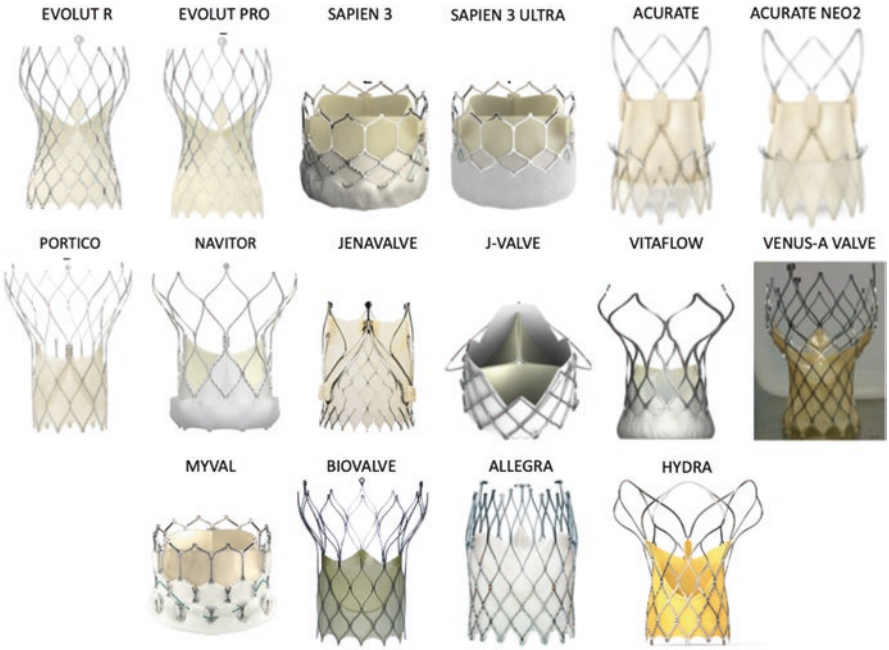


**Fig. 11.4** Overview of the transcatheter heart valve systems

recommendations and MDCT-derived annulus and vascular access size (Table 11.4). In case of borderline annulus size, a poor sizing decision may result in oversizing or undersizing depending on the degree of calcification and the size of the SOV, ascending aorta and the LVOT [68]. While transfemoral access is the default strategy, alternative access may be considered in patients with unfavorable femoral access (see above).

### *11.5.2 Transfemoral TAVI: Procedural Steps*

The generic steps involved in performing TAVI are outlined below:

1. *Anesthesia*: The TAVI procedure can be done under general anesthesia or local anesthesia with or without conscious sedation.
2. *Antithrombotic therapy*: Activated clotting times between 250 and 300 seconds should be achieved and maintained through heparin administration. Typically, pre-procedural loading with low-dose aspirin is also recommended.
3. *Antibiotic prophylaxis*: Performed according to the hospital protocol.
4. *Temporary pacemaker implantation*: A temporary pacemaker is placed via internal jugular into the right ventricular apex. Pacemaker function is assessed under rapid pacing at 160–180 beats/min such that systemic arterial pressure is

**Table 11.4** Transcatheter heart valves sizing chart

| | EVOLUT R/PRO/PRO+ | | | | SAPIEN 3/ULTRA | | | | PORTICO/NAVITOR | | | | ACURATE NEO/NEO2 | | |
|---|---|---|---|---|---|---|---|---|---|---|---|---|---|---|---|
| THV size | 23 | 26 | 29 | 34 | 20 | 23 | 26 | 29 | 23 | 25 | 27 | 29 | S | M | L |
| Annulus diameter (mm) | 18–20 | 20–23 | 23–26 | 26–30 | 18.5–20.8 | 20.8–23.4 | 23.4–26.5 | 26.2–29.4 | 19–21 | 21–23 | 23–25 | 25–27 | 21–23 | 23–25 | 25–27 |
| Annulus perimeter (mm) | 56.5–62.8 | 62.8–72.3 | 72.3–81.7 | 81.7–94.2 | 58.2–65.3 | 65.3–73.5 | 73.5–83.1 | 82.4–92.4 | 60–66 | 66–73 | 72–79 | 79–85 | 66–72 | 72–79 | 79–85 |
| Annulus area ($mm^2$) | | | | | 273–345 | 338–430 | 430–546 | 540–683 | 277–346 | 336–415 | 405–491 | 479–573 | | | |
| Area derived diameter (mm) | | | | | 18.6–21 | 20.7–23.4 | 23.4–26.4 | 26.2–29.5 | | | | | | | |
| SOV diameter (mm) | ≥25 | ≥27 | ≥29 | ≥31 | | | | | ≥27 | ≥27 | ≥29 | ≥31 | | | |
| SOV height (mm) | ≥15 | ≥15 | ≥15 | ≥16 | | | | | ≥15 | ≥15 | ≥15 | ≥15 | | | |

*THV* Transcatheter heart valve; *SOV* Sinus of Valsalva; *S* small; *M* medium; *L* large

reduced below 60 mmHg. Alternatively, in patients with low risk of complete heart block, LV pacing approach where the LV wire is used for temporary pacing is a suitable option that in turn eliminates the need for a separate puncture and theoretically reducing the associated risk of pericardial effusion and/or vascular complications while maintaining similar efficacy [69].

5. *Femoral main access* (for delivery of a THV) and contra-lateral femoral or radial access (for aortic root angiography to guide implantation) are typically obtained. Ultrasound-guided needle puncture is recommended to ensure the puncture site is in the common femoral segment over the femoral head avoiding the femoral bifurcation and in a segment free of significant calcification, thus reducing vascular complications [70]. The main access site is pre-closed typically by using one or two suture-based vascular closure devices (ProGlide, Abbott, Abbott Park, Illinois). Alternatively, one 10 Fr Prostar XL percutaneous vascular surgical system (Abbott) or a plug-based vascular closure device (MANTA, Teleflex, Wayne, Pennsylvania) may also be utilized.
6. *Vascular introducer sheath*: A stiff guidewire (i.e., Amplatz Extra Stiff or Super Stiff) should be used for introduction and advancement of the large bore (14–18 Fr) vascular introducer sheath under fluoroscopic guidance. Any resistance encountered while advancing the sheath should be carefully evaluated during the procedure, in order to avoid vascular complications.
7. *Supra-aortic angiogram*: A pigtail catheter is placed in the non-coronary sinus of the aortic root to perform a supra-aortic angiogram. C-arm angulation (derived from MDCT analysis) is set such that the nadir of all three leaflets is coplanar; perpendicular to the viewing angle. BEVs are typically deployed in 3-cusp coplanar angle. For SEV, the cusp-overlap view [56] is the mostly adopted projection.
8. *Crossing the aortic valve*: Using an Amplatz left (AL1) (AL2 in patients with enlarged aortic root, AL2, or Judkins right in patients with vertical annulus [horizontal aorta]) catheter and a standard straight-tipped wire (hydrophilic or metallic), the aortic valve is crossed. Once the wire is viewed to be across the valve, the catheter is carefully advanced into the LV apex. Careful attention should be paid to avoid entrapment of the catheter or wire in the sub-valvular mitral valve apparatus, which is typically facilitated by using a RAO/CAU fluoroscopic projection. The catheter is then connected to manometry and peak left ventricular, aortic systolic, and diastolic pressures measured. Attention should also be focused on the end-diastolic separation distance between the LV and the aorta for assessment of PVL after implantation. Subsequently, a pre-shaped long Amplatz Extra-stiff APEX wire (Cook Medical, Indiana, USA), CONFIDA™ Brecker wire (Medtronic, Minneapolis, Minnesota) or Lunderquist® (Cook Medical, Bloomington, IN) is advanced into the LV. Safari²™ pre-shaped Guidewire (Boston Scientific, Marlborough, MA, USA) is another option available in three different sizes (extra small, small, and large).
9. *THV is checked* for appropriate crimping and loading onto the delivery catheter as well as correct orientation.

10. *Pre-dilation*: In cases of severely calcified aortic valve, extensive commissural fusion, pre-dilation should be considered under rapid pacing to facilitate the THV delivery and expansion. Pre-dilation is mandatory when implanting some SEV THV like Acurate Neo2. Note, the size of the balloon should not exceed the minimum aortic annulus/LVOT diameter obtained from MDCT.
11. *The THV is advanced* over the extra-stiff wire either through the introducer sheath or sheath-less. Specific orientations of delivery systems have been described in order to achieve commissural alignment. The delivery system should be inserted into the patient's femoral artery according to the specific THV type (flush port at 3 o'clock for EVOLUT [71], safety knob at 6 o'clock for Acurate Neo2 [72], and 12 o'clock for Portico THV [73]).
12. Under fluoroscopic guidance, the THV is delivered over the stiff wire with careful attention to the wire position in the LV apex. The system is carefully advanced across the aortic arch avoiding direct interaction with aortic wall by appropriate deflection and/or rotation of the assembly.
13. Once the THV system has been positioned at the aortic valve level, the 3-cusp coplanar view is typically sets. For SEV, the cusp-overlap view or the double S-curve approach can be utilized for eliminating/reducing THV parallax as described previously. Final depth adjustment is performed with a pigtail catheter placed in the non-coronary cusp for reference.
14. *Prosthesis Deployment*:

**EVOLUT R/PRO/PRO+ (Medtronic, Minneapolis, Minnesota) (Fig. 11.5a)**
The valve delivery system is brought into the appropriate implanting position with a target implant depth of 3–5 mm. The first one-third of the THV is deployed by very slow counterclockwise rotation of the actuator, in short increments in the direction of the marked arrows. The valve position is monitored under fluoroscopy throughout deployment, and the position adjusted as necessary until annular contact is achieved. The capsule has a flare feature that enables the valve to self-center as it deploys. A controlled pacing (90–130 bpm) is considered during deployment to increase valve stability. Periodic aortic root injections guide adequate positioning during deployment. If the operator is satisfied with the valve position at annular contact, valve is continually deployed until just before the "point of no recapture." The operator must be cognizant of quick deployment once blood pressure drops, as

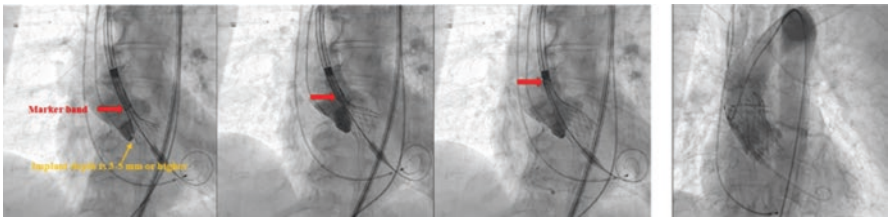


**Fig. 11.5** (**a**) EVOLUT R/PRO/PRO+ THV deployment. (**b**) Sapien 3/Ultra THV deployment. (**c**) Portico/Navitor THV deployment. (**d**) ACURATE Neo/Neo2 THV deployment

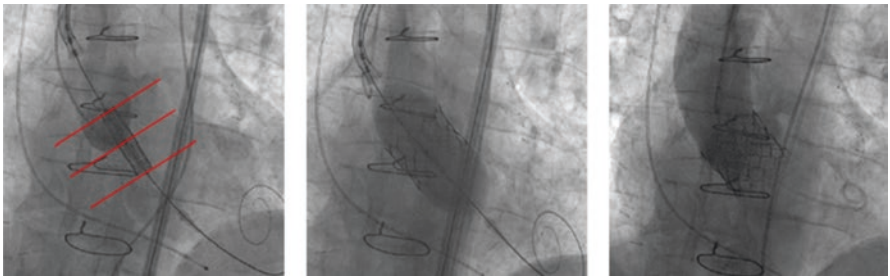

**Fig. 11.5** (continued)

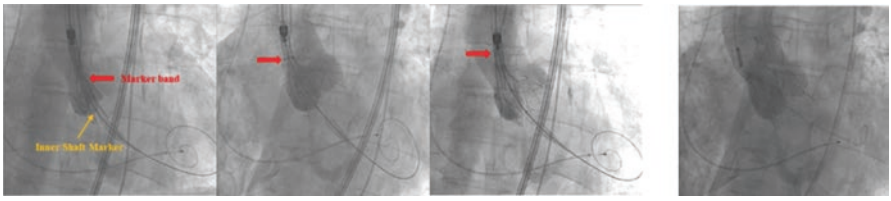


**Fig. 11.5** (continued)

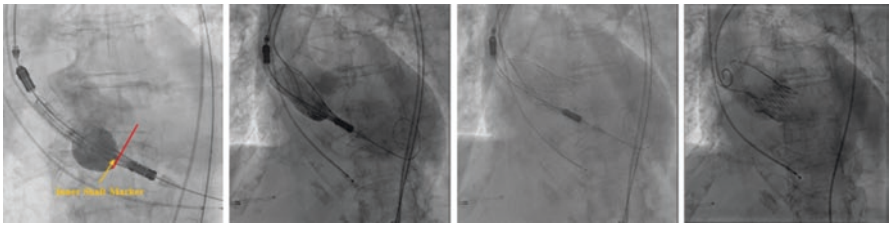

**Fig. 11.5** (continued)

cardiac output is temporarily eliminated as the aortic valve structure is temporarily occluded by the deploying valve. There is a tactile indicator ("rumble strip") that provides feedback to indicate that the capsule is nearing the "point of no recapture." The operator must continue to turn the deployment knob until blood pressure recovers, making sure not to advance past the "point of no recapture." Once blood pressure has recovered, approaching 80% deployment, the implantation depth is once again checked by angiography. Subsequently, tension in the system is released just before full deployment to reduce potential for valve movement by retracting the guidewire, slight forward pushing on the delivery system, and turning the deployment knob very slowly to detach the paddles one at a time. The detachment of frame paddles must be confirmed under fluoroscopy, and the nose cone centered before the delivery system is withdrawn.

**Sapien 3/Ultra (Edwards Lifesciences, Irvine, California) (Fig. 11.5b)**
The current commander delivery system is advanced through the sheath until the prosthesis exits the sheath. Valve alignment is then performed in the descending aorta. Disengage the balloon lock and retract the tip of the Flex Catheter to the center of the triple marker and engage the balloon lock again. The fine adjustment wheel allows for an optimized valve alignment over the balloon. Utilize the Flex wheel to advance the valve all the way up to the aortic valve. After crossing the aortic valve, ensure that the THV is accurately positioned between the alignment markers and the Flex Catheter tip is over the triple marker. Rapid pacing is initiated to reduce the systolic aortic pressure <50 mmHg and the balloon is inflated to deploy the valve. After 4–5 sec, the balloon is deflated and rapid pacing terminated. Finally, the delivery system is dearticulated and retracted back across the aortic arch. Conventionally, the implantation depth is aimed in a ratio of valve frame in the aorta to LVOT of 70:30 or 80:20. Recently, a high deployment technique has been proposed to achieve even higher implantation of the THV, translated in lower rates of PPM implantation, with no differences in PVL [74]. The valve is deployed in the right anterior oblique/caudal fluoroscopy view, removing the parallax after advancing the crimped valve across the aortic valve. The THV is positioned by alignment of the radiolucent line that is located at the superior aspect of the lowest set of stent structs of the valve at the base of the non-coronary cusp.

**Portico/Navitor (Abbott, Abbott Park, Illinois) (Fig. 11.5c)**
Once the THV is advanced across the aortic valve, position the delivery system so that the inner shaft marker band is aligned with the annular plane. Deployment is then initiated by clockwise rotation of the deployment wheel, typically under controlled (90 to 120 bpm) pacing. There is a clicking sound when the delivery system has reached the partial deployment lock. The deployment mechanism will not re-engage until the deployment lock button is depressed. At this point, the imaging projection should be adjusted to remove the parallax in valve inflow and then confirm the valve positioning using aortic root angiography. The ideal depth of implantation is represented by the frame's inflow edge placed 3–4 mm below the aortic annulus. If the appropriate positioning is confirmed, complete valve deployment by pressing the deployment lock button, then turning the deployment wheel in the direction of the arrow on the handle until the valve capsule is fully retracted. The detachment of retainer tabs must be confirmed under fluoroscopy before the system is withdrawn.

**ACURATE Neo 2 (Boston Scientific, Marlborough, Massachusetts) (Fig. 11.5d)**
Due to the lower radial forces of this stent frame, balloon pre-dilation is mandatory to facilitate device expansion. Once the THV has passed the aortic valve, ensure that it is correctly positioned as indicated by the marker band being in the annular plane. It is of utmost importance that the final movement for positioning is in a forward motion (when the final motion of the delivery system is in the aortic direction, upon full release the stent holder will move in an aortic direction and may not disengage from the prosthesis). Deployment can be performed in a two-step manner. The first

step can be initiated by turning the first rotating knob of the release handle counter-clockwise until full stop. This step should be done slowly in order to recognize any inappropriate movement of the device. After the first step, the stabilization arms are fully deployed and the upper crown is partly deployed as well. The positioning of the THV should be verified using aortic root angiography. Note at this stage, it is still possible to adjust the positioning. When a proper device position has been verified, the second step is initiated by removal of the safety knob. Subsequently, knob 2 can be turned counter-clockwise which will release the lower crown for full deployment of the valve. While it is not mandatory, rapid ventricular pacing may facilitate stable valve positioning. After completing step 2, a complete disengagement of the prosthesis from the stent holder should be ascertained under fluoroscopy, and the nose cone centered before the delivery system is withdrawn.

15. *Commissural Alignment*

    With TAVI utilization rapidly spreading across all patient risk groups and younger age patients with longer life expectancy, reliable and reproducible guidance on how to orient the THV to avoid coronary overlap and improve coronary re-access is of utmost importance in order to address concomitant CAD. In this sense, SEV has been mostly studied. The highest likelihood of achieving commissural alignment starts by orienting the THV's delivery system before introducing it in patient's femoral artery, as previously described in Step 11 of TAVI procedure. Subsequently, with EVOLUT platform, the "Hat" marker should be directed to the outer curvature of ascending aorta in 3-cusp coplanar view and center-front position in cusp-overlap view (C-paddle to the right of the screen, in same direction as the native RCC/LCC commissure) [71]. Portico/Navitor and ACURATE Neo2 THVs are typically deployed with one of the commissural posts (visible under fluoroscopy) facing the right side of the fluoroscopic screen in "cusp-overlap view" (Fig. 11.6). After assessing the THV position, if needed, slowly torque the delivery catheter clockwise until reaching the desired position [72]. The application of this technique has been validated in specific trials, showing higher rates of commissural alignment, improving also the rate of selective coronary access after THV [72, 75]. However, despite its simplicity, they are not specific to the patient's anatomy considering that orientation of the native aortic valve differs in every single patient.

16. *Verify implantation position and performance and rule out potential complications*: After THV deployment, a pigtail catheter should be reintroduced into the LV cavity, and simultaneous pressure measurements across the prosthetic valve are then obtained. Measurement of the transvalvular gradient and the diastolic pressure are important to determine the hemodynamic result. Importantly, low aortic diastolic pressure <35 mmHg, elevated LV end-diastolic pressure, or near equalization of the aortic pressures suggest significant PVL. Alternatively, calculation of an AR index may help in quantifying PVL. It is calculated as ratio of the gradient between diastolic blood pressure and LV end-diastolic pressure to systolic blood pressure ×100. An AR index <25 correlates with moderate to severe PVL [76]. Subsequently, it is suggested that an aortic root angiography

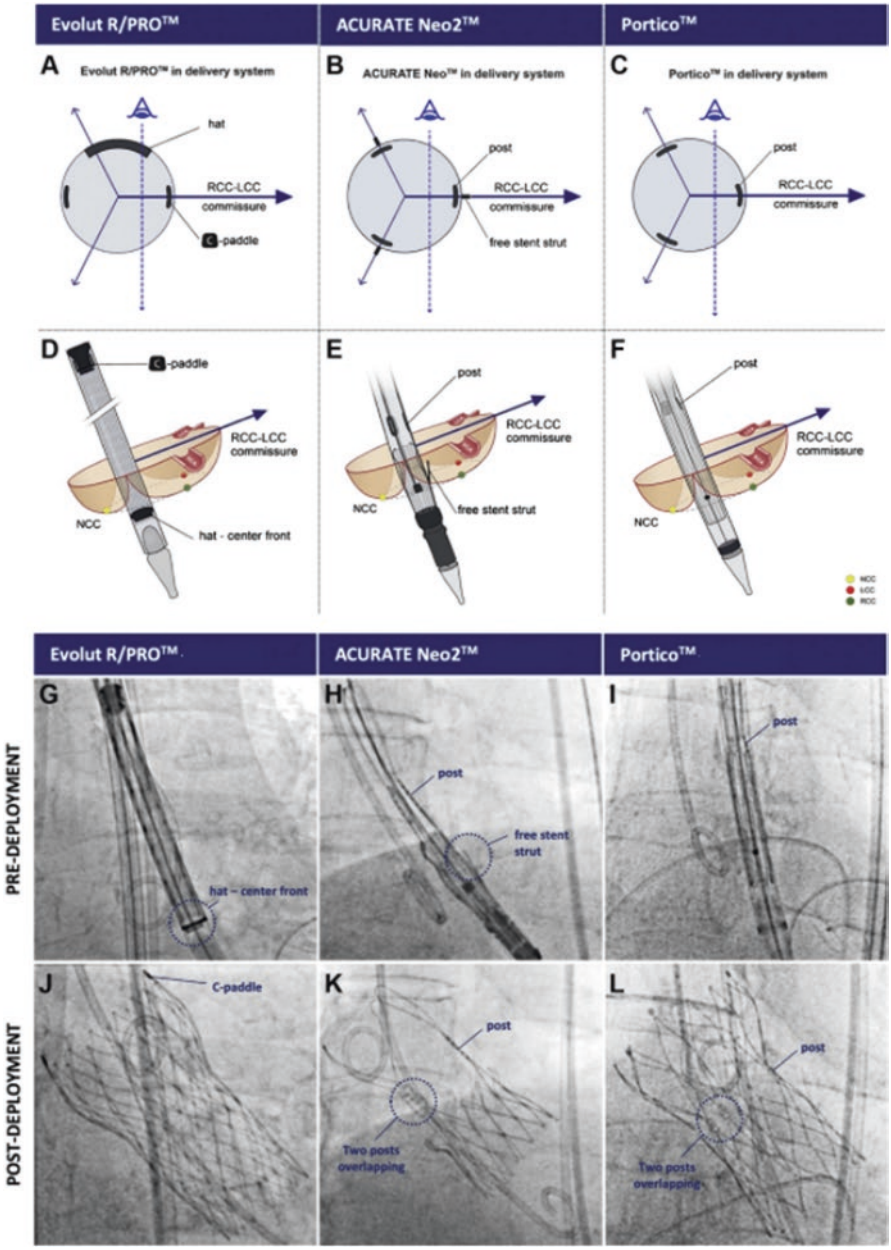


**Fig. 11.6** Neo-commissural alignment: THV-specific instruction for implantation in Cusp-overlap view. Illustration of how the radiopaque THV commissural markers should be oriented in a transversal plane (**a**–**c**) and from a fluoroscopic perspective using RCC/LCC cusp overlap view (**d**–**f**) in order to obtain neo-commissural alignment, and this is for the EVOLUT R/PRO (left column), ACURATE Neo 2 (middle column), and Portico valve (right column). (**g**–**f**) fluoroscopic images from a RCC/LCC cusp overlap view illustrating the THV-specific implantation technique to obtain neo-commissural alignment. THV transcatheter heart valve; RCC/LCC right coronary cusp/left coronary cusp. (Used with permission. Bieliauskas et al. Patient-specific implantation technique to obtain neo-commissural alignment with self-expanding transcatheter aortic valves)

be performed to assess the presence and severity of PVL; as well as to certify that the THV is implanted in an appropriate position, without aortic root rupture or coronary occlusion. Echocardiography may also be utilized for the assessment of PVL among others complications. Cardiac rhythm should also be assessed in all patients; severe bradycardia or high degrees of atrio-ventricular block will require immediate temporary pacing.

17. *Vessel closure and hemostasis*: After confirmation of the optimal result, the TAVI sheath is withdrawn over the extra stiff wire and the pre-closure sutures tightened with the guidewire in place. An additional device such as ProGlide, Angio-seal, or manual compression may be required if bleeding persists. Optionally, the contra-lateral access site may be used to "cross-over" to the main access side. This maneuver may allow for angiographic confirmation of the result upon removal of the TAVI sheath and may serve for bailout balloon angioplasty or covered stent implantation in case of the failure of vascular closure at the main access site.
18. *Post-procedural care*: All TAVI patients should be monitored in an intensive care setting for 24–48 hours. Particular attention should be given to the neurological status, cardiopulmonary function, renal function, and vascular /bleeding complications. Recently, a same-day discharge strategy was described for a very selected group of patients [77]. Nevertheless, echocardiography should routinely be performed before discharge to evaluate early post-procedural prosthetic valve function.

## 11.6 Antithrombotic Management

Recent guidelines recommend life-long single antiplatelet therapy with low-dose aspirin (75–10 mg daily) [12, 13, 78]. A reasonable alternative, particularly for those patients at low risk of bleeding, is to use DAPT during the initial 3–6 months followed by lifelong SAPT [12]. If aspirin is contraindicated, clopidogrel or another P2Y12 inhibitor may serve as an alternative. If there is an established indication for DAPT, the antithrombotic management should follow the recommendations for the indication.

For patients with an established indication for OAC, OAC should be continued after TAVI with no antiplatelet therapy needed [78]. Whether these patients should be treated with DOACs or VKA remains a subject of debate. In patients with indication of both OAC and DAPT, single antiplatelet (preferable clopidogrel) therapy plus OAC appear to be a reasonable strategy.

## 11.7 TAVI-related Complications

Complications associated with TAVI are classified as cardiac or non-cardiac in origin see Table 11.5.

**Table 11.5** Cardiac and non-cardiac complications of transcatheter aortic valve implantation

| |
|---|
| *Cardiac* |
| Paravalvular regurgitation |
| Conduction disturbances |
| Coronary artery obstruction |
| Aortic annular rupture |
| Bioprosthetic valve dysfunction |
| Bioprosthetic valve failure |
| Valve embolization |
| Valve thrombosis |
| Endocarditis |
| Mitral valve injury and mitral valve regurgitation |
| *Non-cardiac* |
| Stroke |
| Vascular complications |

## 11.8 Cardiac Complications

### *11.8.1 Paravalvular Regurgitation*

Currently, the degree of post-implant regurgitation (paravalvular or transvalvular) is observed in about 40% of TAVI recipients [79]. Mechanism of PVL includes THV undersizing [80, 81], mal-apposition, under expansion/recoil of the THV or immobility of the valve leaflets. PVL is typically assessed by post-procedural aortic root angiography and/or TTE or TEE using an integrative approach when quantifying aortic regurgitation [82]. Management of significant PVL depends on the underlying mechanism. If the leak is due to under-expansion of the THV, post-dilation should be performed; note, rarely, a second valve may be needed.

Today, advances in THV such as circumferential outer sealing skirt and repositionable features (in some self-expanding devices) as well as improved THV sizing based on MDCT measurements have remarkably reduced the risk of PVL. In this sense, moderate or severe PVL, which has been consistently associated with increased mortality [83, 84] occurred in 0.8% in the PARTNER 3 trial [9] and in 3.4% in the EVOLUT low risk trial [10].

### *11.8.2 Conduction Disturbances*

The anatomic proximity of the THV position and the conduction system explains the increased risk for conduction disturbances post TAVI [42] (Fig. 11.7). The incidence is higher with SEV compared with BEV. In recent low-risk trials, new PPI was required in 6.5% after BEV TAVI [9] and in 17.4% after SEV [10]. The

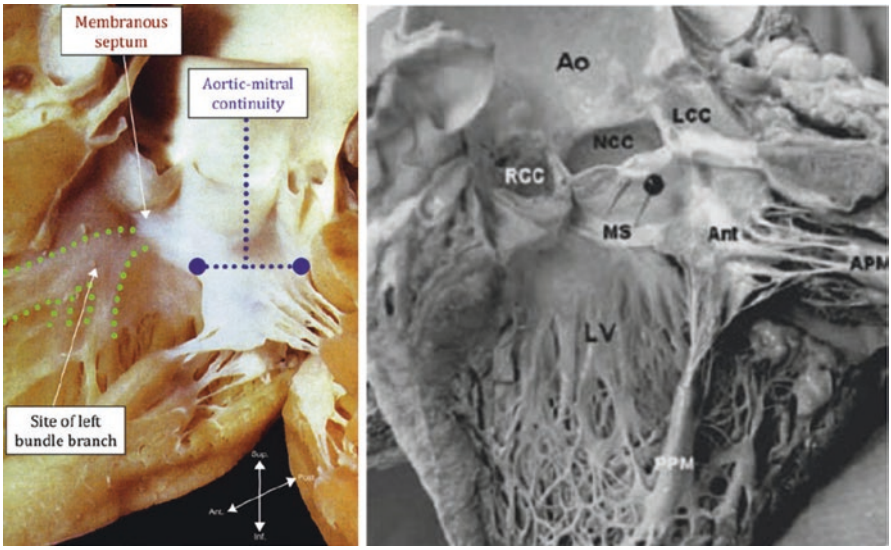


**Fig. 11.7** Relation of aortic valvar complex and the conduction system. Human ear specimen of the left ventricle, aortic valve, and ascending aorta. Note that the left bundle branch exits in the crest of the ventricular septum just beneath the membranous septum

incidence of new LBBB has been reported as 12% to 24% for SAPIEN 3 and 34% Evolut R [85]. Pre-existing right RBBB, short membranous septum length, non-coronary cusp device landing zone calcification, and deep implantation of the THV have been identified as independent predictors of new conduction disturbances [86].

Although the development of AV conduction disturbances usually occurs within 24 hours, it sometimes occurs later than 48 hours after TAVI or even after discharge from the hospital. Therefore, monitoring by telemetry should be continued after the procedure and potential risk assessment of delayed conduction disturbances should be made before discharge [87]. Considering the risks associated with PPI (LV dyssynchrony/dysfunction, lead-induced tricuspid regurgitation, endocarditis, among others), the risk of conduction disturbances should be particularly weighed in lower risk patients with longer life expectancy.

### *11.8.3 Coronary Artery Obstruction*

Coronary artery obstruction is a rare (<1%) but life-threatening complication of TAVI. The left main coronary artery is more commonly involved. Possible mechanisms for coronary obstruction include the following: (1) impingement of the coronary ostia by the valve support structure, (2) displacement of native aortic valve leaflets toward the coronary ostia during valve deployment, and/or (3) embolization from calcium, thrombus, or air. Low coronary height (<10 mm), narrow sinus of

Valsalva, and heavily calcified leaflets are considered as high risk of coronary artery obstruction [88]. Importantly, coronary obstruction is three- to four-fold more common after valve-in-valve (ViV) TAVI when compared with native valve TAVI [52]. Unsurprisingly, it frequently induces sudden hemodynamic compromise and even death. The diagnosis is usually suspected on the basis of hemodynamics, ECG pattern, and/or contrast angiography. Subsequently, the lesion should be treated typically with percutaneous coronary stenting. In patients who are deemed at high risk of coronary artery obstruction, preventive strategies such as coronary protection (Snorkel, chimney stenting) [89, 90] or BASILICA [91] may be considered (see Chap. 13).

### *11.8.4 Aortic Annular Rupture*

Annular rupture is a rare (<1%) but devastating complication that may occur after BEV implantation or aggressive pre/post dilation of any valve type in the setting of a severely calcified valve with extension into the aortic root and LVOT [46]. Depending on its location, rupture may in turn result in the following: (1) a ventricular septal defect, (2) LV to atrial or right atrial shunt, or (3) communication with the extracardiac space [92]. The clinical presentation may vary depending on the location and extent of the injury. Small injuries (contained rupture) may be unrecognized while more extent injuries may induce rapid hemodynamic collapse. In such a case, the presence of annular rupture should be meticulously assessed. Typically, it is identified by aortic root angiography and/or echocardiography with pericardial effusion. The treatment approaches include either surgical or interventional repair. Isolated pericardial drainage and a conservative strategy, depending on the type of rupture, its clinical manifestation, and the patient's background although outcomes remain poor with mortality rates as high as 75% in cases of uncontained rupture [93].

### *11.8.5 Valve Embolization*

Valve dislocation/embolization occurs in approximately 1% of TAVI cases. The incidence has decreased over time attributable to both increasing operator experience and the availability of repositionable THV and refined delivery catheters. Embolization may be caused by the following: (1) undersizing the prosthesis; (2) mal-placement of the prosthesis; (3) improper rapid pacing during valve deployment or post-implant dilation; (4) entanglement of a guidewire across the struts of the prosthesis during valve re-crossing; (5) entanglement of the nose cone with the inflow portion of the prosthesis upon retrieving the delivery catheter, and/or (6) inadequate release of the loading hooks of the frame from the delivery catheter. Non-calcified native aortic valve leaflets, eccentric and asymmetric calcifications,

pre-existing AR, and acute aortic angulation are all considered anatomic risk features related to valve dislocation/embolization. Once it occurs, bailout measures include the following: (1) repositioning attempts using snares, (2) multiple valve implantation, or (3) conversion to surgery.

### *11.8.6 Valve Thrombosis*

Valve thrombosis is relatively rare but considered one of the important causes of bioprosthesis valve dysfunction (BVD) [94]. Valve thrombosis must be distinguished from rapidly progressive structural valve dysfunction (SVD) and endocarditis. Clinical THV thrombosis is defined (VARC-3) in the presence of clinical sequelae of a thromboembolic event (stroke, TIA, retinal occlusion, or other evidence of thromboembolism) or worsening valve stenosis/regurgitation (increasing dyspnea or signs of heart failure). Furthermore, either imaging evidence valve-related thrombus (MDCT or TEE) or hemodynamic valve deterioration stage 2 or 3, or no clinical sequelae but imaging evidence of both valve-related thrombus and hemodynamic valve deterioration stage 3, should be observed during routine interval imaging assessment. Importantly, the use and response of OAC therapy for 2–4 months with reduced gradients and improved symptoms must be carefully documented and provided corroboration of the valve thrombosis diagnosis [94].

Clinical valve thrombosis has been reported to be relatively rare after TAVI with an incidence of <1% [95–98]. In contrast, subclinical leaflet thrombosis (reported ranging from 5% to 40%) [99–103] is most often an incidental finding, characterized by a thin layer of thrombus covering the aortic side of the leaflets causing an increased thickness of the bioprosthesis leaflets as assessed by MDCT. The latter entity is further subcategorized into hypo-attenuated leaflet thickening (HALT) without motion abnormality and in some cases the leaflets mobility is affected therefore termed reduced leaflets motion (RLM) [94]. Importantly, the clinical relevance of this entity as well as its presence leads to clinical valve thrombosis, BVD or thromboembolic events, remains uncertain. Moreover, recent CT substudies of the randomized clinical trials suggested that subclinical leaflet thrombosis may also regress spontaneously without changing antithrombotic therapy [104, 105]. Therefore, tailored strategies are required for patients diagnosed with bioprosthetic valve thrombosis after TAVI.

### *11.8.7 Endocarditis*

Prosthetic valve endocarditis (PVE) is a rare but serious complication associated with valve failure and mortality after TAVI. The diagnosis of PVE can be made using the Duke Criteria for endocarditis; evidence of abscess, pus, or vegetation confirmed as secondary to infection by histological or microbiological studies

during re-operation, or evidence abscess, pus, or vegetation confirmed on autopsy [94]. In a pooled cohort of all patients in the PARTNER I and II trials and continued registries [106], PVE occurred in 107 out of 8530 patients during a mean follow-up of 2.7 years; note this is comparable to its counterpart SAVR. Others registries have reported similar incidence rates [107, 108], with an overall poor prognosis. Current guidelines [12] recommend antibiotic prophylaxis before dental procedures that involve manipulation of gingival tissue, manipulation of the periapical region of teeth, or perforation of the oral mucosa in TAVI recipients.

## 11.9 Non-cardiac Complications

### *11.9.1 Stroke*

Stroke remains one of the most feared complications of TAVI, associated with considerable morbidity and mortality [109]. In a registry including 10,982 patients undergoing TAVI, the incidence of stroke was 2.4% during the first month [109]. However, TAVI portends a 19% lower risk of stroke in patients across all risks throughout 2 years compared with SAVR [110]. Stroke related to TAVI frequently occurs during or within 24–48 hours after the procedure. Patients-related factors such as prior cerebrovascular events, atrial fibrillation, chronic kidney disease, severely calcified aortic valve, concomitant MS, as well as procedural-related factor such as post-dilation, device dislocation/embolization, and lower operator experience has been associated with an increased risk of stroke following TAVI [109, 111, 112]. Optimal anticoagulation therapy during the given TAVI procedure is essential for the prevention of stroke. Moreover, in some specific patients with higher risk of stroke, cerebral embolic protection devices, filters designed to capture or deflect emboli to the brain such as SENTINEL (Boston Scientific, Marlborough, MA, USA), TriGuard (Keystone Heart, Herzliya, Israel), or Embrella (Edwards Lifesciences, Irvine, CA, USA) may be used for the prevention of cerebrovascular events during the procedure.

### *11.9.2 Vascular Complications*

Lower occurrences of vascular complications have been reported, in 2% to 4% of patients in the recent low-risk trials [9, 10] due to smaller and more flexible next-generation delivery systems. However, vascular complications are still common and associated with increased mortality [113]. Vascular injury may include dissection, rupture, thrombosis, stenosis, artery avulsion during sheath retraction, failure of vascular pre-closure, arterial-venous fistula, and/or pseudoaneurysms. The most frequent cause is a closure device failure leading to continued bleeding or stenosis. Factors associated with such adverse outcome are BMI, history of peripheral artery

disease (PAD), the presence of artery calcification, the depth of the skin puncture site, and sheath size [114].

A ≥1.03–1.05 SFAR ratio (sheath diameter to femoral artery minimal luminal diameter) has been also identified as a predictor of major vascular complications and 30-day mortality [115–118]. In non-calcified vessels, the reported ratio is increased to 1.10, and in the presence of calcium, it is decreased to 1.0.

Routine angiography via a crossover catheter to assess for vascular complications after sheath removal may facilitate early recognition. Treatment is cause specific and includes external femoral artery compression, prolonged balloon inflation, covered stent implantation, or surgical repair.

## 11.10 THV Durability

With accumulating evidence, TAVI is increasingly being used among younger and lower-risk patients, who have a longer life-expectancy. Hence, the lifetime management of these patients requires an understanding of THV durability and failure. Favorable data on the durability of THVs have been reported from the randomized clinical trials and large-scale real-world registries, but to date are limited up to 8 years [119–124]. The rates of BVD and bioprosthetic valve failure (BVF) between 5 and 8 years after TAVI ranged from 3.8% to 18.6% and 2.5% to 7.5%, depending on the definitions, the timing, and THV used.

When compared to SAVR valves, the durability of THVs was largely comparable up to 6 years. In the recent US CoreValve High risk trial [122], the rates of severe SVD and BVF were similar between TAVI (SEV) and SAVR. When comparing the rates of moderate BVD between TAVI and SAVR recipients, the latter showed consistently incremented risk among patients within the total risk spectrum. In terms of BVF, the rate was low and similar for both group through 6 years [121]. Moreover, a recent analysis from the CoreValve Pivotal trial and SURTAVI trials (data presented at ACC 2022), evaluated the 5-year incidence and predictors of BVD among high to intermediate risk patients. The incidence of moderate and severe BVD was significantly lower among patients undergoing TAVI compared with SAVR (4.38% vs 2.57, $p$ = 0.0095). The difference was more profound in patients with smaller (<23 mm) annuli. Yet this negative outcome imparted a twofold risk for all-cause mortality ($p$ = <0.001) and hospitalization for aortic valve disease or worsening heart failure ($p$ = <0.01). Lower body surface area, female gender, older patients, prior PCI, or atrial fibrillation were independently associated with lower risk of BVD.

However, according to the BVD and BVF definition utilized in this trial [125], the differences founded were mainly driven by higher gradients in certain SAVR valves which may not be truly indicative of structural valve deterioration (SVD) but PPM. Using the latest definition [94], a dedicated analysis of the population from the PARTNER 2 trial and the PARTNER SAPIEN 3 intermediate-risk observational study [124] showed non-significant differences between the rate of SVD and BVF

among SAPIEN 3 recipients vs a propensity-matched SAVR cohort throughout 5 years (3.9% vs. 3.5%, $p = 0.65$ and 2.6% vs. 1.3%, $p = 0.08$, respectively).

Notable, although promising, the available evidence is limited until 5–8 years of follow-up. Furthermore, bioprosthetic valve deterioration mostly occurs >8–10 years after SAVR. Thus, longer term follow-up using uniform definitions of SVD and BVF are needed.

## 11.11 Emerging Indications

### *11.11.1 TAVI for Bicuspid Aortic Valve Patient*

BAV is the most common congenital heart disease related to AS occurring in 1–2% of the general population [126], and it is a significant risk factor for premature aortic valve disease [127]. Indeed, BAV stenosis and/or regurgitation is the most common indication for SAVR in patients <70 years of age. As there is a shift toward treating younger patients with TAVI, a higher number of BAV in TAVI candidates is expected. Conversely, when the progression of the BAV disease is slow, SAVR may be required in older age groups at higher surgical risk. BAV has important anatomical challenges that may have an impact on short- and long-term prognosis [128–130]. In comparison to TAVI in a stenotic tricuspid aortic valve, the point of highest ellipticity in BAV could be positioned above the aortic annulus, at the level of the commissures and leaflets [131], with large annular dimensions which may impair precise valve location, full apposition and sealing during TAVI, resulting in a relatively greater degree of PVL. Furthermore, more calcified, bulky, and asymmetrical leaflets may interfere with valve expansion and valve hemodynamics with higher transvalvular gradients and PVL. The calcified raphe may place differential stress on the expansion of the valve, increasing the risk of PVL, conduction disturbances, and annular rupture. Moreover, the presence of aortic disease increases the risk of dissection or rupture during valvuloplasty, post-dilation, or implantation of BEV. Finally, the underexpansion and/or the non-circular shape of the THV may ultimately affect long-term durability.

Sizing in BAV based on MDCT includes both an annular sizing and a supra-annular sizing (4 mm above the annular plane). In recent years, various methods of supra-annular sizing have been proposed (i.e., supra-annular tracing, measurement of the intercommissural distance [132], Level of Implantation at the Raphe method (LIRA) [133], Calcium Algorithm Sizing for bicuspid Evaluation with Raphe (CASPER) [i.e., inner leaflet perimeter at the level of the raphe] [134]; yet there remains heterogenicity in clinical practice and concerns of measurements variability. Nonetheless, traditional annular measurements remain the most recognized method for sizing in patients with BAV.

Currently, there are no data supporting the use of a particular TAVI type for patients with BAV AS. Note, new generations THV such as the Venus-A valve

(Venus Medtech, Hangzhou, China) and VitaFlow (Microport, Shanghai, China) have shown excellent performance in a cohort of patients with BAV [135, 136] (Table 11.3 and Fig. 11.4).

To date, BAV has been excluded from the landmark clinical trials involving TAVI. In an analysis of the STS/ACC TVT registry data including 2691 propensity-matched pairs of bicuspid and tricuspid AS, patients with BAV had a comparable mortality at 30 days (2.6% vs. 2.5%, $p = 0.82$) and 1 year (10.5% vs. 12.0%, $p = 0.3$) after TAVI using the SAPIEN 3 THV (31184741). The stroke rate was higher in patients with bicuspid AS at 30 days (2.5% vs. 1.6%, $p = 0.02$), but the differences was not significant at 1 year (3.4% vs. 3.1, $p = 0.16$). There were no significant differences between groups in implant success (99.0% vs. 99.0%, $p = >0.99$) or device success (96.5% vs. 96.6%, $p = 0.87\%$); however, conversion to surgery (0.9% vs. 0.4%, $p = 0.03$) and annular rupture (0.3% vs. 0%, $p = 0.002$) occurred more frequently in patients with bicuspid AS. A recent core laboratory MDCT analysis in a multinational registry ($n = 1034$), identified calcified raphe and excess leaflet calcification in BAV as the risk factors for procedural complications and mid-term mortality after TAVI using current generation devices [137].

Nowadays, surgery remains the treatment of choice for BAV disease, especially in low-risk patients or in the presence of aortic root dilation. TAVI can be an alternative to surgery in patients who are at high surgical risk [138–140].

### *11.11.2 Valve-in-Valve for Surgical Bioprostheses*

Currently, bioprosthetic prostheses represent the majority of all SAVR and are increasingly being implanted in younger patients who can expect the need for valve re-intervention in the future [141]. Clinically relevant SVD of bioprostheses occurs typically at 10–15 years after valve implantation, and then repeat interventions are typically needed for the failed bioprosthesis. Considering the high risk that redo SAVR carries, ViV TAVI has emerged as an attractive alternative for treatment of severe SVD.

Knowledge of the surgical bioprosthesis is critical to determine the feasibility of ViV TAVI and for procedural planning. This information is usually obtained from previous operation records or valve identification cars provided by the manufacturers. The valve-in-valve (aortic) mobile application is an invaluable planning tool to educate operators on the anatomy of surgical aortic valve, assess ViV TAVI feasibility, select the type and size of a THV, and provide guidance on the procedure. The operator should acknowledge particular risks related to a given bioprosthesis design, such as potential coronary obstruction in externally mounted stented valves or stentless valves, valve malapposition or dislocation in stent-less valves, and residual gradients in stented small valves [142–144]. To assess the risk of coronary obstruction in ViV TAVI, a MDCT should be performed and valve-to-coronary (VTC) and valve-to-STJ distances should be measured. VTC distance of <3 mm, would be considered high risk of coronary obstruction in patients with low lying coronary

arteries, and preventive measures such as coronary protection, BASILICA, or snorkel technique should be considered [144] (see Chap. 14). The BASILICA procedure can serve as an adjunctive technique to reduce coronary obstruction risk by splitting the interfering SAV leaflets prior to TAVI [145]. In patients where residual high gradients post ViV TAVI are considered unavoidable (stented valves with small internal diameter), intentional fracture of the bioprosthesis with a non-compliant balloon may be performed before or after the THV implantation to increase the inner diameter of the SAV to allow either a larger THV or a better expanded THV to be implanted potentially reducing the severity of pre-existing PPM [146, 147].

Procedural and clinical outcomes after the ViV procedure for failed bioprostheses have been reported from several dedicated registries [148–152]. To date across these studies, reported overall mortality ranged from 2.1% to 7.6 at 30 days and 11.7% to 16.8% at 1 year among elderly patients (mean age 77–79 years) at an increased surgical risk (mean STS-PROM 7–10%). In a meta-analysis including 5553 patients who underwent TAVI-in-SAV (mean STS-PROM 7.8%, the procedure was successful in 95% of cases. At 30 days, all-cause death occurred in 5%, stroke in 2%, myocardial infarction in 1%, new PPI in 6%, and significant PVL in 7%. At 1 year, the incidence of all-cause mortality death was 12% [153].

Comparative data between TAV-in-SAV versus redo SAVR for the treatment of failed bioprostheses remain scarce and limited to a few observational studies. Yet overall, both therapeutic strategies showed comparable rates of mortality, stroke, acute kidney injury requiring dialysis at 30 days of follow-up [154, 155].

### *11.11.3 Pure Native Aortic Valve Regurgitation*

Although less prevalent than aortic stenosis, AR remains a frequently encountered clinical problem in the adult population, with an estimated prevalence of at least moderate AR of 2.2% in patients older than 70 years [156]. Pure native AR has been considered a relative contraindication to TAVI due to specific anatomic features characterized by the absence of aortic valve calcification, large aortic annulus size and frequent coexistence with dilatations of the aortic root. Moreover, a non-negligible proportion of patients suffering from severe AR have no intervention mainly due elevated surgical risk. Thus, TAVI for pure AR is explored as treatment alternative to surgery.

SEV have been preferred over BEV for the possibility to oversize the prosthesis while preserving a low risk of annular rupture through relying on its radial force to ensure anchoring even in the absence of calcification.

The operator should acknowledge particular limitations of TAVI in AR. Regarding sizing, in patients with associated ascending aorta dilatation, aortic annular dimensions may exceed those recommended by manufacturers of available THV. A greater oversizing is typically performed to minimize the risk of embolization/migration. Device placements can also be difficult with elicitations of increased stroke volume

and a hypercontractile LV [157]. In addition, due to poor visibility of the aortic annulus on fluoroscopy, there is a need for increased contrast volume for opacification, and/or placing one (or two) additional pigtail catheter may help the optimal positioning. All these factors make device positioning and stabilization during deployment very difficult; with the potential risks of device dislodgements and elicitations of subsequent moderate or severe degree of AR.

To date, the scarce data evaluating the outcomes of TAVI in pure AR limited to registries [158–165]. The largest systemic review and meta-analysis on TAVI in AR included 19 studies and 998 patients; the rate of procedural success was 86.2%. Overall mortality at 30 days was 11.9%, but there was a statistically significant reduction in mortality and higher device success when comparing new-generation devices with old-generation devices (9.1% vs 15.3%, $p = 0.02$). Residual moderate-severe AR varied from 0% to 29% with a pooled estimate of 9.2% [166].

The JenaValve (jenaValve Technology, Munich, Germany) is a dedicated SEV system for pure AR that features a clipping mechanism that anchors positioning feelers into the native aortic annulus independent of annular calcification [167]. During release, the native valve leaflets are clipped between the "feelers" and the base of the prosthesis. This mechanism firmly anchors the valve in the correct anatomical position and provides active fixation and resistance to migration. In the JUPITER study, the authors reported a procedural success in 96.7% with only one patient requiring conversion to SAVR because of device embolization. Mortality rate of 10% at 30 days, PVL was none/trivial in 84.6%, and mild in 15.4% while PPM implantation rate was 3.8%. No annular rupture occurred. Survival at 1-year was 79.9% while any stroke was observed at 1-year [168].

## 11.12 Conclusion

TAVI has developed into a mature, safe, and effective therapy across the entire spectrum of patient's presenting with surgical risks, in terms of clinical outcomes during mid-term follow-up (1 to 8 years). Both device innovations/evolutions and increasing operator experiences have led to improved clinical outcomes.

An ever-growing array of clinical studies has improved our understanding of the etiology of cardiac and non-cardiac complications. It is well founded that the role of the multidisciplinary Heart Team is of utmost importance for decision-making in order to achieve optimal patient results.

Compared to SAVR, PVL and conduction abnormalities are still more frequently observed. Certain clinical scenarios such as bicuspid anatomy, pure AR, valve-in-valve TAVI, moderate AS, or asymptomatic severe AS require further studies/procedural refinements in order to clarify the specific roles of TAVI for such patients. Finally, long-term follow-up assessments, in terms of THV durability, will be of utmost importance when indicating TAVI in younger and lower risk populations.

## References


1. Cribier A et al (2002) Percutaneous transcatheter implantation of an aortic valve prosthesis for calcific aortic stenosis: first human case description. Circulation 106:3006–3008
2. Grube E et al (2005) First report on a human percutaneous transluminal implantation of a self-expanding valve prosthesis for interventional treatment of aortic valve stenosis. Catheter Cardiovasc Interv Off J Soc Card Angiogr Interv 66:465–469
3. Leon MB et al (2010) Transcatheter aortic-valve implantation for aortic stenosis in patients who cannot undergo surgery. N Engl J Med 363:1597–1607
4. Smith CR et al (2011) Transcatheter versus surgical aortic-valve replacement in high-risk patients. N Engl J Med 364:2187–2198
5. Adams DH et al (2014) Transcatheter aortic-valve replacement with a self-expanding prosthesis. N Engl J Med 370:1790–1798
6. Leon MB et al (2016) Transcatheter or surgical aortic-valve replacement in intermediate-risk patients. N Engl J Med 374:1609–1620
7. Reardon MJ et al (2017) Surgical or transcatheter aortic-valve replacement in intermediate-risk patients. N Engl J Med 376:1321–1331
8. Thyregod HGH et al (2015) Transcatheter versus surgical aortic valve replacement in patients with severe aortic valve stenosis: 1-year results from the all-comers NOTION randomized clinical trial. J Am Coll Cardiol 65:2184–2194
9. Mack MJ et al (2019) Transcatheter aortic-valve replacement with a balloon-expandable valve in low-risk patients. N Engl J Med 380:1695–1705
10. Popma JJ et al (2019) Transcatheter aortic-valve replacement with a self-expanding valve in low-risk patients. N Engl J Med 380:1706–1715
11. Nishimura RA et al (2014) 2014 AHA/ACC guideline for the management of patients with valvular heart disease: a report of the American College of Cardiology/American Heart Association Task Force on practice guidelines. J Am Coll Cardiol 63:e57–185
12. Otto CM et al (2021) 2020 ACC/AHA guideline for the management of patients with valvular heart disease: executive summary: a report of the American College of Cardiology/American Heart Association Joint Committee on clinical practice guidelines. Circulation 143:e35–e71
13. Vahanian A et al (2022) 2021 ESC/EACTS guidelines for the management of valvular heart disease. Eur Heart J 43:561–632
14. O'Brien SM et al (2009) The Society of Thoracic Surgeons 2008 cardiac surgery risk models: part 2--isolated valve surgery. Ann Thorac Surg 88:S23–S42
15. Wyse RK, Taylor KM (1999) The development of an international surgical registry: the ECSUR project. The European Cardiac Surgical Registry. Eur J Cardio-Thoracic Surg Off J Eur Assoc Cardio-thoracic Surg 16:2–8
16. Nashef SAM et al (2012) EuroSCORE II. Eur J Cardio-Thoracic Surg Off J Eur Assoc Cardio-thoracic Surg 41:734–735
17. Leontyev S et al (2009) Aortic valve replacement in octogenarians: utility of risk stratification with EuroSCORE. Ann Thorac Surg 87:1440–1445
18. Barili F et al (2013) Does EuroSCORE II perform better than its original versions? A multicentre validation study. Eur Heart J 34:22–29
19. Sepehri A et al (2014) The impact of frailty on outcomes after cardiac surgery: a systematic review. J Thorac Cardiovasc Surg 148:3110–3117
20. Stortecky S et al (2012) Evaluation of multidimensional geriatric assessment as a predictor of mortality and cardiovascular events after transcatheter aortic valve implantation. JACC Cardiovasc Interv 5:489–496
21. Green P et al (2015) Relation of frailty to outcomes after transcatheter aortic valve replacement (from the PARTNER trial). Am J Cardiol 116:264–269
22. Afilalo J et al (2017) Frailty in older adults undergoing aortic valve replacement: the FRAILTY-AVR study. J Am Coll Cardiol 70:689–700

23. Okuno T et al (2018) Prognostic impact of computed tomography-derived abdominal fat area on transcatheter aortic valve implantation. Circ J 82:3082–3089
24. Okuno T et al (2019) Evaluation of objective nutritional indexes as predictors of one-year outcomes after transcatheter aortic valve implantation. J Cardiol 74:34–39
25. Mamane S et al (2016) Psoas muscle area and all-cause mortality after transcatheter aortic valve replacement: the Montreal-Munich study. Can J Cardiol 32:177–182
26. Faroux L et al (2019) Coronary artery disease and transcatheter aortic valve replacement: JACC state-of-the-art review. J Am Coll Cardiol 74:362–372
27. Witberg G et al (2017) The prognostic effects of coronary disease severity and completeness of revascularization on mortality in patients undergoing transcatheter aortic valve replacement. JACC Cardiovasc Interv 10:1428–1435
28. Chieffo A et al (2015) Routine screening of coronary artery disease with computed tomographic coronary angiography in place of invasive coronary angiography in patients undergoing transcatheter aortic valve replacement. Circ Cardiovasc Interv 8:e002025
29. Khawaja MZ, Wang D, Pocock S, Redwood SR, Thomas MR (2014) The percutaneous coronary intervention prior to transcatheter aortic valve implantation (ACTIVATION) trial: study protocol for a randomized controlled trial. Trials 15:300
30. Mohr FW et al (2013) Coronary artery bypass graft surgery versus percutaneous coronary intervention in patients with three-vessel disease and left main coronary disease: 5-year follow-up of the randomised, clinical SYNTAX trial. Lancet (London, England) 381:629–638
31. Thalji NM et al (2015) The prognostic impact of concomitant coronary artery bypass grafting during aortic valve surgery: implications for revascularization in the transcatheter era. J Thorac Cardiovasc Surg 149:451–460
32. Khan F et al (2020) Transcatheter aortic valve replacement in patients with multivalvular heart disease. JACC Cardiovasc Interv 13:1503–1514
33. Sinning J-M et al (2013) Transcatheter mitral valve replacement using a balloon-expandable prosthesis in a patient with calcified native mitral valve stenosis. Eur Heart J 34:2609
34. Ribeiro HB et al (2014) Transapical mitral implantation of a balloon-expandable valve in native mitral valve stenosis in a patient with previous transcatheter aortic valve replacement. JACC Cardiovasc Interv 7:e137–e139
35. Wild MG et al (2022) Transapical mitral valve implantation for treatment of symptomatic mitral valve disease: a real-world multicentre experience. Eur J Heart Fail. https://doi.org/10.1002/ejhf.2434
36. Taramasso M et al (2019) Transcatheter versus medical treatment of patients with symptomatic severe tricuspid regurgitation. J Am Coll Cardiol 74:2998–3008
37. Lurz P et al (2021) Transcatheter edge-to-edge repair for treatment of tricuspid regurgitation. J Am Coll Cardiol 77:229–239
38. Delgado V et al (2010) Multimodality imaging in transcatheter aortic valve implantation: key steps to assess procedural feasibility. EuroIntervention J Eur Collab with Work Gr Interv Cardiol Eur Soc Cardiol 6:643–652
39. Schultz CJ et al (2010) Three dimensional evaluation of the aortic annulus using multislice computer tomography: are manufacturer's guidelines for sizing for percutaneous aortic valve replacement helpful? Eur Heart J 31:849–856
40. Schultz CJ et al (2010) Cardiac CT: necessary for precise sizing for transcatheter aortic implantation. EuroIntervention J Eur Collab with Work Gr Interv Cardiol Eur Soc Cardiol 6(Suppl G):G6–G13
41. Stella S et al (2019) Accuracy and reproducibility of aortic annular measurements obtained from echocardiographic 3D manual and semi-automated software analyses in patients referred for transcatheter aortic valve implantation: implication for prosthesis size selection. Eur Hear J Cardiovasc Imaging 20:45–55
42. Piazza N et al (2008) Anatomy of the aortic valvar complex and its implications for transcatheter implantation of the aortic valve. Circ Cardiovasc Interv 1:74–81

43. Tay ELW et al (2011) Outcome of patients after transcatheter aortic valve embolization. JACC Cardiovasc Interv 4:228–234
44. Blanke P et al (2012) Prosthesis oversizing in balloon-expandable transcatheter aortic valve implantation is associated with contained rupture of the aortic root. Circ Cardiovasc Interv 5:540–548
45. Jilaihawi H et al (2014) A revised methodology for aortic-valvar complex calcium quantification for transcatheter aortic valve implantation. Eur Hear J Cardiovasc Imaging 15:1324–1332
46. Okuno T et al (2020) Impact of left ventricular outflow tract calcification on procedural outcomes after transcatheter aortic valve replacement. JACC Cardiovasc Interv 13:1789–1799
47. Van Mieghem NM et al (2012) Incidence, timing, and predictors of valve dislodgment during TAVI with the Medtronic Corevalve system. Catheter Cardiovasc Interv Off J Soc Card Angiogr Interv 79:726–732
48. Abramowitz Y et al (2017) Severe aortic stenosis with low aortic valve calcification: characteristics and outcome following transcatheter aortic valve implantation. Eur Hear J Cardiovasc Imaging 18:639–647
49. Xiong T-Y et al (2018) Transcatheter aortic valve replacement in patients with non-calcific aortic stenosis. EuroIntervention J Eur Collab with Work Gr Interv Cardiol Eur Soc Cardiol. 13:e1756–e1763
50. Webb JG et al (2007) Percutaneous transarterial aortic valve replacement in selected high-risk patients with aortic stenosis. Circulation 116:755–763
51. Ochiai T et al (2020) Coronary access after TAVR. JACC Cardiovasc Interv 13:693–705
52. Ribeiro HB et al (2013) Predictive factors, management, and clinical outcomes of coronary obstruction following transcatheter aortic valve implantation: insights from a large multicenter registry. J Am Coll Cardiol 62:1552–1562
53. Tuzcu EM (2008) Transcatheter aortic valve replacement malposition and embolization: innovation brings solutions also new challenges. Catheter Cardiovasc Interv 72:579–580
54. Bleiziffer S et al (2010) Predictors for new-onset complete heart block after transcatheter aortic valve implantation. JACC Cardiovasc Interv 3:524–530
55. Binder RK et al (2012) Prediction of optimal deployment projection for transcatheter aortic valve replacement: angiographic 3-dimensional reconstruction of the aortic root versus multidetector computed tomography. Circ Cardiovasc Interv 5:247–252
56. Tang GHL et al (2018) 'Cusp-overlap' view simplifies fluoroscopy-guided implantation of self-expanding valve in transcatheter aortic valve replacement. JACC Cardiovasc Interv 11:1663–1665
57. Ben-Shoshan J et al (2021) Double S-curve versus cusp-overlap technique: defining the optimal fluoroscopic projection for TAVR with a self-expanding device. JACC Cardiovasc Interv 14:185–194
58. Pascual I et al (2022) Permanent pacemaker reduction using cusp-overlapping projection in TAVR: a propensity score analysis. JACC Cardiovasc Interv 15:150–161
59. Mendiz OA et al (2021) Impact of cusp-overlap view for TAVR with self-expandable valves on 30-day conduction disturbances. J Interv Cardiol 2021:9991528
60. Patel JS et al (2016) Access options for transcatheter aortic valve replacement in patients with unfavorable aortoiliofemoral anatomy. Curr Cardiol Rep 18:110
61. Lanz J, Greenbaum A, Pilgrim T, Tarantini G, Windecker S (2018) Current state of alternative access for transcatheter aortic valve implantation. EuroIntervention J Eur Collab with Work Gr Interv Cardiol Eur Soc Cardiol 14:AB40–AB52
62. Mack MJ et al (2015) 5-year outcomes of transcatheter aortic valve replacement or surgical aortic valve replacement for high surgical risk patients with aortic stenosis (PARTNER 1): a randomised controlled trial. Lancet (London, England) 385:2477–2484
63. Makkar RR et al (2020) Five-year outcomes of transcatheter or surgical aortic-valve replacement. N Engl J Med 382:799–809

64. Dahle TG, Kaneko T, McCabe JM (2019) Outcomes following subclavian and axillary artery access for transcatheter aortic valve replacement: Society of the Thoracic Surgeons/American College of Cardiology TVT registry report. JACC Cardiovasc Interv 12:662–669
65. Beurtheret S et al (2019) Femoral versus nonfemoral peripheral access for transcatheter aortic valve replacement. J Am Coll Cardiol 74:2728–2739
66. Greenbaum AB et al (2017) Transcaval access and closure for transcatheter aortic valve replacement: a prospective investigation. J Am Coll Cardiol 69:511–521
67. Claessen BE, Tang GHL, Kini AS, Sharma SK (2021) Considerations for optimal device selection in transcatheter aortic valve replacement: a review. JAMA Cardiol 6:102–112
68. Okuno T et al (2021) Heart valve sizing and clinical outcomes in patients undergoing transcatheter aortic valve implantation. Catheter Cardiovasc Interv Off J Soc Card Angiogr Interv 98:E768–E779
69. Faurie B et al (2019) Left ventricular rapid pacing via the valve delivery guidewire in transcatheter aortic valve replacement. JACC Cardiovasc Interv 12:2449–2459
70. Vincent F et al (2020) Ultrasound guidance to reduce vascular and bleeding complications of percutaneous transfemoral transcatheter aortic valve replacement: a propensity score-matched comparison. J Am Heart Assoc 9:e014916
71. Tang GHL et al (2020) Alignment of transcatheter aortic-valve neo-commissures (ALIGN TAVR): impact on final valve orientation and coronary artery overlap. JACC Cardiovasc Interv 13:1030–1042
72. Bieliauskas G et al (2021) Patient-specific implantation technique to obtain neo-commissural alignment with self-expanding transcatheter aortic valves. JACC Cardiovasc Interv 14:2097–2108
73. Tagliari AP et al (2021) Transcatheter aortic valve neo-commissure alignment with the Portico system. EuroIntervention J Eur Collab with Work Gr Interv Cardiol Eur Soc Cardiol 17:e152–e155
74. Sammour Y et al (2021) Systematic approach to high implantation of SAPIEN-3 valve achieves a lower rate of conduction abnormalities including pacemaker implantation. Circ Cardiovasc Interv 14:e009407
75. Tarantini G et al (2022) Coronary access after transcatheter aortic valve replacement with commissural alignment: the ALIGN-ACCESS study. Circ Cardiovasc Interv 15:e011045
76. Sinning J-M et al (2012) Aortic regurgitation index defines severity of peri-prosthetic regurgitation and predicts outcome in patients after transcatheter aortic valve implantation. J Am Coll Cardiol 59:1134–1141
77. Krishnaswamy A et al (2022) Feasibility and safety of same-day discharge following transfemoral transcatheter aortic valve replacement. JACC Cardiovasc Interv 15:575–589
78. Brouwer J et al (2020) Aspirin with or without Clopidogrel after transcatheter aortic-valve implantation. N Engl J Med 383:1447–1457
79. Carroll JD et al (2020) STS-ACC TVT registry of transcatheter aortic valve replacement. J Am Coll Cardiol 76:2492–2516
80. Détaint D et al (2009) Determinants of significant paravalvular regurgitation after transcatheter aortic valve: implantation impact of device and annulus discongruence. JACC Cardiovasc Interv 2:821–827
81. Schultz C et al (2011) Aortic annulus dimensions and leaflet calcification from contrast MSCT predict the need for balloon post-dilatation after TAVI with the Medtronic CoreValve prosthesis. EuroIntervention J Eur Collab with Work Gr Interv Cardiol Eur Soc Cardiol 7:564–572
82. Leon MB et al (2011) Standardized endpoint definitions for transcatheter aortic valve implantation clinical trials: a consensus report from the Valve Academic Research Consortium. Eur Heart J 32:205–217
83. Athappan G et al (2013) Incidence, predictors, and outcomes of aortic regurgitation after transcatheter aortic valve replacement: meta-analysis and systematic review of literature. J Am Coll Cardiol 61:1585–1595

84. Pibarot P et al (2017) Association of Paravalvular regurgitation with 1-year outcomes after transcatheter aortic valve replacement with the SAPIEN 3 valve. JAMA Cardiol 2:1208–1216
85. Scarsini R et al (2019) Impact of complications during transfemoral transcatheter aortic valve replacement: how can they be avoided and managed? J Am Heart Assoc 8:e013801
86. Maeno Y et al (2017) A highly predictive risk model for pacemaker implantation after TAVR. JACC Cardiovasc Imaging 10:1139–1147
87. Rodés-Cabau J et al (2019) Management of conduction disturbances associated with transcatheter aortic valve replacement: JACC Scientific Expert Panel. J Am Coll Cardiol 74:1086–1106
88. Ribeiro HB et al (2013) Coronary obstruction following transcatheter aortic valve implantation: a systematic review. JACC Cardiovasc Interv 6:452–461
89. Abramowitz Y et al (2015) Clinical impact of coronary protection during transcatheter aortic valve implantation: first reported series of patients. EuroIntervention J Eur Collab with Work Gr Interv Cardiol Eur Soc Cardiol 11:572–581
90. Mercanti F et al (2020) Chimney stenting for coronary occlusion during TAVR: insights from the chimney registry. JACC Cardiovasc Interv 13:751–761
91. Lederman RJ et al (2019) Preventing coronary obstruction during transcatheter aortic valve replacement: from computed tomography to BASILICA. JACC Cardiovasc Interv 12:1197–1216
92. Pasic M, Unbehaun A, Buz S, Drews T, Hetzer R (2015) Annular rupture during transcatheter aortic valve replacement: classification, pathophysiology, diagnostics, treatment approaches, and prevention. JACC Cardiovasc Interv 8:1–9
93. Barbanti M et al (2013) Anatomical and procedural features associated with aortic root rupture during balloon-expandable transcatheter aortic valve replacement. Circulation 128:244–253
94. Généreux P et al (2021) Valve academic research consortium 3: updated endpoint definitions for aortic valve clinical research. J Am Coll Cardiol 77:2717–2746
95. Mylotte D et al (2015) Transcatheter heart valve failure: a systematic review. Eur Heart J 36:1306–1327
96. Latib A et al (2015) Treatment and clinical outcomes of transcatheter heart valve thrombosis. Circ Cardiovasc Interv 8:e001779
97. Mangieri A et al (2019) Thrombotic versus bleeding risk after transcatheter aortic valve replacement: JACC review topic of the week. J Am Coll Cardiol 74:2088–2101
98. De Marchena E et al (2015) Thrombus formation following transcatheter aortic valve replacement. JACC Cardiovasc Interv 8:728–739
99. Chakravarty T et al (2017) Subclinical leaflet thrombosis in surgical and transcatheter bioprosthetic aortic valves: an observational study. Lancet (London, England) 389:2383–2392
100. Makkar RR et al (2015) Possible subclinical leaflet thrombosis in bioprosthetic aortic valves. N Engl J Med 373:2015–2024
101. Hansson NC et al (2016) Transcatheter aortic valve thrombosis: incidence, predisposing factors, and clinical implications. J Am Coll Cardiol 68:2059–2069
102. Pache G et al (2016) Early hypo-attenuated leaflet thickening in balloon-expandable transcatheter aortic heart valves. Eur Heart J 37:2263–2271
103. Yanagisawa R et al (2016) Incidence, predictors, and mid-term outcomes of possible leaflet thrombosis after TAVR. JACC Cardiovasc Imaging. https://doi.org/10.1016/j.jcmg.2016.11.005
104. Makkar RR et al (2020) Subclinical leaflet thrombosis in transcatheter and surgical bioprosthetic valves: PARTNER 3 cardiac computed tomography substudy. J Am Coll Cardiol 75:3003–3015
105. Blanke P et al (2020) Bioprosthetic aortic valve leaflet thickening in the Evolut low risk substudy. J Am Coll Cardiol 75:2430–2442
106. Summers MR et al (2019) Prosthetic valve endocarditis after TAVR and SAVR: insights from the PARTNER trials. Circulation 140:1984–1994
107. Bjursten H et al (2019) Infective endocarditis after transcatheter aortic valve implantation: a nationwide study. Eur Heart J 40:3263–3269

108. Stortecky S et al (2020) Infective endocarditis after transcatheter aortic valve replacement. J Am Coll Cardiol 75:3020–3030
109. Vlastra W et al (2019) Predictors, incidence, and outcomes of patients undergoing Transfemoral transcatheter aortic valve implantation complicated by stroke. Circ Cardiovasc Interv 12:e007546
110. Siontis GCM et al (2019) Transcatheter aortic valve implantation vs. surgical aortic valve replacement for treatment of symptomatic severe aortic stenosis: an updated meta-analysis. Eur Heart J 40:3143–3153
111. Auffret V et al (2016) Predictors of early cerebrovascular events in patients with aortic stenosis undergoing transcatheter aortic valve replacement. J Am Coll Cardiol 68:673–684
112. Okuno T et al (2020) Valvular and nonvalvular atrial fibrillation in patients undergoing transcatheter aortic valve replacement. JACC Cardiovasc Interv 13:2124–2133
113. Généreux P et al (2012) Vascular complications after transcatheter aortic valve replacement: insights from the PARTNER (placement of AoRTic TraNscathetER valve) trial. J Am Coll Cardiol 60:1043–1052
114. Chen I-M, Lee T-H, Chen P-L, Shih C-C, Chang H-H (2019) Factors in ProGlide® vascular closure failure in sheath Arteriotomies greater than 16 French. Eur J Vasc Endovasc Surg Off J Eur Soc Vasc Surg 58:615–622
115. Hayashida K et al (2011) Transfemoral aortic valve implantation new criteria to predict vascular complications. JACC Cardiovasc Interv 4:851–858
116. Durand E et al (2021) Standardized measurement of femoral artery depth by computed tomography to predict vascular complications after transcatheter aortic valve implantation. Am J Cardiol 145:119–127
117. Okuyama K et al (2015) Transfemoral access assessment for transcatheter aortic valve replacement: evidence-based application of computed tomography over invasive angiography. Circ Cardiovasc Imaging 8:e001995
118. van Kesteren F et al (2018) Incidence, predictors, and impact of vascular complications after transfemoral transcatheter aortic valve implantation with the SAPIEN 3 prosthesis. Am J Cardiol 121:1231–1238
119. Didier R et al (2018) Five-year clinical outcome and valve durability after transcatheter aortic valve replacement in high-risk patients. Circulation 138:2597–2607
120. Blackman DJ et al (2019) Long-term durability of transcatheter aortic valve prostheses. J Am Coll Cardiol 73:537–545
121. Søndergaard L et al (2019) Durability of transcatheter and surgical bioprosthetic aortic valves in patients at lower surgical risk. J Am Coll Cardiol 73:546–553
122. Gleason TG et al (2018) 5-year outcomes of self-expanding transcatheter versus surgical aortic valve replacement in high-risk patients. J Am Coll Cardiol 72:2687–2696
123. Testa L et al (2020) Long-term clinical outcome and performance of transcatheter aortic valve replacement with a self-expandable bioprosthesis. Eur Heart J 41:1876–1886
124. Pibarot P et al (2020) Structural deterioration of transcatheter versus surgical aortic valve bioprostheses in the PARTNER-2 trial. J Am Coll Cardiol 76:1830–1843
125. Capodanno D et al (2017) Standardized definitions of structural deterioration and valve failure in assessing long-term durability of transcatheter and surgical aortic bioprosthetic valves: a consensus statement from the European Association of Percutaneous Cardiovascular Interve. Eur Heart J 38:3382–3390
126. Fedak PWM et al (2002) Clinical and pathophysiological implications of a bicuspid aortic valve. Circulation 106:900–904
127. Michelena HI et al (2014) Bicuspid aortic valve: identifying knowledge gaps and rising to the challenge from the International Bicuspid Aortic Valve Consortium (BAVCon). Circulation 129:2691–2704
128. Siu SC, Silversides CK (2010) Bicuspid aortic valve disease. J Am Coll Cardiol 55:2789–2800

129. Watanabe Y et al (2015) Comparison of multislice computed tomography findings between bicuspid and tricuspid aortic valves before and after transcatheter aortic valve implantation. Catheter Cardiovasc Interv Off J Soc Card Angiogr Interv 86:323–330
130. Philip F et al (2015) Aortic annulus and root characteristics in severe aortic stenosis due to bicuspid aortic valve and tricuspid aortic valves: implications for transcatheter aortic valve therapies. Catheter Cardiovasc Interv Off J Soc Card Angiogr Interv 86:E88–E98
131. Tchetche D et al (2019) Bicuspid aortic valve anatomy and relationship with devices: the BAVARD Multicenter registry. Circ Cardiovasc Interv 12:e007107
132. Kim W-K et al (2019) Annular versus supra-annular sizing for TAVI in bicuspid aortic valve stenosis. EuroIntervention J Eur Collab with Work Gr Interv Cardiol Eur Soc Cardiol. 15:e231–e238
133. Iannopollo G et al (2020) Supra-annular sizing of transcatheter aortic valve prostheses in raphe-type bicuspid aortic valve disease: the LIRA method. Int J Cardiol 317:144–151
134. Petronio AS et al (2020) Bicuspid aortic valve sizing for transcatheter aortic valve implantation: development and validation of an algorithm based on multi-slice computed tomography. J Cardiovasc Comput Tomogr 14:452–461
135. Liao Y-B et al (2017) Transcatheter aortic valve implantation with the self-expandable venus A-valve and CoreValve devices: preliminary experiences in China. Catheter Cardiovasc Interv Off J Soc Card Angiogr Interv 89:528–533
136. Zhou D et al (2020) VitaFlow™ transcatheter valve system in the treatment of severe aortic stenosis: one-year results of a multicenter study. Catheter Cardiovasc Interv. Off J Soc Card Angiogr Interv 95:332–338
137. Yoon S-H et al (2020) Bicuspid aortic valve morphology and outcomes after transcatheter aortic valve replacement. J Am Coll Cardiol 76:1018–1030
138. Mylotte D et al (2014) Transcatheter aortic valve replacement in bicuspid aortic valve disease. J Am Coll Cardiol 64:2330–2339
139. Yoon S-H et al (2016) Transcatheter aortic valve replacement with early- and new-generation devices in bicuspid aortic valve stenosis. J Am Coll Cardiol 68:1195–1205
140. Yoon S-H et al (2017) Outcomes in transcatheter aortic valve replacement for bicuspid versus tricuspid aortic valve stenosis. J Am Coll Cardiol 69:2579–2589
141. Brown JM et al (2009) Isolated aortic valve replacement in North America comprising 108,687 patients in 10 years: changes in risks, valve types, and outcomes in the Society of Thoracic Surgeons National Database. J Thorac Cardiovasc Surg 137:82–90
142. Webb JG, Dvir D (2013) Transcatheter aortic valve replacement for bioprosthetic aortic valve failure: the valve-in-valve procedure. Circulation 127:2542–2550
143. Duncan A et al (2019) Outcomes following transcatheter aortic valve replacement for degenerative Stentless versus stented bioprostheses. JACC Cardiovasc Interv 12:1256–1263
144. Dvir D et al (2015) Coronary obstruction in transcatheter aortic valve-in-valve implantation: preprocedural evaluation, device selection, protection, and treatment. Circ Cardiovasc Interv 8:e002079
145. Khan JM et al (2021) Preventing coronary obstruction during transcatheter aortic valve replacement: results from the Multicenter International BASILICA Registry. JACC Cardiovasc Interv 14:941–948
146. Chhatriwalla AK et al (2017) Bioprosthetic valve fracture improves the hemodynamic results of valve-in-valve transcatheter aortic valve replacement. Circ Cardiovasc Interv 10:e005216
147. Allen KB et al (2017) Bioprosthetic valve fracture to facilitate transcatheter valve-in-valve implantation. Ann Thorac Surg 104:1501–1508
148. Dvir D et al (2014) Transcatheter aortic valve implantation in failed bioprosthetic surgical valves. JAMA 312:162–170
149. Tuzcu EM et al (2018) Transcatheter aortic valve replacement of failed surgically implanted bioprostheses: the STS/ACC registry. J Am Coll Cardiol 72:370–382
150. Webb JG et al (2017) Transcatheter aortic valve implantation within degenerated aortic surgical bioprostheses: PARTNER 2 valve-in-valve registry. J Am Coll Cardiol 69:2253–2262

151. Webb JG et al (2019) 3-year outcomes after valve-in-valve transcatheter aortic valve replacement for degenerated bioprostheses: the PARTNER 2 registry. J Am Coll Cardiol 73:2647–2655
152. Deeb GM et al (2017) 1-year results in patients undergoing transcatheter aortic valve replacement with failed surgical bioprostheses. JACC Cardiovasc Interv 10:1034–1044
153. Mahmoud AN et al (2020) Systematic review and meta-analysis of valve-in-valve transcatheter aortic valve replacement in patients with failed bioprosthetic aortic valves. EuroIntervention J Eur Collab with Work Gr Interv Cardiol Eur Soc Cardiol 16:539–548
154. Neupane S et al (2018) Meta-analysis of transcatheter valve-in-valve implantation versus redo aortic valve surgery for bioprosthetic aortic valve dysfunction. Am J Cardiol 121:1593–1600
155. Malik AH et al (2020) Valve-in-valve transcatheter implantation versus redo surgical aortic valve replacement. Am J Cardiol 125:1378–1384
156. Singh JP et al (1999) Prevalence and clinical determinants of mitral, tricuspid, and aortic regurgitation (the Framingham heart study). Am J Cardiol 83:897–902
157. Winkel MG, Stortecky S, Wenaweser P (2019) Transcatheter aortic valve implantation current indications and future directions. Front Cardiovasc Med 6:179
158. Roy DA et al (2013) Transcatheter aortic valve implantation for pure severe native aortic valve regurgitation. J Am Coll Cardiol 61:1577–1584
159. Seiffert M et al (2014) Initial German experience with transapical implantation of a second-generation transcatheter heart valve for the treatment of aortic regurgitation. JACC Cardiovasc Interv 7:1168–1174
160. Wendt D et al (2014) Transapical transcatheter aortic valve for severe aortic regurgitation: expanding the limits. JACC Cardiovasc Interv 7:1159–1167
161. Testa L et al (2014) CoreValve implantation for severe aortic regurgitation: a multicentre registry. EuroIntervention J Eur Collab with Work Gr Interv Cardiol Eur Soc Cardiol 10:739–745
162. Schofer J et al (2015) Transfemoral implantation of a fully repositionable and retrievable transcatheter valve for noncalcified pure aortic regurgitation. JACC Cardiovasc Interv 8:1842–1849
163. Yoon S-H et al (2017) Transcatheter aortic valve replacement in pure native aortic valve regurgitation. J Am Coll Cardiol 70:2752–2763
164. De Backer O et al (2018) Usefulness of transcatheter aortic valve implantation for treatment of pure native aortic valve regurgitation. Am J Cardiol 122:1028–1035
165. Anwaruddin S et al (2019) Self-expanding valve system for treatment of native aortic regurgitation by transcatheter aortic valve implantation (from the STS/ACC TVT registry). Am J Cardiol 124:781–788
166. Rawasia WF et al (2019) Safety and efficacy of transcatheter aortic valve replacement for native aortic valve regurgitation: a systematic review and meta-analysis. Catheter Cardiovasc Interv. Off J Soc Card Angiogr Interv 93:345–353
167. Kempfert J, Rastan AJ, Mohr F-W, Walther T (2011) A new self-expanding transcatheter aortic valve for transapical implantation - first in man implantation of the JenaValve™. Eur J Cardio-thoracic Surg. Off J Eur Assoc Cardio-thoracic Surg 40:761–763
168. Silaschi M et al (2018) The JUPITER registry: one-year outcomes of transapical aortic valve implantation using a second generation transcatheter heart valve for aortic regurgitation. Catheter Cardiovasc Interv. Off J Soc Card Angiogr Interv 91:1345–1351

# Chapter 12
# Post-TAVI PCI

**Stefano Cangemi, Paul A. Iaizzo, and Francesco Burzotta**

## 12.1 Introduction

Transcatheter aortic valve implantation (TAVI) is the recommended modality of treatment for old patients affected by symptomatic severe calcific aortic stenosis and other patients with high or prohibitive surgical risk if anatomically suitable [1, 2]. TAVI differently from SAVR doesn't require the removal of the dysmorphic valve but this one is used to anchor the prosthetic valve. Moreover, while the surgical valve is implanted aligning anatomical and surgical commissures in TAVI, the orientation of the prosthesis is often unpredictable. Due to the intrinsic structure of prostheses and their interaction with ascending aorta structures, major issues may arise regarding coronary artery access and management during and after TAVI. The most common coronary problems are represented by TAVI-induced coronary occlusion and difficulties in carrying on angiography (CA) and percutaneous coronary intervention (PCI) after TAVI implantation. Particularly, the possibility of re-access to a coronary artery in TAVI recipients with the selective engagement of a guide catheter is an increasingly important issue because TAVI candidates are becoming younger and coronary artery disease is often concomitant to severe aortic stenosis [3]. A recent registry [4] demonstrated that acute coronary syndrome (ACS) after TAVI happens in 5% of patients within 1 year, moreover ACS post-TAVI has a high rate of mortality (one-third of patients within 30-days from admission), and an invasive approach with coronary angiography and PCI is associated with significantly

S. Cangemi · F. Burzotta (✉)
Dipartimento di Scienze Cardiovascolari, Fondazione Policlinico Universitario A. Gemelli IRCCS, Rome, Italy

Università Cattolica del Sacro Cuore, Rome, Italy

P. A. Iaizzo
Visible Heart® Laboratories, Department of Surgery, Institute for Engineering in Medicine, University of Minnesota, Minneapolis, MN, USA

© The Author(s), under exclusive license to Springer Nature Switzerland AG 2023

P. A. Iaizzo et al. (eds.), *Heart Valves*, https://doi.org/10.1007/978-3-031-25541-0_12

lower mortality rate. Transcatheter aortic valves are usually divided into three groups: self-expanding valves prosthesis (SEP), balloon-expandable valves prosthesis (BEP), and mechanically expandable valves prosthesis (MEP). The transcatheter aortic valves more used in clinical practice are the SEP and the BEP. Below we will make a brief summary of the main characteristics of each class of transcatheter aortic valve prostheses:

- Balloon-Expandable Valves

The most used BEP valves are the Sapien XT and Sapien 3 (Edwards Lifesciences, Irvine, California) [5]. These prostheses are implanted intra-annularly [5]. The frame of this valve is shorter compared to SEP. Sapien valves are mounted around a catheter balloon which, once placed at the level of the aortic valve, is inflated [5]. They rarely extend beyond the sinotubular junction. It should be noted that in a real-world registry Sapien 3 valves were associated with a lower risk of a coronary obstruction than Sapien XT [6]. Moreover, a recent study demonstrated that a systematic approach of high implantation of Sapien 3 significantly reduces conduction abnormalities without an increase in coronary obstruction [7]. On the other hand, this type of prosthesis has been associated with a higher risk of aortic root valve rupture than SEP [8, 9]. Coronary artery cannulation is usually performed easier than SEP and MEP with the same catheter selection (JR4 6F for right coronary artery and JL 3.5/4 6F for left coronary artery) used in non-TAVI recipients [5]. The worst scenario with Sapien valves is when in a patient with low coronary arteries origin, the prosthetic valve is implanted high and prosthetic commissures face the coronary ostium. In the last scenario, it could be helpful to try to engage the coronary ostium from above through the upper row of cells, sometimes can be used a coronary guidewire [5] or a guide extension catheter.

- Mechanically Expandable Valves (LOTUS):

The mechanically expandable valves (Lotus valves, Boston Scientific, Marlborough, MA, USA) were retired from the market in 2020. They were biological valves within a nitinol frame and a specific mechanism of deployment which allowed complete retrieval and repositioning [10, 11]. After the deployment of the valve, the nitinol frame was transformed into a compressed state [10, 11]. Rapid ventricular pacing was unnecessary during expansion because the deployment did not impede the transaortic blood flow [10, 11]. This valve was usually deployed below the ostia of the coronary arteries. Because the nitinol frame is compressed, the coronary catheter cannot pass through the valve, so the catheter needs to engage the coronary ostium from above or go outside the frame. Even if this valve was usually deployed below the ostia of the coronary arteries, a recent Japanese study demonstrated that half of 41 Lotus valve recipients who underwent multidetector computed tomography (MDCT) had coronary arteries in an unfavorable position [12] (coronary ostium under the valve frame with small space between them). It often requires a 5F coronary catheter to engage coronary ostia, little is known about the best coronary catheter to use [12].

- Self-Expanding Valves Prosthesis (SEP):

Among the self-expanding prosthesis, we have Evolut R and Evolut Pro (Medtronic, Minneapolis, MN, USA), ACURATE neo 2 (Boston Scientific, Marlborough, Massachusetts), and Portico (Abbott, Abbott Park, Illinois). These prostheses have minor differences regarding the deployment technique, the frame size, and the size of the cells but they have in common the fact that they are tall valves (high longitudinal extension) which invariably implies coronary take-off coverage. Evolut family (Evolut R and Evolut PRO, Medtronic, Minneapolis, MN, USA) is very popular and its efficacy has been supported by large randomized trials [13, 14]. This valve consists of a tall nitinol frame with a porcine valve [5] inside (Fig. 12.1). The frame can be divided into three portions [5]: (a) the Inflow tract with the skirt which exerts radial force and ideally anchors the valve to the annulus; (b) the waist, the concave intermedium tract to reduce the incidence of coronary occlusion and allow coronary catheters engagement; (c) outflow tract, the widest part in contact with ascending aorta. The valve delivery system allows full retrieval and repositioning of the prosthesis in order to obtain the optimal valve position. Yet, the structure of Evolut (R and PRO) self-expanding prosthesis (ESEP) implies that coronary management issues like post-TAVI coronary procedures or coronary protection during TAVI have to invariably deal with the ESEP characteristics. Figure 12.1 shows the key ESEP structural features that may influence coronary procedures. Evolut prostheses have numerous advantages over BEP such as they can be used in many different aortic valve anatomy (aortic regurgitation [15], small

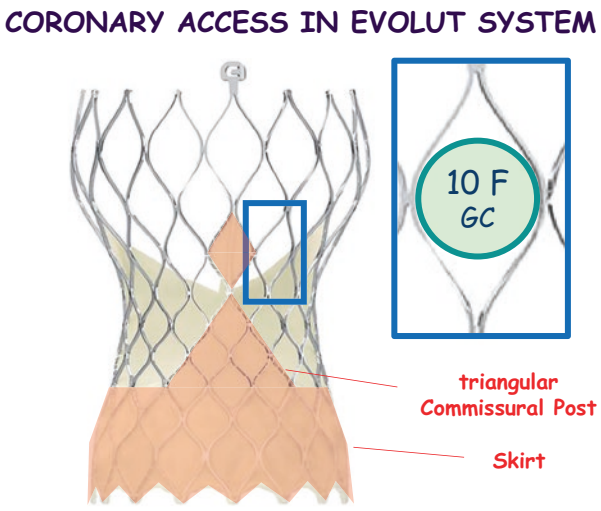


**Fig. 12.1** Evolut (R and PRO) self-expandable prosthesis characteristics that may influence coronary management during and after TAVI. Red color highlights asymmetric areas where the ESEP frame is covered so that its crossing with coronary devices is impossible. Blue boxes highlight an ESEP rhombus-shaped closed cell with maximal and minimal dimensions (green) and the geometrical relationship with a 6 F guiding catheter (GC) (inscribed yellow circle)

aortic annulus [16]) and have a minor rate of aortic rupture [8, 9] and coronary obstruction [17]. The relative disadvantage of ESEP are the relatively high atrioventricular conduction disturbance rate [13, 14], but recent studies and technique improvements are significantly reducing this rate [18, 19] and a higher rate of coronary access failure post-TAVI [5].

In this chapter, we reviewed the main coronary management issues that may occur with ESEP using a unique multimodal imaging in reanimated swine hearts [20, 21] in the Visible Heart® Laboratory. Briefly, 80–90 kg healthy swine were anesthetized and intubated. A sternotomy was performed and a pretreatment solution was injected into the pericardium and allowed to incubate for 1 hour. Cardioplegia was induced with a high potassium solution and the heart was then explanted and cannulated. The heart was then set up on an ex vivo cardiac perfusion apparatus (Visible Heart® methodologies), where it was warmed by the perfusion of Krebs at 36 °C and reanimated with a 30 J direct current shock (LifePack, Physio-Control, Redmond, WA, USA). Once reanimated, the heart was placed in a dedicated catheterization laboratory where a series of TAVI procedures and coronary management techniques were practiced by experienced interventional cardiologists. The procedures were simultaneously recorded using fluoroscopy and videoscopes located in ascending aorta and left ventricle. The coronary interventions were performed using commercially available materials as previously described [21]. Of note, the Visible Heart® laboratory was recently used to perform both PCI and TAVI in reanimated human heart [21, 22] successfully.

## 12.2 Coronary Access After TAVI Implantation

Coronary angiography and PCI might be necessary after TAVI due to the suspected or ascertained ischemic heart disease development [23]. When needed, such coronary procedures might be technically challenging so not even a minor procedure failure rate due to coronary access issues has been reported [24–39]. Table 12.1 summarizes the frequency of unplanned coronary procedures and their failures observed in the available studies. Coronary cannulation is the key to successful coronary interventions. Coronary cannulation after TAVI is affected by the individual patient's anatomy (like coronary take-off height, sinus of Valsalva, and sinotubular junction size), implantation depth of prosthesis, and the orientation of the prosthesis as regard to coronary ostia [5, 29, 30, 40–43]. When dealing with ESEP, computed tomography allowed to recognize as adverse orientations two conditions: coronary ostium below the skirt and coronary ostium behind triangular commissural post [40]. In the same study, as high as 34.8% of patients have been found to have such "unfavorable" coronary access features after ESEP. A higher implantation depth is associated with a higher coronary access failure [25]. This is important because the recent cusp-overlap technique [44, 45], which demonstrated to significantly reduce the rate of atrioventricular conduction disturbance post-TAVI, aims to implant TAVI higher to reduce left bundle branch damage. Tang et al. [43] first

**Table 12.1** Overview of coronary angiography and PCI after TAVI

| Study | Prosthesis type | Coronary procedures attempted | Failure |
|---|---|---|---|
| Faroux (2021) [24] | Medtronic Evolut R/PRO<br>Edwards SAPIEN XT/3/ULTRA<br>Inovare<br>Boston Scientific Acurate neo<br>Abbott Portico<br>Centera<br>Lotus | 102 PCI attempted in STEMI after TAVI patients<br>103 CA | PCI:<br>14 failure (5 failure to cannulate coronary ostium)<br>18 nonselective injection<br>9 guide catheter extension<br>Coronary angiography:<br>0 failure.<br>Left coronary artery:<br>>2 catheters used 6<br>Nonselective injection 23<br>Right coronary artery:<br>>2 catheters used 11<br>Nonselective injection 25<br>Significant higher rate of nonselective cannulation, PCI failure, use of catheter guided extension than control NON-TAVI patient |
| Barbanti et al. (2020) [25] | Medtronic Evolut R/PRO<br>Edwards SAPIEN 3/ULTRA<br>Boston Scientific Acurate neo<br>Abbott Portico | 123 (CA)<br>96 (CA)<br>72 (CA)<br>9 (CA) | 22<br>1<br>0<br>0 |
| Nai Fovino et al. (2020) [26] | Edwards Lifesciences, Sapien 3 and Ultra<br>Medtronic, Evolut R and Pro Boston Scientific, Acurate Neo | 72 (CA)<br>23 (CA)<br>39 (CA) | 0<br>0<br>0 |
| Tarantini et al. (2020) [27] | Edwards Lifesciences, Sapien 3 | 68 (CA)<br>50 (PCI) | 0 (CA)<br>1 (PCI) due to coronary guidewire perforation |
| Faroux et al. (2020) [28] | Self-expanding valves<br>Balloon-expandable valves<br>Valve-in-Valve | 163 (CA)<br>90 (PCI) | Self-expanding valves (CoreValve or Evolut R):<br>4 Nonselective CA (3 RCA; 1 LM)<br>2 PCI failure due to coronary access issues |
| Couture et al. (2020) [29] | Medtronic Evolut R, Pro | 10 (CA)<br>2 (PCI) | 6 (RCA) and 4 (LCA) with nonselective injection<br>1 (PCI) inability to selectively cannulate the RCA |

(continued)

**Table 12.1** (continued)

| Study | Prosthesis type | Coronary procedures attempted | Failure |
|---|---|---|---|
| Faroux et al. (2020) [30] | Edwards Sapien XT or Sapien 3 | 53 (CA)<br>23 (PCI) | 3 (LCA) and 20 (RCA) nonselective injection<br>2 (PCI) inability to selectively cannulate |
| Gonçalves et al. (2020) [31] | Medtronic CoreValve, Evolut R, Pro<br>Edwards Sapien XT, 3 | 11 PCI | 4 |
| Tanaka et al. (2019) [32] | Medtronic Corevalve and Evolut R | 32 (CA)<br>30 (PCI) | (16 RCA coro; 4 LM coro)<br>2 (PCI) |
| Htun et al. (2017) [33] | Medtronic CoreValve and Evolut R | 43 (CA)<br>29 (PCI) | 1 (LM coro)<br>3 (RCA coro)<br>0 (PCI) |
| Boukantar et al. (2017) [34] | Medtronic Corevalve | 16 (CA)<br>7 (PCI) | 7<br>1 |
| Zivelonghi et al. (2016) [35] | Medtronic Evolut R<br>Edwards Sapien 3 | Evolut R: 25 CA, 6 PCI<br>Sapien 3: 41 (CA), 13 (PCI) | Evolut R: 1 (coro) 0 (PCI)<br>Sapien 3: 0 (coro); 0 (PCI) |
| Chetcuti et al. (2016) [36] | Medtronic Corevalve | 190 (CA)<br>113 (PCI) | 4 (CA)<br>10 (PCI) |
| Chakravarty et al. (2016) [37] | Medtronic Corevalve<br>Edwards Sapien | Corevalve/Evolut R: 4 PCI LM<br>Edwards Sapien: 5 PCI LM | 0<br>0 |
| Allali et al. (2016) [38] | Medtronic Corevalve | 24 (PCI) | 1 |
| Blumenstein et al. (2015) [39] | Edwards Sapien XT<br>Medtronic Corevalve<br>Symetis<br>Jenavalve Jena<br>Abbott Portico | Sapien XT:<br>19 selective CA; 8 PCI<br>CoreValve:<br>10 CA<br>Symetis:<br>4 CA, 1 PCI<br>Jena:<br>1 CA;<br>Portico:<br>1 CA; 1 PCI | Sapien XT:<br>0 CA; 0 PCI<br>CoreValve:<br>1 failure CA, 6 nonselective CA<br>Symetis:<br>2 nonselective CA, 0 PCI<br>Jena:<br>0 CA<br>Portico:<br>0 CA: 0 PCI |

*CA* coronary angiography, *LM* left main artery, *PCI* percutaneous coronary intervention, *RCA* right coronary artery, *TAVI* transcatheter aortic valve implantation

described a technique that permits to improve neo-commissures alignment rate during TAVI with Evolut devices; this technique has been further improved by Bieliauskas et al. [46] with a patient-specific technique. The width of Sinus of Valsalva is a critical parameter to evaluate before TAVI implantation because a

reduced width is associated with a higher rate of procedural coronary obstruction (due to acute occlusion of a coronary ostium by a native valve leaflet or prosthetic frame) and increased difficulty in post-TAVI coronary ostia cannulation (a wider sinus of Valsalva allows more space for manipulation of the catheter) [5]. The other fundamental anatomical parameter is the height of the coronary ostia, in general, the lower they are, the greater the risk of them being hidden by the valve prosthesis frame. Numerous studies and registries have shown greater difficulty in performing coronary angiography after TAVI in patients with SEP [24–39]. Algorithms have been proposed in choosing the coronary catheter in patients undergoing TAVI with Evolut valves [5]. In general, with regard to left main coronary angiography, the JL3.5 or the JL3.0 catheters should be used as the first choice (usually it's required a smaller catheter than usual) and in case of failure, a left guide catheter (FL3, EBU3, or XB3) Ikari Right 1.0/1.5 catheter or JR4 catheter must be used with the help of the coronary guidewire. If it is impossible to cannulate the coronary arteries during a coronary angiography selectively, it is always possible to perform an aortography with non-selective coronary angiography. The first choice is always the JR4 catheter for the right coronary catheter engagement. In case of failure with the JR4 and if the commissure of the prosthesis is in front of the ostium (i.e., the catheter cannot enter the cell of the frame in front of the ostium) or the skirt of the frame is high, it is useful to use a Multipurpose (MP) or Ikari Right 1.5 with the help of the coronary guidewire [5]. If the commissural posts are away from coronary ostia, it can use an AR2 catheter as a second line [5]. Guide extension catheter is a helpful tool for PCI in TAVI recipient [47, 48].

Figure 12.2 shows the post-TAVI appearance of a right coronary artery (RCA) ostium with low take-off from a small Sinus of Valsalva (SOV) with the triangular commissural post that is very close. It is evident that this configuration may hinder coronary cannulation since the ostium cannot be reached navigating outside the ESEP frame (no space between the Aorta wall and prosthesis) and the neo-cusp commissural edges may interfere with the rotation of the catheter. In this condition, after having experienced difficulties in rotating the catheter at the level of RCA take-off, successful selective cannulation is obtained by rotating the catheter at a higher level and then pushing it into the upper "jailing" prosthesis' cell Fig. 12.2. The image allows also us to recognize how a 6 F guiding catheter may fit well even into the half of a jailing cell. Once such selective cannulation is achieved, high-quality coronary angiography and eventual PCI can easily be performed.

Another specific setting associated with coronary access concern is represented by "TAV-in-TAV" configuration. This technique represents an established option for the bail-out treatment of suboptimal TAVI acute results [49]. Furthermore, "TAV-in-TAV" has recently started to be considered as a selective treatment to be offered for patients with failed TAVI prosthesis [50]. When TAV-in-TAV is performed using two ESEPs, the overlapping frames cannot be perfectly aligned, and this creates new cells with unpredictable shapes and sizes. Figure 12.3 shows the appearance of a right coronary artery (RCA) ostium after TAV-in-TAV was performed by implanting an ESEP after too low first ESEP implantation. The figure allows appreciation

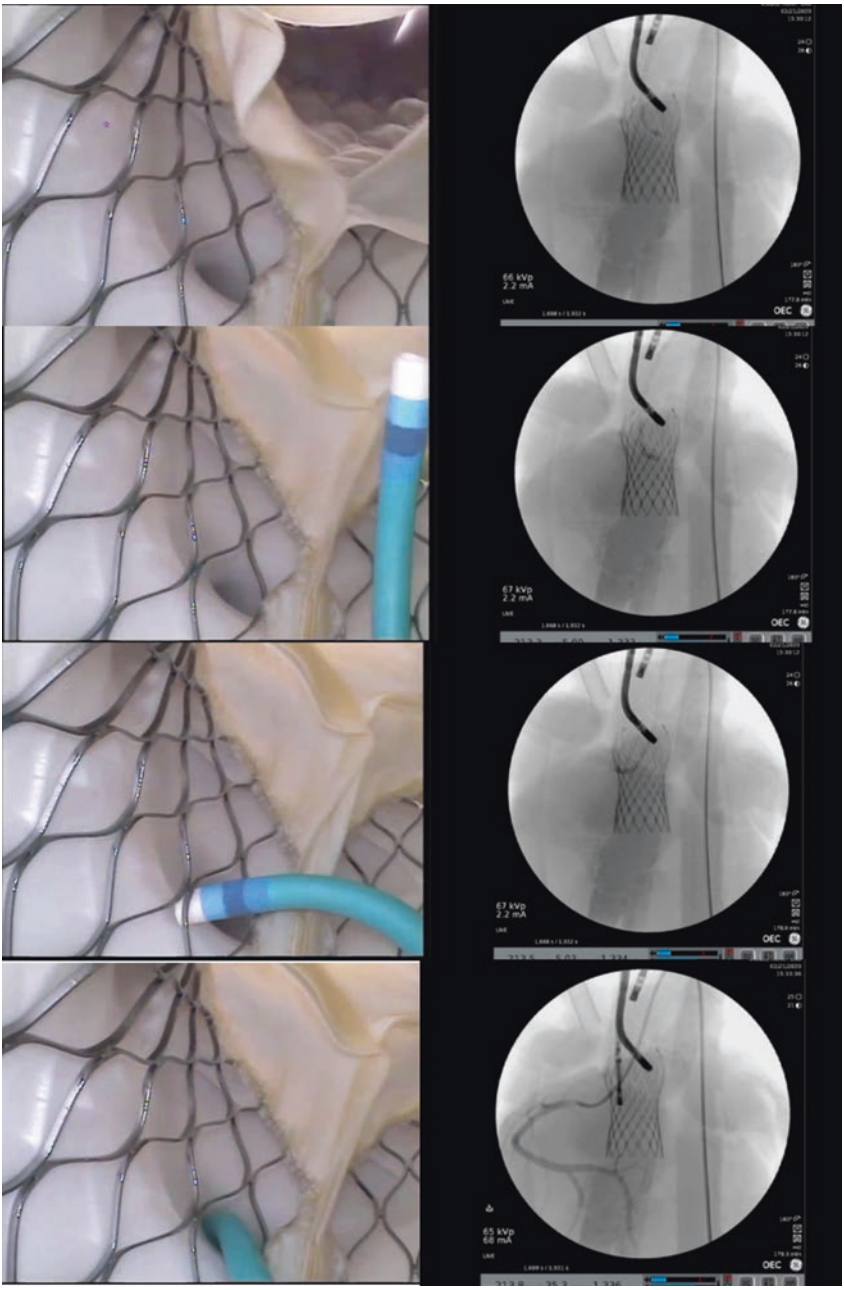


**Fig. 12.2** Selective coronary angiography in a right coronary artery after implantation of Evolut self-expandable prosthesis with unfavorable orientation

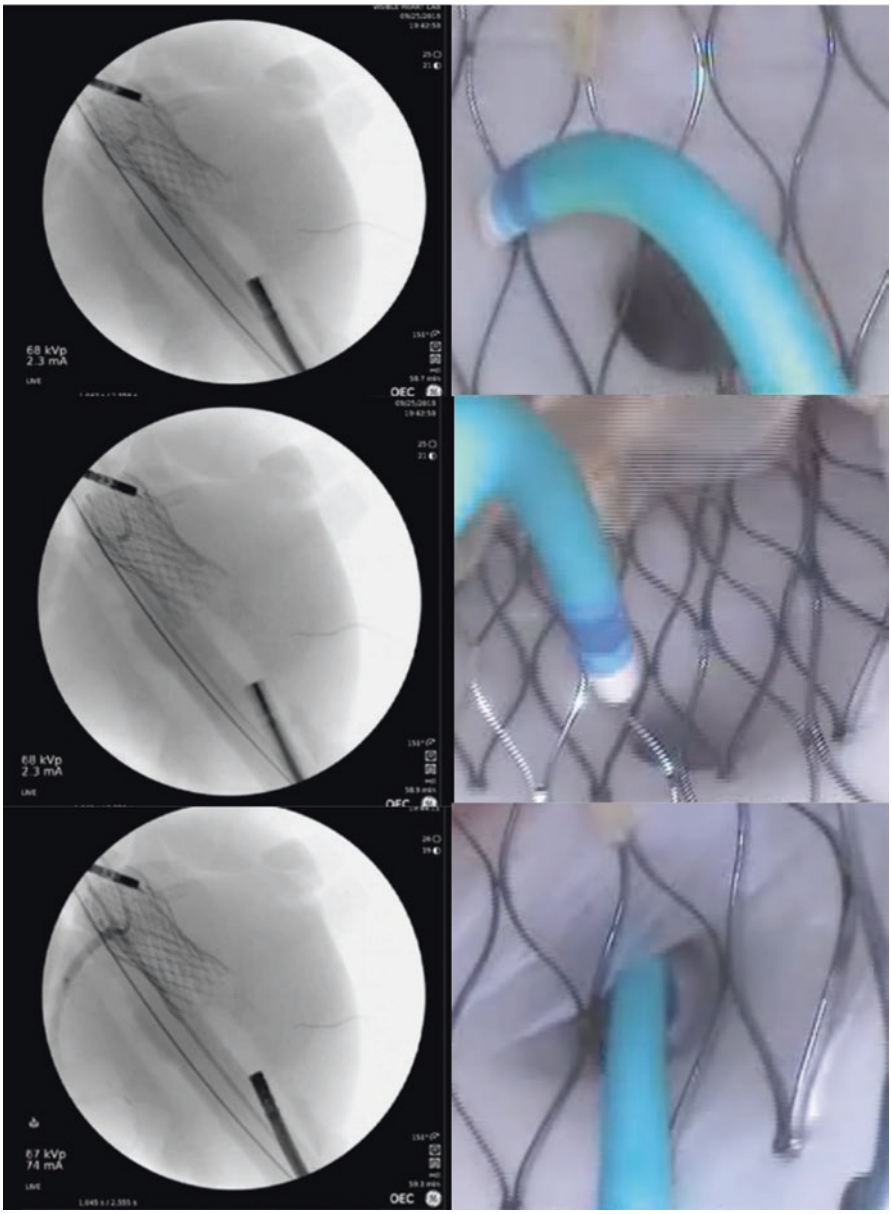


**Fig. 12.3** Selective coronary angiography in a right coronary artery after TAV-in-TAV with two Evolut self-expandable prostheses

of the overlapping ESEP frames causing new, smaller cells to cover the coronary ostium. Of note, the resulting cells are large enough to allow 6F guiding catheter crossing so that selective coronary angiography is performed Fig. 12.3.

## 12.3 Coronary Artery Occlusion Prevention

Coronary artery obstruction (CAO) represents a well-recognized, major complication of TAVI [51]. More recently, it has been highlighted that CAO may occur later after successful TAVI [52]. Table 12.2 shows an overview of coronary occlusion occurrence during TAVI [53–64]. Many factors [65] have been associated with an increased risk of coronary artery occlusion. The most important factors are: low coronary ostium height (<12 mm), shallow sinus of Valsalva (<30 mm), bulky and focal calcified aortic leaflets, previous surgical aortic valve (especially if externally mounted bioprosthetic valve leaflets, stentless bioprosthetic valves, or planned bioprosthetic valve fracture), leaflet length greater than corresponding coronary height and reduced virtual transcatheter valve to ostium (VTC) width (<4 mm). When the risk of CAO is recognized as not negligible, different technical strategies for coronary patency protection might be considered [65].

The less invasive coronary protection technique is represented by the placement of a coronary guiding catheter (usually with a guidewire and eventually with an uninflated stent) inside the coronary artery with high occlusion risk. Although obviously less effective than preventive ostial stenting [66], this technique has the advantage of avoiding implant stents in those patients who, despite baseline risk, did not develop CAO.

Figure 12.4 shows ESEP implantation with guiding catheter protection in low left main take-off. According to this technique, the decision to implant a stent is made after having implanted the prosthesis and the possibility of delivering the stent is warranted by the "jailed" guiding catheter. Of note, the possibility of having delayed CAO occurring after guidewire and guiding catheter removal does exist [66] and should be taken into account.

When the risk of CAO is unacceptable, preventive coronary stent implantation represents a valuable option that has recently been documented to be associated with good long-term outcome [66].

To date, stent implantation from the coronary ostium to the aorta outside the TAVI prosthesis according to the Chimney/Snorkel technique [67] represents a widely adopted strategy [68].

Figure 12.5 shows the steps of the Chimney/Snorkel technique to protect the low-take-off left main during ESEP implantation (with adverse prosthesis orientation). After balloon removal, the delivered stent is able to displace the ESEP from the aortic wall, and this should warrant coronary flow maintenance. Yet, the final configuration of the coronary stent and the ESEP frame looks extremely complex (Fig. 12.5) making repeat coronary angiography cumbersome. Moreover, the occurrences of Chimney/Snorkel stent external compression by the ESEP [69] and sinus

**Table 12.2** Overview of coronary occlusion occurrence during TAVI

| Study | Prosthesis type | Coronary occlusion | Management |
|---|---|---|---|
| Mangieri et al. (2022) [53] | Corevalve, Evolut R, and Evolut PRO (139 Valve-in-Valve TAVI) | 4 (acute coronary occlusion) | PCI without sequelae |
| Low Risk Bicuspid Study (2021) [54] | Evolut or Evolut PRO (150 with bicuspid aortic valve) | 1 | Emergency CABG |
| Gallo et al. (2021) [55] | 160 TAVI-in-TAVI Evolut valves, Sapien valves | 0.6% | No specified the management |
| Carrol et al. (2020) [56] | All device available in USA from 2010 to 2019 (276.316) | No data on coronary occlusion but:<br>PCI (30-days): 1.9%, 572<br>CPB: 0.4% | We have only indirect data.<br>In 2019 BASILICA was performed 166. |
| Evolut Low Risk Trial (2019) [14] | CoreValve, Evolut R, or Evolut PRO (725 attempted, 706 per protocol) | 0.9% (6.5 patients) | 2 death after attempted CABG |
| Partner 3 Trial (2019) [57] | Sapien 3 (496 assigned, 495 treated) | 1 | PCI without sequelae |
| Evolut R U.S. Study (2017) [58] | Evolut R (241) | 1 | PCI without sequelae |
| Surtavi Trial (2017) [59] | CoreValve (724), Evolut R (139) | 0.2% (1.7 patients) | 0 deaths. No specified the management |
| Bicuspid AS TAVI Multicenter Registry (2017) [60] | Sapien, Sapien 3 CoreValve, Evolut R Lotus<br>(546 Bicuspid TAVI matched with 546 Tricuspid TAVI) | 5 (Bicuspid)<br>3 (Tricuspid) | No specified the management |
| Partner 2 Trial (2016) [13] | Sapien XT (2032 TAVI) | 4 | 1 death. No specified the management |
| Holmes et al. (2015) [61] | CoreValve and Sapien/ Sapien XT (26.378) | 1.743 (both Sapien and CoreValve) | Data no available |
| CoreValve Study (2014) [62] | CoreValve (795) | 0 | 0 |
| Ribeiro et al. (2013) [63] | Balloon-expandable valve: Sapien/Sapien XT (4580)<br>Self-expandable valve: CoreValve (2073) | Sapien/Sapien XT 37<br>CoreValve 7 | PCI (75% of the patients) with success rate of 81.8%.<br>Urgent CABG or mechanical hemodynamic support (14%) |
| Partner Trial (2010) [64] | Sapien (179) | 0 | / |

*CABG* coronary artery bypass graft surgery, *CPB* cardiopulmonary bypass, *PCI* percutaneous coronary intervention, *TAVI* transcatheter aortic valve implantation

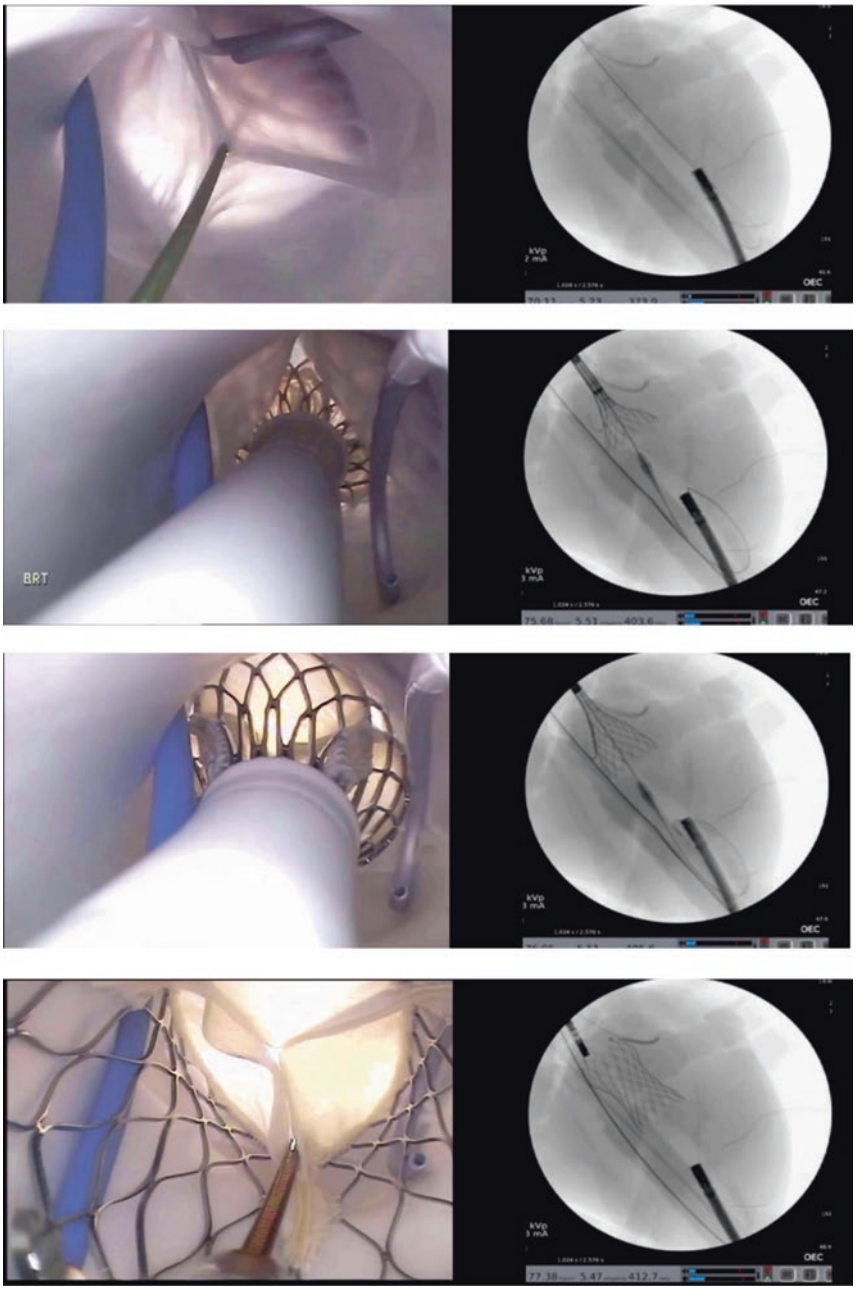


**Fig. 12.4** "Protection" of the left main coronary with 6F Judkins guiding catheter and coronary guidewire during TAVI

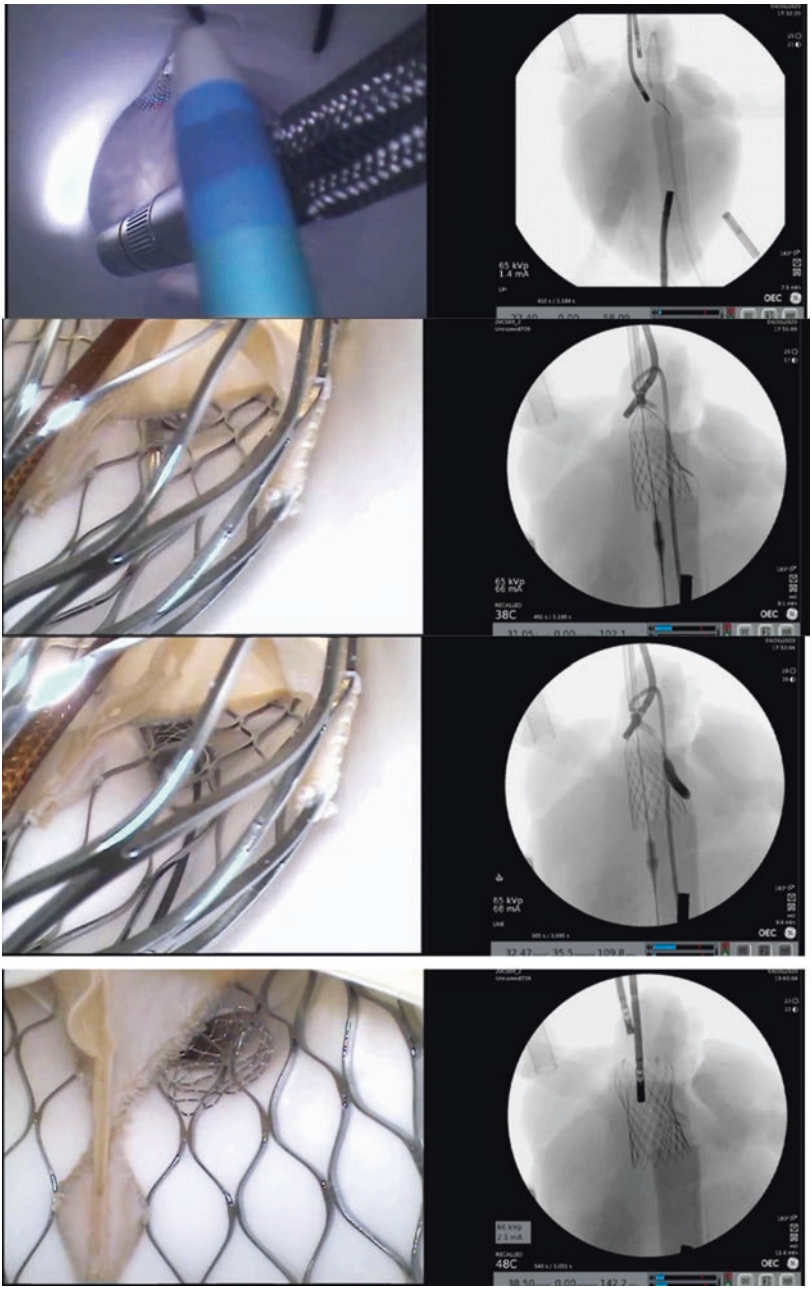


**Fig. 12.5** Chimney/Snorkel technique to protect low-take-off left main during ESEP implantation (with adverse prosthesis orientation)

of Valsalva thrombosis [70] due to impaired blood flow have been recently described. The need to implant a stent on a not diseased Left Main artery in a position with impaired blood flow has reduced enthusiasm for this technique and sought to find new possibilities.

## 12.4 Ostial Coronary Stenting Through the Prosthesis Frame

During the clinical practice, the need to stent the coronary ostia may emerge in conditions where Chimney/Snorkel technique may not be practiced. These conditions include the development of new disease in the proximal artery segment and the occurrence of CAO after TAVI conducted without the set-up for the Chimney/Snorkel technique. Anytime decision to implant the coronary stent after ESEP implantation, it is reasonable attempting this by re-accessing the coronary artery from the inner part of the prosthesis.

Figure 12.6 shows the bail-out management of post-TAVI partial coronary obstruction due to dislodgement of the native aortic leaflet. The partially occluded ostium and the corresponding prosthesis frame are crossed with a guiding catheter and guidewire. Then, a stent of the appropriate length to reach the prosthesis frame is delivered. Due to the more "anatomical" configuration (as compared with the Chimney/snorkel technique) of the stent/prosthesis frame achieved, this technique, named "Orthotopic" Snorkel-Stenting Technique [71], has been recently, electively practiced to maintain coronary patency during high-risk TAVI with transcatheter aortic valve replacement with ESEP.

Basilica Technique: An alternative technique to Chimney/Snorkel technique in preventing coronary artery obstruction during TAVI is BASILICA (Bioprosthetic or native Aortic Scallop Intentional Laceration to prevent Iatrogenic Coronary Artery obstruction during TAVI) technique [72]. This technique consists of the intentional laceration by the electricity of native or prosthetic leaflets before transcatheter prosthesis implantation [65, 73]. The target aortic leaflet is traversed with a guidewire supported by a microcatheter in order to insulate the guidewire. Once the guidewire crosses the leaflet, its distal end is captured using snare retrieval. Then the guidewire is electrified using an electrosurgical generator. The resulting laceration allows the leaflet to splay open [74] (Fig. 12.7). BASILICA technique has outcomes similar to Chimney/Snorkel technique, but it has never been performed a study to compare them. It is associated with an increased risk of periprocedural stroke [75], so it has been suggested to use a cerebral protection device when it is performed. One-year outcomes are reassuring [76]. One of the main limitations of this procedure is the complexity and the absence of clear predictive parameters. It reduces neosinus and sinus stasis [77]. It is actually performed only in a few centers at very high volume, but it potentially could resolve periprocedural coronary obstruction avoiding implantation of stents in the left main coronary not diseased.

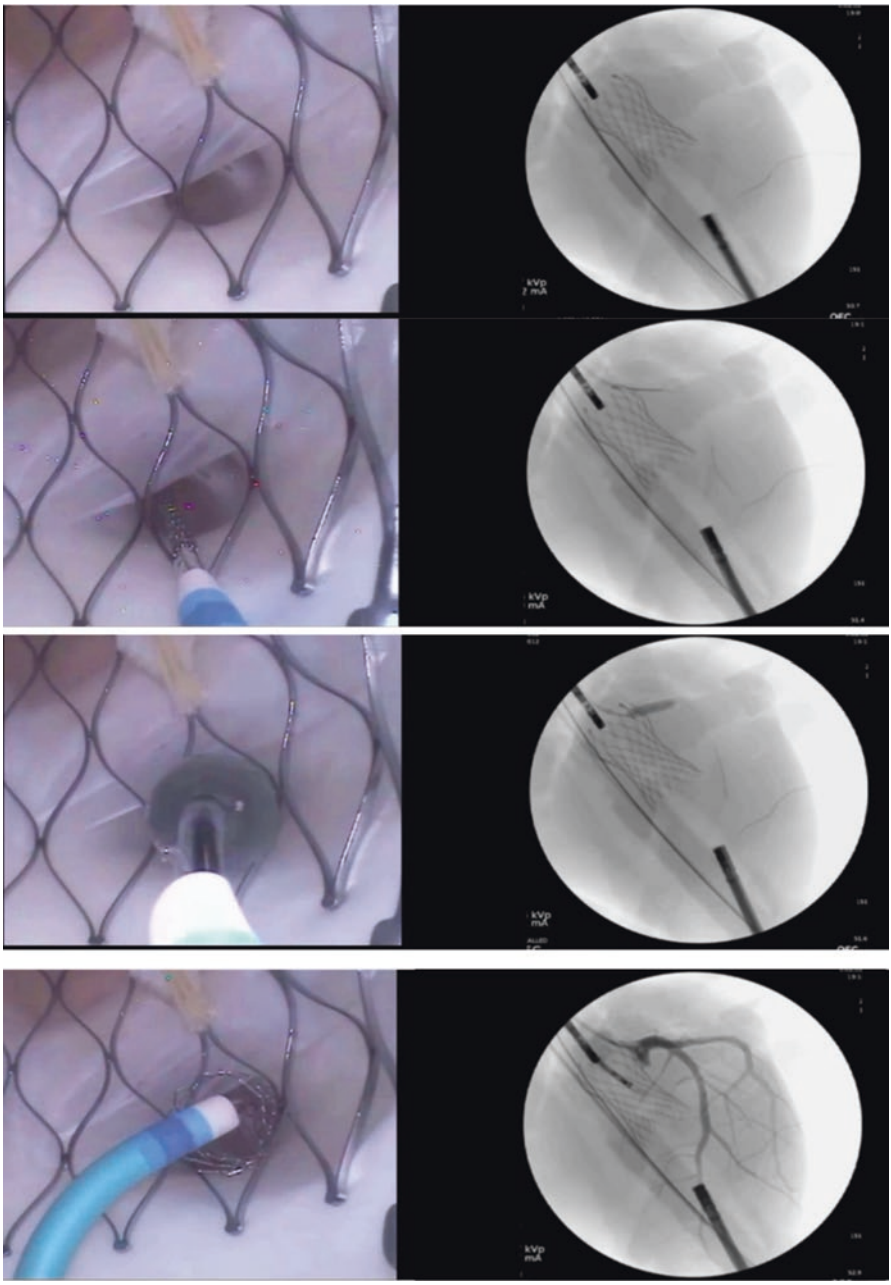

**Fig. 12.6** "Inner-snorkel" technique for bail-out management of post-TAVI partial coronary obstruction. Incomplete obstruction of a RCA with low take-off is caused by dislodgement of the native aortic leaflet. The partially occluded cell is crossed with a guiding catheter and guidewire. A stent of appropriate length to reach the prosthesis frame is selected and delivered to achieve "inner-snorkel" configuration with good angiographic result

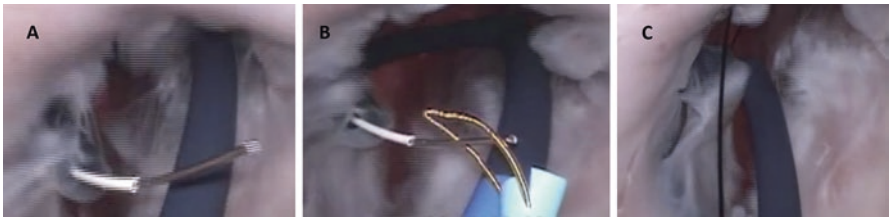


**Fig. 12.7** BASILICA technique. (**a**) An electrified guidewire perforates the leaflet. (**b**) The guidewire distal end is snared. (**c**) Laceration of the leaflet

## 12.5 Conclusion

TAVI with ESEP creates new anatomy where the geometrical relationship between individual patient anatomy and implanted prosthesis location and orientation may hinder coronary access and cause coronary obstruction. Coronary techniques standardization, deep understanding, and standardization represent a pivotal aspect of improving the management of patients treated by TAVI, which may benefit from procedure simulations in a beating heart model.

**Authors' Disclosures** Francesco Burzotta, received speaker's fees from Abbott, Medtronic, and Abiomed. Other authors have no conflicts of interest.

## References

1. Vahanian A, Beyersdorf F, Praz F, ESC/EACTS Scientific Document Group, ESC Scientific Document Group et al (2022) 2021 ESC/EACTS guidelines for the management of valvular heart disease. Eur Heart J 43:561–632
2. Otto CM, Nishimura RA, Bonow RO, Writing Committee Members et al (2021) 2020 ACC/AHA guideline for the management of patients with valvular heart disease: executive summary: a report of the American College of Cardiology/American Heart Association Joint Committee on clinical practice guidelines. J Am Coll Cardiol 77:450–500
3. Cangemi S, Aurigemma C, Romagnoli E et al (2022) Management of concomitant coronary artery disease and aortic valve stenosis in the era of transcatheter aortic valve treatment. Minimally invasive Surg 6:3
4. Mentias A, Desai MY, Saad M et al (2020) Incidence and outcomes of acute coronary syndrome after transcatheter aortic valve replacement. JACC Cardiovasc Interv 13(8):938–950
5. Yudi MB, Sharma SK, Tang GHL, Kini A (2018) Coronary angiography and percutaneous coronary intervention after transcatheter aortic valve replacement. J Am Coll Cardiol 71(12):1360–1378
6. Arai T, Lefèvre T, Hovasse T et al (2017) Incidence and predictors of coronary obstruction following transcatheter aortic valve implantation in the real world. Catheter Cardiovasc Interv 90(7):1192–1197
7. Sammour Y, Banerjee K, Kumar A et al (2021) Systematic approach to high implantation of SAPIEN-3 valve achieves a lower rate of conduction abnormalities including pacemaker implantation. Circ Cardiovasc Interv 14(1):e009407

8. Coughlan JJ, Kiernan T, Mylotte D, Arnous S (2018) Annular rupture during transcatheter aortic valve implantation: predictors, management and outcomes. Interv Cardiol 13(3):140–144
9. Walther T, Hamm CW, Schuler G, Berkowitsch A, Kötting J, Mangner N, GARY Executive Board et al (2015) Perioperative results and complications in 15,964 transcatheter aortic valve replacements: prospective data from the GARY registry. J Am Coll Cardiol 65(20):2173–2180
10. Solomonica A, Choudhury T, Bagur R (2018) The mechanically expandable LOTUS Valve and LOTUS Edge transcatheter aortic valve systems. Expert Rev Med Devices 15(11):763–769
11. Buellesfeld L, Gerckens U, Grube E (2008) Percutaneous implantation of the first repositionable aortic valve prosthesis in a patient with severe aortic stenosis. Catheter Cardiovasc Interv 71:579–584
12. Moriyama N, Shishido K, Yokota S et al (2022) Coronary access after TAVR with a cylindrical shaped valve: learning from LOTUS. Cardiovasc Revasc Med 37:23–33
13. Leon MB, Smith CR, Mack MJ et al (2016) Transcatheter or surgical aortic-valve replacement in intermediate-risk patients. N Engl J Med 374:1609–1620
14. Popma JJ, Deeb GM, Yakubov SJ, Evolut Low Risk Trial Investigators et al (2019) Transcatheter aortic-valve replacement with a self-expanding valve in low-risk patients. N Engl J Med 380:1706–1715
15. De Backer O, Pilgrim T, Simonato M et al (2018) Usefulness of transcatheter aortic valve implantation for treatment of pure native aortic valve regurgitation. Am J Cardiol 122(6):1028–1035
16. Hase H, Yoshijima N, Yanagisawa R, OCEAN-TAVI Investigators et al (2021) Transcatheter aortic valve replacement with Evolut R versus Sapien 3 in Japanese patients with a small aortic annulus: the OCEAN-TAVI registry. Catheter Cardiovasc Interv 97(6):E875–E886
17. Ribeiro HB, Nombela-Franco L, Urena M et al (2013) Coronary obstruction following transcatheter aortic valve implantation: a systematic review. JACC Cardiovasc Interv 6(5):452–461
18. Sengupta A, Alexis SL, Lee T et al (2021) Cusp overlap technique: should it become the standard implantation technique for self-expanding valves? Curr Cardiol Rep 23(11):154
19. Jilaihawi H, Zhao Z, Du R, Staniloae C et al (2019) Minimizing permanent pacemaker following repositionable self-expanding transcatheter aortic valve replacement. JACC Cardiovasc Interv 12(18):1796–1807
20. Chinchoy E, Soule CL, Houlton AJ et al (2000) Isolated four-chamber working swine heart model. Ann Thorac Surg 70(5):1607–1614
21. Valenzuela TF, Burzotta F, Iles TL, Lassen JF, Iaizzo PA (2021) Assessment of single and double coronary bifurcation stenting techniques using multimodal imaging and 3D modeling in reanimated swine hearts using Visible Heart® methodologies. Int J Cardiovasc Imaging 37(9):2591–2601
22. Sanchez JZ, Burzotta F, Valenzuela T, Lassen JF, Iles T, Iaizzo PA (2021) Direct visualization of TAVR-related coronary artery management techniques in reanimated beating hearts. JACC Cardiovasc Interv 14(9):e87–e91
23. Lawton JS, Tamis-Holland JE, Bangalore S et al (2022) 2021 ACC/AHA/SCAI guideline for coronary artery revascularization: a report of the American College of Cardiology/American Heart Association Joint Committee on clinical practice guidelines. J Am Coll Cardiol 79(2):e21–e129
24. Faroux L, Lhermusier T, Vincent F et al (2021) ST-segment elevation myocardial infarction following transcatheter aortic valve replacement. J Am Coll Cardiol 77(17):2187–2199
25. Barbanti M, Costa G, Picci A et al (2020) Coronary cannulation after transcatheter aortic valve replacement: the RE-ACCESS study. JACC Cardiovasc Interv 13(21):2542–2555
26. Nai Fovino L, Scotti A, Massussi M et al (2020) Coronary angiography after transcatheter aortic valve replacement (TAVR) to evaluate the risk of coronary access impairment after TAVR-in-TAVR. J Am Heart Assoc 9(13):e016446
27. Tarantini G, Nai Fovino L, Le Prince P et al (2020) Coronary access and percutaneous coronary intervention up to 3 years after transcatheter aortic valve implantation with a balloon-expandable valve. Circ Cardiovasc Interv 13(7):e008972

28. Faroux L, Munoz-Garcia E, Serra V et al (2020) Acute coronary syndrome following transcatheter aortic valve replacement. Circ Cardiovasc Interv 13(2):e008620
29. Couture T, Faroux L, Junquera L et al (2020) Interaction between self-expanding transcatheter heart valves and coronary ostia: an angiographically based analysis of the Evolut R/Pro valve system. J Invasive Cardiol 32(4):123–128
30. Faroux L, Couture T, Guimaraes C et al (2020) Interaction between balloon-expandable valves and coronary ostia: angiographic analysis and impact on coronary access. J Invasive Cardiol 32(6):235–242
31. Gonçalves M, de Araújo Gonçalves P, Campante Teles R et al (2021) Low rate of invasive coronary angiography following transcatheter aortic valve implantation: real-world prospective cohort findings. Cardiovasc Revasc Med 28:42–49
32. Tanaka A, Jabbour RJ, Testa L et al (2019) Incidence, technical safety, and feasibility of coronary angiography and intervention following self-expanding transcatheter aortic valve replacement. Cardiovasc Revasc Med 20(5):371–375
33. Htun WW, Grines C, Schreiber T (2018) Feasibility of coronary angiography and percutaneous coronary intervention after transcatheter aortic valve replacement using a Medtronic™ self-expandable bioprosthetic valve. Catheter Cardiovasc Interv 91(7):1339–1344
34. Boukantar M, Gallet R, Mouillet G et al (2017) Coronary procedures after TAVI with the self-expanding aortic bioprosthesis Medtronic CoreValve™, not an easy matter. J Interv Cardiol 30(1):56–62
35. Zivelonghi C, Pesarini G, Scarsini R et al (2017) Coronary catheterization and percutaneous interventions after transcatheter aortic valve implantation. Am J Cardiol 120(4):625–631
36. Chetcuti S, Kleiman NS, Matthews R, Popma JJ, Moore J (2016) TCT-743: percutaneous coronary intervention after self-expanding transcatheter aortic valve replacement (abstr). J Am Coll Cardiol 68(Suppl B):B300–B301
37. Chakravarty T, Sharma R, Abramowitz Y et al (2016) Outcomes in patients with transcatheter aortic valve replacement and left main stenting: the TAVR-LM registry. J Am Coll Cardiol 67(8):951–960
38. Allali A, El-Mawardy M, Schwarz B et al (2016) Incidence, feasibility and outcome of percutaneous coronary intervention after transcatheter aortic valve implantation with a self-expanding prosthesis. Results from a single center experience. Cardiovasc Revasc Med 17(6):391–398
39. Blumenstein J, Kim WK, Liebetrau C et al (2015) Challenges of coronary angiography and intervention in patients previously treated by TAVI. Clin Res Cardiol 104(8):632–639
40. Ochiai T, Chakravarty T, Yoon SH et al (2020) Coronary access after TAVR. JACC Cardiovasc Interv 13(6):693–705. https://doi.org/10.1016/j.jcin.2020.01.216
41. Abdelghani M, Landt M, Traboulsi H, Becker B, Richardt G (2020) Coronary access after TAVR with a self-expanding bioprosthesis: insights from computed tomography. JACC Cardiovasc Interv 13(6):709–722
42. Rogers T, Greenspun BC, Weissman G et al (2020) Feasibility of coronary access and aortic valve reintervention in low-risk TAVR patients. JACC Cardiovasc Interv 13(6):726–735
43. Tang GHL, Zaid S, Fuchs A et al (2020) Alignment of transcatheter aortic-valve neocommissures (ALIGN TAVR): impact on final valve orientation and coronary artery overlap. JACC Cardiovasc Interv 13(9):1030–1042
44. Pascual I, Hernández-Vaquero D, Alperi A et al (2022) Permanent pacemaker reduction using cusp-overlapping projection in TAVR: a propensity score analysis. JACC Cardiovasc Interv 15(2):150–161
45. Tang GHL, Zaid S, Michev I et al (2018) "Cusp-overlap" view simplifies fluoroscopy-guided implantation of self-expanding valve in transcatheter aortic valve replacement. JACC Cardiovasc Interv 11(16):1663–1665
46. Bieliauskas G, Wong I, Bajoras V et al (2021) Patient-specific implantation technique to obtain neo-commissural alignment with self-expanding transcatheter aortic valves. JACC Cardiovasc Interv 14(19):2097–2108
47. Bharadwaj AS, Bhatheja S, Sharma SK, Kini AS (2018) Utility of the guideliner catheter for percutaneous coronary interventions in patients with prior transcatheter aortic valve replacement. Catheter Cardiovasc Interv 91(2):271–276

48. Jackson M, Williams PD (2018) Coronary access following TAVI – selective coronary engagement using balloon-assisted tracking of a guide catheter extension. Cardiovasc Revasc Med 19(3 Pt B):384–389
49. Witkowski A, Jastrzebski J, Dabrowski M, Chmielak Z (2014) Second transcatheter aortic valve implantation for treatment of suboptimal function of previously implanted prosthesis: review of the literature. J Interv Cardiol 27(3):300–307
50. Tchétché D, Siddiqui S (2020) TAV-in-TAV for failed prosthesis: the new frontier. EuroIntervention 16(2):e100–e102
51. Akinseye OA, Jha SK, Ibebuogu UN (2018) Clinical outcomes of coronary occlusion following transcatheter aortic valve replacement: a systematic review. Cardiovasc Revasc Med 19:229–236
52. Jabbour RJ, Tanaka A, Finkelstein A et al (2018) Delayed coronary obstruction after transcatheter aortic valve replacement. J Am Coll Cardiol 71:1513–1524
53. Mangieri A, Khokhar AA, Petronio AS et al (2022) Valve-in-valve implantation of Medtronic CoreValve prosthesis in patients with failing bioprosthetic aortic valves: mid-term outcomes from the Italian CoreValve clinical service project. J Invasive Cardiol 34(2):E73–E79
54. Forrest JK, Ramlawi B, Deeb GM et al (2021) Transcatheter aortic valve replacement in low-risk patients with bicuspid aortic valve stenosis. JAMA Cardiol 6(1):50–57
55. Gallo M, Fovino LN, Blitzer D et al (2022) Transcatheter aortic valve replacement for structural degeneration of previously implanted transcatheter valves (TAVR-in-TAVR): a systematic review. Eur J Cardiothorac Surg 61(5):967–976
56. Carroll JD, Mack MJ, Vemulapalli S et al (2020) STS-ACC TVT registry of transcatheter aortic valve replacement. J Am Coll Cardiol 76(21):2492–2516
57. Mack MJ, Leon MB, Thourani VH, PARTNER 3 Investigators et al (2019) Transcatheter aortic-valve replacement with a balloon-expandable valve in low-risk patients. N Engl J Med 380(18):1695–1705
58. Popma JJ, Reardon MJ, Khabbaz K et al (2017) Early clinical outcomes after transcatheter aortic valve replacement using a novel self-expanding bioprosthesis in patients with severe aortic stenosis who are suboptimal for surgery: results of the Evolut R U.S. study. JACC Cardiovasc Interv 10(3):268–275
59. Reardon MJ, Van Mieghem NM, Popma JJ, SURTAVI Investigators et al (2017) Surgical or transcatheter aortic-valve replacement in intermediate-risk patients. N Engl J Med 376(14):1321–1331
60. Yoon SH, Bleiziffer S, De Backer O et al (2017) Outcomes in transcatheter aortic valve replacement for bicuspid versus tricuspid aortic valve stenosis. J Am Coll Cardiol 69(21):2579–2589
61. Holmes DR Jr, Nishimura RA, Grover FL, STS/ACC TVT Registry et al (2015) Annual outcomes with transcatheter valve therapy: from the STS/ACC TVT Registry. J Am Coll Cardiol 66(25):2813–2823
62. Adams DH, Popma JJ, Reardon MJ, U.S. CoreValve Clinical Investigators et al (2014) Transcatheter aortic-valve replacement with a self-expanding prosthesis. N Engl J Med 370(19):1790–1798
63. Ribeiro HB, Webb JG, Makkar RR et al (2013) Predictive factors, management, and clinical outcomes of coronary obstruction following transcatheter aortic valve implantation: insights from a large multicenter registry. J Am Coll Cardiol 62(17):1552–1562
64. Leon MB, Smith CR, Mack M, PARTNER Trial Investigators et al (2010) Transcatheter aortic-valve implantation for aortic stenosis in patients who cannot undergo surgery. N Engl J Med 363(17):1597–1607
65. Lederman RJ, Babaliaros VC, Rogers T et al (2019) Preventing coronary obstruction during transcatheter aortic valve replacement: from computed tomography to BASILICA. JACC Cardiovasc Interv 12(13):1197–1216. https://doi.org/10.1016/j.jcin.2019.04.052. PMID: 31272666; PMCID: PMC6724191
66. Palmerini T, Chakravarty T, Saia F et al (2020) Coronary protection to prevent coronary obstruction during TAVR: a multicenter international registry. JACC Cardiovasc Interv 13:739–747

67. Fetahovic T, Hayman S, Cox S, Cole C, Rafter T, Camuglia A (2019) The prophylactic Chimney snorkel technique for the prevention of acute coronary occlusion in high risk for coronary obstruction transcatheter aortic valve replacement/implantation cases. Heart Lung Circ 28(10):e126–e130
68. Mercanti F, Rosseel L, Neylon A et al (2020) Chimney stenting for coronary occlusion during TAVR: insights from the chimney registry. JACC Cardiovasc Interv 13:751–761
69. Ristalli F, Meucci F, Bonechi F et al (2020) Severe compression of a left main coronary stent implanted using a chimney technique. JACC Cardiovasc Interv 13:141–142
70. Mangieri A, Gallo F, Popolo Rubbio A et al (2020) Outcome of coronary ostial stenting to prevent coronary obstruction during transcatheter aortic valve replacement. Circ Cardiovasc Interv 13(6):e009017
71. Burzotta F et al "Inner-snorkel" technique to maintain coronary patency during high-risk transcatheter aortic valve replacement with self-expandable prostheses. Cardiovasc Revasc Med. Jul;28S:94–97
72. Khan JM, Dvir D, Greenbaum AB et al (2018) Transcatheter laceration of aortic leaflets to prevent coronary obstruction during transcatheter aortic valve replacement: concept to first-in-human. JACC Cardiovasc Interv 11(7):677–689
73. Bruce CG, Greenbaum AB, Babaliaros VC, Rogers T, Lederman RJ, Khan JM (2021) Safeguards and pitfalls for bioprosthetic or native aortic scallop intentional laceration to prevent iatrogenic coronary artery obstruction during transcatheter aortic valve replacement-the BASILICA technique. Ann Cardiothorac Surg 10(5):700–707
74. Zhingre Sanchez JD, Iles TL, Dvir D, Iaizzo PA (2020) Direct visualisation of the BASILICA technique post TAVR to enhance coronary flow. EuroIntervention 16(8):680–681
75. Khan JM, Greenbaum AB, Babaliaros VC et al (2019) The BASILICA trial: prospective multicenter investigation of intentional leaflet laceration to prevent TAVR coronary obstruction. JACC Cardiovasc Interv 12(13):1240–1252
76. Khan JM, Greenbaum AB, Babaliaros VC et al (2021) BASILICA trial: one-year outcomes of transcatheter electrosurgical leaflet laceration to prevent TAVR coronary obstruction. Circ Cardiovasc Interv 14(5):e010238
77. Hatoum H, Maureira P, Lilly S, Dasi LP (2019) Impact of leaflet laceration on transcatheter aortic valve-in-valve washout: BASILICA to solve neosinus and sinus stasis. JACC Cardiovasc Interv 12(13):1229–1237

# Chapter 13
# Tissue-Engineered Heart Valves


**Jillian B. Schmidt, Zeeshan H. Syedain, and Robert T. Tranquillo**

## 13.1 Introduction

Mechanical and biological prosthetic heart valves and cryopreserved homograft valves have been used successfully to replace diseased and damaged heart valves in patients for several decades. However, drawbacks such as the limited long-term durability of bioprosthetic valves, the short supply of cryopreserved homografts, and the requirement of anticoagulation drug therapy for recipients of mechanical prosthetic valves motivate innovative improvement in heart valve replacement technologies [1]. In addition, mechanical and bioprosthetic valves are unable to grow with the patient, thus pediatric and young adult patients require multiple surgeries to replace the previously implanted prosthetic valves as they are outgrown. With these shortcomings in mind, researchers have begun work to develop a living TEHV that could be used as a replacement valve, particularly for young patients.

Design criteria for a TEHV include long-term durability, non-calcific, minimal regurgitation and systolic pressure drop, and the capacity to grow and adapt with the patient. The TEHV must also be non-thrombogenic and non-immunogenic to prevent clot formation and immune rejection, respectively. While the biomechanics of native heart valves are relatively well understood [2, 3], the goal of most TEHV researchers is to produce a tissue or regenerative scaffold at implantation that is much simpler than the tri-layer structure of the native leaflets [4] but is still functional. These design criteria are demanding, but researchers in the field of heart valve tissue engineering are becoming well-equipped to confront many of these issues.

J. B. Schmidt
Missouri University of Science and Technology, Rolla, MO, USA

Z. H. Syedain · R. T. Tranquillo (✉)
Department of Biomedical Engineering, University of Minnesota, Minneapolis, MN, USA
e-mail: tranquil@umn.edu

© The Author(s), under exclusive license to Springer Nature Switzerland AG 2023

P. A. Iaizzo et al. (eds.), *Heart Valves*, https://doi.org/10.1007/978-3-031-25541-0_13

In general, a TEHV is produced by forming a degradable scaffold material into the valve geometry then either seeding or entrapping a relevant cell type during in vitro culture or implanting the cell-free scaffold and recruiting cells to the scaffold in situ. Some approaches rely on seeded cells to produce extracellular matrix (ECM) components during an in vitro culture period, before removing these cells through a decellularization process and implanting the cell-free ECM [5–11]. The cell produced ECM components, specifically collagen, provide the mechanical strength necessary to maintain valve structure and function, and the TEHV undergoes further remodeling as cells repopulate the matrix in vivo. Many different combinations of scaffold materials, geometries, cells, and culture methods are possible, so research groups have developed different approaches to meet the TEHV design criteria. This chapter will provide an overview of the different methods currently employed for producing TEHVs. The chapter will conclude with results from recent preclinical and clinical studies and a discussion of the future directions and trends in TEHV research.

## 13.2 Current Methods of Heart Valve Tissue Engineering

Research groups around the world are working on developing TEHVs, using various types of cells, scaffolds, and culture methods. There are many possible combinations of materials and stimuli, and the interactions between the different components of tissue-engineered constructs are complex. Thus, the "optimal" TEHV fabrication and culture process has yet to be determined, and there is likely more than one way to produce an adequate TEHV, that is, one which is able to meet the aforementioned design criteria. Two main approaches will be discussed in this section: (i) TEHVs consisting of cell-produced ECM, requiring in vitro culture and (ii) TEHVs fabricated from bioresorbable synthetic polymeric scaffolds eliminating the need for in vitro culture. While there is also ongoing work investigating the use of decellularized valve homografts [12–19] and xenografts [20–27] for heart valve replacement, these approaches are considered out of the scope of this chapter.

### *13.2.1 Tissue-Engineered Matrix TEHVs*

Several research groups utilize a tissue-engineered matrix (TEM) approach to fabricate TEHVs. In this approach, relevant cells are seeded on or entrapped within a degradable scaffold material in the correct geometry. Then, during a period of in vitro culture, this scaffold is degraded and replaced by cell-produced ECM, crucially collagen, which provides the mechanical strength for the valve function. The scaffold must degrade at a rate that balances with the rate of ECM production, so that the cells are always provided with sufficient mechanical support. While early approaches focused on using possible autologous cell sources during TEHV

fabrication to create a patient-specific valve [28–32], more recent approaches have utilized allogeneic cells for matrix production and then decellularized the TEHVs prior to implantation [5–11]. This latter approach allows for the TEHVs to be utilized as "off-the-shelf" replacements, if the TEM induces recellularization post-implantation to achieve long-term durability.

Multiple groups are utilizing the TEM approach, but their choice of scaffold material, cell source, and culture conditions differ. One current approach to fabricating TEHVs is to seed cells onto a synthetic, degradable polymeric scaffold made from polyglycolic acid (PGA), polylactic acid (PLA), the PLGA copolymer, or polyhydroxyalkanoate polymers [6, 28, 33–37]. The synthetic polymer mesh is formed into a tri-leaflet valve geometry and vascular derived cells [6, 28, 33, 36], dermal fibroblasts [34, 35], or mesenchymal stem cells [37] are seeded onto the polymer mesh. The synthetic polymers provide the initial mechanical strength and stiffness and degrade in a period of weeks or months. The initial strength and stiffness of the synthetic polymer scaffolds are greater than the strength and stiffness of native heart valve tissue, but after several weeks of in vitro culture, TEHV mechanical properties become more similar to those of native heart valve tissue as the synthetic polymer degrades [28]. Upon completion of the in vitro culture process, these TEHVs can be decellularized using a detergent solution and can either be implanted cell-free [34–36] or re-seeded with a cell source such as autologous mesenchymal stem cells [6]. Figure 13.1 shows a decellularized TEHV created using this method.

In contrast to this synthetic polymer scaffold approach, fibrin, a biopolymer, can be used as a scaffold material. A fibrin gel is a highly hydrated network of entangled protein fibrils in which cells are entrapped, producing a completely biological TEHV [5, 7, 10, 11, 29, 31, 38–43]. Fibrin scaffolds are additionally advantageous, because the cell-mediated fibrin gel contraction can be used to achieve fiber alignment and anisotropy similar to that of native heart valve root and leaflets [11, 31]. With this method of TEHV fabrication, dermal fibroblasts are suspended in fibrinogen, and the addition of thrombin causes a fibrin gel to form. The suspension can be cast into a mold with the desired geometry, and the cells contract the fibrin gel around the mold surfaces. A fibrin gel is much weaker than native heart valve tissue,


**Fig. 13.1** Decellularized synthetic polymer-based TEM valve in closed (**a**), open (**b**), and cross-section (**c**) views. Vascular-derived cells were seeded on PGA/P4HB synthetic polymer matrix and cultured in vitro to allow for the deposition of cell-produced matrix components. Following the in vitro culture period, the TEHV was decellularized prior to implantation. (Reprinted from Driessen-Mol et al. [36] with permission from Elsevier. This article was published in Driessen-Mol et al. [36], Copyright American College of Cardiology Foundation (2014))

even after cell-mediated contraction of the fibril network. A significant challenge in the production of fibrin-based TEHVs is obtaining sufficient mechanical properties for in vivo function by inducing the cells to convert the aligned fibrin into aligned ECM of appropriate stiffness and sufficient strength, and optimized in vitro culture conditions and bioreactor conditioning are often utilized to accelerate this process. Similar to the PGA/P4HB-based TEHV discussed previously, the fibrin-based TEHVs can also be decellularized using a detergent solution, enabling "off-the-shelf" availability [5, 7, 10, 11].

Some fibrin-based approaches have utilized a mold for the fibrin gel that recreates the entire root and leaflet geometry [29, 31, 38–41], recently there has been increased focus on using this approach to create simpler geometries. For example, utilizing tubular tissues and sewing these tubes into a suitable valve geometry after the in vitro remodeling process is complete [5, 7, 10, 11, 42, 43]. Reimer et al. demonstrated the feasibility of a "tube-in-tube" design in which two of these engineered matrix tubes were sewn together to form the root and leaflet structures [7], and Syedain et al. utilized three tubes to create a tri-tube design (Fig. 13.2) with improved commissure stability [11]. There are no frames or stents present in these designs and because the sutures used are degradable, these TEHVs are intended to be suitable for a pediatric patient were growth is required.

In an alternative approach, researchers have developed a method of printing hydrogels in the geometry of a heart valve using a 3D printer [44–50]. By printing various compositions of the hydrogels and modifying photo-crosslinked molecules by UV light upon ejection from the print head, they are able to tune the stiffness of the printed hydrogels. This enables them to print a scaffold with spatially varying mechanical properties, although the fabrication process is more intensive than the

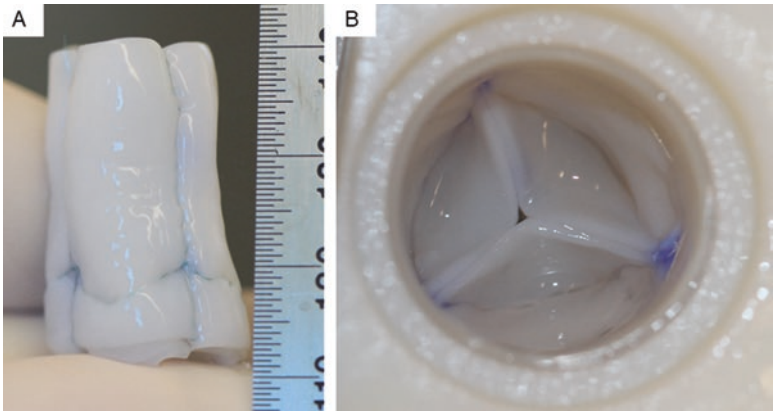


**Fig. 13.2** Photograph of tri-rube decellularized fibrin-based TEM valve showing (**a**) side view of construction with suture lines and (**b**) top view with three coapting leaflets. Dermal fibroblasts entrapped within a fibrin scaffold were cultured in vitro to form the TEM. After in vitro culture, the tubes were decellularized and sewn into the configurations shown. (From Syedain et al. [11]. Reprinted with permission from AAAS)

commonly used techniques of synthetic polymer seeding or biopolymer casting approaches.

Hockaday et al. printed a hydrogel TEHV consisting of polyethylene glycol diacrylate (PEGDA) both with and without an interpenetrating collagen fibrillar network. The root and leaflet portions of the anatomically accurate aortic valve geometry were printed with different molecular weight PEGDA solutions, so that the two distinct regions had differing mechanical strength and stiffness. Porcine aortic valve interstitial cells cultured on these PEGDA and collagen/PEGDA scaffolds for up to 21 days were viable and exhibited spread morphology, demonstrating the feasibility of using a photo-crosslinked polymer scaffold for TEHV applications [45].

Duan et al. used a similar 3D printing process to print hybrid methacrylated hyaluronic acid (Me-HA) and methacrylated gelatin (Me-Gel) in a tri-leaflet valve geometry and found that by adjusting the composition of this hybrid solution thus altering the stiffness of the scaffold, the response of the encapsulated porcine aortic valve interstitial cells could be regulated [46]. While this study only utilized a short in vitro culture period of 7 days after printing, cell viability both inside the scaffold and on the surface was preserved, and there was early evidence of in vitro remodeling of the printed hydrogel scaffold. Recent work in the area of 3D printing for TEHV applications has investigated optimization and modification of hydrogel materials to promote cell attachment and attain desirable cell phenotypes [47, 48], optimizing cell viability during the photo-crosslinking process [49], and investigating in vivo remodeling of 3D printed hydrogel constructs [50].

### *13.2.2 In Vitro Culture of Tissue-Engineered Matrix TEHVs*

The in vitro culture environment can profoundly affect the final TEHV properties for valves created using tissue-engineered matrix. Biochemical molecules such as growth factors, ascorbic acid, and insulin have been shown to have significant effects on the resulting TEHVs. Ramaswamy et al. were able to nearly double the amount of collagen produced per MSC in their synthetic polymer-based constructs by supplementing their standard growth medium with basic fibroblast growth factor and ascorbic acid-2-phosphate [37]. In fibrin-based constructs, Neidert et al. demonstrated that collagen deposition by human dermal fibroblasts could be increased 20-fold by supplementing their medium with transforming growth factor-beta, plasmin, and insulin [51]. Depending on the cell type and scaffold material involved, each laboratory uses different combinations of culture medium and supplements in an attempt to optimize ECM production and maturation.

Using a bioreactor for the mechanical conditioning of TEHVs is another approach that can optimize the in vitro culture environment. A TEHV is a complex, 3D structure that can be mechanically stimulated in multiple ways. Flow through a TEHV results in combinations of leaflet flexure and stretch, shear stress, and root distension. Because the system is so complex, the optimal stimulation protocol is still

unknown, and research groups have developed several different types of bioreactors to improve the mechanical properties of their constructs.

Several groups have designed and implemented pulse duplicator systems to condition entire TEHVs using physiological pulsatile pressure waveforms. The details of the bioreactors differ, but all share some key features. These include a pump to induce pulsatile fluid motion, a medium reservoir to replenish the system, a section in which the TEHV can be mounted, a fluid capacitance for energy dissipation (to mimic arterial elasticity), and a tunable resistance element to control the pressure in the system [52]. In addition, these systems must be sterilizable, allow for gas exchange, fit in a cell culture incubator, and minimize the volume of culture medium used in order to reduce operational cost.

Hoerstrup et al. [53] developed a pulsatile bioreactor for conditioning their synthetic polymer-based TEHVs that consisted of an air chamber and a medium chamber separated by a silicone membrane. A ventilator was used to pump air into the air chamber, cyclically displacing the silicone membrane and thereby generating pulsatile flow in the medium chamber. The TEHV was mounted onto a tube in the medium chamber, with a minimal amount of culture medium above the valve and below. By changing the stroke volume and rate of the ventilator, they were able to vary the pressure drop and flow rate across the valve. With this system, they achieved pressures of 10–240 mm Hg and flow rates of 50–2000 mL/min. In one study [28], TEHVs made from myofibroblasts and endothelial cells (ECs) seeded on PGA/P4HB scaffolds were subjected to flow conditions gradually increasing from 35 to 50 mm Hg and 135 to 750 mL/min over 28 days. Compared to controls that were cultured statically, the bioreactor conditioned TEHVs were more robust, contained more collagen, had higher suture retention strengths, and maintained structural integrity throughout the culture period. An additional benefit of this system was the ability to test the TEHVs at physiological pressures immediately before implantation to ensure function.

Hildebrand et al. developed a pulse duplicator system that was similar to the system described above, but had several novel features including electronic control of all components and a precise pneumatic system for waveform generation. The system, shown in Fig. 13.3, consisted of a flow loop containing an atrial chamber that filled a ventricular chamber through a mechanical valve. The ventricular chamber was controlled by a pneumatic system which could generate physiological waveforms to eject culture medium through the TEHV mounted downstream. An electronically controlled resistance element was used to achieve the desired system pressure. Pressure and flow through the system was measured using a pressure transducer and ultrasonic flow probe, respectively [54].

In a study to validate the benefits of this system, TEHVs made from MSCs seeded onto synthetic polymer scaffolds were cultured statically for weeks 1–3 then subjected to physiological pulmonary valve pressure and flow conditions for weeks 4–6, and a four-fold increase in collagen content was observed compared to 6 week static culture samples [37]. It is clear that pulse duplicator systems can have beneficial effects for TEHV growth and remodeling. However, despite providing well-defined pressure waveforms, the applied mechanical stimuli are complex and

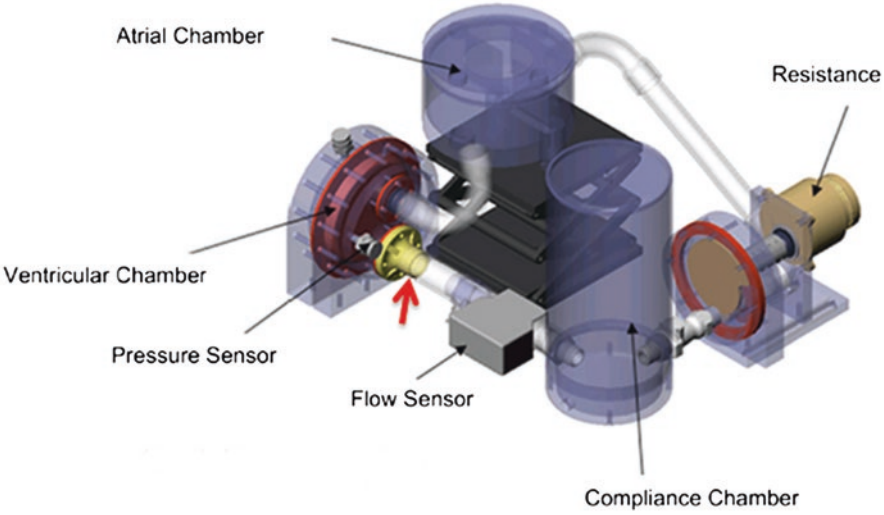


**Fig. 13.3** Schematic of the pulse duplicator bioreactor designed by Hildebrand et al. [54]. The location of the TEHV is indicated by the red arrow. (Reprinted from Ramaswamy et al. [37] with permission from Elsevier. This article was published in Ramaswamy et al. [37], Copyright Elsevier (2010))

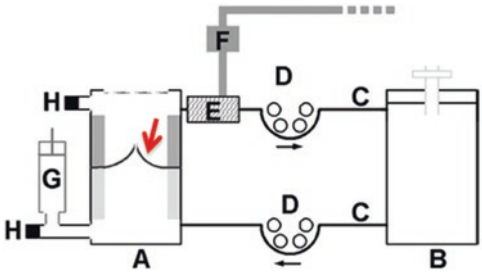


**Fig. 13.4** Schematic of Diastolic Pulse Duplicator consisting of a bioreactor chamber (**a**) and a medium chamber (**b**). The location of the TEHV is indicated by the red arrow. The bioreactor and medium chambers are connected by tubing (**c**) and flow is driven by roller pumps (**d**). Part of the tubing is encased in a polycarbonate cylinder (**e**), and the injection of air into the cylinder through a magnet valve (**f**) compresses the tubing and applies cyclic back pressure to the TEHV. A syringe acts as compliance chamber (**g**), and pressure is monitored by sensors on either side of the TEHV (**h**). (Reprinted from Mol et al. [33] by permission from Springer Nature: Mol et al. [33], Copyright (2005))

difficult to control. The leaflet properties and deformation behavior change as the tissue remodels in vitro, the mechanical stimuli applied by these systems are time-dependent and poorly defined.

Instead of attempting to replicate physiological operating conditions, several research groups have developed bioreactors to apply well-defined mechanical stimulation to TEHVs. A Diastolic Pulse Duplicator (DPD) bioreactor (Fig. 13.4) was

developed in which cyclic pulses of backpressure were applied resulting in coaptation of the TEHV leaflets by compressing and releasing silicone tubing containing culture medium [33]. The leaflet strain in this system depended on the mechanical properties of the tissue, which varied with time as the tissue matured, an inherent complication as noted above. The dynamic strain in the leaflets increased from 8% to 20% from weeks 2 to 4 in culture as the polymer scaffold degraded and the stiffness of the construct decreased. No significant improvements in collagen production or mechanical properties were observed in the dynamically strained samples compared to TEHVs which were exposed to constant, low flow rate at medium circulation in the DPD system. This lack of improvement may have been because the applied strains in the later weeks of the culture period were too large, as the applied load remained constant while the tissue stiffness decreased. However, Kortsmit et al. proposed a method of implementing a volumetric deformation-controlled feedback loop in which the applied load in the DPD bioreactor was automatically adjusted to achieve the desired deformation [55]. By controlling the overall volumetric deformation of the coapting leaflets, they were able to apply defined average cyclic strain to their TEHV leaflets.

In the Tranquillo research group, a cyclic stretch bioreactor was used to apply controlled pulsatile circumferential deformation to the fibrin-based tubular constructs used to create TEHVs [5, 7, 10, 11]. Previous studies demonstrated increased collagen content and improved mechanical strength and stiffness of fibrin-based vascular grafts subjected to cyclic distension in a similar system [56, 57], and this concept was adapted for the larger tubular constructs used to fabricate TEHVs. After an initial static culture period, the fibrin-based tube is placed over an elastic latex tube for support and mounted between two end pieces then placed in a jar containing culture medium. A reciprocating syringe pump injects medium into one end of the mounted tube, causing the elastic support and tubular construct to distend. The pumped fluid then flows out of a small hole in the other end piece and into the jar of medium surrounding the tubular structure [57, 58]. The distension magnitude can be controlled by the stroke volume of the syringe pump to apply controlled cyclic stretching throughout culture as shown in Fig. 13.5.

In addition to the development of bioreactors to promote in vitro tissue formation, bioreactor devices can also be used to seed and dynamically condition seeded cells on TEHVs prior to implantation [59, 60]. Sierad et al. developed a bioreactor based on the pulse duplicator system of Hoerstrup et al. [28], which they used to dynamically condition porcine aortic endothelial cells that were seeded on decellularized porcine aortic valves. This resulted in viable and spread cells after 17 days of dynamic conditioning under physiological pulmonary conditions [59]. Using the same system, Kennamer et al. dynamically conditioned decellularized porcine aortic valves seeded with human adipose-derived stem cells. Although the bioreactor performed as intended, at the conclusion of the 24-day study, the majority of the seeded cells had died, highlighting the challenging task of determining the appropriate conditioning regimen for a particular cell type and scaffold combination [60]. As researchers strive to fabricate TEHVs reproducibly with properties suitable for implantation, bioreactor conditioning for both tissue

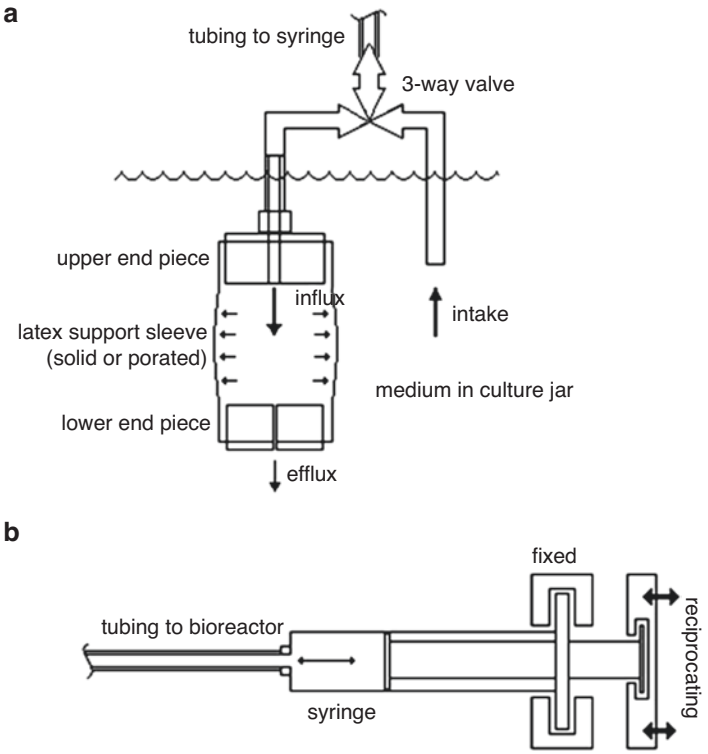


**Fig. 13.5** Cyclic stretch bioreactor for TEM tubes. Schematic of (**a**) bioreactor components and (**b**) reciprocating syringe pump. Culture medium is pumped down through the center of the latex support sleeve and out through the small efflux hole in the lower end piece resulting in cyclic distension of the latex. The TEM tube is placed outside the support sleeve and is cyclically stretched along with the latex. (Reprinted from Schmidt and Tranquillo [58] by permission from Springer Nature: Schmidt and Tranquillo [58], Copyright (2016))

formation and cell conditioning continues to play an important role during fabrication of engineered matrix TEHVs.

### *13.2.3 Bioresorbable Polymer TEHVs*

Recently, there has been interest in using bioresorbable polymer scaffolds as a basis for "in situ tissue engineering." In this approach, in vitro culture is not required to degrade the polymer scaffold and replace it with cell-produced ECM. Rather, the polymer scaffold is either implanted directly into the patient, cell-free [61–66] or pre-seeded with an autologous cell source such as bone marrow mononuclear cells [67]. Once implanted, the patient's own cells are recruited to the scaffold and remodel it in situ as the scaffold is absorbed by the body and replaced with ECM.

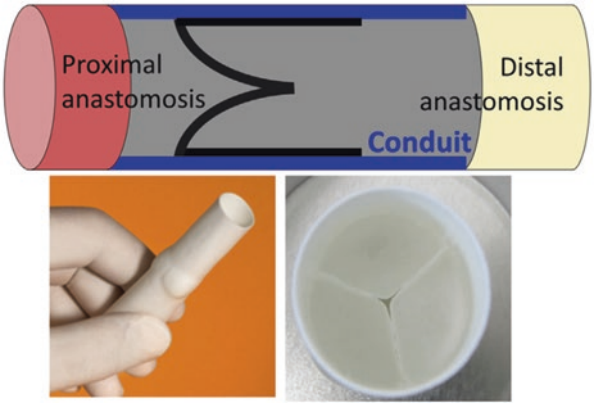


**Fig. 13.6** Xeltis Pulmonary Valved Conduit (XPV). The XPV consists of a UPy synthetic biopolymer scaffold implanted without prior in vitro culture or cell seeding. (Reprinted from Bennink et al. [64] with permission from Elsevier. This article was published in Bennink et al. [64], Copyright American Association for Thoracic Surgery (2018))

An advantage to this approach is the ability to reproducibly fabricate scaffolds with the desired geometry, porosity, mechanical properties, and chemical composition. Using this approach, Kluin et al. designed a bioresorbable polymer scaffold comprised of electrospun bis-urea-modified polycarbonate (PC-BU). The PC-BU electrospun tubes were sewn over a polyether ether ketone (PEEK) frame and coated with fibrin [61]. Coyan et al. similarly fabricated a bioresorbable polymer TEHV scaffold from electrospun polycarbonate urethane urea, which was mounted on a degradable magnesium stent [62]. Capulli et al. utilized a Rotary Jet Spinning system to deposit P4HB and gelatin composite fiber scaffolds, creating the bioresorbable JetValve, which supported valve interstitial cell infiltration in vitro [63]. The Xeltis Pulmonary Valved Conduit (XPV) shown in Fig. 13.6 is another example of a bioresorbable polymer valve, consisting of 2-ureido-4[1H]-pyrimidinone (U-Py), with different formulations of U-Py using the root and leaflet structures to give the desired properties [64–66].

Synthetic polymers offer the promise of consistency and scalability, making this approach attractive for “off-the-shelf” valve replacement technologies, however, this approach does rely heavily on the remodeling response in vivo, which can vary from patient to patient and are not yet fully understood.

## 13.3 In Vivo Results: Preclinical and Clinical Studies

The ovine model is the current gold standard for preclinical heart valve replacement studies [68]. In a 1995 study designed to explore the feasibility of using TEHVs as replacement heart valves, Shinoka et al. demonstrated that tissue-engineered single leaflets consisting of autologous cells seeded onto a synthetic polyglactin/PGA

scaffold functioned well for up to 4 weeks in the pulmonary position in lambs [69]. While a single tissue-engineered leaflet has limited applications, this preliminary study demonstrated that it was possible to implant at least a portion of a TEHV for a short-term in vivo study and paved the way for future pre-clinical ovine model studies.

To date, several research groups utilizing both the TEM and bioresorbable polymer approaches have implanted their TEHVs into sheep to evaluate in vivo performance and remodeling. While the ovine model is the most commonly used, non-human primate and porcine models have also been utilized in TEHV preclinical trials. In the majority of these preclinical studies, TEHVs have been implanted in the pulmonary position, although several groups have studied performance in the aortic position as well. Both surgical and transcatheter approaches have been utilized, depending on the TEHV design.

Table 13.1 provides a summary of recent preclinical studies using TEM TEHVs grouped by approach. In an early study investigating the recellularization potential, Weber et al. implanted a TEM valve, fabricated using human vascular-derived fibroblasts seeded on a PGA/P4HB scaffold, in the pulmonary position in a non-human primate model [9]. Significant leaflet shortening was observed at 8 weeks, resulting in increasing pulmonary regurgitation. However, the TEM valve showed increased recellularization potential compared to decellularized human native heart valve controls, demonstrating the promise of a TEM scaffold for in vivo remodeling. Using a similar approach, Mol et al. implanted an ovine-derived TEM valve as a pulmonary valve replacement in sheep [36]. Although these TEHVs demonstrated good early performance and recellularization potential, by 16 weeks mild regurgitation had developed, progressing to moderate regurgitation at 24 weeks. This degraded valve performance was hypothesized to be caused by a reduction in leaflet mobility due to fusion of the leaflets with the valve wall.

In an effort to overcome the issues of leaflet retraction, Motta et al. utilized a more anatomically relevant valve geometry, incorporating Valsalva sinuses into their stented TEHV design [34, 70]. It was hypothesized that the inclusion of this feature would create hemodynamic conditions more similar to those in the native pulmonary valve and prevent abnormal loading that may promote a contractile phenotype of the infiltrating cells. Ovine-derived TEM valves with Valsalva sinuses were created using a PGA/P4HB scaffold and ovine vascular derived cells, and the resulting TEHVs were implanted in sheep. Although the Valsalva sinus TEHV design was able to be safely implanted, leaflet retraction and increasing regurgitation continued to be an issue, motivating additional optimization of TEHV geometry and stent design [34]. Emmert et al. utilized a computationally driven geometry, which incorporated leaflet belly curvature and an increased coaptation area in an ovine-derived TEM valve design, similarly aiming to produce a more physiological mechanical environment for cells as they repopulate and remodel the TEHV in vivo [8]. TEHVs fabricated in this geometry were implanted in the pulmonary position in sheep, and 9 of 10 implanted TEHVs maintained function at the 52-week follow-up point with trivial to mild insufficiency. The dependence of the cells' remodeling response on the mechanical environment demonstrated in this study motivates

**Table 13.1** Summary of preclinical studies with tissue-engineered matrix (TEM) valves

| TEHV design [Ref] | Animal model | TEHV position | Implantation method | Study end points | Summary |
|---|---|---|---|---|---|
| *Biopolymer (fibrin-based) scaffold* | | | | | |
| Ovine TEM (fibrin-based) [11] | Sheep | Pulmonary | Surgical | 12, 20, 36, and 52 weeks | A tri-tube design implanted in growing lamb model demonstrated root growth. Commissure separation due to rapid root growth relative to leaflets led to Gen2 design with supporting external tube. No leaflet thickening, recellularization from root into leaflets, reduced calcification and improved function compared to bioprosthetic control. Gen2 valves showed trivial to moderate regurgitation after 52 weeks. |
| Ovine TEM (fibrin-based) [7] | Sheep | Pulmonary | Surgical | 12–22 weeks | Tube-in-tube design implanted in growing lambs. Substantial cell infiltration in root and on leaflet surfaces. Good function up to 8 weeks, then insufficiency increased due to leaflet shortening, hypothesized to be a result of commissure instability. |
| Ovine TEM (fibrin-based) [10] | Sheep | Aortic | Surgical | 12 and 24 weeks | Tubular framed valve design implanted in aortic position. Substantial recellularization and no evidence of calcification at 24 weeks. Mild-to-moderate insufficiency in 3 of 4 valves after 12 weeks, thought to be due to problems near top of frame struts |
| *Synthetic polymer scaffold* | | | | | |
| Human TEM (PGA/P4HB) [34] | Sheep | Pulmonary | Transcatheter | Acute | Demonstrated valve with anatomical Valsalva sinus created from human TEM. Good acute function, evidence of early cell infiltration |
| Ovine TEM (PGA/P4HB) [8] | Sheep | Pulmonary | Transcatheter | 52 weeks | Computationally driven design with belly curvature and increased leaflet coaptation area. More physiological mechanical environment resulted in quiescent cell phenotype and reduced insufficiency compared to previous designs. 9/10 TEHVs maintained function at 52 weeks with only trivial-to-mild insufficiency and showed substantial recellularization and remodeling. |

(continued)

**Table 13.1** (continued)

| TEHV design [Ref] | Animal model | TEHV position | Implantation method | Study end points | Summary |
|---|---|---|---|---|---|
| Ovine TEM (PGA/P4HB) [70] | Sheep | Pulmonary | Transcatheter | 16 weeks | Design incorporating Valsalva sinus used. Good acute performance, no paravalvular leakage. Substantial recellularization, but contractile phenotype of infiltrating cells resulted in significant leaflet shortening. |
| Human TEM (PGA/P4HB) [35] | Sheep | Aortic | Transcatheter | Acute | Demonstrated good acute function of human TEM valve in the aortic position with transcatheter delivery. No paravalvular leakage or stenosis observed. |
| Ovine TEM (PGA/P4HB) [36] | Sheep | Pulmonary | Transcatheter | 1 day, 8, 16, and 24 weeks | Substantial recellularization. Good early performance with mild central regurgitation observed at 16 weeks progressing to moderate insufficiency by 24 weeks. Degraded valve performance likely due to leaflet fusion with valve wall. |
| Human TEM (PGA/P4HB) [9] | Baboon | Pulmonary | Transcatheter | 4 and 8 weeks | Human TEM valve implanted in non-human primate model. Increased recellularization potential compared to decellularized homografts. Mild-to-moderate insufficiency after 8 weeks due to leaflet shortening. |

continued investigation into in vivo loading conditions and the use of computational tools to optimize TEHV geometry.

In the Tranquillo laboratory, they have tested fibrin-based TEM TEHVs in several different geometries in the ovine model. This TEM is fabricated using ovine dermal fibroblasts entrapped in a sacrificial fibrin gel cast around a mandrel in a tubular mold and the resulting ovine-derived TEM tubes are decellularized prior to implantation. Syedain et al. implanted TEHVs consisting of a single TEM tube sutured over a Mitroflow® frame (Sorin Group) in the first long-term (6 month) study of a TEM valve in the aortic position [10]. TEHVs were repopulated with interstitial-like cells, and there was evidence of endothelialization and tissue remodeling after 6 months in vivo. No stenosis was observed, however, three of four TEHVs exhibited increasing aortic insufficiency at 3 months that stabilized and remained unchanged until explant. Gross pathology of the valve at explant showed

small tears in two of the valves at the frame post, leading to leaflet prolapse, and the entire tube sagged downward around the frame in one of the valves. These frame attachment issues were likely the cause of the observed mild-to-moderate regurgitation.

Building on the demonstrated regenerative potential of this fibrin-based TEM, Reimer et al. surgically implanted their previously discussed "tube-in-tube" design TEHV in the pulmonary position in a growing lamb model [7]. These TEHVs functioned well up to 8 weeks, demonstrating fusion between the tubes after degradation of the suture, but after 8 weeks, pulmonary insufficiency increased. This insufficiency was likely a result of the combined effects of root growth in the growing lamb model without accompanying leaflet growth leading to leaflet shortening, as well as due to inadequate fusion between the two TEM tubes. To address the issue of commissure stability, Syedain et al. developed the previously mentioned "tri-tube" design, in which the loading under diastolic pressure was primarily carried by the matrix rather than the suture line [11]. TEHVs with the tri-tube design (Gen 1) were implanted in the pulmonary position in four growing lambs. Although the Gen 1 tri-tube valves functioned well immediately upon implantation, as the diameter of the valve root increased in the growing lambs (from ~19 to 25 mm over 1 year), tissue growth between the TEM tubes created gaps at commissures, resulting in regurgitation and degraded performance long-term, even though initial leaflet height was maintained.

In an effort to slow the "commissure separation," a sleeved tri-tube TEHV (Gen 2) was developed, in which a fourth tube was placed around the tri-tube design acting as a sleeve to counteract the faster root growth compared to leaflet growth. Two of the three Gen 2 TEHVs had only trivial to mild regurgitation up to 1 year even as the pulmonary artery grew from 19 to 25 mm, and the third Gen 2 valve developed moderate regurgitation due to a larger-than-expected increase in diameter of the pulmonary artery, again attributed to tissue growth between TEM tubes creating a gap at one commissure. As shown in previous studies, this TEM was suitable for recellularization in vivo, as all explanted TEHVs showed substantial repopulation by interstitial cell types and the presence of an endothelium throughout the length of the root and progressing from the base of the leaflet. Although sparse evidence of microcalcification was present in some leaflet regions at explant, it was noted that both Gen 1 and Gen 2 valves had less calcification and improved function compared to bioprosthetic controls (Hancock 150 valved conduit and Contegra 200 valved conduit) implanted in the same growing lamb model. Figure 13.7 shows representative images of the explanted Gen 2 TEHVs after 12 months in vivo in sheep.

There have been multiple preclinical studies utilizing bioresorbable polymer TEHVs as well. Recent studies using this approach are summarized in Table 13.2. Early efforts investigating the bioresorbable polymer approach utilized PGA/P4HB scaffolds seeded with autologous bone marrow mononuclear cells [71–74]. Although these early studies had relatively short follow-up periods of 1 month or less, they demonstrated the feasibility of implanting a bioresorbable polymer scaffold to serve as a platform for in situ remodeling. Even in these short-term in vivo studies, there was evidence of cell infiltration and remodeling of the matrix, although mild leaflet

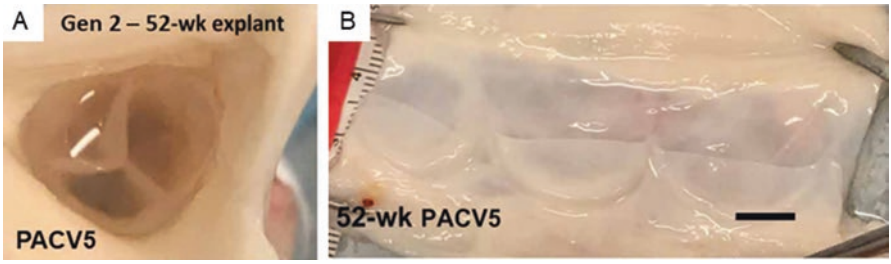


**Fig. 13.7** Explanted Gen 2 tri-tube TEHV after 12-month implantation in a growing lamb. (**a**) Distal view and (**b**) cut open view showing the three leaflets. (From Syedain et al. [11]. Reprinted with permission from AAAS)

shortening resulting in progressive regurgitation was observed [74]. Coyan et al. [62] and Capulli et al. [63] also demonstrated promising acute function in their bioresorbable polymer TEHVs, although additional studies are necessary to investigate long-term function and in situ remodeling.

In a long-term study, bioresorbable polymer valves based on PC-BU scaffolds have been implanted for up to 1 year in sheep with and without pre-seeding with autologous bone marrow mononuclear cells. Unseeded PC-BU TEHVs demonstrated acceptable function up to 1 year, with extensive recellularization with both interstitial-like cells and endothelial cells [61]. The deposited matrix components consisted of collagen, glycosaminoglycans (GAGs), and elastin, including mature elastin fibers. Although some absorption of the biopolymer scaffold had occurred 1 year post implant, scaffold material still remained in the explanted valves, especially in the less cellular regions. In a follow-up study, Fioretta et al. found that pre-seeding this same PC-BU scaffold with autologous bone marrow mononuclear cells was detrimental to long-term function [67]. Pre-seeded TEHVs demonstrated maladaptive remodeling including calcification and leaflet fusion which ultimately led to degraded performance after only 24 weeks in vivo. In addition, Fioretta et al. observed differences in remodeling of the leaflets, even within the same valve and concluded that further investigation into the in situ remodeling process is necessary to ensure the safety of this approach prior to clinical translation. Seeking to better understand the cell–scaffold interaction in PC-BU valves, Uiterwijk et al. implanted unseeded PC-BU TEHVs with randomly oriented or circumferentially oriented polymer fibers [75]. Contrary to their hypothesis, the circumferentially oriented fibers in the initial scaffold did not result in circumferentially oriented collagen deposition, and in fact, explanted scaffolds at 6 and 12 months exhibited isotropic properties regardless of the initial scaffold orientation. The authors additionally noted that there was heterogeneous remodeling of TEHVs in both study groups, again highlighting the need for a better understanding of the in situ remodeling process for bioresorbable polymer TEHVs.

Several preclinical studies have been performed with the Xeltis Pulmonary Valved Conduit in adult sheep, using both transcatheter [76] and surgical [64, 66] approaches. Bennink et al. surgically implanted XPVs in the pulmonary position in

**Table 13.2** Summary of preclinical studies with bioresorbable polymer valves

| TEHV design [Ref] | Animal model | Pre-seeded cell type | TEHV position | Implantation method | Study end points | Summary |
|---|---|---|---|---|---|---|
| *Acellular (non-seeded) scaffolds* | | | | | | |
| PC-BU [75] | Sheep | None | Pulmonary | Surgical | 1, 6, and 12 months | TEHVs with randomly oriented fibers and circumferentially oriented fibers were implanted. At 6 and 12 months, all explanted valves exhibited isotropic properties. Variability in remodeling response within study group. |
| Polycarbonate urethane urea [62] | Pig | None | Pulmonary | Surgical | Acute | Good acute performance with no evidence of thrombosis, platelet activation, or structural damage. |
| UPy (XPV) [64] | Sheep | None | Pulmonary | Surgical | 2, 6, and 12 months | Degradation of XPV beginning at 2 months. Acceptable function throughout 1 year study. Compared to Hancock valve controls, XPV showed reduced calcification and neointimal thickening. |
| P4HB/Gelatin [63] | Sheep | None | Pulmonary | Transcatheter | Acute | Good acute performance demonstrated with no evidence of damage to the TEHV after transcatheter delivery. No thrombosis detected in acute trial. |

(continued)

**Table 13.2** (continued)

| TEHV design [Ref] | Animal model | Pre-seeded cell type | TEHV position | Implantation method | Study end points | Summary |
|---|---|---|---|---|---|---|
| PC-BU [61] | Sheep | None | Pulmonary | Transcatheter | 2, 6, and 12 months | Acceptable valve function up to 1 year. Scaffold was repopulated by interstitial and endothelial cells. PC-BU scaffold was not fully degraded after 12 months. |
| UPy (XPV) [66] | Sheep | None | Pulmonary | Surgical | Acute, 3, 6, 12, and 24 months | XPV functioned up to 24 months with trace-to-mild regurgitation in most cases. |
| UPy (XPV) [76] | Sheep | None | Aortic | Transcatheter | Acute | After transcatheter delivery, XPV demonstrated good acute function in the aortic position with all TEHVs exhibiting mild (or less) regurgitation. |
| *Pre-seeded scaffolds* | | | | | | |
| PC-BU [67] | Sheep | aBMMNCs | Pulmonary | Transcatheter | Acute, 4 and 24 weeks | TEHVs seeded with aBMMNCs demonstrated maladaptive remodeling including leaflet fusion resulting in increasing regurgitation and calcification. Maladaptive remodeling was absent in non-seeded controls. |

(continued)

**Table 13.2** (continued)

| TEHV design [Ref] | Animal model | Pre-seeded cell type | TEHV position | Implantation method | Study end points | Summary |
|---|---|---|---|---|---|---|
| PGA/P4HB [71] | Sheep | aBMMNCs | Aortic | Transcatheter | Acute | aBMMNC seeded TEHVs were implanted transapically into the aortic position. TEHVs were able to withstand loading and no rupture was observed. Paravalvular leakage and aortic regurgitation was present in some animals. |
| PGA/P4HB [72] | Sheep | aBMMNCs | Aortic | Transcatheter | Acute, 2 days, 2 weeks | TEHV implanted using transcatheter approach without structural damage. Cellular infiltration and remodeling shown after 2 weeks. |
| PGA/P4HB [73] | Sheep | aBMMNCs | Aortic | Transcatheter | Acute | Demonstrated feasibility of transcatheter aortic valve implantation. No evidence of tissue damage. |
| PGA/P4HB [74] | Baboon | aBMMNCs | Pulmonary | Transcatheter | Acute, 1 month | At 1 month, scaffold showed recellularization and remodeling potential. Mild-to-moderate regurgitation observed and minimal shortening of cusps. |

sheep for up to 1 year [64]. Degradation and remodeling of the UPy bioresorbable polymer scaffold began around 2 months and continued throughout the 1-year study. XPVs demonstrated acceptable function up to 1 year, and compared with Hancock bioprosthetic valve controls, XPVs showed reduced calcification and neointimal thickening. In a study by Soliman et al., XPVs were shown to be functional with only trace-to-mild regurgitation in most cases 2 years after surgical implantation into sheep [66].

Building on the promising results in the preclinical studies, the first clinical trial with the XPV in children is currently ongoing [65, 77]. Two designs of the XPV were used in this study, with the second design being a modification of the first to address issues observed during early follow up. The original XPV-1 design was surgically implanted in the pulmonary position in 12 children (median age 5) and followed up to 12 months with echocardiography. The modified XPV-2 design with a more homogeneous leaflet thickness was implanted in an additional six children (median age 5) and followed up to 12 months with echocardiography for comparison with the original design. At 12 months post operation, all 18 children were in New York Heart Association (NYHA) functional class 1, with no limitation of physical activity. At 12 months, five patients with the XPV-1 design developed severe regurgitation caused by leaflet prolapse, while only one patient with the XPV-2 design developed more than trace-to-mild regurgitation. One patient with XPV-2 required reoperation due to stenosis that was attributed to a hyperinflammatory response.

Children with the XPV-1 design have completed their 24-month follow up [77]. At 24 months, 9 of 12 children are in NYHA class I and the remaining three children are in NYHA class 2. None of the patients have required reoperation, although five patients have severe pulmonary valve regurgitation due to the leaflet prolapse previously mentioned. While the outcome of this first human study with bioresorbable polymer TEHVs is promising, future work must continue to address valve regurgitation and investigate the growth potential of these grafts in longer term studies.

## 13.4 Future Directions

TEHVs are an exciting and attractive alternative to traditional mechanical and bioprosthetic replacement heart valves. Although great progress has been made, there are still challenges that must be overcome before TEHVs are suitable for routine clinical use. The in situ remodeling process is not yet fully understood even in a healthy patient and the remodeling response may be species and age dependent and affected by the disease state of the recipient. Work is ongoing to investigate the variable remodeling observed in both preclinical and clinical trials, as obtaining a predictable and consistent remodeling result will be necessary for the clinical translation of TEHVs [78].

Although longer term preclinical and clinical trials with TEHVs are being conducted, currently full regeneration of the TEHV scaffold with native cells and ECM components has not been demonstrated, in part due to slower recellularization of the leaflets compared to the TEHV root. The challenging task of inducing and accelerating recellularization of leaflets, both for repair and durability in adult applications and for growth in pediatric applications, remains to be solved. Substantial work is still required to understand the factors contributing to the in situ recellularization and remodeling process. Computational models can predict the initial valve function well and such models should be used to optimize design with respect to typical factors like valve performance metrics, solid stress concentration, and hemodynamic factors affecting endothelial phenotype [8, 11]. However, accurate patient-specific prediction of remodeling, yet alone growth, of the implanted material requires further understanding of complex regenerative processes.

In designing a TEHV for pediatric applications, only the growth potential of the root has been clearly demonstrated in the growing lamb model [11, 79, 80]. Although Syedain et al. showed indications of leaflet growth in a growing lamb model (i.e., increase of leaflet-free edge length), the leaflet growth lagged root growth resulting in commissure separation. However, it should be noted that the growth rate of lambs is faster than what would be expected in a pediatric patient [11]. The challenging task of balancing the rate of growth of the patient with the recellularization and growth rate of TEHV leaflets must be addressed in future pediatric TEHV designs. To date, longer-term studies of TEHVs with growth potential have used surgically implanted valves, and while there has also been investigation into the use of biodegradable stents for transcatheter delivery of TEHVs for pediatric applications, these designs have only been tested in acute preclinical studies and regeneration of the protein nanofiber scaffold has yet to be proven [62].

Another area of future investigation is the hemocompatibility and necessary anticoagulation regimen for both TEM and bioresorbable polymer TEHVs. Although endothelization was reported after implantation in most previously discussed studies, all preclinical and clinical trials discussed used some form of anti-coagulation regimen at implantation, and it is not yet known when or if these treatments can be reduced or terminated. The best strategy to ensure hemocompatibility is likely specific to a particular TEHV material and design. Overall, the long-term outcome for TEHVs is not yet certain, and future studies will seek to determine when regeneration is “complete” and assess the long-term durability, biocompatibility, and hemocompatibility of each TEHV design.

The new approach of 3D bioprinting enables the fabrication of TEHVs with more complex architectures that better mimic native valves and valve mechanics. This approach can create TEHVs with spatially varying mechanical properties and size a TEHV specifically for an individual patient. Despite the potential advantages of this approach, the regenerative capacity of printed TEHVs with the current bioinks has not yet been demonstrated [44–50].

In addition to these design-related challenges, there are manufacturing, economic, and regulatory hurdles that must be overcome before TEHVs are available for routine clinical use. As discussed previously, TEHVs can be fabricated using a

variety of scaffold materials (bioresorbable polymers or TEM) and cell types (cell free, autologous cells entrapped, or pre-seeded). Especially for cell-based materials, there are significant challenges related to reproducibility and quality control during manufacturing. While bioresorbable polymer TEHVs have an advantage here, standardized manufacturing procedures must be developed to ensure a consistent and safe end product.

The regulatory pathway for TEHVs with regenerative potential, even acellular TEHVs, is unclear, and if TEHVs are classified and regulated as a biological product rather than a medical device, this pathway may be more challenging. Currently, preclinical testing is directed by ISO-5840 from the International Organization for Standardization [81, 82], which was initially designed for traditional mechanical and bioprosthetic valves. Unlike currently available heart valve replacement options, TEHVs undergo extensive in vivo remodeling, and this process will likely result in variability in performance among patients. Factors such as genetic variation, comorbidities, and medications may lead to heterogeneity in the remodeling response and thus differences in device performance. This patient-specific interaction between device and patient may require additional study and regulatory principles beyond those required for traditional replacement heart valves [83]. In addition, attention must be paid to determining appropriate durability standards for TEHVs in light of the scaffold degradation and remodeling process. The ISO-5840 guidelines require heart valves to last 200 million cycles, but it is unclear whether this standard is appropriate for TEM or synthetic polymer valves where substantial remodeling is expected well before that many cycles.

In terms of cost-effectiveness, as TEHVs are not currently commercially available and fabrication methods vary widely, it is difficult to obtain a good estimate of TEHV cost. Market value depends on performance, unproven yet clinically relevant for TEHVs. From a cost standpoint, it will be difficult for TEHVs to compete with bioprosthetic valves, but they may be able to displace mechanical valves if 20+ year durability without the need for sustained anticoagulation therapy is proven. For pediatric patients, a TEHV would become the dominant valve if growth potential is demonstrated (at least of the root) and at least 5-year function and durability are proven, even if sustained anticoagulation is needed, as the number of cardiopulmonary bypass procedures would be reduced by at least one [84].

## 13.5 Summary

The development of a TEHV as a living heart valve replacement offers great promise, particularly for pediatric patients who require a prosthetic valve that can grow and adapt. This chapter provided a brief overview of the methods currently employed for TEHV fabrication, including both the tissue-engineered matrix approach and the bioresorbable polymer approach. Preclinical studies have demonstrated good short-term function and in vivo remodeling capability of THEVs, and an initial clinical trial with a bioresorbable polymer TEHV is currently ongoing. However, despite

promising early results, these studies have also elucidated several key issues that must be addressed in future work before TEHVs are suitable for clinical use, and there are a number of manufacturing, regulatory, and economic hurdles that must be overcome.

## References


1. Senthilnathan V, Treasure T, Grunkemeier G et al (1999) Heart valves: which is the best choice? Cardiovasc Surg 7:393–397
2. Sacks MS, Merryman WD, Schmidt DE (2009) On the biomechanics of heart valve function. J Biomech 42:1804–1824
3. Sacks MS, Yoganathan AP (2007) Heart valve function: a biomechanical perspective. Philos Trans R Soc Lond Ser B Biol Sci 362:1369–1391
4. Hinton RB, Yutzey KE (2010) Heart valve structure and function in development and disease. Annu Rev Physiol 17:29–46
5. Syedain ZH, Meier LA, Reimer JM et al (2013) Tubular heart valves from decellularized engineered tissue. Ann Biomed Eng 41:2645–2654
6. Dijkman PE, Driessen-Mol A, Frese L et al (2012) Decellularized homologous tissue-engineered heart valves as off-the-shelf alternatives to xeno- and homografts. Biomaterials 33:4545–4554
7. Reimer JM, Syedain ZH, Haynie BH et al (2015) Pediatric tubular pulmonary heart valve from decellularized engineered tissue tubes. Biomaterials 62:88–94
8. Emmert MY, Schmitt BA, Loerakker S et al (2018) Computational modeling guides tissue-engineered heart valve design for long-term in vivo performance in a translational sheep model. Sci Transl Med 10:eaan4587
9. Weber B, Dijkman PE, Scherman J et al (2013) Off-the-shelf human decellularized tissue-engineered heart valves in a non-human primate model. Biomaterials 34:7269–7280
10. Syedain Z, Reimer J, Schmidt J et al (2015) 6-month aortic valve implantation of an off-the-shelf tissue-engineered valve in sheep. Biomaterials 73:175–184
11. Syedain ZH, Haynie B, Johnson SL et al (2021) Pediatric tri-tube valved conduits made from fibroblast-produced extracellular matrix evaluated over 52 weeks in growing lambs. Sci Transl Med 13:eabb7225
12. Tudorache I, Horke A, Cebotari S et al (2016) Decellularized aortic homografts for aortic valve and aorta ascendens replacement. Eur J Cardiothorac Surg 50:89–97
13. Sarikouch S, Horke A, Tudorache I et al (2016) Decellularized fresh homografts for pulmonary valve replacement: a decade of clinical experience. Eur J Cardiothorac Surg 50:281–290
14. Cebotari S, Tudorache I, Ciubotaru A et al (2011) Use of fresh decellularized allografts for pulmonary valve replacement may reduce the reoperation rate in children and young adults: early report. Circulation 124:S115–S123
15. Boethig D, Horke A, Hazekamp M et al (2019) A European study on decellularized homografts for pulmonary valve replacement: initial results from the prospective ESPOIR Trial and ESPOIR Registry data†. Eur J Cardiothorac Surg 56:503–509
16. da Costa FD, Costa AC, Prestes R et al (2010) The early and midterm function of decellularized aortic valve allografts. Ann Thorac Surg 90:1854–1860
17. Helder MR, Kouchoukos NT, Zehr K et al (2016) Late durability of decellularized allografts for aortic valve replacement: a word of caution. J Thorac Cardiovasc Surg 152:1197–1199
18. Burch PT, Kaza AK, Lambert LM et al (2010) Clinical performance of decellularized cryopreserved valved allografts compared with standard allografts in the right ventricular outflow tract. Ann Thorac Surg 90:1301–1305

19. da Costa FDA, Etnel JRG, Torres R et al (2017) Decellularized allografts for right ventricular outflow tract reconstruction in children. World J Pediatr Congenit Heart Surg 8:605–612
20. Zafar F, Hinton RB, Moore RA et al (2015) Physiological growth, remodeling potential, and preserved function of a novel bioprosthetic tricuspid valve: tubular bioprosthesis made of small intestinal submucosa-derived extracellular matrix. J Am Coll Cardiol 66:877–888
21. van Rijswijk JW, Talacua H, Mulder K et al (2020) Failure of decellularized porcine small intestinal submucosa as a heart valved conduit. J Thorac Cardiovasc Surg 160:e201–e215
22. Mosala Nezhad Z, Poncelet A, de Kerchove L et al (2017) CorMatrix valved conduit in a porcine model: long-term remodelling and biomechanical characterization. Interact Cardiovasc Thorac Surg 24:90–98
23. Gilbert CL, Gnanapragasam J, Benhaggen R et al (2011) Novel use of extracellular matrix graft for creation of pulmonary valved conduit. World J Pediatr Congenit Heart Surg 2:495–501
24. Perri G, Polito A, Esposito C et al (2012) Early and late failure of tissue-engineered pulmonary valve conduits used for right ventricular outflow tract reconstruction in patients with congenital heart disease. Eur J Cardiothorac Surg 41:1320–1325
25. Simon P, Kasimir MT, Seebacher G et al (2003) Early failure of the tissue engineered porcine heart valve SYNERGRAFT in pediatric patients. Eur J Cardiothorac Surg 23:1002–1006
26. Rüffer A, Purbojo A, Cicha I, Cesnjevar RA et al (2010) Early failure of xenogenous decellularised pulmonary valve conduits--a word of caution! Eur J Cardiothorac Surg 38:78–85
27. Gonzalez BA, Pour Issa E, Mankame OV et al (2020) Porcine small intestinal submucosa mitral valve material responses support acute somatic growth. Tissue Eng Part A 26:475–489
28. Hoerstrup SP, Sodian R, Daebritz S et al (2000) Functional living trileaflet heart valves grown in vitro. Circulation 102:III44–III49
29. Flanagan TC, Cornelissen C, Koch S et al (2007) The in vitro development of autologous fibrin-based tissue-engineered heart valves through optimised dynamic conditioning. Biomaterials 28:3388–3397
30. Mol A, Rutten MC, Driessen NJ et al (2006) Autologous human tissue-engineered heart valves: prospects for systemic application. Circulation 114:I152–I158
31. Robinson PS, Johnson SL, Evans MC et al (2008) Functional tissue-engineered valves from cell-remodeled fibrin with commissural alignment of cell-produced collagen. Tissue Eng Part A 14:83–95
32. Sutherland FW, Perry TE, Yu Y et al (2005) From stem cells to viable autologous semilunar heart valve. Circulation 111:2783–2791
33. Mol A, Driessen NJB, Rutten MCM et al (2005) Tissue engineering of human heart valve leaflets: a novel bioreactor for a strain-based conditioning approach. Ann Biomed Eng 33:1778–1788
34. Motta SE, Lintas V, Fioretta ES et al (2019) Human cell-derived tissue-engineered heart valve with integrated Valsalva sinuses: towards native-like transcatheter pulmonary valve replacements. NPJ Regen Med 4:14
35. Lintas V, Fioretta ES, Motta SE et al (2018) Development of a novel human cell-derived tissue-engineered heart valve for transcatheter aortic valve replacement: an in vitro and in vivo feasibility study. J Cardiovasc Transl Res 11:470–482
36. Driessen-Mol A, Emmert MY, Dijkman PE et al (2014) Transcatheter implantation of homologous "off-the-shelf" tissue-engineered heart valves with self-repair capacity: long-term functionality and rapid in vivo remodeling in sheep. J Am Coll Cardiol 63:1320–1329
37. Ramaswamy S, Gottlieb D, Engelmayr GC Jr et al (2010) The role of organ level conditioning on the promotion of engineered heart valve tissue development in-vitro using mesenchymal stem cells. Biomaterials 31:1114–1125
38. Flanagan TC, Sachweh JS, Frese J et al (2009) In vivo remodeling and structural characterization of fibrin-based tissue-engineered heart valves in the adult sheep model. Tissue Eng Part A 15:2965–2976
39. Syedain ZH, Tranquillo RT (2009) Controlled cyclic stretch bioreactor for tissue-engineered heart valves. Biomaterials 30:4078–4084

40. Syedain ZH, Lahti MT, Johnson SL et al (2011) Implantation of a tissue-engineered heart valve from human fibroblasts exhibiting short term function in the sheep pulmonary artery. Cardiovasc Eng Technol 2:101–112
41. Weber M, Gonzalez de Torre I, Moreira R et al (2015) Multiple-step injection molding for fibrin-based tissue-engineered heart valves. Tissue Eng Part C Methods 21:832–840
42. Weber M, Heta E, Moreira R et al (2014) Tissue-engineered fibrin-based heart valve with a tubular leaflet design. Tissue Eng Part C Methods 20:265–275
43. Moreira R, Velz T, Alves N et al (2015) Tissue-engineered heart valve with a tubular leaflet design for minimally invasive transcatheter implantation. Tissue Eng Part C Methods 21:530–540
44. Filho ALL, Cheung PYC, Noritomi PY et al (2010) Construction and adaptation of an open source rapid prototyping machine for biomedical research purposes-a multinational collaborative development. In: Bartolo PJ et al (eds) Innovative developments in design and manufacturing: advanced research in virtual and rapid prototyping. CRC Press Taylor & Francis Group, London, pp 469–474
45. Hockaday LA, Kang KH, Colangelo NW et al (2012) Rapid 3D printing of anatomically accurate and mechanically heterogeneous aortic valve hydrogel scaffolds. Biofabrication 4:035005
46. Duan B, Kapetanovic E, Hockaday LA et al (2014) Three-dimensional printed trileaflet valve conduits using biological hydrogels and human valve interstitial cells. Acta Biomater 10:1836–1846
47. Ma N, Cheung DY, Butcher JT (2022) Incorporating nanocrystalline cellulose into a multifunctional hydrogel for heart valve tissue engineering applications. J Biomed Mater Res A 110(1):76–91
48. Hockaday LA, Duan B, Kang KH et al (2014) 3D-printed hydrogel technologies for tissue-engineered heart valves. 3D Print Addit Manuf 1:122–136
49. Kang LH, Armstrong PA, Lee LJ et al (2017) Optimizing photo-encapsulation viability of heart valve cell types in 3D printable composite hydrogels. Ann Biomed Eng 45:360–377
50. Maxson EL, Young MD, Noble C et al (2019) In vivo remodeling of a 3D-bioprinted tissue engineered heart valve scaffold. Bioprinting 16:e00059
51. Neidert MR, Lee ES, Oegema TR et al (2002) Enhanced fibrin remodeling in vitro with TGFbeta 1, insulin and plasmin for improved tissue-equivalents. Biomaterials 23:3717–3731
52. Berry JL, Steen JA, Koudy Williams J et al (2010) Bioreactors for development of tissue engineered heart valves. Ann Biomed Eng 38:3272–3279
53. Hoerstrup SP, Sodian R, Sperling JS et al (2000) New pulsatile bioreactor for in vitro formation of tissue engineered heart valves. Tissue Eng 6:75–79
54. Hildebrand DK, Wu ZJ, Mayer JE Jr et al (2004) Design and hydrodynamic evaluation of a novel pulsatile bioreactor for biologically active heart valves. Ann Biomed Eng 32:1039–1049
55. Kortsmit J, Rutten MC, Wijlaars MW et al (2009) Deformation-controlled load application in heart valve tissue engineering. Tissue Eng Part C Methods 15:707–716
56. Syedain ZH, Weinberg JS, Tranquillo RT (2008) Cyclic distension of fibrin-based tissue constructs: evidence of adaptation during growth of engineered connective tissue. Proc Natl Acad Sci U S A 105:6537–6542
57. Syedain ZH, Meier LA, Bjork JW et al (2011) Implantable arterial grafts from human fibroblasts and fibrin using a multi-graft pulsed flow-stretch bioreactor with noninvasive strength monitoring. Biomaterials 32:714–722
58. Schmidt JB, Tranquillo RT (2016) Cyclic stretch and perfusion bioreactor for conditioning large diameter engineered tissue tubes. Ann Biomed Eng 44:1785–1797
59. Sierad LN, Simionescu A, Albers C et al (2010) Design and testing of a pulsatile conditioning system for dynamic endothelialization of polyphenol-stabilized tissue engineered heart valves. Cardiovasc Eng Technol 1:138–153
60. Kennamer A, Sierad L, Pascal R et al (2016) Bioreactor conditioning of valve scaffolds seeded internally with adult stem cells. Tissue Eng Regen Med 13:507–515

61. Kluin J, Talacua H, Smits AI et al (2017) In situ heart valve tissue engineering using a bioresorbable elastomeric implant – from material design to 12 months follow-up in sheep. Biomaterials 125:101–117
62. Coyan GN, D'Amore A, Matsumura Y et al (2019) In vivo functional assessment of a novel degradable metal and elastomeric scaffold-based tissue engineered heart valve. J Thorac Cardiovasc Surg 157:1809–1816
63. Capulli AK, Emmert MY, Pasqualini FS et al (2017) JetValve: rapid manufacturing of biohybrid scaffolds for biomimetic heart valve replacement. Biomaterials 133:229–241
64. Bennink G, Torii S, Brugmans M et al (2018) A novel restorative pulmonary valved conduit in a chronic sheep model: mid-term hemodynamic function and histologic assessment. J Thorac Cardiovasc Surg 155:2591–2601.e3
65. Morales DL, Herrington C, Bacha EA et al (2021) A novel restorative pulmonary valve conduit: early outcomes of two clinical trials. Front Cardiovasc Med 7:583360
66. Soliman OI, Miyazaki Y, Abdelghani M et al (2017) Midterm performance of a novel restorative pulmonary valved conduit: preclinical results. EuroIntervention 13:e1418–e1427
67. Fioretta ES, Lintas V, Mallone A et al (2019) Differential leaflet remodeling of bone marrow cell pre-seeded versus nonseeded bioresorbable transcatheter pulmonary valve replacements. JACC Basic Transl Sci 5:15–31
68. Iaizzo PA (2009) Handbook of cardiac anatomy, physiology, and devices, 2nd edn. Springer, New York, p 398
69. Shinoka T, Breuer CK, Tanel RE et al (1995) Tissue engineering heart valves: valve leaflet replacement study in a lamb model. Ann Thorac Surg 60:S513–S516
70. Motta SE, Fioretta ES, Dijkman PE et al (2018) Development of an off-the-shelf tissue-engineered sinus valve for transcatheter pulmonary valve replacement: a proof-of-concept study. J Cardiovasc Transl Res 11:182–191
71. Emmert MY, Weber B, Behr L et al (2014) Transcatheter aortic valve implantation using anatomically oriented, marrow stromal cell-based, stented, tissue-engineered heart valves: technical considerations and implications for translational cell-based heart valve concepts. Eur J Cardiothorac Surg 45:61–68
72. Emmert MY, Weber B, Wolint P et al (2012) Stem cell-based transcatheter aortic valve implantation: first experiences in a pre-clinical model. JACC Cardiovasc Interv 5:874–883
73. Emmert MY, Weber B, Behr L (2011) Transapical aortic implantation of autologous marrow stromal cell-based tissue-engineered heart valves: first experiences in the systemic circulation. JACC Cardiovasc Interv 4:822–823
74. Weber B, Scherman J, Emmert MY et al (2011) Injectable living marrow stromal cell-based autologous tissue engineered heart valves: first experiences with a one-step intervention in primates. Eur Heart J 32:2830–2840
75. Uiterwijk M, Smits AIPM, van Geemen D et al (2020) In situ remodeling overrules bioinspired scaffold architecture of supramolecular elastomeric tissue-engineered heart valves. JACC Basic Transl Sci 5:1187–1206
76. Miyazaki Y, Soliman OII, Abdelghani M et al (2017) Acute performance of a novel restorative transcatheter aortic valve: preclinical results. EuroIntervention 13:e1410–e1417
77. Prodan Z, Mroczek T, Sivalingam S et al (2022) Initial clinical trial of a novel pulmonary valved conduit. Semin Thorac Cardiovasc Surg 34(3):985–991
78. Fioretta ES, Motta SE, Lintas V et al (2021) Next-generation tissue-engineered heart valves with repair, remodelling and regeneration capacity. Nat Rev Cardiol 18:92–116
79. Syedain Z, Reimer J, Lahti M et al (2016) Tissue engineering of acellular vascular grafts capable of somatic growth in young lambs. Nat Commun 7:12951
80. Tudorache I, Theodoridis K, Baraki H et al (2016) Decellularized aortic allografts versus pulmonary autografts for aortic valve replacement in the growing sheep model: haemodynamic and morphological results at 20 months after implantation. Eur J Cardiothorac Surg 49:1228–1238

81. International Organization for Standardization (2021) Cardiovascular implants – cardiac valve prostheses – part 1: general requirements (ISO 5840-1)
82. International Organization for Standardization (2021) Cardiovascular implants – cardiac valve prostheses – part 2: surgically implanted heart valve substitutes (ISO 5840-2)
83. Zhang BL, Bianco RW, Schoen FJ (2019) Preclinical assessment of cardiac valve substitutes: current status and considerations for engineered tissue heart valves. Front Cardiovasc Med 6:72
84. Huygens SA, Rutten-van Molken M, Noruzi A et al (2019) What is the potential of tissue engineered pulmonary valves in children? Ann Thorac Surg 107:1845–1853

# Chapter 14
# Anticoagulation Management for Mechanical Valves in the On-X Era


**Monique Bethel and Vishal Arora**

## 14.1 Introduction

The first mechanical valve was placed into a 30-year old woman in 1952 [1]. The first generation of this innovation was a ball-in-cage design and was implanted not at the location of the native aortic valve, but in the descending aorta. Ultimately, 200 patients received this mechanical valve [2]. During these early years of valve replacement surgery, there were reports of thrombus forming around the valve construct [3]. As the engineering of mechanical heart valves and surgical survival improved, the technology was able to be expanded for use in the aortic, and eventually, the mitral positions. Follow-up studies of these early valves showed that thromboembolic events were quite common. In the 1960s, the Starr-Edwards mechanical ball-in-cage valve was introduced and could be placed in the aortic position (at the aortic root) and in the mitral position [4]. Interestingly, thromboembolic events were again quite common in these early valves, with reported rates of up to 27% of valves in the aortic position [5] and rates of up to 70% for valves placed in the mitral position [6]. Systemic anticoagulation to prevent thromboembolic events was already widespread [5, 7]. Improvements in the materials composing the valves and the overall valve design have led to changes in anticoagulation management for patients with mechanical valves. The purpose of this chapter is to review the current indications, complications, and guidelines for the use of anticoagulation for mechanical valves in the aortic and mitral positions.

M. Bethel · V. Arora (✉)
Department of Medicine, Augusta University, Augusta, GA, USA
e-mail: mbethel@augusta.edu; varora@augusta.edu

© The Author(s), under exclusive license to Springer Nature Switzerland AG 2023

P. A. Iaizzo et al. (eds.), *Heart Valves*, https://doi.org/10.1007/978-3-031-25541-0_14

## 14.2 Risk of Mechanical Valve Thrombotic and Thromboembolic Complications

Thromboembolic phenomena after placement of a mechanical valve include systemic thrombosis, transient ischemic attacks (TIA), and/or cerebrovascular accidents (stroke) [8]. While these events were more common during the early days of valve replacement, the improved design of later generation mechanical valves and systemic anticoagulation have made these relatively rare events. For example, in the 1960s, Akbarian et al. reported on TE events after a mean follow-up of 20 months and found a 24% rate of events involving the caged ball valve [5]. This compares to a lower incidence of events among patients receiving the St. Jude bi-leafet valve, at 3.71%/person-year, reported after examining outcomes from the years 1978 and 1982 [9]. More recently, Labaf et al., using a database of Swedish patients who both received a mechanical valve between the years 2005 and 2011 and were on anticoagulation, reported an annual incidence of TIA/stroke of 1.3 per 100 person-years for mechanical aortic valves and 1.6 for mechanical mitral valves [8]. In this study, there was no statistically significant difference between the incidence of TE events between valves in the aortic or mitral position, although multiple other studies have shown that the incidence of valve thrombosis and thromboembolic phenomena are more common with mechanical mitral valves [8, 10–17]. The LOWERING-IT trial conducted in Germany also showed low rates of thromboembolic events in patients with bi-leaflet mechanical aortic valves, this despite less aggressive INR goals, with no significant difference in the event rate for those with an average INR of 1.9 vs 2.6 [18].

The most severe TE event that can occur is thrombosis of the valve itself. This causes malfunction of the valve and can lead to life-threatening sequelae [16]. Patients who have formed thrombus may be completely asymptomatic; or, in the case of acute formation of a large thrombus, may present with cardiogenic shock [16]. Pannus, which is an inflammatory tissue that may form over time and obstruct flow through the valve, may present similarly to thrombus or may be accompanied by thrombus; however, it is important to distinguish the two, because the treatments are completely different [19]. It can be difficult to distinguish between the two based on symptoms alone. Fortunately, there are now several imaging options to aid in the diagnosis including transesophageal echocardiography (TEE), valve fluoroscopy, and/or computed tomography (CT) [19].

TEE is a more invasive modality than the other options but has the advantage of avoiding exposure to ionizing radiation. Tanis et al. reviewed the literature regarding TEE and fluoroscopy and found that in cases of prosthetic valve thrombosis (PVT) there was more likely to be a mass visualized on TEE and restricted leaflet movement on fluoroscopy, compared to the presence of pannus, where these findings were much less likely [19]. Hsu et al. point out the limitations in the use of echocardiography to determine valve obstruction, as pressure gradients suggesting valve obstruction may be erroneous [20]. They postulated that CT may be an ideal alternative, as this modality has the capability for superior spatial resolution along with the provision of cine images, which allow visualization of the heart throughout the cardiac cycle [20].

Should a thrombus be identified and the patient is hemodynamically stable, then the first treatment option is to optimize or intensify anticoagulation [16]. If this is unsuccessful or, if dealing with a large thrombus, then more aggressive therapy with thrombolytics can be considered [21]. The final option, if more conservative methods are unsuccessful, is repeat valve surgery which is the least desirable option due to the increased risk in repeating open heart.

## 14.3 What Determines the Thrombotic Risks of the Mechanical Valve

There are three factors that contribute to the thrombogenic potential of any prosthetic material in the body. First, the properties of the biomaterial itself perhaps play the largest role in the thrombogenic potential of an implant. Second, the hemodynamic changes introduced to the body by the design, placement, and shape of the valve. Finally, patient-related factors including the use of anticoagulants, genetics, and associated comorbidities may affect the local milieu surrounding the valve and the propensity to form clot [22]. Each of these will be discussed in further detail.

### *14.3.1 Biomaterials*

As any foreign material placed in to the body, the materials that compose prosthetic valves are all to some degree thrombogenic [22]. The Starr Edwards ball-in-cage valve was composed of a silicone-based ball within a stellite cage, surrounded by a fabric sewing ring [2]. One of the earlier models of this valve had a Dacron (a synthetic polyester material) coating on the metal struts [23]. In vitro studies showed that both platelets and plasma proteins such as von Willebrand factor, fibrinogen, and fibronectin become absorbed by Dacron [24]. In addition to these materials absorbing platelets, in patients with prosthetic valves, more circulating platelets are in the activated state [25]. Activated platelets are able to aggregate and help stabilize nascent thrombus and are therefore critical components of the coagulation cascade [26]. Furthermore, the presence of prosthetic materials induces activation of other proteins involved in the extrinsic [27] and intrinsic [28] pathways of the coagulation cascade. Warfarin, a vitamin K antagonist (VKA), inhibits hepatic synthesis of coagulation factors involved in both pathways of the coagulation cascade (factors II, XII, IX, and X). Therefore, warfarin, and other VKAs, have been keystones in counteracting the thrombogenic state induced by mechanical valves [29].

The evolution of the mechanical valve has also included an evolution of the biomaterials used to construct the valve leaflets, sewing ring, and struts. After the Starr Edwards valve, other valves began to incorporate materials such as titanium and pyrolytic carbon [2]. Both of these materials are less thrombogenic than the

materials that composed the earliest mechanical valves; however, a synthetic material able to perfectly mimic the non-thrombogenic properties of human endothelium cells has remained elusive [28].

### *14.3.2 Hemodynamics*

A diseased native heart valve produces negative hemodynamic effects. At the point these effects produce symptoms or cause detrimental changes to the heart itself, it is time to consider replacement of the valve [30]. Mechanical prostheses are an improvement over a diseased native valve, but they too alter the fluid dynamics in the immediate area, and this contributes to their thrombogenic potential. It is important to consider the three general types of mechanical valve constructs when discussing how they alter hemodynamics. There is the first-generation caged-ball construct, which has been previously introduced. With time, two other general constructs emerged, the disk/tilting disk and, lastly, the bi-leaflet mechanical valve which is most commonly in use today [31].

In terms of fluid dynamics, the caged-ball construct performed the worst. When open to flow, a circumferential, high-velocity jet forms, leaving a central region with little to no flow [30]. This central area of low or no flow may reverse and flow back toward the valve during cardiac systole [30]. The differential flow speeds between these two jets creates turbulence that encourages the formation of thrombus [30]. The high-velocity jet also causes increased shear stress along the vessel wall [30]. High shear stress may damage the endothelial cells, which can activate the coagulation cascade [32]. The turbulent flow also causes imbalances in procoagulant cellular elements and anti-thrombotic cytokines released by the endothelium that can favor thrombus formation in low flow states [28]. One positive characteristic of these first-generation mechanical valves was that the ball seals the orifice nearly completely in diastole, therefore, there is very little regurgitant flow to create additional turbulence [30].

The tilting disk valve creates a major and minor orifice, with two tracts for blood flow [30]. Flow from the larger orifice has a slightly higher velocity, but the velocities of these two jets are generally similar [30]. Like the caged ball, if there is enough of a differential in flow velocity between the two orifices, an area of reverse flow can form and cause turbulence [30]. Additionally, leakage jets can form in the small spaces between the sewing ring and the disks, though these small jets can have the benefit of “washing” the disk and discouraging the formation of thrombus [33]. However, if these jets become sufficiently large, they may cause significant leakage across the valve and require repair or replacement. Generally, the shear stress from the jets in a properly functioning disk valve is lower than that formed in the caged ball construct and causes less endothelial damage [30].

The bi-leaflet valve forms two lateral and one central orifice, allowing three paths for forward flow [30]. The velocities of flow from the lateral orifices are slightly higher than the central orifice [30]. There are small areas of decreased/reverse flow

around the hinge points of the semicircular leaflets. There is also slightly more regurgitant flow than a disk valve, however, this may be beneficial as a "washing" jet [30]. Nevertheless, this area remains an area vulnerable to thrombus formation due to turbulence [30]. The bi-leaflet valves produce the lowest shear stress levels among the three valve constructs, but tends to develop high-velocity turbulent flows in the central jet which may cause endothelial damage further downstream [30].

### *14.3.3 Cavitation*

Small microbubbles of gas form in the blood stream and can grow relatively large with local drops in pressure [30]. If the pressure changes quickly, these bubbles can collapse, causing a shock wave that can strike valve leaflets and cause small defects called pits. This process is called cavitation. Small imperfections such as these can encourage the formation of thrombus [34] and/or damage to blood cells [35]. Cavitation pits have been observed on mechanical valves in the mitral position [30]. Tilting disk valves have been shown to be more susceptible to cavitation damage than other valve constructs [34].

### *14.3.4 Patient Factors*

The individual patient characteristics that may affect the coagulant state are likely innumerable. There are some characteristics predisposing to valve thromboembolism that have been defined in the literature and may be useful in terms of identifying patients at higher risk of TE events.

A small prospective case-control study compared 18 patients who developed PVT despite a therapeutic or near-therapeutic INR compared to 18 that did not [36]. The authors reported that those with PVT had significantly higher markers of platelet reactivity. The authors hypothesized that such patients may benefit from the addition of antiplatelet therapy to standard anticoagulation. These assays are not commonly performed in clinical practice but are examples of how patient-specific factors may effect thrombotic risk.

Kalpana et al. performed polymerase chain reaction experiments on 91 consecutive patients with mechanical valves in the aortic and mitral positions and PVT [17]. The primary outcome was to examine expression of certain genes known to be associated with response to anticoagulation. Compared to controls with rheumatic heart disease or mechanical valve prostheses without thrombosis, expression of the homozygous recessive gene *CYP4F2* was associated with a fivefold increase in having PVT. The investigators also noted that female gender and smaller valve size were associated with an increased risk of PVT. These data further support a genetic predisposition to thromboembolic (TE) events.

Other patient characteristics, such as having a non-"O" blood type [37], congenital or acquired thrombophilias [38, 39], female gender [14, 17], and/or older age [40] have all been associated with higher rates of valve thrombosis or TE events. Clinical comorbidities such as severe left ventricular systolic dysfunction or congestive heart failure [12, 37], atrial fibrillation [10], enlarged left atrium [10], and/or vascular disease [8] are also associated with increased risk of valve thrombosis or TE events. Pregnancy is another known hypercoagulable state and will be discussed further below.

## 14.4 INR Targets for Mechanical Valves

INR targets were established early in the history of valve replacements and have been relatively stable. In a historical analysis published in 1993, Albertal et al. defined "moderate intensity anticoagulation" in patients with mechanical valves, including the caged ball valve and the tilting disk valve [41]. Moderate intensity anticoagulation was defined as an INR target of 2.5–3.5 with the addition of a daily 100–325 mg dose of aspirin [41]. With this regimen, the reported incidence of thromboembolic events was 3.3%. Several years later, the American College of Cardiology and the American Heart Associateion (ACC/AHA) published the first guidelines on anticoagulation therapy for patients with mechanical valves [42]. These initial recommendations closely adhered to the previous study and included an INR goal of 2.5–3.5 for all valves in the first 3 postoperative months, followed by 2.0–3.0 for valves in the aortic position (or 2.5–3.5 if additional risk factors are present), and maintaining an INR goal of 2.5–3.5 for valves in the mitral position [42]. The addition of low-dose aspirin to all patients was granted a IIa indication, signifying that the benefits probably outweigh the risk, and it would be a reasonable treatment [42].

As the design of mechanical valves has evolved to make them less thrombogenic, the question has arisen of whether the anticoagulation targets should remain the same. Kido and Ball examined this issue for mechanical aortic valves with a meta-analysis. This meta-analysis included studies from 1946 to 2017 and found that the INR target should be based on several factors, including the type of valve [43]. Additionally, consideration should be given to the overall risk of TE. Those deemed to be at higher risk, including those with atrial fibrillation, prior TE events, decreased LV function, first-generation mechanical valves, and older age should maintain a higher INR goal, while those at lower risk may have more lenient INR targets [43]. This has been reflected in the guidelines over time. The 2014 ACC/AHA guidelines recommend that a patient with a newer generation valve in the aortic position (i.e., tilting disk or bi-leaflet) and no other risk factors can safely target an INR of 2.5, while a patient with any mechanical valve in the mitral position should have an INR target of 3.0 [44]. Of note, in the 2017 update to the 2014 guidelines, it was recommended that each patient should be given a specific INR target instead of a range, to avoid INR values consistently at the upper or lower threshold of the therapeutic window [45].

The European Society of Cardiology (ESC) guidelines on the management of valvular heart disease, published in 2017, are similar to the ACC/AHA guidelines, but differ on a few points. The ESC approach first considers the thrombogenicity profile of the specific mechanical valve, and risk is categorized as low, medium, or high [46]. Then, patient characteristics increasing the risk of TE events are included, and a high risk patient is considered as having one or more of the following: a mitral prosthesis, LVEF <35%, atrial fibrillation, or previous TE events [46]. Applying this paradigm, a patient with a high-risk prosthesis combined with a high-risk clinical profile would have a target INR of 4.0. The ESC guidelines recommend low dose aspirin in addition to warfarin only in cases of TE events occurring in the face of a therapeutic INR or concomitant atherosclerotic disease, where aspirin is a separately indicated therapy [46].

## 14.5 The On-X Mechanical Valve and Newer Generation Bi-Leaflet Valves

For the newest generation of mechanical valve placed in the aortic position, there has been consideration for even lower INR targets. The On-X valve (On-X Life Technologies Inc., Austin, TX) is a bi-leaflet mechanical valve which was engineered to minimize the risk of TE events [47]. It was first implanted into patients in 1996 and can be implanted at the aortic and mitral positions [47]. Part of its unique design is the pyrolytic carbon material from which the leaflets are constructed. Pyrolytic carbon is a pure carbon compound [48] produced through manufacturing processes to ensure that it is durable and less thrombogenic than materials used in previous valve constructs [49]. Formerly, older valves were constructed in part from silicone, due to its biocompatibility and strength [50]. Some earlier generation mechanical valves also had a pyrolytic carbon coating [31]. The St. Jude bi-leaflet valve is constructed in part from pyrolytic carbon, but was shown to have a higher incidence of valve thrombosis and a smaller effective orifice area than the On-X [51]. Furthermore, the On-X design was found by some authors to allow for less turbulent flow. Gao et al. found that there was specifically less turbulent flow around the hinges, even compared to other bi-leaflet valves [52]. Mirkhani et al. designed a computer simulation model to study fluid mechanical properties of the On-X valve and found that such models predict less turbulence and a smaller transvalvular gradient [53]. Conversely, other studies have shown that the On-X valve has a similar, but not superior, hemodynamic profile to other bi-leaflet valves currently available on the market [54], and it does not consistently reduce turbulent flow across when the valve was in the aortic position [55].

The On-X valve has performed well clinically. Early follow-up was published by Moidl et al. sharing their 5-year experience in the United States and Europe [47]. Over 500 patients having isolated aortic or mitral valve replacement were included. In this study, patients were anticoagulated with warfarin to an INR goal of 2.0–3.0

for valves in the aortic position and 2.5–3.5 for valves in the mitral position. Notably, in both the "early" (<30 days following surgery) and "late" (≥30 days following surgery) postoperative periods, there were no instances of valve thrombosis. Rates of both early and late TE events were low, with a maximum of 1.3% of patients having an early TE event and 1.7% having a late TE event. This confirmed that the On-X valve performed better at preventing events than previous valves, at least in the early postoperative period.

Longer term 12-year follow-up of 691 patients receiving single or dual valve replacement was published in 2013 [56]. Rates of events were similarly low with stroke, TIA, and valve thrombosis occurring at rates less than 1% per patient-year. Taken together, these design characteristics and outcome data led to studies to investigate if the On-X valve was appropriate for a lower INR target.

The Prospective Randomized On-X Anticoagulation Trial (PROACT), initiated in 2006, examined the safety of a lower target INR for patients with an On-X valve in the aortic position [57]. This study included patients who would be considered at higher risk for TE events, including those in atrial fibrillation, reduced LV systolic function (<30%), and a history of prior events. This study included 375 patients who were randomized to standard warfarin therapy to an INR goal of 2.0–3.0 versus 1.5–2.0 in the experimental group. The mean INR in the experimental group was 1.89 and after 4 years of follow-up, bleeding events were significantly lower in the experimental group. While there was significantly less bleeding in the lower INR group, the rate of thrombotic events between the groups was the same. These results have been replicated in other studies [58] and the long-term results support the lower INR threshold [59]. The U.S. Federal Drug Administration approved the lower INR range for the On-X valve in the aortic position in 2015 [60].

For other newer generations of mechanical valve placed in the aortic position, there has also been consideration for lower INR targets. The LOWERING-IT trial was a single-center, open-label, prospective trial of individuals deemed at low risk for TE and receiving a single bi-leaflet mechanical aortic valve [18]. Subjects were randomized to a low INR (1.5–2.5) and standard INR (2.0–3.0) group. The study enrolled 396 individuals and after a median follow-up of 5.6 years, there was no difference in TE events between the groups, but bleeding events were significantly higher in the standard INR group [18].

Limitations of these studies included small sizes and open-label designs. Therefore, recommendations for a lower INR were included in the most recently published U.S. guidelines, but received only a class IIb indication, signifying that the benefits may outweigh the risks and the treatment may be considered [62]. In its latest guidelines, published in 2021, the ESC surmises that there is insufficient evidence to lower the INR threshold for the On-X valve [61].

Most recently, Rubino et al. repeated a prospective study with patients receiving an Abbott bi-leaflet valve in the aortic position, with tighter INR goals of "low" (INR-2.0) and "conventional" (INR 2.5) [63]. With a propensity weighted analysis, the findings still favored the lower INR target, with fewer events (a composite of bleeding and TE events) in the lower INR group [63]. Larger randomized trials may

be needed before a major change in the guidelines, but it may be considered reasonable to have a lower INR target for low-risk patients with the newer-generation mechanical aortic valves [43].

## 14.6 Complications of Anticoagulation in Mechanical Valve Replacements

Great care must be taken to avoid TE events in patients with a mechanical valve. Another potentially devastating complication is the risk of hemorrhagic events associated with the requisite anticoagulation. Historically, the rate of major bleeding with the use of vitamin K antagonists (VKA) was low. In 1994, Cannegieter et al. published a meta-analysis of 46 studies from the years 1970–1992 including over 13,000 patients, 53,000 patient years of data, and multiple types of mechanical valves. The rate of major bleeding, defined as intracranial bleeding, bleeding requiring hospitalization, or causing death, was 1.4 per 100 patient-years [11]. The addition of antiplatelet therapy increased the risk of bleeding slightly to 2.2 per 100 patient years [11]. In a more contemporary analysis of Swedish registry data, the incidence of major bleeding was slightly higher. The incidence of major bleeding was 3.9 per 100 patient years with mechanical valves in the mitral position. Major bleeding with valves in the aortic position was lower at 2.6 per 100 patient years [8]. Older age and previous major bleeding episodes were independent predictors of bleeding [8]. The risk of major bleeding may be particularly high for patients with mechanic valves at both the aortic and mitral positions. One small study reported an incidence of major bleeding double that of patients with single valves at either position [64].

Time in therapeutic range (TTR) may contribute heavily to the risk of both bleeding and thrombotic events. TTR is defined by the percentage of time that INR values are within the therapeutic range for a given patient [65]. The goal for TTR should be >70% [65]. Grzymala-Lubanski et al. found that TTR values less than 70% were associated with a significantly higher risk of bleeding and other complications in an analysis of Swedish registry data [66]. As another measure of the deleterious effects of INR instability, an INR variation of ≥0.4 between measurements has been associated with bleeding events [67]. The worst bleeding outcomes have been documented with both TTR and INR variation were abnormal [67]. This raises the question of safety and efficacy of the use of direct oral anticoagulants (DOACs) in mechanical valves.

## 14.7 Are DOACS a Reasonable Option?

The introduction of DOACs into the market revolutionized the treatment of atrial fibrillation and venous thromboembolic phenomena. This class of medication has demonstrated efficacy in preventing strokes and VTE events, with fewer bleeding

complications, and less follow-up monitoring than warfarin [68]. However, DOACs are contraindicated for anticoagulation in the setting of mechanical valves in the European and US guidelines [62]. There have been several published studies that can help explain the current guidelines.

The RE-ALIGN trial was published in the *New England Journal of Medicine* in 2013 and was a phase-II dose validation trial [69]. Participants either had to be receiving a mechanical valve in the aortic or mitral position within 1 week of enrollment (group A) or had received one least 3 months ago (group B). Participants were randomized to dabigatran or warfarin with an INR target based on TE risk. The primary outcome was the trough level of dabigatran, but other safety outcomes were analyzed, including TE events, MI, VTE, bleeding, and death. The study was terminated early due to an excess number of strokes in the participants receiving dabigatran. Greater rates of asymptomatic valve thrombosis and the composite outcome of MI, stroke, TIA, systemic embolism, or death all occurred more frequently in the participants receiving dabigatran. Additionally, there were also greater numbers of major bleeding in the dabigatran group. The majority of complications occurred in group A, the group receiving a new valve or valves. These results were disappointing; however, there were some important take-aways from the RE-ALIGN trial. Critics have pointed to a possibly inappropriate target trough level for dabigatran [70]. Furthermore, as the majority of complications occurred in group A, the group receiving a new valve, it has been argued that the levels of dabigatran in the direct vicinity of the valve were insufficient to prevent thrombosis around the sewing ring, but were high enough to encourage postsurgical bleeding at remote sites [71]. Perhaps due to the popularity and benefits of the DOAC class of medications over warfarin, investigators have pursued additional studies of DOACs in mechanical valves.

A porcine model of a bi-leaflet mechanical aortic valve compared the efficacy of apixaban and warfarin in reducing thrombus burden [72]. Of the animals receiving apixaban, 60% (three of five formed thrombus on the valve, while 66.7% [two of three animals]) receiving warfarin had evidence of clot [72]. Oral apixaban also resulted in higher thrombus burden compared to warfarin [72]. With such small sample sizes in an animal model, the benefit to humans was far from proven, but this study did show that oral apixaban provided some protection from thrombotic events. The ARISTOTLE trial examined the use of apixaban in patients with atrial fibrillation and valvular heart disease. In a sub-analysis of the data from this trial collected from patients with moderate to severe valvular disease or previous valve surgery, apixaban was non-inferior to warfarin in terms of reducing stroke risk or causing bleeding complications [73]. Again, evidence of benefit from large, randomized trials was lacking and the recommendations against the use of DOACs for mechanical valves remained in place.

A pilot study published in 2020 revisited the question of safety and efficacy of DOACs in ten patients receiving mechanical aortic valves [74]. These patients were started on 20 mg of rivaroxaban on the third postoperative day and were continued at this dose for 6 months and then switched to a VKA. After 180 days, none of the ten patients suffered any major thrombotic or bleeding events. There were also no

deaths. The results of this small study suggest that rivaroxaban may be safe for anticoagulation for aortic mechanical valves, but more data will be needed. A small study of patients with mechanical valves offered newer insights into why the DOACs have underperformed compared to warfarin. Plasma was drawn from three groups of patients with mechanical valves: a group treated with warfarin; another group treated with one of either apixaban, rivaroxaban, or dabigatran; and the final group with the combination of rivaroxaban and dabigatran. The plasma from each patient was subjected to an in vitro thrombin generation assay showing that the "mean endogenous thrombin potential" (ETP) was higher in plasma treated with dabigatran, rivaroxaban, and apixaban vs the plasma of the patients taking warfarin [75]. In the discussion, the authors suggested that mechanical valves induce the formation of factor Xa (the final step in both the intrinsic and extrinsic pathways of the coagulation cascade prior to the generation of thrombin) in concentrations that overwhelm the therapeutic potential of the DOACs. A study comparing the safety and efficacy of apixaban to warfarin in On-X valves in the aortic position is on the horizon [76].

Currently, there very limited evidence suggesting that the DOACs may be effective for anticoagulation of mechanical valves in the aortic position but may not be adequate for mechanical valves in the mitral position. Further studies are needed to help determine the most appropriate therapy for patients in these situations.

## 14.8 Anticoagulation Considerations in Special Populations

### *14.8.1 Anticoagulation in the Pregnant Patient with a Mechanical Valve*

Due to risks both to the developing fetus and mother, pregnancy presents unique challenges for managing anticoagulation with mechanical valves, and there is delicate balance in anticoagulation management that is required to keep both mother and baby safe. During pregnancy, there are multiple factors leading to a prothrombotic state. These include impaired fibrinolysis, and additionally, there are decreased levels of protein S and resistance to protein C, both of which are innate anticoagulants [77]. These factors compound the already added risk of thrombotic events from the presence of a mechanical valve. In a fully anticoagulated patient, the risk thrombotic events must be balanced against the risk of significant bleeding during a vaginal or Caesarean delivery. It is in part due to these factors that the presence of a mechanical valve is associated with an increased risk of poor pregnancy outcomes. Batra et al. reported that up to two-third of pregnant patients with a mechanical valve experienced pregnancy loss either through spontaneous or induced abortion [78]. Thrombosis of a mechanical valve in a pregnant patient is a devastating complication with reported mortality of up to 20% [79]. Furthermore, delivery was associated with a doubling of the risk needing a valve reoperation [78].

Warfarin is able to cross the placenta and can be teratogenic if used between the 6th and 12th weeks of pregnancy [80]. Warfarin can cause a fetal syndrome consisting of skeletal malformations and nasal hypoplasia [81]. The nasal hypoplasia may cause airway and feeding difficulties in early life [82]. There are also case reports of fetal intracranial hemorrhaging [83] and diaphragmatic hernias [84] with the use of warfarin. Even if a patient avoids the use of warfarin during the vulnerable period in the first trimester, the risk of embryopathy remains throughout pregnancy if warfarin is used [82]. Unfractionated heparin (UFH) does not cross the placenta [80] and is therefore a safer option for the developing fetus, but can only be administered intravenously and would be a difficult therapy to manage for outpatients. Low molecular weight heparin (LMWH) can be administered subcutaneously and thus is convenient for long-term use in the outpatient setting. There have been concerns about the overall safety of LMWH in pregnancy [85]; however, this is controversial. In a meta-analysis of pregnant patients with mechanical valves, Steinberg et al. showed that VKAs were associated with better maternal outcomes, while LMWH was associated with better fetal outcomes [77]. Conversely, there was also evidence that LMWH was associated with improved outcomes compared to UFH [77]. The 2021 ESC/EACTS guidelines recommend warfarin therapy throughout pregnancy if the daily dose is 5 mg or less. If the daily dose is more, it is recommended to transition to LMWH [61]. Aspirin is considered to be a safe medication and can be continued during a pregnancy [77]. Aspirin has been shown to reduce TE events in pregnant women, but this comes at the expense of some increased risk of bleeding [79]. The 2014 ACC/AHA guidelines recommended aspirin during the second and third trimesters [44], however, the updated guidelines published in 2020 only comment on safety but do not specifically recommend aspirin unless there is another indication, such as pre-eclampsia [62]. The ESC/EACTS recommendations do not address aspirin use in pregnant women. There is no one recommended strategy for anticoagulation in pregnant women with mechanical valves, several strategies are acceptable and there should be shared decision making between the woman and her provider about the best course of action [79]. If LMWH is used, the dosing should be monitored closely with anti-Xa levels [86].

As the time for delivery draws near, if warfarin is in use, it is usually discontinued and replaced with heparin [86]. Patients already on LMWH may be switched to UFH when hospitalization and delivery is imminent. In expectant mothers for whom a C-section delivery is anticipated or for whom surgery is required for other reasons, the same paradigm is followed. When bleeding risk has been minimized, the patient may then resume whatever anticoagulation was in use before surgery/delivery. There is some variability when anticoagulation is restarted after delivery, but it is generally within 24 hours [87], with some advocating delaying restarting of warfarin for 48 hours [86]. If delivery is early or unplanned, the use of vitamin K analogs to reverse warfarin has not been well studied and therefore no specific recommendations have been made in that regard. It has been noted that use of vitamin K analogs may possibly precipitate TE events in the mother and there is no way to monitor its effects on the fetus [88]. Nevertheless, bridging anticoagulation is mandatory for pregnant patients with a mechanical valve. Stringent laboratory monitoring of anticoagulation efficacy is required throughout pregnancy.

## 14.9 Perioperative Management of Anticoagulation in Patients with Mechanical Valves

Patients with mechanical valves undergoing procedures or surgery may have an increased risk of bleeding necessitating temporary cessation of anticoagulation. Tafur et al. designed the BleedMAP scoring system that assesses risk of major perioperative bleeding in patients on chronic anticoagulation therapy [89]. A diagnosis of cancer, prior major bleeding event, mechanical valve in the mitral position, and thrombocytopenia (platelet count <150,000 cells/μL) are all factors that raise the risk of major bleeding in the perioperative period [89]. In this scoring paradigm, each risk factor is equally weighted with a score of one and a score of two or more points is considered to be at elevated risk for perioperative bleeding [89]. In patients taking warfarin, the rate of periprocedural bleeding has been reported to be as high as 7.1% [90]. Conversely, the risk of periprocedural thromboembolic events, while lower than bleeding events, is also elevated [90, 91]. The American College of Chest Physicians released a set of guidelines in 2012 [92] to provide guidance to clinicians on the perioperative management of anticoagulation prior to high-risk surgeries or procedures. Other non-surgical procedures with an increased risk of bleeding are gastrointestinal polyp resection and implantation of intracardiac devices such as pacemakers or defibrillators. Superficial dermatological procedures, cataract removal, and venography do not require interruption of anticoagulation [93]. The category of dental procedures and endoscopic procedures are discussed in further detail below.

### *14.9.1 Dental Procedures*

The issue of warfarin interruption has been extensively studied in common dental procedures such as tooth extractions. Multiple strategies have been studied, including no interruption, limited interruption 2–3 days prior to the procedure, and full 5-day interruption. In 2002, Evans et al. performed a small randomized controlled trial comparing a group that continued warfarin therapy prior to a dental extraction to those who discontinued warfarin 2 days prior to the procedure [94]. They found no difference in bleeding between the groups. Several years later, Bajkin et al. conducted another small randomized study of anticoagulated patients undergoing tooth extraction [95]. In this study, the patients were randomized to continuation of warfarin (group A) vs discontinuation and bridging with LMWH (group B). Approximately one-third of all patients in the study had a prosthetic valve as the indication for anticoagulation. In group A, receiving continued warfarin, the average INR was 2.45 and an absorbable collage sponge was used for hemostasis at the time of extraction. Group B did not receive this method of hemostasis. Both at the time of extraction and in the 7-day post-procedure observation period, there was no significant difference in reported bleeding rates. Similar findings have been observed

in multiple studies [96–98] suggesting that only mild bleeding can be expected from minor dental procedures [99] and if it does become problematic, it can be controlled with topical hemostatic agents.

### *14.9.2 Endoscopic Procedures*

Endoscopic procedures, with or without biopsy, are generally low risk in terms of bleeding and warfarin can be continued in these situations [91]. Data were examined from a sample of individuals undergoing colonoscopy and taking warfarin enrolled in the Clinical Outcomes Research Initiative. These data showed a 2% rate of major bleeding events in this sample of patients. The extraction of polyps seems to increase the risk of bleeding [100, 101]; however, the need for discontinuing anticoagulation for all polypectomies is controversial as data suggests that small polyps can be safely removed in patients with a therapeutic INR [102]. Nevertheless, the gastroenterology guidelines advocate holding warfarin prior to a procedure in which polypectomy is anticipated [93, 103]. Anticoagulation management is also predicated upon the urgency of the procedure and the risk of TE events [104]. Interestingly, it seems that adherence to the guidelines for warfarin management is suboptimal, with a substantial percentage of physicians improperly following the guidelines [105]. There is some evidence that medications are incorrectly held specifically prior to lower endoscopy [105], although the same anticoagulation management applies for upper endoscopy, esophagogastroduodenoscopy (EGD), and endoscopic retrograde cholangiopancreatography (ERCP). If there are underlying factors that raise the risk of bleeding such as suspicion of cancer, or underlying liver disease with variceal formation as these procedures carry risk of complications that may not be able to be treated endoscopically, then that may justify discontinuation of anticoagulation [104].

If undergoing a non-cardiac procedure with high risk for bleeding, it is recommended that patients on warfarin therapy stop the anticoagulant 5 days prior to the anticipated procedure. Bridging anticoagulation is mandatory in patients with a mechanical valve who are deemed to be of at least moderate risk of TE events [106]. This can be achieved with LMWH, unless there is significant renal insufficiency [106] or with UFH in the inpatient setting. UFH should be stopped 4–6 hours before the anticipated procedure. LMWH should be discontinued 12–24 hours prior to the procedure, with some advocating dose adjustment by administering a lower dose the day prior to surgery [107]. Interestingly, if LMWH is stopped 12 hours prior to the procedure, there is evidence that a substantial number of patients have a therapeutic levels of LMWH as measured by anti-factor Xa level [108]. Patients with mechanical heart valves who are at low risk for TE events should *not* receive bridging anticoagulation [93]. Anticoagulation therapy should be resumed fairly rapidly, no more than 12–24 hours after surgery [93]. Patients receiving aspirin should have the medication discontinued 7–10 days prior to a surgery/procedure with high risk for bleeding but aspirin should not be interrupted for minor procedures [93].

In the case of emergency non-cardiac surgery, or other cases of life-threatening bleeding, there is a paucity of evidence-based guidelines. Moia and Squizzato proposed a 7-component model for treatment of life-threatening bleeding in the setting of anticoagulant use. The first action would be withdrawing the anticoagulant, followed by resuscitation with IV fluids, while simultaneously measuring blood counts, liver and renal function, and coagulation studies, then transfusion of blood products and local hemostatic measures if possible, and finally administration of reversal agents [109]. In the case of warfarin, this may be achieved with oral or IV vitamin K, or if immediate reversal is needed, then administration of fresh frozen plasma or non-activated prothrombin complex concentrates [109].

## 14.10 Atrial Fibrillation and Mechanical Valves

Mechanical heart valves pose inherent thrombotic risks, but added to this, the presence of atrial fibrillation and mitral valve disease requiring a mechanical valve raises those risk even higher. Atrial fibrillation in the presence of a mechanical heart valve may complicate the proposed anticoagulation strategy. In an observational study of approximately 10,000 patients with atrial fibrillation, mechanical valves were present in 3% of these patients [110]. As the prevalence of atrial fibrillation is already high and expected to grow higher with the aging population of Western countries, this represents a substantial number of patients [111]. Additionally, atrial fibrillation has been cited as the most significant risk factor for TE events after mechanical mitral valve replacement [112]. The CHADS2-VASc score, which is typically used to determine stroke risk in patients with atrial fibrillation, may underestimate the risk of TE events in patients with mechanical valves [113]. Melgaard et al. found that even for those who would be considered at low risk for stroke, i.e., a CHADS2VASC score of 1 or 0, in the presence of a mechanical valve, the observed risk of stroke was high enough to suggest these individuals would benefit from full anticoagulation [114]. The time in therapeutic range (TTR) is important in the use of warfarin for anticoagulation, and indeed in patients with atrial fibrillation, a mechanical valve, and a subtherapeutic INR, there was a 1.1–1.4% incidence of TE events within 14 days of the subtherapeutic INR measurement [115].

Still today, the incidence of postoperative atrial fibrillation following valve surgery is quite high. Kalra et al. reported that approximately 31% of patients developed atrial fibrillation following mechanical aortic valve replacement [116]. These authors site several conditions in the postoperative period which may incite atrial fibrillation, including a hyperadrenergic state, volume overload, and inflammation surrounding the surgical site [116]. In an outcome study of patients undergoing aortic mechanical valve replacement, the prevalence of atrial fibrillation was 18.2% after a median follow-up of 7.8 years [117]. There is also evidence that the incidence of atrial fibrillation is higher after mechanical vs bioprosthetic valve replacement, especially in the mitral position. Jin et al. followed 150 patients with rheumatic mitral stenosis undergoing surgical mitral valve replacement and found that the

incidence of early postoperative atrial fibrillation was 39% and 21% of patients 1 year out from surgery [118]. The incidence may be extremely high after multiple valve surgery, up to 74% [119].

### *14.10.1 Anticoagulation in Patients with a Mechanical Valve, Atrial Fibrillation, and Coronary Disease*

There is also the potential for coronary artery disease in this patient population, and if percutaneous intervention becomes necessary, then so-called "triple therapy" with aspirin, a $P2Y_{12}$ inhibitor such as clopidogrel, and warfarin may be indicated. The question then becomes how to safely balance the risks of bleeding on triple therapy and the risks of valve or stent thrombosis when anticoagulation and antiplatelet therapies are inadequate. Triple therapy is associated with a high risk of major and minor bleeding events, as much as 16% annually [120]. Generally, patients are continued on triple therapy for 1–6 months following PCI, but there have not been robust clinical trials to determine the optimal length of therapy. One example of studies in this area include the WOEST trial, in which patients already receiving warfarin therapy and subsequently undergoing stent placement were randomized to dual therapy with clopidogrel and warfarin vs triple therapy. The safety in terms of bleeding events of dual- vs triple-therapy were compared, but the study was not powered to determine efficacy. There were significantly fewer bleeding events in the dual-therapy group vs the triple-therapy group, 19.4% vs 44.4% (HR 0.36) [120]. The WOEST trial suggests that the dual therapy strategy may be effective, but there were no patients with mechanical valves in the sample. Other studies that have compared dual- vs. triple therapy, such as AUGUSTUS [121] and the RE-DUAL PCI [122], have also excluded those with mechanical valves. In their 2017 guidelines, the ESC recommends dual therapy for anticoagulated patients who undergo PCI but who are at higher risk of bleeding; however, the population of patients with mechanical valves are not specifically addressed [123]. The optimal approach to addressing antiplatelet and anticoagulation therapy in patients with mechanical valves and symptomatic coronary disease requiring stents has yet to be defined.

## 14.11 Anticoagulation with Allergies/Adverse Reactions

Although not a true allergy, treatment with warfarin may result in skin lesions ranging from minor to severe [124] and which may be lethal on occasion [125]. These lesions have been called "warfarin-induced skin necrosis" and this adverse reaction was first described in 1943 [126]. It typically begins with sensations of paresthesias, followed by poorly demarcated erythema, which then devolves into hemorrhagic

petechia, bullae, or full skin thickness necrosis [127]. The lesions have a predilection for areas with a large mass of soft tissue, such as the breasts, thighs, buttocks, penis, and nose, although any area may be affected [124]. It is fortunately very rare, affecting only 0.01–0.1% of patients using warfarin [127]. The lesions typically become manifest in the first several days of warfarin use [127] however, there are case reports of this occurring after long term-term use of warfarin [128, 129]. The pathogenesis of this reaction has not been fully described, but it is thought that the initial procoagulant state induced by warfarin use, which inhibits endogenous anticoagulants proteins C and S, is one of the inciting factors [130]. Indeed, it appears that inherent protein C and S deficiencies are associated with approximately one-third of the cases of warfarin-induced skin necrosis [131]. The early pathogenic changes that manifest have rarely been documented histologically, but when the lesions are advanced, there has been demonstration of necrotic lesions and infarctions in the small capillaries and veins [124]. In advanced lesions, evidence of vasculitis or arterial involvement is usually absent [124].

Small lesions may be treated with withdrawal of warfarin alone, though larger lesions may require surgical debridement. Withholding warfarin in the case of a mechanical valve is often not an option. In such situations, anticoagulation could be achieved with LMWH injections as an outpatient, or UFH infusions for inpatients. Warfarin has been successfully re-initiated in patients who have developed skin necrosis [132].

Heparin-induced thrombocytopenia (HIT) is another potential adverse effect of anticoagulation that may be seen in patients receiving heparin. This syndrome can cause a dramatic drop in platelet levels, but paradoxically, thrombotic events occur and are a hallmark of this syndrome [133, 134]. Clinically, this situation may be only relevant for patients in the postoperative period after receiving a mechanical valve or those requiring interruption of warfarin for other surgeries or acute bleeding events. Bivalirudin [135], fondaparinux [133], and argatroban [136] have all been used as alternative anticoagulants for patients with mechanical valves in the case of HIT. LMWH is associated with lower incidence of HIT [137, 138], however, LMWH may also aggravate HIT and due to high levels of cross reactivity, it should not be used in patients with a known history of HIT [137, 139]. There are also reports of associated complications of heparin therapy in patients with warfarin skin necrosis raising the question of whether or not the two are related syndromes [140].

## 14.12 Concluding Remarks

Mechanical valves have evolved over time which have lead to reduce thromboembolic events, but perhaps the ideal valve has yet to be constructed. Many patients with mechanical valves require lifelong anticoagulation with a vitamin K antagonist, although improvements in valve design have resulted in reduced anticoagulation theraputic intensity for patients with mechanical valves in the aortic position. This

may present challenges in managing anticoagulation in pregnant patients, patients needing surgeries or procedures, and/or patients who have adverse reactions to commonly used anticoagulants. Initial studies of the DOACs were disappointing and this class of medications remains contraindicated for appropriate anticoagulation of mechanical valves, but additional testing of the newer DOACs is expected and may significantly change the management of patients with mechanical valves, especially in the aortic position.

## References


1. Mechanical Heart Valve 2008. Available from: http://www.pages.drexel.edu/~nag38/History.html
2. Gott VL, Alejo DE, Cameron DE (2003) Mechanical heart valves: 50 years of evolution. Ann Thorac Surg 76(6):S2230–S2239
3. Butany J, Ahluwalia MS, Fayet C, Munroe C, Blit P, Ahn C (2002) Hufnagel valve-the first prosthetic mechanical valve. Cardiovasc Pathol 6(11):351–353
4. Matthews AM (1998) The development of the Starr-Edwards heart valve. Tex Heart Inst J 25(4):282
5. Akbarian M, Austen WG, Yurchak PM, Scannell JG (1968) Thromboembolic complications of prosthetic cardiac valves. Circulation 37(5):826–831
6. Macmanus Q, Grunkemeier G, Thomas D, Lambert L, Starr A (1977) The Starr-Edwards model 6000 valve. A fifteen-year follow-up of the first successful mitral prosthesis. Circulation 56(4):623–625
7. Gadboys HL, Litwak RS, Niemetz J, Wisch N (1967) Role of anticoagulants in preventing embolization from prosthetic heart valves. JAMA 202(4):282–286
8. Labaf A, Grzymala-Lubanski B, Stagmo M, Lovdahl S, Wieloch M, Sjalander A et al (2014) Thromboembolism, major bleeding and mortality in patients with mechanical heart valves- a population-based cohort study. Thromb Res 134(2):354–359
9. Horstkotte D, Schulte H, Bircks W, Strauer B (1993) Unexpected findings concerning thromboembolic complications and anticoagulation after complete 10 year follow up of patients with St. Jude Medical prostheses. J Heart Valve Dis 2(3):291–301
10. Renzulli A, Deluca L, Caruso A, Verde R, Galzerano D, Cotrufo M (1992) Acute thrombosis of prosthetic valves – a multivariate-analysis of the risk-factors for a LIFE-threatening event. Eur J Cardiothorac Surg 6(8):412–421
11. Cannegieter S, Rosendaal F, Briet E (1994) Thromboembolic and bleeding complications in patients with mechanical heart valve prostheses. Circulation 89(2):635–641
12. Mustapha R, Philip I, Bohm G, Depoix JP, Enguerand D, Debauchez M et al (1994) Thromboses of heart-valve prostheses – predisposing and prognostic factors based on a study of 41 patients. Ann Chir 48(3):243–247
13. Rizzoli G, Guglielmi C, Toscano G, Pistorio V, Vendramin I, Bottio T et al (1999) Reoperations for acute prosthetic thrombosis and pannus: an assessment of rates, relationship and risk. Eur J Cardiothorac Surg 16(1):74–80
14. Durrleman N, Pellerin M, Bouchard D, Hebert Y, Cartier R, Perrault LP et al (2004) Prosthetic valve thrombosis: twenty-year experience at the Montreal Heart Institute. J Thorac Cardiovasc Surg 127(5):1388–1392
15. Bourguignon T, Bergoend E, Mirza A, Ayegnon G, Neville P, Aupart MR et al (2011) Risk factors for valve-related complications after mechanical heart valve replacement in 505 patients with long-term follow up. J Heart Valve Dis 20(6):673–680
16. Lim WY, Lloyd G, Bhattacharyya S (2017) Mechanical and surgical bioprosthetic valve thrombosis. Heart 103(24):1934–1941

17. Kalpana S, Bharath G, Simran Jain NM, Satvic CM (2019) Prosthetic valve thrombosis–association of genetic polymorphisms of VKORC1, CYP2C9 and CYP4F2 genes. Medicine 98(6):e14365
18. Torella M, Torella D, Chiodini P, Franciulli M, Romano G, De Santo L et al (2010) LOWERing the INtensity of oral anticoaGulant Therapy in patients with bileaflet mechanical aortic valve replacement: results from the "LOWERING-IT" Trial. Am Heart J 160(1):171–178
19. Tanis W, Habets J, van den Brink RB, Symersky P, Budde RP, Chamuleau SA (2014) Differentiation of thrombus from pannus as the cause of acquired mechanical prosthetic heart valve obstruction by non-invasive imaging: a review of the literature. Eur Heart J Cardiovasc Imaging 15(2):119–129
20. Hsu C, Bourganos K, Zafar MA, Huber S, Buntin J, Ziganshin BA et al (2020) Cine-computed tomography for the evaluation of prosthetic heart valve function. Cardiology 145(7):439–445
21. Gunduz S, Kalcik M, Gursoy MO, Guner A, Ozkan M (2020) Diagnosis, treatment & management of prosthetic valve thrombosis: the key considerations. Expert Rev Med Devices 17(3):209–221
22. Hoffman AS (1982) Blood—biomaterial interactions: an overview. In: Cooper SL et al (eds) Biomaterials: interfacial phenomena and applications advances in chemistry. American Chemical Society, Washington, DC
23. National Museum of American History. Starr-Edwards heart valve. Available from: https://americanhistory.si.edu/collections/search/object/nmah_1726277
24. Roald H, Barstad R, Bakken I, Roald B, Lyberg T, Sakariassen K (1994) Initial interactions of platelets and plasma proteins in flowing non-anticoagulated human blood with the artificial surfaces Dacron and PTFE. Blood Coagul Fibrinolysis 5(3):355–363
25. Pumphrey C, Dawes J (1983) Platelet alpha granule depletion: findings in patients with prosthetic heart valves and following cardiopulmonary bypass surgery. Thromb Res 30(3):257–264
26. Yun S-H, Sim E-H, Goh R-Y, Park J-I, Han J-Y (2016) Platelet activation: the mechanisms and potential biomarkers. Biomed Res Int 2016:9060143
27. Chan NC, Weitz JI, Eikelboom JW (2017) Anticoagulation for mechanical heart valves: will oral factor Xa inhibitors be effective?. Am Heart Assoc, vol 37, pp 743–745
28. Edmunds LH Jr (1996) Is prosthetic valve thrombogenicity related to design or material? Tex Heart Inst J 23(1):24
29. Tiede DJ, Nishimura RA, Gastineau DA, Mullany CJ, Orszulak TA, Schaff HV (1998) Modern management of prosthetic valve anticoagulation. Mayo Clin Proc 73(7):665–680. Elsevier
30. Yoganathan AP, He ZM, Jones SC (2004) Fluid mechanics of heart valves. Annu Rev Biomed Eng 6:331–362
31. DeWall RA, Qasim N, Carr L (2000) Evolution of mechanical heart valves. Ann Thorac Surg 69(5):1612–1621
32. Yau JW, Teoh H, Verma S (2015) Endothelial cell control of thrombosis. BMC Cardiovasc Disord 15(1):1–11
33. Kumar UD, Nareppa U, Shetty SP, Wali M (2015) Transvalvular mitral regurgitation following mitral valve replacement a diagnostic dilemma. Ann Card Anaesth 18(4):584
34. Johansen P, Andersen TS, Hasenkam JM, Nygaard H, Paulsen PK (2014) Mechanical heart valve cavitation in patients with bileaflet valves. Annu Int Conf IEEE Eng Med Biol Soc 2014:5655–5658. IEEE
35. Lee H, Taenaka Y, Kitamura S (2005) Mechanisms of mechanical heart valve cavitation in an electrohydraulic total artificial heart. ASAIO J 51(3):208–213
36. Bouganim T, Shapira Y, Sagie A, Vaturi M, Battler A, Kornowski R et al (2009) Platelet reactivity in patients with a history of obstructive prosthetic valve thrombosis. Am J Cardiol 103(12):1760–1763
37. Astarcıoğlu MA, Kalçık M, Yesin M, Gürsoy MO, Şen T, Karakoyun S et al (2016) AB0 blood types: impact on development of prosthetic mechanical valve thrombosis. Anatol J Cardiol 16(11):820

38. Pegoraro C, Biasiolo A, Iliceto S, Pengo V (2003) Mechanical prosthetic heart valve thrombosis despite optimal anticoagulation in a patient with congenital thrombophilia (factor V Leiden). Clin Appl Thromb Hemost 9(1):89–90
39. Gencbay M, Turan F, Degertekin M, Eksi N, Mutlu B, Unalp A (1998) High prevalence of hypercoagulable states in patients with recurrent thrombosis of mechanical heart valves. J Heart Valve Dis 7(6):601–609
40. Jamieson WRE, Miyagishima RT, Grunkemeier GL, Germann E, Henderson C, Lichtenstein SV et al (1999) Bileaflet mechanical, prostheses for aortic valve replacement in patients younger than 65 years and 65 years of age or older: major thromboembolic and hemorrhagic complication. Can J Surg 42(1):27–36
41. Albertal J, Sutton M, Pereyra D, Segura E, Aramburu D, Lardani H et al (1993) Experience with moderate intensity anticoagulation and aspirin after mechanical valve replacement. A retrospective, non-randomized study. J Heart Valve Dis 2(3):302–307
42. Bonow RO, Carabello B, de Leon AC Jr, Edmunds LH Jr, Fedderly BJ, Freed MD et al (1998) Guidelines for the management of patients with valvular heart disease: executive summary. A report of the American College of Cardiology/American Heart Association Task Force on Practice Guidelines (Committee on Management of Patients with Valvular Heart Disease). Circulation 98(18):1949–1984
43. Kido K, Ball J (2019) Optimal intensity of warfarin therapy in patients with mechanical aortic valves. J Pharm Pract 32(1):93–98
44. Nishimura RA, Otto CM, Bonow RO, Carabello BA, Erwin JP, Guyton RA et al (2014) 2014 AHA/ACC guideline for the management of patients with valvular heart disease: a report of the American College of Cardiology/American Heart Association Task Force on Practice Guidelines. J Am Coll Cardiol 63(22):e57–e185
45. Nishimura RA, Otto CM, Bonow RO, Carabello BA, Erwin JP, Fleisher LA et al (2017) 2017 AHA/ACC focused update of the 2014 AHA/ACC guideline for the management of patients with valvular heart disease: a report of the American College of Cardiology/American Heart Association Task Force on Clinical Practice Guidelines. J Am Coll Cardiol 70(2):252–289
46. Baumgartner H, Falk V, Bax JJ, De Bonis M, Hamm C, Holm PJ et al (2018) 2017 ESC/EACTS Guidelines for the management of valvular heart disease. Kardiol Pol (Polish Heart J) 76(1):1–62
47. Moidl R, Simon P, Wolner E (2002) The On-X prosthetic heart valve at five years. Ann Thorac Surg 74(4):1312–1317
48. Ely JL, Emken MR, Accuntius JA, Wilde DS, Haubold AD (1998) Pure pyrolytic carbon: preparation and properties of a new material, On-X° carbon for mechanical heart valve. J Heart Valve Dis 7(6):626–632
49. CryoLife. On-X pyrolytic carbon. CryoLife, Kennesaw. Available from: https://www.cryolife.com/products/contract-manufacturing/on-x-pyrolytic-carbon/
50. Coulter FB, Schaffner M, Faber JA, Rafsanjani A, Smith R, Appa H et al (2019) Bioinspired heart valve prosthesis made by silicone additive manufacturing. Matter 1(1):266–279
51. Mostafa EA, El Midany AA, Taha AS, El-Aasy SR, Doghish AA, Helmy A et al (2017) On-X versus St Jude Medical mechanical prosthesis in mitral position: are we moving forward in design technology? J Cardiovasc Surg 59(2):252–258
52. Gao Z, Hosein N, Dai F, Hwang N (1999) Pressure and flow fields in the hinge region of bileaflet mechanical heart valves. J Heart Valve Dis 8(2):197–205
53. Mirkhani N, Davoudi MR, Hanafizadeh P, Javidi D, Saffarian N (2016) On-X heart valve prosthesis: numerical simulation of hemodynamic performance in accelerating systole. Cardiovasc Eng Technol 7(3):223–237
54. Algarni KD, Hassan E, Arafat AA, Shalaby MA, Elawad HH, Pragliola C et al (2021) Early hemodynamic profile after aortic valve replacement-a comparison between three mechanical valves. Braz J Cardiovasc Surg 36:10–17
55. Hatoum H, Maureira P, Dasi LP (2020) A turbulence in vitro assessment of On-X and St Jude Medical prostheses. J Thorac Cardiovasc Surg 159(1):88–97

56. Chambers JB, Pomar JL, Mestres CA, Palatianos GM (2013) Clinical event rates with the On-X bileaflet mechanical heart valve: a multicenter experience with follow-up to 12 years. J Thorac Cardiovasc Surg 145(2):420–424
57. Puskas J, Gerdisch M, Nichols D, Quinn R, Anderson C, Rhenman B et al (2014) Reduced anticoagulation after mechanical aortic valve replacement: interim results from the prospective randomized On-X valve anticoagulation clinical trial randomized Food and Drug Administration investigational device exemption trial. J Thorac Cardiovasc Surg 147(4):1202–11. e2
58. Teshima H, Ikebuchi M, Miyamoto Y, Tai R, Sano T, Kinugasa Y et al (2017) 10-year results of On-X bileaflet mechanical heart valve in the aortic position: low target INR regimen in Japanese. Gen Thorac Cardiovasc Surg 65(8):435–440
59. Puskas JD, Gerdisch M, Nichols D, Fermin L, Rhenman B, Kapoor D et al (2018) Anticoagulation and antiplatelet strategies after On-X mechanical aortic valve replacement. J Am Coll Cardiol 71(24):2717–2726
60. On-X Life Technologies Inc (2015) FDA aprroval: On-X aortic valves with less warfarin. Life Science Connect, Erie. Available from: https://www.fdanews.com/articles/170615-fda-grants-expanded-labeling-claim-to-on-x-aortic-heart-valve
61. Vahanian A, Beyersdorf F, Praz F, Milojevic M, Baldus S, Bauersachs J et al (2022) 2021 ESC/EACTS Guidelines for the management of valvular heart disease. Developed by the Task Force for the management of valvular heart disease of the European Society of Cardiology (ESC) and the European Association for Cardio-Thoracic Surgery (EACTS). Eur Heart J 43(7):561–632
62. Members WC, Otto CM, Nishimura RA, Bonow RO, Carabello BA, Erwin JP III et al (2021) 2020 ACC/AHA guideline for the management of patients with valvular heart disease: a report of the American College of Cardiology/American Heart Association Joint Committee on Clinical Practice Guidelines. J Am Coll Cardiol 77(4):e25–e197
63. Rubino AS, Torella M, Della Ratta EE, Galbiati D, Della Corte A, Bancone C et al (2020) Safety of low intensity oral anticoagulant therapy in patients with bileaflet mechanical aortic valve prosthesis: a propensity weighted study. Int J Cardiol 317:139–143
64. Schapkaitz E, Jacobson B, Becker P, Conway G (2006) Thrombo-embolic and bleeding complications in patients with mechanical valve replacements-a prospective observational study. S Afr Med J 96(8):710–713
65. Members ATF, Camm AJ, Lip GY, De Caterina R, Savelieva I, Atar D et al (2012) 2012 focused update of the ESC Guidelines for the management of atrial fibrillation: an update of the 2010 ESC Guidelines for the management of atrial fibrillation. Developed with the special contribution of the European Heart Rhythm Association. Eur Heart J 33(21):2719–2747
66. Grzymala-Lubanski B, Labaf A, Englund E, Svensson PJ, Själander A (2014) Mechanical heart valve prosthesis and warfarin–treatment quality and prognosis. Thromb Res 133(5):795–798
67. Grzymala-Lubanski B, Svensson PJ, Renlund H, Jeppsson A, Själander A (2017) Warfarin treatment quality and prognosis in patients with mechanical heart valve prosthesis. Heart 103(3):198–203
68. Lopez-Lopez JA, Sterne JAC, Thom HHZ, Higgins JPT, Hingorani AD, Okoli GN et al (2017) Oral anticoagulants for prevention of stroke in atrial fibrillation: systematic review, network meta-analysis, and cost effectiveness analysis. Br Med J 359:j5058
69. Eikelboom JW, Connolly SJ, Brueckmann M, Granger CB, Kappetein AP, Mack MJ et al (2013) Dabigatran versus warfarin in patients with mechanical heart valves. N Engl J Med 369:1206–1214
70. Roberts A (2013) Results of RE-ALIGN disappoint. Nat Rev Cardiol 10(11):617
71. Alberio L (2014) The new direct oral anticoagulants in special indications: rationale and preliminary data in cancer, mechanical heart valves, anti-phospholipid syndrome, and heparin-induced thrombocytopenia and beyond. Semin Hematol 51(2):152–156. Elsevier
72. Lester PA, Coleman DM, Diaz JA, Jackson TO, Hawley AE, Mathues AR et al (2017) Apixaban versus warfarin for mechanical heart valve thromboprophylaxis in a swine aortic heterotopic valve model. Arterioscler Thromb Vasc Biol 37(5):942–948

73. Avezum A, Lopes RD, Schulte PJ, Lanas F, Gersh BJ, Hanna M et al (2015) Apixaban in comparison with warfarin in patients with atrial fibrillation and valvular heart disease: findings from the apixaban for reduction in stroke and other thromboembolic events in atrial fibrillation (ARISTOTLE) trial. Circulation 132(8):624–632
74. Roost E, Weber A, Alberio L, Englberger L, Reineke D, Keller D et al (2020) Rivaroxaban in patients with mechanical heart valves: a pilot study. Thromb Res 186:1–6
75. Jaffer IH, Fredenburgh JC, Stafford A, Whitlock RP, Weitz JI (2020) Rivaroxaban and dabigatran for suppression of mechanical heart valve–induced thrombin generation. Ann Thorac Surg 110(2):582–590
76. Jawitz OK, Wang TY, Lopes RD, Chavez A, Boyer B, Kim H et al (2020) Rationale and design of PROACT Xa: a randomized, multicenter, open-label, clinical trial to evaluate the efficacy and safety of apixaban versus warfarin in patients with a mechanical On-X Aortic Heart Valve. Am Heart J 227:91–99
77. Steinberg ZL, Dominguez-Islas CP, Otto CM, Stout KK, Krieger EV (2017) Maternal and fetal outcomes of anticoagulation in pregnant women with mechanical heart valves. J Am Coll Cardiol 69(22):2681–2691
78. Batra J, Itagaki S, Egorova NN, Chikwe J (2018) Outcomes and long-term effects of pregnancy in women with biologic and mechanical valve prostheses. Am J Cardiol 122(10):1738–1744
79. Van Hagen IM, Roos-Hesselink JW, Ruys TP, Merz WM, Goland S, Gabriel H et al (2015) Pregnancy in women with a mechanical heart valve: data of the European Society of Cardiology Registry of Pregnancy and Cardiac Disease (ROPAC). Circulation 132(2):132–142
80. Yurdakök M (2012) Fetal and neonatal effects of anticoagulants used in pregnancy: a review. Turk J Pediatr 54(3):207
81. Ferreira S, Costa R, Malveiro D, Vieira F, Tuna M (2018) Warfarin embryopathy: balancing maternal and fetal risks with anticoagulation therapy. Pediatr Neonatol 59(5):534–535
82. Mason J, Jardine A, Gibbin K (1992) Foetal warfarin syndrome—a complex airway problem. J Laryngol Otol 106(12):1098–1099
83. Starling LD, Sinha A, Boyd D, Furck A (2012) Fetal warfarin syndrome. BMJ Case Rep 2012:bcr2012007344
84. Vilhena C, Gameiro C, Tomás C, Santos A, Ilgenfritz R (2015) Warfarin-associated diaphragmatic hernia: an unusual diagnosis. Case Rep Obstet Gynecol 2015:987940
85. Ginsberg JS, Chan WS, Bates SM, Kaatz S (2003) Anticoagulation of pregnant women with mechanical heart valves. Arch Int Med 163(6):694–698
86. Nishimura RA, Warnes CA (2015) Anticoagulation during pregnancy in women with prosthetic valves: evidence, guidelines and unanswered questions. Heart 101(6):430–435
87. Irani RA, Santa-Ines A, Elder RW, Lipkind HS, Paidas MJ, Campbell KH (2018) Postpartum anticoagulation in women with mechanical heart valves. Int J Womens Health 10:663–670
88. Alshawabkeh L, Economy KE, Valente AM (2016) Anticoagulation during pregnancy: evolving strategies with a focus on mechanical valves. J Am Coll Cardiol 68(16):1804–1813
89. Tafur A, Mcbane R 2nd, Wysokinski W, Litin S, Daniels P, Slusser J et al (2012) Predictors of major bleeding in peri-procedural anticoagulation management. J Thromb Haemost 10(2):261–267
90. Kovacs M, Kearon C, Rodger M, Anderson D, Turpie A, Bates S et al (2004) Single-arm study of bridging therapy with low-molecular-weight heparin for patients at risk of arterial embolism who require temporary interruption of warfarin. Circulation 110(12):1658–1663
91. Wysokinski WE, McBane RD (2012) Periprocedural bridging management of anticoagulation. Circulation 126(4):486–490
92. Ioannidis G, Pallan S, Papaioannou A, Mulgund M, Rios L, Ma J et al (2014) Glucocorticoids predict 10-year fragility fracture risk in a population-based ambulatory cohort of men and women: Canadian Multicentre Osteoporosis Study (CaMos). Arch Osteoporos 9(1):1–8
93. Douketis JD, Spyropoulos AC, Spencer FA, Mayr M, Jaffer AK, Eckman MH et al (2012) Perioperative management of antithrombotic therapy: antithrombotic therapy and prevention of thrombosis: American College of Chest Physicians evidence-based clinical practice guidelines. Chest 141(2):e326S–e350S

94. Evans I, Sayers M, Gibbons A, Price G, Snooks H, Sugar A (2002) Can warfarin be continued during dental extraction? Results of a randomized controlled trial. Br J Oral Maxillofac Surg 40(3):248–252
95. Bajkin BV, Popovic SL, Selakovic SD (2009) Randomized, prospective trial comparing bridging therapy using low-molecular-weight heparin with maintenance of oral anticoagulation during extraction of teeth. J Oral Maxillofac Surg 67(5):990–995
96. Borea G, Montebugnoli L, Capuzzi P, Magelli C (1993) Tranexamic acid as a mouthwash in anticoagulant-treated patients undergoing oral surgery: an alternative method to discontinuing anticoagulant therapy. Oral Surg Oral Med Oral Pathol 75(1):29–31
97. Al-Belasy FA, Amer MZ (2003) Hemostatic effect of n-butyl-2-cyanoacrylate (histoacryl) glue in warfarin-treated patients undergoing oral surgery. J Oral Maxillofac Surg 61(12):1405–1409
98. Carter G, Goss A (2003) Tranexamic acid mouthwash—a prospective randomized study of a 2-day regimen vs 5-day regimen to prevent postoperative bleeding in anticoagulated patients requiring dental extractions. Int J Oral Maxillofac Surg 32(5):504–507
99. Sacco R, Sacco M, Carpenedo M, Moia M (2006) Oral surgery in patients on oral anticoagulant therapy: a randomized comparison of different INR targets. J Thromb Haemost 4(3):688–689
100. Hui AJ, Wong RM, Ching JY, Hung LC, Chung SS, Sung JJ (2004) Risk of colonoscopic polypectomy bleeding with anticoagulants and antiplatelet agents: analysis of 1657 cases. Gastrointest Endosc 59(1):44–48
101. Gerson LB, Michaels L, Ullah N, Gage B, Williams L (2010) Adverse events associated with anticoagulation therapy in the periendoscopic period. Gastrointest Endosc 71(7):1211–7. e2
102. Friedland S, Sedehi D, Soetikno R (2009) Colonoscopic polypectomy in anticoagulated patients. World J Gastroenterol: WJG 15(16):1973
103. Khor CJ, Hartono JL (2012) Current guidelines for endoscopy in patients receiving antithrombotic medication. Gastrointest Interv 1(1):58–62
104. Anderson MA, Ben-Menachem T, Gan SI, Appalaneni V, Banerjee S, Cash BD et al (2009) Management of antithrombotic agents for endoscopic procedures. Gastrointest Endosc 70(6):1060–1070
105. Bruno M, Marengo A, Elia C, Caronna S, Debernardi-Venon W, Manfrè SF et al (2015) Antiplatelet and anticoagulant drugs management before gastrointestinal endoscopy: do clinicians adhere to current guidelines? Dig Liver Dis 47(1):45–49
106. Tan CW, Wall M, Rosengart TK, Ghanta RK (2019) How to bridge? Management of anticoagulation in patients with mechanical heart valves undergoing noncardiac surgical procedures. J Thorac Cardiovasc Surg 158(1):200–203
107. Abbas S, Abu-Amer Y (2003) Dominant-negative IkappaB facilitates apoptosis of osteoclasts by tumor necrosis factor-alpha. J Biol Chem 278(22):20077–20082
108. O'Donnell MJ, Kearon C, Johnson J, Robinson M, Zondag M, Turpie I et al (2007) Brief communication: preoperative anticoagulant activity after bridging low-molecular-weight heparin for temporary interruption of warfarin. Ann Intern Med 146(3):184–187
109. Moia M, Squizzato A (2019) Reversal agents for oral anticoagulant-associated major or life-threatening bleeding. Intern Emerg Med 14(8):1233–1239
110. Thomas KL, Jackson LR, Shrader P, Ansell J, Fonarow GC, Gersh B et al (2017) Prevalence, characteristics, and outcomes of valvular heart disease in patients with atrial fibrillation: insights from the ORBIT-AF (outcomes registry for better informed treatment for atrial fibrillation). J Am Heart Assoc 6(12):e006475
111. Hald J, Poulsen PB, Qvist I, Holm L, Wedell-Wedellsborg D, Dybro L et al (2017) Opportunistic screening for atrial fibrillation in a real-life setting in general practice in Denmark – The Atrial Fibrillation Found On Routine Detection (AFFORD) non-interventional study. PLoS One 12(11):e0188086
112. Bando K, Kobayashi J, Hirata M, Satoh T, Niwaya K, Tagusari O et al (2003) Early and late stroke after mitral valve replacement with a mechanical prosthesis: risk factor analysis of a 24-year experience. J Thorac Cardiovasc Surg 126(2):358–363

113. Çınar T, Hayıroğlu MI, Tanık VO, Aruğaslan E, Keskin M, Uluganyan M et al (2018) The predictive value of the CHA2DS2-VASc score in patients with mechanical mitral valve thrombosis. J Thromb Thrombolysis 45(4):571–577
114. Melgaard L, Overvad TF, Jensen M, Lip GY, Larsen TB, Nielsen PB (2020) Thromboembolic risk in nonanticoagulated patients with atrial fibrillation and valvular heart disease. JACC Clin Electrophysiol 6(13):1672–1682
115. Dentali F, Pignatelli P, Malato A, Poli D, Di Minno MND, Di Gennaro L et al (2012) Incidence of thromboembolic complications in patients with atrial fibrillation or mechanical heart valves with a subtherapeutic international normalized ratio: a prospective multicenter cohort study. Am J Hematol 87(4):384–387
116. Kalra R, Patel N, Doshi R, Arora G, Arora P (2019) Evaluation of the incidence of new-onset atrial fibrillation after aortic valve replacement. JAMA Intern Med 179(8):1122–1130
117. Bozso SJ, White A, Kang JJ, Hong Y, Norris CM, Lakey O et al (2020) Long-term outcomes following mechanical or bioprosthetic aortic valve replacement in young women. CJC Open 2(6):514–521
118. Jin Y, Wang Y, Zhang J, Yue F, Yin Z, Zhu Y et al (2020) Left atrial mechanical function predicts postoperative AF in patients with rheumatic mitral valve disease who underwent mitral valve surgery. Heart Surg Forum 23(6):E907–E912
119. Khan J, Khan N, Loisa E, Sutinen J, Laurikka J (2016) Increasing occurrence of postoperative atrial fibrillation in contemporary cardiac surgery. J Cardiothorac Vasc Anesth 30(5):1302–1307
120. Dewilde WJ, Oirbans T, Verheugt FW, Kelder JC, De Smet BJ, Herrman J-P et al (2013) Use of clopidogrel with or without aspirin in patients taking oral anticoagulant therapy and undergoing percutaneous coronary intervention: an open-label, randomised, controlled trial. Lancet 381(9872):1107–1115
121. Lopes RD, Heizer G, Aronson R, Vora AN, Massaro T, Mehran R et al (2019) Antithrombotic therapy after acute coronary syndrome or PCI in atrial fibrillation. N Engl J Med 380(16):1509–1524
122. Cannon CP, Bhatt DL, Oldgren J, Lip GY, Ellis SG, Kimura T et al (2017) Dual antithrombotic therapy with dabigatran after PCI in atrial fibrillation. N Engl J Med 377(16):1513–1524
123. Valgimigli M, Bueno H, Byrne RA, Collet J-P, Costa F, Jeppsson A et al (2017) 2017 ESC focused update on dual antiplatelet therapy in coronary artery disease developed in collaboration with EACTS. Kardiol Pol (Polish Heart J) 75(12):1217–1299
124. Fred HL (2017) Skin necrosis induced by coumarin congeners. Tex Heart Inst J 44(4):233–236
125. Nalbandian RM, Mader IJ, Barrett JL, Pearce JF, Rupp EC (1965) Petechiae, ecchymoses, and necrosis of skin induced by coumarin congeners: rare, occasionally lethal complication of anticoagulant therapy. JAMA 192(7):603–608
126. Flood E, Reddish M, Bociek S, Shapiro S (1943) Thrombophlebitis migrans disseminata: case in which gangrene of the breast occurred. N Y State J Med 43:1121–1124
127. Chan Y, Valenti D, Mansfield A, Stansby G (2000) Warfarin induced skin necrosis. J Br Surg 87(3):266–272
128. Goldberg SL, Kessler CM, Yalisove BL, Elgart ML, Orthner CL (1991) Skin necrosis following prolonged administration of coumarin in a patient with inherited protein S deficiency. Am J Hematol 38(1):64–66
129. Teepe RG, Broekmans AW, Vermeer BJ, Nienhuis AM, Loeliger EA (1986) Recurrent coumarin-induced skin necrosis in a patient with an acquired functional protein C deficiency. Arch Dermatol 122(12):1408–1412
130. Pourdeyhimi N, Bullard Z (2014) Warfarin-induced skin necrosis. Hosp Pharm 49(11):1044–1048
131. Kakagia DD, Papanas N, Karadimas E, Polychronidis A (2014) Warfarin-induced skin necrosis. Ann Dermatol 26(1):96–98
132. Jillella AP, Lutcher CL (1996) Reinstituting warfarin in patients who develop warfarin skin necrosis. Am J Hematol 52(2):117–119

133. Baroletti SA, Goldhaber SZ (2006) Heparin-induced thrombocytopenia. Circulation 114(8):e355–e3e6
134. Tugulan C, Chang DD, Bates MJ (2021) Heparin-induced thrombocytopenia after mitral valve replacement. Ochsner J 21(2):200–204
135. Klein M, Tomer A, Swartz A, Koyffman L, Weksler N (2006) Bivalirudin for anticoagulation in mechanical aortic valve replacement and heparin-induced thrombocytopenia. Blood Coagul Fibrinolysis 17(4):331–333
136. Li Y-C, Wang R, Xu H, Ding L-P, Ge W-H (2020) Anticoagulation resumption in a patient with mechanical heart valves, antithrombin deficiency, and hemorrhagic transformation following thrombectomy after ischemic stroke. Front Pharmacol 11:549253
137. Warkentin TE, Levine MN, Hirsh J, Horsewood P, Roberts RS, Gent M et al (1995) Heparin-induced thrombocytopenia in patients treated with low-molecular-weight heparin or unfractionated heparin. N Engl J Med 332(20):1330–1336
138. Kim GH, Hahn DK, Kellner CP, Komotar RJ, Starke R, Garrett MC et al (2009) The incidence of heparin-induced thrombocytopenia type II in patients with subarachnoid hemorrhage treated with heparin versus enoxaparin. J Neurosurg 110(1):50–57
139. Magnani H (1993) Heparin-induced thrombocytopenia (HIT): an overview of 230 patients treated with orgaran (Org 10172). Thromb Haemost 70(10):554–561
140. Abdel-Wahab OI, Rosovsky RP, Warth JA (2008) Warfarin-induced skin necrosis in a patient with heparin-induced thrombocytopenia: two diseases or one? Acta Haematol 120(2):117–122

# Part III
# Testing, Regulatory and Training Issues

# Chapter 15
# In Vitro Testing of Heart Valve Substitutes


**Timothy A. Kelley, Sal Marquez, Eric L. Pierce, Carl F. Popelar, and Matthew C. Ziebol**

## Abbreviations

| | |
|---|---|
| AWT | Accelerated wear test |
| bpm | Beats per minute |
| COF | Chronic outward force |
| CT | Computed tomography |
| DFM | Dynamic failure mode |
| DTA | Damage tolerance analysis |
| EOA | Effective orifice area |
| FCG | Fatigue crack growth |
| FDA | Food and Drug Administration |
| FEA | Finite element analysis |

T. A. Kelley (✉)
Medtronic, Santa Rosa, CA, USA
e-mail: tim.kelley@medtronic.com

S. Marquez
Edwards Lifesciences, Irvine, CA, USA
e-mail: Sal_Marquez@edwards.com

E. L. Pierce
Medtronic, Santa Rosa, CA, USA

Medtronic, Santa Ana, CA, USA
e-mail: eric.pierce@medtronic.com

C. F. Popelar
Southwest Research Institute, San Antonio, TX, USA
e-mail: carl.popelar@swri.org

M. C. Ziebol
Medtronic, Mounds View, MN, USA
e-mail: matthew.c.ziebol@medtronic.com

© The Author(s), under exclusive license to Springer Nature Switzerland AG 2023

P. A. Iaizzo et al. (eds.), *Heart Valves*, https://doi.org/10.1007/978-3-031-25541-0_15

| | |
|---|---|
| IFU | Instructions for use |
| ISO | International Organization for Standardization |
| MDCT | Multi-detector computed tomography |
| RRF | Radial resistive force |
| RWT | Real-time wear testing |
| S/N | Stress/life |
| ε/N | Strain/life |

## 15.1 Introduction

Specifications of the comprehensive set of appropriate qualification tests and methods for a device under evaluation are to be derived from the risk analysis for the given device with consideration to the target patient population, disease state to be treated, valve implant position, and system design. The results from the in vitro testing effort provide a substantial and critical part of the risk assessment and regulatory submission package for the device prior to clinical implantation [1] and later in support of device labeling, device claims, and Instructions For Use (IFU).

The landscape of heart valve substitutes has evolved significantly over the past decade and a half, from mechanical and tissue heart valves implanted surgically via open chest procedures to a number of newly developed heart valve substitutes delivered via minimally invasive transcatheter approaches. For treatment of severe symptomatic aortic stenosis, transcatheter aortic valve replacement (TAVR) therapies have transitioned from treatment of extreme-risk patients to treatment of low-risk patients and are on their way to becoming standard of care for patients at all risk levels [2]. Ongoing clinical studies with an expanding portfolio of devices seem destined to expand indications for TAVR towards lower risk, younger, and asymptomatic populations [3–5]. In addition, transcatheter heart valve therapies are also approved for treatment of pulmonary stenosis (Medtronic Melody® and Edwards Sapien 3 ® devices); the indication for these devices is primarily for treatment of a dysfunctional Right Ventricular Outflow Tract (RVOT) conduit or a failed bioprosthetic valve. The Medtronic Harmony™ device is currently the only transcatheter device approved in the United States for treatment of pulmonary insufficiency [6]; the indication for this device is primarily treatment of severe pulmonary regurgitation in patients with a failed native or surgically repaired RVOT. Numerous transcatheter heart valve replacement therapies for treatment of severe mitral valve regurgitation [7] and severe tricuspid insufficiency [8] are approved for limited clinical indications or are currently in clinical trials.

The basic functional requirements for a heart valve substitute are the same independent of whether the device is implanted surgically or via transcatheter approaches. However, given the design differences between heart valves implanted via surgical and transcatheter approaches, different in vitro test methods may be required to evaluate the performance characteristics for each design and to adequately assess potential risks.

Detailed guidelines for in vitro testing and evaluations of heart valve prostheses have long been established by the US Food and Drug Administration (FDA) [9] and the International Organization for Standardization (ISO) [10] for surgically

implanted heart valve substitutes. Evaluation requirements for transcatheter heart valves have developed and evolved over the past several years by leveraging surgical heart valve testing and evaluation requirements in addition to learnings from initial clinical experience with transcatheter heart valves. From these efforts, recent revisions to the ISO 5840 series of standards have been released that define minimum performance and in vitro test requirements for evaluating surgical [11] and transcatheter heart valve substitutes [12] for all valve positions.

When developing any new device, the fundamental questions to be asked prior to beginning the design process are as follows: (1) ***What*** *are the intended functions of the device*? (2) ***Where*** *must the device perform its functions*? and (3) ***How long*** *must the device perform its functions*? Having the answers in hand to these three fundamental questions provides a solid framework for engineering a reliable device. While the answers to these questions may seem straightforward, there can be substantial challenges in obtaining them—especially in defining and characterizing use conditions for devices implanted within the human heart. Considerations for addressing each of these questions, as applicable to a heart valve substitute, are framed out in the following sections.

## 15.2 Primary Functions of a Heart Valve Substitute

The primary function of a heart valve substitute is to provide unidirectional blood flow into or out of the left or right ventricle of the heart. There are several performance requirements associated with this primary function that must be satisfied. Forward flow through the valve must be attained with acceptably small pressure drop or energy loss. Retrograde flow across the closed valve must be acceptably small, including paravalvular leakage. The device must be biocompatible and should minimize potential for hemolysis and thrombus formation. After implantation, the device must remain securely fixed in place, resisting migration and embolization. Lastly, the device must maintain structural and functional integrity during its expected lifetime. The expected operational lifetime for a heart valve substitute can range from a few years to a few decades, depending on the intended patient population and device design. Published literature has documented patient follow-up after surgical heart valve replacement with mechanical valves up to four decades post implantation [13, 14], with tissue valves in excess of two decades post implantation [15–18], and with transcatheter valves over 8 years post implantation [19].

In order for a heart valve substitute to perform its intended function within the heart, it must first be safely and effectively implanted within the target implant location. The procedural aspects associated with safe and effective implantation of the heart valve substitute must be defined. The delivery tools and accessories provided for device implantation must permit consistent, accurate, and safe access, delivery, placement, and securement of the heart valve substitute to the intended implant site. As such, the delivery tools, accessories, and defined implant procedure must be appropriately included as part of the in vitro test program for the heart valve system. A schematic of the various elements comprising a heart valve substitute system is shown in Fig. 15.1.

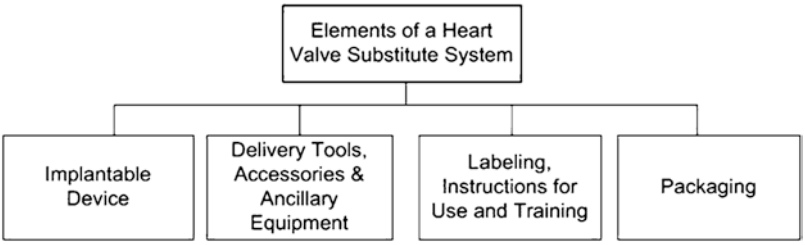


**Fig. 15.1** Schematic diagram representing the various elements comprising a heart valve substitute system

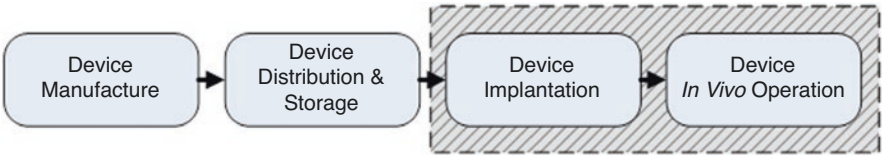


**Fig. 15.2** Exposure environments for heart valve substitutes during the device life cycle. The shaded box represents the aspects that will be covered in detail in this chapter

## 15.3 Heart Valve Substitute Use Conditions

Understanding the environments and conditions under which the device is expected to function is critical for reliable operation and performance of a heart valve substitute. It is through a detailed understanding of the use conditions for a heart valve substitute that a robust product can be engineered. Figure 15.2 depicts typical exposure environments for a heart valve substitute over the course of the device life cycle. For the intent of this chapter, only the use conditions associated with device implantation and in vivo operation will be discussed in detail. However, it is important to consider other aspects of device manufacturing and distribution/storage environments that is relevant for conditioning devices prior to in vitro testing. This will also be described to ensure that all factors which may affect device performance have been appropriately assessed.

### *15.3.1 Device Implantation*

Surgical heart valve substitutes (Fig. 15.3) are typically supplied within the device packaging pre-attached to a holder which serves to protect the device during shipment and during the implantation procedure. Instruments are typically provided to facilitate transfer of the device from the sterile packaging to the sterile surgical field. The instruments are intended to securely hold the heart valve substitute while the surgeon places sutures through the sewing cuff and then facilitate "parachuting" the heart valve substitute down into the implant site. Prior to implantation, the implant

**Fig. 15.3** Representative images of currently marketed surgical heart valve substitutes (left to right): stented porcine aortic valve, stented bovine pericardial valve, bileaflet mechanical valves, and stentless porcine valve

| | Acurate (Boston Scientific) | Allegra (NVT) | Centera (Edwards) | Evolut PRO (Medtronic) | Evolut R (Medtronic) | JenaValve (JenaValve) | Portico (St Jude) | Sapien 3 (Edwards) | VenusA (Venus Medtech) |
|---|---|---|---|---|---|---|---|---|---|
| |  |  |  |  |  |  |  |  |  |
| Design (leaflets, frame and delivery) | Porcine pericardium Nitinol Self-expanding | Bovine pericardium Nitinol Self-expanding | Bovine pericardium Nitinol Self-expanding | Porcine pericardium Nitinol Self-expanding | Porcine pericardium Nitinol Self-expanding | Porcine pericardium Nitinol Self-expanding | Bovine pericardium Nitinol Self-expanding | Bovine pericardium Cobalt-chromium Balloon-expandble | Porcine pericardium Nitinol Self-expanding |
| Delivery routes and sheath size | TF, TA, TS 18 Fr/19 Fr | TF 18 Fr | TF, TS 14 Fr | TF, TAo, TS 16 Fr | TF, TAo, TS 14 Fr | TF, TA 18 Fr | TF, TA 18 Fr/19 Fr | TF, TA, TAo 14 Fr/16 Fr | TF, TA, TS 18 Fr/20 Fr |
| CE mark (years) | 2011 | 2017 | Awaited | 2017 | 2013 | 2011 (AS) 2013 (AR) | 2012 | 2014 | NA |
| Specific advantages | Low PPM requirement | Resheathable up to 70% of deployment | Resheathable up to 85% deployment. PTFE skirt to reduce PVL. Motorized delivery system | Resheathable up to 80% deployment Double layer porcine pericardial skirt | Resheathable up to 80% deployment. Upcoming RCT data in low risk population | Active fixation for use in AR | Resheathable up to 85% deployment | External skirt to reduce PVL. Upcoming RCT data in low risk population | Experience in bicuspid valve population in China; reduced cost |

AR, aortic regurgitation; AS, aortic stenosis; PPM, permanent pacemaker; PVL, paravalvular leak; TA, transapical; TAo, transaortic; TF, transfemoral; TS, trans-subclavian.

**Fig. 15.4** A comparative overview of selected transcatheter aortic heart valve substitutes (commercially available, in-development, or no longer in development). (Reproduced from Cahill et al. [3])

site is surgically prepared to create an optimum landing zone for the valve; this may involve complete removal of the diseased native valve leaflets and debridement of calcium deposits that may interfere with the function of the heart valve substitute. During implantation, the heart valve substitute components may be manipulated to facilitate tying of sutures or to ensure no unintended interactions with adjacent anatomical structures. Following implantation of the heart valve substitute, the holder is removed, leaving the heart valve substitute securely affixed in position. After the device holder is removed, the functionality of the heart valve substitute can be confirmed by ensuring valve leaflets fully open and close without unintended interaction with anatomical structures.

By design, transcatheter valves (Figs. 15.4, 15.5, 15.6, and 15.7) are delivered via vascular access sites and then tracked through potentially very calcified and tortuous vasculature to the target implant site. Necessarily, these devices must be compressed to a very small diameter to facilitate loading the device on the

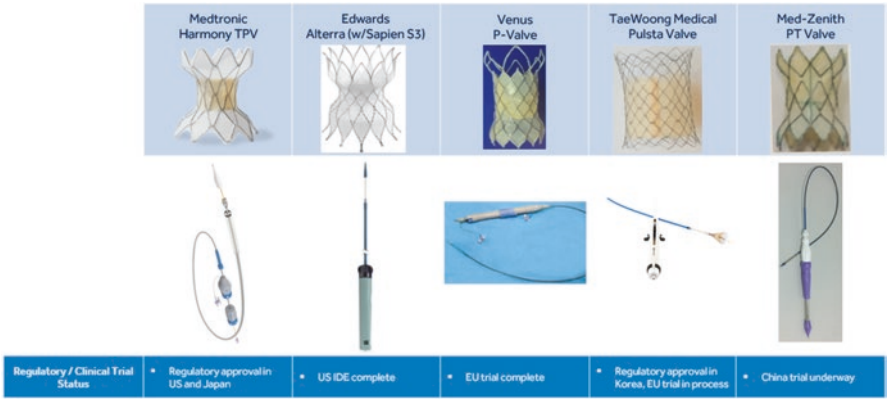


**Fig. 15.5** Overview of transcatheter pulmonary heart valve substitutes for treatment of pulmonary insufficiency within the native RVOT


**Fig. 15.6** Current landscape of transcatheter mitral heart valve substitutes. Most systems shown are currently under development and/or clinical evaluation; the Abbott Tendyne system has obtained CE mark approval. (**a**) CardiAQ/EVOQUE (Edwards Lifesciences Inc.); (**b**) Tiara (Neovasc Inc.); (**c**) FORTIS (Edwards Lifesciences Inc.); (**d**) Tendyne (Abbott Inc.); (**e**) Intrepid (Medtronic Inc.); (**f**) Caisson (LivaNova); (**g**) HighLife Bioprosthesis and Subannular Implant (HighLife SAS); (**h**) SAPIEN M3 (Edwards Lifesciences Inc.); (**i**) Cardiovalve (Cardiovalve); (**j**) NaviGate (NaviGate Cardiac Structures Inc.). (Reproduced from Testa et al. [20])

delivery catheter or similar tool. Although typical transfemoral system profiles range from 18 to 24 Fr (6–8 mm) for TAVR and TPV devices, system profiles for TMVR and TTVR devices currently in early feasibility studies may be much larger (≥30 Fr).

It is imperative that transcatheter heart valves be subjected to all use conditions that the device would encounter prior to and during clinical implantation such that the test articles include any effects of loading, crimping, tracking through the vasculature, recapture, etc., on measured device performance. These use conditions can subject the tissue, tissue attachment interface, and the device frame to potentially

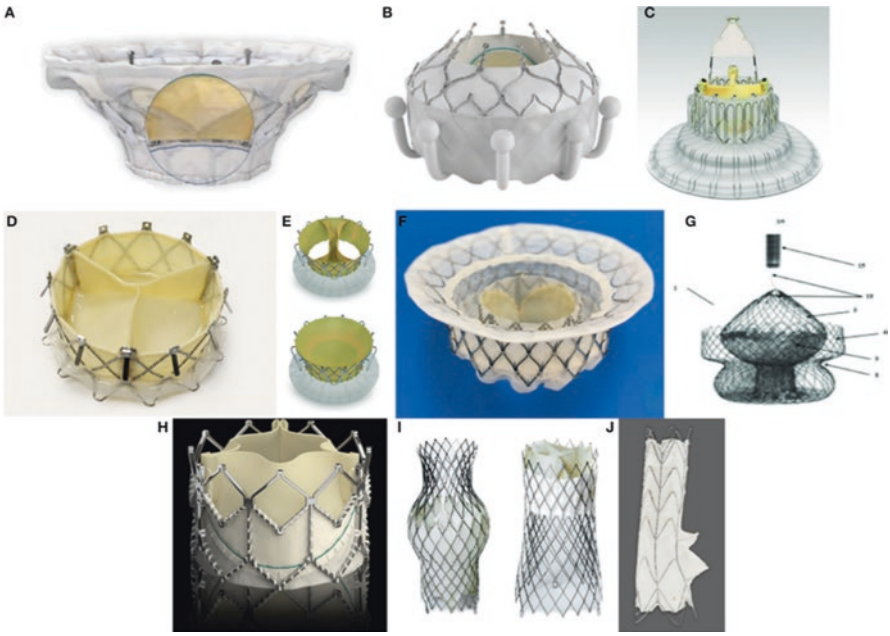


**Fig. 15.7** Transcatheter tricuspid heart valve substitutes currently under development and clinical evaluation. Orthotopic transcatheter valves: (**a**) Cardiovalve (Boston Medical, Shrewsbury, MA, USA). (**b**) Evoque (Edwards Lifescience, Irvine, CA, USA). (**c**) LUX-Valve (Jenscare Biotechnology, Ningbo, China). (**d**) NaviGate (NaviGate Cardiac Structures Inc., Lake Forest, CA, USA). (**e**) Trisol (Trisol Medical, Yokneam, Israel). (**f**) Intrepid (Medtronic Plc, Minneapolis, MN, USA). (**g**) Tricares (TRiCares SAS, Paris, France). Heterotopic transcatheter valves: (**h**) Sapien XT (Edwards Lifescience, Irvine, CA, USA). (**i**). TricValve (P + F Products + Features, Vienna, Austria) (**j**). Tricento (New Valve Technology, Hechingen, Germany). (Reproduced from Goldberg et al. [8])

significant stresses/strains. For valves utilizing balloon-expandable frames, the device is compressed onto the balloon catheter using a crimper, or it may be crimped manually by the physician depending on the specific device design and IFU. This compression of the device results in plastic deformation of the frame, allowing the device to securely conform to the balloon catheter. The delivery system for balloon-expandable devices may or may not utilize a sheath to cover the valve since it is not required to constrain the device. Once the delivery system has been tracked to the anatomical valve location and the device is positioned within the desired implant location, the constraining sheath is retracted (if utilized) and the balloon catheter is inflated, expanding the heart valve substitute within the native diseased valve. The heart valve substitute is deployed to a diameter that is larger than the native annulus diameter to create an interference fit with the annulus and surrounding anatomy to firmly affix the device in place, thus maximizing valve orifice area and mitigating against both paravalvular leakage and device migration. During inflation of the balloon catheter to expand the device, rapid ventricular pacing is typically employed to

decrease cardiac output and prevent large shifts in position of the heart valve substitute resulting from changes in chamber pressure when the valve orifice is occluded.

In the case of a valve with a self-expanding frame, the device may be compressed using a crimper or via loading funnels/cones. For self-expanding frames fabricated from superelastic Nitinol, the crimping and loading process is typically conducted with the device immersed in a cold saline bath such that the frame material is in its low-temperature martensitic phase (see Sect. 15.5.1). This material phase makes the frame malleable and facilitates loading of the device onto the delivery system in a controllable manner. After loading the device onto the delivery system catheter, a sheath is placed over the device to constrain it so that it remains firmly attached and contained within the delivery system. Once the delivery system has been tracked with the appropriate medical image to the anatomical location and the device is positioned in the desired implant location, the constraining sheath is retracted. At body temperature (37 °C), the frame expands to its preformed configuration via the shape memory effect. The device expands until it opposes the valve annulus, creating an interference fit with the surrounding anatomy. As with balloon-expandable devices, the heart valve substitute size is selected such that the deployed diameter of the valve is larger than the native annulus diameter in order to create an interference fit with the annulus and surrounding anatomy. This sizing helps to firmly affix the device in place, maximizing valve orifice area and mitigating against both paravalvular leakage and device migration.

### *15.3.2 Device In Vivo Operation*

After device implantation within the target implant site, heart valve substitutes can be subjected to a combination of loading modes. These loading modes vary as a function of implant site (aortic, mitral, tricuspid, pulmonary), valvular disease etiology, and device design.

Since the primary function of the heart valve substitute is to control blood flow into and out of the heart, forces associated with pressure loading across the valve are one of the primary cyclic loading conditions to which a heart valve substitute is subjected. The differential pressure across the closed heart valve substitute under hypertensive blood pressure conditions represents the most significant pressure loading condition, relative to the heart valve substitute components from a structural performance. However, from a valve functional performance perspective, low cardiac output and hypotensive pressure conditions may also pose a challenge, i.e., the valve leaflets must open and close under low cardiac output and low-pressure conditions. The range of hemodynamic conditions for hypotensive to hypertensive patients to be considered when evaluating a heart valve substitute are listed in Table 15.1 based on the guidelines contained in ISO 5840 [10].

In addition to the pressure loading on the heart valve substitute, other anatomical loading conditions are imposed as well. Since the perimeters of the native valve annuli are comprised of both ventricular myocardium and fibrous tissue, dynamic

**Table 15.1** Heart valve substitute operational environment for right and left side of heart for the adult population [10]

| Parameter | Description | | | |
|---|---|---|---|---|
| Heart rate | | 30–200 bpm | | |
| Cardiac output | | 3–15 Lpm | | |
| Forward flow volume | | 25–100 mL | | |
| Patient blood pressure condition | Peak differential pressure across closed valve (mmHg) | | | |
| | Pulmonary | Tricuspid | Aortic | Mitral |
| Hypotensive | 10 | 15 | 50 | 60 |
| Normotensive | 19 | 27 | 100 | 120 |
| Hypertensive | | | | |
| Mild | 28–34 | 40–49 | 115–129 | 140–159 |
| Moderate | 35–42 | 50–59 | 130–144 | 160–179 |
| Severe | 43–59 | 60–84 | 145–164 | 180–209 |
| Very severe | ≥60 | ≥84 | ≥165 | ≥210 |

*bpm* beats per minute

mechanical loading is applied to a device implanted within the valve annulus throughout the cardiac cycle. In addition, the motion of the heart within the chest cavity may subject the heart valve substitute to additional mechanical forces. The physiological loading conditions to which a heart valve substitute is subjected may include (1) radial dilatation and compression, (2) torsion, (3) bending, (4) axial tension and compression, and (5) linear/transverse compression (e.g., crushing) [10]. These combined loading conditions create a challenging fatigue environment for heart valve substitutes.

There is very limited quantitative information in the scientific literature regarding the potential magnitudes of the anatomical forces that may be generated within each of the four primary valve positions. For the mitral valve, there are limited publications that provide estimates of forces generated within the mitral annulus of healthy pigs and sheep [21–24]. The pulmonary valve is the most anterior of the four heart valves, and as such it is the valve position in closest proximity to the chest wall. This creates the potential for a device implanted in this position to be subjected to cyclic compressive loading, as it is compressed between the anterior chest wall and the heart. As reported by Peng et al. [25], the substernal implant position was identified as a notable risk factor for stainless steel stent fracture; nearly 90% of observed fractured stents in this study were implanted directly below the sternum.

One method that may be employed for identification and quantification of various loading modes and magnitudes to which an implanted transcatheter heart valve may be subjected is the coupling of reconstructed multi-detector computed tomography (MDCT) data to finite element analysis [26, 27]. Obtaining MDCT data from patients implanted with a device of known mechanical characteristics (e.g. stiffness) and performing reconstructions of the deformed device throughout the cardiac cycle provides information that can be used to develop boundary condition estimates for that specific device within the target patient population. The deformation data

obtained from the CT reconstructions can be used in conjunction with a finite element model of the implanted device to (1) predict the stress/strain distribution within the specific device under the measured boundary conditions or (2) estimate reaction force magnitudes that would result in the measured deformation of the specific device. The resolved reaction force estimates may provide boundary condition input for other devices that are intended for implantation in the same valve position and intended patient population; differences in geometry and mechanical response must be appropriately accounted for relative to the applicability of boundary conditions derived from another device.

Ultimately, the device manufacturer must identify and justify the appropriate in vivo loading conditions for a heart valve substitute based on the device design in the context of the target implant site. In addition, consideration must be given to associated anatomic variability and pathological changes. Due to significant differences in anatomy, geometry, and cardiac dynamics for each of the four valve positions, loading information for one valve position (e.g., aortic) offers limited applicability to another valve position (e.g., mitral).

Other considerations that may impact in vivo performance of both balloon-expandable and self-expanding devices include nonuniform deployment of the heart valve substitute, under- or over-deployment, canting, and high or low deployment (with respect to intended implant position). These variations can potentially impact device performance and should be accounted for as part of the in vitro evaluation program.

## 15.4 Risk Assessment

Risk assessment plays a critical role in any device evaluation program. ISO 14971 [28] provides guidance and requirements for implementing a risk management program for a medical device. As described by ISO 14971, the risk assessment is comprised of risk analysis and risk evaluation. The risk analysis process begins by defining the intended use and operational environment for the device and by identifying the characteristics related to the safety of the heart valve substitute. Next, known and foreseeable hazards associated with the heart valve substitute system are identified, and an initial risk estimate for each hazardous situation is made.

The testing and analysis necessary to better estimate or refine the risk estimate associated with each hazard are then determined from information regarding the nature of the hazard and the corresponding failure modes/causes. This information provides input for the overall in vitro test strategy for the heart valve substitute. The in vitro test and analysis requirements not only serve as a basis for verification and validation but are also used to facilitate risk estimation for identified hazards through failure mode identification and/or failure probability quantification. The risk estimates for each identified hazard are then evaluated against the manufacturer's established risk acceptance criteria to determine if associated risk levels are acceptable.

## 15.5 In Vitro Evaluations

The purpose of in vitro evaluations is to verify that the device meets the specified design requirements. The series of in vitro tests and analyses described herein provide quantitative and qualitative measures of the performance of the heart valve substitutes implanted via either surgical or transcatheter approaches.

It is important that the materials, valves, and delivery systems for evaluation are the final designs and manufacturing processes intended for clinical product. It is also critical that the valves and delivery systems to be used for verification testing have been conditioned in a manner representative of the worst-case conditions that the device may encounter during its life cycle (e.g., sterilization cycles, shipping and storage conditions, crimp diameter, crimp time, crimp cycles, deployed size/geometry, and in vivo deformations/loading conditions). These considerations ensure that the valves being tested represent the condition of the valves that will be implanted into patients. For component-level tests, the extent of pre-conditioning should be considered and applied as appropriate based on the intent and scope of the test.

Of equal importance, the test methods themselves demand engineering rigor. In developing each test method, the engineering team should identify any anatomic/physiologic/use conditions that are relevant to the performance parameter(s) under interrogation and ensure they are adequately represented by the test method. The test method should be appropriately validated (e.g., demonstrated to be sufficiently repeatable and reproducible and to have tolerable uncertainty) in accordance with established standards. Other test method quality considerations to be accounted for include, but are not limited to, training of operators, installation qualification of equipment, and calibration of instrumentation.

Note, any specific test levels cited in the following sections refer to those recommended for an adult population; pediatric test levels may vary. For further guidance, refer to ISO 5840 [10–12].

### *15.5.1 Component Material and Mechanical Property Testing*

It is critical that the constituent materials of all components of the heart valve substitute system (e.g., frame, valve leaflets, and delivery system) be characterized in their different states as applicable to the specific design of the system. This data confirms the appropriateness of the proposed materials for use in the specific design.

It is important to characterize mechanical properties at various stages of manufacture, as applicable, for (a) the component raw materials, (b) the device components in their final manufactured state, and (c) the finished device after applicable exposure to simulated use conditions. The stress–strain response should be characterized under monotonic and cyclic load-unloading conditions to understand the cyclic response of the material. The generated mechanical property data can provide

material input information for use in finite element analyses (FEA) in order to determine in vivo induced stresses or strains within the structural components.

There have been numerous material combinations utilized over the years in the design and manufacture of heart valve substitutes. Typical materials used in commercially released surgical and transcatheter heart valve substitutes are summarized in Tables 15.2 and 15.3, respectively; however, these tables are not intended to be an exhaustive list.

The materials that comprise the primary elements of currently marketed prosthetic heart valve substitutes typically consist of conventional metal alloys, pyrolytic carbon, various polymers, porcine or bovine heart tissue, and nickel-titanium alloys (e.g., superelastic Nitinol). These materials exhibit a range of mechanical behavior, as shown schematically in Fig. 15.8a for pyrolytic carbon, steel, and nickel-titanium and in Fig. 15.8b for polymers and tissue.

**Table 15.2** Typical materials used in commercially released surgical heart valve substitutes

| Surgical valves | | | |
|---|---|---|---|
| Frame | Leaflets | Joining materials | Sewing cuff |
| Pyrolytic carbon | Pyrolytic carbon | Polyester suture | Polyester fabric |
| Polymers | Bovine pericardium | PTFE suture | |
| Titanium alloys | Porcine aortic valve tissue | Nickel-titanium alloys | |
| Cobalt-chromium alloys | Porcine pericardium | | |

**Table 15.3** Typical materials used in commercially released transcatheter heart valve substitutes

| Transcatheter valves | | | |
|---|---|---|---|
| Frame | Leaflets | Joining materials | Skirt/Wrap |
| Nickel-titanium alloys | Bovine pericardium | Polyester suture | Porcine pericardium |
| Stainless steel alloys | Porcine pericardium | PTFE suture | Polyethylene terephthalate |
| Platinum-iridium alloys | Bovine jugular | Polyethylene suture | Polyester |
| Cobalt-chromium alloys | | | Polycarbonate urethane |

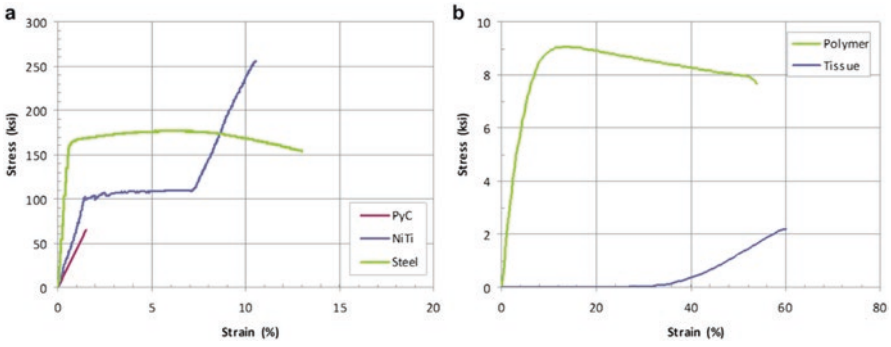


**Fig. 15.8** Representative stress–strain response for pyrolytic carbon (PyC), nickel-titanium alloys (NiTi), and steel (**a**). Representative stress–strain response for polymer and valve tissue material (**b**)

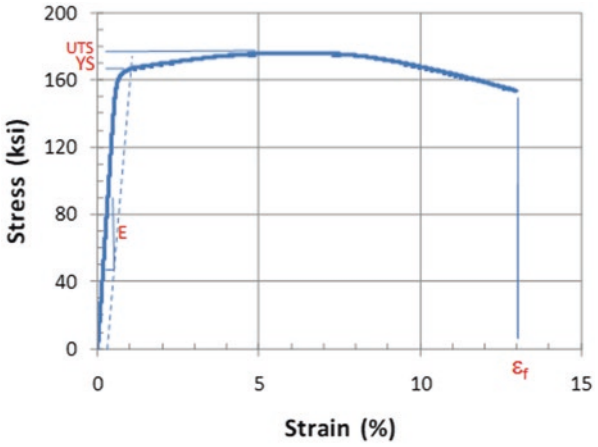


**Fig. 15.9** Representative stress–strain response for engineering alloy with relevant parameters noted. $\varepsilon_f$ elongation at failure; *E* elastic modulus; *UTS* ultimate tensile strength; *YS* yield strength

***Metallic alloys*** Conventional metallic alloys are materials commonly used as structural elements of heart valve substitutes, and their mechanical (stress–strain) response is one of the most fundamental and well characterized. A typical stress–strain response is shown in Fig. 15.9. The initial response is characterized by an elastic region in which the stress is proportional to the strain. Beyond a certain limit, defined as the yield point, permanent (plastic) deformation occurs, which is not recoverable upon unloading. Continued loading will ultimately result in failure. The following is a list of typical mechanical properties that characterize conventional metal alloys: (1) elastic modulus (*E*), (2) yield strength (YS), (3) ultimate tensile strength, (4) elongation at failure (*e*f), and (5) Poisson's ratio.

***Pyrolytic carbon*** Pyrolytic carbon has been used successfully for decades in mechanical heart valve substitutes due to its biocompatibility, thromboresistance, and durability [29]. Like ceramics, the mechanical behavior of pyrolytic carbon is linear elastic and exhibits no appreciable plastic deformation (Fig. 15.8), while also exhibiting high strength and better ductility than most ceramics. However, due to the lack of plastic deformation, the material is relatively brittle and very sensitive to defects. As such, measures of strength are typically performed on a statistical basis on samples that are prepared to be representative of manufacturing processes specifically designed to remove surface defects.

***Polymers*** Surgical tissue valve frames are commonly fabricated from polymeric materials. Although their mechanical stress–strain behavior may appear similar to metals (Fig. 15.8), polymers are not as strong but can withstand far more deformation than most metals. Being viscoelastic, these materials will creep or continue to deform under constant load and will relax under constant deformation [30]. As such, their response is very sensitive to the loading rate, and their characterization should consider rates that will be experienced in vivo.

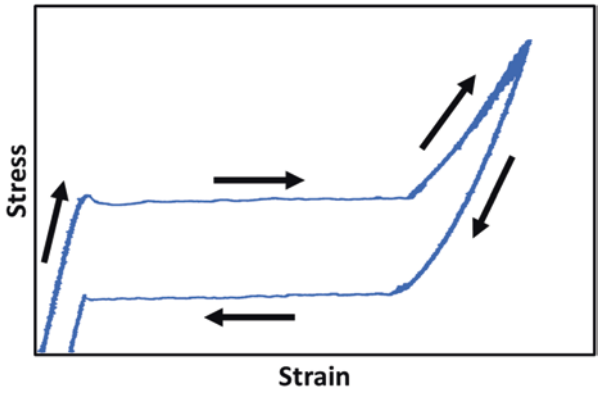


**Fig. 15.10** Typical stress–strain curve for superelastic Nitinol depicting "flag-shaped" hysteresis curve

***Nickel-titanium alloys*** Some metals, such as Nitinol (an alloy of approximately equiatomic nickel and titanium content), when combined and processed in specific ways exhibit unique mechanical behavior that is particularly well suited for medical devices. An example of a Nitinol stress–strain curve, depicting its unique behavior, is shown in Fig. 15.10. Unlike conventional metals that exhibit permanent (plastic) deformation after about 0.5% deformation, Nitinol is capable of deformations up to 8% without permanent set. This "superelastic" behavior makes Nitinol particularly attractive for vascular stents and transcatheter valves. The superelastic behavior is the result of a microstructural shape change that occurs when the stress level is sufficient to cause the initial austenitic phase to transform to martensite along the upper plateau stress. Unloading before reaching approximately 8% strain causes a reverse transformation from martensite back to austenite along the lower plateau stress and full recovery can be achieved. Continued loading beyond 8% strain results in plastic behavior typical of traditional metals.

Nitinol frames possess unique metallurgical and mechanical properties that facilitate (1) the loading of the device onto the delivery system, (2) the transcatheter delivery and implantation procedure, and (3) the mechanical performance of the valve post-implantation. When processed appropriately, Nitinol exhibits a shape memory effect. This effect describes the ability of a frame made out of a shape memory alloy like Nitinol to revert to its original shape and configuration upon heating after being severely deformed at a sufficiently low temperature. With slightly different processing, a shape memory alloy can also exhibit superelasticity. In the superelastic condition, a frame can undergo large mechanical deformations and instantly revert to its original configuration upon unloading at a specified temperature. Both the shape memory effect and the superelastic behavior are the result of reversible martensitic phase transformations. The phase transformation stimuli could be a change in temperature (shape memory effect) for example, or the application of a mechanical stress (superelasticity).

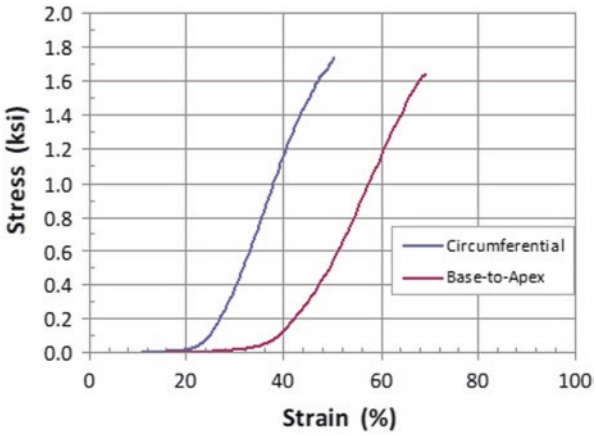


**Fig. 15.11** Stress–strain diagram depicting typical glutaraldehyde-treated bovine pericardium tensile behavior in the circumferential and radial directions

***Bovine and porcine heart tissue*** Bovine and porcine pericardium and porcine aortic valve tissues are used to construct leaflets in heart valve substitutes. In addition, some heart valve substitutes are comprised of a native bovine jugular vein and valve. All animal tissues are subjected to various fixation processes, which are typically glutaraldehyde-based, to impart desirable mechanical properties and to promote durability of the tissue during in vivo operation. Due to the oriented fibril nature of the collagen, tissue behavior is typically anisotropic (Fig. 15.11) and is often characterized under biaxial loadings [31]. These tissues can undergo extensive deformation (~100–200%) with minimal force before ultimately stiffening and rupturing. Furthermore, given their high water content, they exhibit incompressible, viscoelastic behavior.

## *15.5.2 Device Acute Performance Testing*

Verification and characterization testing of the acute performance of the heart valve substitute is critical to ensure that it can withstand the forces to which it will be subjected, with no detrimental impact to valve function. As previously stated, the complete test program is to be defined based on the device product specification and risk assessment. The tests discussed below are not intended to be all inclusive but rather a description of typical performance characterization tests that are conducted for heart valve substitutes.

#### 15.5.2.1 Frame/Housing Crush Resistance

The crush resistance testing characterizes the deformation of the frame/housing as a function of applied load, with the typical output for this test being a load–displacement plot. This test is typically conducted using a curved or parallel plate test setup with the compressive load applied normal to the flow axis of the valve. A schematic of a representative test setup along with an example test output is shown in Fig. 15.12. Using a bileaflet mechanical valve as a specific example, by applying the load along the vertical axis of the valve leaflets, the load and displacement at which the leaflets fail to freely rotate can be quantified. Conversely, by applying the load normal to the vertical axis of the valve leaflets, the load and displacement at which the leaflets no longer remain captured within the housing can also be determined. Testing of this type can mitigate against these two potential device failure modes by ensuring sufficient resistance to leaflet binding and leaflet escape.

For transcatheter valves, flat plate crush resistance testing is performed in a similar manner as for surgical valves and is typically conducted using parallel plates to measure the ability of the frame to resist permanent deformation along the entire length of the device when subjected to a uniformly applied load. The typical output for this test is a load–displacement plot as shown in Fig. 15.12. For self-expanding frames, the testing is conducted at expected operating temperatures (37 °C), and the maximum crush displacement is typically set equal to 50% of the fully expanded frame diameter. For frames exhibiting a variation in stiffness along the length, this testing may be performed for each region of the frame as well as for the entire frame length. The testing is conducted for each device over a deployed diameter range that encompasses the range of deployed diameters recommended per the device labeling.

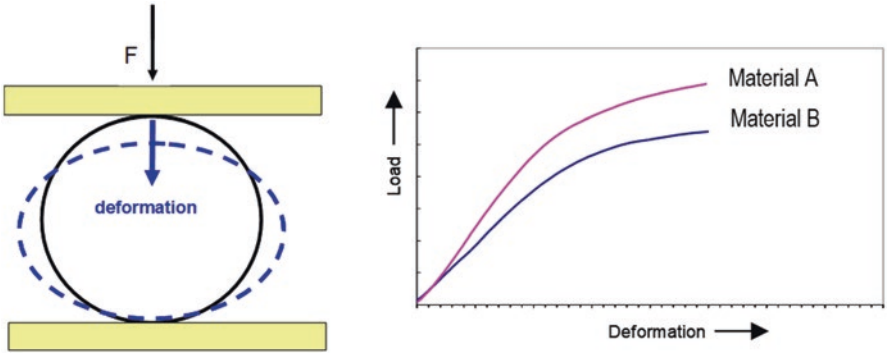


**Fig. 15.12** Representative schematic of a flat plate test setup and an example of a load-deformation plot output for a given frame of two material options

#### 15.5.2.2 Frame Deflection

Frame deflection testing measures the amount of frame deformation as a function of applied backpressure loading across the closed valve. This test is performed on valves under varying pulsatile pressure-loading conditions. The device is anchored within a holder and placed within a pulsatile flow chamber that allows full visualization of the valve (pulsatile flow tester design is discussed in Sect. 15.5.2.8). Small markers may be affixed to the outflow aspect of the frame in specific locations such that the position of each marker can be continuously tracked throughout the cardiac cycle. This testing is typically performed at a beat rate of 70 bpm, cardiac output of 5–7 Lpm, and at increasing differential pressures ranging from normotensive up to severe hypertensive patient conditions, as defined in Table 15.1. High-speed imaging is typically used to capture the frame deflections throughout the cardiac cycle, and motion analysis software is used to process the resultant images and compute the relative displacements of each marker position. The deflection data provide quantitative input into corresponding computational analysis (e.g., FEA) for the device under evaluation and input into fatigue test methods for the heart valve substitute frame.

#### 15.5.2.3 Sewing Ring Integrity

Sewing ring integrity testing is performed to determine the force required to cause sewing ring separation from the heart valve substitute housing or body. This testing ensures that the device can withstand the axial loading to which it may be subjected during implantation and in vivo operation. In this testing, the valve is typically sutured within a holding fixture and then subjected to axial loading via a linear test setup. The forces required to separate the device from the sewing ring via either cuff fabric tearing or suture pullout are measured for comparison to those load magnitudes expected during use.

#### 15.5.2.4 Frame Creep

Frame creep characterization of bioprosthetic valve frames is performed to quantify potential creep deformation of polymeric stent posts under continuous cyclic loading conditions. The purpose of this testing is to ensure that the valve frame geometry remains stable over the expected lifetime, maintaining proper valve function. This testing is typically conducted using appropriately pre-conditioned stent components in a simulated physiological environment under cyclic stent post deflections representing worst-case differential pressure-loading conditions.

#### 15.5.2.5 Radial Stiffness, Recoil, Radial Resistive Force (RRF), and Chronic Outward Force (COF)

Radial stiffness testing of balloon-expandable frames measures the radial deformation of the frame when subjected to a circumferentially uniform radial load/pressure. The typical output for this test is a plot of the change in frame diameter as a function of uniformly applied external radial pressure. Radial strength measures the ability of a balloon-expandable frame to resist permanent deformation/collapse when subjected to a circumferentially uniform radial load. The radial strength represents the load/pressure magnitude at which frame collapse occurs.

The recoil of balloon-expandable frames represents the percent reduction in the frame outer diameter between full balloon inflation and balloon deflation. Recoil is a function of frame design, frame material, and frame material condition. Excessive recoil can result in improper sizing and improper function of the heart valve substitute frame (i.e., poor migration resistance). Standard test methods for measuring recoil are described in American Society for Testing and Materials (ASTM) F2079 [32].

For self-expanding frames, radial stiffness is the elastic response of the frame to radial loading and provides a measure of the valve's ability to resist diametrical loss during such loading. Unlike most metals that exhibit a single elastic response behavior during both loading and unloading, a self-expanding Nitinol frame exhibits two distinctly different behaviors in these conditions. This behavior is termed "biased stiffness" and is a unique property of Nitinol that results in the chronic outward force (COF) and radial resistive force (RRF) observed. Figure 15.13 is a schematic diagram showing radial force plotted as a function of frame diameter. The graph resembles a typical stress–strain graph of self-expanding Nitinol exhibiting fairly flat (force) plateaus during both loading and unloading and although idealized, the graph serves to illustrate these effects.

The RRF is the force exerted by the self-expanding Nitinol frame as it resists radial compression from its relaxed diameter. The RRF provides resistance to imposed frame radial deformations, thus facilitating valve shape and efficacy. The COF is the force exerted by the self-expanding Nitinol frame on the surrounding anatomy as it attempts to expand to its relaxed diameter after being radially compressed during the crimping operation. The COF exerted by the Nitinol frame on the valve anatomy acts to prevent acute and chronic migration alleviating the need for positive anchoring, and also mitigating paravalvular leakage. This force is relatively constant over a large range of diameters as schematically shown in Fig. 15.13. Some frames are specifically designed to possess different radial force responses along the frame length. If a self-expanding heart valve substitute allows for multiple crimp or recapture cycles, the radial force response should be characterized accordingly to account for any OD loss associated with each crimp or recapture cycle.

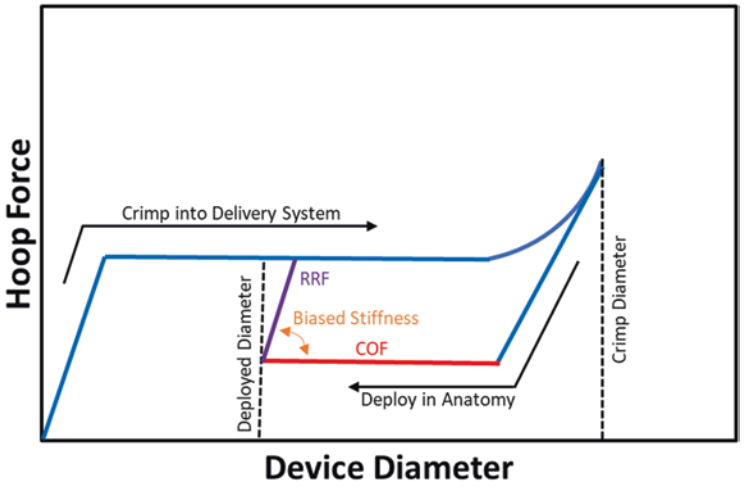


**Fig. 15.13** Schematic hoop force vs. diameter plot for a self-expanding Nitinol frame demonstrating chronic outward force (COF), radial resistive force (RRF), and biased stiffness. The loading curve represents compression of the frame from fully expanded diameter to minimum crimp diameter. The unloading curve represents expansion of the frame from its fully compressed diameter [32]

#### 15.5.2.6 Device Integrity

Device integrity testing is performed to confirm that the use conditions associated with crimping the device to the delivery system diameter, loading it onto the delivery catheter or balloon, tracking the delivery catheter and loaded device around a tortuous vasculature, and then deploying/expanding the device will not result in damage to the device. Plastic deformation of the frame during loading or balloon expansion may cause cracks or other damage. Crimping and compressing the valve assembly may result in damage to the heart valve substitute tissue or attachment sutures.

Typically, optical and scanning electron microscopy is used for visual inspection of the device to confirm there is no damage to the valve components. These inspections are performed after the device has been subjected to worst-case conditions (durations and geometries) of crimping, tracking, and expansion to the largest diameter (balloon-expandable frames) or to the unconstrained diameter (self-expanding frames). If the implant procedure allows for multiple crimping operations or if the device is intended to be recapturable, the devices must be inspected after conditioning to the maximum number of crimping or recapturing cycles.

#### 15.5.2.7 Corrosion

Corrosion of the implantable device components can cause or contribute to structural component failure. In addition, corrosion by-products that are detected during in vitro testing could cause adverse biological and tissue responses. Many types of corrosion mechanisms might occur, often simultaneously, on the device over time. While some corrosion mechanisms are predominantly related to material properties, surface finish, and manufacturing of the component (e.g., uniform corrosion, pitting corrosion, and intergranular corrosion), others relate more to the device design (e.g., crevice corrosion and galvanic corrosion) or the operational conditions (e.g., fretting corrosion, corrosion fatigue, and stress corrosion cracking). The planning, selection, design, and execution of corrosion tests should ensure that all relevant corrosion mechanisms and their interactions are identified and assessed to obtain the information needed to evaluate the device performance during its service life.

Corrosion testing can include a variety of electrochemical, microscopic, and gravimetric methods [33]. Often combinations of qualitative observations, quantitative measurements, and statistical analyses are needed to provide an overall assessment of corrosion. Standard corrosion tests developed by ASTM, NACE (Corrosion Society), and ISO address the technical requirements specified in the test method but may need to be modified to address conditions applicable to device applications.

Commonly used standard methods for medical device components include, but are not limited to, ASTM F2129 and ASTM F746. Nondestructive methods, such as electrochemical impedance spectroscopy (ASTM G106) and electrochemical noise measurements (ASTM G199), might be advantageous for monitoring corrosion properties and events during accelerated or real-time fatigue testing.

The corrosion mechanisms are often applicable to materials and conditions representative of implantable heart valve substitutes, although other mechanisms are possible. The manufacturer should provide rationale for the selected test methods and justify that all applicable corrosion mechanisms and conditions have been addressed through testing or theoretical assessments.

#### 15.5.2.8 Hydrodynamic Performance

A prosthetic valve's most fundamental performance requirement is to restore effective flow control. To this end, hydrodynamic testing quantifies the extent to which the device permits forward flow and prevents leakage (i.e., regurgitation or retrograde flow). A few key metrics are of interest during hydrodynamic performance testing, as follows.

***Pressure Gradient (ΔP)*** Computed as (downstream pressure–upstream pressure) and studied during forward flow. Per Ohm's Law, a valve that opens more will offer less resistance to flow, resulting in a lower pressure drop. This benefits circulation overall. In the pulsatile flow setting, $\Delta P$ may be evaluated in terms of *peak* gradient

throughout the cardiac cycle, but is more often evaluated in terms of the *mean* gradient, i.e., the mean of the positive pressure gradient period.

***Effective Orifice Area (EOA)*** Like $\Delta P$, EOA again describes the extent to which the valve permits forward flow. However, whereas $\Delta P$ is necessarily dependent on the applied flow rate, EOA is less flow-dependent, and thus approaches describing an *intrinsic* opening capability of the valve. In vitro, EOA is calculated as:

$$\mathrm{EOA} = \frac{Q_{\mathrm{RMS}}}{51.6 * \sqrt{\frac{\Delta P}{\rho}}}$$

where $\Delta P$ refers to the mean gradient, $Q_{\mathrm{RMS}}$ is the root-mean-square forward flow during the same period, and $\rho$ is fluid density. Despite EOA's noted advantages over $\Delta P$, it does suffer from poor repeatability in the event of very low gradients [34]. This may occur with large valves and/or low flow rates. Ultimately, both $\Delta P$ and EOA have useful roles in hydrodynamic performance assessment.

***Regurgitant Fraction (RF)*** RF is computed as (regurgitant volume/forward flow volume) for a single cardiac cycle. As demonstrated in Fig. 15.14, regurgitation volume is the sum of *closing volume* (retrograde flow as the valve leaflets are still reaching their closed position) and *leakage volume* (retrograde flow thereafter).

Note, RF is only measurable in the pulsatile setting; in the steady back pressure testing, a leakage rate is assessed instead. Further detail follows below.

When fixturing samples for hydrodynamic testing, the approach may differ significantly based on whether the test sample is a surgical or transcatheter valve. Surgical valves are typically sewn onto compliant gaskets that simulate the patient's annulus. The cloth of the valve is sealed against the fixture to simulate the biological reaction to the cloth.

For transcatheter valves, the fixturing method is much more complex. Because the patient's diseased valve is not removed during a transcatheter valve procedure, the in vitro landing zone must simulate the diseased valve (especially the annulus and leaflets). Numerous other anatomic features may also need to be simulated, depending on the intended patient population and the implant's specific manner of engaging with the anatomy. These may include a specific annular aspect ratio, discrete calcium nodules, anatomic material properties, and more. Also, because the transcatheter valve has the potential to be implanted at a range of depths relative to the annulus, and because its final configuration may be under-expanded, over-expanded, and/or distorted (e.g., out-of-round), multiple test fixtures are typically required, to evaluate performance across the range of potential configurations. ISO 5840-3 provides guidance on many key fixture parameters [12], but this guidance is not comprehensive. Ultimately, the manufacturer must identify and justify an appropriate fixturing approach.

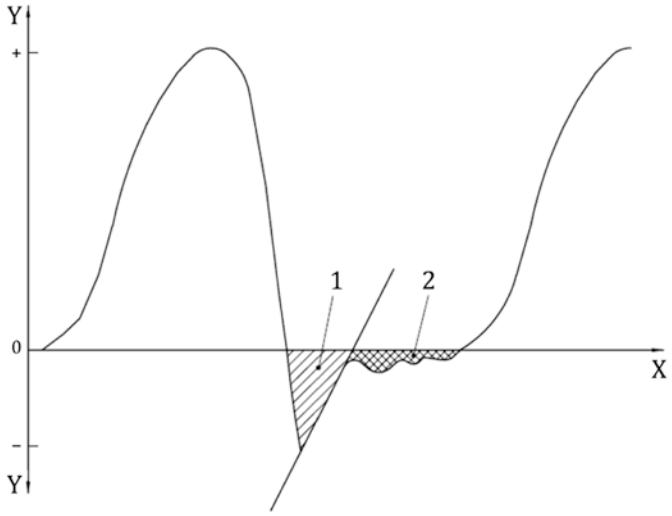


**Fig. 15.14** A representative flow waveform, highlighting the two volumes that comprise regurgitant volume. (Reproduced with permission from ISO 5840-1:2021 [10])

Hydrodynamic performance may be investigated either under pulsatile flow, to simulate beating of the heart, or under steady flow. Each is required by ISO 5840 [10–12], and each is summarized herein.

***Pulsatile flow testing*** Although pulse duplicator system designs and modes of operation vary, some core elements are universal.

- The ventricle has a drive mechanism (typically electromechanical or pneumatic) that can provide stroke volume from approximately 25–150 mL/beat and beat rates of 45–120 beats per minute (bpm). Its inlet and outlet connections must accommodate insertion of two heart valves: mitral and aortic valves for left heart testing or tricuspid and pulmonic valves for right heart testing.
- When operating the system, the test specimen resides at one valve position, while another passive valve must occupy the other position. A commercially available mechanical heart valve is often used, but the same effect can be achieved through other durable valve designs. This second valve is necessary to achieve physiologically accurate dynamics.
- Calibrated sensors are installed to monitor temperature, flow rate, and pressures. In order for the flow probe to accurately report flow through the test specimen, the flow area between it and the test specimen must have no compliant elements. With respect to pressure transducers, two must be placed at appropriate distances upstream and downstream of the test specimen. Also, a pressure transducer must

be placed to measure arterial pressure. In the case of aortic or pulmonic valve testing, the transducer downstream of the test specimen may serve this purpose. For mitral or tricuspid testing, a third pressure transducer is required for this purpose.

- Downstream of the aortic/pulmonic valve position, the system has adjustable compliance and resistance elements. These mimic the bulk compliance and resistance of the peripheral vasculature. By tuning these elements in combination with the ventricular actuation, the operator modulates the pressure and flow waveforms to achieve desired conditions for measurement. Downstream of these elements, fluid typically drains into an open reservoir, whose height provides a modest pressure head. This pressure head represents atrial pressure and drives ventricular filling during diastole.
- Typically, a heating subsystem is necessary, targeting fluid temperature of 37 °C to be representative of the in vivo use condition.
- Test media may vary, and the specific choice requires justification. Physiologic saline is common, due to its relative ease of production/use, and due to the fact that its low viscosity, relative to blood, poses a worst-case test condition for regurgitation. Viscosity-matched solutions, such as a glycerol–saline mixture, may also be considered.

An example schematic of a pulse duplicator system is provided in Fig. 15.15. Given such complexity, it is understandable that specific pulse duplicator implementations and their specific methods of operation can vary. To understand the impact of this variability on test outcomes, a study by Wu et al. [35] asked a group of 13 testing laboratories to test the same set of valves (St. Jude Medical Masters Series), under specified hydrodynamic conditions. This round-robin study concluded that "significant variability" existed and that system tuning is a blend of science and art. The *average* test outcomes from this study constitute valuable reference data, to help to benchmark the performance of a pulse duplicator system. This characterization activity is recommended by ISO 5840 [11, 12].

A new heart valve substitute is required to satisfy a set of minimum performance requirements under nominal hydrodynamic conditions (5.0 L/min, 70 bpm, 35% systolic duration, normotensive), according to ISO 5840. Minimum performance requirements for aortic and mitral valve substitutes, relating to EOA and RF, are provided in ISO 5840-2 (for surgical valves) and 5840-3 (for transcatheter valves) [11, 12]. These requirements are provided below (Table 15.4). The distinction between surgical and transcatheter valves is that transcatheter valves may experience leakage around their perimeter (paravalvular leakage). Recognizing this, a pulsatile hydrodynamic test fixture for a transcatheter valve must not intentionally seal the perimeter, but the maximum allowable RF is also greater. For tricuspid and pulmonic valve substitutes, the manufacturer is tasked to define and justify the performance requirements utilized.

Additionally, ISO 5840 states that pressure drop (i.e., forward flow dynamics) should be characterized at four cardiac outputs between 2 and 7 L/min (at 35% systolic duration and 70 bpm). Regurgitation dynamics should be characterized

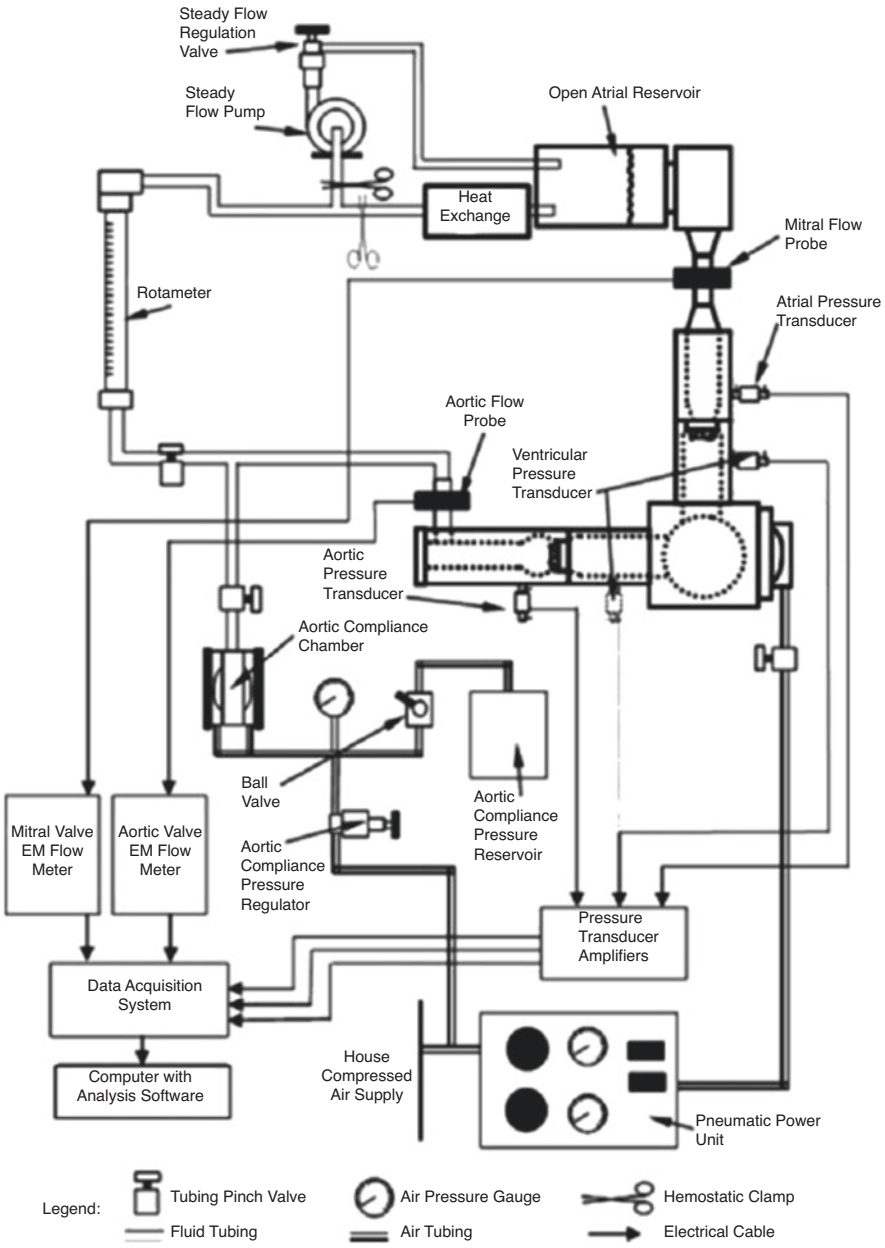


**Fig. 15.15** Representative schematic diagram of a pulse duplicator

**Table 15.4** Minimum hydrodynamic performance requirements for heart valve substitutes

| | Aortic | | | Mitral | | |
|---|---|---|---|---|---|---|
| | EOA lower limit ($cm^2$) | RF upper limit (%) | | EOA lower limit ($cm^2$) | RF upper limit (%) | |
| Valve size (mm)[a] | – | Transcatheter valves | Surgical valves | – | Transcatheter valves | Surgical valves |
| 17 | 0.70 | 20 | 10 | NA | | |
| 19 | 0.85 | 20 | 10 | NA | | |
| 21 | 1.05 | 20 | 10 | NA | | |
| 23 | 1.25 | 20 | 10 | 1.05 | 20 | 15 |
| 25 | 1.45 | 20 | 15 | 1.25 | 20 | 15 |
| 27 | 1.70 | 20 | 15 | 1.45 | 20 | 15 |
| 29 | 1.95 | 20 | 20 | 1.65 | 20 | 20 |
| 31 | 2.25 | 20 | 20 | 1.90 | 20 | 20 |
| 33 | NA | | | 2.15 | 20 | 20 |

Adapted from ISO 5840 [11, 12]

[a]For transcatheter heart valve substitutes, valve size is defined as the area-derived diameter after deployment within the implant site

across a specific range of beat rates, systolic durations, and pressure levels (each at 5 L/min).

***Steady flow testing*** Relative to pulsatile flow testing, steady flow testing is much simpler in design and execution. Two variants exist. In *steady forward flow testing,* a series of constant flow rates (typically 5–30 L/min) are applied, and at each level, the resultant pressure drop is measured and EOA computed. In *steady back pressure testing,* a series of constant back pressures (e.g., 40–200 mmHg for left heart valves for adults) is applied, and at each level, the resultant leakage rate is measured. Although the lack of pulsatility comprises a severe departure from the physiologic condition, the simplicity of steady flow testing leads to a much greater degree of accuracy and repeatability. It is thus a useful complementary tool to further describe a valve's hydraulic performance; such characterization is required by ISO 5840 [10].

To benchmark the steady flow test system, ISO 5840 provides dimensions for a pair of standard rigid nozzles (one for each test variant), along with target output measurements when they are tested. Benchmark data stems from prior work completed via a round robin testing by test labs participating as members of the ISO 5840 technical committee for the 2005 revision of ISO 5840 [36].

#### 15.5.2.9 Migration Resistance

For transcatheter valves, a key performance attribute is the ability of the device to resist migration and embolization after being deployed in the target implant location (e.g., native valve or pre-existing prosthesis). To properly evaluate migration

resistance, special test chambers are developed that simulate critical characteristics of the target implant site. As in the other tests, this evaluation must take into consideration worst-case conditions for sizing, geometry, pressure loading, etc. Migration resistance testing is typically performed using a specialized form of a pulse duplicator system used for valve hydrodynamic testing. Migration testing is generally performed under pulsatile pressure loading representing hypertensive patient conditions with the deployed valve configuration representing minimum radial interference between the valve and simulated implant location (in accordance with prescribed valve sizing criteria). When developing fixtures for migration testing, it is critical to meaningfully represent device–tissue interaction characteristics that influence migration resistance (e.g., native valve leaflets, degree and distribution of calcification, and implant site mechanical properties). The minimum duration for migration testing has not been established within ISO 5840; nonetheless, the test duration should be sufficient to demonstrate stability of the deployed device under simulated use conditions through a reasonable post-implant duration (e.g., 1000–10,000 cycles).

#### 15.5.2.10 Thrombogenic and Hemolytic Potential

ISO 5840 requires characterization of the potential for the heart valve substitute to induce thrombosis or hemolysis. Thrombosis will generally result from areas of low flow and/or low shear stress, whereas hemolysis will generally result from the inverse. Other factors, such as chemical interactions between the implant's materials and the blood, may also play a role. There exist multiple potentially informative tools. In no particular order, these include the following:

- Computational flow field assessments, using Computational Fluid Dynamics (CFD), Fluid Structure Interaction (FSI), or similar methods. These tools are beyond the scope of this chapter.
- Ex vivo flow testing. The test specimen is subjected to a pulsatile flow field using blood (appropriately anticoagulated) as the test media. At intervals, the extent of thrombosis and hemolysis is directly assessed through methods such as visual inspection, weight of the test specimen, pressure drop across the test specimen, and quantitative blood assays (platelet count, hematocrit, activated clotting time, clotting time, maximum clotting firmness, base excess, and plasma-free hemoglobin). Typically, the full test matrix will include the bookend valve sizes, low and high flow rates, and a range of relevant valve configurations.
- Experimental flow field assessment, through such tools as Particle Image Velocimetry (PIV) in combination with a pulse duplicator. In PIV, the test media is spiked with fluorescent particles. Typically, a thin laser sheet is used to illuminate a planar region of interest, such as the midplane of the region downstream of the valve. The illuminated particles are imaged via high-speed camera through a precise protocol. Post-processing algorithms can convert video data into velocity fields, shear stress fields, and more, to highlight regions of disturbed flow. Typically, the full test matrix will span multiple valve sizes/configurations,

regions of the flow field, planes of interest, hemodynamic conditions, and acquisition routines.

- Notably, for transcatheter valves, the "neo-sinus" is one important area for evaluation of thrombogenic potential (Fig. 15.16) [37, 38]. For further guidance on PIV investigations, additional reading is recommended [39, 40].

Each of the above modalities presents its own advantages and disadvantages. Also, unlike pulsatile hydrodynamic performance testing, in which clear minimum requirements are defined, there remain no clear specifications for thrombogenic or hemolytic potential assessment. In consideration of these facts, ISO 5840 recommends an "integrated" approach, in which one or more of these modalities are employed [10]. The test setup for each assessment is carefully informed by upfront definition of the relevant in vivo boundary conditions. Reference valves are typically necessary, to aid interpretation of results. The manufacturer must ultimately justify the appropriateness of the heart valve substitute's thrombogenic and hemolytic potential, in consideration of *all* data generated, including experimental, computational, and pre-clinical in vivo evidence.

#### 15.5.2.11 Cavitation Potential

For mechanical heart valve substitutes, assessment of cavitation potential during hydrodynamic testing is also important. Cavitation is a known failure mode for this class of device; during in vitro evaluation, it is indicated by the formation of vapor bubbles on valve closure caused by localized negative pressure regions. Violent collapse of these vapor bubbles adjacent to the valve leaflet or housing can result in

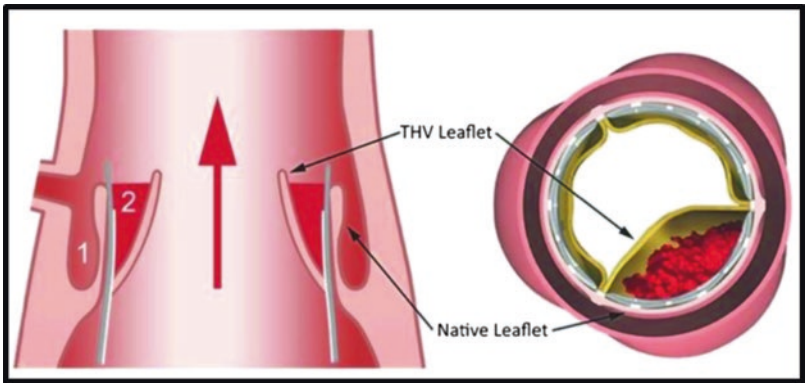


**Fig. 15.16** Transcatheter aortic valve (TAV) implantation displaces the native leaflets and the native sinus area (region 1) and creates a "neo-sinus", i.e., the region bounded by the TAV leaflets and the pinned native leaflets (region 2). Thrombus in the neo-sinus, which impacts TAV leaflet thickness and mobility, has been reported. This risk should be assessed for novel transcatheter valves, whether for the aortic position or elsewhere. (Reproduced with permission from Midha et al. [37])

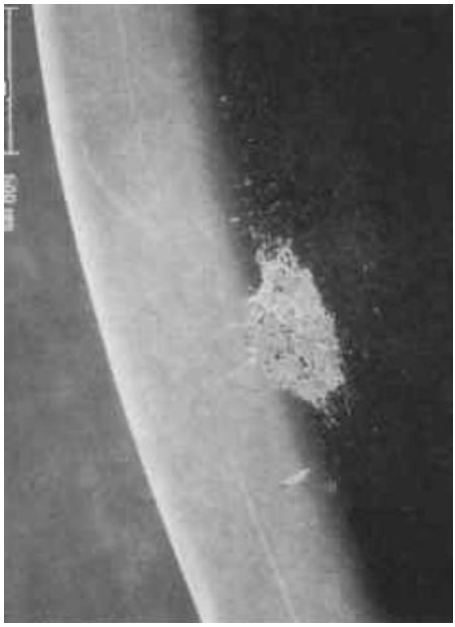

**Fig. 15.17** Cavitation erosion on a mechanical heart valve leaflet. (Reproduced with permission from Richard and Cao [41])

erosion of the material surface, degrading the structural integrity of the device. An example of cavitation erosion along the inflow edge of a pyrolytic carbon heart valve leaflet is shown in Fig. 15.17. For further information, refer to reviews by Johansen or Qian et al. [42, 43].

### *15.5.3 Fatigue Assessment*

At an average rate of 72 bpm, a heart valve substitute is subjected to approximately 40 million opening and closing cycles per year in a demanding physiological operating environment. In addition to pressure loading due to blood flow, the heart valve substitute is subjected to a combination of loading modes during each heartbeat associated with the systolic and diastolic action of the heart. The loading modes to which a heart valve is subjected are a function of device design, valve implant position (aortic, mitral, pulmonary, or tricuspid), and disease etiology.

Depending on the target patient population, the heart valve substitute could be expected to maintain its function for one or more decades, readily approaching one billion cycles. In order to evaluate the risks associated with potential structural and durability-related failure modes under the aggressive implant environment, an assessment of the ability of the implant to withstand the loading cycles and/or deformations to which it will be subjected over the expected implant duration is required. This is typically accomplished through a combination of acute testing of the heart valve substitute assembly (Sect. 15.5.2), fatigue testing of the heart valve

substitute's structural components, and valve durability testing of the finished heart valve substitute. Fatigue testing is discussed in this section; for valve durability see Sect. 15.5.4.

For the heart valve substitute structural components (i.e., housing, frame), testing is required to demonstrate reasonable assurance that the frame will remain functional for a minimum of 400 million cycles (10 years) for critical loading modes per ISO 5840 requirements [10] or for 600 million cycles (15 years) per US FDA requirements [9]. Historically, US FDA requirements for structural component testing have been more stringent as compared to the ISO requirements.

As depicted in Fig. 15.18, the structural analysis process begins by characterization and quantification of the loading conditions to which the device will be subjected. As discussed in Sect. 15.3, the loading conditions vary as a function of the valve implant position, disease state, and device design. Next, the mechanical properties of the structural components of the device are characterized (Sect. 15.5.1). The boundary condition data and mechanical property data provide critical inputs into the finite element model which is then used to predict the stress or strain distribution within the device during loading of the device onto the delivery system, deployment within the target implant site, and in vivo operation. In addition, the boundary condition data provide input into the device-level fatigue test methods (i.e., deployed shape and deformation targets).

Material fatigue characterization testing is conducted to determine the material fatigue strength at 400M (ISO) and 600M cycles (FDA). For a stress- or strain-life fatigue assessment, the FEA results are then evaluated in conjunction with the material fatigue strength data to compute fatigue safety factors for the device or to compute the likelihood of fracture within the expected lifetime. Lastly, device-level

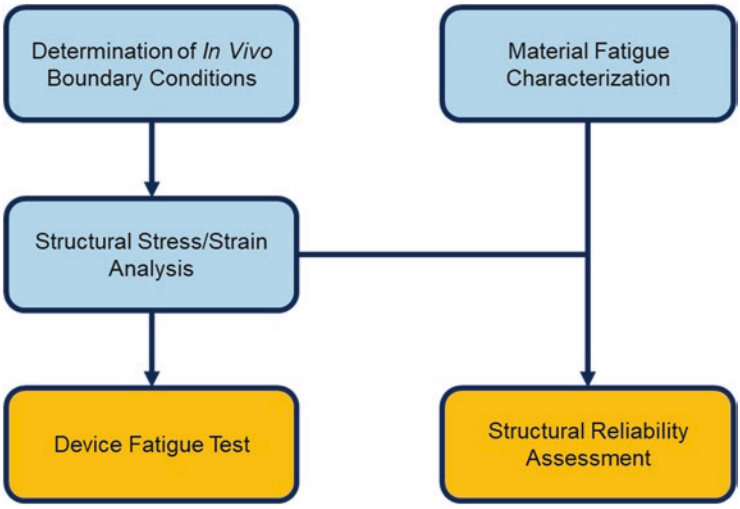


**Fig. 15.18** Schematic example of the elements comprising a device fatigue assessment process. (Adapted from ISO 5840-1:2021 [10])

fatigue tests are conducted at test conditions representing worst-case in vivo loading or deformation conditions (conducted to 400M or 600M cycles) as confirmatory fatigue tests for comparison to structural reliability predictions. Alternatively, device-level fatigue tests may be conducted over a range of test conditions to 400M or 600M cycles to quantify the fatigue capability of the device under physiological as well as hyperphysiological conditions.

In the case of a damage tolerance-based analysis, the FEA results are evaluated in conjunction with the crack growth parameters for the device structural components to predict the minimum structural lifetime and/or compute the maximum allowable flaw size/geometry that can be tolerated by the device to satisfy minimum lifetime requirements.

#### 15.5.3.1 Stress or Strain Analysis

Appropriately validated stress/strain analyses, typically in the form of a FEA, are performed to quantify the stress/strain distribution within all structural components of the heart valve substitute under in vivo loading conditions. Although stress analyses are primarily intended to quantify the driving force for failure, a detailed understanding of the failure mechanism particular to the loading and material is needed in order to identify the most relevant parameter that governs fatigue failure of the component. In many cases, this is some measure of stress, which will be assumed throughout this discussion. However, measures of strain or other parameters such as the stress intensity factor, $K$, may be more relevant. A more in-depth description of the use of numerical simulation in the design of heart valve substitutes is provided in the proceeding chapters.

Analyses should represent the full range of loading conditions associated with the implant position, anatomical variations, disease state, and pathological changes. In addition to the pressure loading due to the blood flow, the heart valve substitute is subjected to a combination of loading modes during each heartbeat associated with the systolic and diastolic action of the heart (Sect. 15.3.2). While it may not be feasible to simulate all loading modes in a single analysis, the potential for coupled effects should be considered if the results of individual analyses are to be superimposed.

#### 15.5.3.2 Material Fatigue Characterization

While stress analysis is performed to quantify the driving forces, material fatigue characterization is performed to quantify the resistance of the material to fatigue failure. Fatigue characterization typically falls into one of three main categories: (1) stress/life (S/N) for use with classical stress/life assessment, (2) strain/life (ε/N) for use with classical strain/life assessment, and (3) fatigue crack growth (FCG) for use in damage tolerance analysis (DTA), depending on the nature of the material.

Regardless of the approach, test specimens should be produced in such a way as to ensure material that is representative of the actual material in the heart valve substitute component (e.g., microstructure, crystallinity, density). Test conditions such as frequency and environment, including test temperature and physiologically representative fluid, should be representative of the in vivo environment.

***Stress/life (S/N) characterization*** Classical S/N characterization is commonly used for traditional engineering alloys and polymers. Coupons test specimens are typically cycled at constant stress amplitude until failure, and failure data are generated for stress amplitudes spanning or approaching the levels encountered in vivo. Thus, test durations will approach or exceed intended implant durations, which may approach one billion cycles. Since these durations typically far exceed conventional fatigue characterizations, endurance limits, as classically defined, might not exist, and extrapolating fatigue behavior from shorter duration testing may be nonconservative.

Testing is often performed at cyclic frequencies far exceeding in vivo conditions in order to minimize test duration. However, these accelerated frequencies can influence the fatigue behavior of polymers given their viscoelastic nature. Thus, care must be taken to ensure that the resulting S/N characterization is representative of the behavior at in vivo conditions. As shown in Fig. 15.19 using the time-temperature superposition principle, accelerated S/N testing at higher frequencies can be performed at appropriately elevated temperatures in order to preserve the in vivo fatigue behavior [44].

***ε/N characterization*** Stress has traditionally been the basis for controlling fatigue tests and as a means of monitoring fatigue performance and failure for conventional engineering materials. However, for materials such as Nitinol, given the superelastic behavior, an ε/N approach provides a more practical and appropriate means of characterizing fatigue performance. Figure 15.20 provides an exemplary constant-life diagram characterized using laser-cut electropolished medical grade Nitinol fatigue specimens which were thermally processed and electro-polished similar to endovascular stents [45]. Conditions that survived the 400 million cycle testing are shown as open circles, whereas cyclic conditions that led to fracture are represented with Xs or diamonds for fracture less than ten million cycles. Depending on the exact material processing and test parameters, the variation in fatigue life as a function of mean strain is monotonic yet nonlinear.

Analogous to stress/life, testing is performed at constant strain amplitudes. Testing should span a sufficient range of both strain amplitude and mean strain conditions in order to establish and characterize the fatigue response of the material, encompassing the worst-case anticipated in vivo strains experienced by the component.

***FCG characterization*** Damage tolerance approaches have traditionally been employed for materials, such as pyrolytic carbon, whose fatigue performance is governed by the growth of crack-like defects [29]. FCG characterization relates the

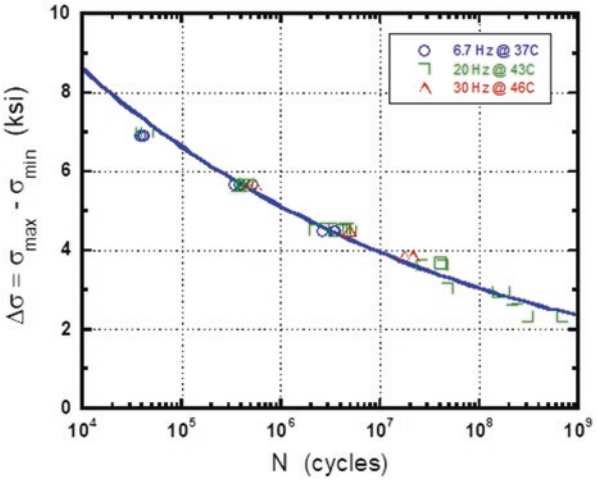


**Fig. 15.19** Typical stress/life behavior for an acetyl polymer at various combinations of temperatures and test frequencies [44]

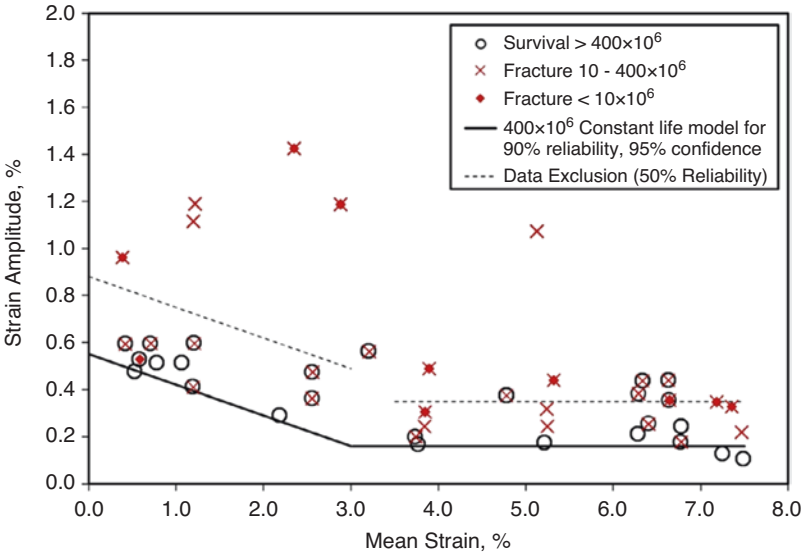


**Fig. 15.20** Constant-life diagram from laser-cut Nitinol test specimens for a life of 400 million cycles where the various conditions of mean strain and strain amplitude are plotted. (Reproduced from Cao [45])

rate of crack growth, d*a*/d*N*, to an appropriate measure of the cycling crack driving force (commonly taken as the cyclic stress intensity factor) that is determined for the component material.

FCG testing is performed by cycling a specimen containing a crack and measuring the rate of crack growth (Fig. 15.21). It is common and convenient to use a standard fracture mechanics specimen for which the crack driving force is readily known. However, testing can be performed on actual components so long as the crack driving force can be calculated.

Testing is performed to span the full range of FCG behavior from threshold crack driving forces below which no measurable crack growth occurs to driving forces approaching the fracture toughness of the material where instantaneous fracture occurs. Threshold behavior is often difficult to obtain, and not all materials exhibit threshold behavior, particularly in corrosive environments.

#### 15.5.3.3 Structural Reliability Assessment

Based on material fatigue characterization, lifetime assessments of the structural components are performed in order to evaluate risks associated with fatigue-related failure modes. Fatigue assessments are typically based on traditional stress (or strain)-life approach or by using a DTA. In traditional stress (strain)-life approaches, the in vivo loading (stress or strain) derived from the stress analysis are compared with the material fatigue characterization to predict the fatigue life of the component. In DTA approaches, the FCG behavior is used to predict the life of a component associated with the growth of an assumed initial flaw size to failure. Safety margins are associated with the degree to which the predicted lifetime exceeds the intended lifetime.

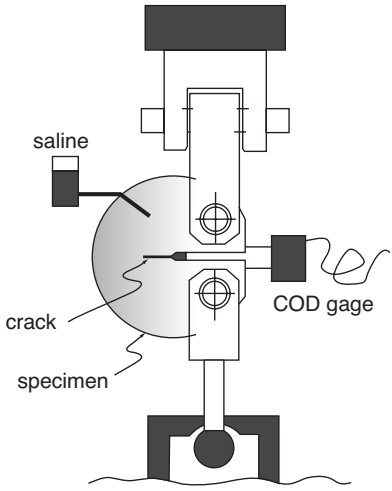


**Fig. 15.21** Schematic of fatigue crack growth (FCG) test setup with disc specimen to determine FCG behavior of pyrolytic carbon [29]

***Stress/life (S/N) or strain/life (ε/N) assessments*** Traditional fatigue life assessments are performed by using the material fatigue characterization to predict the lifetime of the component associated with the in vivo loading derived from the stress or strain analysis. A stress/life approach is often used for heart valve substitute structural components fabricated from traditional alloys and polymers. The strain/life approach is often used for heart valve substitute structural components fabricated from Nitinol.

For a stress/life or strain/life fatigue assessment, the FEA results are evaluated in conjunction with the material fatigue strength data to compute the fatigue safety factor for the device. Historically, a deterministic-based approach has been used to compute a fatigue safety factor by dividing the fatigue strength (at 400M or 600M cycles) by the peak alternating stress or strain amplitude as predicted by FEA. These fatigue safety factors provide a margin of safety estimate for the likelihood of frame fracture due to fatigue. A fatigue safety factor of >1 implies that a margin of safety exists for the performance of the device under the specified in vivo deformations. Probabilistic approaches may also be employed for fatigue life assessments in order to reflect the inherent variability in the fatigue data as well as a measure of confidence in the stress or strain analysis.

Variability in the fatigue characterization data and uncertainties in the stress or strain analysis are important considerations in any fatigue assessment. Fatigue data are typically more variable than most quasi-static material properties, which gives rise to uncertainty in the fatigue strength at a given stress or strain. Furthermore, the confidence in the fatigue strength when extrapolating from short-term testing can decrease significantly. Similarly, there are uncertainties associated with the stress or strain analysis. In addition to errors and uncertainties due to model approximations and assumptions, there are uncertainties and variability associated with the in vivo loading conditions. As such, neither the resulting stress or strain nor the fatigue strength is known with absolute confidence. From a deterministic perspective, the safety margin may be assessed by comparing estimates of the upper bound of the in vivo stress to lower bounds of the fatigue strength. Fatigue safety margins may also be assessed with reliability methods in which the probability that the fatigue strength exceeds the applied stress (or strain) at the expected lifetime is quantified.

***Damage tolerance analysis (DTA)*** Damage tolerance analyses are used to quantify component life due to fatigue crack propagation and have been used for pyrolytic heart valve substitute components [46]. Typically in a DTA, the component is assumed to contain a crack-like defect. The size of this defect is often based on the minimally detectable flaw size associated with inspection methods or based on the maximum size that would survive proof testing (testing during manufacturing that is specifically designed to result in catastrophic failure of parts with unacceptable defects).

The stress analysis is used to determine the in vivo crack driving force associated with the presence of a flaw located in a heart valve substitute component. The material FCG characterization is used to predict the rate of crack growth associated with

the in vivo driving force. As the fatigue crack continues to grow, the crack driving force increases. Eventually, as the crack length increases and the driving force approaches the fracture toughness, the crack will become sufficiently long and the driving force so high that the component would no longer be able to support further FCG. The fatigue life of the component is the life associated with FCG to this critical length. Similar to stress/life approaches, probabilistic analyses can be used to address uncertainties with in vivo loading conditions and variability in FCG behavior.

Damage tolerance analyses can also be used to determine the maximum allowable flaw size for a given component. Additionally, DTA can be used to determine the initial flaw size associated with a particular design life. Knowing this maximum allowable initial flaw size, inspection methods and proof tests can be specified and developed in order to ensure that the intended life of the device is achieved. This flaw size information provides input into establishing proof test levels to ensure flaws greater than the maximum allowable size is rejected during component manufacturing.

#### 15.5.3.4 Component Fatigue Demonstration Testing

To confirm structural reliability predictions from the FEA and material fatigue data, component-level testing is typically conducted under the primary device-loading modes at test conditions (displacements or loads) that meet or exceed those that the device would be predicted to experience during in vivo operation. These component-level fatigue tests are conducted to 400M or 600M cycles as confirmatory fatigue tests for comparison to structural reliability predictions. Historically, these types of fatigue tests are conducted using a "test-to-success" paradigm in which a sample of devices are tested without failure to a specific cycle count (i.e., 400M or 600M cycles); these fatigue test results may be utilized to demonstrate a minimum survival at a specified confidence level. Alternatively, unit cells or complete devices can be tested at multiple levels in a "test to fracture" methodology in order to fully characterize the fatigue response of the device; the test levels would typically include a "test to success" level to the expected lifetime of the device [47]. Although component-level fatigue testing is typically conducted as separate fatigue tests for the primary device-loading modes, it may be feasible to conduct this testing under a combination of primary-loading modes.

As for other tests, the fatigue test specimens must represent, as closely as possible, the finished product as supplied for clinical use, including exposure to the worst-case number of recommended sterilization cycles, process chemicals, aging effects, and any catheter crimping, loading, and deployment steps in accordance with manufacturing procedures and IFU. In addition, the effects of anticipated variations in the deployed device shape on device fatigue performance should also be taken into consideration. It is also important that the fatigue tests be conducted at the intended operating temperatures (37 °C) and in a representative physiological environment (e.g., phosphate-buffered saline).

It is critical that the fatigue test methods be sufficiently validated to confirm that the test is applying loads/deformations to the device under test in the manner intended and that the test conditions remain stable over the duration of the test. As part of the test method validations, a sample of specimens may be subjected to exaggerated stress or strain levels to generate fatigue fractures for comparison of the predicted areas of high stress or strain from computational analyses to the observed fracture areas. This testing is typically performed on the worst-case device size (i.e., size with the highest potential for fracture).

As shown in Fig. 15.22, the 4D CT data has been reconstructed and used to define in vivo boundary conditions imposed on the device within the aortic root. The boundary conditions were then applied in the finite element model of the implanted device to estimate the stress/strain distribution within the frame under simulated in vivo conditions. The finite element model results can be used for fatigue assessment of the implanted device and for defining in vitro fatigue test conditions.

### *15.5.4 Valve Durability Assessment*

In addition to the requirements to investigate structural reliability and fatigue, which are detailed in Sect. 15.5.3, it is also necessary to assess durability of the finished implant. A heart valve substitute must be designed to function for hundreds of millions of cycles. Verification of this durability is challenging, and no single tool or test method will provide a comprehensive picture. To this end, ISO 5840 calls for an integrated durability assessment, which brings together multiple complementary

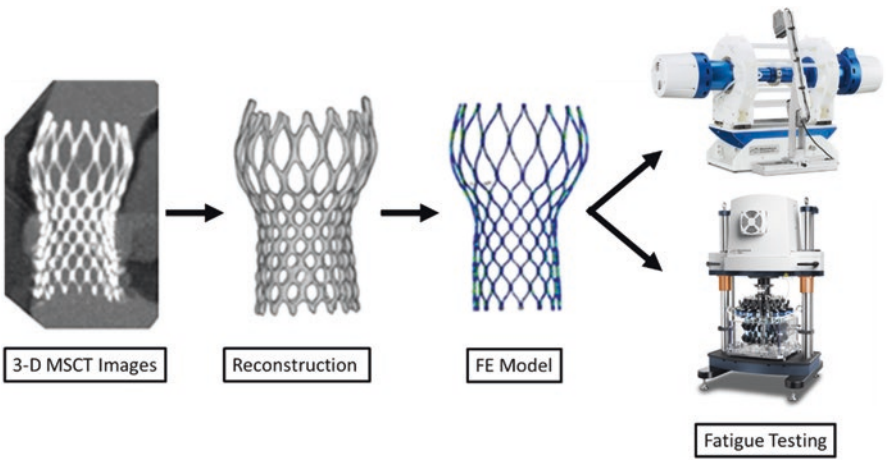


**Fig. 15.22** Example of an implanted transcatheter aortic valve (TAV) frame and 3D reconstruction from multi-slice CT (MSCT) images. This 3D geometry was used as an input to a finite element model. Finally, the outputs from the finite element (FE) model were used as input into device fatigue evaluations [26]

sources of evidence [10]. An example of such an approach is provided in Fig. 15.23. Table 15.5 summarizes the required durations of each in vitro durability test from Fig. 15.23. These methods are then described further in Sects. 15.5.4.1, 15.5.4.2, and 15.5.4.3.

If the labeling for a particular heart valve substitute includes an explicit statement about anticipated in vivo device lifetime, evidence must be generated to support the labeling claim, potentially beyond the extents given in Table 15.5. For example, if labeling states the expected lifetime of the device is 10 years, then evidence to support a claim of 400 million cycles would need to be provided.

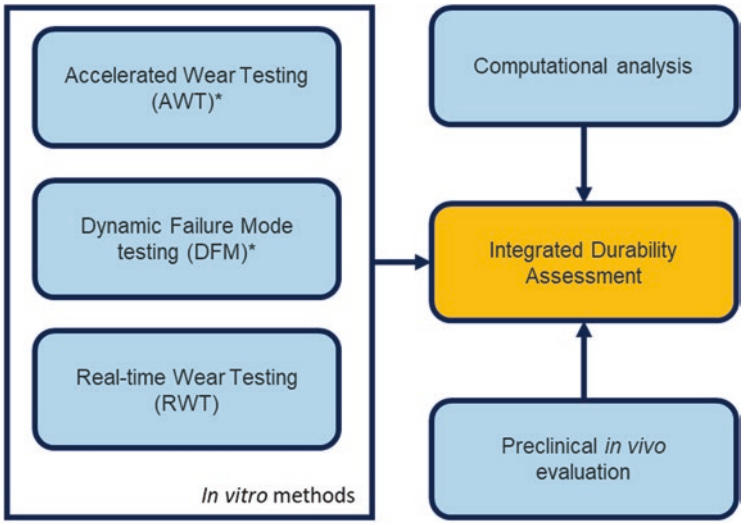


**Fig. 15.23** Example of an integrated approach to durability assessment. (Adapted from ISO 5840-1 [10]. *Required by ISO 5840)

**Table 15.5** Minimum durability test durations per ISO 5840 and US FDA heart valve guidance [9, 10]

| Source | AWT for valves with gradual failure modes | AWT for valves with catastrophic failure modes | DFM Testing | RWT for valves with established materials and processing methods | RWT for valves with novel materials or processing methods |
|---|---|---|---|---|---|
| ISO 5840 | 200M (5 years) | 400M (10 years) | Until failure or exit[a] | None | 50M (1.25 years) |
| US FDA | 200M (5 years) | 600M (15 years) | None | None | None |

For tests to success, durations are provided in terms of cycle number and equivalent implant duration in years

[a]See Sect. 15.5.4.2 for exit criteria

#### 15.5.4.1 Accelerated Wear Testing (AWT)

In any product life testing, engineers seeking to gain reliability results more quickly than can be achieved under normal operating conditions may consider accelerated tests. The two forms of acceleration are *usage rate acceleration* and *overstress acceleration*. AWT is the central test-to-success that must be passed in order to establish adequate durability performance of the heart valve substitute. It is a usage rate-accelerated test, targeting normotensive peak pressures at cycle rates of ranging from 10 to 25 Hz (600–1500 bpm).

With any accelerated life test, caution must be taken that the acceleration does not introduce unrealistic failure mechanisms. To this end, the chosen cycle rate during AWT must be justified.

The AWT equipment is best understood with reference to the pulse duplicator design concepts detailed in Sect. 15.5.2.8. Because the intent of AWT is to subject a group of test specimens to hundreds of millions of cycles of pressure loading and the full range of leaflet motion, certain departures from a complete pulse duplicator design are appropriate or even necessary. The key distinguishing features of an AWT system are as follows:

- The specific method of actuation may vary but must enable oscillations within the desired cycle rate. To achieve the necessary movement of fluid, common approaches include direct actuation via a linear motor (e.g., voice coil with piston) or indirect actuation via a rotary motor (e.g., with a cam mechanism to convert to linear motion).
- While the pulse duplicator requires a second passive valve to enable physiologic pressure and flow waveforms, the AWT system has no such second valve. This is an appropriate design simplification given that these waveforms cannot possibly be physiologic at the accelerated rates.
- Because the requirements for valid AWT cycling pertain to pressures and leaflet kinematics, it is necessary to have pressure transducers at the valve's inflow and outflow, as well as a high-speed camera capable of clearly demonstrating leaflet kinematics. AWT systems require the control and monitoring of temperature but not flow. The test system must be able to demonstrate the number of *valid* cycles accumulated (validity is defined by ISO 5840 and is discussed further below).
- The need for efficiency in AWT, resulting from the months-long test durations, shows up in system design. Specifically, testers typically have multiple (4–8) test stations, which are controlled independently or semi-independently.
- Various elements of the AWT system can be adjusted during cycling. Aside from the actuator itself (which may be adjusted in terms of stroke length, cycle frequency, and in some cases even motion profile), one or more adjustable compliance elements and resistance elements are typically also present. The resistance element (e.g., a ball valve) gates flow through a bypass channel for fluid to move *around* the test specimen.

When preparing to undertake an AWT study, the engineering team should carefully investigate the system's dynamics. Output parameters of interest include peak

pressures and leaflet kinematics and may also include motion of the implant's structural components, pressure loading profile, and more. Each test input may impart a unique combination of effects on the set of relevant output parameters. These inputs include not only the *tester* controls but also fixture design. If these dynamics are not well-controlled, the AWT study faces undue risk of artifactual test failures. The long test duration only heightens this risk, by creating opportunity for bioburden-related phenomena. In view of the high monetary, resource, and time costs of running an AWT study, all of the above variables and risks demand careful attention before a formal test is endeavored.

With respect to test matrix, ISO 5840 requires a minimum of five AWT samples per labeled valve size, with one possible exception. For products having more than three sizes, it may be acceptable to only test the smallest, largest, and an intermediate size, provided sufficient engineering justification. For transcatheter valves in particular, given the well-established potential for sample configuration to impact durability-related outcomes [48, 49], the worst-case(s) from across the range of possible deployed configurations must be tested (e.g., ellipticities, deployed sizes). When multiple configurations are included, the requirement is to test at least three samples per configuration, per labeled valve size. With respect to the test fixtures themselves, design considerations are generally analogous to those for hydrodynamic test fixtures. However, ISO 5840 provides far less specific guidance than it does for hydrodynamic testing; the manufacturer is expected to justify the fixture design.

A reference valve of established clinical performance may prove useful to contextualize AWT results and/or to detect test execution errors, but is not required.

Required AWT durations vary according to the type of heart valve substitute, as delineated above (Table 15.5). For those whose failure modes have been demonstrated to result in gradual degradation of valve function (i.e., tissue or polymer), it is required by both ISO 5840 and US FDA guidelines that testing be conducted to demonstrate the valves will remain functional for 200 million cycles (equivalent 5-year implant duration) [9, 10]. For those whose failure modes have the potential to result in immediate total loss of valve function (i.e., mechanical heart valves), demonstration of functionality is required through 400 million cycles (equivalent 10-year implant duration) per ISO 5840 requirements or through 600 million cycles (equivalent 15-year implant duration) per US FDA requirements. The longer test duration requirements for valves with potential immediate total loss of valve function are due to the potential patient harms associated with catastrophic failure of the heart valve substitute.

Per ISO 5840, a valid test cycle is one in which (a) test media temperature is $37 \pm 2$ °C, (b) the test specimen experiences the full range of leaflet motion (opening and closing), and (c) the test specimen experiences normotensive differential pressure conditions for at least 5% of the cycle's duration (e.g., for an aortic valve, at least 5% of the cycle having a backpressure of at least 100 mmHg) [10]. Test specimens must be investigated, via both visual inspection and hydrodynamic testing, at intervals not exceeding 50 million cycles. Damage patterns must be characterized. Although ISO 5840 requires the manufacturer to establish a clear definition of

failure prior to initiation of the study, it is noted that failure is "characterized by excessive structural damage and/or functional impairment" (Fig. 15.24).

#### 15.5.4.2 Dynamic Failure Mode (DFM) Testing

Because AWT pressure peaks align with normotensive in vivo levels, AWT failures may not present for months or years of real testing time. DFM testing aims to address this challenge, by inducing rapid failure of the heart valve substitute under higher stress conditions than experienced during AWT.

Typically, DFM testing manifests as a high-pressure variant on AWT. Peak pressures may step up gradually over the course of the study or may remain fixed. DFM testing may prove an invaluable design iteration tool early in a heart valve substitute's development process. The specific locations and modes of failure can indicate focal areas for design improvements. Putative design improvements can then be readily assessed by the resultant gains in time to failure during further DFM testing.

Section 15.5.4.1 described that accelerated product life testing may take either an *usage rate acceleration* and/or an *overstress acceleration* approach and AWT takes the former. DFM, in contrast, combines both approaches. As such, DFM presents a high risk of creating unrealistic failure modes. As one hypothetical example, extreme peak pressures could introduce artificially high frame deflection amplitudes, which could unnaturally abrade sutures and induce suture breaks that would never occur in vivo. Unrecognized, such unrealistic failure modes may misdirect the product design team toward solving false product performance shortcomings.

As it relates to final design verification, DFM is a requirement of ISO 5840 [10]. A successful AWT study will only culminate in valves that have not failed. Thus, the formal DFM study serves a critical complementary role to AWT, providing insight regarding specific anticipated durability-related failure modes of the heart valve substitute. This characterization testing must cover the range of relevant valve sizes

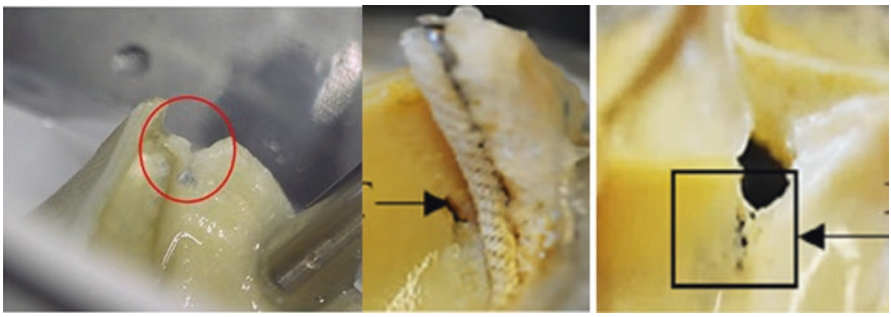

**Fig. 15.24** Representative examples of AWT tears at the leaflet commissure, sewing margin, or free margin. Tears are only one of many potential damage modes that can occur during AWT. (Images reproduced with permission from Vriesendorp et al. and Sritharan et al. [48, 50])

and configurations, with at least one specimen per size/configuration used in AWT and at least three samples per labeled valve size.

The formal DFM study concludes when each sample has met either of two exit criteria: (1) the sample has demonstrated functional failure or (2) the sample has survived at least 200M total DFM cycles, with at least 50M cycles having peak pressures of at least 1.5 times the very severe hypertension condition for the intended anatomic valve position (e.g., 248 mmHg for an aortic valve implant). One efficient path to fulfilling these exit criteria is to utilize test samples that have completed the full AWT study. Alternatively, non-AWT cycled valves may be used after appropriate pre-conditioning.

#### 15.5.4.3 Real-Time Wear Testing (RWT)

For heart valve substitutes whose materials and/or processing methods have established clinical history, the risk of unrealistic AWT outcomes is generally regarded as tolerable with sufficient due diligence (i.e., frequency justification). For valves having novel materials and/or processing methods, however, this risk can be addressed through a limited duration of RWT. For these valve types, ISO 5840 requires that RWT be considered, and decisions to forego RWT be scientifically justified.

Where RWT is required, ISO 5840 provides some direction [10]. Testing may not conclude until at least 50 million valid cycles have been accumulated. Visual and hydrodynamic outcomes must be compared to analogous outcomes from corresponding cycle counts during AWT, with conclusions being drawn on the appropriateness of the AWT methodology.

A valid RWT cycle requires is one in which (a) test media temperature is 37 ± 2 °C, (b) the test specimen experiences the full range of leaflet motion, (c) the test specimen experiences normotensive differential pressure conditions for at least 20% of the cycle's duration, and (d) the cycle rate does not exceed 200 bpm. If constructed appropriately, either a pulse duplicator or an AWT system may be suitable for RWT. Alternatively, a specialized RWT system may be employed.

ISO 5840 requires testing of at least the smallest, largest, and one intermediate labeled valve size. A minimum of three test samples must be tested, with the selected configuration(s) also being used in AWT, to enable direct comparison of wear patterns.

### *15.5.5 System Testing*

Since heart valve substitutes are designed to be used with accessory devices simulated use evaluations of the usability assessment/device and delivery system interaction testing of the entire system must be conducted in addition to evaluating valve functionality. Guidance for usability testing is provided in ANSI/AAMI/IEC 62366 (*Medical Devices Application of usability engineering to medical devices*). This

assessment should evaluate potential user error and provide mitigations where possible. Some methods to gather information on device/user interactions include wet labs with target end users, acute animal studies, and clinical experience with earlier generation devices. The results of such tests should be fed back into the risk analysis and in vitro test protocols.

For surgically implanted valves, this system might be comprised of the valve, packaging, holder, handle, sizers, and sutures. Simulated use evaluations should be conducted to ensure that these accessories do not damage the heart valve substitute in any way during use. This may be accomplished via detailed characterization and inspection of the heart substitute before and after simulated use testing. The following are examples of aspects that should be evaluated, as applicable: (1) inserting the handle into the holder for potential damaging forces on the valve, (2) suture insertion forces that could cause the holder to slip and damage a leaflet, (3) valve insertion forces (parachuting) that could deform or damage the valve, and (4) any foreseeable mishandling that could lead to the holder damaging the leaflets.

For transcatheter valves, this usability assessment should validate that users can use system components safely and effectively to deliver and deploy the valve utilizing the entire delivery system. The delivery system is often comprised of a crimper, valve, delivery catheter, dilators, sheaths, balloons, and other accessories. This assessment can be rather complex due to the multitude of accessories and access/pathways for implantation. Detailed evaluations of interactions between the implant and delivery system during use should be conducted. This assessment should include all elements of the transcatheter heart valve system and all associated procedural steps required to facilitate delivery and implantation of the implantable device. The focus of these evaluations should be on user error and clinical situations that could damage the device or result in patient or user injury. This may be accomplished via detailed characterization and inspection of the heart substitute before and after simulated use testing. The following are examples of aspects that should be evaluated, as applicable: (1) crimping/loading and attachment of device to delivery system, (2) loading device into delivery sheath, (3) positioning/deployment of device within target implant site, (4) repositioning/recapturing of device (if applicable) including damage to valve if intended for immediate reuse, (5) withdrawal of delivery system from the patient, and (6) component dimensional compatibility with ancillary devices.

### *15.5.6 Packaging Testing*

Packaging testing is conducted to ensure that the device is protected against damage and deterioration during transport, handling, and storage; damage includes compromise of device sterility if a device is packaged and shipped in sterile condition. Package testing is designed to simulate the conditions the package could encounter and typically consists of shock/drop testing, vibration testing, temperature and humidity excursions, and crush testing. Applicable ASTM or IEC test methods [51,

52] may be appropriate. It may be appropriate to precondition design verification test devices via simulated distribution testing to ensure that any effects of shipping/distribution on device performance are accounted for.

## 15.6 Summary

The primary purpose of this chapter was to familiarize the reader with basic in vitro test methods to verify the design and manufacturing of a heart valve substitutes. This chapter highlights those in vitro tests intended to characterize the primary device functions and performance parameters. Many descriptions of the scientific principles and test methods have been simplified for clarity. It is noted that there are many additional in vitro test methods beyond those described that are applicable to other elements of a heart valve substitute system.

A robust in vitro testing program is intended to demonstrate that a newly developed or modified device satisfies defined performance specifications and is a critical step in the process of demonstrating device safety. As described in this chapter, an in vitro test program includes evaluation of all system components and associated interactions to which the device may be exposed. The in vitro test methods described within this chapter were based on guidance documents and standards for surgical valves, transcatheter valves, and associated delivery systems.

The requirements discussed within this chapter were defined with reference to current commercially released heart valve substitutes. Definition of a comprehensive set of appropriate qualification tests and methods for new devices are derived from the risk assessment for the specific device with consideration to the target patient population, valve implant position, and system design.

## References

1. Kaplan AV, Baim DS, Smith JJ, Feigal DA, Simons M, Jefferys D, Fogarty TJ, Kuntz RE, Leon MB (2004) Medical device development from prototype to regulatory approval. Circulation 109(25):3068–3072
2. Carroll JD, Mack MJ, Vemulapalli S, Herrmann HC, Gleason TG, Hanzel G, Deeb GM, Thourani VH, Cohen DJ, Desai N, Kirtane AJ, Fitzgerald S, Michaels J, Krohn C, Masoudi FA, Brindis RG, Bavaria JE (2021) STS-ACC TVT registry of transcatheter aortic valve replacement. Ann Thorac Surg 111(2):701–722
3. Cahill TJ, Chen M, Hayashida K, Latib A, Modine T, Piazza N, Redwood S, Søndergaard L, Prendergast BD (2018) Transcatheter aortic valve implantation: current status and future perspectives. Eur Heart J 39(28):2625–2634
4. Popma JJ, Deeb GM, Yakubov SJ, Mumtaz M, Gada H, O'Hair D, Kleiman NS et al (2019) Transcatheter aortic valve replacement with a self-expanding valve in low risk patients. N Engl J Med 380(18):1706–1715
5. Mack MJ, Leon MB, Thourani VH, Makkar R, Kodali SK, Russo M, Pibarot P et al (2019) Transcatheter aortic valve replacement with a balloon-expandable valve in low risk patients. N Engl J Med 380(18):1695–1705

6. FDA. FDA approves first in the world device to treat patients with congenital heart disease, US FDA, 26 Mar 2021. [Online]. Available: https://www.fda.gov/news-events/press-announcements/fda-approves-first-world-device-treat-patients-congenital-heart-disease
7. Fiorilli PN, Herrmann HC, Szeto WY (2021) Transcatheter mitral valve replacement: latest advances and future directions. Ann Cardiothorac Surg 10(1):85–95
8. Goldberg YH, Ho E, Chau M, Latib A (2021) Update on transcatheter tricuspid valve replacement therapies. Front Cardiovasc Med 8:619558–619558
9. Food and Drug Administration (2010) Draft replacement heart valve guidance
10. ISO 5840-1:2021 (2021) Cardiovascular implants – cardiac valve prostheses – part 1: general requirements
11. ISO 5840-2:2021 (2021) Cardiovascular implants – cardiac valve prostheses – part 2: surgically implanted heart valve substitutes
12. ISO 5840-3:2021 (2021) Cardiovascular implants – cardiac valve prostheses – part 3: heart valve substitutes implanted by transcatheter techniques
13. Vlahakes GJ (2007) Mechanical heart valves the test of time. Circulation 116(16):1759–1760
14. Svennevig JL, Abdelnoor M, Nitter-Hauge S (2007) Twenty-five–year experience with the Medtronic-Hall valve prosthesis in the aortic position a follow-up cohort study of 816 consecutive patients. Circulation 116(16):1795–1800
15. David TE, Armstrong S, Maganti M (2010) Hancock II bioprosthesis for aortic valve replacement: the gold standard of bioprosthetic valves durability? Ann Thorac Surg 90(3):775–781
16. Jamieson WE, Burr LH, Miyagishima RT, Germann E, MacNab JS, Stanford E, Chan F, Janusz MT, Ling H (2005) Carpentier-Edwards supra-annular aortic porcine bioprosthesis: clinical performance over 20 years. J Thorac Cardiovasc Surg 130(4):994–1000
17. Mykén PS, Bech-Hansen O (2009) A 20-year experience of 1712 patients with the Biocor porcine bioprosthesis. J Thorac Cardiovasc Surg 137(1):76–81
18. Yankah CA, Pasic M, Musci M, Stein J, Detschades C, Siniawski H, Hetzer R (2008) Aortic valve replacement with the Mitroflow pericardial bioprosthesis: durability results up to 21 years. J Thorac Cardiovasc Surg 136(3):688–696
19. Jørgensen TH, Thyregod HGH, Ihlemann N, Nissen H, Petursson P, Kjeldsen BJ, Søndergaard L et al (2021) Eighth-year outcomes for patients with aortic valve stenosis at low surgical risk randomized to transcatheter vs surgical aortic valve replacement. Eur Heart J 42(30):2912–2919
20. Testa L, Rubbio AP, Casenghi M, Pero G, Latib A, Bedogni F (2019) Transcatheter mitral valve replacement in the transcatheter aortic valve replacement era. J Am Heart Assoc 8(22):e013352
21. Hasenkam JM, Nygaard H, Paulsen PK, Kim WY, Hansen OK (1994) What force can the myocardium generate on a prosthetic mitral valve ring? An animal experimental study. J Heart Valve Dis 3(3):324–329
22. Shandas R, Mitchell M, Conrad C, Knudson O, Sorrell J, Mahalingam S, Fragoso M, Valdes-Cruz L (2001) A general method for estimating deformation and forces imposed in vivo on bioprosthetic heart valves with flexible annuli: in vitro and animal validation studies. J Heart Valve Dis 10(4):495–504
23. Jensen MO, Jensen H, Nielsen SI, Smerup M, Johansen P, Yoganathan AP, Nygaard H, Hasenkam JM (2008) What forces act on a flat rigid mitral annuloplasty ring. J Heart Valve Dis 17(3):267
24. Siefert AW, Jimenez JH, Koomalsingh KJ, West DS, Aguel F, Shuto T, Gorman RC, Gorman JH, Yoganathan AP (2012) Dynamic assessment of mitral annular force profile in an ovine model. Ann Thorac Surg 94(1):59–65
25. Peng LF, McElhinney DB, Nugent AW, Powell AJ, Marshall AC, Bacha EA, Lock JE (2006) Endovascular stenting of obstructed right ventricle–to–pulmonary artery conduits a 15-year experience. Circulation 113(22):2598–2605
26. Schoenhagen P, Hill A, Kelley T, Popovic Z, Halliburton SS (2011) In vivo imaging and computational analysis of the aortic root. Application in clinical research and design of transcatheter aortic valve systems. J Cardiovasc Transl Res 4(4):459–469
27. Xiong T-Y, Stoppani E, Beule MD, Chen F, Li Y-J, Liao Y-B, Feng Y, Jaegere PD, Chen M (2021) Force distribution within the frame of self-expanding transcatheter aortic valve: insights from in-vivo finite element analysis. J Biomech 128:110804

28. ISO 14971:2019 (2019) Medical devices – application of risk management to medical devices
29. Cao H (1996) Mechanical performance of pyrolytic carbon in prosthetic heart valve applications. J Heart Valve Dis 5 Suppl 1:S32–S49
30. Ferry JD, Rice SA (1962) Viscoelastic properties of polymers. Physics Today 15(1):3, 76–78. https://doi.org/10.1063/1.3057989
31. Sacks MS, Sun W (2003) Multiaxial mechanical behavior of biological materials. Annu Rev Biomed Eng 5(1):251–284
32. ASTM F3067 Guide for radial loading of balloon expandable and self-expanding vascular stents
33. Baboian R (2005) Corrosion tests and standards: application and interpretation, vol 20. ASTM International, West Conshohocken
34. Floersch J, Evans MC, Midha PA (2021) Ineffective orifice area: practical limitations of accurate EOA assessment for low-gradient heart valve prostheses. Cardiovasc Eng Technol 2021:1–8
35. Wu C, Saikrishnan N, Chalekian AJ, Fraser R, Ieropoli O, Retta SM, Joseph R, Lee S, Marquez S, Mester D, Pan N (2019) In-vitro pulsatile flow testing of prosthetic heart valves: a round-Robin study by the ISO cardiac valves working group. Cardiovasc Eng Technol 10(3):397–422
36. ISO 5840:2005 (2005) Cardiovascular implants – cardiac valve prostheses
37. Midha PA, Raghav V, Sharma R, Condado JF, Okafor IU, Rami T, Kumar G, Thourani VH, Jilaihawi H, Babaliaros V, Makkar RR (2017) The fluid mechanics of transcatheter heart valve leaflet thrombosis in the neosinus. Circulation 136(17):1598–1609
38. Makkar RR, Fontana G, Jilaihawi H, Chakravarty T, Kofoed KF, De Backer O, Asch FM, Ruiz CE, Olsen NT, Trento A, Friedman J (2015) Possible subclinical leaflet thrombosis in bioprosthetic aortic valves. N Engl J Med 373(21):2015–2024
39. Raffel M, Willert CE, Scarano F, Kahler C, Wereley ST, Kompenhans J (2018) Particle image velocimetry: a practical guide. Springer International Publishing, Cham
40. Raghav V, Sastry S, Saikrishnan N (2018) Experimental assessment of flow fields associated with heart valve prostheses using particle image velocimetry (PIV): recommendations for best practices. Cardiovasc Eng Technol 9(3):273–287
41. Richard G, Cao H (1996) Structural failure of pyrolytic carbon heart valves. J Heart Valve Dis 5 Suppl 1:S79–S85
42. Johansen P (2004) Mechanical heart valve cavitation. Expert Rev Med Devices 1(1):95–104
43. Qian JY, Gao ZX, Hou CW, Jin ZJ (2019) A comprehensive review of cavitation in valves: mechanical heart valves and control valves. Bio-Des Manuf 2(2):119–136
44. Popelar C, Hoang T (2003) On the temperature-accelerated fatigue characterization of polymers. In: Fourth international conference on mechanic of time dependent materials, Lake Placid
45. Cao H, Wu MH, Zhou F, McMeeking RM, Ritchie RO (2020) The influence of mean strain on the high-cycle fatigue of Nitinol with application to medical devices. J Mech Phys Solids 143:104057
46. Ryder JK, Cao H (1996) Structural integrity assessment of heart valve prostheses: a damage tolerance analysis of the CarboMedics Prosthetic Heart Valve. J Heart Valve Dis 5 Suppl 1:S86–S96
47. Pelton AR, Schroeder V, Mitchell MR, Gong X-Y, Barney M, Robertson SW (2008) Fatigue and durability of Nitinol stents. J Mech Behav Biomed Mater 1(2):153–164
48. Sritharan D, Fathi P, Weaver JD, Retta SM, Wu C, Duraiswamy N (2018) Impact of clinically relevant elliptical deformations on the damage patterns of sagging and stretched leaflets in a bioprosthetic heart valve. Cardiovasc Eng Technol 9:351–364
49. Sun W, Li K, Sirois E (2010) Simulated elliptical bioprosthetic valve deformation: implications for asymmetric transcatheter valve deployment. J Biomech 43(16):3085–3090
50. Vriesendorp MD, de Lind van Wijngaarden RAF, Rao V, Moront MG, Patel HJ, Sarnowski E, Vatanpour S, Klautz RJM (2020) An in vitro comparison of internally versus externally mounted leaflets in surgical aortic bioprostheses. Interact Cardiovasc Thorac Surg 30(3):417–423
51. ASTM D4169 – 16 (2016) Standard practice for performance testing of shipping containers and systems
52. IEC 60068-2:2021 (2021) Environmental testing – part 2: tests – all parts

# Chapter 16
# Perspectives on Heart Valve Modelling: Contexts of Use, Risk, Validation, Verification and Uncertainty Quantification and End-to-End Example


**Cahal McVeigh, Frank Harewood, Patrick King, Mark Driscoll, Sanjeev Kulkarni, Tina Zhao, Mark Goodin, and Tinen L. Iles**

## Abbreviations

| | |
|---|---|
| CFD | Computational fluid dynamics |
| CUO | Context of use |
| FEA | Finite element analysis |
| QOI | Quantity of interest |
| VVUQ | Verification, validation and uncertainty quantification |

## 16.1 Introduction to VV40

Device manufacturers are increasingly reliant on computational modelling to demonstrate the safety, performance and durability of heart valve devices, across a highly variable patient population, prior to clinical evaluation and commercialization. More

C. McVeigh (✉) · F. Harewood · P. King
Medtronic, Dublin, Ireland
e-mail: cahal.mcveigh@medtronic.com

M. Driscoll
McGill University, Montreal, QC, Canada

S. Kulkarni
Permobil, Inc., Lead Test & Simulation Engineer – V&V, Lebanon, TN, USA

T. Zhao
Edwards Lifesciences, Irvine, CA, USA

M. Goodin
SimuTech Group, Rochester, NY, USA

T. L. Iles
University of Minnesota, Department of Surgery, Minneapolis, MN, USA

© The Author(s), under exclusive license to Springer Nature Switzerland AG 2023

P. A. Iaizzo et al. (eds.), *Heart Valves*, https://doi.org/10.1007/978-3-031-25541-0_16

recently, patient-specific models have been considered as supplements to clinical trial evidence and used as individual patient procedural planning tools. As modelling capabilities evolve to facilitate digital twins and personalized medicine, the risk profile of modelling is evolving, prompting additional focus on model credibility.

Bringing together researchers, medical device manufacturers and regulatory agencies, the ASME VVUQ40 subcommittee (Assessing Credibility of Computational Modeling Through Verification and Validation: Application to Medical Devices) has developed a risk-based approach to identifying the level of verification and validation activities required when modelling is used to assess medical devices. This standard (VV40), recognized by FDA, builds on the validation frameworks outlined in ASME VVUQ10 (V&V in Computational Solid Mechanics) and VVUQ20 (V&V in Computational Fluid Dynamics and Heat Transfer) [1–3].

The VV40 standard outlines a risk-based framework through which modellers can assess whether their models are sufficiently credible, relative to the context of use and model risk (Fig. 16.1). This framework inherently recognizes the wide range of contexts in which modelling is used by device manufacturers, academia and clinicians. The process starts by defining the question of interest that the model is intended to answer. The context of use (COU) defines the role and scope of the model in addressing the question of interest. The COU has an associated model risk, characterized by considering both the influence of the model, relative to other available evidence, and the consequence of an incorrect model prediction, most often in terms of potential patient harm. A number of verification and validation activities are suggested; these can be performed to varying degrees to demonstrate that model credibility is appropriate for the COU and commensurate with the model risk [1].

## 16.2 Context of Use (COU) and Model Risk for Heart Valve Modelling

Computational modelling is used by device manufacturers, academics and clinicians through the full product life cycle and for all components of the heart valve replacement system, including delivery catheter, packaging, accessories and implant. A well-formulated context of use is foundational to successful execution of

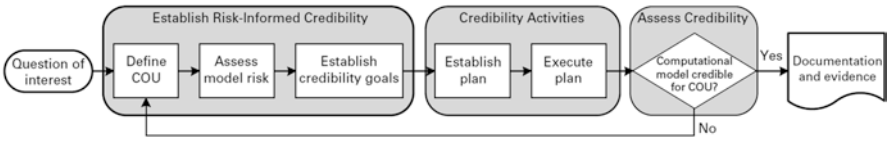


**Fig. 16.1** ASME VV40 framework

the subsequent model risk assessment and VVUQ activities. The following are several examples of contexts of use for heart valve modelling:

**Ideation** Modelling used for ideation and concept evaluation may employ lower resolution structural elements (e.g. beams, shells) to facilitate a rapid exploration of a large design space. These models may occur before formal design controls (CFR 820.30 Design Controls) are in place. The risk associated with models used in this context is typically low because they are not used as part of the formal risk mitigation process, and the benefits of speed often outweigh the burden of performing extensive VVUQ activities [6].

**Optimization** Once a concept is selected, modelling can be used to optimize the structure/material/geometry/topology to meet specific design objectives (often before physical prototyping has occurred). This typically requires higher credibility, often carrying higher risk if the model results are used to make critical design decisions which can impact product quality and product development timelines. Optimization model results (along with other sources of evidence) can influence a device manufacturer's decision to freeze a device design and progress to the next phase of product development [8].

**Design verification and ISO5840** Modelling used by manufacturers during design verification (CFR 820.30 Design Controls – (f) Design Verification) has a significant risk of impacting product quality and patient safety. ISO5840-1:2021 [4] is an international standard recognized by heart valve manufacturers and regulators as the approach for verifying heart valve designs through risk management. In the Fatigue Assessment Annex of ISO5840-1, the standard calls for a stress/strain analysis of the structural components under simulated in vivo conditions, specifically requiring validation in line with ASME VVUQ40: *Validation of the stress/strain analysis shall be performed in order to demonstrate confidence in the predicted results (ASME V&V 40).* Regardless of the model risk determined by the manufacturer, the standard requires that: *While it is left to the manufacturer to develop and justify the validation approach, the validation shall include comparisons of predicted FEA results against independent experimental measurements.* This requirement is often fulfilled by comparing device radial force derived from the model to real-world radial force recorded in benchtop tests. More sophisticated methods of directly measuring strains in heart valve devices are gaining prominence. Digital image correlation can be used to measure surface deformation on devices which are physically loaded on the bench. Identical loading can be applied in the model, facilitating a comparison of predicted strain versus experimentally measured strain. This technique offers a method to improve the relevance of the quantities of interest from the validation activities to the quantities of interest for the context of use (see ASME VV40 5.3.1 Relevance of QOIs).

ISO5840-1:2021 also identifies computational fluid dynamics (CFD) as a tool which can contribute to understanding of thrombogenic and haemolytic potential, in conjunction with experimental techniques. The standard recognizes the importance of model credibility: *The computational tools developed are validated using*

*experimental data by comparing relevant metrics and observations in the conditions studied*. The model risk (in particular the model influence) in this context would depend on other sources of evidence available, such as particle image velocimetry (PIV), evidence of thrombus formation, blood loops or clinical data.

**Preoperative (patient-specific) planning** Modelling is increasingly used as a tool to understand the unique device-anatomy interaction that will present in a specific patient under consideration for treatment. This may occur when patients are receiving an investigational device as part of a clinical trial or being implanted with a commercially available device. Modelling may be used to screen candidates for anatomical suitability and to select the appropriate device type or device size. Some models may be appropriate for providing procedural recommendations to the treating physician (e.g. optimal implant positioning within the anatomy). The risk associated with these models is highly dependent on the model influence (relative to other sources of evidence) and likelihood of harm to the patient due to an inaccurate model prediction [5–8].

Some modelling applications in this context of use may overlap with the concept of software as a medical device, SaMD (US), or medical device software, MDS (EU). Care should be taken as the model/software may fall under the scrutiny of regulatory bodies as a medical device in its own right (Guidance on Qualification and Classification of Software in Regulation (EU) 2017/745 – MDR and Regulation (EU) 2017/746 – IVDR, https://ec.europa.eu/docsroom/documents/37581), or as non-Device Clinical Decision Support (CDS) Software (https://www.fda.gov/regulatory-information/search-fda-guidance-documents/clinical-decision-support-software). This is a fast-evolving space, and efforts have been made by IMDRF (International Medical Device Regulators Forum) to harmonize the treatment of SaMD regulation internationally.

**In silico trials** Although not common in the heart valve industry, modelling may facilitate in silico clinical trials of heart valves in the future [9, 10]. The objective of researchers in this area is to use computer models to supplement or eventually replace clinical evaluation of medical devices. Given that clinical trials represent the ultimate regulatory evaluation of device safety and efficacy, the model risk associated with in silico models is higher than many other contexts of use (https://avicenna-isct.org/).

**Other COUs** Many other COUs can arise in the heart valve life cycle. For example, modelling can be used to understand failure modes (root cause investigations), make marketing claims, identify hazards or estimate the risk of hazardous situations, identify worst case scenarios, justify sample sizes in tests, improve manufacturing processes and identify appropriate manufacturing specifications.

**Decision consequence and influence** The risk associated with each context of use will inform the subsequent credibility goals and VVUQ activities. To reduce overall product risk, medical device manufacturers use quality tools to identify hazards and evaluate the probability of potential consequences. In particular, failure modes and

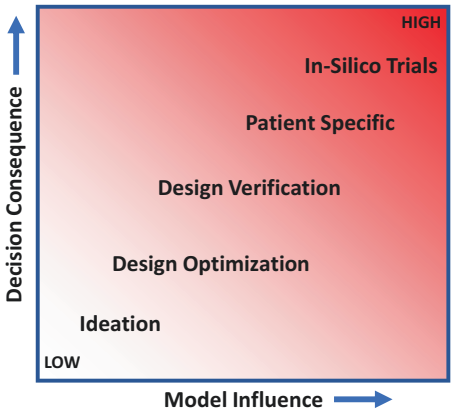


**Fig. 16.2** Examples of model risk for various potential contexts of use (COU) applications

effects analysis (FMEA) is commonly used to estimate potential patient harm. When assessing *model* risk, the FMEA risk analysis can be leveraged to determine the model decision consequence (see Fig. 16.2). Model influence should take account of the other available sources of evidence. Model results are often used alongside predicate device clinical data, cadaveric studies, preclinical (animal) studies and benchtop studies.

### *16.2.1 Challenges of Validating Patient-Specific Models*

Patient-specific models are often developed with a goal of predicting clinical outcomes (e.g. device apposition to the anatomy or flow conditions in the vicinity of the valve). Several challenges arise when validating this type of model, relative to available clinical data:

(a) Models may not be sophisticated enough to directly simulate the clinical outcome of interest (e.g. thrombus formation) and instead are tasked with outputting a more basic engineering surrogate or marker (e.g. wall shear stress). In this case, a direct comparison cannot be made between the model's engineering output and the clinical condition. Instead, the user may resort to demonstrating an association or correlation between the model and clinical outputs to demonstrate credibility of the prediction.
(b) Available clinical data used to build the patient-specific model may be of low quality, or key boundary conditions may be ill-defined. Uncertainty in the clinical imaging (e.g. preoperative CT images of the patient's anatomy) should be well understood. ASME VV40 offers a framework to account for this uncertainty (See ASME VV40 5.2.1.2.2 Quantification of Uncertainties) when assessing model credibility and describes potential associated form error.
(c) Available clinical data used to validate the model output may be limited (e.g. due to restrictions on the use of confidential patient data) or may consist of

lower-quality imaging or diagnostic data, from which subjective measurements (often involving considerable intra-observer error) are made. The uncertainty in the clinical output (e.g. PVL grades or transvalvular pressure gradient) should be accounted for when validating the model versus real-world clinical data (See ASME VV40 5.2.3.2.3 Output Comparison).

Well-controlled bench testing methods can be used to supplement and improve validation of patient–specific models. For example, as a surrogate for a clinical procedure, patient-specific anatomies could be 3D printed and experimented on with heart valve devices. The model's ability to replicate the experimental observations can demonstrate a degree of credibility prior to validation versus less-controllable real-world clinical outcomes. However, because synthetic materials are used in the validation exercises, the applicability of the validation activities to the intended patient-specific context of use is again compromised.

### *16.2.2 Model V&V Reporting*

Models used in the heart valve life cycle encompass a range of contexts of use and model risks. Device manufacturers, and others using modelling which could impact patient safety, should ensure procedures exist which codify when and how the ASME VV40 standard is followed in their organization. Regulators increasingly expect models to be validated in a manner which is commensurate with the model risk. FDA recognizes the ASME VV40 standard and further provides a guidance document on Reporting of Computational Modeling Studies in Medical Device Submissions. It is notable that this guidance document recommends concisely identifying the context of use of the modelling study reinforcing the foundational nature of the COU statement.

## 16.3 Summary and Conclusion

The rapid expansion of modelling and simulation across the heart valve life cycle has necessitated codification of a risk-based framework for model VVUQ. ASME VV40, recognized by the FDA, provides this framework. The framework is flexible in its implementation and can be applied to models spanning a wide range of contexts of use and risk levels. It is ultimately up to the end-user to ensure that model credibility is commensurate with the risk associated with the model. It is good practice to initiate modelling activities with a clear question or interest and context of use; these are foundational to a successful model VVUQ. Two COUs can particularly benefit from the application of the ASME VV40 framework:

(i) Design verification, in accordance with ISO5840, is a critical element of all heart valve manufacturers' product development processes. ISO5840 requires models to be validated consistently with the ASME VV40 risk-based framework. This

will improve conformity of heart valve V&V across manufacturers, resulting in improved overall model credibility.

(ii) Patient-specific modelling has unique challenges in relation to validating model outputs versus clinical data sets. Although focused more on benchtop-derived comparator data sets, the ASME VV40 framework and concepts can generally be applied to validation of patient-specific models.

## Appendix I: End-to-End Example VVUQ Transcatheter Valve

### *Background*

This example demonstrates the application of the ASME V&V 40 standard to the credibility assessment of a transcatheter aortic valve (TAV) FEA model, used in design verification (21CFR 820.30(f)) activities. In particular, the FEA model is utilized in the context of a structural component stress/strain (fatigue) analysis, in accordance with practices outlined in ISO5840-1:2021. This condensed example is for conceptual illustration only; model credibility activities for actual design verification purposes should be commensurate with model risk and sufficient to satisfy applicable industry standards and regulatory expectations.

The TAV device is designed to replace the native or surgical bioprosthetic aortic heart valve without open-heart surgery and without concomitant surgical removal of the failed valve. The TAV bioprosthesis in this example consists of a tissue valve mounted on a self-expanding (Nitinol) frame for catheter delivery in patients diagnosed with severe aortic stenosis. The implant is deployed within the target landing zone of the aortic root and remains in place due to oversizing, i.e. the original diameter of the implanted device is larger than the patient's aortic annular diameter resulting in an interference fit (Fig. 16.3).

Finite element analysis (FEA) is an integral part of the strategy to demonstrate structural integrity of the transcatheter aortic valve. Simulation of the device under in vivo loading is performed to quantify the material fatigue strains (referred to as *structural component stress/strain analysis* in ISO5840). Structural component fatigue testing is then typically performed at (or above) the in vivo fatigue strain level. FEA can also be used to determine the structural component fatigue test loading conditions, required to achieve the targeted fatigue strain level.

The process diagram of the risk-informed credibility assessment framework, as outlined in ASME V&V 40-2018 [4] is followed in this example (Fig. 16.1).

### *Question of Interest*

Three questions of interest were defined for the TAV finite element model:

1. What are the crimp strains and fatigue strains (strain amplitude and mean strain) and peak locations in the TAV under simulated in vivo conditions?

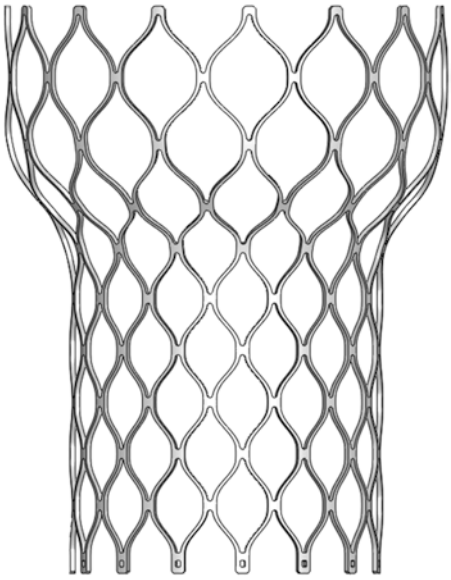

**Fig. 16.3** Generic self-expanding TAV frame model replicated from Confluent Medical's open-source project (https://confluentmedical.github.io/nitinol-design-concepts/120-open-frame-fatigue/)

2. What test conditions are required to replicate in vivo strain amplitudes (and mean strains) for structural component fatigue testing?
3. Will the TAV survive 600 M cycles under in vivo loading, without fracture?

Question 1 is answered with an 'in vivo' FEA model. Question 2 is answered with a similar model, which simulates the bench fatigue test. Question 3 is answered by demonstrating survival of structural components tested at or above in vivo fatigue strains levels. The ratio of test strain amplitude and in vivo strain amplitude (i.e. the fatigue factor of safety) is a key quantity of interest referred to throughout this example.

## *Define Context of Use (COU)*

The COU of the FEA model is to predict the fatigue strains in multiple device sizes under in vivo loading conditions. Results are used to identify the worst-case device size, location of peak fatigue strains and test conditions required to reproduce in vivo strain levels in a benchtop structural component fatigue test.

## *Assess Model Risk*

Model risk is assessed based on the influence of the model and the consequence of an adverse outcome resulting from an incorrect decision. The Model Influence and Decision Consequence classification systems are presented in Tables 16.1 and

**Table 16.1** Model influence scale

| Model influence | Description | Rank |
|---|---|---|
| Negligible | Model simulation results are a negligible factor in the decision | 1 |
| Minor | Model simulation results are a minor factor in the decision and augment other relevant data (e.g. test, predicate, literature, etc.) | 2 |
| Major | Model simulation results are a major factor in the decision but are supported by other relevant data (e.g. test, predicate, literature, etc.) | **3** |
| Primary | Model simulation results are the primary factor in the decision but are supported by other relevant data (e.g. test, predicate, literature, etc.) | 4 |
| Exclusive | Model simulation results are the exclusive factor in the decision | 5 |

**Table 16.2** Decision consequence scale

| Decision consequence | Description | Rank |
|---|---|---|
| Negligible | An incorrect decision may result in inconvenience or temporary discomfort | 1 |
| Minor | An incorrect decision may result in temporary injury or impairment not requiring medical intervention, or minor property or environmental damage | 2 |
| Major | An incorrect decision may result in injury or impairment that requires medical intervention (e.g. infection), or serious property or environmental damage | 3 |
| Critical | An incorrect decision may result in permanent impairment or life-threatening injury, or critical property or environmental damage | **4** |
| Catastrophic | An incorrect decision may result in patient or operator death, or catastrophic property or environmental damage | 5 |

16.2, respectively. A five-level ranking scale was adopted to assess the model influence and the decision consequence. The decision consequence rating is related to the severity ranking in the design failure mode and effect analysis (DFMEA) for the device. A decision consequence rating of 4, or critical, is assigned for the model.

A model influence of 3, or major, is assigned as the model will be used to define fatigue test conditions. The choice of a ranking of 3 is also supported by existence of clinical data for a predicate device with a similar design, showing no reported cases of fracture. Further, modelling results are used to inform subsequent benchtop testing, which is used to finally confirm device performance.

Model influence and decision consequence are mapped to a three-level risk schema as shown in Table 16.3.

**Table 16.3** Model risk classification matrix

| Model influence | Negligible | Minor | Major | Critical | Catastrophic |
|---|---|---|---|---|---|
| Exclusive | | | | | |
| Primary | | | | | |
| Major | | | | X | |
| Minor | | | | | |
| Negligible | | | | | |

Decision consequence

Red = high, yellow = medium, green = low

## *Establish Credibility Goals*

Credibility goals are defined, based on the COU and the model risk rating, to demonstrate an appropriate level of confidence in the model. A detailed list of example gradations and associated credibility levels adapted from ASME V&V 40-2018 is provided in Table 16.4. Credibility goals targeted here are highlighted in Table 16.4, commensurate with the risk identified in Table 16.3. Activities that correspond to a credibility of medium or high were completed for most credibility factors. The credibility activities are summarized in the following sections

## *Model Description*

In vivo *frame model:* Non-linear static analyses were performed using the Abaqus FEA code, using the Abaqus/standard implicit solver. The generic TAV frame FEA model is meshed with 3D hexahedral elements. In this example, a biased mesh was assigned to the geometry with smaller elements at the surface of the strut and towards the connectors of the frame where high strains are localized (Fig. 16.4).

A nominal 180° in vivo FEA model was created, using mean anatomical loading conditions, for use in model validation activities. The largest size device was modelled, and the results are assumed to be applicable for the smaller sizes due to the similar structure and strut dimensions. The in vivo loading consisted of a simulated crimp and deploy, followed by applying deformation to the Nitinol frame through contact with constraining rings (Fig. 16.5), to mimic motion of the device over the cardiac cycle.

A superelastic-plastic material model was used, allowing residual stresses and strains following device loading and deployment to be retained during cyclic loading.

*Bench fatigue test model:* FEA is also used to determine the test conditions required to reproduce (or exceed) the predicted in vivo fatigue strain levels. The benchtop fatigue test is modelled using the same frame model as is used in the

**Table 16.4** Example gradation of activities (adapted from ASME VV40-2018) and the credibility level which was assumed for this work
**Credibility factors and required activity for this work are highlighted**
[a]Wording has been adapted from ASME V&V40 to apply to this specific example. Wording in V&V 40 is "The numerical solution was compared to an accurate benchmark solution from another verified code
[b]Two comparators were used: Radial force test data and fatigue test data. This goal applies to the radial force comparator. For the fatigue comparator, multiple test samples were used but not enough to be statistically relevant, and a qualitative comparison was performed between FEA results and test data

| Activities | | Credibility factors | Example gradation of activities | Credibility level |
|---|---|---|---|---|
| Verification | Code | Software quality assurance | (a) Very little or no SQA procedures were specified or followed | Low |
| | | | (b) SQA procedures were specified and documented | Medium |
| | | | (c) SQA procedures were specified and documented; the software anomaly list and the software development environment were fully understood, and the impact on the COU was analysed and documented; quality metrics were tracked | High |
| | | Numerical code verification | (a) NCV was not performed | Low |
| | | | (b) The numerical solution, for an applicable benchmark problem, was compared to the exact analytical solution[a] | Low |
| | | | (c) Discretization error was quantified by comparison to an exact solution, and a grid convergence study demonstrated that the numerical solution asymptotically approached the exact solution as the discretization was refined | Medium |
| | | | (d) In addition to the quantification of discretization error and the execution of a grid convergence study as described in (c), the observed order of accuracy was quantified and compared to the theoretical order of accuracy | High |
| | Calculation | Discretisation error | (a) No grid or time-step convergence analysis was performed to estimate the discretization error | Low |
| | | | (b) Applicable grid or time-step convergence analyses were performed, and their respective convergence behaviours were observed to be stable, but the discretization error was not estimated | Medium |
| | | | (c) Applicable grid or time-step convergence analyses were performed, and discretization error was estimated | High |

[1] Wording has been adapted from ASME V&V40 to apply to this specific example. Wording in V&V 40 is "The numerical solution was compared to an accurate benchmark solution from another verified code."

**Tab. 16.4** (continued)

| Activities | | Credibility factors | Example gradation of activities | Credibility level |
|---|---|---|---|---|
| | | Numerical solver error | (a) No solver parameter sensitivity was performed | Low |
| | | | (b) No solver parameter sensitivity was performed. Solver parameters were established based on values from a previously verified computational model | Medium |
| | | | (c) Problem-specific sensitivity study was performed on solver parameters, confirming that changes in simulation results due to changes in the solver parameters were negligible relative to the model accuracy goal | High |
| | | Use error | (a) Inputs and outputs were not verified | Low |
| | | | (b) Key inputs and outputs were verified by the practitioner | Low |
| | | | (c) Key inputs and outputs were verified by internal peer review | Medium |
| | | | (d) Key inputs and outputs were verified by reproducing simulations as part of an external peer review | High |
| Validation | Computational model | Model form | (a) Influence of model form assumptions was not explored | Low |
| | | | (b) Influence of expected key model form assumptions was explored | Medium |
| | | | (c) Comprehensive evaluation of model form assumptions was conducted | High |
| | | Model input–quantification of sensitivities | (a) Sensitivity analysis was not performed | Low |
| | | | (b) Sensitivity analysis on expected key parameters was performed | Medium |
| | | | (c) Comprehensive sensitivity analysis was performed | High |
| | | Model input–quantification of uncertainties | (a) Uncertainties were not identified | Low |
| | | | (b) Uncertainties on expected key inputs were identified and quantified but were not propagated to quantitatively assess the effect on the simulation results | Medium |

**Tab. 16.4** (continued)

| Activities | | Credibility factors | Example gradation of activities | Credibility level |
|---|---|---|---|---|
| | | | (c) Uncertainties on all inputs were identified and quantified and were propagated to quantitatively assess the effect on the simulation results | High |
| | Comparator | Test samples – quantity of test samples | (a) A single sample was used | Low |
| | | | (b) Multiple samples were used, but not enough to be statistically relevant | Medium |
| | | | (c) A statistically relevant number of samples were used[b] | High |
| | | Test samples – range of characteristics of test samples | (a) One or more samples with a single set of characteristics were included | Low |
| | | | (b) Samples representing a range of characteristics near nominal were included | Low |
| | | | (c) Samples representing the expected extreme values of the parameters were included | Medium |
| | | | (d) Samples representing the entire range of parameters were included | High |
| | | Test samples – measurements of test samples | (a) Test samples were not measured and/or characterized | Low |
| | | | (b) One or more key characteristics of the test samples were measured | Medium |
| | | | (c) All key characteristics of the test samples were measured | High |
| | | Test samples – uncertainty of test sample measurements | (a) Samples were not characterized or were characterized with gross observations, and measurement uncertainty was not addressed | Low |
| | | | (b) Uncertainty analysis incorporated instrument accuracy only | Low |
| | | | (c) Uncertainty analysis incorporated instrument accuracy and repeatability (i.e., statistical treatment of repeated measurements) | Medium |

[2] Two comparators were used: Radial force test data and fatigue test data. This goal applies to the radial force comparator. For the fatigue comparator, multiple test samples were used but not enough to be statistically relevant, and a qualitative comparison was performed between FEA results and test data.

**Tab. 16.4** (continued)

| Activities | | Credibility factors | Example gradation of activities | Credibility level |
|---|---|---|---|---|
| | | | (d) Uncertainty analysis incorporated a comprehensive uncertainty quantification, which included instrument accuracy, repeatability, and other conditions affecting the measurements | High |
| | | Test conditions – quantity of test conditions | (a) A single test condition was examined | Low |
| | | | (b) Multiple (two to four) test conditions were examined | Medium |
| | | | (c) More than four test conditions were examined | High |
| | | Test conditions – range of test conditions | (a) A single test condition was examined | Low |
| | | | (b) Test conditions representing a range of conditions near nominal were examined | Low |
| | | | (c) Test conditions representing the expected extreme conditions were examined | Medium |
| | | | (d) Test conditions representing the entire range of conditions were examined | High |
| | | Test conditions – measurements of test conditions | (a) Test conditions were qualitatively measured and/or characterized | Low |
| | | | (b) One or more key characteristics of the test conditions were measured | Medium |
| | | | (c) All key characteristics of the test conditions were measured | High |
| | | Test conditions – uncertainty of test condition measurements | (a) Test conditions were not characterized or were characterized with gross observations; measurement uncertainty was not addressed | Low |
| | | | (b) Uncertainty analysis incorporated instrument accuracy only | Low |
| | | | (c) Uncertainty analysis incorporated instrument accuracy and repeatability (i.e., statistical treatment of repeated measurements) | Medium |
| | | | (d) Uncertainty analysis incorporated a comprehensive uncertainty quantification, which included instrument accuracy, repeatability, and other conditions affecting the measurements | High |
| | Assessment | Equivalency of input parameters | (a) The types of some inputs were dissimilar | Low |

**Tab. 16.4** (continued)

| Activities | | Credibility factors | Example gradation of activities | Credibility level |
|---|---|---|---|---|
| | | | (b) The types of all inputs were similar, but the ranges were not equivalent | Medium |
| | | | (c) The types and ranges of all inputs were equivalent | High |
| | | Output comparison – quantity | (a) A single output was compared | Low |
| | | | (b) Multiple outputs were compared | High |
| | | Output comparison – equivalency of output parameters | (a) Types of outputs were dissimilar | Low |
| | | | (b) Types of outputs were similar | Medium |
| | | | (c) Types of outputs were equivalent | High |
| | | Output comparison – rigor of output comparison | (a) Visual comparison was performed | Low |
| | | | (b) Comparison was performed by determining the arithmetic difference between computational results and experimental results | Medium |
| | | | (c) Uncertainty in the output of the computational model or the comparator was used in the output comparison | Medium |
| | | | (d) Uncertainties in the output of the computational model and the comparator were used in the output comparison | High |
| | | Output comparison – agreement of output comparison | (a) The level of agreement of the output comparison was not satisfactory for key comparisons | Low |
| | | | (b) The level of agreement of the output comparison was satisfactory for key comparisons, but not all comparisons | Medium |
| | | | (c) The level of agreement of the output comparison was satisfactory for all comparisons | High |

**Tab. 16.4** (continued)

| Activities | Credibility factors | Example gradation of activities | Credibility level |
|---|---|---|---|
| Applicability | Relevance of the quantities of interest | (a) The QOIs from the validation activities were related, though not identical, to those for the COU | Low |
| | | (b) A subset of the QOIs from the validation activities were identical to those for the COU | Medium |
| | | (c) The QOIs from the validation activities were identical to those for the COU | High |
| | Relevance of the validation activities to the COU domain | (a) There was no overlap between the ranges of the validation points and the COU | Low |
| | | (b) There was partial overlap between the ranges of the validation points and the COU | Low |
| | | (c) The COU encompassed some of the validation points | Medium |
| | | (d) The COU encompassed all validation points, and the validation points spanned the entire COU space | High |

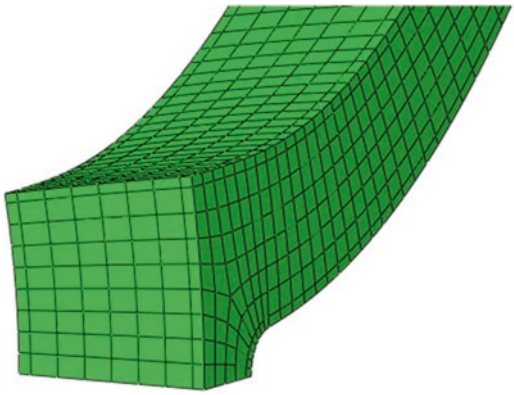

**Fig. 16.4** Cross-section through the frame strut showing the biased mesh

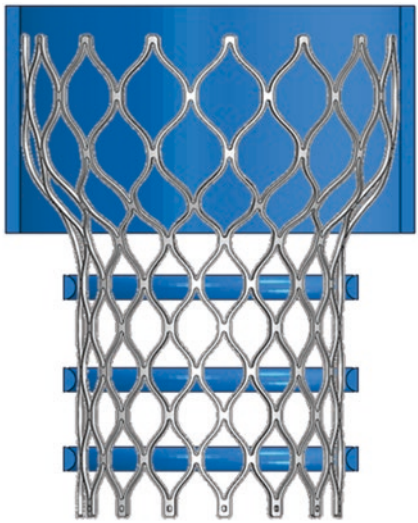

**Fig. 16.5** Half-frame (180°) symmetry was modelled. Anatomical loading conditions applied through constraining rings

in vivo model; the mesh density, material model and other analysis settings are identical to the in vivo model. Details of the bench fatigue test and associated FEA model are beyond the scope of this example problem (Fig. 16.6).

## *Credibility Activities*

**Code verification (ASME V&V 40 5.1.1)** Dassault Systemes, makers of the Abaqus FEA software used in this study, have a strong history of quality control and are certified to ISO 9001:2015. The Abaqus installation process includes a verification procedure which runs verification problems and compares the results to reference values. This confirms that the software has been successfully installed and can

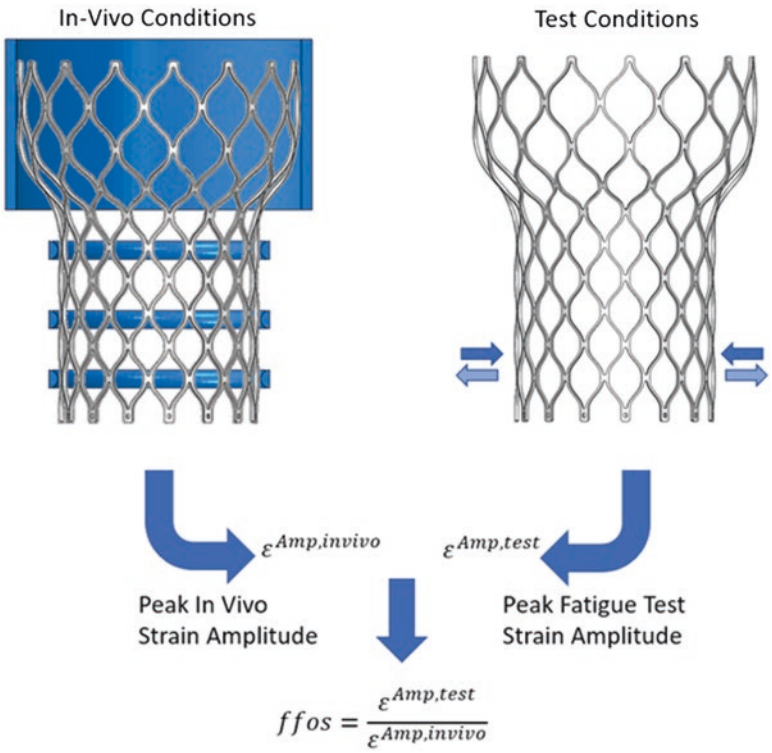


**Fig. 16.6** The same model is used to predict in vivo and test strain levels. In this example, the ratio (fatigue factor of safety) is the quantity of interest when determining structural integrity

operate correctly on the computer resource and software environment in which it will be used. Code verification was performed on the machines used to run the analyses detailed in this example.

To demonstrate numerical code verification, the numerical solution for an applicable benchmark problem was compared to the exact analytical solution. The qualification process for new Abaqus releases includes running and verifying results for all problems in the Abaqus Verification Guide and the Abaqus Benchmarks Guide. An applicable benchmark problem from the Abaqus Benchmarks Guide was identified (geometrically nonlinear analysis of a cantilever beam). The problem involves large displacement, geometrically non-linear analysis of a cantilever beam. Using reduced-integration linear elements (C3D8R), with enhanced hourglass control, the FE model displacement results were shown to match an exact analytical solution.

**Calculation verification, discretization error (ASME V&V 40 5.1.2.1)** A study was performed to assess the sensitivity of model outputs to different levels of discretization error (i.e. mesh refinement). In vivo simulations were performed with five mesh densities (Fig. 16.7). Fatigue test simulations were performed using the

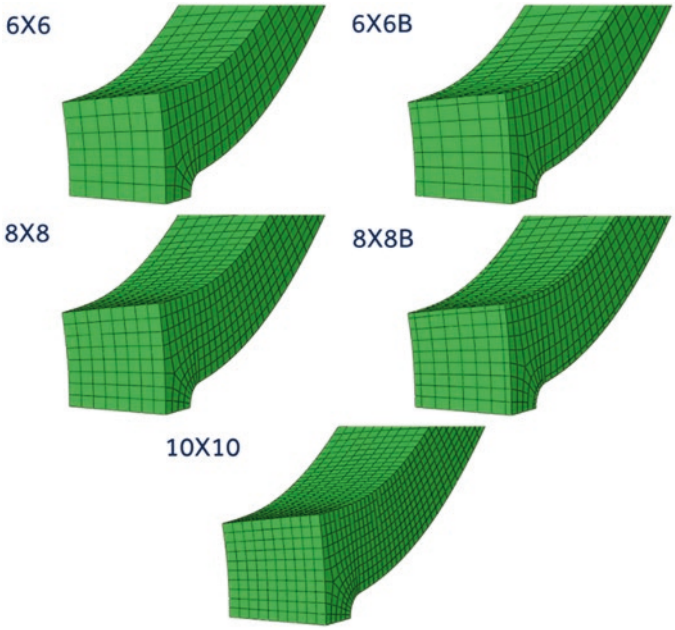


**Fig. 16.7** Mesh configurations. The 6 × 6, 8 × 8 and 10 × 10 meshes consist of uniform element size through the frame cross-section. The 6 × 6B and 8 × 8B meshes contain smaller elements on the frame surface

**Table 16.5** Test/in vivo strain amplitude ratio results for the mesh refinement sensitivity study

| Metric | 6 × 6 | 6 × 6B | 8 × 8 | 8 × 8B | 10 × 10 |
|---|---|---|---|---|---|
| In vivo strain amplitude [%] | 0.11% | 0.11% | 0.11% | 0.12% | 0.12% |
| Test strain amplitude [%] | 0.12% | 0.12% | 0.12% | 0.13% | 0.12% |
| Test/in vivo ratio [−] | 1.11 | 1.10 | 1.08 | 1.07 | 1.03 |
| Difference relative to 10 × 10 [%] | 8% | 6% | 4% | 3% | – |

The 'difference' row compared the test/in vivo ratio results with the 10 × 10 results

same meshes. The quantity of interest used to demonstrate acceptable mesh error is the apparent fatigue factor of safety, i.e. the ratio of test/in vivo peak strain amplitudes. These were calculated for each mesh density as shown in Table 16.5.

The lowest ratio value was observed with the 10 × 10 mesh configuration. The values calculated with the 8 × 8B and 8 × 8 mesh configurations are within 5% of that calculated with the 10 × 10 mesh configuration. Computational cost of the 10 × 10 mesh configuration was approximately two times that of the 8 × 8B mesh.

Based on the results of this mesh refinement sensitivity study, it is concluded that the 8 × 8B mesh configuration should be used. The test/in vivo alternating strain ratio values for the 8 × 8B mesh configuration were within 3% of that of the 10 × 10

mesh configuration. The 8 × 8B mesh configuration with smaller elements towards the surface ensures that surface strains are captured more accurately with greater computational efficiency.

**Calculation verification, numerical solver error (ASME V&V 40 5.1.2.2)** Sensitivity analyses were performed to gauge the effect of (a) implicit analysis convergence criteria and (b) the presence of volume proportional damping (automated stabilization) in the model. Reducing the convergence criteria by a factor of 2 had no significant impact on model results (crimp strain, fatigue strains, test/in vivo strain amplitude ratio). Removal of the automatic stabilization algorithm resulted in a change in the predicted test/in vivo strain amplitude ratio of 1.8%. It is concluded that the automatic damping algorithm may be used, with default convergence settings, to overcome model convergence issues caused by local instabilities.

**Calculation verification, use error (ASME V&V 40 5.1.2.3)** Model inputs and outputs were verified by both the practitioner and an internal peer review. The peer review was documented and attached as a supportive document to the FEA engineering report.

**Computational model validation, model form (ASME V&V 40 5.2.1)** Key model form assumptions were identified, and their influence on model outputs was assessed. Assumptions that give rise to the model form were evaluated, and the important contributors to model form uncertainty were identified. The following model form assumptions were investigated: choice of solver, element type, Nitinol material model, frame geometry, square strut edges, model symmetry, valve loading and anatomic loading method.

Choice of solver: The FEA described here are non-linear static analyses, and all analyses are carried out using the Abaqus/standard implicit solver. The lowest structural eigenfrequency is significantly greater than five times the loading frequency. Thus, inertia forces can be assumed to be negligible, and in vivo simulations can be treated as static. It is concluded that the Abaqus/standard solver is suitable for use in this study.

Element type: Reduced integration, linear, hexahedral elements with enhanced hourglass control (Abaqus element type: C3D8R) are used to model the TAV frame in this example. 3D elements are chosen as the geometry of the TAV frame is complex. Hexahedral elements are used as they have a good convergence rate. Reduced integration elements reduce computational cost and do not suffer from shear or volumetric locking. Enhanced hourglass control provides increased resistance to hourglassing for non-linear materials.[1] C3D8R elements with enhanced hourglass control have been shown to produce accurate results for large-displacement geometrically non-linear analyses.[2]

[1] Dassault Systemes, 2019, 'Abaqus Elements Guide', Providence.

[2] Dassault Systemes, 2019, 'Abaqus Benchmarks Guide', Providence.

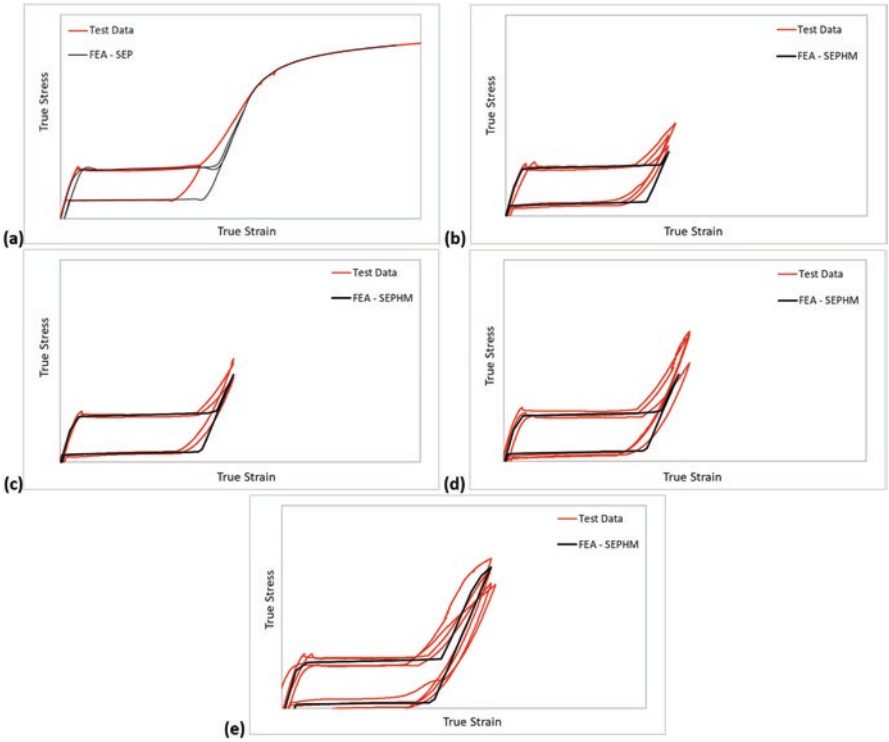


**Fig. 16.8** Verification of the SEPHM constitutive model. The stress-strain response from a single-element uniaxial analysis (black curve) is compared with experimental data (red curves) at different levels of uniaxial strain

Nitinol material model: Abaqus version 2019 offers constitutive models to simulate Nitinol as superelastic only (SE) and with plasticity and hardening modifications (SEPHM) included, allowing the upper and lower transformation stress plateaus to be a function of plastic strain. The constitutive models were calibrated based on tensile data from coupons heat treated equivalently to the TAV frame. Material verification was conducted using a single element uniaxial tension analysis. Incrementally increasing strains were applied to verify that transformation stress levels shifted as a function of plastic strain (Fig. 16.8).

The sensitivity of strain amplitude results to the SE and SEPHM constitutive models was analysed. The sensitivity of the test/in vivo strain amplitude ratio to the material model choice was quantified (Table 16.6). Results show that the SEPHM material model produces marginally more conservative results (lower ratio). Therefore, the SEPHM material model is used for the TAV frame FEA in this example.

**Table 16.6** Material model sensitivity – test/in vivo strain amplitude ratio results

| Metric | Superelastic (SE) | Superelastic-plastic with hardening modifications (SEPHM) |
|---|---|---|
| In vivo strain amplitude [%] | 0.12% | 0.14% |
| Test strain amplitude [%] | 0.13% | 0.14% |
| Test/in vivo ratio [−] | 1.07 | 1.01 |
| Difference [%] | 6% | |

The Nitinol material model used in this example does not account for cyclic stabilization but does account for the impact of pre-straining during crimping of the device [13].

Frame geometry: In this example, the final 3D model of the Nitinol frame was used as a starting point for simulations. In practice, antecedent FEA modelling is performed to generate the 3D FEA model. The manufacturing process of the frame is mimicked by simulating a multi-stage expansion process of a laser-cut stent structure. Stress removal is simulated subsequent to each expansion step, and the final structure is assumed to be stress-free. Modelling the expansion process ensures the final shape is accurately captured [11–14]. In this example, the model dimensions of the final 3D TAV frame were compared with those from component qualification inspection of actual parts. The strut width and thicknesses and the frame diameter measurement data from a number of manufacturing lots were found to be comparable to the nominal FEA model.

Square strut edges: In the FEA model, the TAV frame struts are idealized with square edges. In reality, the frames are electropolished during the manufacturing process, and the strut edges are rounded. The sensitivity of predicted crimp strain, strain amplitude, mean strain and test/in vivo strain amplitude ratio results to this assumption was assessed. The radius of the rounded edge, determined from cross-sections of the struts, was modelled using the submodelling technique. Due to the curvature of the strut edge, a refined mesh was required to capture the geometry. A square-edge model with equivalent mesh density was also simulated for comparison (Fig. 16.9).

The percentage difference between outputs from the square- and rounded-edge models was less than 2%. The contour plots show similar strain amplitude distributions for square-edge and rounded-edge models. Including rounded strut edges in the model has a negligible effect on fatigue results (Table 16.7 and Fig. 16.10).

Model symmetry: The anatomical loading applied to the TAV is generated based on analysis of multiphase CT of the device in vivo. The observed deformation at the inflow, waist and outflow supports the decision to simulate the frame using 180° symmetry.

Valve loading: During the cardiac cycle, the valve (consisting of leaflets and skirt) is subjected to a differential pressure load. These loads are transferred to the

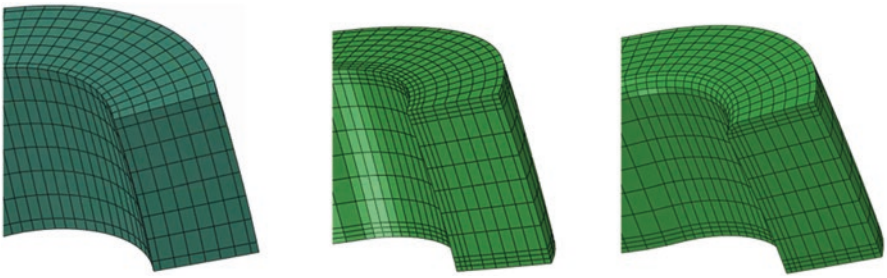

**Fig. 16.9** Global model mesh (left), square-edge submodel mesh (middle), rounded-edge submodel mesh (right)

**Table 16.7** Test/in vivo strain amplitude ratio for the rounded strut edge sensitivity study

| Metric | Square edge | Rounded edge |
|---|---|---|
| In vivo strain amplitude [%] | 0.141% | 0.141% |
| Test strain amplitude [%] | 0.140% | 0.142% |
| Test/in vivo ratio [−] | 1.00 | 1.01 |
| Difference [%] | 1.59% | |

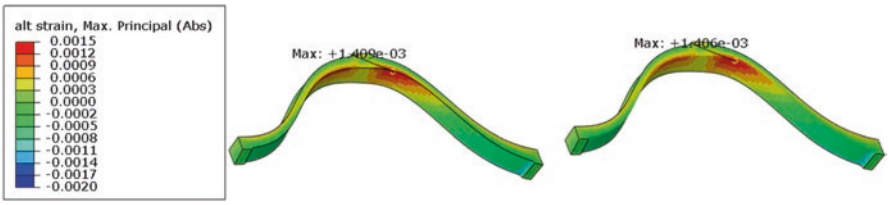


**Fig. 16.10** In vivo submodel: Strain amplitude contour plot, square edge (left), rounded edge (right)

TAV frame, resulting in frame deflections. Various methods of applying both skirt and leaflet loads have been investigated numerically. The final method results in pressure-driven frame deflections which are consistent with benchtop hydrodynamic and clinical observations (Fig. 16.11).

Anatomic loading method: The analysis loading method in this example makes use of constraining rings which contact the frame outer surface. The rings are morphed to drive local frame deformations, as observed clinically from post-implant CT scans, for nominal and extreme patients. The deformed device model was compared to detailed measurements of the device from clinical CT to verify that realistic deformations were achieved. The differences between the FEA model and the CT-derived measurements were typically within the CT inter-/intra-observer error. Additionally, FEA and CT device geometries were overlaid visually to allow for a

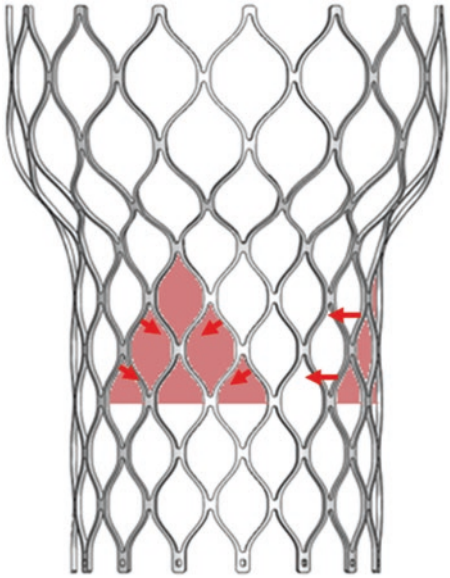

**Fig. 16.11** Example of applying valve and skirt loads in the frame-only model

qualitative assessment of the results. Good overall agreement was achieved between FEA and CT deformations.

**Computational model validation: Model input – quantification of sensitivities (ASME V&V 40 5.2.1.2.1)** Sensitivity analyses were performed to assess the degree to which the computational model outputs are sensitive to key model inputs. The results of these sensitivity analyses are presented in this section. The following model inputs were considered: leaflet loads, frame dimensions, Nitinol material properties and in vivo use conditions.

Leaflet loads: Hydrodynamic implant testing was performed to measure the frame deflections in the vicinity of the leaflet attachment points (to the frame) over a simulated cardiac cycle (for six devices). The frame deflections from each test were applied as boundary conditions in six separate FEA models of the device. The resulting strain amplitudes are plotted in Fig. 16.12, with an average of 0.15% (test deflections). The average test deflections were applied in a seventh simulation, resulting in a strain amplitude of 0.15% (mean deflections). Peak strain amplitude for the individual test simulations varies by up to 12% from the averaged simulation.

Frame dimensions: The TAV frame was modelled with the nominal specification dimensions. The dimensional variability from a number of manufacturing lots was quantified. Sensitivity analyses were performed to assess the sensitivity of model results to this variation (±1 standard deviations was simulated). For the variation of strut width and thickness, two models were created: one with upper strut dimensions and one with lower strut dimensions. The ratio of predicted test/in vivo strain amplitude was calculated. There is a 12% decrease in the ratio for a reduction of one

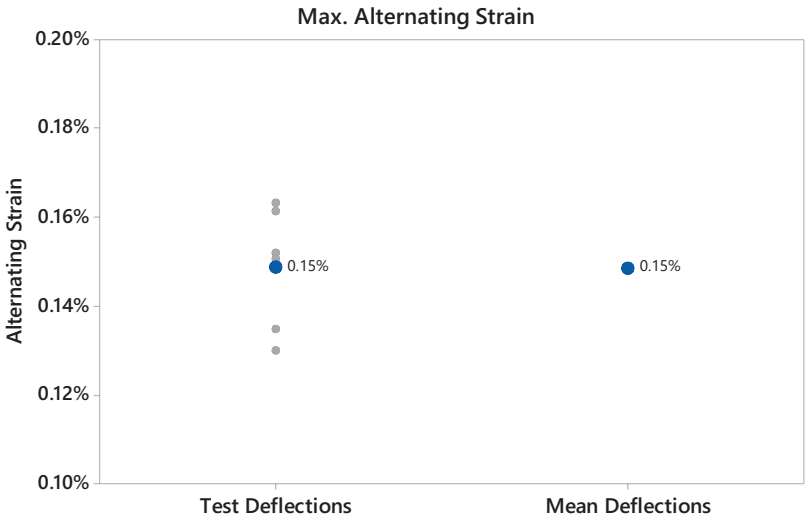


**Fig. 16.12** Strain amplitude results for 6 bench test simulations and mean deflection simulation

standard deviation in strut width and thickness. There is a 14% increase in the ratio for an increase of one standard deviation in strut width and thickness. The effect of overall frame diameter was also assessed (±1 standard deviation). The test/in vivo strain amplitude ratio is reduced by 6% when frame diameters are reduced by one standard deviation.

Nitinol material properties: The sensitivity of the model results to $A_f$ temperature was simulated. Manufacturing data from a number of frame lots showed a standard deviation of approximately 1 °C. To simulate a change in $A_f$ temperature of +1 °C, the loading and unloading plateau stresses of the baseline material model were reduced by 6.9 MPa and vice versa [15]. Analysis results indicate that a change of 1 °C in the $A_f$ temperature leads to a change in the test/in vivo alternating strain ratio of approximately 3%.

In vivo use conditions: A one-factor-at-a-time (OFAT) study was performed to assess the sensitivity of strain amplitude, mean strain and test/in vivo strain amplitude ratio to the variation in applied anatomical (in vivo) loading.

The 50th and 90th percentiles of 12 deformation modes (e.g. static and cyclic perimeter, ellipticity and offset at the device inflow and outflow) were identified based on regression modelling from a CT dataset of implanted devices. FEA simulations were performed to quantify the impact of loading variability. Mean deformation modes were imposed in the baseline model.

The sensitivity of strain amplitude to variability (from the 50th to 10th/90th %ile) in each deformation mode is illustrated in Fig. 16.13. The results of this sensitivity analysis may also be useful when defining appropriate in vivo loading conditions for the structural component stress/strain analyses.


**Fig. 16.13** Strain amplitude results from the in vivo loading sensitivity study

**Computational model validation: Model input – quantification of uncertainties (ASME V&V 40 5.2.1.2.2)** The uncertainty in model inputs was quantified by examining the gauge errors in the measurement systems from which the model inputs are obtained. This is quantified as part of test method validation that occurs prior to design verification testing. The gauge repeatability and reproducibility standard deviation quantifies the uncertainty in the measurement system. The measurement system uncertainty was quantified for the following model inputs: frame dimensions, frame deflection under valve loading, Nitinol tensile test data and inter-/intra-observer error from implanted device CTs.

**Comparator (ASME V&V 40 5.2.2)** Simulation results were evaluated against TAV frame radial compression bench test data and test fatigue data. Details of the frame radial compression data comparison are presented; quantity, range, measurement and measurement uncertainty are discussed.

Radial compression comparator, test samples: Radial compression (force) data from design verification testing of three frame sizes were used as the comparator. For each frame size, data for 12 samples drawn from two lots were used. The validation goal is for the prediction to be within three standard deviations of the mean test value. For a one sample t-test, with a power of 90%, a minimum sample size of four is required to detect a difference of three standard deviations, at a significance level of 0.05, as shown in Fig. 16.14. Therefore, the sample size of 12 is assumed to be statistically relevant.

The samples used in radial compression testing were processed identically to commercial frames. Random frames were selected to obtain a spread of characteristics representative of the commercial product. All key characteristics of the test samples were measured and were within the specifications. Validation of the

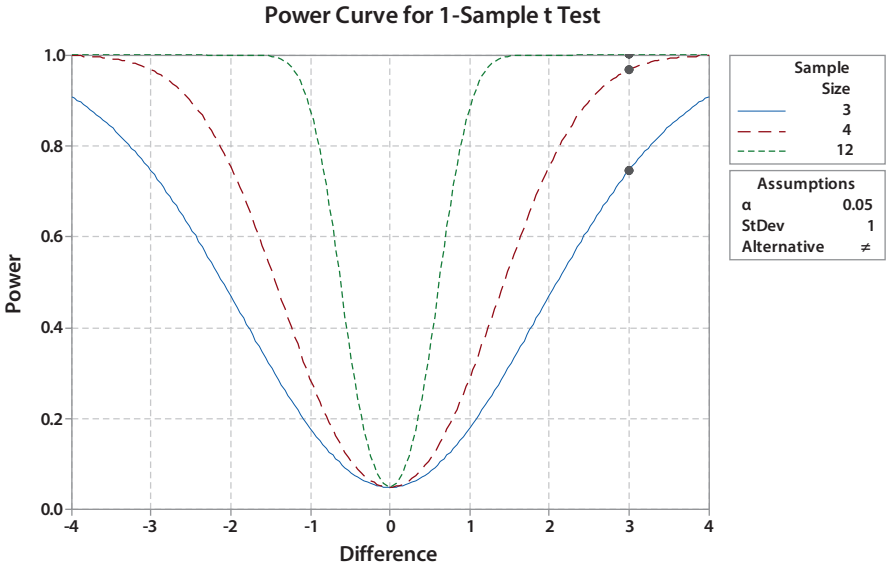


**Fig. 16.14** Power curves for one-sample T-test, produced using Minitab

frame dimensional measurement system was completed during component qualification. Measurement system repeatability and reproducibility was successfully demonstrated.

Radial compression comparator, test conditions: Radial compression of the full frame and the inflow section of the frame was performed at 37 °C using a validated radial compression test method. The results were compared with FEA simulation of the same conditions. Test conditions representing the expected extreme conditions were examined. Frames were radially compressed to the delivery system ID, and radial force measurements spanning the entire aortic valve annulus diameter range were obtained.

## *Assessment (ASME V&V 40 5.2.3)*

Equivalency of input parameters: Diameters applied in the FEA model (of the radial compression test) are equivalent to those applied during testing. Simulations assumed a temperature of 37 °C – the applied test temperature is 37 ± 2 °C. The loading rate is low and can be considered to be static; therefore, static analyses were used to simulate the test.

Output comparison: Chronic outward forces (COF) at multiple diameters and for multiple frame sizes were used to evaluate the model. The output parameter from test and FEA models was identical (applied radial force versus applied diameter in both). Comparison was performed by determining the arithmetic difference between

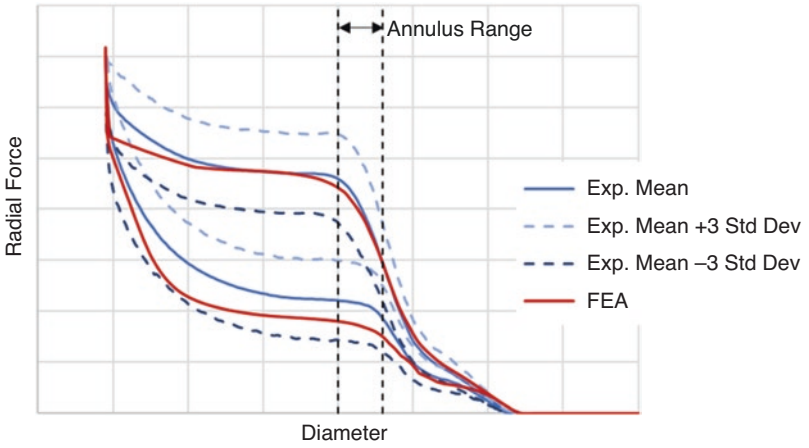


**Fig. 16.15** Full-frame radial force validation results

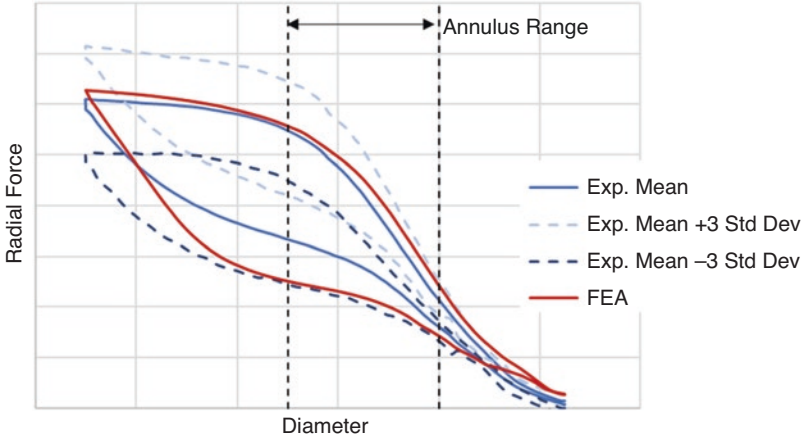


**Fig. 16.16** Frame inflow radial force validation results

computational results and experimental results. COF, within the treatable annulus range for each TAV size, were compared to test data.

An example of the output results from radial force testing and FEA is presented in Fig. 16.15 for the full frame, and in Fig. 16.16, for the inflow only test. The predicted COF is within three standard deviations of the mean experimental value, within the treatable annulus range.

Test fatigue comparator: Fatigue testing was performed at highly elevated test levels, resulting in consistent fracture observations. Fracture locations from the bench test data were compared to predicted hotspot locations in the FEA simulations,

under the same simulated conditions. Locations of high strain amplitude and mean strains corresponded closely to fracture locations observed in fatigue tests.

### *Applicability (ASME V&V 40 5.2.3)*

Relevance of the quantities of interest (QOI): The quantities of interest (QOI) for the context of use are strain amplitude, location of peak strain amplitude (potential fracture) and, more broadly, the ratio of strain amplitude in the bench test versus the in vivo model (the apparent fatigue factor of safety). The quantities of interest for the validation models (radial compression and fatigue test models) are force and locations of fracture. Therefore, in this example, only a subset of the QOIs from the validation activities were identical to those for the COU.

Relevance of the validation activities to the COU domain: The range and type of loading applied during the validation activities (compression to clinically relevant diameters in the radial force test and cyclic loading in the fatigue test) are highly relevant to the quantities of interest for the context of use.

Credibility assessment: In accordance with the model classification and risk identified for this example study, credibility requirements have been established (Table 16.4), and verification and validation activities have been conducted and reported. The model risk rating is medium. The credibility level of all credibility goals is medium or high, with two exceptions. The credibility level for the factor 'test samples – range of characteristics of test samples' is low. The test samples used were all processed identically to commercial frames, and random frames were selected to obtain a spread of characteristics representative of the commercial product. The credibility level of the factor 'numerical code verification' is low. Abaqus is a commercially available software which has been verified using a large number of benchmark problems. Overall, the credibility levels associated with the verification and validation goals are commensurate with the model risk rating.

Based on the results of the verification and validation studies described in this example, the in vivo and fatigue test FEA models are determined to be acceptable for use in this context, i.e. structural component stress/strain analyses.

## References

1. Assessing credibility of computational modeling through verification and validation: applications to medical devices (2018) ASME. ISBN: 9780791872048
2. Standard for verification and validation in computational solid mechanics V V 10 (2019) ASME. ISBN: 9780791873168
3. ASME V and V 20-2009 Standard for verification and validation in computational fluid dynamics and heat transfer. ASME. ISBN: 9780791832097
4. International Standards: ISO 5840-1:2021 cardiovascular implants – cardiac valve prostheses – Part 1: general requirements

5. Morrison TM, Hariharan P, Funkhouser CM, Afshari P, Goodin M, Horner M (2019) Assessing computational model credibility using a risk-based framework: application to hemolysis in centrifugal blood pumps. ASAIO J 65(4):349–360. https://doi.org/10.1097/MAT.0000000000000996. Erratum in: ASAIO J. 2019;65(8):e100. PMID: 30973403; PMCID: PMC6493688
6. Bateman MG, Durfee WK, Iles TL, Martin CM, Liao K, Erdman AG, Iaizzo PA (2020) Cardiac patient-specific three-dimensional models as surgical planning tools. Surgery 167(2):259–263. https://doi.org/10.1016/j.surg.2018.11.022. Epub 2019 Feb 18. PMID: 30792012
7. Prisco AR, Aguado-Sierra J, Butakoff C, Vazquez M, Houzeaux G, Eguzkitza B, Bartos JA, Yannopoulos D, Raveendran G, Holm M, Iles T, Mahr C, Iaizzo PA (2021) Concomitant respiratory failure can impair myocardial oxygenation in patients with acute cardiogenic shock supported by VA-ECMO. J Cardiovasc Transl Res:1–10. https://doi.org/10.1007/s12265-021-10110-2. Epub ahead of print. PMID: 33624260; PMCID: PMC7901681
8. Mineroff J, McCulloch AD, Krummen D, Ganapathysubramanian B, Krishnamurthy A (2019) Optimization framework for patient-specific cardiac modeling. Cardiovasc Eng Technol 10(4):553–567. https://doi.org/10.1007/s13239-019-00428-z. Epub 2019 Sep 17. PMID: 31531820; PMCID: PMC6868335
9. Luraghi G, Rodriguez Matas JF, Migliavacca F (2021) In silico approaches for transcatheter aortic valve replacement inspection. Expert Rev Cardiovasc Ther 19(1):61–70. https://doi.org/10.1080/14779072.2021.1850265. Epub 2020 Dec 31. PMID: 33201738
10. Viceconti M, Pappalardo F, Rodriguez B, Horner M, Bischoff J, Tshinanu FM (2021) In silico trials: verification, validation and uncertainty quantification of predictive models used in the regulatory evaluation of biomedical products. Methods 185:120–127. https://doi.org/10.1016/j.ymeth.2020.01.011. Epub 2020 Jan 25. PMID: 31991193; PMCID: PMC7883933
11. Soffel F, Lin Y, Keller D, Egorov S, Wegener K (2021) Laser remelting process simulation and optimization for additive manufacturing of nickel-based super alloys. Materials (Basel) 15(1):177. https://doi.org/10.3390/ma15010177. PMID: 35009327; PMCID: PMC8746250
12. Del Rosso S, Iannucci L, Curtis PT (2019) Finite element simulation of the braiding process. Mech Adv Mater Mod Process 5(1):1. https://doi.org/10.1186/s40759-019-0041-4. Epub 2019 Jan 23. PMID: 30873338; PMCID: PMC6383729
13. Marrey R, Baillargeon B, Dreher ML, Weaver JD, Nagaraja S, Rebelo N, Gong XY (2018) Validating fatigue safety factor calculation methods for cardiovascular stents. J Biomech Eng. 140(6). https://doi.org/10.1115/1.4039173. PMID: 29392299; PMCID: PMC6352986
14. Asri RIM, Harun WSW, Samykano M, Lah NAC, Ghani SAC, Tarlochan F, Raza MR (2017) Corrosion and surface modification on biocompatible metals: a review. Mater Sci Eng C Mater Biol Appl 77:1261–1274. https://doi.org/10.1016/j.msec.2017.04.102. Epub 2017 Apr 20. PMID: 28532004
15. Pelton AR et al (2009) Optimisation of processing and properties of medical grade Nitinol wire. Minim Invasive Ther Allied Technol 9(2):107–118

# Chapter 17
# Numerical Methods for Design and Evaluation of Prosthetic Heart Valves


**Michael J. Schendel, Carl F. Popelar, and David Martin**

## Abbreviations

| | |
|---|---|
| CT | Computed tomography |
| FEA | Finite element analysis |
| FSI | Fluid–structure interaction |
| MRI | Magnetic resonance imaging |
| V&V | Verification and validation |

## 17.1 Brief History of Analyses of Prosthetic Heart Valves

The need for mechanical analyses in heart valve prosthesis development was recognized in the mid-1900s as Dr. Hufnagel began the development and introduction of prosthetic heart valves [1]. It was recognized that the "ball valve" designs diverted the blood flow from a central flow to a flow around the ball occluder. This can cause damage to the blood cells and elevated pressure gradients across the heart valve, causing the heart to work harder. Tilting disc prosthetic heart valves helped restore the desirable central flow, reducing the damage to blood cells. However, one design (the Bjork–Shiley valve) developed a reliability issue which resulted in multiple

M. J. Schendel
Medtronic Cardiovascular, Medtronic, Inc., Mounds View, MN, USA
e-mail: michael.james.schendel@medtronic.com

C. F. Popelar
Southwest Research Institute, San Antonio, TX, USA

D. Martin (✉)
Medtronic Cardiovascular, Medtronic Inc., Parkmore West Business Park, Galway, Ireland
e-mail: David.m.martin@medtronic.com

© The Author(s), under exclusive license to Springer Nature Switzerland AG 2023

P. A. Iaizzo et al. (eds.), *Heart Valves*, https://doi.org/10.1007/978-3-031-25541-0_17

fatal events; this reliability issue was related to the weld used for the struts, and the valve was removed from the market by 1986. Later structural finite element analyses (FEA) were completed to quantify the stresses related to the failures and to develop differing methods of failure detection [2, 3]. The methods for failure detection involved acoustic and harmonic analyses. Experimentally, the resonant frequencies for intact and fractured struts were measured and were found to be significantly different. A modal analysis of the Bjork–Shiley valve was completed, and the responses compared favorably to the experimental studies [4–6]. Chondros (2010) improved on these acoustic methods and suggested a method of monitoring fatigue crack propagation in the valve strut [6]. Well-validated methods like this would be useful in identification of broken valve struts prior to any clinical symptoms.

The mechanical bi-leaflet valve was introduced in 1979. As a mechanical valve, this valve prevails today and reproduces the central flow quite well. These mechanical heart valves require an anticoagulation therapy for the life of the patient because of the potential for thrombus formation. Due to this propensity for thrombus formation, the hemodynamics of these mechanical bi-leaflet heart valves have been studied extensively [7]. A sparse number of reports in the public domain have focused on the structural integrity of these valves or the leaflets under the repeated impact loads endured during valve closure. Yuan et al. simulated the loading on valve leaflets during closure using an FEA model [7]. This study focused on a design optimization and stresses in the acetal homopolymer leaflets. A fatigue analysis method for mechanical heart valves was developed using FEA to investigate the impact stress and loading from cavitation in heart valve prostheses with pyrolytic carbon as the material for the leaflet construction. The finite element method for this fatigue assessment was programmed into a scripting language for ease of use [8]. In 2009, Hong et al. examined the effects of valve rotation within the vessel using fluid–structure interaction (FSI) simulations [9].

Simultaneously with the development of the mechanical heart valves, bioprosthetic valves were developed. Some of the earliest structural FEA of heart valve prostheses were with the simulation of the stresses and deformation in the valve leaflets under the pressures on a closed valve [10, 11]. These valves are constructed from porcine aortic valves or preserved bovine pericardial tissue and do not require an anticoagulation regimen. However, these valves may suffer a mechanical degradation and typically need to be replaced in about 12 years on average. Numerical analysis has been used to monitor the degradation of the leaflets by measuring the frequency of heart sounds in patients [12]. Leaflet failure in bioprosthetic heart valves has been related to the regions of high stress concentration during function [13–15]. FSI methods are designed to capture all events affecting the bioprosthetic heart valve and have been employed by some researchers. Makhijani et al. simulated a bioprosthetic heart valve in 3D using symmetry assumptions [16]. The leaflets were modelled as an isotropic hyperelastic material and the coaptation occurred on the symmetry plane.

Over the past two decades, transcatheter heart valve (THV) replacement has emerged as a minimally invasive alternative to surgical heart valve replacement. Transcatheter valves generally consist of a bioprosthetic valve assembly that is

attached to a metallic frame. These devices are reduced in diameter to a low profile and introduced to the vasculature via a delivery catheter. They are introduced percutaneously through a peripheral blood vessel and tracked to the target anatomy in the heart. The THV is then deployed in vivo and replaces the function of the diseased native heart valve. These valves are manufactured in multiple sizes to accommodate a broad range of patient anatomies and are classified according to their deployment mechanism. "Balloon-expandable" valves are manufactured from conventional alloys and are deployed in situ through the dilatation of a balloon-tipped catheter. "Self-expandable" valves are manufactured from shape memory alloys (e.g., Nitinol) and are deployed in situ by retracting a sheath on the delivery catheter and allowing the frame to expand to its intended shape. One of the earliest numerical studies of a transcatheter heart valve was performed by Schievano et al. who used fluoroscopy images and structural FEA to simulate the in vivo deformations of a novel balloon-expandable pulmonary valve [17, 18]. This work provided a more realistic assessment of the stresses in the device under in vivo loading conditions and identified deficiencies with benchtop fatigue tests. The learnings from this work would later inform an FEA-driven optimization study for a next-generation pulmonary valve [19] (Fig. 17.1).

During the past decade, transcatheter aortic valve replacement (TAVR) has been established as a noninferior alternative to surgery in the treatment of severe symptomatic aortic stenosis in patients of all-risk categories [20–24]. Paravalvular leakage (PVL) was identified as a major complication of first-generation TAVR devices; this refers to regurgitant flow around the implanted valve and is associated with increased mortality. Bosi et al. used structural FEA to simulate the deployment of commercial TAVs in a range of patient-specific aortic anatomies and successfully predicted PVL by identifying regions of poor apposition between the TAV and the anatomy [25, 26]. De Jaegere et al. took the deformed domain from similar patient-specific FEA models and performed computational fluid dynamics (CFD) analyses to predict both the occurrence and severity of PVL for a large sample of patients [27]. Conduction disturbances are another potential complication of TAVR procedures that can result in pacemaker implantation. Rocatello et al. used patient-specific

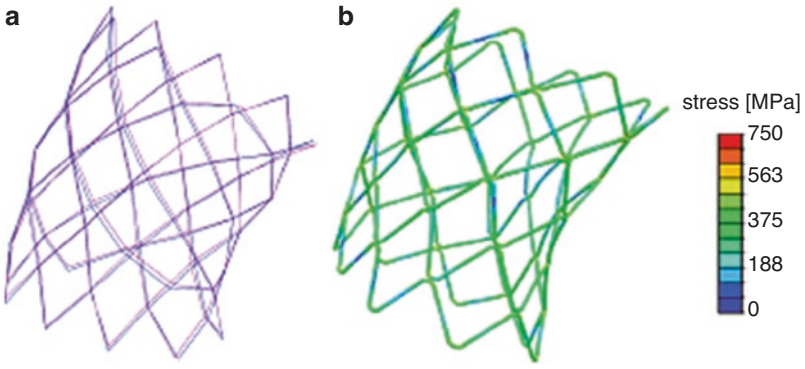


**Fig. 17.1** 3D stent reconstructions from fluoroscopy images in diastole (**a**) and stress distribution predicted in a pulmonary valve frame when deployed in a patient's RVOT/pulmonary trunk (**b**)

structural FEA models to show that interactions between TAVR devices and the membranous septum may be linked to conduction abnormalities after TAVR implantation [28]. A small number of studies have considered both the structural and fluid mechanics analyses simultaneously in complex FSI models. Luraghi et al. proposed a Lagrangian–Eulerian method to simulate pulsatile blood flow through a TAVR device after a simulated deployment in a patient-specific anatomy [29]. Pasta et al. completed a similar study in which structural FEA and smooth particle hydrodynamic (SPH) methods were coupled to evaluate the severity of PVL following TAVR implantation in bicuspid aortic anatomies [30]. With the continuing advancement in computing power, finite element methods are being used to combine patient-specific modelling and design optimization techniques. Rocatello et al. proposed a framework to optimize the design of a transcatheter aortic valve through patient-specific finite element and fluid dynamics simulation [31] (Fig. 17.2).

The previous paragraphs illustrate some of the numerical modeling completed in the public realm. There also exists a large volume of modeling work completed in the private sector, typically by the manufacturer or in collaboration with consultants. These analyses are designed to increase the confidence in a particular design and to aid in addressing reliability questions posed by regulatory agencies.

ISO5840-1:2021 provides guidance on structural analyses for heart valve prostheses [32]. It requires that a validated stress/strain analysis be performed for all structural components under in vivo loading conditions. The critical inputs to this process are the component geometry, the mechanical properties, and the boundary conditions to which the device is subjected. All device sizes and configurations (e.g., deployment diameters) should be considered unless a worst-case size and configuration can be identified. For transcatheter valves, the entire stress/strain history of the device should be considered and residual stresses/strains resulting from manufacturing, loading, and deployment should be included. Validation of the analyses should be performed to demonstrate confidence in the predicted results and should provide comparison to experimentally measured quantities. ASME V&V40:2018 proposes a risk-based credibility assessment framework for identifying the verification and validation activities required when numerical simulation is applied to

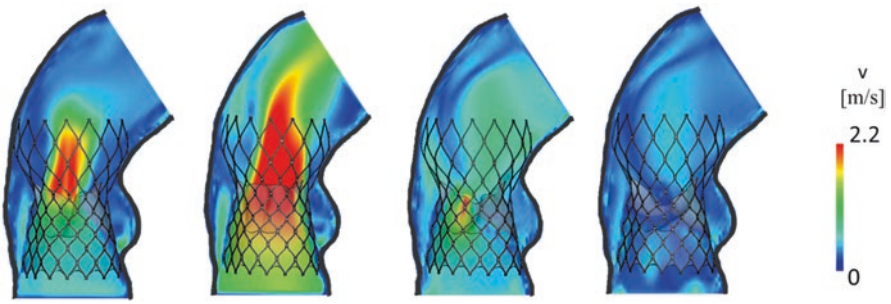


**Fig. 17.2** Contour plots of the velocity magnitude predicted in a patient-specific FSI model of a self-expanding valve at four time points during a simulated cardiac cycle [29]

medical devices [33]. This standard (VV40) builds on the validation frameworks outlined in ASME VVUQ10 (V&V in Computational Solid Mechanics) and VVUQ20 (V&V in Computational Fluid Dynamics and Heat Transfer) [34, 35].

## 17.2 Best Practices in Modeling Valve Prostheses

One of the first documented suggestions that "...nonlinear finite element analysis can significantly accelerate product development cycles while helping manufacturers... avoid costly mistakes" was made by Haridas and Haynes [36]. FEA has proven to be an invaluable tool in predicting device performance and is used widely in the industry to generate design verification evidence to regulatory agencies. However, the credibility of any computational model relies on quantifying the sources of uncertainty. One major source of uncertainty is the device loading conditions. Babuska et al. pointed out the importance of quantification of the uncertainty around all input data to models [37].

The following "mantra" for robust design and evaluation of medical implants has been developed. When contemplating a design, developers should consider three questions:

- What is the device intended to do?
- Where must the device perform its function?
- How long must the device perform its function?

The first question centers on the therapy to be provided, while the second question addresses the use environment including the thermal and mechanical loading conditions. The third question addresses the longevity (expected lifetime) that the device must survive when exposed to the loading conditions. Addressing these three questions in the design phase should lead to robust designs. Unfortunately, sometimes these questions cannot be completely answered. Numerical analyses can be used to help address all three questions; however, analysis alone cannot provide complete answers. It is important to identify how numerical models can aid in addressing these questions and more importantly what is missing in the use of the current models.

There are nine important aspects which need to be addressed by any numerical analysis; each will be discussed in more detail in this chapter:

- Problem definition
- Material and constitutive models
- Geometry/mesh/element type
- Loading conditions (constraints and loads)
- Physics/solution method
- Model verification and validation
- Interpretation
- Documentation
- Peer review

### 17.2.1 Problem Definition

One of the most important tasks for the analyst is to clearly define the problem to be solved. At this point the analyst should meet with stakeholders to clearly define (a) the purpose and scope of the analyses, (b) the key questions of interest, (c) key inputs and outputs and (d) validation and verification requirements. By doing this properly, the purpose of the work is clear to all, and it is easier to determine the steps required to validate the model. Too often it is natural to believe that a model will directly address project goals when the reality is that oftentimes it will not. Modeling is often a necessary, but incomplete, part of the solution to addressing the project goals. For example, when considering the structural integrity of a heart valve prosthesis, the "project goal" may be to evaluate whether the valve design subjected to certain loading conditions will fail due to a specific failure mode (e.g., fracture due to crack growth). By itself, a structural FEA cannot directly address this project goal. Rather, a priori knowledge of the failure mode, the governing parameter or metric, and the failure criterion is also required.

FEA is typically used to quantify the driving force, or propensity for failure, while testing or other physics are needed to establish the resistance to failure (i.e., the failure criterion) (see Chap. 16 for more information). Thus, the model goal, or objective of the model, is distinct from the project goal. For example, the model goal for a pyrolytic carbon leaflet would be to accurately quantify the stress intensity factor, K, while the project goal remains unchanged: will the valve fail due to crack growth (i.e., is $K > K_{IC}$?)?

As stated by Box [38], "all models are wrong, but some are useful." By their very definition, all models are approximations. Further, the solutions to many models often require additional simplification, which imposes certain limitations on their applicability. These approximations and simplifications result in model error. It is important to understand these sources of error and to establish acceptable bounds on the accuracy of the model, as these errors affect the confidence in the model solution and the validation strategy.

### 17.2.2 Materials and Constitutive Models

Understanding the material properties and their variability are critical inputs to any analysis of heart valve prostheses. In particular, the tissue leaflets cannot be modelled accurately without a clear understanding of their material behavior. This is also true when modeling the large deformations of the metallic frames used for transcatheter valves. There has been much research in identifying constitutive models and mechanical properties for these materials, and the following paragraphs will summarize some of this work.

#### 17.2.2.1 Balloon-Expandable Transcatheter Frames

Balloon-expandable frames for transcatheter valves are typically manufactured from stainless steel, cobalt-chromium, or platinum-iridium alloys and are designed to yield and deform plastically to maintain their shape following crimp and expansion. The mechanical behavior of balloon-expandable frames is typically described using elastic–plastic constitutive models and an idealized uniaxial stress–strain curve is shown in Fig. 17.3. Initially, the response is elastic, but once the yield stress is exceeded, the material deforms plastically to a maximum stress state. If the applied load is removed and the stress is reduced to zero, the material recovers the initial elastic deformation but retains the permanent plastic deformation. If the load is then reapplied, the material deforms elastically, with the same elastic modulus as in the initial loading. This elastic response continues until the prior maximum stress is exceeded. At this point, the material yields and plastic deformation occurs. This increase in yield stress between the initial and subsequent loading step is referred to as strain (or work) hardening and is a result of dislocations in the material during the initial plastic deformation.

Care is required when defining the yield criterion and hardening law for elastic–plastic materials. In particular, the hardening law defines how the yield surface changes with plastic deformation. With isotropic hardening, the yield surface is fixed in stress space and increases in size as plastic strain is accumulated [39]. This

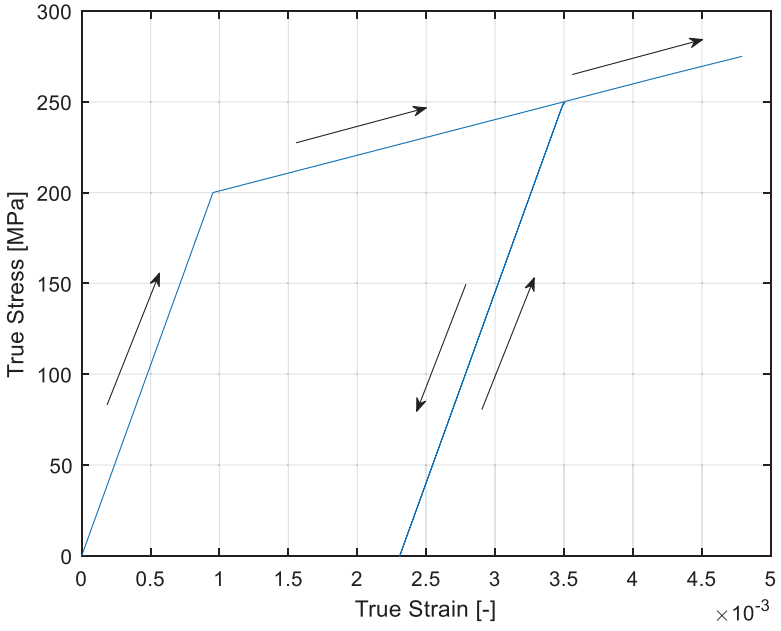


**Fig. 17.3** Schematic of uniaxial stress–strain response for an elastic–plastic constitutive material model

is intended for problems in which the applied load is monotonic. In problems where the applied loading is reversed, the yield stress in the reverse direction is typically reduced, known as the Bauschinger effect. This can be captured with kinematic hardening, where the size of the yield surface is fixed, but it can move in stress space as plastic strain is accumulated [39]. The difference between isotropic and kinematic hardening is demonstrated in Fig. 17.4. Here, the material is loaded beyond yield (200 MPa) in tension to a maximum stress (250 MPa). The material is then released and loaded to the same target stress in compression. For isotropic hardening, the yield stress in compression is equal to the hardened yield stress in tension (250 MPa). However, for kinematic hardening, the yield stress in compression is reduced (−150 MPa) by the difference between the initial (200 MPa) and hardened (250 MPa) yield stress in tension. In many cases, the observed hardening behavior will be neither isotropic or kinematic, and a combined (or mixed) hardening law may be required.

Balloon-expandable frames undergo several hardening steps and load reversals in manufacturing, assembly, crimping, and deployment and are subject to long-term cyclic in vivo loading. To accurately predict the plastic deformation and subsequent residual stresses in these devices, it is critical that constitutive models are well calibrated to appropriate test data and all relevant conditioning steps are accounted for.

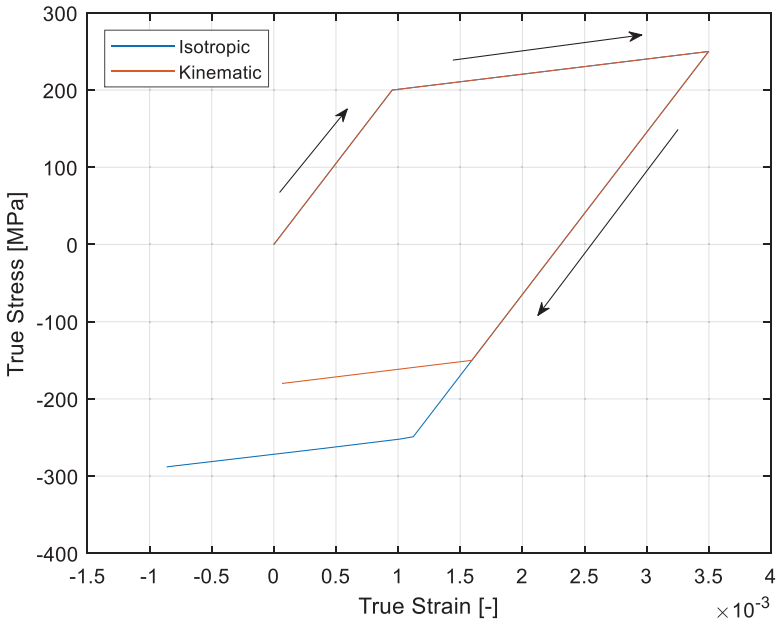


**Fig. 17.4** Schematic of uniaxial stress–strain response for an elastic–plastic constitutive material model under reversed loading comparing isotropic (blue) and kinematic (orange) hardening laws

#### 17.2.2.2 Self-Expandable Transcatheter Frames

Self-expandable frames for transcatheter valves have traditionally been manufactured from nickel-titanium alloys (i.e., Nitinol) which exhibit shape memory and superelastic properties. These unique material properties occur due to reversible transformations between austenite and martensite phases which can be driven by an applied load or a change in temperature. The martensite finish-phase transformation temperature and austenite finish-phase transformation temperature are material properties inherent to the superelastic material and are controlled through the material processing and heat treatment recipe [40, 41]. The shape memory effect is observed when Nitinol is cooled below the martensite finish temperature. In this state, large deformations are easily imposed, and the material will hold its deformed shape on load removal. When heated above the austenite finish temperature, the Nitinol then transforms back to austenite and recovers its original shape. Self-expandable frames may be designed to be loaded onto the delivery catheter system at lower temperatures to exploit the shape memory properties of Nitinol and to facilitate ease of use. When deployed in vivo, the frames are then raised above the austenite finish temperature and so regain their original "trained" shape and stiffness.

The superelastic effect is observed when Nitinol is exposed to high strains at temperatures above the austenite finish temperature [40]. In this state, the application of a load results in a local stress-induced phase transformation from austenite to martensite. Upon load removal, the material transforms back to austenite, regaining its original "trained" shape. Self-expandable frames are designed to operate above the austenite finish temperature when deployed in vivo and can exhibit superelastic behavior up to 6–8% strain. This behavior is modeled in FEA using superelastic constitutive material models and an idealized uniaxial stress–strain curve is shown in Fig. 17.5. Here, the initial response is elastic and is defined by an austenite elastic modulus. As the transformation stress is exceeded, austenite-to-martensite phase transformation begins, and large reversible strains occur with minimal changes in stress. This transformation continues until the material is fully martensite. At this point, the response is elastic as defined by the martensite elastic modulus up to the point of yield and plastic deformation. On unloading, transformation occurs in reverse in a similar manner, though the transformation stresses are lower, defining a lower plateau. Most superelastic constitutive models present in the commercial FEA codes are based on the work of Auricchio and Taylor [42, 43]. When calibrating the constitutive material model to test data, it is important that the test conditions and test specimens mimic those of the device operating conditions (e.g., testing at 37 °C of coupons that have been processed in an identical manner to the implant).

When modeling self-expanding valves, it is important to be aware that the material is path dependent. To provide accurate results, structural FEA models should account for the full loading history of the device (e.g., crimping, implantation, and in vivo loading). For example, it is possible to achieve different stresses at certain strains due to the hysteresis in the material response. It is also important to accurately simulate conditioning steps for self-expanding valves as they can have a

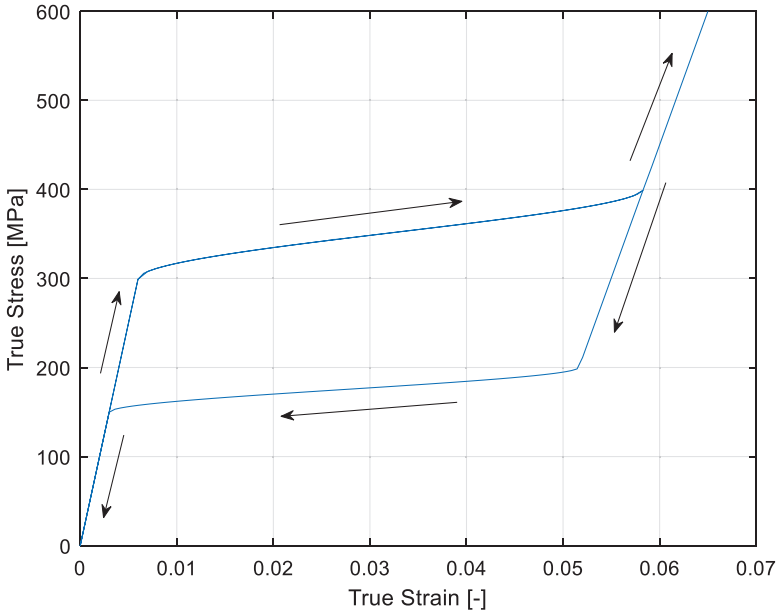


**Fig. 17.5** Schematic of uniaxial stress–strain response for a superelastic constitutive material model

notable effect on fatigue. Senthilnathan et al. demonstrated that plastic deformation during conditioning causes residual stresses that can influence fatigue performance [44]. It is also important to consider all potential deployment diameters for self-expanding prostheses, giving particular attention to high interference configurations. Cao et al. suggested that increased mean strain may result in reduced fatigue performance for Nitinol components [45]. These last two points demonstrate why caution is advised when trying to apply fatigue data (e.g., constant life diagrams) from the literature that may not properly reflect the strain history of the device being analyzed. This is reinforced in ISO 5840-1:2021 where "the use of material fatigue characterization data from the literature without sufficient justification is not acceptable" when assessing fatigue performance of the device.

#### 17.2.2.3 Tissue Leaflets

Some of the earliest analysis of leaflets in heart valve prostheses involved numerical methods with assumptions of purely linear elastic materials [46, 47]. These methods used linear expressions for the calculation of membrane stresses; however, the native aortic valve leaflet is a tri-layered structure [48]. This leaflet tissue has a noted anisotropic mechanical behavior due to the circumferential orientation of the collagen fibers and the radial orientation of the elastin fibers [13]. To begin to account for this nonlinear material behavior, there have been many advances in

material testing and modeling of heart valve tissue. Biaxial testing has become widely accepted for tissue material property assessment. These data provide input for constitutive models of the leaflet material. More recently, heart valve researchers have developed more customized constitutive models for valve leaflet mechanics. A good overview of leaflet constitutive models is given by Weinberg and Kaazempur–Mofrad [49], and new element formulation is also progressing. These formulations attempt to capture all aspects of the tissue in a heart valve. Weinberg and Kaazempur–Mofrad introduced a specialized shell element formulation for heart valve leaflets [50] designed to be compatible with commercial FEA codes. Sun et al. also described the necessity for accurate constitutive models when attempting to simulate the leaflets of a bioprosthetic valve [51]. This is echoed in the ISO 5840 guidance document which calls for an "...appropriate constitutive model for each material..." and that the parameters be established experimentally from material processed in the same manner as used for manufacture [32].

### *17.2.3 Geometry/Mesh/Element Type*

Properly capturing the correct geometry is as important as the proper material definition. If one is simulating a manufactured prosthetic valve, this "geometry" may seem easy to attain, but there are several features that make it more difficult. The biggest feature is variability; this becomes most important when the design is developed using automated manufacturing processes, which often include some surface finishing that is not included on the CAD drawings. For a more accurate geometric representation of a prosthetic valve, direct measurements from samples can be useful. This is true when the implant design has small features that may not be specified on the device drawing. If prototypes are available, a microcomputed tomography (μCT) scan may be used to aid in the quantification of the actual macro-dimensions of a design.

Occasionally, the analyst would like to simulate the actual geometry of the annular region or the vessel walls. These boundaries are then used in finite element models to simulate loading stress and strain developed from the actual implanted environment. These data are typically obtained using magnetic resonance imaging (MRI), CT, 3D ultrasound, or other imaging methods. Typically, these data are collected from healthy subjects; the datasets are then converted to surfaces or element representation using various commercial software packages. These image-to-mesh methods are also touted for "patient-specific" modeling [52]. Determining geometries from data collected with these imaging methods is not without error. Uncertainties arising from imaging errors have been quantified and should be included when simulating the boundaries for heart valve prostheses.

Another consideration when representing the valve prosthesis and/or associated anatomy is symmetry. Models often rely on symmetry to reduce the number of elements in the model. Complex three-dimensional geometries will require many elements to gain reasonable accuracy. Considering the materials are typically nonlinear

and sometimes the analysis is dynamic, the assembly and solution time for these simulations can quickly become enormous. To make solution times reasonable, analysts often will rely on model symmetry. This is a powerful feature in finite element modeling, but the analyst must use caution and heed guidelines for the use of symmetry when creating a model. One requirement is that the geometry of the device (heart valve prosthesis) is symmetric; this is coupled with another requirement which demands that the loading conditions also are symmetric. The ISO 5840 guidance document notes that valve motion and closure is not always symmetric and recommends that analyses be performed on full valve geometries [32]. Analysts should also consider any nonuniformities that can arise in the diseased state of the anatomy. Disease can create asymmetric boundaries that invalidate the use of symmetry in a model. The FDA guidance document for Reporting of Computational Modeling Studies in Medical Device Submissions also requires a rationale of the appropriateness of any model simplifications (e.g., the use of symmetry) in the computational model [53]. These documents also suggest examining different size implants and investigating the sensitivity of the frame to the manufacturing tolerances allowed for the device.

The type of element should be considered carefully when creating the finite element model. It is obvious to choose elements capable of using the appropriate constitutive model as described above (Sect. 17.2.2). Some elements will perform better than others under specific loading or contact conditions. The choice and rationale for the element type should be documented in the final report.

### *17.2.4 Loading Conditions (Constraints and Loads)*

Properly defining the loading conditions on the prosthetic heart valve may arguably be the most difficult task facing the analyst. It is desirable for a prosthetic heart valve to perform for the lifetime of the recipient. Minimum recommended targets for device performance have been established by the regulatory bodies. ISO suggests that the heart valve prosthesis be designed to withstand loads from the human body for a minimum of 10 years, while the US regulatory body, the FDA, requires 15 years, which translates into 400 and 600 million cycles, respectively. This high cycle fatigue performance can be affected by all initial manufacturing, handling, and surgical processes; knowledge of these steps is imperative for a thorough analysis. This is specifically true if any initial procedure has the propensity to change the starting stress state in the device. For example, this can occur if a device is loaded past the material yield point during processing or handling, resulting in the development of a residual stress in the device. Therefore, before simulation of the physiologic loading on a prosthetic heart valve, one must consider the entire load history that the device will encounter prior to implant. Some of these loads may need to be included in the physiologic loading simulation because they influence the stress state. This is the case with some stented heart valves, and the FDA guidance highlights the consideration of all loading steps [53, 54]. The FDA specifically

recommends consideration of the crimping, expansion/deployment, and any stent recoil as these steps could result in the development of a residual stress state in the stented heart valve prosthesis.

This is a good time to reflect on the Problem Definition section (Sect. 17.2.1) to reinforce the distinction between the project goal and the model goal. The recommendations established by the regulatory bodies help establish the project goals of prosthesis survival after 400 or 600 million cycles under physiologic loading; this is a fatigue assessment requirement, and currently structural finite element models cannot address this directly. FEA can, and is used to, quantify the driving force (strain amplitude, stress amplitude, stress intensity, etc.) for failure under physiologic loading. Knowledge of the fatigue strength of the material is also required to complete the project goal.

Physiologic loading conditions are then applied to the model after the simulation of any preimplant loading. Often the analyst is faced with the derivation of loads from assumptions on the in vivo conditions. When new devices are being examined, previously discounted loading conditions can then become important. For example, in a bi-leaflet mechanical valve prosthesis with a rigid housing, the propensity for radial deformations or bending is small and assumed insignificant. Depending on the design, this may not be the case for more compliant stent-based transcatheter valve prostheses where these loadings may be more significant. Analysts should consider each loading condition and determine the contribution of these conditions to the overall combined load and ultimately to the material stress/strain.

The importance of these combined loadings is highlighted in the ISO 5840 guidance document [32]. For transcatheter heart valves, ISO 5840 guidance recommends using blood pressures associated with moderate hypertension at a minimum and suggests that the manufacturer has the responsibility to identify and justify appropriate in vivo loading conditions. While it may appear simple to apply blood pressure changes in a simulation, the true use condition loads and boundary conditions are much more complex. The prostheses are implanted in a diseased environment; annular deformations and vessel calcification change the boundary conditions and add variability. It is difficult to quantify these properties by measurements in healthy animals or humans, and there is a dearth of research focused on measuring these quantities for the diseased state.

### *17.2.5 Physics/Solution Method*

The solution methods for most commercial FEA codes typically fall into one of two categories: implicit or explicit. Implicit solvers are generally used for linear or mildly nonlinear analyses and rely on an iterative scheme to develop a converged solution for each increment. The advantage of these implicit solvers is that they allow for very large load increments, making this solver attractive for many quasi-static structural, heat transfer, and diffusion simulations. However, the iterative scheme can be computationally expensive and time consuming and can fail for

highly nonlinear problems, such as those involving complex contact or material, and geometric nonlinearities. This method requires some tolerance adjustments to overcome the nonlinearity.

Explicit solvers operate on the dynamic equations of motion by using a central difference integration scheme to explicitly develop a solution at the next time increment. This approach does not require any iteration or convergence scheme within an increment, so each increment is relatively computationally inexpensive. These solvers are particularly attractive for dynamic simulations and highly nonlinear simulations. Because no iteration is involved, a solution (good or bad) is nearly always achieved, making this solver particularly attractive for highly nonlinear quasi-static analyses typical of many implantable medical devices. Since this formulation is a wave propagation problem, certain care is needed in obtaining a quasi-static solution. It is recommended to monitor the ratio of kinetic energy in the model to the internal energy to ensure that the inertia forces do not contribute to the model response. However, since time is explicitly modeled, the time increment is related to the wave speed of the material and element size and is typically very short. For models with significant mesh refinement, time increments can be impractically small, requiring an unreasonable number of increments.

A variety of solution methods have been developed and implemented. Each method was designed to address a specific class of problems, with certain advantages and limitations. Selection of a solution method is important, and it is incumbent upon the user to understand these methods to select the most appropriate method.

### *17.2.6 Model Verification and Validation*

Using computer predictions for prosthetic heart valve designs carries enormous importance. Therefore, prior to accepting the results from a finite element simulation, an appropriate level of verification and validation is required to quantify confidence in the ability of the model to answer the question of interest. Most of the referenced simulations in this document have provided some form of validation.

Verification and validation—these two words are often referenced when speaking about numerical simulations. Unfortunately, these words are often used interchangeably despite having two very distinct meanings and guides that have been established as early as 1998 [55, 56]. Verification ensures that the equations are solved as intended. Validation ensures that the right equations are solved. ASME V&V40:2018 clearly defines and distinguishes the terms verification and validation and proposes a risk-based framework for identifying the verification and validation activities required when modeling is used to assess medical devices [33]. An end-to-end example of how the framework proposed in V&V40 can be applied to a heart valve computational model is provided in Chap. 14.

Verification is the process of determining if the computational model and code correctly represent the mathematical model and its solution with sufficient accuracy. It is important to note that verification does not ensure accurate prediction of a

physical event. Structural FEA and computational fluid dynamics involve the discretization of the domain into elements, and the order, type, and distribution (or bias) of these elements in large part govern the integrity and accuracy of the solution; solutions typically converge as the mesh is refined. Thus, mesh refinement is often one very important element in model verification.

A Grid Convergence Index based on Richardson extrapolation [57] has been developed and established to estimate mesh convergence error and facilitate determination of an appropriate level of mesh refinement. Adaptations by Schwer [58] allow for nonuniform grid refinement ratios. This is especially important for analyses requiring highly biased, nonuniform meshes to more effectively model areas of high gradients where an accurate assessment is needed.

With increased mesh refinement comes increased computational time and expense. As such, there is often a trade-off between mesh refinement and the desired accuracy of the solution. For example, models used for general comparative purposes that focus more on trends in behavior may not require the same level of accuracy and convergence as models intended to predict actual behavior. Additionally, a finer mesh is required when stresses and strains are the quantities of interest, whereas a coarser mesh is sufficient when force is the quantity of interest. Analysts are responsible for establishing and verifying an appropriate level of convergence and solution accuracy commensurate with the intended context of use for the model [59].

While verification focuses on the ability of the model to appropriately represent the underlying mathematical model, validation is concerned with the ability of the model to represent reality. Validation is defined as the process of determining the degree to which a model is an accurate representation of reality with respect to its intended use [33]. Similarly, Knepell and Arangno define validation as the demonstration that a computer model has accuracy which is satisfactory with respect to the intended use of the model and within the intended range of application [60]. Here, the "intended use of the model" is the model goal as defined above in Sect. 17.2.1.

Validation typically employs physical experiments and the comparison of these results with those predicted by the model. While there is no recipe for validation, it typically relies on experimentally measurable parameters for comparison to the simulations. In many instances, such as with stress or stress intensity factors, the variable of interest cannot be measured directly. In such cases, parameters that can be measured and are closely related to the parameter of interest can be compared (e.g., compare measured and predicted strain fields ahead of a crack tip). Another approach is to use a validated surrogate model to compute the experimentally derived parameter from actual measurements to compare to the model prediction (e.g., use measured strain fields to calculate an experimentally derived $K$ for comparison to the predicted $K$).

In studies of bioprosthetic valves, early researchers relied on experimental displacement measurements for validation data [11, 61]. Newer technology promises to provide more and higher fidelity data for validation of these leaflet models. Gao et al. quantified bioprosthetic valve leaflet motion using dual-camera stereo

photogrammetry [62]. Many techniques for measuring the fluid flow through these prosthetic valves have been developed and are cited in Chandran [13] and Abbas [63].

Assessing whether the model possesses the required accuracy is not always straightforward; there is error and uncertainty in experimental results as well as error in the simulation. Thus, validation activities often require statistical or probabilistic analyses to assess model accuracy and confidence. This may entail several replicate tests and quantification of the variability in various model inputs. In doing so, one could assess the distribution of model predictions resulting from variability in model inputs to the range of experimental measurements.

It is also important to note that the project model may also be a model that requires validation. While the computational model can be verified and validated with respect to the model goals, often the project goals involve another overarching model that contains the numerical model. In the case of our example of the pyrolytic carbon leaflet, the numerical model was intended to develop the stress intensity factor $K$, while the project model was to compare $K$ to a critical value, the material toughness $K_{IC}$, to assess the propensity for failure due to unstable crack growth. In principle, this project model may also require both verification and validation, though a model as simple as this example requires no verification. As a model (a failure model, in this case), it does require validation as it is certainly possible to have a project model defined such that it does not accurately represent reality. In the case of our example, the governing failure model may be controlled by, for example, an elastoplastic fracture process for which $K$ is not valid despite the level of accuracy of the model to predict $K$. Alternatively, failure may occur due to net-section collapse and not unstable crack growth, something not necessarily realized without validation testing carefully designed to test the project goal.

This concept begins to define a hierarchical approach to verification and validation (V&V) [33]. In many instances, satisfactorily achieving the overall project goal is dependent on a system or collection of models, some of which may contain submodels. In these cases, the recommended V&V approach is to develop a model hierarchy and work from the bottom up to identify the appropriate level of accuracy of each model to meet the overall project goal. Verification and validation activities would then start at the lowest levels and work from the bottom up through the hierarchy. For each model, verification should precede validation; it does not make sense to attempt validation prior to appropriate verification. Similarly, it does not make sense to attempt V&V on a higher-level model if one or more of its submodels have not been appropriately verified and validated.

Finally, the level or degree of V&V must be considered. The primary objective of V&V is to establish confidence in the ability of the computational model to predict reality. Generally, it will not be possible to completely verify and validate a model; thus, V&V activities are performed to assure a certain level of confidence in the ability of the model to represent reality. The level of V&V should be established, commensurate with the consequences of being incorrect.

### 17.2.7 Interpretation

One of the most important steps in the FEA process begins after the model has been built and executed—this step is "interpretation of the results." This step is necessary to address the project goal to determine if any design changes are needed to satisfy the project goals. The first part of interpretation is to simply think about the results and see if they physically make sense. Some articles offer some insight into "interpretation" [64, 65]. Modern FEA software provides a myriad of various results which can generally be plotted and are available for further post-processing. It is the responsibility of the analyst to choose the proper stress or strain variables to query when addressing the project objective. When concerned with the structural integrity of a pyrolytic carbon leaflet of a prosthetic heart valve, for example, the analyst would be concerned with the maximum principal stress over the cardiac cycle. Materials exhibiting more ductile failure would rely on a von Mises stress or a maximum shear stress, and superelastic Nitinol material is typically examined by quantification of the strain, both mean and amplitude, in the model. Variable contour patterns and gradients should be considered, specifically when contact, symmetry, or special elements like shells and beams are used. Occasionally these can cause abrupt concentrations or discontinuities in field variable contours.

Fortunately, these potential model issues should be identified during previous V&V work or the final peer review. The identification of the proper metric to address the project goal is the responsibility of the team and/or the analyst and is an important part of the FEA results interpretation.

### 17.2.8 Documentation

It is imperative that analysts document their results in a clear and concise fashion. Without documentation, the logic and assumptions used in the analysis become lost, and the results of analyses may errantly be given more, or less, credibility than appropriate. When striving for technical rigor in a report documenting the model, one must remember four criteria: (1) clarity, (2) concision, (3) completeness, and (4) correctness. This will enhance readability when reviewing the results.

A well-documented analysis will allow others to repeat the analyses, if necessary, and can highlight sections where more information would be beneficial to improving the credibility of the analysis. Regulatory agencies have published guidance documents to provide recommendations on the formatting, organization, and content of reports of CM&S studies of medical devices [53]. Companies that manufacture and distribute heart valve prostheses will have some type of document control system, and FEA reports should be stored in this type of system. It is a recommended practice to also store the source FEA files to ensure traceability of the model results.

If the prosthesis being simulated is based on a stent as a support frame, the FDA has a guidance document to follow for the documentation of the FEA results [53]. All the suggestions made in this guidance document are included as topics in the attached appendix, except for a specific request for information regarding contact elements. Additionally, the guidance document recommends an indication of "...if mesh refinement analysis was performed..." Note that this is a mandatory step unless one can illustrate model verification by another means. The analyst should always consult the appropriate guidance documents when preparing the final report.

### *17.2.9 Peer Review*

The final stage in the analysis is the peer review, an important step that is closely linked to the documentation of the analysis results. Two aspects of technical rigor are completeness and correctness. While not entirely infallible, peer review is designed to help ensure these aspects of the analyses. Fortunately for the analyst, working within a medical device manufacturing company, quality systems employed for compliance require some type of review and approval of the documented work. Regardless, this is a best practice for any analyst. If the analysis is properly designed, performed, and documented, a thorough peer review will add confidence to the work completed. Of course, the need for peer review is not limited to analyses completed within the realm of product development in a medical device company. Academic and industrial researchers must also submit their analysis work to a complete peer review; this should be completed before any submission for publication. Often the reviewers of manuscripts for publication only see a portion of the work behind the overall paper, which prevents a thorough technical review of the analysis.

## 17.3 Summary and Conclusions

The use of numerical methods to simulate native and prosthetic heart valves will likely continue to expand. These tools, combined with new anatomical data, tissue mechanical properties, and methods for failure prediction enable analysts to simulate heart valve prostheses more accurately. To truly advance the field of simulation for prosthetic heart valves, development of data and methods to assist in addressing the project goals are essential. Examples of this would be studies that can assist in the translation of mechanical loads predicted by FEA to physiologic effects on the vessels, valve leaflets, and ultimately the patients. Some of this work has been performed for bioprosthetic valves. Researchers are attempting to isolate mechanical variables to predict calcification of heart valve leaflets [15]. Developing some type of metric to predict paravalvular leakage or other clinical sequelae for transcatheter heart valve prostheses is required for attempts to simulate the overall therapy. This may require the use of FEA, FSI, or possibly more complex multiphysics simulation

methods and tools [66]. The development and improvement of methods for in vitro or direct in vivo measurements of loading on implants will aid the field by providing more accurate input loading conditions for FEA models. Some of these measurements have already been made in animals for pulmonary valve applications, while others have developed methods for in vitro measurements on aortic stent prostheses [67]. Perfection of the material constitutive models for metal alloys with inclusion of the post-plastic work hardening regime would make it easier to simulate any residual stresses that develop during prosthesis use. This would help with true simulation of loads on the devices and prediction of failures due to fatigue loading.

Simulation methods for device structural integrity should be improved and validated. Improved validation has been achieved using probabilistic methods that account for the fact that fatigue is not a stochastic event [68]. Boundary conditions, material properties, and device geometry have their own variability, and there is often considerable uncertainty in the in vivo boundary conditions in addition to model error. Thus, simulations of heart valve prostheses will be enhanced by probabilistic methods to assess valve reliability and confidence. The latest revision of ISO 5840:2021 acknowledges the benefits of adopting a probabilistic approach, where the distributions of the fatigue strength and the stress/strain are characterized, rather than taking single values of strength and stress.

During these exciting times, advances in computer performance and sophistication of the methods used have made numerical analyses a critical tool for the design and evaluation of new prosthetic heart valves. Yet, along with these advances comes a higher responsibility for the analyst. “Ease of use” can translate into “ease of misuse.” Following a structured approach, such as described in this chapter, should help those simulating the prosthetic heart valves perform meaningful and accurate simulations. In closing, remember the saying by Box (1976) “All models are wrong, some are useful” [38]. Ultimately, it is the responsibility of all researchers and analysts to strive to make their FEA models of native or prosthetic heart valves useful.

## References

1. Chaikof EL (2007) The development of prosthetic heart valves—lessons in form and function. N Engl J Med 357:1368–1371
2. McMeeking RM, He MY, Chia R (1996) Structural analysis of the Björk-Shiley Delrin heart valve occluder. J Heart Valve Dis 5(Suppl 2):S229–S237
3. Fontaine AA, Ellis JT, Healy TM (1996) Identification of peak stresses in cardiac prostheses. A comparison of two-dimensional versus three-dimensional principal stress analyses. ASAIO J 42:154–163
4. Plemons TD, Hovenga M, Reeder H (1993) Classification of Bjork-Shiley convexo-con-cave valve status by detection of the intact outlet strut resonant frequency. In: Proceedings of the 15th annual international conference of the IEEE, pp 389–390
5. Udpa S (2002) New electromagnetic methods for the evaluation of prosthetic heart valves. J Appl Phys 91:1–5
6. Chondros TG (2010) Fatigue fracture of the Björk–Shiley heart valve strut and failure diagnosis from acoustic signatures. Theor Appl Fract Mech 54:71–81

7. Yuan Q, Xu L, Ngoi BK (2003) Dynamic impact stress analysis of a bileaflet mechanical heart valve. J Heart Valve Dis 12:102–109
8. Mohammadi H, Klassen RJ, Wan W-K (2008) A finite element model on effects of impact load and cavitation on fatigue crack propagation in mechanical bileaflet aortic heart valve. J Eng Med 222:1115–1125
9. Hong TH, Choi CR, Kim CN (2009) Characteristics of hemodynamics in a bi-Leaflet mechanical heart valve using an implicit FSI method. Eng Technol 49:679–684
10. Thubrikar M (1990) The aortic valve. CRC Press, Boca Raton, p 221
11. Rousseau EPM, van Steenhoven AA, Janssen JD (1988) A mechanical analysis of the closed Hancock heart valve prosthesis. J Biomech 7:545–564
12. Hamid MS, Sabba HN, Stein PD (1987) Vibrational analysis of bioprosthetic heart valve leaflets using numerical models: effects of leaflet stiffening, calcification, perforation. Circ Res 61:687–694
13. Chandran KB (2010) Role of computational simulations in heart valve dynamics and design of valvular prostheses. Cardiovasc Eng Technol 1:18–38
14. Thubrikar MJ, Deck JD, Nolan SP (1983) Role of mechanical stress in calcification of aortic bioprosthetic valves. J Thorac Cardiovasc Surg 86:115–125
15. Sacks MS, Schoen FJ (2002) Collagen fiber disruption occurs independent of calcification in clinically explanted bioprosthetic heart valves. J Biomed Mater Res 62:359–371
16. Makhijani VB, Yang HQ, Dionne PJ (1997) Three-dimensional coupled fluid–structure simulation of pericardial bioprosthetic aortic valve function. ASAIO J 43:M386–M392
17. Schievano S, Petrini L, Migliavacca F (2007) Finite element analysis of stent deployment: understanding stent fracture in percutaneous pulmonary valve implantation. J Interv Cardiol 20:546–554
18. Schievano S, Taylor AM, Capelli C (2010) Patient specific finite element analysis results in more accurate prediction of stent fractures: application to percutaneous pulmonary valve implantation. J Biomech 43:687–693
19. Schievano S, Taylor A, Capelli C (2010) First-in-man implantation of a novel percutaneous valve: a new approach to medical device development. EuroIntervention 5:745–750
20. Popma JJ, Adams DH, Reardon MJ et al (2014) Transcatheter aortic valve replacement using a self-expanding bioprosthesis in patients with severe aortic stenosis at extreme risk for surgery. J Am Coll Cardiol 63:1972–1981
21. Reardon MJ, Van Mieghem NN, Popma JJ et al (2017) Surgical or transcatheter aortic-valve replacement in intermediate-risk patients. N Engl J Med 376:1321–1331
22. Leon MB, Smith CR, Mack MJ et al (2016) Transcatheter or surgical aortic-valve replacement in intermediate-risk patients. N Engl J Med 374:1609–1620
23. Mack MJ, Leon MB, Thourani VH et al (2019) Transcatheter aortic-valve replacement with a balloon-expandable valve in low-risk patients. N Engl J Med 380:1695–1705
24. Popma JJ, Deeb GM, Yakubov SJ et al (2019) Transcatheter aortic-valve replacement with a self-expanding valve in low-risk patients. N Engl J Med 380:1706–1715
25. Bosi G, Capelli C, Cheang M et al (2020) A validated computational framework to predict outcomes in TAVI. Sci Rep 10:9906
26. Bosi G, Capelli C, Cheang M et al (2018) Population-specific material properties of the implantation site for transcatheter aortic valve replacement finite element simulations. J Biomech 71:236–244
27. De Jaegere P, De Santis G, Rodriguez-Olivares R (2016) Patient-specific computer modeling to predict aortic regurgitation after transcatheter aortic valve replacement. JACC Cardiovasc Interv 9:508–512
28. Rocatello G, El Faquir N, De Santis G (2018) Patient-specific computer simulation to elucidate the role of contact pressure in the development of new conduction abnormalities after catheter-based implantation of a self-expanding aortic valve. Circ Cardiovasc Interv 11:e005344
29. Luraghi G, Migliavacca F, García-González A (2019) On the modeling of patient-specific transcatheter aortic valve replacement: a fluid-structure interaction approach. Cardiovasc Eng Technol 10:437–455

30. Pasta S, Cannata S, Gentile G (2020) Simulation study of transcatheter heart valve implantation in patients with stenotic bicuspid aortic valve. Med Biol Eng Comput 58:815–829
31. Rocatello G, De Santis G, De Bock S et al (2019) Optimization of a transcatheter heart valve frame using patient-specific computer simulation. Cardiovasc Eng Technol 10:456–468
32. Standards, International. ISO 5840-1:2021 cardiovascular implants – cardiac valve prostheses – Part 1: general requirements
33. ASME (2018) Assessing credibility of computational modeling through verification and validation: applications to medical devices. ASME
34. ASME (2019) Standard for verification and validation in computational solid mechanics V V 10-2019. ASME
35. ASME (2009) ASME V and V 20-2009 Standard for verification and validation in computational fluid dynamics and heat transfer. ASME
36. Haridas B, Haynes C (1999) Predictive analysis at the forefront of medical product development. Med Dev Diagn Ind 3:112–119
37. Babuska I, Oden T (2005) The reliability of computer predictions: can they be trusted? Int J Numer Anal Model 1:1–18
38. Box G (1976) Science and statistics. J Am Stat Assoc 71:791–799
39. MacDonald BJ (2007) Practical stress analysis with finite elements. Glasnevin Publishing
40. Pelton AR, Russell SM, DiCello J (2003) The physical metallurgy of nitinol for medical applications. JOM 55:33–37
41. Robertson SW, Pelton AR, Ritchie RO (2012) Mechanical fatigue and fracture of Nitinol. Int Mater Rev 57:1–37
42. Auricchio F, Taylor RL (1996) Shape-memory alloys: modeling and numerical simulations of the finite-strain superelastic behavior. Comput Methods Appl Mech Eng 143:175–194
43. Auricchio F, Lubliner J (1997) Shape-memory alloys: macromodelling and numerical simulations of the superelastic behavior. Comput Methods Appl Mech Eng 146:281–312
44. Senthilnathan K, Shamimi A, Bonsignore C (2019) Effect of prestrain on the fatigue life of superelastic nitinol. J Mater Eng Perform 28:5946–5958
45. Cao H, Wu MH, Zhou F (2020) The influence of mean strain on the high-cycle fatigue of Nitinol with application to medical devices. J Mech Phys Solids 143:104057
46. Ghista DN, Reul H (1977) Optimal prosthetic aortic leaflet valve: design parametric and longevity analyses. Development of the Avcothane-51 leaflet valve based on the optimal design analysis. J Biomech 10:313–323
47. Christie GW, Medland JC. A non-linear finite element stress analysis of bioprosthetic heart valves. Simon BR, Johnson PC, Gross JF, Gallagher RH. Finite elements in biomechanics. Wiley, Chichester 1982
48. Sacks MS, Yoganathan AP (2007) Heart valve function: a biomechanical perspective. Philos Trans R Soc Lond Ser B Biol Sci 362:1369–1391
49. Weinberg EJ, Kaazempur-Mofrad MR (2005) On the constitutive models for heart valve leaflet mechanics. Cardiovasc Eng 5:37–43
50. Weinberg EJ, Kaazempur-Mofrad MR (2007) A finiteshell element for heart mitral valve leaflet mechanics, with large deformations and 3D constitutive material model. J Biomech 40:705–711
51. Sun W, Abad A, Sacks MS (2005) Simulated bioprosthetic heart valve deformation under quasi-static loading. J Biomech Eng 127:905–914
52. Hashim S, Richens D (2006) Finite element method in cardiac surgery. Interact Cardiovasc Thorac Surg 5:5–8
53. Document, FDA Guidance (2016) Reporting of computational modeling studies in medical device submissions. FDA
54. Document, FDA Guidance (2010) Non-clinical engineering tests and recommended labeling for intravascular stents and associated delivery systems – guidance for industry and FDA staff. FDA
55. AIAA (1998) Guide for the verification and validation of computationalfluid dynamics simulations. American Institute of Aeuronautics and Astronautics: AIAA-G-077-1998

56. Babuska I, Oden JT (2004) Verification and validation in computational engineering and science: basic concepts. Comput Methods Appl Mech Engg 193:4057–4066
57. Roache PJ (1998) Verification and validation in computational science and engineering. Hermosa Publishers, Albuquerque
58. Schwer LE (2008) Is your mesh refined enough? Estimating discretization error using GCI. LS-Dyna Anwenderforum, Bamberg
59. Honkala KA (2000) Adequate mesh refinement for accurate stresses. BENCHmark, pp 4–9
60. Knepell PL, Arangno DC (1993) Simulation validation: a confidence assessment methodology. IEEE Computer Society Press
61. Thubrikar M, Skinner JR, Eppink RT (1982) Stress analysis of porcine bioprosthetic heart valves in-vivo. J Biomed Mater Res 16:811–826
62. Gao ZB, Pandya S, Hosein N (2000) Bioprosthetic heart valve leaflet motion monitored by dual camera stereo photogrammetry. J Biomech 33:199–207
63. Abbas SS, Nasif MS, Al-Waked R (2022) State-of-the-art numerical fluid–structure interaction methods for aortic and mitral heart valves simulations: a review. Simulation 98:3–34
64. Williams B What all engineers need to know before using finite element analysis
65. Baguley D, Hose DR (1997) How to interpret FEA results. NAFEMS Publication
66. Baillargeon B, Rebelo N, Fox DD et al (2014) The Living Heart Project: a robust and integrative simulator for human heart function. Eur J Mech A Solids 48:38–47
67. Contil JC, Strope ER (2000) Evaluating the in situ loading and accelerated durability of barbs located on bifurcated aorto-iliac stent-grafts. Biomed Sci Instrum 36:93
68. Bonsignore C (2017) Present and future approaches to lifetime prediction of superelastic Nitinol. Theor Appl Fract Mech 92:298–305

# Chapter 18
# Animal Models for Cardiac Valve Research

**Sarah E. Ahlberg, Michael G. Bateman, Michael D. Eggen, Jason L. Quill, Eric S. Richardson, Paul A. Iaizzo, and Priya Nair**

## Abbreviations

| | |
|---|---|
| ECG | Electrocardiogram |
| FDA | Food and Drug Administration |
| GLP | Good laboratory practices |
| TCV | Transcatheter valve |

S. E. Ahlberg · M. D. Eggen
Medtronic, Inc., Mounds View, MN, USA
e-mail: sarah.ahlberg@medtronic.com

M. G. Bateman
Cardiovascular Solutions Incorporated, Minneapolis, MN, USA
e-mail: MBateman@csi360.com

J. L. Quill
Anteris Technologies, Eagan, MN, USA

E. S. Richardson
Department of Biomedical Engineering, Pratt School of Engineering, Duke University, Durham, NC, USA
e-mail: eric.s.richardson@duke.edu

P. A. Iaizzo
Visible Heart® Laboratories, Department of Surgery, Institute for Engineering in Medicine, University of Minnesota, Minneapolis, MN, USA
e-mail: iaizz001@umn.edu

P. Nair (✉)
Medtronic Inc., Santa Rosa, CA, USA
e-mail: priya.nair@medtronic.com

© The Author(s), under exclusive license to Springer Nature Switzerland AG 2023

P. A. Iaizzo et al. (eds.), *Heart Valves*, https://doi.org/10.1007/978-3-031-25541-0_18

## 18.1 Introduction

The modern era of cardiac valve repair and replacement has its foundations rooted in the pioneering research completed by surgeons, scientists, and engineers in animal research laboratories. Today, animal models are required for the preclinical assessment of drugs and invasive medical device prior to human clinical studies and/ or medical usage. More importantly, these advances in medical technology have also benefited countless subjects in the field of veterinary science, with recent cases reporting heart valve and hip replacement procedures in domestic dogs. The use of animal experimentation in medical research has resulted in the development of a multitude of cancer, diabetes, and heart disease treatments and vaccines for domestic pets and wildlife [1].

In the field of cardiac valve research, preclinical in vivo testing is designed to critically assess the performances of a replacement valve or surgical procedure in a beating heart. These analyses include assessments of a given therapy's effect on hemodynamic performance, the biocompatibility and mechanical durability of the device, and the efficacy and ease of the developed implantation procedure. It is essential that any preclinical in vivo testing be designed to replicate the environment in which the procedure under review will be applied to human patients. Such attention to detail ensures the collection of more relevant data and maximizes the likelihood of the successful transition of any therapy to clinical trials.

### *18.1.1 Acute Versus Chronic Testing*

Within the field of cardiac valve repair and replacement, preclinical in vivo animal testing essentially falls into two distinct categories: acute (i.e., short-term: study initiation and termination in the same procedure) and chronic (i.e., long-term: study termination occurring days, weeks, or months after initiation).

Acute animal testing generally focuses on the immediate fits and functions of the valve therapy within the environment of the contracting heart. Since the animal is sacrificed shortly after the procedure, it is typical to perform multiple methods of invasive monitoring to capture the maximum amount of data. This can include the recording of hemodynamic factors such as pressure gradients across the valve, blood flow parameters, valvular insufficiencies, paravalvular leaks, pressure-volume loops, and/or electrophysiological measurements such as intracardiac electrical monitoring. Other important measurements made to assess the fit and function of the valve are the effective orifice areas of the functioning prosthesis; i.e., the area available for blood to pass through the valve. These measurements can help to determine whether the device is functioning as expected and, thus, better quantify its influences on physiological parameters. For example, accurately measuring such parameters for the native valve prior to the procedure and after the valve prosthesis has been implanted provides the design engineer with valuable information regarding prosthesis performance with respect to native anatomy.

Conversely, the protocol for a typical chronic animal experiment is primarily designed to test the long-term biocompatibility, function, and durability of a valve therapy. In such studies, the surgical procedure or implantation under review is conducted in the same manner as the intended human procedure, and the animals are monitored postoperatively until a predetermined endpoint. Consequently, invasive monitoring is kept to a minimum, prioritizing the condition of the animal during the surgery and maximizing the chances of survival. Commonly, the performances of a repair device or implanted prosthesis are assessed at one or more timepoints in the duration between the initial procedures the final experimental endpoints, and again upon reaching the planned experimental endpoints before a given animal is sacrificed. Typically, the primary parameters assessed include the following: (1) the location and function of the device (e.g., did the prosthetic valve migrate from its implanted position, is the prosthetic device performing as intended?); (2) the immune response of the host, the healing/level of inflammation of the tissue surrounding the implant; and (3) the overall health of the animal (i.e., was the systemic health of the animal compromised by the therapy?). In the instance where an animal does not reach the experimental endpoint, a postmortem investigation is conducted to determine whether the tested procedure directly caused the mortality.

### *18.1.2 Regulations*

Prior to commencing any animal experimentation, a study protocol must be approved by an independent regulatory body that ensures that investigators comply with the following goals [2]:

- Procedures are to be designed and performed with due consideration of their relevance to human or animal health, the advancement of knowledge, or the good of society.
- The selection of appropriate species and the minimum number of animals to be used to achieve valid results (including using alternate forms of testing, such as in vitro testing and computer simulations).
- The avoidance or minimization of animal discomfort, distress, and pain when consistent with sound scientific practices.
- The appropriate use of sedation, analgesia, or anesthesia during procedures that involve more than momentary or slight pain to the animal (acute studies should terminate with a painless ending of the animal's life).
- Appropriate living conditions and care for the animals and proper training for investigators.

These regulatory guidelines were initially defined by the Animal Welfare Act of 1966 and have since been updated through the Health Research Extension Act of 1985, and most recently updated in 2015 with the Public Health Service Policy on Humane Care and Use of Laboratory Animals. In educational organizations in the USA where research using animals is performed, the standard governing body is known as the *Institutional Animal Care and Use Committee* (see www.iacuc.org).

Additionally, documentation from the US National Academy of Sciences entitled the "Guide for the Care and Use of Laboratory Animals" has been created to assist investigators who plan to utilize animal research in the experimental design and subject choice for their research [2]. In addition to defining the regulations for animal research, these committees and guidelines also stress the need to investigate nonanimal research alternatives, such as in vitro or in silico testing, as well as the importance of determining what information can be garnered from previous research. By adhering to these regulations, investigators ensure that every effort is made to maximize health advancements while minimizing the distress that animals experience during the procedures and the number of animal experiments performed.

At this time, there are no computer simulations and/or adequate in vitro tests capable of mimicking the complete complex physical and biological system responses of the human body. Therefore, preclinical testing of cardiac valve repair procedures and replacement technologies are not only necessary but also essential since they provide the most accurate ways to screen potential therapies and/or devices prior to human use.

## 18.2 Choosing the Correct Animal Model

The choice of animal model should be primarily based on three determining factors [3]:

1. The scientific hypotheses to be answered
2. The similarity of the native anatomy to the relevant human anatomy
3. The laboratory's capability to safely employ the model in the chosen species (i.e., appropriate animal housing and care, equipment, and laboratory resources)

### *18.2.1 Spontaneously Occurring Animal Models of Congenital Valve Disease*

Still today, the commercial availability of animals with naturally occurring cardiac pathologies for use in cardiac valve repair and replacement research purposes is extremely limited. Although great advances have been made into the investigation of the pathophysiological mechanisms of cardiac disease with the use of transgenic mice and mice with gene deletions, these models do not lend themselves well to valve repair and replacement research [3]. While mice and rats can work well for specific tissue and metabolic work, due to obvious technical limitations, most testing of procedures for the repair and replacement of valves in humans takes place on large animal models. Advances have been made in various transgenic swine models, but these have had limited use in preclinical valve studies.

The lack of naturally occurring models of valve disease and the need for standardized models for regulatory approval have led to the use of iatrogenic models of valve disease. Research has been ongoing into the induction of various cardiac

disease states that can affect valve function, such as functional mitral or tricuspid valve regurgitation because of dilated cardiomyopathy. An excellent example is the use of chronic high-rate pacing, or tachypacing, to create animal models of dilated cardiomyopathy [4, 5]. Researchers looking at creating chronic heart failure models by pacing the heart at two to four times the intrinsic rate from either the atria or ventricles discovered that an increase in chamber volume leads to a dilation of the atrioventricular valve annuli and subsequent mitral and tricuspid valve regurgitation. Aortic supravalvular stenosis, as well as aortic valvular stenosis, has been commonly induced in the canine model (dog) [6, 7], while graded stenosis in the aortic and mitral valves has been produced in the ovine model (sheep) by banding the aorta in young animals [8]. Additionally, more direct interventions, such as the incision of chordae tendineae, have been used to create anatomical abnormalities that disrupt the hemodynamics across a valve [9]. However, most valve implantation studies approved for human use are completed in healthy animals, and their primary goals are to strictly examine valve performance (Fig. 18.1) [3].

### *18.2.2 Species-to-Species Variability*

The three most common large animal models for cardiac investigations are the canine (dog), swine (pig), and ovine (sheep). Thus, the remainder of this section will focus on these three models and compare their native cardiac anatomy to that of a human.

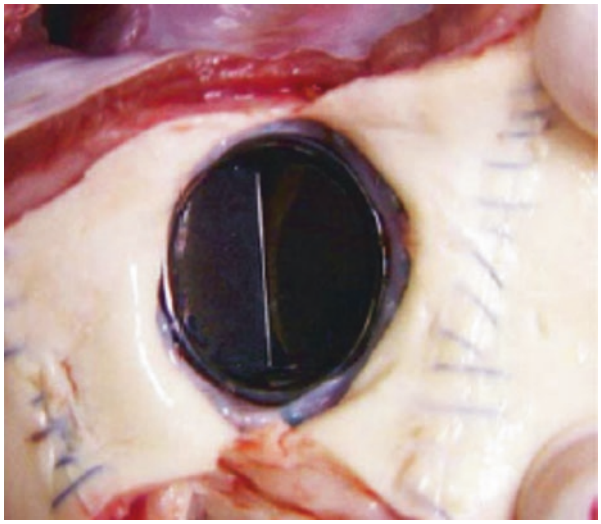

**Fig. 18.1** Implantation of a St. Jude bileaflet mechanical valve in an ovine model (St. Jude Medical, St. Paul, MN). (Reprinted with kind permission from Springer Science & Business Media [30])

#### 18.2.2.1 Comparative Anatomy

Detailed descriptions regarding comparative cardiac anatomy between canine, ovine, swine, and humans have been published by Hill and Iaizzo [10] and Michaëlsson and Ho [11]. Consequently, we will describe the major differences in cardiac anatomy between animals and humans in the context of valve repair and replacement procedures.

***Canine model*** For years, valvular studies using the canine model has proved to be excellent since the animals typically have good temperament and can be trained to sit still during postoperative examinations: no sedation required or agents that might alter native physiology. Yet, it has been reported that the atrioventricular valves in canines can exhibit leaflet fusion and variabilities in the numbers and positions of the papillary muscles [11, 12]. It should also be recognized that the canine hearts have an unusually large amount of collateral coronary circulation, which is only similar to humans who present with a slowly progressing end-stage chronic heart failure [10].

***Swine model*** Swine have emerged as an excellent model for acute cardiac device testing. Swine have similar cardiac anatomies to humans with respect to the conduction system, cardiac valves, and coronary arteries [10]. However, when considering this species for the testing of aortic valve therapies, notable differences include the presence of excess myocardial tissue at the ventricular septum under the right coronary leaflet, low coronary ostia [13], and a short ascending aorta. It should be noted that swine are not often used in chronic studies that require invasive surgical procedures due to sensitivity to anesthesia, and frequent intra- and postoperative complications such as cardiac arrhythmias and sudden death [14]. Yet, swine might be an interesting model to employ for accelerated growth studies as they can grow 10 or more pounds per week (see below).

***Ovine model*** The ovine model is currently accepted as the gold standard for valve replacement research using defined survival surgeries that meet Food and Drug Administration (FDA) requirements. Normal cardiovascular physiological parameters of sheep approximate those of humans in blood pressures, heart rates, cardiac outputs, and intracardiac pressures [15]. In addition, the anatomies of the adult heart provides valve orifice diameters that are similar to humans [13]. The use of animals of similar age and weight (8–12 months, 30–40 kg) allows for the testing of replacement valves using a single orifice size for comparison of valve performance to an appropriate standard. Although the heart and vessels are small in animals within this weight range, the sheep's relatively large left and right atria allow for straightforward surgical approaches to either the mitral or tricuspid valves [3]. In general, sheep as experimental animals allow for easy handling and long-term husbandry. The ovine model is also characterized by a higher immune response than other animals. This means that in many cases a thrombolytic event will be observed in the

sheep more prominently than in swine or dogs and, therefore, may provide investigators with better ideas of what the failures will look like in humans. Importantly, specific attention to gastric decompression, perioperative antibiotics, sterile techniques, and minimally invasive interventions in the postoperative period will all increase the success of valve implantation studies in the ovine model [16].

#### 18.2.2.2 Rate of Growth

The variability between species in terms of each animal's rate of growth is an important consideration when choosing the correct chronic animal model. Although the rate of growth is dependent on the environment and varies between individuals within each species, it can be predicted relatively accurately. In studies where a specific heart size is required, estimates have been established for each species comparing the excised heart weight to body weight. In general, the heart weight to body weight ratios for adult dogs, pigs, and sheep are 7, 2.5, and 3 g/kg, respectively [17]. For comparison, the heart weight to body weight ratio of humans is approximately 5 g/kg. It should be noted that, for swine, a more realistic heart weight to body weight ratio may be obtained by using younger animals [18] or mini-pigs [19].

In addition to the relative heart size of each species, the overall growth rate and mature animal size should be considered as larger animals become difficult to manage. All three species reach mature size by approximately 12–18 months of age. However, the comparatively large mature size of swine results in a higher growth rate which, in turn, makes the results of chronic studies with these animals harder to interpret, i.e., the heart continues to enlarge with the size of the animal. This accelerated growth rate can cause the animal to outgrow its prosthetic implant, resulting in valvular dysfunction during the postimplantation test periods, as compared to the ovine model [14]. Yet, in rare cases, this accelerated growth rate can be beneficial to the researcher, for example, when determining the ability of therapies designed for the pediatric population to adapt with the growing patient.

Another important parameter to consider when choosing the appropriate animal model for a study is the impact of the growth rate on the process of calcification. This is particularly important in the realm of prosthetic tissue valves due to the propensity of these devices to calcify over time, a process that can impact valve function. The high growth rate within juvenile animals tends to increase the rate of calcification on an implanted device [20]. Therefore, if looking to assess the performance of a novel anti-calcification treatment, choosing a juvenile animal model is encouraged in order to provide a good challenge condition for the treatment. Conversely, if the assessment of calcification is not an endpoint of the study, then an adult animal model is more appropriate to eliminate the concern of the model outgrowing the prosthesis.

## 18.3 Basic Experimental Design

As previously mentioned, any preclinical, in vivo testing protocols should be designed to replicate the environments in which the eventual device/procedure under review will be applied to human patients. This section will briefly discuss some of the fundamental topics that need to be considered when designing a surgical or interventional procedure with animal subjects.

### *18.3.1 Anesthetics and Monitoring*

The choice of anesthetic(s) to be administered in a given study protocol depends on several factors:

1. The species of animal model used.
2. The nature and duration of the planned intervention, including the amount of pain or distress involved.
3. Whether the subject will be recovered after the procedure.

It should be noted that general guidelines for the choice of anesthesia can be found on the Animal Welfare Information Center website (https://www.nal.usda.gov/awic). Most cardiac valve procedures require either surgical or catheter access to the heart, and it is usually deemed necessary to intubate and ventilate the subject. With ventilation, the subjects can be anesthetized using the inhaled delivery of volatile anesthetics rather than intravenous delivery of liquid anesthetics, facilitating the sedation process.

All animals should be closely monitored during anesthesia. At a minimum, a three-lead electrocardiogram (ECG) should be continuously monitored, and the blood pressure should be assessed often (e.g., using noninvasive cuff or direct arterial line). An excessively high heart rate, high blood pressure, and/or animal movement (blink reflex) can be signs that the anesthesia is too low (the animal is *light*). Conversely, a low pressure and low heart rate may be indicators that the animal is receiving too much anesthesia. However, during most invasive surgical procedures, a combination of parameters is monitored to ensure the subject remains under a stable level of anesthesia (employ anesthetic monitoring if available). Examples of commonly monitored parameters include end tidal $CO_2$ level, cardiac output, anesthetic concentration, core temperature, and arterial $O_2$ and pH values.

### *18.3.2 Accessing the Heart*

Cardiac valve therapies are usually administered via surgical or vascular access to the heart. For percutaneous interventions that require device delivery through the large vessels such as the femoral arteries or veins in humans, the carotid artery or

subclavian vein approach can be used in animals. Access can be gained by using the Seldinger technique after the vessel is exposed via a direct surgical cutdown. Surgical access to the heart is usually gained via a thoracotomy or a sternotomy. A thoracotomy is generally described as a surgical window between two ribs within which a rib spreader, or retractor, is placed to gain access to the heart. The site of the incision is critical as the relatively small window exposes only a small section of the heart during the procedure. A medial sternotomy, on the other hand, is the most invasive method of accessing the heart but provides the investigator complete access to almost all surfaces. Access to the thoracic cavity is gained by transecting the exposed sternum and retracting the ribcage laterally.

If the animal is to be recovered from a thoracic surgery, extreme care must be taken to use aseptic techniques as any subsequent chest infections (mediastinitis) have a very high associated mortality rate for most large animal cardiovascular models. In general, the closure procedure, including the placement of chest tubes, can be complicated, and the animal requires postoperative monitoring. Furthermore, recovery from thoracic surgery may take anywhere from a few days to several weeks and can be associated with considerable pain. Therefore, appropriate pain medication and antibiotics must be given to help ensure the comfort and survival of these animals. An excellent resource for more detailed information on these procedures can be found in David Gross' *Animal Models in Cardiovascular Research* [21].

Today, highly specialized research laboratories (academic, within a given company or for hire) offer the same surgical technologies and standards of care as hospital operating rooms. This can include current surgical techniques and expertise such as bypass surgery, clinical imaging capabilities, and state-of-the-art pathology services.

## 18.4 Replacement Heart Valve Testing

The significant morbidity and mortality associated with heart valve disease and the limitations and inherent dangers of direct surgical correction have created a highly lucrative and competitive market for manufactured prosthetic valves. Efforts to develop the ideal replacement heart valve have focused on producing a device that functions like the native valve (Table 18.1) [3].

As previously mentioned, the FDA and the International Standards Organization (ISO) have provided the medical device industry with guidelines for prosthetic valve manufacturing in the form of guidance documents, advice, reporting, premarket approval, development of standards, and third-party reviews. These guidelines define the parameters for all in vitro and benchtop testing protocols and outline the needs for in vivo testing of the device in a living host. Consequently, all replacement heart valves, both surgical and transcatheter, undergo a preclinical animal study with implantation in the orthotopic (anatomically normal) positions for a required minimum of 20-week period of evaluation [22]. During these in vivo studies, a multitude of variables, outlined in Table 18.2, are investigated depending on the design

**Table 18.1** Qualities of the ideal device for heart valve replacement

| |
|---|
| Durable |
| Does not leak |
| Biologically inert |
| Non-thrombogenic |
| Facilitates laminar flow |
| Easily implanted by the surgeon |
| Quiet |

**Table 18.2** Parameters for data collection as recommended by the FDA [22]

| |
|---|
| Study of acute hemodynamic performance |
| Ease of handling and surgical implantation |
| Hemodynamic performance (catheter data as well as echocardiography) |
| Leaflet motion (by echocardiography and angiography) |
| Presence of stenosis or regurgitation |
| Study of chronic hemodynamic performance |
| Ease of handling and surgical implantation |
| Hemodynamic performance (catheter data as well as echocardiography) |
| Leaflet motion (by echocardiography and angiography) |
| Presence of stenosis or regurgitation |
| Blood studies, imaging studies of leaflet motion, and regurgitation |
| In situ photos of inflow and outflow regions and valve surfaces |
| Necropsy and gross pathology |
| Explanted valve analysis (including histology of the valve and surrounding tissue) |
| Hemodynamic performance assessments |
| Peak and mean pressure gradient |
| Effective orifice area regurgitation |
| A description of instrumentation and test methods |
| Laboratory results |
| Complete blood count and chemistry analysis should include the following: |
| Red blood cell count |
| White blood cell count (with differential) |
| Hematocrit |
| Free hemoglobin |
| Serum lactate dehydrogenase |
| Haptoglobin |
| Reticulocyte count |
| Platelet count |
| For flexible leaflet valves, in addition to the tests listed above, you should include the following: |
| Serum calcium |
| Serum phosphorous |
| Leaflet calcium |
| Phosphate |

and build of the prosthesis and the nature of the test [23]. For example, surgically implanted mechanical valves are known to cause more hemolysis and thrombosis than surgically implanted tissue valves placed in the same cardiac position. However, tissue valves are known to be sensitive to calcium deposition on the valve leaflets, affecting the performances of these prostheses over time. Therefore, in vivo testing regulations for the two valve types differ, with mechanical valves being scrutinized for thrombus formations and tissue valves undergoing strict postmortem histological investigations to determine the levels of leaflet calcification [3].

### *18.4.1 Percutaneously Placed Valve Testing*

In vivo testing of transcatheter valves (TCV) generally occurs in one of two animal models: ovine or swine. These animals have vasculature and major vessels that are similar in sizes and structures to humans and are fairly robust in recovering from cardiac procedures. The most common type of TCV undergoing testing in today's market is the transcatheter aortic valve, which will be referenced throughout this section. These valves can be implanted from several access points: femoral, direct aortic, and/or brachiocephalic.

The main considerations when choosing an animal model for TCV testing are the anatomical measurements of the structures in and around the vessel surrounding the valve of interest. For instance, when implanting a transcatheter aortic valve, the diameter of the annulus of the native valve is of utmost importance. If the TCV is placed in an annulus that is too small, the TCV is considered "oversized" and will not function properly, as the valve leaflets will not be able to fully expand and may have redundancies. This can cause non-physiological stresses thereby impacting gradients and possible leaflet prolapse. If the TCV is placed in an annulus that is too large (i.e., the valve is "undersized"), it may not seat appropriately as the frame will not have sufficient contact with the surrounding anatomy. The result can be paravalvular leak and/or valve migration, both of which have very serious consequences. The annular diameter of different breeds of swine can vary greatly relative to the heart size, making it critical to understand the anatomical measurements of each breed before choosing a model to implant and/or anatomic assessments of a given animal prior to use.

Another critical anatomical considerations when implanting an aortic TCV are the locations/ heights of the coronary artery ostia with respect to the commissures of the native and implanted valves, as occlusions of the coronary arteries can result in sudden cardiac death. The left coronary ostium heights in animals are much lower than that seen in humans (~9 vs. ~17 mm, respectively). For this reason, prescreenings of animals are essential to understanding the landing zones for the intended TCV implantation.

In vivo imaging techniques, such as echocardiography and computed tomography (CT), are commonly used to prescreen animals prior to implantation. While echocardiography can be used to prescreen and measure certain areas of interest

(e.g., annular diameter) for more critical analysis of the associated cardiac anatomy, the use of contrast-enhanced CT screening is considered the most accurate, providing an effective way to look at a number of factors that can impact the relative fit and function of a valve prior to implantation. Anatomical prescreening enables the selection of the best candidate in terms of device fit, which will allow for the best function and evaluation of the test device. Some of the measurements that are made during prescreening in an animal model include the following: annulus diameter, sinotubular junction height, sinotubular junction diameter, basal plane to brachiocephalic height, and coronary artery height and depth.

As discussed in Sect. 18.2.2.2, the relative growth rate of the recipient animal must be considered when choosing the correct model for TCV implantation. For example, the implantation of a TCV in the aortic position in a juvenile swine model for more than 60 days could mean that the animal would likely outgrow the device, thereby compromising the results for device fit and function. Consequently, if a juvenile swine model is preferred over another species for annular diameter purposes, the time duration of the proposed study should be carefully considered, as means to minimize the possibility of the subject outgrowing the prosthesis. In general, preferred duration for animal testing of a TCV is to perform a 140-day study to prove safety and efficacy in the intended implantation site for new devices, per ISO 5840 Parts 2 and 3. Because a great deal of healing occurs within the first 90 days of implantation, a 90-day study is becoming a possibility in some cases, depending on the opinion of the pertinent regulatory body.

Humans requiring aortic TCV replacement often elicit severe cases of aortic stenosis. They generally occur in elderly patients (80+ years); however, in 2019, the FDA expanded aortic TCV replacement to patients who are at low risk for surgery thereby decreasing the mean age. In patients with calcific aortic stenosis, the leaflets of the native valve are highly calcified, meaning they are covered in a rigid, often bulbous crust. Importantly, it is this crust that actually helps to anchor the TCV frame by providing some resistance to migration. The animal models that are used to test TCVs are generally young and healthy, meaning their aortic leaflets are not calcified and this aforementioned resistance to migration is not present, for anchoring assistance. Nevertheless, there are other mechanisms present in these animal models that can assist in the successful implantation of TCV replacements, including the septal wall muscle shelves found in both swine and ovine models. This helps to keep the device in place long enough for some ingrowth of surrounding tissue (pannus) to secure the device.

While there are many trade-offs that need to be considered when selecting the appropriate animal model for TCV testing, recoverability and manageability of the animal postimplant in a chronic procedure should be taken into consideration. If the animal cannot tolerate an invasive procedure, desired results will not be achievable, in spite of a good device fit.

### *18.4.2 Surgically Placed Valve Testing*

When selecting the appropriate animal model to use for the surgical implantation of replacement valves, there are three main considerations that need to be addressed:

1. The materials used in the valve design, i.e., mechanical vs. tissue valves.
2. The ability of the species to cope with the invasive nature of cardiac surgery.
3. The ability of the bioprosthesis to fit in the anatomical location of interest.

Historically, surgically implanted valves undergoing preclinical trials were ball and cage, tilting disk, or bileaflet mechanical valve designs. Due to their robust nature, sheep were preferred as the preclinical model in these studies. However, studies to determine chronic performance and biocompatibility of devices, such as the Medtronic Parallel™ valve, showed poor correlations of thrombus formation between preclinical and clinical trial data [24]. The resulting investigations into these phenomena presented data that suggested platelet activity in the ovine model was considerably lower than that of humans [25]. This inspired researchers to overcome the limitations involved with using swine in surgical implantation procedures, predominantly the incidence of postoperative arrhythmias and high rates of thrombus formation [22]. However, the long-term assessment of surgically implanted mitral replacements in swine was inhibited by the need for high levels of anticoagulation treatment, individualized to each subject. In addition to distorting the recorded data, these high levels of blood thinners resulted in a greater instance of hemorrhagic complications [19].

The introduction of tissue valves shifted the requirements of how the preclinical animal model reacted to an implanted prosthesis. As previously mentioned, thrombus formation associated with the two valve designs is considerably different. Additionally, the need to assess the calcification of tissue valve leaflets drew researchers back to the ovine model [26]. Finally, thrombus formation concerns have been allayed with data from Sato et al., suggesting that when considering platelet activity in a dynamic rather than static model, sheep provide a satisfactory medium for the study of blood compatibility with implanted prostheses [27].

As with transcatheter-delivered valves, both ovine and swine models have and continue to be used for the in vivo testing of implanted replacement valves. This is largely due to the favorable anatomical features of these two species. However, when considering new surgical valve replacement therapies, the ability of the surgeon to access the valve annulus remains as an important factor. When considering the surgical approach to the aortic valve, the length of the ascending aorta must be considered. This anatomical dimension is much greater in a human than in a swine or ovine model (~110 vs. ~40 vs. ~30 mm, respectively); therefore, when trying to implant a surgical aortic valve, the space for an aortotomy for placement of the valve is limited. In cases where the incision is too close to the valve annulus, the implanted valve will interact with the incision resulting in severe bleeding and irritation to the surrounding vasculature. As noted above, the large atria in the ovine model facilitate access to study both mitral and tricuspid valves therapies.

## 18.5 Good Laboratory Practice and FDA Submission

It is important to note that the FDA strongly encourages that data from preclinical laboratory studies is collected in accordance with 21 CFR Part 58, the Good Laboratory Practice (GLP) for Nonclinical Laboratory Studies [28]. This document has been created to embody *a set of principles that provides a framework within which studies are planned*, *performed*, *monitored*, *recorded*, *reported and archived* [29]. When considering the preclinical testing of heart valve replacement systems, *GLP helps assure regulatory authorities that the data submitted are a true reflection of the results obtained during the study and can therefore be relied upon when making risk/safety assessments* [29].

In addition to the published documents, the FDA provides a series of recommendations specific to the study design and data collection, analysis, and reporting of valve testing to increase the relevance of any data collected from the GLP studies [25]. Many of these recommendations, such as the chronic study duration, the timing and parameters involved in valve assessment, and the rationale for animal selection and number, have been discussed previously in this chapter.

Once all preclinical animal testing under GLP conditions has been completed, a report of the laboratory tests summarizing all data collected and recommending the clinical safety and performance of the device must be prepared for submission to an unbiased third-party observer (outside auditor). The report must include all details regarding the device being tested and the implant location, the experimental design, details regarding the animal model and individual animal identifications, all data collection and results, and any circumstances that resulted in device failure or deviation from the predefined experimental protocol. Finally, it is strongly recommended that an explanation of how the animal models and medications adequately represent the intended patient population and anticipated clinical experience is provided.

## 18.6 Summary

A well-designed, executed, and reported preclinical animal testing protocol addresses the factors required to predict the safety and efficacy of clinical use of a novel valve repair or replacement therapy. This is achieved by completing a series of GLP studies in a sufficient number of animals of the same species, and preferably the same gender and age, receiving both experimental and control devices. The number of studies is best determined based upon the risk analyses of the device(s) and the statistical significance sought by the experimental design. The duration of the preclinical experiment design is typically specified in accordance with the parameter under investigation, and each animal must undergo a macroscopic and microscopic postmortem examination.

Common goals of a preclinical study are to report the following:

- Any detectable pathological consequences around the device implant or in the major organs of the body.

- Any macro- or microscopically detectable structural alterations in the device itself.
- Histological assessment of any thromboembolic material, inflammatory reactions, or degenerative process.
- Fit and function of the implanted prosthesis.

The FDA requires that every invasive device used clinically today has been tested in a large animal model prior to the use of clinical trials, and it is generally considered that the continued use of animal models will ensure the successful development of the next generation of valve therapies.

## References

1. NIH Publication Number 08-6436. Medical research with animals. Available at: https://grants.nih.gov/grants/policy/air/AnimalResearchFS06.pdf
2. National Research Council (2011) Guide for the care and use of laboratory animals, 8th edn. National Academies Press, Washington, DC. https://doi.org/10.17226/12910
3. Bianco RW, Gallegos RP, Rivard AL et al (2009) Animal models for cardiac research. In: Iaizzo PA (ed) The handbook of cardiac anatomy, physiology, and devices, 2nd edn. Springer, New York, pp 147–158
4. Power JM, Raman J, Byrne MJ et al (2005) Efficacy of the Acorn cardiac support device in animals with heart failure secondary to high rate pacing. Heart Fail Rev 10:117–123
5. McGinley JC, Berretta RM, Bratinov GD et al (2005) Subvalvular alterations promote increased mitral valve regurgitation in progressive dilated cardiomyopathy. J Card Fail 11:343–350
6. Su-Fan Q, Brum JM, Kaye MP et al (1984) A new technique for producing pure aortic stenosis in animals. Am J Phys 246:H296–H301
7. Rogers WA, Bishop SP, Hamlin RL (1971) Experimental production of supravalvular aortic stenosis in the dog. J Appl Physiol 30:917–920
8. Taylor DE, Whamond JS (1975) A method of producing graded stenosis of the aortic and mitral valves in sheep for fluid dynamic studies. J Physiol 244:16P–17P
9. Kunzelman KS, Linker DT, Sai S et al (1999) Acute mitral valve regurgitation created in sheep using echocardiographic guidance. J Heart Valve Dis 8:637–643
10. Hill AJ, Iaizzo PA (2009) Comparative cardiac anatomy. In: Iaizzo PA (ed) The handbook of cardiac anatomy, physiology, and devices, 2nd edn. Springer, New York
11. Michaëlsson M, Ho SY (2000) Congenital heart malformations in mammals: an illustrated text. Imperial College Press, London/River Edge
12. Evans HE (1993) The heart and arteries. In: Miller ME, Evans HE (eds) Miller's anatomy of the dog, 3rd edn. Saunders, Philadelphia, pp 586–602
13. Sands MP, Rittenhouse EA, Mohri H et al (1969) An anatomical comparison of human pig, calf, and sheep aortic valves. Ann Thorac Surg 8:407–414
14. Grehan JF, Hilbert SL, Ferrans VJ et al (2000) Development and evaluation of a swine model to assess the preclinical safety of mechanical heart valves. J Heart Valve Dis 9:710–719. discussion 719–720
15. Barnhart GR, Jones M, Ishihara T et al (1982) Bioprosthetic valvular failure. Clinical and pathological observations in an experimental animal model. J Thorac Cardiovasc Surg 83:618–631
16. Salerno CT, Droel J, Bianco RW (1998) Current state of in vivo preclinical heart valve evaluation. J Heart Valve Dis 7:158–162
17. Lee JC, Taylor FN, Downing SE (1975) A comparison of ventricular weights and geometry in newborn, young, and adult mammals. J Appl Physiol 38:147–150
18. Hughes HC (1986) Swine in cardiovascular research. Lab Anim Sci 36:348–350

19. Fox JG (2002) Laboratory animal medicine, 2nd edn. Academic Press/Elsevier, San Diego
20. Flameng W, Meuris B, Yperman J et al (2006) Factors influencing calcification of cardiac bioprostheses in adolescent sheep. J Thorac Cardiovasc Surg 132:89–98
21. Gross DR (1985) Animal models in cardiovascular research. Nijhoff, Boston
22. Gallegos RP, Nockel PJ, Rivard AL et al (2005) The current state of in-vivo pre-clinical animal models for heart valve evaluation. J Heart Valve Dis 14:423–432
23. http://www.fda.gov/medicaldevices/deviceregulationandguidance/guidancedocuments/ucm193096.htm#12. Accessed 25 July 2012
24. Bodnar E (1996) The Medtronic Parallel valve and the lessons learned. J Heart Valve Dis 5:572–573
25. Goodman SL (1999) Sheep, pig, and human platelet material interactions with model cardiovascular biomaterials. J Biomed Mater Res 45:240–250
26. Barnhart GR, Jones M, Ishihara T et al (1982) Failure of porcine aortic and bovine pericardial prosthetic valves: an experimental investigation in young sheep. Circulation 66:I150–I153
27. Sato M, Harasaki H (2002) Evaluation of platelet and coagulation function in different animal species using the xylum clot signature analyzer. Am Soc Artif Intern Organs J 48:360–364
28. https://www.ecfr.gov/current/title-21/chapter-I/subchapter-A/part-58. Accessed 28 Oct 2021
29. http://www.mhra.gov.uk/Howweregulate/Medicines/Inspectionandstandards/GoodLaboratoryPractice/Structure/index.htm. Accessed 25 July 2012
30. Iaizzo PA (ed) (2010) The handbook of cardiac anatomy, physiology, and devices, 2nd edn. Springer Science & Business Media, p 397

# Chapter 19
# The Preclinical Uses of Isolated Heart Models and Anatomic Specimens as Means to Enhance the Design and Testing of Cardiac Valve Therapies

**Emma A. Schinstock, Michael D. Eggen, and Paul A. Iaizzo**

## Abbreviations

| | |
|---|---|
| CT | Computed tomography |
| MRI | Magnetic resonance imaging |
| VR | Virtual reality |

## 19.1 Introduction

An intricate understanding of human cardiac anatomy remains one of the most important fundamentals for both cardiovascular medicine and the cardiac device industry [1, 2]. The successful deployment and performance of cardiac valve therapies is often impacted by the ability of the device to adapt to the anatomic landscape within the heart, specifically the anatomical variations that may exist for given human cardiac structures. Further, with transcatheter therapies, one also needs to understand optimal individualized delivery pathways and approaches. In other words, a well-developed understanding of the relevant cardiovascular anatomies (in relation to both vascular approaches and within the heart itself) is critical at all levels of device design and development processes [3–5].

E. A. Schinstock, MS, PhD (✉)
Medtronic Inc.,, Minneapolis, MN, USA
e-mail: schin139@umn.edu

M. D. Eggen, MS, PhD · P. A. Iaizzo
Visible Heart® Laboratories, Department of Surgery, Institute for Engineering in Medicine, University of Minnesota, Minneapolis, MN, USA
e-mail: michael.d.eggen@medtronic.com; iaizz001@umn.edu

© The Author(s), under exclusive license to Springer Nature Switzerland AG 2023

P. A. Iaizzo et al. (eds.), *Heart Valves*, https://doi.org/10.1007/978-3-031-25541-0_19

The study of both fixed and reanimated human hearts, using the various methodologies described here, has provided vital insights as to the details of human cardiac anatomies. The Visible Heart® methodologies have provided a unique perspective on functional cardiac anatomies. By reanimating human hearts not deemed viable for transplant, we have been able to visualize functional anatomies using a variety of imaging modalities, including endoscopes placed directly within the various heart chambers and/or within the large diameter vessels. This database of images exemplifies the large degree of variability that exists in all four human valve and chamber anatomies, from both a static and functional perspective [6]. Additionally, such imaging techniques allow one to better visualize anatomical alterations that occur with various pathologies and/or those that may occur following the deployment of devices into various positions within the heart. The unique combinations of direct visualization using endoscopic cameras with relevant clinical imaging has further allowed researchers and physicians the capabilities to fully understand the implications of a large variety of device implantations.

The recent advances in intracardiac interventions have increased the need for an even greater understanding of the anatomical complexities of the given human heart prior to the respective procedure. The utilization of technologies such as transcatheter valve replacement is expected to further intensify as clinicians become more comfortable with the delivery of novel devices within beating hearts and outcomes continue to show positive results. This is highlighted today by the highly competitive field of transcatheter aortic valve implants and the emerging field of transcatheter atrioventricular valve repairs and replacements, where competing designs attempt to provide the most effective treatment in a package that enables physicians to administer the advanced therapy comfortably and reliably with less trauma and improved outcome for the patient. Consequently, it becomes more critical than ever for device developers to have a thorough understanding of the following: (1) the variations of cardiac valve anatomies that will occur in the patient populations they treat and (2) the results they obtain from in vitro and in vivo testing of next generation therapies.

This chapter will discuss the multiple uses of anatomical specimens and isolated heart preparations as important methods to provide an educational foundation in the fields of cardiac valve design, development, and deployment.

## 19.2 Anatomical Specimens and Static Imaging

Throughout history, anatomists such as Galen, Vesalius, da Vinci, and more recently Hunter, Gray, and Netter have recreated their knowledge gained from the dissection of animal and human cadavers in elegant treatises. With the advent of high-resolution noninvasive imaging in the past century, understanding of the functional internal anatomy of the human body has progressed rapidly. Most recently, the field of cardiac anatomy has undergone a shift to correct the perceived orientation of the organ's anatomical features to align with the overall anatomy of the human

body—attitudinally correct anatomy [7]. This shift has been driven by the need for anatomists, surgeons, radiologists, cardiologists, echocardiographers, and biomedical engineers to be able to communicate using common anatomical terms. Refer to Chaps. 1 and 2 for specific descriptions of the anatomy and morphology of the cardiac valves.

Combined with the advances in anatomical nomenclature, there have also been major advances in the preparation of anatomical specimens for research. The techniques for embalming bodies date back to the ancient Egyptians as part of the ritual preparation of their deceased kings for burial. However, through the ages, human cadavers used for medical dissections were not typically preserved in embalming solutions. In the mid-nineteenth century, the discovery of glutaraldehyde and formaldehyde allowed for the complete preservation of cadavers. Such preparation techniques extended the periods of time that anatomists could study a particular specimen and increased their integrations into anatomical classes for medical education. However, the fixation of the heart within the body as prepared for an anatomical study typically preserves the myocardium in a state of rigor; usually with the various heart chambers collapsed and potentially full of clotted materials (blood). In 1978, researchers at the Mayo Clinic in Rochester, Minnesota, adapted a formalin pressure perfusion system used in the study of pulmonary disorders to prepare hearts for anatomical studies [8, 9]. However, this reported technique was time-consuming and did not become more commonly used until Thomas and Davies reported the use of a simple apparatus to allow for the perfusion fixation of fresh cardiac specimens [10]. This technique has since been used extensively over the years by leading cardiac morphologists, such as Robert Anderson [11], and was adopted by the Visible Heart® laboratories as the preferred method of preparation for the cardiac specimens for many years [5]. However, more recently, a newer system for formalin fixation has been developed and utilized to better preserve the valvular structures within the human hearts stored in the Visible Heart® specimen library [12]. This new system utilizes multiple pressure heads to elicit physiologic pressure differences across the atrioventricular valves and the semilunar valves. Figure 19.1 illustrates the mechanisms for dilated fixation with valve coaptation.

## 19.3 The Visible Heart® Human Specimen Library

Our laboratory has the privilege to obtain fresh human heart and heart-lung bloc specimens for educational and research purposes from the following: (1) organ donors whose hearts are not deemed viable for transplantation and are donated for research (via LifeSource, the Upper Midwest Organ Procurement Organization) and (2) bodies donated to the University of Minnesota's Anatomy Bequest Program. After excision, these fresh, unfixed specimens are subsequently carefully dissected and then perfusion fixed in 10% buffered formalin by first attaching the cannulated aorta and pulmonary artery of each heart to the system previously described, to pressurize the chambers of the heart as well as maintain pressure differences across

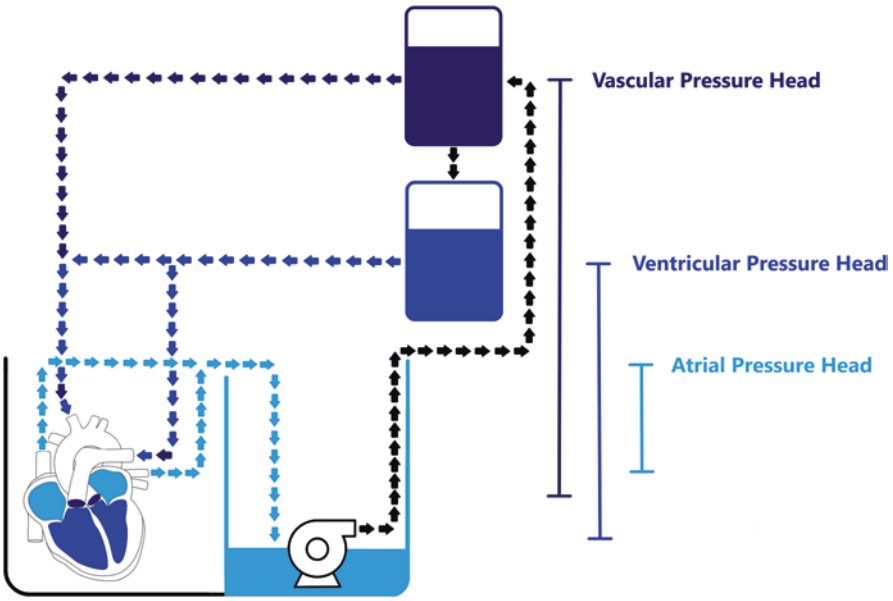


**Fig. 19.1** Each reservoir pressurizes the corresponding area of the heart: the vascular pressure head pressurizes the pulmonary artery and aorta at approximately 70–90 mmHg, the ventricular pressure head pressurizes the ventricles at approximately 30–40 mmHg, and the atrial pressure head pressurizes the atria at approximately 10–15 mmHg

the valves. This technique fixes the hearts in an approximation of the end-diastolic state, providing unique insights into the anatomical dimensions of a given specimen. Figure 19.2 demonstrates images that can be acquired from these specimens and shows some of the valve pathologies that can be subsequently visualized.

To date, our library of more than 830 hearts continues to provide researchers with the ability to gain insights into how potential valve therapies/technologies may interact with the surrounding cardiac anatomies. In addition to anatomical investigations, this library of real specimens allows for the placement of prototype devices and the rapid comparison of how given devices may interact with the surrounding cardiac anatomies in a variety of human anatomies, both diseased and normal [13, 14]. Fresh cadaver hearts received by the Visible Heart® laboratory are documented at each stage of the acquisition process to record any global anatomical changes during the fixation process, such as tissue weight and overall dimensions. Images of the fresh preparation and more recently 3D external object scans (using a Artec Space Spider object scanner), the resulting fixed specimen and the nondestructive imaging of one specimen from the library (adapted from the Atlas of Human Cardiac Anatomy [15]), can be seen in Fig. 19.3. When available, the medical history of each specimen's donor and their specific pathologies is stored in a de-identified database which allows researchers to evaluate therapies and devices in a specific patient population.

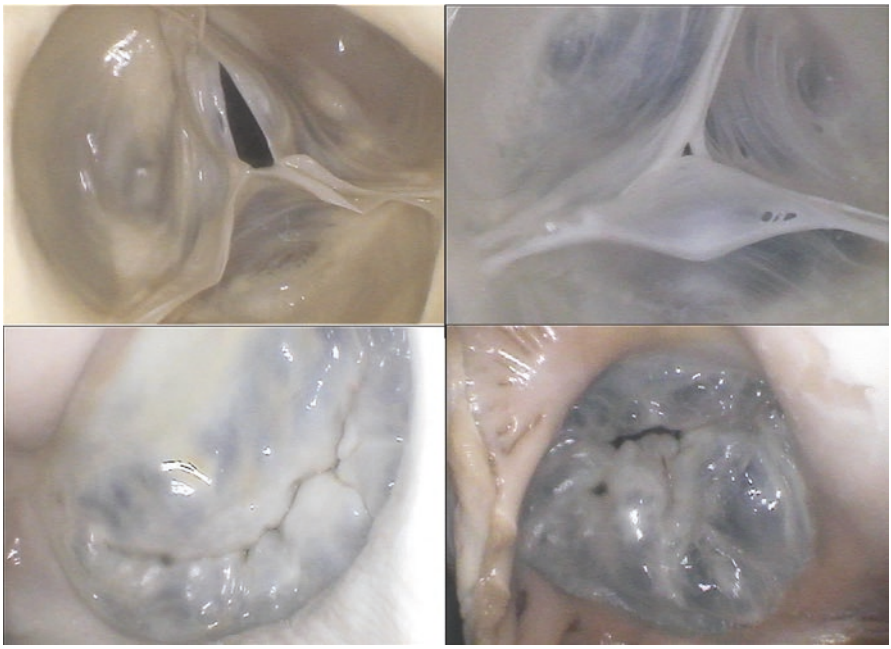

**Fig. 19.2** Images from perfusion fixed hearts from the Visible Heart® Laboratory's library: (1) calcified aortic valve (upper left panel), (2) pulmonary valve (upper right panel), (3) mitral valve (lower left panel), and (4) tricuspid valve from the right atrium (lower right panel)

Recent advances in high-resolution noninvasive cardiac imaging have fostered extensive work in the in vivo analyses of anatomical variations from patient to patient using a variety of imaging modalities:

1. Cardiac ultrasound (e.g., transthoracic, transesophageal, intracardiac, 2D, 3D, and/or 4D) [16]
2. Computed tomography (CT) [17]
3. Microcomputed tomography (μCT)
4. Multi-slice computed tomography [18]
5. Magnetic resonance imaging (MRI, e.g., 1.5T, 3T, or greater; diffusion tensor, DTMRI) [19]

Nondestructive imaging of specimens from the Visible Heart® library via photography, object scans, ultrasound, CT, μCT, and MRI has been used to collate a digital database of these hearts for educational and research purposes. The perfusion fixed specimens are typically prepared for scanning by suspending them in an agar gel medium, allowing for a full complement of multimodal imaging to be performed on the hearts without changing the orientation [20]. Obtaining high-resolution images has allowed for detailed analyses of cardiac anatomies for a variety of both

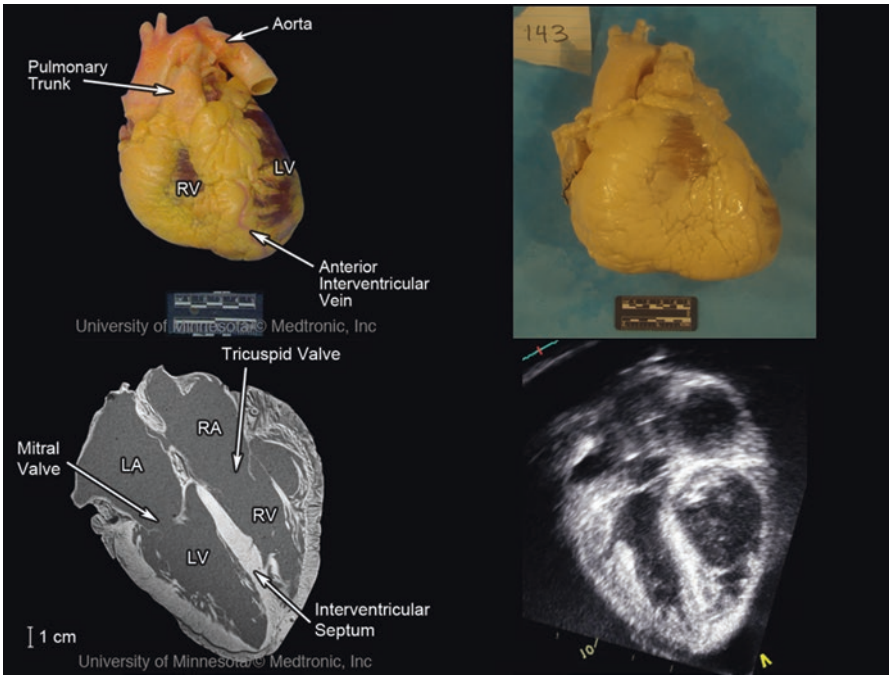


**Fig. 19.3** Images of a heart received by the Visible Heart® library and imaged fresh (upper left panel), after perfusion fixation (upper right panel) and scanned in a 3T Siemens MRI scanner (bottom left panel) and GE Vivid I ultrasound (lower right panel) in the four-chamber long-axis view. (Modified from the Atlas of Human Cardiac Anatomy [15])

normal and pathologic specimens; many of these high-resolution images are considered not possible with available clinical imaging protocols. In addition to studying the clinically accepted images, virtual models can be created from the preserved hearts and studied or 3D printed to highlight or explore specific anatomy: e.g., used to develop mixed reality educational modules. These virtual models can also be implemented into simulated environments to investigate the anatomy's effect on hemodynamic or electrical properties.

Such studies that use fixed specimen data have included studies on anatomic variation [21], digital anatomy measurements [22, 23], and the effects of anatomy on hemodynamic parameters [24] and the analyses of fiber orientations of specimens obtained from patients in end-stage heart failure, using DTMRI [25]. Such studies have shown the breadth of research these fixed specimens are invaluable for.

It has also been possible to compare the ability of different imaging modalities to assess the anatomical characteristics of specific cardiac pathologies, such as aortic stenosis, thus building on the work of other researchers [26].

## 19.4 In Vitro Isolated Heart Models

A comprehensive understanding of the cardiac valve anatomy provides device designers with fundamental information regarding the anatomical dimensions and variations of the environment into which the device or therapy will be delivered. However, these static human heart specimens do not address the complications surrounding the delivery and function of a device or therapy in a beating heart. Before embarking upon complex and expensive chronic animal testing protocols which are required to prove the efficacy of novel prosthetic valves, there is exceptional value in testing cardiac devices in reanimated beating heart models. Our laboratory at the University of Minnesota has reanimated over 2000 large mammalian hearts (canine, ovine, swine, mini-pigs, and human) for such studies in the last two decades. There have been several other academic institutions and private companies that have developed in vitro large mammalian heart models, with many groups effectively developing systems based upon the mechanical reanimation of cadaveric large mammalian hearts. For example, Richards et al. were able to consistently and reliably quantify mitral regurgitation across a range of severities in explanted porcine hearts and investigate the efficacy of various repair techniques [27]. Further, two other groups have succeeded in studying the electrophysiology of explanted human hearts by sustaining the heart with a pressurized coronary flow of oxygen saturated salt solution via Langendorff perfusion [28, 29]. However, it should be noted that the true "reanimation" of large mammalian hearts (whereby the heart functions independently of any mechanical or electrical assistance) has only been achieved by a small number of research groups. Araki et al., Nagoya University, Japan, reported that they were able to complete optical and hemodynamic analyses of cardiac valves in reanimated swine hearts [29]. Weger et al., at the Leiden University Medical Center, Netherlands, have monitored transcatheter valve implantations in reanimated swine hearts using their described *PhysioHeart system* [30]. However, it should be noted that in both of these aforementioned preparations, the researchers were limited by the amount of time the heart remained viable, a factor considered key to the accessibility of the heart for device testing. Transmedics® has created the first and only FDA-reviewed heart perfusion system for clinical use. Their system aims to increase the time a human heart is viable for transplant by utilizing Langendorff perfusion to decrease the ischemic damage to the myocardium. However, this system does not retain the full physiologic functions of the heart and is only useful for transportation purposes [31].

As noted above, the Visible Heart® laboratories partnered with Medtronic, Inc. in 1997 to develop the Visible Heart® methodologies which consist of a large mammalian isolated heart model that can be controlled to function in either Langendorff [32], right-side working, or four-chamber working modes [33, 34]. Over this time and continuing today, we have been developing/optimizing these systems for reanimating hearts whereby isolated large mammalian hearts are perfused and then actively pump a clear crystalloid perfusate in the place of blood. Further modifications have allowed us to fully submerge the heart in saline or buffer to collect

external electrical signals from the heart for electrical mapping or arrythmia identification (e.g., using external mapping catheters or a Medtronic CardioInsight non-contact mapping system). External images of a human heart connected to the Visible Heart® apparatus can be seen in Fig. 19.4. This approach has allowed our group to visualize what occurs inside the heart during device deployment procedures and subsequently to determine how such devices interact with the specific anatomies of the heart throughout all the phases of the cardiac cycle. Further, we can visualize how variations in human valvular anatomies can play a critical role in such: e.g., our laboratory recently described that in a large percentage of human hearts, the right atrioventricular valve is actually quadricuspid with additional papillary muscles [21].

Briefly, our approach includes the initial step of removing hearts from humans or animals using standard cardioplegia procedures [33, 34]. Once isolated, cannulae are inserted into the great vessels allowing the placement of endoscopes or devices into all four working chambers as well as the connection of the vessels to perfusion pathways (a double bypass system with preload and afterload chambers). Following reanimation, cardiac and systemic pressures and outputs can be monitored and preloads and afterloads adjusted accordingly to simulate systemic vascular pathologies such as hypertension. Additionally, the isolated heart apparatus allows researchers to quickly switch the perfusion system to operate in Langendorff, right-side working, or four-chamber working modes. During the Langendorff mode, the left-side afterload is held constant with a coronary perfusion pressure of approximately 90 mmHg [33]; thus, the flow through the coronaries is determined by dilation or constriction of the coronary arteries. Right-side working mode combines Langendorff retrograde aortic perfusion with antegrade, or physiologic, flow through the right atrium and right ventricle with a preload range of 5–40 mmHg, with normal or augmented cardiac outputs. During four-chamber working mode, the flow through a heart is normally determined by its intrinsic heart rate, preloads, afterloads, and the relative contractilities of the various heart chambers. By controlling the orientation of the heart in our apparatus and determining the preload and afterload pressures exerted on the specimen, we can recreate specific cardiac states. Interestingly, the intrinsic heart rate and hemodynamic performance can be modified by altering the temperature of the buffer or by adding pharmacological agents

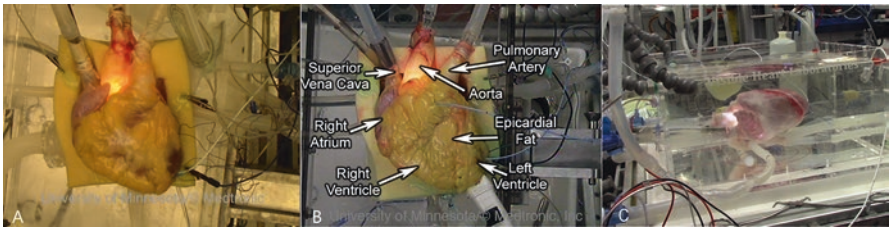


**Fig. 19.4** Images of a human heart connected to the Visible Heart® apparatus from an approximation of the anterior-posterior aspect (**a**) and from the left anterior oblique aspect (**b**) and an image of a fully submerged swine heart from the right oblique aspect (**c**)

(e.g., catecholamines or anesthetics), which are discussed later in this chapter [35]. The buffer can also be altered to more closely mimic the viscosity of blood to allow researchers to more accurately examine the flow through devices or anatomies. Although no model can perfectly mimic in vivo conditions, to date our apparatus has allowed researchers to simulate a broad range of particular physiological environments that are observed in various clinical settings and study numerous device-tissue interactions.

In addition to reanimated hearts, the Visible Heart® methodologies can also be modified slightly and utilized for the perfusion of fixed specimens. Although no intrinsic heartbeat is observed in these models, as noted above, the anatomical information can be invaluable to device designers and physicians. For example, interventional cardiologists have placed stents in diseased coronary arteries of perfusion fixed hearts in a study that imaged all stages of a bifurcated stenting procedure [36].

## 19.5 How Can an Isolated Heart Prep Augment and Compliment Benchtop Testing?

The combination of a "live" functional anatomy within a controlled "benchtop" experimental setting provides a unique stepping stone between in vitro preclinical device testing and in vivo implantations required for implantable medical devices. Figure 19.5 shows how the typical stages of device testing and development compare in terms of the relevance of the testing environment to the intended functional environment and the relative cost of performing such investigations. It can easily be observed that as the relevance of a particular testing methodology increases, the relative costs will dramatically increase. It is also noteworthy that as cost increases, the likely number of possible iterations decreases. Consequently, any possible

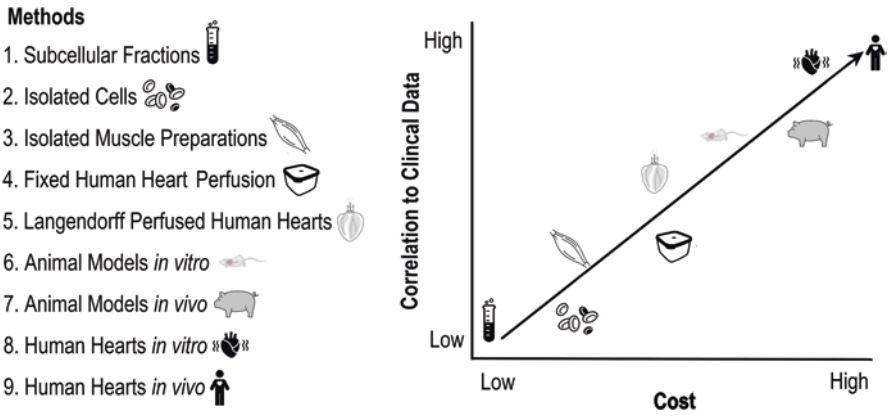


**Fig. 19.5** The relationship between cost and correlation to clinical data of multiple methods of model preparation

augmentations to device testing prior to chronic animal implants (e.g., via isolated beating heart preps) can, in turn, greatly reduce the overall product development costs and speed clinical uses of novel valve repairs, implants, and/or their associated delivery systems.

A variety of conditions and augmentations can be evaluated in a single heart on an isolate preparation. Heart performance and perfusion characteristics can be changed effortlessly using methods such as pharmacologic delivery, pressure manipulations, manual tissue manipulations, and electrical interventions. These changes should always be related back to in vivo models, however. For example, let us consider accelerated wear testing and fatigue testing which are required gold standards for the assessment of cardiac valve durability (see Chap. 17). As such, in accelerated wear testing, the hydrodynamic conditions are tightly controlled and easily varied, allowing the durability of the valve leaflets to be assessed under a variety of predetermined conditions. Similarly, the boundary conditions imposed on the valve frame or commissure posts during fatigue testing can assess frame durability. Isolated heart preparations, including the Visible Heart® methodologies, will never replace these forms of testing, but unique information regarding the device-tissue interactions in the latter, can be observed in real time using multimodal imaging. It should be noted that since the hydrodynamics of isolated heart preparations are typically less aggressive environments than what is experienced during accelerated wear testing, the boundary conditions observed for a device in such studies are not always directly transferable to accelerated wear testing test fixtures. Yet on the other hand, they can serve as means to obtain additional information to ascertain the validity of any boundary conditions within the accelerated testing protocol. More specifically, in fatigue testing, the frames should be tested to the anticipated worst-case conditions, which would not likely be observed using our Visible Heart® apparatus. Nevertheless, observations from this in vitro approach, in which the implanted device can be directly visualized, have helped to ensure that all forms of boundary conditions have been considered. Most importantly, such experimentation has provided us with a so-called physiological link between benchtop testing of devices and in situ or in vivo, acute or chronic preclinical animal testing. In other words, acute phenomena observed during accelerated wear testing and the insights gained with both invasive and noninvasive imaging techniques in animal studies may be directly observed during a valve implant study in vitro. For example, a procedural issue observed under fluoroscopy during an in vivo animal implant could be recreated by employing the Visible Heart® approach (under direct visualization) with simultaneous fluoroscopy, thus gaining a better understanding of potential adverse issues. We consider that having the Visible Heart® apparatus as a tool for device design has allowed us to obtain a more rapid understanding of phenomena observed in both benchtop and preclinical settings; as such, it is an invaluable tool for a device designer, especially at the early stages of development, ideation, and prototype testing.

## 19.6 The Importance of Species Selection in In Vitro Cardiac Valve Research

The ultimate utility of studies performed with Visible Heart® methodologies, such as transcatheter valve development, is in part determined by the heart chosen for reanimation. We suggest that the criteria for species selection for acute in vitro studies are slightly different from those for chronic valve assessments (Chap. 16) due to the elimination of all systemic factors that may contribute to device performance. In other words, the species of the donor can be chosen specifically for its relative cardiac anatomies, such as valve sizes rather than for factors such as thrombogenesis, immune response, and/or growth rates.

For years, the canine heart has been used for such experimentation and has provided useful information. Yet, it should be recognized that canine hearts have an unusually large amount of collateral coronary circulation (similar to humans in end-stage chronic heart failure), and this in turn results in the inconsistent creation of ischemic (infarct) regions [37]. Sheep have been historically employed for chronic valve implantation studies, as valve function and valve orifice sizes observed in sheep are very similar to those of a human heart. Additionally, the relatively large atria of the sheep's heart allow for straightforward surgical approaches to the atrioventricular valves. However, it has recently been proposed that swine are an excellent model for acute cardiac device testing, as porcine hearts have very similar anatomies to those of humans with respect to the cardiac valves, conduction system, coronary arteries, and great vessels. Nevertheless, it is important to note that there are some specific variations in animal valve anatomies that should be known; such interindividual and interspecies variations have been extensively researched by Michaëlsson and Ho [38], and other investigators have highlighted the impact of such work in medical device testing [33–37, 39]. For example, when testing aortic valve therapies in the swine model, it should be considered that there are several interspecies differences in leaflet morphologies and coronary ostia positioning, resulting in an increased likelihood of interaction between these two structures [37]. Additionally, in swine, (1) the ascending aorta is typically shorter, i.e., the branch of the brachiocephalic artery and the start of the aortic arch are closer to the aortic annulus than in humans; (2) there are only two primary arteries exiting the arch; and (3) there typically are no plaques present or calcific stiffening of the aorta [37]. Anatomical variations in the mitral and tricuspid valve anatomies are also noteworthy, e.g., there can be primary differences in the number of leaflets and the structures of the subvalvular apparatus. Interestingly, these variations are more often attributed to interindividual differences rather than interspecies variation [37, 38].

Importantly for those interested in transcatheter-delivered valves, the relationship between the various valves themselves and the cardiac conduction system is comparable between swine and human anatomies. Hill et al. have theorized that the interaction between an aortic prosthesis, the mitral valve, and the conduction systems within the interventricular system can be quantified to a reasonable extent in the swine model [23].

Due to their specific anatomical similarities with human hearts and the relative ease of procurement (excision and reanimation), the mainstay of cardiac valve research done in the Visible Heart® laboratory has and will continue to be completed using swine hearts. Nevertheless, as previously mentioned, our laboratory has also had the privilege to obtain fresh human heart specimens for reanimation, for both educational and research purposes. Such hearts, if received in a timely manner and with complete anatomies including the great vessels, have been reanimated using the same methodologies as previously described for swine hearts. By reanimating these hearts using a clear perfusate, visualization of the internal cardiac anatomy has provided novel insights into the relative variations of human cardiac anatomies (in healthy and diseased individuals) and has highlighted the alterations that occur with various pathologies. Finally, this approach provides the unique opportunity to deliver existing or novel devices within functional human anatomies without the concerns and considerations required in clinical trials; thus, it has allowed researchers to garner invaluable knowledge about their device designs that otherwise could not be generated using animal models. It should be noted that our research team were able to recently perform numerous TAVR, coronary bifurcation studies, and post-TAVR PCI studies in human hearts [36, 40, 41].

## 19.7 Understanding and Modulating Heart Function In Vitro

When studying cardiac valves, it is important to understand how the heart functions in both systole and diastole (Chaps. 1 and 2). When working with a specimen in vitro, the performance of the reanimated heart can be influenced by several additional mechanisms. For example, subsequent cardiac function will be compromised by the amount of cell injury that occurs, governed in part by the amount of time between heart explant and reanimation. It is considered that if this period exceeds 6 hours, performance will be compromised, even if the heart is stored under ideal conditions. To reduce such time-associated myocardial injury due to global ischemia, we have investigated the use of cardioprotective agents delivered before explanting the heart [42]. Most recently, we have been investigating the effect of omega-3 polyunsaturated fatty acids administered before explant on the acute function upon reanimation [43]. Utilizing a clear perfusate, one removes all red blood cells; hence, the oxygen delivery capacity is greatly compromised relative to when blood is utilized for reanimation: this in turn causes global ischemia and reduced the length of cardiac viability.

Because of the isolation process, the reanimated heart has no direct parasympathetic or sympathetic innervation and thus is not affected by any signals from the autonomic nervous system. However, pharmaceuticals/hormones such as dobutamine and epinephrine can be administered to the circulating perfusate. These catecholamines work by stimulating the $\beta_1$ receptor on the myocytes, acting as

chronotropes and inotropes, increasing heart rates and contractility and, thus, overall cardiac output. Furthermore, the ionic balance of the circulating buffer can have very dramatic effects; e.g., increasing the calcium $Ca^{2+}$ concentration in the buffer will act as a potent inotrope by increasing the $Ca^{2+}$ inside the cell during the action potential. Thus, frequent buffer changes are also recommended to remove metabolites. We will often utilize such inotropic agents shortly after deploying a valve within an isolated heart to increase cardiac output and ejection fraction and therefore optimize function of the implanted prosthesis. Pharmacologic agents are also often delivered to modulate the function of the heart to simulate specific states. Nitroglycerin is typically introduced into the perfusate to improve myocardium uptake of nutrients through coronary dilation and/or maintain dilation when large amounts of contrast agents are administered [44].

It should be noted that by utilizing our Visible Heart® methodologies, the reanimated heart tissue is alive on the apparatus and the heart rate is driven by the sinoatrial node. However, pacing to ensure a consistent heart rate may be required during an experiment. Additionally, pacing the heart allows for rapid ventricular pacing, a technique often used to reduce cardiac output and wall movement during the implantation of balloon-delivered transcatheter valves.

Several factors indicate heart performance, and experts such as physicians and perfusionists often evaluate several parameters to determine the overall performance of the heart. These parameters include pressure waveforms, ECG waveforms, coronary perfusion, metabolite production, and ventricular contractility. These parameters can be routinely evaluated, and the development of an algorithms to evaluate these parameters and provide a functional score is ongoing in the Visible Heart® laboratories [44].

## 19.8 Comparative Imaging in the Visible Heart® Apparatus

The ability to reanimate, control, and optically visualize human hearts has allowed for the collection of unique videoscopic footage of the functional human heart [40, 41, 45, 46]. By utilizing endoscopic video systems (2.4, 4, and 6 mm videoscopes) in conjunction with clinically relevant imaging modalities, such as fluoroscopy (continuous X-ray), cardiac ultrasound (echocardiography), optical coherence tomography (OTC), and high-speed imaging, we have been able to create novel comparative anatomy footage [23, 36, 39]. This has provided a direct visualization of what the physician would see in the clinical setting and has also provided valuable insights into device and delivery system performance and, in some case, the utilizations of clinical imaging. With recent advances in echocardiography, one can evaluate heart stresses, strains, and flows in real time. In addition, OCT can be used to image small vessels during stenting procedures, including the effects of stenting post-TAVR implantation [40]. Examples of the imaging capabilities of the Visible Heart® methodology within a human specimen can be seen in Fig. 19.6. In addition to video images of the functional anatomies, extensive footage of device

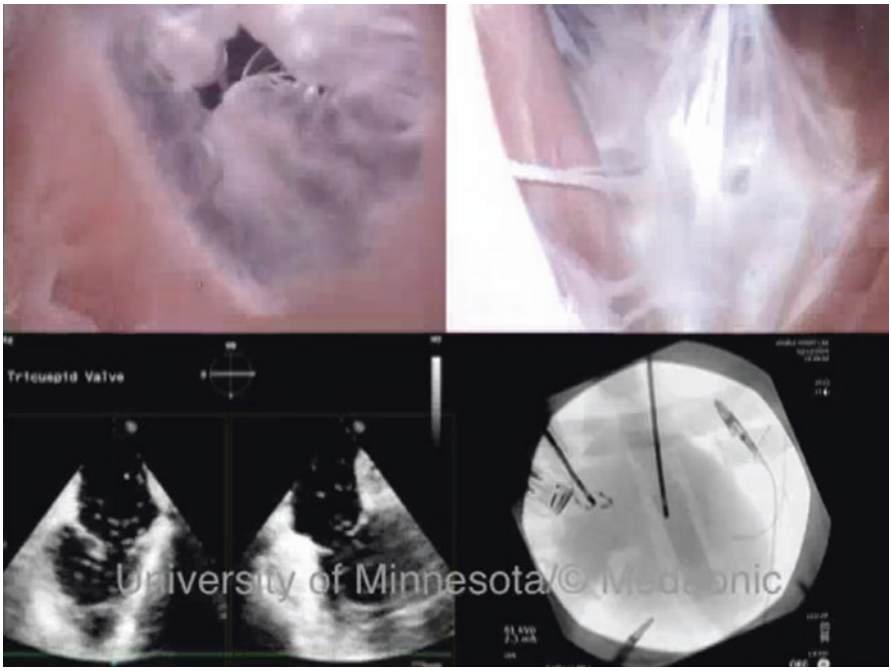


**Fig. 19.6** Unique views of the tricuspid valve within a reanimated human heart imaged using the following: (1) an endoscope placed within the right atrium (upper left panel), (2) an endoscope placed within the right ventricle (upper right panel), (3) fluoroscopy with an anterior-posterior orientation (lower left panel), and (4) ultrasound (lower right panel). (Modified from the Atlas of Human Cardiac Anatomy [29])

implantations has been obtained utilizing Visible Heart® methodologies, including transcatheter-delivered devices to the pulmonary and aortic positions as seen in Fig. 19.7. Such visualization of the delivery of a transcatheter pulmonic valve has provided new information to assist designers in the adaptation of the valve leaflets in the pulmonary position to accommodate the low-pressure gradients that may be encountered in this location [45]. Furthermore, the implantation of transcatheter aortic valve replacements into the native aortic root of human hearts has highlighted the interaction of the frame with native leaflets and the mitral apparatus, thus illustrating the importance of precise frame sizing and positioning in order to avoid interaction with the anterior leaflet of the mitral valve and excessive pressure on the cardiac conduction system [41]. Our laboratory also has performed post-procedure analyses of the performed procedures using both CT and microCT imaging (with resolution down to 20 microns), to study the nuances of the device-tissue interfaces.

Our employed Visible Heart® approach can be used to capture unique internal and/or external images of device implantations at wide ranges of hemodynamic conditions (e.g., left ventricular systolic pressures of 20–120 mmHg). To date, images obtained using Visible Heart® methodologies have allowed for collaborating

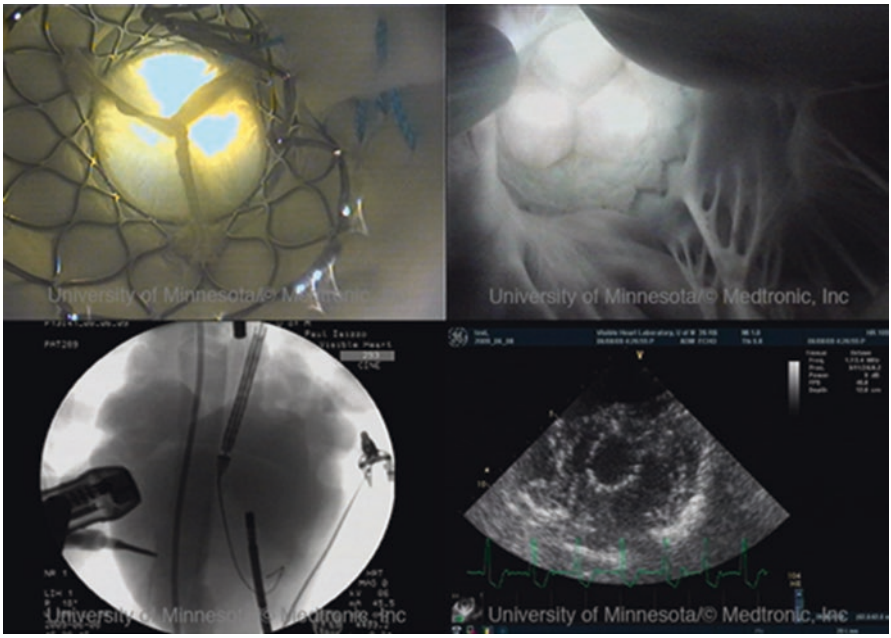


**Fig. 19.7** Images of a transcatheter-delivered aortic valve imaged using the following: (1) an endoscope placed within the ascending aorta (upper left panel), (2) an endoscope placed within the left ventricle (upper right panel), (3) fluoroscopy with an anterior-posterior orientation (lower left panel), and (4) ultrasound (lower right panel). (Modified from Iaizzo et al. [34])

clinicians, engineers, and scientists to evaluate many aspects of transcatheter device design, such as delivery catheters, deployed frame lengths, frame shapes, relative valve attachments, valve in valve implantations, post-TAVR PCI interaction of these devices with native or conduit anatomies, and/or others [36, 40, 41].

## 19.9 A Portable Visible Heart® or "VH Mobile"

Due to the inherent advantages of MRI and CT for assessment of native valve function and anatomy in vivo, it was considered desirable for our group to develop a portable Visible Heart® system which would allow MR or CT imaging of an isolated beating heart through the whole cardiac cycle. Such a portable system would enable physiologic perfusion of an isolated large mammalian heart during simultaneous MR or CT imaging. The full details of the development of a portable apparatus and associated methodologies for isolated heart imaging in CT and MRI environment were described by Eggen et al. [47]. Briefly for MRI studies, one needs to first consider the strong magnetic field in the MR environment that poses specific design challenges; we considered that this required us to construct a two-unit system to

remove all ferromagnetic materials from the proximity of the MR scanner. Yet, the apparatus needs to contain the necessary preload and afterload chambers required for physiological cardiac function (i.e., in Langendorff or four-chamber working modes) and allow for independent controls of the chambers in order to augment the pressure gradients across the valves. Furthermore, for any such system, it should allow for the isolated heart to be placed safely on the patient bed and fit appropriately within the MR or CT scanner (Fig. 19.8).

To date, this mobile approach has been successfully used to obtain MR and CT images in both swine and human hearts (Figs. 19.9 and 19.10) [47, 48]. We consider that some of the advantages of isolating and reanimating a heart within the MRI/CT environment for valve testing with such a portable system include the following:

- High-resolution studies of use conditions or device-tissue interactions (i.e., valve strut or aortic stent deformation) with precise controls over physiological

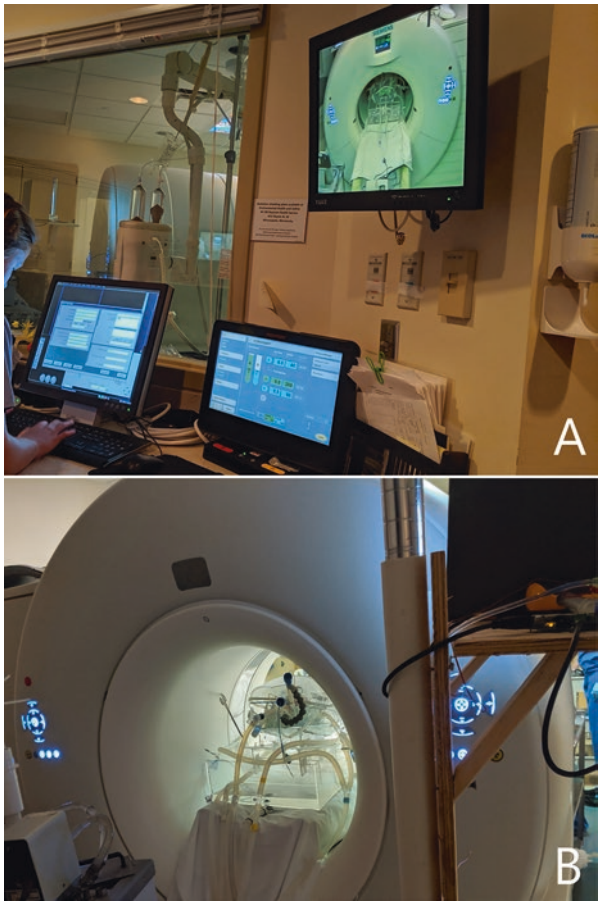


**Fig. 19.8** Portable Visible Heart® apparatus: the capsule and containment system placed within the University of Minnesota hospital CT scanner as seen from the radiologists' control room (**a**) and directly behind the CT scanner (**b**)

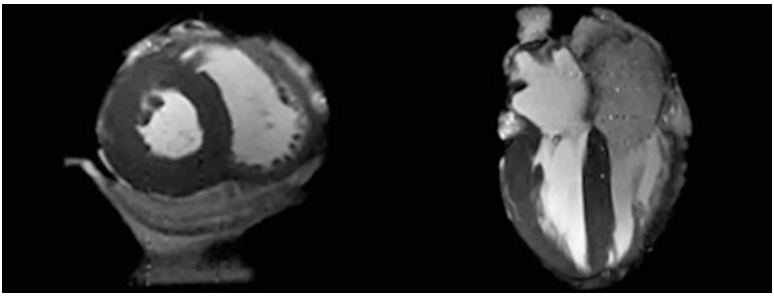

**Fig. 19.9** MRI images obtained from a reanimated human heart placed in a 1.5T MRI scanner: short-axis view (left) and long-axis view (right)

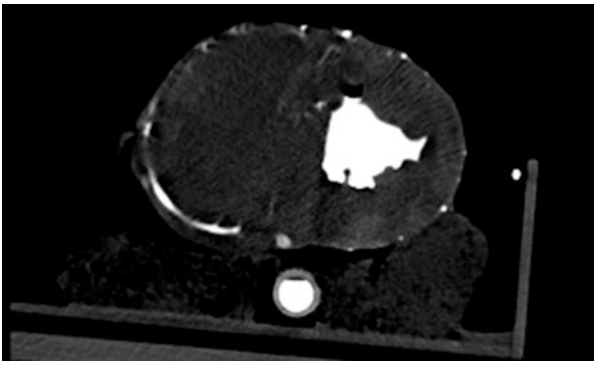

**Fig. 19.10** Contrast-enhanced CT image of an isolated swine heart. The right coronary artery, aorta, and left ventricular endocardium are enhanced

conditions throughout the cardiac cycle. For example, the independently controlled preload and afterload chambers allow pressure across the valves to be changed in order to simulate a variety of disease states, and the effect of the pressure gradients on stented valve deformations can be determined. As such, without the need for breath holds as is required for the intact animal or human scan sessions, image averaging and sequence times can be increased, thereby increasing the ultimate signal-to-noise ratios.

- Comparative imaging. Direct imaging methods (i.e., endoscope) can be subsequently compared to MRI/CT imaging of valve anatomy or interaction with devices as a means to evaluate the best clinical imaging modalities for the desired target variable/interaction of interest. In several cases, we have utilized endoscopes to place devices while the heart has been situated within the CT scanner.
- Multiple device implantation studies can be conducted under endoscopic visualization before analyzing the implantations using MRI/CT imaging without requiring an XRM suite, or combination CT-X-ray surgical suite.
- Virtual reality (VR) scenes can be created to aid in education of cardiac devices as the move within functional anatomies [49].

## 19.10 Limitations of Visible Heart® Methodologies

The Visible Heart® methodologies are not without known limitations. For example, ischemic time prior to reanimation can compromise reanimated cardiac function, specifically contractility and thus pressure generation. Additionally, the lack of a pericardium may contribute to overexpansion of the atrial chambers, slightly different respective anatomical orientations of the great vessels and chambers, and/or differences in contractility compared to in vivo performance; however, it should also be noted that one can isolate these large mammalian hearts for use with the pericardium primarily intact [50]; yet, it is rare to obtain a human heart for reanimation with intact pericardium due to the extensive diaphragmatic connections. Additionally, the relative positioning of a given heart on the apparatus may also affect its overall performance. Furthermore, as noted above, the use of a clear perfusate, without a specific oxygen carrier (i.e., a hemoglobin substitute like a perfluorocarbon), will lead to progressive global ischemia and the development of tissue edema which has effects on the long-term viability of these reanimated hearts. The acellular buffer on the Visible Heart® apparatus causes progressive edema and slow ischemic damage after several hours of reanimation. Yet, submersion of the heart in a lower ionic salt buffer may help to minimize such.

The altered hydrodynamic state of the heart and progressive edema that occurs during reanimation on the Visible Heart® apparatus may limit the use of these methodologies for certain types of valve testing. Such deterioration of the tissue does not allow for extended periods of valve testing and limits most investigations related to the acute consequences of device implantations. Additionally, as previously mentioned, benchtop tests such as accelerated wear testing have established guidelines for testing valves (see Chap. 17), which cannot be reliably reproduced on the Visible Heart® apparatus. Valve testing conducted in animals typically includes an artificially induced "challenge" state, which produces hemodynamic profiles that can be unattainable on the isolated heart preparation. In other words, while the Visible Heart® methodologies in its current form does not replicate or replace benchtop or preclinical testing, it can provide unique comparative imaging of functional anatomy and details of the device-tissue interface which are not available in benchtop or preclinical animal testing.

## 19.11 Acute Testing of Pathological Animal Models

The successful reanimation of human hearts using the Visible Heart® approach described in this chapter requires a level of cardiac health not always present in the available specimens (nonviable for transplant). Additionally, it is considered that the therapies for a specific category of pathologies often cannot be adequately or ideally tested by using "healthy" swine hearts as a model (e.g., valve calcification). Consequently, to further the ability of the in vitro model to test specific devices/prototypes, there has been ongoing work by our laboratory and collaborators to develop models specifically designed to simulate certain pathological states.

Recent advances in transcatheter-delivered pulmonary valve technologies have also initiated the development of therapies for individuals with previous repairs for congenital defects and/or other specific patient populations. For example, it is well understood that valvular heart disease is a major cause of morbidity and mortality in patients who survive surgical correction for tetralogy of Fallot [51], and the pathologies associated with this disorder display wide variations in their morphologies of the right ventricular outflow tracts [52]. As such, planned therapies for these unique clinical scenarios need to adapt to a large variety of anatomical configurations, thus requiring extensive in vitro and in vivo testing before starting clinical studies. Here, we describe the surgical adaptation of the swine model to approximate the right ventricular anatomy of such patients; a beating heart model of the relevant anatomy is created by compromising the pulmonary valve and dilating the outflow tract and annulus (unpublished data). Once created in vivo, such models can be transferred to the Visible Heart® apparatus for in vitro study, e.g., visualization of the device-tissue interaction within this altered anatomy (Fig. 19.11).

To date, the Visible Heart® has also been used extensively in investigations on percutaneous edge-to-edge mitral valve repair devices. In order to validate such techniques and to determine if mitral stenosis occurs after edge-to-edge repair, the swine model can be surgically adapted by cutting a strut chordae in the P2 region of the posterior leaflet under visual guidance (Fig. 19.12) [53]. Subsequently, these in vitro models have since been used to determine the effectiveness of percutaneous devices at capturing prolapsing leaflets and restoring valve function. We have also looked at various minimally or transcatheter therapies for the right atrioventricular valve (tricuspid or quadricuspid).

With the intense interest in percutaneous aortic valve repair and/or replacement, there have been considerable advances in the design and development of transcatheter-delivered prosthetic aortic valves. Our laboratory has been fortunate to utilize Visible Heart® methodologies to provide a beating heart model for the testing

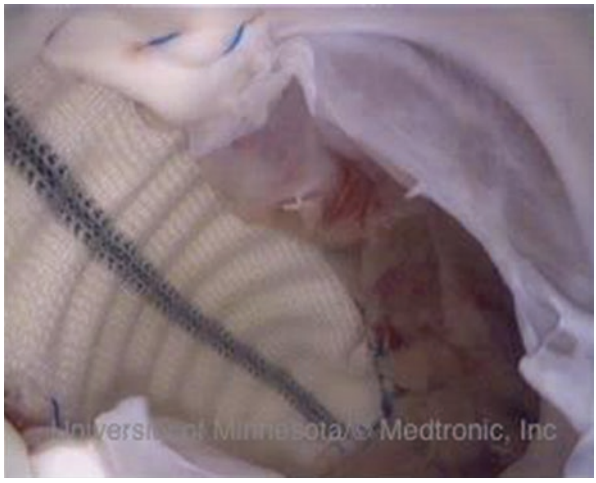


**Fig. 19.11** Image of the surgically created right ventricular outflow tract dilation of a swine heart; the remnants of the pulmonary valve can be seen in the foreground. (Modified from Bateman et al. [6])

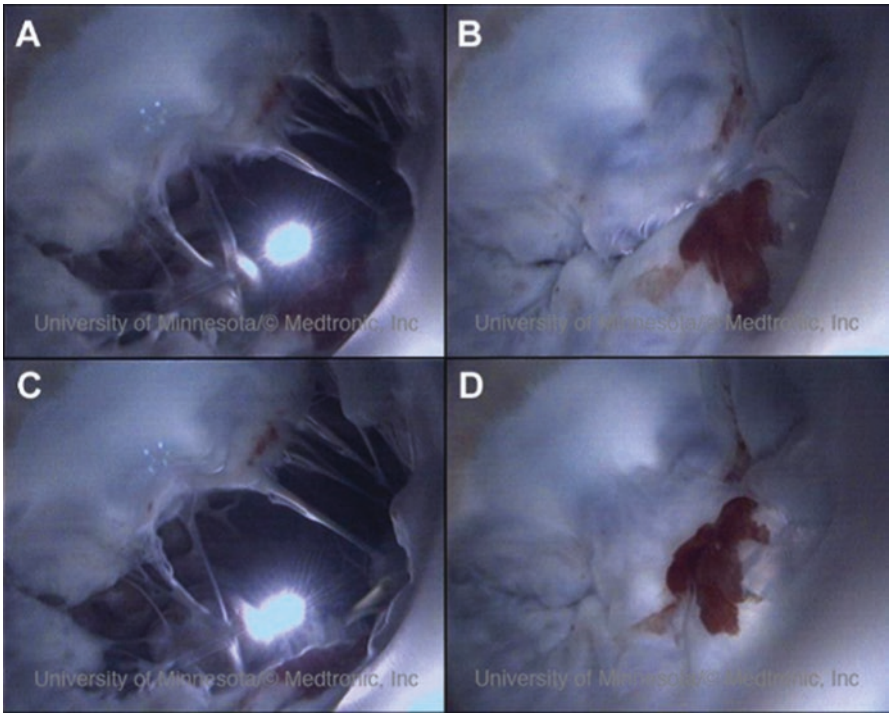


**Fig. 19.12** A mitral valve visualized during diastole (a and c) and systole (b and d) for the normal (a and b) and prolapsed state created by cutting a strut chordae of the P2 region (c and d). (Modified from Quill et al. [40])

of such devices and their delivery systems. Nevertheless, it should be again noted that the testing of such devices in healthy swine anatomy does not always satisfactorily approximate the anatomical environment of the devices' intended patient population. As such, our group has been working on developing various models for severe aortic stenosis, e.g., one with the specific aim of determining how large calcific deposits on the leaflets affect the deployment and function of such devices. To approximate severe stenosis of the aortic valve, we have (1) directly adhered plastic models of calcifications to the leaflets to reduce leaflet motions and (2) partially adhered the leaflet commissures to reduce the effective orifice areas of these valves. To date, such models have allowed for expanded procedural testing of these devices, e.g., from balloon valvuloplasty to device deployment. Interestingly, such studies have provided useful insights into the potential interaction of deployed devices and the calcific deposits relative to the native anatomy.

## 19.12 Future Directions

As anatomical resources and functional in vitro cardiac systems such as the Visible Heart® library and apparatus continue to grow and evolve respectively, so will the research possibilities within the realm of anatomical visualization and in vitro reanimation. The initiation of successful collaborations with the University of Manchester (UK) has been cultivated to determine the particular anatomical structure of the cardiac conduction system and thus provide new insights into why particular valve therapies may elicit detrimental electrophysiological effects on the heart [54, 55]. Additionally, continued imaging should provide further anatomical information on cardiac disease states highlighting how disease management could, in turn, be effecting reverse remodeling on a cellular scale as well as a global scale of cardiac anatomy. Currently, all collected datasets (videoscopic, CT, echocardiographic, and MRI) are being used to create a digital database of these human anatomies by rendering 3D computational models using software packages such as Mimics (Materialise, Leuven, Belgium); ultimately, we aim to use such datasets to create physical representations of given specimens via 3D printing [16]. Along with the plastination of select specimens, such work is creating real-life and computational 3D models that will pave the way for ongoing investigations and provide anatomically correct models for investigations related to device design and/or for educational purposes.

The Visible Heart® methodologies continue to be expanded to accommodate minimally invasive techniques as well. Development of a radial access pathway has been 3D printed from a model developed from a cadaver's anatomy. Using similar methods, minimally invasive techniques can be iteratively developed for education or device design. Moreover, procedures to reproduce the results from complex medical device implants can be evaluated [56].

In addition, our laboratory as a whole is constantly improving the Visible Heart® methodologies, e.g., with systems designed to optimize the physiological function and control of the heart to improve the reproducibility, longevity, and utility of the investigations. New pericardial target therapies, cardioplegia solutions, and perfusate solutions are being tested as means to better protect the heart from ensuing global ischemia and edema (some of which may be delivered as the pretreatment to specimens before extraction). Further, there is a continuing need to modify the setup/apparatus itself, e.g., to better accommodate various delivery system designs (such as subclavian and femoral access systems). It should also be noted that the use of Visible Heart® methodologies to augment chronic studies has allowed for the validation of surgically created anatomies and the direct visualization of chronic device implants that were not previously possible. We consider that the utilization of both fixed specimens and Visible Heart® methodologies for device evaluation should be used in a complementary fashion with other techniques that utilize in vivo or in vitro methods to test the reliability, durability, biocompatibility, and/or other design parameters of newly developed transcatheter devices. There is little doubt that the continued testing of novel cardiac valve prostheses via in vitro and in vivo

studies will provide scientists, engineers, and/or clinicians working in this field with the needed tools to drive the required research and development of the next generation of transcatheter-delivered cardiac devices.

## 19.13 The Atlas of Human Cardiac Anatomy

As novel therapies become clinically available and thus are implanted by more and more physicians, individuals will require continued education in the techniques required to navigate and deploy such devices. In response to this need, our laboratory has created a free access web site, the Atlas of Human Cardiac Anatomy, which can be utilized by cardiac device developers and clinical implanters to gain insights on the relative variabilities in functional cardiac anatomies [15]. This web site uniquely includes downloadable movie clips of functional cardiac anatomies, comparative imaging using echo, fluoroscopy, and MRI, digital reconstruction images, or VR scenes obtained from the human hearts of organ donors whose hearts were deemed not viable for transplant.

## 19.14 Conclusion

In summary, the study of fixed and reanimated human hearts, using the various methodologies described here, should provide an individual with novel insights on normal and pathological human cardiac anatomies. Additionally, one can better visualize anatomical alterations that occur with specified pathologies and/or those that may occur following the deployment of devices within the heart. More specifically, the Visible Heart® methodologies to reanimate large mammalian hearts have provided unique perspectives as to functional cardiac anatomies, including the cardiac valves and their associated structures. By reanimating such hearts using a clear perfusate, we are able to visualize functional anatomy with endoscopes placed directly within various heart chambers and/or within the large diameter vessels of the heart. We believe that such anatomic knowledge is critical for device designers and developers, as well as clinicians who utilize these less invasive cardiac repair approaches for patients with acquired or congenital structural heart defects. Furthermore, when direct visualization is simultaneously coupled with clinically employed imaging modalities, it provides further critical insights that can be used to more quickly and precisely advance such technologies. We consider that the utilization of both fixed specimens and Visible Heart® methodologies for device evaluation should be used in a complementary fashion with other techniques that utilize in vivo or in vitro methods to test the reliability, durability, biocompatibility, or other parameters of newly developed transcatheter devices. The continued testing of novel cardiac valve prostheses via in vitro and in vivo studies will provide scientists and engineers working in this field with tools to drive the required research and development of the next generation of transcatheter-delivered cardiac devices.

## References


1. Anderson RH, Becker AE (1993) The heart: structure in health and disease. Gower Medical Pub, London/New York
2. Weinhaus AJ, Roberts KP (2009) Anatomy of the human heart. In: Iaizzo PA (ed) The handbook of cardiac anatomy, physiology, and devices, 2nd edn. Humana Press, Totowa
3. Loukas M, Sullivan A, Tubbs RS et al (2010) Chiari's network: review of the literature. Surg Radiol Anat 32:895–901
4. Maselli D, Guarracino F, Chiaramonti F et al (2006) Percutaneous mitral annuloplasty: an anatomic study of human coronary sinus and its relation with mitral valve annulus and coronary arteries. Circulation 114:377–380
5. Anderson SE, Quill JL, Iaizzo PA (2008) Venous valves within left ventricular coronary veins. J Interv Card Electrophysiol 23:95–99
6. Bateman MG, Iaizzo PA (2011) Comparative imaging of cardiac structures and function for the optimization of transcatheter approaches for valvular and structural heart disease. Int J Cardiovasc Imaging 27:1223–1234
7. Anderson RH, Cook AC (2002) Attitudinally correct nomenclature. Heart 87:503–506
8. Tajik AJ, Seward JB, Hagler DJ et al (1978) Two dimensional real-time ultrasonic imaging of the heart and great vessels. Mayo Clin Proc 53:271–303
9. Edwards WD, Tajik AJ, Seward JB (1981) Standardized nomenclature and anatomic basis for regional tomographic analysis of the heart. Mayo Clin Proc 56:479–497
10. Thomas AC, Davies MJ (1985) The demonstration of cardiac pathology using perfusion-fixation. Histopathology 9:5–19
11. Kilner PJ, Ho SY, Anderson RH (1989) Cardiovascular cavities cast in silicone rubber as an adjunct to post-mortem examination of the heart. Int J Cardiol 22:99–107
12. Zhingre Sanchez JD, Schinstock EA, Bateman MG, Iaizzo PA (2019) The development and testing of a fixation apparatus for inducing the coaptation of the cardiac atrioventricular valves. ASME
13. Quill JL, Hill AJ, Laske TG et al (2009) Mitral leaflet anatomy revisited. J Thorac Cardiovasc Surg 137:1077–1081
14. Quill JL, Geesling AG, Iaizzo PA (2009) Transcatheter aortic valve deployment: interactions between native leaflets and coronary ostia. J Med Devices Trans ASME 3:027530
15. http://www.vhlab.umn.edu/atlas/index.shtml. Accessed 15 Mar 2021
16. Ton-Nu T, Levine RA, Handschumacher MD et al (2006) Geometric determinants of functional tricuspid regurgitation: insights from 3-dimensional echocardiography. Circulation 114:143–149
17. Plass A, Valenta I, Gaemperli O et al (2008) Assessment of coronary sinus anatomy between normal and insufficient mitral valves by multi-slice computer tomography for mitral annuloplasty device implantation. Eur J Cardiothorac Surg 33:583–589
18. Tops L, Wood D, Delgado V et al (2008) Noninvasive evaluation of the aortic root with multislice computed tomography implications for transcatheter aortic valve replacement. JACC Cardiovasc Imaging 1:321–330
19. Salton CJ, Chuang ML, O'Donnell CJ et al (2002) Gender differences and normal left ventricular anatomy in an adult population free of hypertension. J Am Coll Cardiol 39:1055–1060
20. Eggen MD, Bateman MG, Iaizzo PA (2011) Methods to prepare perfusion fixed cardiac specimens for multimodal imaging: the use of formalin and agar gels. J Med Devices Trans ASME 5:027539
21. Hołda MK, Zhingre Sanchez JD, Bateman MG, Iaizzo PA (2019) Right atrioventricular valve leaflet morphology redefined: implications for transcatheter repair procedures. JACC Cardiovasc Interv 12(2):169–178
22. Mattson AR, Soto MJ, Iaizzo PA (2018) The quantitative assessment of epicardial fat distribution on human hearts: implications for epicardial electrophysiology. Clin Anat 31(5):661–666

23. Sanchez JZ (2021) Anatomical, structural, and device-tissue characterizations of the atrioventricular valves, and associated structures: implications for transcatheter valve repairs and/or replacement therapies. PhD dissertation, Department of Surgery, University of Minnesota, Minneapolis
24. Sacco F et al (2018) Left ventricular trabeculations decrease the wall shear stress and increase the intra-ventricular pressure drop in CFD simulations. Front Physiol 9:458
25. Eggen MD, Swingen CM, Iaizzo PA (2009) Analysis of fiber orientation in normal and failing human hearts using diffusion tensor MRI. In: 2009 IEEE international symposium on biomedical imaging: from nano to macro, pp 642–645
26. Messika-Zeitoun D, Serfaty J-M, Brochet E et al (2009) Multimodal assessment of the aortic annulus diameter. J Am Coll Cardiol 55:186–194
27. Richards AL, Cook RC, Bolotin G et al (2009) A dynamic heart system to facilitate the development of mitral valve repair techniques. Ann Biomed Eng 37:651–660
28. Nanthakumar K, Jalife J, Masse S et al (2007) Optical mapping of Langendorff-perfused human hearts: establishing a model for the study of ventricular fibrillation in humans. Am J Physiol Heart Circ Physiol 293:H875–H880
29. Araki Y, Usui A, Kawaguchi O et al (2005) Pressure–volume relationship in isolated working heart with crystalloid perfusate in swine and imaging the valve motion. Eur J Cardiothorac Surg 28:435–442
30. de Weger A, van Tuijl S, Stijnen M et al (2010) Direct endoscopic visual assessment of a transcatheter aortic valve implantation and performance I the physioheart, an isolated working heart platform. Circulation 121:e261–e262
31. Transmedics. OCS heart for HCP's – Transmedics [Online]. Available: https://www.transmedics.com/ocs-hcp-heart/. Accessed 30 Apr 2021
32. Langendorff O (1895) Untersuchungen am uberlebenden Saugenthierherzen [Investigations on the surviving mammalian heart]. Pflugers Arch 61:291–332
33. Chinchoy E, Soule CL, Houlton AJ et al (2000) Isolated four-chamber working swine heart model. Ann Thorac Surg 5:1607–1614
34. Hill AJ, Laske TG, Coles JA Jr et al (2005) In vitro studies of human hearts. Ann Thorac Surg 79:168–177
35. Sigg DC, Iaizzo PA (2006) In vivo versus in vitro comparison of swine cardiac performance: induction of cardiodepression with halothane. Eur J Pharmacol 543(1–3):97–107
36. Valenzuela TF, Burzotta F, Iles TL, Lassen JF, Iaizzo PA (2021) Assessment of single and double coronary bifurcation stenting techniques using multimodal imaging and 3D modeling in reanimated swine hearts using Visible Heart® methodologies. Int J Cardiovasc Imaging 37(9):2591–2601
37. Sands MP, Rittenhouse EA, Mohri H et al (1969) An anatomical comparison of human, pig, calf, and sheep aortic valves. Ann Thorac Surg 8:407–414
38. Michaëlsson M, Ho SY (2000) Congenital heart malformations in mammals: an illustrated text. Imperial College Press, London/River Edge
39. Hill A, Iaizzo PA (2009) Comparative cardiac anatomy. In: Iaizzo PA (ed) The handbook of cardiac anatomy, physiology, and devices, 2nd edn. Humana Press, Totowa, pp 87–108
40. Sanchez JZ, Iles T, Dvir D, Iaizzo P (2020) Direct visualisation of the BASILICA technique post TAVR to enhance coronary flow. EuroIntervention 16(8):680–681
41. Zhingre Sanchez JD, Bateman MG, Iaizzo PA (2019) Multimodal imaging of a self-expanding transcatheter aortic valve replacement (TAVR) procedure in a reanimated human heart and post-implant analyses. Int J Cardiovasc Imaging 35(11):2135–2137
42. Sigg DC, Coles JA, Oeltgen PR et al (2002) Role of δ-opioid receptor agonists on infarct size reduction in swine. Am J Physiol Heart Circ Physiol 282:H1953–H1960
43. Iles TL et al (2016) Testing the efficacy of pharmacological agents in a pericardial target delivery model in the swine. J Vis Exp 113:52600
44. Schinstock E, Ramirez D, Iaizzo PA (2020, July) The development of pharmacologic control algorithms to optimize heart physiological functions during ex-vivo heart perfusion. Poster

presentation in the annual international conferences of the IEEE Engineering in Medicine and Biology Society in conjunction with the annual conference of the Canadian Medical and Biological Engineering Society, Montreal, QC, Canada
45. Quill JL, Laske TG, Hill AJ et al (2007) Direct visualization of a transcatheter pulmonary valve implantation within the Visible Heart®: a glimpse into the future. Circulation 116:e548
46. Iaizzo PA, Hill AJ, Laske TG (2008) Cardiac device testing enhanced by simultaneous imaging modalities: the Visible Heart®, fluoroscopy, and echocardiography. Expert Rev Med Devices 5:51–58
47. Eggen M, Swingen C, Matta P et al (2009) Design of a novel perfusion system to perform MR imaging of an isolated beating heart. J Med Devices Trans ASME 3:027536
48. Eggen MD, Bateman MG, Rolfes CD et al (2010) MRI assessment of pacing induced ventricular dyssynchrony in an isolated human heart. J Magn Reson Imaging 31:466–469
49. Holm MA, Mattson A, Mattison L, Gaasedelen E, Zhingre Sanchez J, Iaizzo PA (2018) A portable ex vivo heart perfusion apparatus for cardiac CT imaging: Visible Heart(R) mobile. Paper presented at 2018 Design of Medical Devices Conference, DMD 2018, Minneapolis, MN, USA
50. Richardson E, Hill AJ, Skadsberg ND et al (2009) The pericardium. In: Iaizzo PA (ed) The handbook of cardiac anatomy, physiology, and devices, 2nd edn. Humana Press, Totowa, pp 125–136
51. Wren C, O'Sullivan J (2001) Survival with congenital heart disease and need for follow up in adult life. Br Med J 85:438–443
52. Schievano S, Coats L, Migliavacca F et al (2007) Variations in right ventricular outflow tract morphology following repair of congenital heart disease: implications for percutaneous pulmonary valve implantation. J Cardiovasc Magn Reson 9:687–695
53. Quill JL, Bateman MG, St. Louis JL et al (2010) Edge-to-edge repairs of P2 prolapsed mitral valves within isolated swine hearts. J Heart Valve Dis 20:5–12
54. Dobrzynski H, Li J, Tellez J et al (2005) Computer three-dimensional reconstruction of the sinoatrial node. Circulation 111:846–854
55. Chandler N, Aslanidi O, Buckley D et al (2011) Computer three-dimensional anatomical reconstruction of the human sinus node and a novel paranodal area. Anat Rec (Hoboken) 294:970–979
56. Zhingre Sanchez JD, Iaizzo PA (2020) A novel transcatheter edge-to-edge suturing technique and prototype for repairing tricuspid valve regurgitation. ASME

# Chapter 20
# Clinical Trial Requirements for Cardiac Valves


**Sonia Diaz de Leon, Larry Lambrecht, Jenna C. Iaizzo, and Anna T. F. Lovas**

## Abbreviations

| | |
|---|---|
| CE | "Conformité Européenne" or European Conformity |
| CEC | Clinical Events Committee |
| CFR | Code of Federal Regulations |
| DSMB | Data Safety Monitoring Board |
| EC | Ethics Committee |
| EOA | Effective orifice area |
| FDA | Federal Drug Administration |
| GCP | Good Clinical Practice |
| IDE | Investigational device exemption |
| IRB | Institutional Review Board |
| ISO | International Organization for Standardization |
| OPC | Objective performance criteria |
| PMA | Pre-market approval |
| PMCF | Post-market clinical follow-up |

S. D. de Leon (✉) · L. Lambrecht
Medtronic, Inc., Structural Heart & Aortic, Minneapolis, MN, USA
e-mail: sonia.diaz.de.leon@medtronic.com

J. C. Iaizzo
Medtronic, Inc., Structural Heart & Aortic, Minneapolis, MN, USA

Edwards LifeSciences, Irvine, CA, USA

A. T. F. Lovas
Medtronic, Inc., Structural Heart & Aortic, Minneapolis, MN, USA

Lutonix, Inc., CR Bard, Minnetonka, USA

© The Author(s), under exclusive license to Springer Nature Switzerland AG 2023

P. A. Iaizzo et al. (eds.), *Heart Valves*, https://doi.org/10.1007/978-3-031-25541-0_20

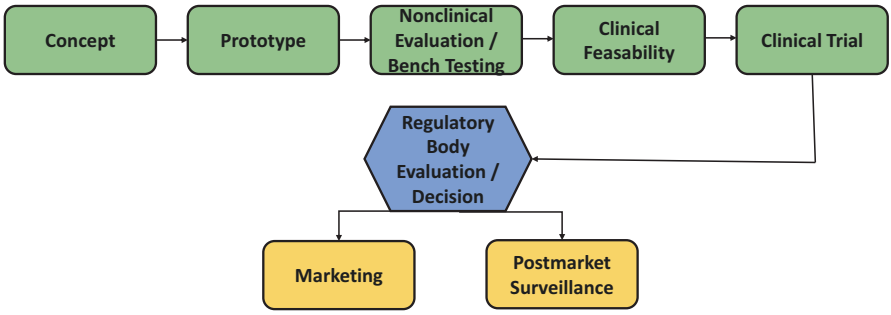


**Fig. 20.1** Timeline of medical device development

## 20.1 Introduction

Clinical trials play a very crucial part in the process of bringing devices, specifically heart valves, to the market and for providing continued scientific clinical data after commercialization (Fig. 20.1). Nevertheless, prior to executing a clinical trial, researchers do not know how the newly developed valve will perform in a human body. Further, it should be noted that many patients that receive these class III life-sustaining devices will likely have many other clinical complications that, in some cases, may adversely affect the potential success of novel technologies. Therefore, carrying out a carefully designed clinical trial is an important opportunity to examine outcomes of the new valve in humans and to provide resultant clinical data to patients, physicians, and the entire scientific community. Yet today, the primary purpose of such a clinical trial is to provide valid scientific evidence about the safety and/or efficacy of a device, resulting in clinical evidence for future use or retraction of a therapy.

There are various types of heart valve clinical trials, from trials where a novel valve technology is being used for the first time ("first in human" studies) to post-market trials in which a valve therapy has obtained regulatory approval and studied further to examine long-term effects and/or to obtain more specific information about the overall therapy. Clinical evidence is vital not only to demonstrate safety and effectiveness of a device therapy in humans but also to further examine how well the device performs compared to other devices and/or concomitant treatments. In the specific case of a newly developed heart valve, clinical studies will often be designed to compare the new valve against the native valve, other heart valve devices, and/or standard-of-care treatments including guideline-directed medical therapy. This chapter provides a general overview of the present state of human heart valve clinical trials, including an overview of the following: (1) the current positions of regulatory bodies that oversee trials, (2) specific features of a trial design, and (3) the many necessary considerations involved in the proper implementation of heart valve clinical trials.

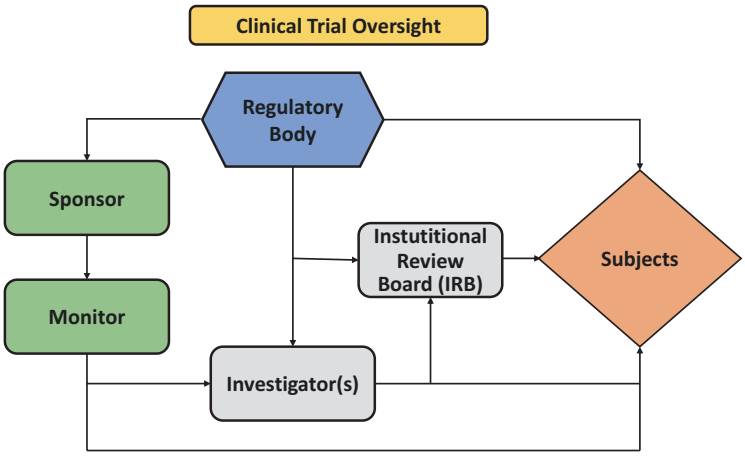


**Fig. 20.2** Clinical trial oversight

Today, for any designed heart valve trial, the following groups/individuals can be identified, each with their specific role(s) (Fig. 20.2) [1]:

***Sponsor(s)*** Person who initiates but does not actually conduct the investigation. Typically, this includes the developer of the technology seeking approval for market release.

***Investigator(s)*** Individual who actually conducts the clinical investigation or, if the investigation is conducted by a team, is the responsible leader of that team. More specifically, this includes nonbiased individual(s) that will not only implant/deploy the novel technology but will also be responsible for individual patient follow-ups.

***Monitor(s)*** Individuals designated by the sponsor or contract research organization to oversee the progress of an investigation (responsible to ensure that the trial is performed in an ethical and proper fashion). Regulatory bodies also have their own process for auditing sponsors and investigators through their bioresearch monitoring group(s).

***Institutional Review Board (IRB)/Ethics Committees (ECs)*** The board, committee, or other group designated by the institution that is ultimately responsible to review research involving subjects for ensuring that the clinical protocol is appropriate, and that the institutional investigators perform the study in a proper and ethical manner in conformance with part 56 of the Code of Federal Regulations. These boards may have different names according to the institutional structure.

***Subjects*** Individual patients who participates in an investigation and deemed appropriate to be enrolled (meeting all inclusion and none of the exclusion criteria) and provided informed consent.

## 20.2 Regulatory Bodies

Regulations and the regulatory bodies that govern heart valve clinical trials play an important role in how heart valve technologies reach the market. A solid partnership between a sponsor and regulatory body, aided by clear communication, can affect whether technology can reach the market in an expeditious manner. International regulatory bodies are important as they ensure that there is consistency in clinical trials and that they are run properly in order to provide the supportive scientific evidence required. Specifically, there are numerous regulatory bodies that provide oversight for heart valve clinical trials throughout the world. A brief overview of regulatory bodies from different geographies is provided, yet our discussion focuses mainly on the Food and Drug Administration (FDA) in the United States and European Economic Area.

### *20.2.1 Food and Drug Administration (United States)*

The FDA oversees clinical trials exclusively within the United States. The FDA's mission statement consists of the following: (1) "Promoting public health by ensuring the safety, efficacy, and security of human and veterinary drugs, biological products, and medical devices"; and (2) "Advancing the public health by helping to speed innovations that make medical products more effective, safer, and more affordable and by helping the public get the accurate, scientific-based information they need to use medical product and foods to maintain and improve their health" [2]. The Center for Devices and Radiological Health is the branch that oversees devices (including heart valves).

In the United States, there are three regulatory classes of devices based on the considered levels of risk involved with a given device. All class I–III devices are subject to general controls, meaning the FDA looks at factors like labeling, registrations, etc. Class I devices have the lowest amount of risk and regulatory controls (e.g., devices such as elastic bandages and surgical gloves). Class II devices must meet specific performance standards in addition to all class I requirements (e.g., devices such as surgical drapes). Most stringently, class III devices require premarket approvals to ensure both their safety and effectiveness. As such, class III devices are also considered as the riskiest category of devices such as implantable pacemakers and heart valves.

It should be noted that the FDA regulations for medical device products are detailed in Title 21 of the Code of Federal Regulations (CFR). The most applicable parts of CFR 21 that apply to heart valve clinical trials include Part 812 (Investigational Device Exemption, or IDE) and Part 814 (Premarket Approval or PMA). Most new heart valves are required to undergo IDE clinical trials before receiving FDA approval unless iterative change to an already approved device that do not constitute a significant change in design or basic principles of operation (i.e., change to sewing ring dimension or addition of radiopaque markers).

According to CFR Part 812, an approved IDE "permits a device that otherwise would be required to comply with a performance standard or to have premarket approval to be shipped lawfully for the purpose of conducting investigations of that device" [1]. Furthermore, Part 812 provides procedures for the conduct of clinical investigations of devices. If data is used to support the IDE or device marketing application from outside the United States, the investigation needs to be conducted in accordance with good clinical practice.

### *20.2.2 Other Regulatory Bodies*

In Europe, each country has their own competent authority (CA), who has the ownership for review and approval of clinical trials that are conducted in their individual country. In addition, manufacturers need to work with a notified body, who is responsible for the commercial approval of the device, which includes the review of the clinical data generated from the clinical trial(s).

The most prevalent regulatory oversight applies to the countries in the European Economic Area; these are countries required to obtain a CE mark ("Conformité Européenne" or European Conformity). While the criteria to receive a CE mark in Europe are notably different than receiving FDA approval, both geographies follow the International Organization for Standardization (ISO) ISO 5840 as a general principle for approving heart valve therapies. ISO 5840 is broken into three parts: Cardiovascular implants – Cardiac valve prothesis – General requirements (5840-1: 2021), Surgical Implanted Heart Valve Substitutes (5840-2: 2021), and Heart Valve Substitutes Implanted by Transcatheter Techniques (5840-3: 2021). These standards provide requirements for clinical investigations including study design, ethical considerations, and clinical data requirements for surgical and transcatheter valves, respectively [3–5].

The Medical Device Directive (MDD) was developed to harmonize requirements for medical devices in the European Union. Manufacturers were required to meet MDD requirements to manufacture and legally place a medical device on the European market. On May 26, 2021, the MDD was replaced with Medical Device Regulation (MDR) which is intended to add more rigor to the regulations focused on the protection of health for patients and users and establishing a high standard for safety and clinical performance of the device, along with improving traceability of medical devices, and transparency for patients [6].

These standards, directives, and regulations can pose different obstacles when moving into other geographies and may influence the intended quality and importance of every clinical trial completed for the new device. It is also important to note many geographies require or prefer the investigational product to be tested in their local country or similar patient population.

**Table 20.1** Thirteen principles of Good Clinical Practice

| |
|---|
| *Ethics* |
| 1. Ethical conduct of clinical trials |
| 2. Benefits justify risks |
| 3. Rights, safety, and well-being of subject prevail |
| *Protocol and science* |
| 4. Nonclinical and clinical information supports the trial |
| 5. Compliance with a scientifically sound, detailed protocol |
| *Responsibilities* |
| 6. Institutional Review Board/Independent Ethics Committee approval prior to initiation |
| 7. Medical care and decisions by qualified physician |
| 8. Each individual qualified (education, training, experience) to perform his/her tasks |
| *Informed consent* |
| 9. Freely given from every subject prior to participation |
| *Data quality and integrity* |
| 10. Accurate reporting, interpretation, and verification |
| 11. Protects confidentiality of records |
| *Investigational products* |
| 12. Conform to good manufacturing practice and used per protocol |
| *Quality control/quality assurance* |
| 13. Systems with procedures to ensure quality of every aspect of the trial |

### *20.2.3 Good Clinical Practice Oversight*

Good Clinical Practice (GCP) is "an international ethical and scientific quality standard for designing, conducting, recording, and reporting trails that involve the participation of human subjects" [7]. This standard was developed by a collaborative group of regulatory authorities of various worldwide geographies including the European Union, Japan, and the United States by the International Conference on Harmonisation (ICH). Good Clinical Practice was finalized in 1996 and became effective in 1997; it provides international assurance that data and results of clinical investigations are credible and accurate and that the rights, safety, and confidentiality of participants in the clinical research studies are respected and protected. More specifically, GCP consists of 13 principles (Table 20.1).

## 20.3 The Generalized Clinical Trial Cycle/Process

Addressing all aspects of a clinical trial in depth is an enormous undertaking and beyond the scope of this chapter; thus, the following sections will highlight some of the foundational methods and processes of a typical heart valve clinical trial. As shown in Table 20.2 from ICH, there are many tasks that need to be addressed with the development and execution of a clinical trial (some tasks may occur simultaneously) [7].

**Table 20.2** Standardized clinical research process

| |
|---|
| 1. Prepare a clinical plan |
| 2. Recruit investigators |
| 3. Prepare protocol |
| 4. Prepare case report forms |
| 5. Prepare informed consent form |
| 6. Perform investigator site visit |
| 7. One-on-one investigator reviews, including clinical plan, protocol, case report forms, and informed consent form |
| 8. Obtain an investigator agreement |
| 9. Obtain IRB approvals for each participating institution |
| 10. File an IDE |
| 11. Obtain an IDE approval |
| 12. Perform periodic investigator meetings |
| 13. Conduct the clinical study, i.e., a multicenter study |
| 14. Monitor the multicenter study |
| 15. Conclude study |
| 16. Compile data from each institution |
| 17. Analyze overall collected data |
| 18. Write final clinical report |

### *20.3.1 Features of a Trial Design for a Newly Developed Heart Valve*

Prior to planning and execution of a heart valve trial, it is important to research and understand all current published information and relevant heart valve trial data including previous trial designs and subsequent outcomes associated with those trials. For gaining FDA approval for any cardiac device, the importance of clinical evidence cannot be stressed enough. The beginning stages of planning a clinical trial design, associated publications, and previous research can help shape important components for the new trial, such as patient inclusion/exclusion criteria, statistical designs employed in such trials, and/or the general patient populations to be studied.

A well-controlled clinical investigation includes a clear objective and defined methods of analyses. ISO 5840-2:2021 and ISO 5840-3:2021 state that for new heart valve systems, studies should be designed to evaluate the system for its intended use and should include adverse event assessments for risk to the device and procedure. The bias for the selection of the primary objectives includes clinical relevancy to safety and effectiveness aspects of the investigational system, objectively defined and measurable, and consistent with current recommendations for endpoints in valve replacement studies [4, 5]. More specifically, the objective should address the proposed medical claims for the given investigational device, and these should be refined to specifically address the safety and effectiveness of the heart valve in a defined population. Next, it is important to structure a trial so there can be

a valid comparison to controls. A control group gives the trial results a meaningful comparison to an existing therapy or treatment. For example, in current transcatheter valve therapy trials, a new transcatheter valve is directly compared to an approved transcatheter valve(s) as a control. Often, an appropriate control group can be identified by performing a careful and thorough literature search. Furthermore, performing prior research on the specific disease or conditions that the newly designed heart valve will be intended to treat is equally important, in order to understand the natural progression of the disease or condition and the current benefits or limitation of other treatments. It should be noted that often this step of researching the disease or condition is completed in earlier phases of prototyping of the actual heart valve, but it is recommended that it be reviewed once again just prior planning the clinical trial. Finally, literature searches on similar treatments/heart valves can also assist in identifying the appropriate disease populations and justifying the inclusion and exclusion criteria for the trial.

When the patient population and treatment/control cohorts are clearly identified, one needs to consider the next set of factors to impact the ultimate design. First, the type of trial design must be determined such as randomization vs single arm, non-inferiority vs superiority, hypothesis testing, etc. Each of the designs may strengthen the significance of the obtained results, while also minimizing bias and providing comparability of groups. Well-defined trial endpoints are also of great significance for the overall success of a clinical trial. For example, typical heart valve trial endpoints should encompass both safety and effectiveness measures. Note that adverse events often comprise the safety endpoint for a given trial. Typically, effectiveness endpoints are found in the form of the presence or absence of a clear, and the definite effect on a patient which for heart valve trials may include the following:

- Rate of death, stroke, and heart failure rehospitalization
- Reduction in mean pressure aortic gradient or increase in effective orifice area postimplantation (device performance)
- Improvement in functionality (e.g., quality of life via New York Heart Association (NYHA) classification or Kansas City Cardiomyopathy Questionnaire (KCCQ), or improvement in 6-minute walk test)

Table 20.3 provides a list of key steps to consider in designing a clinical trial for the development of a new heart valve technology.

An often-overlooked aspect of the early execution or startup of a clinical trial is a high degree of physician involvement or engagement. Physicians play a major role throughout the execution of the trial, and it is important to gain their insights into the overall design and planning early in the process. Given physicians are ultimately the users of the heart valve being studied, their clinical knowledge can be used to create a well-thought through trial design.

**Table 20.3** General steps in the development of a clinical study design

| |
|---|
| Develop the study objectives which includes research objectives, device claims, and pilot of feasibility study. |
| Note that the study objectives should be phrased as a research question posed to address medical claims for the device. |
| Refine the research question to specifically address the safety/effectiveness of the given device in a well-defined patient population for one or more outcomes. |
| Perform a pilot or feasibility study; if claims are inadequately known, conduct a pilot or feasibility study on a small subgroup of patients or subjects. As such, the pilot study objectives are to identify claims more precisely, test study procedures, and/or obtain estimates of properties of outcome and/or other variables. |
| Properly identify and select variables/parameters. |
| Define the study population(s) and appropriate clinical controls. |
| For example, defined prior to study by rigorous inclusion/exclusion criteria. |
| Define a subset of the general population representing the target population for the device. |
| List all parameters of the specific study design. |
| Define the study masking (i.e., your bias control). |
| Define the number of study sites and potential investigators. |
| Fit the needs for a sufficient number of eligible patients in a timely fashion. |
| The center must be capable of processing patients. |
| Engage competent staff members who work well on the trial. |
| Identify investigators willing to recruit patients and conduct the study as specified in the protocol. |
| All center individuals need to be qualified to perform trial parameters. |
| Determine the proper patient sample size, i.e., the study is properly statistically powered. |

### *20.3.2 Reimbursement and Payer Information*

While the process for the development of clinical trials is essential to understanding the appropriate use of medical interventions of all types, it is also important for payers to understand the potential coverage for the device. Routine costs in clinical trials (including the investigational device) may be covered by Medicare for qualifying clinical trials in accordance with The National Coverage Determination for Routine Costs in Clinical Trials [8].

### *20.3.3 Clinical Trial Site Selection*

By definition, investigational sites include all centers implanting the valve that submit data as part of the investigation. The initial selection of the proper hospitals/institutions and physicians to participate in a clinical trial is a key step toward success. After time and money have been invested in creating a clinical trial design and protocol, there is no doubt that the actual execution can affect the outcome of the trial. All possible steps should be taken to eliminate extraneous variables such as

reeducation or elimination of a site that does not abide by the set protocol. Furthermore, it is critical to qualify the experience of the physicians relative to their ability to utilize novel or investigational therapies similar to the device you are investigating. It would be strategic to identify and recruit physicians already well established in the related therapy or device being investigated. It is also important for physicians to have experience in clinical research and have the infrastructure to conduct a clinical study at their institution including qualified support staff and adequate facilities and storage. It is good practice to check the hospital/site's previous clinical trial performances and confirm they are not participating in competing studies to avoid patient selection bias. Finally, it is essential to make sure the physician investigators have not been disbarred, banned, or excluded from participating in any type of clinical trial.

Another crucial variable to consider when selecting sites is the actual geographic location. The clinical trial design and projected subject population(s) are helpful when identifying the number of sites needed in the trial. As such, typically large metropolitan area hospitals are chosen to participate in clinical trials given they should be able to quickly recruit the desired patients. However, there are regional hospitals that receive a high number of referrals; thus, these hospitals may be able to effectively contribute to enrollment. Sites that have experience working with and successfully recruiting the appropriate patient populations can be immensely helpful in enrolling subjects in a timely manner to complete a trial. In addition, the FDA encourages a diverse population including representative of relevant age and racial and ethnic subgroups consistent with the intended use of the device. Ensuring participation from a diverse background in clinical research is critical to advancing health equity [9].

The potential for conflicts of interest is also something to consider when choosing the clinical sites for a trial. Heart valve clinical trials typically involve a high level of physician engagement in the trial and device being tested. Therefore, in order to legitimize their participation in such a trial, it is important to rule out potential biases with regard to trial execution and the quality of the data being captured. It should be noted that many sponsors and clinical sites have built-in regulations or processes to cover any potential conflicts of interest.

### *20.3.4 Clinical Trial Execution*

Throughout the execution of a given clinical trial, there are multiple activities happening simultaneously that all need to be managed. For example, it is important to design a trial with multiple follow-up visits in order to capture long-term (typically 10+ years) data on the subject population(s). With clinical evidence being the primary end product of a given clinical trial, it is crucial to ensure that one captures both valid and quality data in a highly efficient manner. The trial data are captured on what most clinical trial sponsors called *case report forms*. Nearly all trial data are collected electronically (sites enter data directly into an online case report form and

the sponsor can see the data in real time). It will be critical to keep up with the ever-evolving technologies that are being developed and deployed to ensure the integrity, quality, and efficiency of clinical trials.

An interesting trend in recent transcatheter heart valve trials is the development and utilization of screening committees. A screening committee for a heart valve transcatheter trial would typically be comprised of well-established, objective cardiac surgeons, and interventional cardiologists. As such, it is imperative that each individual involved would also be familiar with the details of heart valve technologies, trial design, and patient population which the trial is enrolling including specific inclusion/exclusion criteria (i.e., those described in the clinical investigational plan or protocol). The screening committee could also be used to assist in determining and identifying the right patients for a properly designed trial. It is critical that one recruits an overall subject population that is highly consistent but encompassing of the target population; this is especially important when multiple clinical sites/hospitals are participating in the trial.

Assuming the trial has progressed to the point of near completion, there are several other factors that one needs to consider. For example, all subjects should be completely accounted for in the final clinical report. It is recommended that complete subject accounting, on a per subject basis, for each cohort is provided. The report should include the following: (1) the total number of subjects expected for follow-up, (2) all subjects discontinued because of death or device removal or withdrew participation, and (3) the numbers of subjects that were actually evaluated at each evaluation pre-planned time point.

It should also be noted that depending on the type of trial and the primary endpoints listed in the protocol, submitting for regulatory approval may happen before the designed trial is fully complete. For example, in an IDE study with primary endpoints at 1 year of subject follow-up, an application for premarket approval may be submitted and granted prior to the end of all subject follow-up (depending on the accepted trial design). As further described in Sect. 20.3.7, the FDA expects long-term data for most IDE heart valve trials, allowing for the investigational valve to be commercialized prior to the end of all follow-up visits. However, regular reports will need to be submitted to regulatory bodies containing the long-term data. Finally, the overall timeline for submission for regulatory approval will ultimately depend on the study design, statistical methods, and analytical processes laid out in the final trial protocol. It is important that this section of the device trial protocol be carefully followed, as it is agreed upon by the FDA or regulatory body prior to initiation.

### *20.3.5 Data Collection Within the Clinical Trial*

As clinical evidence to support the use of the investigative heart valve is the ultimate product of conducting a clinical trial, the remainder of this chapter will focus on the collection of data and various regulations one needs to consider related to clinical evidence.

As described in ISO 5840-3:2021, Clinical Data Requirements, "clinical data (including adverse events) shall be recorded for all subjects in the study as required by [ISO] 14155." This standard also instructs the manufacturer to develop systems to ensure that all adverse events and device deficiencies are received, evaluated, and communicated to interested parties in accordance with ISO 14155. Further details on adverse event data collection requirements, definitions, and classification of causal relationships are provided in Annex G [5].

CFR 812.140 (Records) states participating investigator(s) shall maintain accurate, complete, and current documentation relating to the investigator's participating in the investigation. This includes but not limited to records of receipt, use or disposition of the investigational device, records of subject's case history (including case report forms and informed consent), and reasons for deviation from the protocol [1].

### *20.3.6 Data Collected for Each Subject Enrolled into a Clinical Trial*

Each subject enrolled in the study should be followed, and appropriate data should be collected according to the study protocol. Additionally, follow-up data should be collected for each subject until the entire study is terminated and data is typically collected during office, clinic, or hospital visits. Telephone follow-up visits may also be considered to minimize loss to follow-up, and allowance of telephone visits should be specified in the study protocol. Accordingly, an informed consent must be received documenting the planned follow-up period and assessments from all subjects (21 CFR 50.25(a)) [10]. Any subject not willing to fully participate in the study, including the follow-up period, should not be enrolled. Most institutions have a thorough consent process, as governed by regulatory bodies and their own IRBs. However, trial attrition still occurs, and there is the potential for patients to enroll in a clinical trial to obtain the latest technologies, with little or no intent of participating in a follow-up period.

ISO 5840-3:2021, Clinical Data Requirements, goes into more detail about specific data to be collected [5]. For example, follow-up data for most heart valves should include data collected approximately 30 days, at least one specific time point between 3 months and 6 months, at 1 year, and minimum annually thereafter until investigational is completed (in accordance with the clinical investigational plan). Physical examination is also recommended along with hemodynamic evaluation by Doppler echocardiography, functional assessment, cardiovascular medication collection, and evaluations for adverse events.

Additionally, enrolled patients may be followed after the procedure by their personal cardiologists (not the implant surgeon/interventionalist), especially in large referral centers. Therefore, the study investigators should work in conjunction with the patients' physicians to collect all appropriate data from the correct time periods. This may be better accomplished if the study investigator or the sponsor obtains

contact information for the following physician, so she/he can be advised of the actual study protocol. It is important to note that study procedures (outside of the standard of care scope) should only be performed by investigators trained on the trial protocol.

### *20.3.7 Clinical Trial Sample Size and Follow-Ups*

As stated in Sect. 20.3.6, it is important to plan for potential attrition in the statistical plan by having an adequate population enrolled greater than the minimum patients needed for an appropriate analysis. It is helpful to determining the appropriate subject population by referring to the term *follow-up in patient-years.* For example, ISO 5840-3:2021 states for a new transcatheter heart valve system, in a population with acceptable surgical risk, the sample size shall include a minimum number of 150 patients for each indicated valve location, each of whom is intended to be studied for at least 1 year. In addition, at least 400 patient-years of data are required in a pre-market setting to assess late adverse events. Anticipated adverse event rates also need to be considered when calculating the patient-year follow-up [5].

For surgical heart valves, there are historical data on a multitude of surgical heart valve that can serve as a reference for how a new device should perform in terms of safety outcomes. These objective performance criteria (OPCs) have been summarized and listed in Annex I of ISO 5840-2 and in Table 20.4. The occurrence of late (>30 days postimplant) complications that are observed with a new valve should be numerically less than twice the OPC. For a single-position valve (aortic or mitral), a minimum sample size of 150 patients followed to a year with at least 800 patient-years of follow-up is required. If the investigational valve is for use in both the aortic and mitral positions, there should be a minimum of 150 patients for each location followed for a year, and the data shall be broken out by valve position. A minimum of 400 patient-years is required for each valve position; however, it is recommended that more than 400 patient-years are collected in both (aortic and mitral) positions, if possible, to enable more reliable comparisons to the OPC [4].

**Table 20.4** Objective performance criteria for surgical heart valve substitutes

| | Bioprosthetic | | Mechanical | |
|---|---|---|---|---|
| Adverse event (endpoint) | Aortic | Mitral | Aortic | Mitral |
| Thromboembolism | 1.5 | 1.3 | 1.6 | 2.2 |
| Valve thrombosis | 0.04 | 0.03 | 0.1 | 0.2 |
| Major hemorrhage | 0.6 | 0.7 | 1.6 | 1.4 |
| Major paravalvular leak | 0.3 | 0.2 | 0.3 | 0.5 |
| Endocarditis | 0.5 | 0.4 | 0.3 | 0.3 |

Linearized rates (% per valve-year)

ISO 5840-3:2021 also provides guidance on total duration of the study. The study duration should be based on specific purposes of the study (i.e., intended applications and outcomes measured). Prolonged post-market clinical follow-up (PMCF) is considered essential to collected long-term data on valve performance and long-term adverse events, such as structural valve deterioration. A PMCF study includes following the initial cohort of patients included in the pre-market investigation in a post-market setting. A minimum of 10 years postimplantation should be used in pivotal studies with collection of safety, performance, and effectiveness data. However, ISO recognizes that the expected longevity of the study population should be considered for long-term study duration. For example, follow-up may be limited to 5 years for a patient population that are classified as high or extreme risk to surgery. It may also be appropriate to obtain clinical data in a real-world clinical setting. If this is conducted, the study should enroll patients prospectively in a PMCF study to minimize bias patient selection and retrospective reporting [5].

### *20.3.8 Complications and Management of Adverse Events*

The types of complications to expect from patients treated with newly developed valve technologies may include the following: valve thrombosis, major hemorrhage, perivalvular leak, permanent pacemaker implant, valve endocarditis, stroke, thromboembolism, as well as other access-site related events. Additionally, it is typical that the complication data include all-cause reoperation, valve-related reoperation, explant, all-cause death, and valve-related death along with events related to cardiac damage, implant procedure, organ damage, and the device.

The clinical trial sponsors are ultimately responsible for ensuring proper monitoring of the investigation and must select non-biased monitors qualified by appropriate training and experience. A sponsor can establish a Data Safety Monitoring Board (DSMB), also known as Data Monitoring Committees (DMCs), to review adverse events and recommend study termination if safety concerns warrant. DSMBs are generally recommended for any controlled study that compares rates of mortality or major morbidity. A DSMB may not be required for studies at early stage of product development or for studies addressing lesser outcomes such as short-term relief of symptoms. The patient population is also a factor when determining the need for a DSMB (i.e., vulnerable populations such as children or terminally ill). The DSMB should establish criteria for recommending study termination for safety reasons before the study begins, and meeting frequency is dependent on expected event occurrence rate and should be described in the study protocol. It is recommended that the DSMB should have members who are independent from the study sponsors and investigators and comprised of clinicians with expertise in the relevant therapies as well as at least one biostatistician [11].

For a clinical trial for a novel valve technology, it is also recommended that the sponsor establish a Clinical Events Committee (CEC) to review important endpoints reported in the clinical study and determine which endpoints meet

protocol-defined criteria. A CEC may be important when endpoints are subjective or require the use of complex definitions [11]. Similar to the DSMB, the CEC should have members who are independent from the study sponsors as well as selected clinical investigators.

The aforementioned topics outline some of the areas considered in the general clinical trial cycle/process. With the ever-changing regulatory environment and concerns for ensuring safety of cardiac valves, the clinical trial process will continually evolve. It is important to keep up to date on additional requirements and landmark trials testing devices similar to the new heart valves being developed today. The FDA provides great resources on their website along with a repository for most clinical trials that are occurring in the United States (www.clinicaltrials.gov).

## 20.4 Summary/Conclusion

Clinical trials are an important and critical step in bringing new technologies (including heart valves) to the market. As detailed above, there are many pieces comprising the development, execution, and ultimately the results of a clinical trial. This chapter provides a high-level overview of these aspects, which may vary from product to product. Setting up robust, well-designed trial and performing it correctly will affect the ability to successfully market a developed heart valve. The clinical trial requirements along with the regulatory and reimbursement landscape are vast and constantly changing. When designing a clinical trial, it is important to keep in mind the various global regulatory requirements, good clinical practices, physician and institution selection, data collection, identification of prespecified endpoints, and overall execution of the trial. With such a heavily regulated environment and the intricacies of heart valves, ensuring proper conduct to ensure high quality and integrity of data is crucial.

## References

1. U.S Food and Drug Administration Code of Federal Regulations Title 21. Part 812: Investigational device exemptions. https://www.accessdata.fda.gov/scripts/cdrh/cfdocs/cfcfr/CFRsearch.cfm?CFRPart=812. Accessed 11 October 2022
2. U.S. Food and Drug Administration (November 28, 2010) What we do. U.S. Department of Health & Human Services. http://www.fda.gov/AboutFDA/WhatWeDo/default.htm. Accessed 11 October 2022
3. International Organization for Standardization (ISO) (2021) ISO 5840:2005: Cardiovascular implants – cardiac valve prostheses – Part 1: General considerations, 2nd edn. ISO
4. International Organization for Standardization (ISO) (2021) ISO 5840:2005: Cardiovascular implants – cardiac valve prostheses – Part 2: Surgically implanted heart valve substitutes, 2nd edn. ISO

5. International Organization for Standardization (ISO) (2021) ISO 5840:2005: Cardiovascular implants – cardiac valve prostheses – Part 3: Heart valve substitutes implanted by Transcatheter Techniques, 2nd edn. ISO
6. Medical Device Regulation (MDR) – CE Certification MDR (EU) 2017/745. https://www.dekra.com/en/medical-device-regulation/. Accessed 11 October 2022
7. ICH E6 Guideline: Guideline for good clinical practice (E6R1) (1998)
8. Centers for Medicare & Medicaid Services (2012) National coverage determination (NCD) for routine costs in clinical trials (310.1) – current policy – July 2007 NCD. Medicare Clinical Trial Policies. https://www.cms.gov/ClinicalTrialPolicies/. Accessed 11 October 2022
9. U.S. Food and Drug Administration (September 2017) Evaluation and reporting of age-, race-, and ethnicity – specific data in medical device clinical studies: guidance for industry and Food and Drug Administration staff. https://www.fda.gov/regulatory-information/search-fda-guidance-documents/evaluation-and-reporting-age-race-and-ethnicity-specific-data-medical-device-clinical-studies. Accessed 11 October 2022
10. U.S. Food and Drug Administration Code of Federal Regulations Title 21. Part 50 – Protection of human subjects. https://www.ecfr.gov/current/title-21/chapter-I/subchapter-A/part-50. Accessed 11 October 2022
11. U.S. Food and Drug Administration (March 2006) Establishment and operation of clinical trial data monitoring committees: guidance for clinical trial sponsors. https://www.fda.gov/regulatory-information/search-fda-guidance-documents/establishment-and-operation-clinical-trial-data-monitoring-committees. Accessed 11 October 2022

# Chapter 21
# Clinical Applications of 3D Modeling and Printing for Intracardiac Valves

**Amanda C. Tenhoff**

## 21.1 Introduction: A Brief History of 3D Modeling and Printing

In order to fully appreciate the progress made in the last few decades – as well as the projected future applications for 3D modeling and printing as an invaluable technological resource in medicine – it is important to understand the associated history and development of this technology. Within this section, we describe a brief history of 3D printing as well as an overview of the various 3D printing technologies as they have applied to medical uses.

### *21.1.1 3D Printing Background*

Within this section, we detail the historical background of 3D printing as it relates to clinical applications, as well as its context today.

#### 21.1.1.1 3D Printing History

3D printing is a form of additive manufacturing, whereby material is added together to form a final product. By contrast, previous manufacturing techniques were primarily subtractive manufacturing (e.g., carving, cutting, or milling) or formative manufacturing (e.g., injection molding). Additive manufacturing methods, such as

A. C. Tenhoff, Ph.D. (✉)
Structural Heart - Anatomy-Device Interactions, Implant Group, Medtronic, Minneapolis, MN, USA
e-mail: tenho004@umn.edu

© The Author(s), under exclusive license to Springer Nature Switzerland AG 2023

P. A. Iaizzo et al. (eds.), *Heart Valves*, https://doi.org/10.1007/978-3-031-25541-0_21

3D printing, are largely utilized for rapid prototyping, since the nature of additive manufacturing allows for swifter creation of a final product as compared to subtractive manufacturing [1]. Thus, 3D printing has been greatly influential in shaping rapid prototyping and additive manufacturing processes [2].

Although previous studies had been conducted by others using a similar technology, 3D printing is largely recognized to have been invented by engineering-physicist Charles "Chuck" Hull in the early 1980s [1, 3]. In 1984, the first patent for the stereolithography (SLA) printing technology was filed by Hull, and the first 3D printer was made commercially available 4 years later through Hull's own company, 3D Systems [3, 4]. Since then, 3D printing has grown to include several different additive manufacturing technologies – most notably, selective laser sintering (SLS) by Carl Deckard in 1987 and fused deposition modeling (FDM), patented by S. Scott Crump of Stratasys in 1989 [5].

In the mid-1990s, preliminary applications of 3D printing for head and neck reconstruction were being explored – an endeavor developed and funded by the US military [6]. However, the breakthrough usage for 3D modeling and printing in the clinical realm was in the field of dentistry and orthodontia, when researchers first 3D printed various scaffold structures for synthetic bone growth in the early to mid-2000s [3, 7, 8]. Since then, 3D prints have been utilized for various clinical purposes ranging from cell growth structures, rapid prototyping of medical devices, anatomical organ modeling, and more – as to be discussed in further depth in Sect. 21.2.1.

In the cardiovascular space, 3D printing was first utilized in the early 2000s, mainly for the purposes of aiding in treatment planning and procedural planning of structural heart diseases [9–11]. The field has since grown to utilize 3D printing for rapid prototyping of medical devices in development, morphological study of anatomy, and even patient-specific medical device manufacture. These applications and more will be discussed in Sect. 21.2.

#### 21.1.1.2 Printing Processes and Materials

As mentioned in Sect. 21.1.1.1, various printing modalities are currently available, and each is compatible with a select variety of printing materials. These methodologies and materials exhibit a wide range of assets as well as drawbacks. Therefore, the optimal printing approach for a given project is ultimately driven by the functional needs and intended purpose of the 3D print. For example, if one desired only a detailed anatomical understanding of a heart for educational purposes, a relatively low-resolution, low-cost, hard plastic print would be sufficient. However, if one desired to practice a surgical procedure on a realistic anatomical 3D print of the heart, the aforementioned hard plastic print would not suffice. In this latter example, one would require a higher-resolution, more costly, flexible plastic print in order to meet the needs of the project. Therefore, it is important to consider the trade-offs of various printing modalities and materials – such as print resolution, cost, time constraints of the project, post-processing, and other needs defined by intended print

functionality – when deciding on 3D printing methods for a given project. This is discussed in more detail in Sect. 21.1.1.3.

3D prints are created through the aggregation of layers. No matter the modality or material, before a 3D model can be printed, a software program is used to slice the model into layers. As each layer is printed sequentially on top of one another, they aggregate to form the final 3D print. Photographs of these layers visible in a 3D print are shown in Fig. 21.1.

In general, there are two main types of layering methods within the printing processes, which we will define as two-dimensional (2D) layering and one-dimensional (1D) layering. In 2D layering modalities – such as material jetting (MJ) and stereolithography (SLA) – prints are created such that an entire two-dimensional area of one layer is completed at once. For MJ printing specifically, heated photopolymer droplets are sprayed onto the print bed, where they then cure to form the layer [12]. This process may also include UV light sources for curing. An example of this printing process is shown in Fig. 21.2.

In SLA printing – or, more specifically, vat polymerization – a print bed sits atop or at the bottom of a vat of liquid resin, and a laser is drawn over the area of interest. As the laser passes through the resin, it polymerizes it into one cohesive structure, which bonds to the print bed. The print bed then lifts away from – or descends into, depending on the printer – the vat of resin, such that uncured liquid resin can then

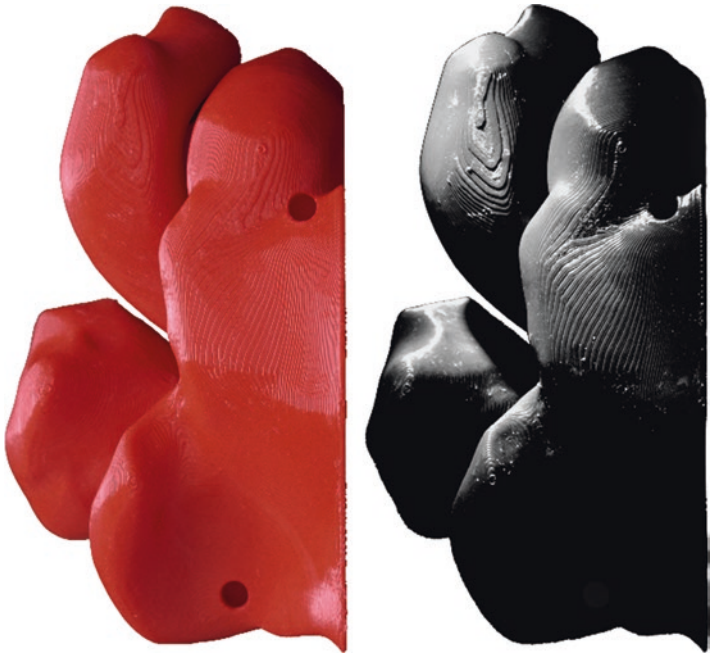

**Fig. 21.1** Visible layers (striations) in 3D print. Partial cardiac blood volume model, printed with PLA using FDM. Right image is digitally enhanced to better illustrate layers

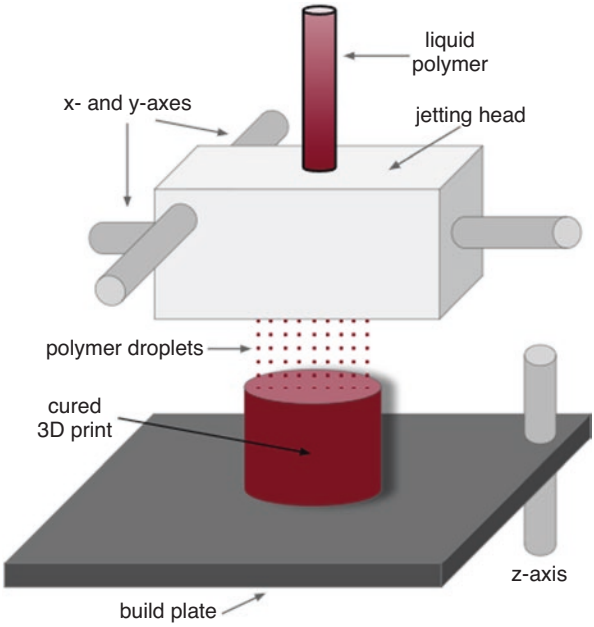


**Fig. 21.2** Simplified diagram showing material jetting 3D printing process

move between the laser source and the cured resin, for the polymerization and creation of the next layer. Most often, this process is done through projection of a 2D light map to print an entire layer at once, rather than tracing a singular laser point [13]. For these 2D light map cases, SLA printing can be considered to be a form of 2D layering.

By contrast, for 1D layering – such as selective laser sintering (SLS), fused deposition modeling (FDM), and single laser point SLA – a singular line or point approach is taken: the laser head or extrusion nozzle traces over the area of interest and consequently extrudes one line of material point-by-point until the area for one layer has been printed. This is illustrated in Fig. 21.3.

For SLS printing, a laser passes over a bed of material while following the path dictated by the layer geometry of the model slice. SLS is the process of sintering – or heating and combining – powdered material, usually nylon and other polymers or metal. Between layers, the print bed lowers and a fresh layer of powder is laid across the printing area as raw build material for the next layer to be sintered [12, 14].

In FDM printing, as illustrated in Fig. 21.3, filament material is heated to just above its glass transition temperature and then extruded out of a nozzle. In addition to the printing of the model itself, if needed, there may also be a support material printed alongside with the 3D print, in order to help the print maintain its structure as it cools into a solid piece. This support material may or may not be the same as the printed model material – often, the support material is dissolvable for easy removal. Unlike the simplified illustration in Fig. 21.3, it should be noted that 3D prints made by FDM are often not solid inside. This inner volume of the print, called

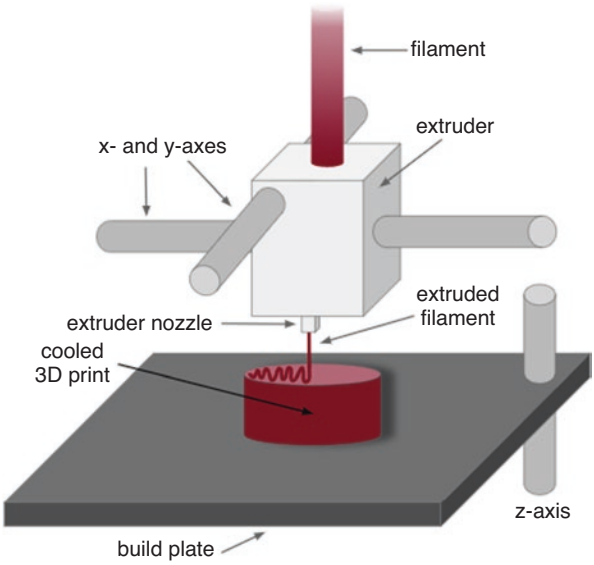


**Fig. 21.3** Simplified diagram showing FDM 3D printing process

the print infill, is a variable parameter. Depending on the needs of the 3D print, this infill may be modified in shape, structure, or density, in addition to surrounding wall thickness. This is also true for any support material that may be used in this printing process. Changing these parameters – for both the print material itself and the support material – can help to conserve both print material and printing time, therefore also minimizing overall printing costs.

Although FDM may be more tedious and have longer associated print times than other printing modalities, an advantage to this printing technique is that any thermoplastic may be used as filament [12]. Other printing methods (SLA, SLS, MJ) have a more limited range of print materials available for use, often due to the chemical or light curing process involved.

Generally, however, 2D layering modalities are advantageous over 1D layering in terms of printing time. This is especially true if multiple models are to be printed at once using the same printer, as the total print time for 2D layering modalities is solely dependent on the number of layers in the build, rather than the cumulative surface area of the layers. That is to say, for example, that if one SLA 3D print of layer height $Y$ took $T$ time to print, a number $N$ of these prints – printed at the same time and on the same printer – would still take the same total amount of time, $T$, to print. This is because an entire layer, $y$, can be formed within all $N$ prints simultaneously. The printing time for each layer is independent of the total print area of that layer. By contrast, the length of time needed to complete 3D prints through 1D layering techniques, such as FDM, scales directly with the number of prints being printed at the same time. In other words, a number $N$ prints would take at least $N \times T$ time to print, if $T$ was the time needed to print for $N = 1$. This is because each individual layer of each 3D print cannot be printed simultaneously, since the print

material is only being extruded from one location. This difference in print times is important to consider when deciding the appropriate printing approach for a given need, especially if multiple copies of the same print are desired.

#### 21.1.1.3 Considerations, Advantages, and Disadvantages for Clinical Use Cases

As one might expect, the plethora of printing processes and materials all have their own unique advantages and disadvantages, depending on the intended application for the final product. This is especially pertinent in the clinical space, where 3D models and prints may be used for a broad range of purposes. In deciding which 3D print modality is best for a given application, it is important to consider whether the final product will be implanted, blood-contacting, worn outside the body, or will have no long-term contact with the body.

From there, it is important to assess the intended function of the print: Is this meant to be a structural part, such as those used in facial reconstruction? Will it need to be bioinert, or would it be best to incorporate bioactive properties and tissue scaffolding structures? Will the print be undergoing any repeated stresses, or repeated deformations? If not being used for any sort of implant, important considerations regarding function include the following: the necessary accuracy or spatial resolution of the print, replication of tissue-like material properties, and anticipated handling of the print.

Additionally, it is important to consider the costs of the various printing modalities – including those of the printers themselves – and printing materials, as well as availability of printers/materials for utilization. Another associated factor with cost is necessary print turn-around time. If a print is needed as soon as possible for an emergent pre-procedural planning case, this will limit which printing modalities and materials may be suitable choices. In addition to the time it takes for prints to run, there may also be associated post-processing needed of the print, which can add significant time to the workflow. Furthermore, if a print is outsourced to another facility, there may be an increase in lead time due to travel or any other processing by the facility. Sometimes, these processes may be able to be expedited, but not without an increase in price. These and other cost considerations are discussed more generally in Sect. 21.1.3.

The printing modalities described in Sect. 21.1.1.2, as well as typical applications and associated advantages and disadvantages, are summarized in Table 21.1. It should be noted that this is not an exhaustive list, but this is intended to represent very common materials and printing modalities.

### *21.1.2 Clinical Workflow: From Scan to Model and Beyond*

In general, for the creation of a 3D print to be used for clinical purposes, the workflow will follow the same general progression: obtain the clinical imaging, import images into appropriate segmentation software, segment the desired anatomical

**Table 21.1** Comparison of printing modalities

| Print modality | Modality type | Material | Typical application | Advantages | Disadvantages |
|---|---|---|---|---|---|
| Stereolithography (SLA) | Vat polymerization | Resin | Bioimplants, tissue engineering, pre-procedural planning [14, 15] | High accuracy, fast printing time, can print complex structures | High cost, post-processing needed, very difficult to print using multiple materials [14] |
| Selective laser sintering (SLS) | Powder bed fusion | Nylon | Artificial bone structures (e.g., hip, skull), device prototypes, implants, cell scaffolds, drug delivery [14, 15] | Incorporation of bio structures, no support material, easy post-processing, easier to print difficult structures (e.g., channels, overhangs) [12, 14] | Very high cost [16], only one material per print [17] |
| | | Metal | Artificial bone structures (e.g., hip, skull) [15] | Material strength, no support material, easy post-processing, easier to print difficult structures (e.g., channels, overhangs) [12, 14] | Very high cost [16], only one material per print [17] |
| Fused deposition modeling (FDM) | Material extrusion | Polylactic acid (PLA) | Pre-procedural planning, education | Low cost, can be printed with water-soluble support (PVA) | Lowest accuracy, cannot encapsulate cells [14] |
| | | Acrylonitrile butadiene styrene (ABS) | Pre-procedural planning, education | Low cost, more durable than PLA | Lowest accuracy, cannot encapsulate cells [14], more difficult to work with than PLA |

(continued)

**Table 21.1** (continued)

| Print modality | Modality type | Material | Typical application | Advantages | Disadvantages |
|---|---|---|---|---|---|
| | | Nylon | Orthotics, braces, surgical guides [18, 19] | More pliable than PLA or ABS [18] | Difficult to store [18], higher cost compared to other materials and machine needs [19] |
| PolyJet (PJ) | Material jetting (MJ) | Acrylic-based polymers | Pre-procedural planning, practice surgery | High accuracy, can replicate tissue-like material properties, can print multiple materials at once | High cost [16], requires support material and post-processing [17] |

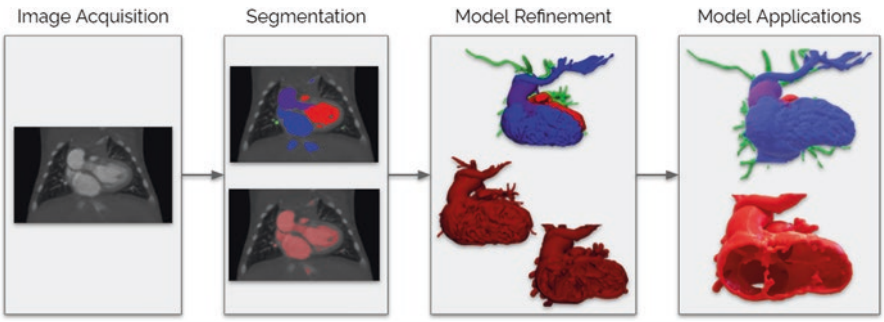


**Fig. 21.4** 3D model generation workflow. Illustration shows various segmentations and resultant models created from a single DICOM dataset (CT scan)

features into masks, export the resultant 3D reconstruction to mesh refinement software, refine the mesh, and prepare the final model. After the final model has been achieved, depending on the needs for the model, the result may or may not be 3D printed. Other clinical applications for a finalized 3D model include – but are not limited to – computational simulations, such as fluid flow analyses, and virtual or augmented reality integration. The workflow diagram in Fig. 21.4 illustrates this process.

Clinical or research image acquisition can be done through computed tomography (CT), microCT (μCT) scanning, magnetic resonance imaging (MRI), ultrasound or echocardiography, or any other type of multidimensional imaging, such as

those following the Digital Imaging and Communications in Medicine (DICOM) imaging format standard. For clinical cardiac cases, models are typically created from CT or MRI scans, although 3D echocardiography can also be utilized for the incorporation of valve segmentation [12]. Echocardiography is considered to be the best imaging modality for valve leaflets themselves, due to their relatively thin structure as well as dynamic motions resulting in difficulties in direct segmentation through other modalities [20]. Contrast-enhanced CT, in which a CT scan is performed while radiocontrast is injected into the bloodstream in the regions of interest, is greatly beneficial for the segmentation and modeling of the chamber and vascular blood volumes from the surrounding tissue of the heart. It is important to mention, however, that the models created from such datasets can ultimately only be as good as the imaging quality itself. Therefore, in order to best utilize these anatomical models, it is imperative to acquire the best imaging possible for the situation. Yet, one does need to consider the health impacts of radiocontrast and radiation exposure to the given patient. It should be noted that although radiation exposure from CT imaging can potentially increase risk of cancer, the impact is relatively small as compared to normal background radiation exposure [21]. Still, out of an abundance of caution, it is generally considered best practice to limit these exposures wherever possible [22].

A few of the main factors in determining imaging quality are the spatial resolution, or voxel (volume pixel) depth, the 2D pixel size, the brightness contrast between the blood and surrounding tissues, and the brightness contrast between varying tissue types. Limiting factors for image quality include the size and somatotype of the given patient being imaged, the amount of time available for imaging or otherwise the exposure time necessary for the imaging, and the ability to use radiocontrast. Especially for small or newborn patients, clinicians will want to expose these patients to as little radiation and as little chemical radiocontrast as possible, as both of these elements – although greatly beneficial for imaging quality and resultant anatomical modeling – can potentially be harmful to the pediatric patient in large or prolonged quantities [22].

As mentioned previously, in the context of heart valve modeling, it is important to recognize that valve leaflets are relatively thin and therefore difficult to resolve and distinguish from the blood volume and surrounding tissue when segmenting. Therefore, it can be particularly useful to augment CT or MRI data with echocardiographic imaging, as it can be easier to distinguish the valve leaflets and identify the annulus through echocardiography [23–25]. Additionally, it can be helpful to acquire electrocardiogram-gated (ECG-gated) CT imaging in order to determine the timing of the cardiac cycle and resultant valve positioning in the imaging [26].

Segmentation, then, is the process of separating the areas of interest from other elements within the images. Often, segmentation is performed manually by an anatomical expert; however, segmentation can also be completed automatically through the use of trained neural networks [25, 27, 28]. Typically, the initial segmentation will result in one or more masks, which are reconstructions of the selected areas of interest. As such, the segmentation process involves the creation of an initial mask through brightness thresholding – usually determined by voxel Hounsfield unit

(HU) intensity values. This mask is then edited through various software tools (automatically or manually) in order to achieve a result that best represents the patient's anatomy [29, 30].

An example of segmentation of several masks, each representing a different anatomical structure, is shown in Fig. 21.5. The lungs are represented by a peach-colored mask, the blood volume by a red mask, and the bones by a blue mask. Materialise Mimics© was used to read the patient's CT images and create these masks.

For the creation of cardiac 3D models and prints, especially in patients with septal defects or other intracardiac or vessel abnormalities, it should be noted that it may be most useful to create the 3D model from direct segmentation of the blood volume from the imaging. This is advantageous for a few reasons: It may be easier to get a more accurate model of the blood volume than the tissue, due to the contrast of the blood, and blood volume models can better elucidate intracardiac structural defects, especially in the case of congenital heart disease (CHD). If the vessel wall or chamber wall thickness is not important for the needs of the model or print, but an accurate representation of the intracardiac morphology is desired, this can be achieved through creating a blood volume model and then using software segmentation and modeling tools to create a hollow shell around this model.

After an appropriate mask or masks have been segmented, the next step is 3D reconstruction and post-processing. Masks can be created into volumetric 3D reconstructions – hereby referred to as models – and exported as stereolithography/standard tessellation language (STL) files for post-processing. The purpose of this step is to clean up model details (e.g., repair broken surfaces, smooth the model, trim unwanted sections, hollow the model) as well as to refine the model's structural mesh. Note, these types of modification require both a strong cardiac anatomical background and specific understanding of the given clinical case. Especially when

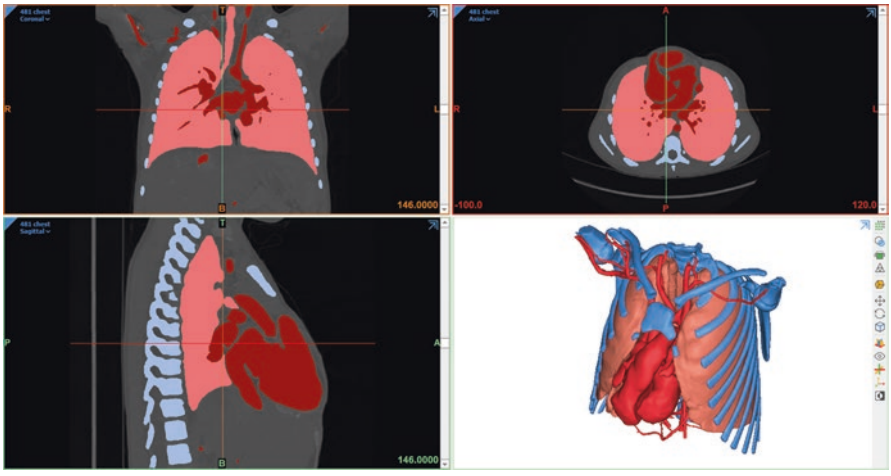

**Fig. 21.5** Multiple mask segmentation in Materialise Mimics© software. Red mask represents blood volume, peach mask represents the lung tissue, and blue mask represents the bone tissue

planning to 3D print the model, this step is crucial, because smoother contiguous surfaces with fewer hills and valleys will result in better-looking 3D prints with faster print times. A smoother print can also help to reduce the amount of support material needed for the print, thereby reducing the overall cost. This smoothing step is especially pertinent to models to be used in computational fluid flow applications as well, as smooth models will aid in decreasing the total mesh, thus decreasing the computation time needed to solve.

Once the model has been prepared through post-processing, it is ready for its various applications. As described previously, models are commonly 3D printed at this stage. Other applications – especially for cardiac or cardiovascular models – include computational fluid dynamics (CFD), model visual manipulation tools, and virtual reality (VR) integration. When preparing the model for VR, a common file format for the model is an object (OBJ) file. A model file can either be directly exported as an OBJ from the modeling software, or the mesh can be converted from the file format used by the modeling software – such as STL – into an OBJ file. This OBJ file can then be integrated into an appropriate VR software for use in the VR format.

Another way in which to create 3D anatomical models is to use a 3D object scanner. 3D models can easily be created from object scans of explanted hearts, such as those allocated for research purposes or those utilized in and recovered from preclinical studies. Once the object has been appropriately scanned, the procedure to the final application follows relatively the same workflow of post-processing as outlined above.

### *21.1.3 3D Printing Access*

As briefly described in Sect. 21.1.1.3, varied printing processes will have varied associated costs. Limitations may also exist in resource allocation for clinical 3D printing. For instance, a smaller or more rural hospital or medical center may not have the capability to create detailed 3D models or prints for their patients. By contrast, larger urban medical centers may have dedicated 3D printing centers, with designated staff for patient-specific 3D modeling and printing. This is especially true for centers with associated universities, such as Johns Hopkins Hospital (in association with the Carnegie Center for Surgical Innovation) and Stanford Health Care medical center, among others discussed in Sect. 21.3.1 [31, 32].

Medical care centers that do not have devoted 3D printing staff but still have resources for 3D printing may do so by outsourcing the print. As an example, the University of Minnesota Twin Cities campus and associated hospitals do not have hospital staff dedicated to anatomical 3D printing services; however, there are several groups within the university who partner with clinical care teams in order to deliver 3D models and prints for direct clinical needs. Here at the Visible Heart® Labs, we collaborate with clinical staff at the Masonic Children's Hospital and Children's Minnesota to provide patient-specific 3D models and 3D prints on an

as-needed basis, at no cost to the hospitals. This is done as part of an educational collaboration, funded through our partnership with Medtronic (Minneapolis, MN, USA) and an unrestricted educational grant with Stratasys (Eden Prairie, MN, USA). In addition, other hospitals and medical institutions can outsource their 3D modeling and printing needs directly to commercial companies, such as Stratasys, Materialise, Hubs, Craftcloud®, and many others. However, there are associated fees with utilizing these services, which may vary between vendors and between material, print modality, and print order volume.

Still, there remain a number of medical centers who are unable to afford in-house or even outsourced 3D modeling and 3D printing. For these centers, although they are not necessarily patient-specific models for the centers in need, there exist a number of online resources for viewing 3D anatomical models. One such resource is the Atlas of Human Cardiac Anatomy – an open-access website built, supported, and maintained by the Visible Heart® Labs [33]. Through the Atlas, visitors can learn about cardiac anatomy and physiology through studying models of real patients, in additional to a multitude of translational animal models. The Atlas is particularly useful for understanding complex disease states. Due to their anatomical complexity and morphological individuality in presentation, many complex disease states – particularly those of congenital heart defects – are better understood through individual patient models, rather than through a generalized textbook description and cartoon. Although these models may not be exactly what a practitioner is seeing in their own patient, the variety of patient-specific models offered through the Atlas is intended to aid in educational understanding of the disease state at hand [34]. In addition, as of the writing of this chapter, we are aiming to incorporate an option to download these 3D models for printing or computational use on an as-needed basis. This effort is particularly aimed at allowing access to 3D modeling and printing that some medical centers may otherwise not have.

To conclude, access to 3D modeling and printing capabilities for medical centers is still not universal. Some centers may have in-house 3D printing; others may outsource their 3D printing. Still, others may not have the resource availability for providing 3D prints at all. Especially for these facilities, anatomical 3D models available online can prove to be a powerful educational tool.

## 21.2 3D Modeling and Printing for Cardiac Clinical Applications

Within this section, we detail the clinical applications of 3D modeling and 3D printing specifically within the realm of cardiac anatomy and physiology. Generally, these purposes can be for the fulfillment of a direct clinical need (e.g., patient-specific cardiac models for pre-procedural planning), an educational or research resource, or for industry use.

### *21.2.1 Overview of Cardiac Clinical Applications*

From the clinical perspective, 3D modeling and printing can be used for three main purposes: (1) rapid prototyping in medical device design, (2) patient-specific medical device design, and (3) patient-specific anatomical modeling and virtual prototyping. Many of the potential uses for 3D modeling and printing in the clinical realm have been outlined in Table 21.1, from Sect. 21.1.1.3. Within this section, the specific cardiac applications are highlighted and described in further detail.

#### 21.2.1.1 Rapid Prototyping in Medical Device Design

As mentioned previously, rapid prototyping of devices is the defining advantage of utilizing 3D modeling and printing in general. Within the realm of clinical applications, there are many regulatory standards in place – and more are continuing to be developed, even as this chapter is being written. In short, regulations exist in the production of all medical devices in order to help standardize their production and guarantee their safety. With the rise in 3D printing technology being used in the medical field, it became imperative that new standards were assessed and implemented [35]. This is to be discussed in further detail in other chapters within this publication, particularly the ASME Verification and Validation (V&V 40) standard newly published in 2018 as well as other regulatory standards and processes [36].

Due to the nature of 3D printing technology itself, it is usually more economically feasible to utilize other means for larger-scale production. Thus, the rapid prototyping offered by 3D printing is more often performed on an as-needed basis or in low-count batches – such as in the early stages of product development. If large volumes of product are needed, such as for commercial manufacture, then formative manufacturing such as injection molding or other approaches should be considered. Rapid prototyping, as the name would suggest, is instead greatly useful for research and design (R&D) applications.

In the cardiac space, rapid prototyping has a multitude of applications, including 3D anatomical modeling for device sizing, device testing, or even rapid manufacture and cost-effective design and proof-of-concept testing of early device prototypes. It should be noted that this approach can be applied to both preclinical (animal) and early feasibility studies. More specifically for intracardiac valve applications, rapid prototyping has been used for creating anatomical structures for benchtop modeling of valves, as well as for ex vivo valve function analysis, the testing of valve hemodynamics, and other research and educational endeavors [26]. However, since all of these applications require models that ultimately depend on imaging, it is imperative that proper images with appropriate spatial and temporal resolution are acquired. As mentioned previously, due to their thin structure and changing morphology, intracardiac valves are difficult to image and replicate, so care must be taken to ensure optimal image quality. Limitations in both imaging technology and 3D printing materials pose the greatest limitations on rapid prototyping in valvular disease.

#### 21.2.1.2 Patient-Specific Medical Devices and Implants

Perhaps one of the main drivers for the utilization of 3D modeling and printing in the cardiac space – and, more generally, in the medical field – is the ability to create patient-specific models and device designs. By modeling real patient anatomies, corresponding medical devices and implants can be designed to complement the given patient's critical anatomies in association with the device-tissue interface. By extension, since these devices are designed for specific patients, the aim is that the devices would be more efficacious with improved long-term outcomes. This is especially pertinent to patient-specific computational models, which allow for rigorous testing in a simulated environment before deployment or implantation in any patients – such as in the case of finite element analysis (FEA) and fluid-structure interaction (FSI) for the investigation of patient-specific bioprosthetic aortic valve replacements [37, 38]. Computational processes such as FEA, FSI, and computational fluid dynamics (CFD) are all essential components of patient-specific medical device design and testing. These methods, along with their regulatory compliance, are explained in further detail in other chapters within this publication.

#### 21.2.1.3 Patient-Specific Anatomical Modeling and Virtual Prototyping

Arguably today, patient-specific anatomical modeling and virtual prototyping are the major applications for 3D modeling and printing in the cardiac space – especially for intracardiac valve studies. Patient-specific anatomical models are advantageous for pre-procedural planning, in general, and are especially useful for planning in cases of transcatheter valve replacement, aortic or pulmonary stenosis, or the treatment of other valvular dysfunction [39]. Models can be printed and used in these cases for patient education, treatment discussion among the care team, specific treatment planning (such as valve sizing), or for procedural practice [40]. Another valuable application for patient-specific anatomical models is in the determination of candidacy for clinical trials of devices, such as the Edwards Alterra® prestent and SAPIEN 3® implantable valve system (Edwards Lifesciences, Irvine, CA, USA) [41].

Additionally, anatomical models can be used for virtual prototyping [42]. Virtual prototyping is a method by which 3D models of a device prototype are virtually implanted through computational means into a 3D anatomical model. This can lead to valuable insights about how a given device or multiple devices may fit within a heart or surrounding vessels, in a more cost-effective manner than through large-animal or cadaveric models – especially when considering that multiple anatomical models may be used to study variances of device fittings between patients [42]. Consequentially, virtual prototyping should be considered as an invaluable part of the iterative design process, such as in the creation of an implantable pulmonic valve replacement [43]. Additionally, virtual prototyping can be useful not only in the design process of the device itself but also in the device delivery approach, such as in cases of pre-procedural planning or for general clinical procedural training [43, 44].

Another growing area in patient-specific anatomical modeling and virtual prototyping is virtual and mixed realities. In virtual reality, any 3D anatomical model can be incorporated into a virtual environment for users to experience in fully immersive 3D scenes. These scenes may have more than just static 3D models – they may also include incorporated videos, programmed fly-throughs, or other interactive elements. Virtual models have been shown to be an advantageous teaching tool but can also be useful for patient-specific treatment planning due to their manipulability [34, 45]. Specifics about and applications of virtual and mixed realities for cardiac study are also discussed in more depth in other chapters of this publication.

Although not fully immersive, another useful application of these models is incorporation into open-access model visual manipulation tools, such as Sketchfab©. Through tools such as these, 3D models can be shared in an environment where they can easily be visualized and manipulated by end users – such as clinical teams or medical trainees – in a low-cost, easy-to-access manner.

### *21.2.2 Usage Cases: Intracardiac Valve Modeling*

One important application for cardiovascular 3D modeling and printing is intracardiac valve modeling. Especially as imaging and computing technologies continue to advance, the ability to model and print intracardiac valves and the surrounding anatomy is becoming a more accessible reality. This is an important and exciting development for specific use cases such as implantable valve sizing, evaluation of valve replacement candidacy, and bioprinting of implantable valves [15]. Within this section are discussions of two specific examples of intracardiac valve modeling: a pediatric case evaluating candidacy for transcatheter pulmonary valve replacement (TPVR) [47], and a retrospective study determining the utility of preoperative patient-specific 3D prints in adult cases of transcatheter aortic valve replacement (TAVR) [46].

#### 21.2.2.1 Pediatric Case: Evaluation for TPVR

One example in which 3D modeling and printing were used clinically for valve study was in the case of a pediatric patient who was exhibiting significant pulmonary valve insufficiency and was being evaluated as a candidate for transcatheter pulmonary valve replacement, or TPVR [47]. The print was desired in this case because, in addition to assessing proper valve frame sizing, the clinician wanted to ensure that the implantation of this new valve would not consequently obstruct flow in the ascending aorta nor would it cause occlusion of the right or left coronary arteries. Figure 21.6 illustrates the relevant anatomy that would raise this concern. Implantation of a valve in the area of the native pulmonary valve (PV), especially if the implanted valve was too oversized, could result in partial or full occlusion of the right coronary ostium (RCO) or the left coronary artery (LCA).

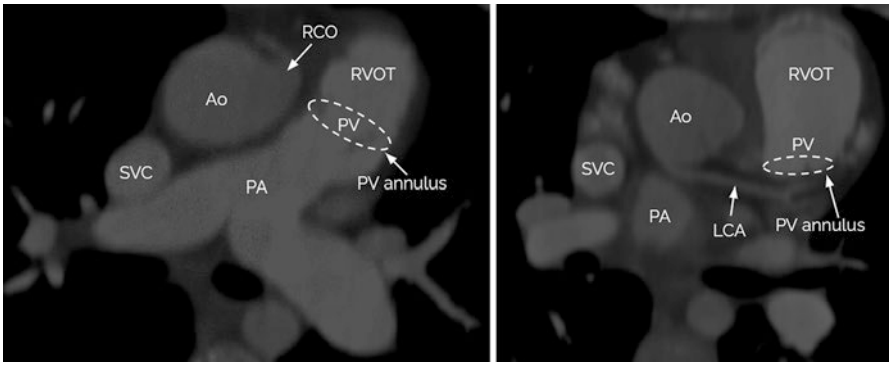


**Fig. 21.6** Inferior views of axial plane slices from patient CT scan. LEFT: location of RCO relative to PV annulus. RIGHT: location of LCA relative to PV annulus. Nomenclature from left to right: SVC, superior vena cava; Ao, aorta; PA, pulmonary artery; RCO, right coronary ostium; PV, pulmonary valve; RVOT, right ventricular outflow tract; LCA, left coronary artery

In order to best evaluate the anatomy in this case, it was decided to print three distinct 3D anatomical models: a reference model of the blood volume, a hollow outwardly shelled blood volume model, and a tissue-based model [47]. The two hollow models were used to take measurements and practice valve deployment, whereas the blood volume model was used as a guide to understanding the blood flow pathway within the heart. A comparison of these masks and resultant models is shown in Fig. 21.7.

It should be noted that the valves themselves were not included with these models. When segmenting the imaging, it was difficult to determine the leaflets apart from the blood volume due to the image resolution and timing of the image capture relative to the phase of the cardiac cycle. Additionally, resources were not available for replicating the leaflet tissue mechanical properties, and there was concern about how this might impact valve deployment and resultant conclusions, being that the printed valve leaflets would not correlate well with the patient's true physiology. As to be discussed in Sect. 21.3, this is one limitation that advanced imaging and computing technologies can help to obsolete.

#### 21.2.2.2 Adult Case: Prediction of TAVR Complications

Another usage case for patient-specific 3D valve modeling is postoperative – or even postmortem – study. In 2019, researchers from Shanghai and Liaoning, China, published a study in which four adults were studied after fatal complications subsequent to receiving transcatheter aortic valve replacement (TAVR) intervention [46]. The aim of this study was to determine if the deaths of these patients could have been predicted beforehand, through the utilization of patient-specific 3D models.

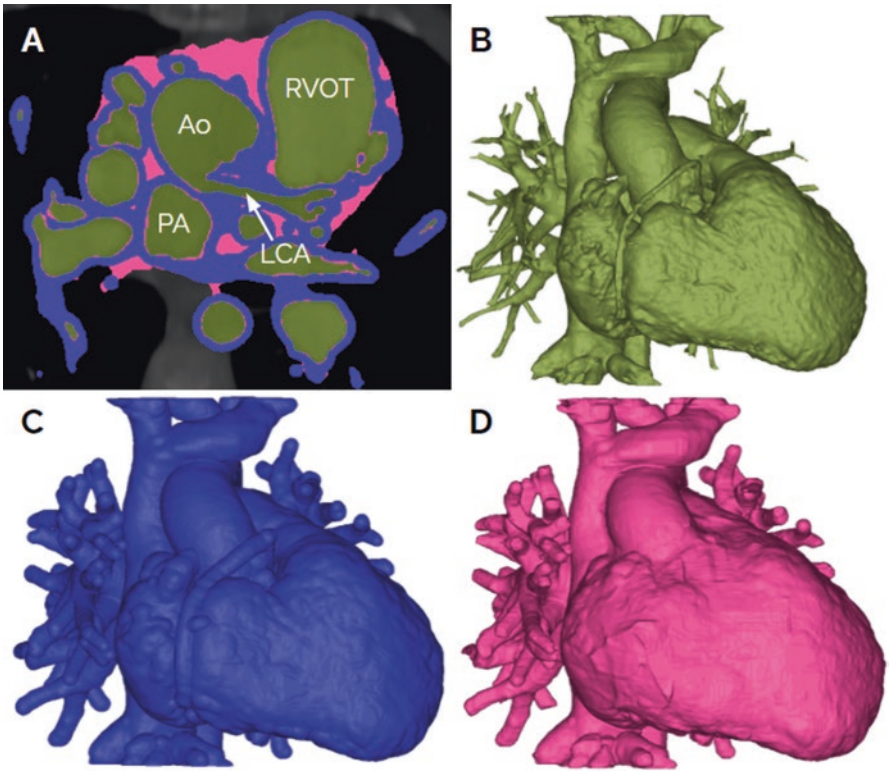


**Fig. 21.7** The different masks and resultant models for the TPVR case. (**a**) Inferior view of axial slice, as shown in Fig. 21.6. The green mask represents the blood volume, the blue mask represents a 2 mm shell around the blood volume, and the pink mask represents the cardiac tissue. (**b**) The blood volume model. (**c**) The hollow shell model. (**d**) The tissue model

Patients were chosen for this study who had died after undergoing TAVR but whose pre-procedural CT angiography (CTA) imaging had not indicated any complications [46]. Models were created from the pre-procedural CTA data that was available, in order to replicate the scenario. These models were segmented from the blood volume in the CTA imaging. From there, a 2 mm shell was created around the blood volume, and a 1 mm valve with calcifications was manually incorporated into the model. This shell model, with the imitation valve and calcium, became the final model used for benchtop testing.

The resultant models were printed using flexible material that mimicked the material properties of the aortic vessel and of the calcium [46]. Non-valved stent frames consistent with those used in the patients were then deployed into their respective patient-specific 3D prints. In all four prints, the result from the deployment – either coronary ostium obstruction or aortic annulus rupture – was consistent with and replicated the events seen in the respective patients during their TAVR procedures [46].

The conclusion of this study was that for these four cases, preoperative patient-specific 3D models may have been helpful in avoiding adverse outcomes for the patient by allowing for benchtop simulation to inform treatment planning. Thus, 3D models were shown in these cases to be a useful – if not critical – supplement to diagnostic imaging for patient treatment planning and care.

## 21.3 Today and Tomorrow: Where Are We Now, and Where Are We Headed?

Throughout this chapter, the utility of 3D modeling and printing for intracardiac valves has been made evident. However, multiple limitations have also come to light, such as difficulty and expense of printing materials with realistic tissue-like material properties, imaging quality, biocompatibility of materials, and regulation of 3D modeling and printing processes within the clinical realm. In an effort to excel past these limitations, researchers and organizations around the world are making advances in 3D modeling and printing technology every day. Even at our own home institution, the University of Minnesota (Minneapolis, MN, USA) has multiple teams of researchers working on 3D modeling and printing technologies for a multitude of applications. To name just a few, the Visible Heart Labs® (led by Dr. Paul Iaizzo), the System Regeneration Lab (led by Dr. Brenda Ogle), the McAlpine lab (led by Dr. Michael McAlpine), and the Medical Devices Center (led by Dr. Art Erdman) at the University of Minnesota are all committed to research for advancing clinical 3D printing in the cardiac space.

### *21.3.1 Current Technologies and Ongoing Research*

Since the invention of 3D printing technology in the 1980s, technological growth and scientific advancements continue to redefine the landscape for what comes next. Currently, one of the main areas of research and growth in this area is 3D bioprinting. Bioprinting technology involves creating structures from, or that are embedded with, living cells. Applications for bioprinting vary but can be greatly useful in patient-specific grafting or replacement of damaged tissues, such that the structure can be utilized as an implant that is both biocompatible and bioactive within the body of the recipient.

For a real-world example, researchers from the System Regeneration Lab, the Talkachova Lab (led by Prof. Elena Tolkacheva, University of Minnesota, Minneapolis, MN, USA), and the McAlpine Lab recently created a 3D bioprinted two-chambered beating heart organoid [48]. This was created by way of embedding hydrogel extracellular matrix material with cellularized gelatin bioink. The result was a beating, two-chambered heart pump at a tenth of the scale of an adult human heart [48]. Differentiation of the cardiomyocytes in situ was a significant

breakthrough for cardiac bioprinting and shows promise for future functional bioprinting.

Looking more specifically at intracardiac valves, the McAlpine lab recently teamed with the Visible Heart® Labs to create a patient-specific model of an aortic root that contained embedded sensors [49]. This print was used for understanding contact pressures between a TAVR implant and the surrounding tissue-like material, which is valuable for assessing device sizing and placement in a potential patient. In addition to these embedded sensors, this print was also unique in that it featured three varying types of materials in order to mimic the tissue properties of the aorta itself, the surrounding myocardium of the left ventricle, and the calcifications within the left ventricular outflow tract (LVOT) and leaflets [49].

Here at the Visible Heart® Labs, researchers are working on 3D printing alongside virtual and mixed realities integration in order to educate patients and their families as well as clinical care team members and training cardiology fellows on diseased cardiac anatomy and physiology [34, 42]. Within the lab, there is a long history of 3D modeling and printing in these contexts – from pre-procedural planning tools to educational post-procedural analysis, to benchtop modeling of anatomical-device interaction, and beyond [50–53]. In addition, these models and resources are being made available worldwide through an open-access website: the Atlas of Human Cardiac Anatomy, as discussed in Sect. 21.1.3 [33, 34].

The Visible Heart® Labs also houses over 600 formalin-fixed human hearts, procured through LifeSource (Minneapolis, MN, USA) and graciously donated by organ donors whose hearts were unable to be transplanted to living recipients. These hearts were perfused in an end-diastolic morphology, while they were being chemically fixed in a 10% formalin solution, such that the atria and ventricles remained dilated; thus, the valves and other intracardiac structures could be easily visualized postfixation [54–56].

Outside of the University of Minnesota, separate research teams at Cornell University (Ithaca, NY, USA) and Sabanci University (Istanbul, Turkey) have each successfully printed biocompatible aortic valves within a hydrogel structure [15, 57, 58]. Having biocompatible and bioactive valves may allow for these structures to continue to grow and change with the recipient, so that they would not need a replacement as their bodies naturally change over time. Evidently, researchers around the world are working to advance cardiovascular bioprinting.

Technological advances in clinical 3D printing are not limited to academia. Industry professionals in healthcare – from both engineering and medical contexts – are also working to push 3D printing to the next level. As of the publication of this chapter, Materialise (Leuven, Belgium) Mimics® software suite remains the industry standard for image processing and modeling from DICOM images, and they and others are working to automate cardiac image segmentation in order to streamline the workflow from imaging to model. This can also help to standardize anatomical models, which can vary slightly between users. Convolutional neural networks (CNN) are being developed for this purpose and have been shown to be successful in healthy adult human heart segmentation [25, 27, 28].

The next step in the workflow – 3D printing itself – is seeing industry advancements as well. 3D printing companies such as Stratasys (Rehovot, Israel) are working to create materials which mimic mechanical properties of varying tissue types. This can be difficult not only in achieving specific properties but also in the integration and cohesion of multiple types of tissues and their various properties in one print. Still, printers such as the Stratasys J750 Digital Anatomy printer are able to print with a wide variety of mechanical properties and colors, for applications such as realistic surgical practice and education – a very exciting development from the humble SLA beginnings of 3D printing in 1986.

Additionally, the practice of clinical 3D printing is expanding to be an incorporated part of medical schools and hospitals – in some institutions, it can even be a part of the protocol for patient care, as discussed in Sect. 21.1.3. At institutions such as the Henry Ford Hospital in Detroit, MI, the creation of a patient-specific model for evaluation of TAVR candidacy and treatment planning is a frequent part of the protocol for patients exhibiting aortic valve insufficiency, as well as for other structural heart diseases [17, 59]. Additionally, institutions such as the University of South Florida have dedicated staff in their Department of Radiology whose primary job is to create patient-specific anatomical models for pre-procedural usage, at the request of doctors and surgeons at the university [60].

As with any advancing technology, in order to bridge the gap between the research realm and clinical implementation, the next step is the development of appropriate regulatory processes. As mentioned in Sect. 21.2.1.1, the key to these regulations and subsequent discussions was the Verification and Validation standard published in 2018 [36]. These and other regulatory information are discussed in more detail in other chapters within this publication.

### *21.3.2 Future Advancements*

3D modeling and printing in the clinical realm is predicted to continue to grow, continuing to advance with associated technologies and meet as of yet unmet clinical needs. As previously mentioned, bioprinting in particular tends to be the main focus area for research and growth in clinical 3D printing.

Some difficulties faced in advancing bioprinting include maintaining cellular viability, differentiation of cell types, maintenance of mechanical tissue properties, and maintenance of electrical tissue properties, if applicable [57]. However, working to overcome these hurdles will be extremely advantageous for all future patients – and especially valuable for pediatric patients. Generally, it can be difficult to create patient-specific devices or implants for pediatric cases since the child is anticipated to grow and change anatomically, much more so than a fully grown adult. Therefore, the creation of devices – such as the implantable valves previously discussed – that can grow with the patient would be of great value for the treatment of pediatric valve insufficiencies (and other congenital or structural heart diseases) in the future.

Alongside those of biotechnology, advances in computing are pivotal in shaping the future of 3D modeling and 3D printing for clinical applications. Additionally, advancements in imaging technology and associated post-processing software will consequently lead to improved model accuracy and usability [61]. Especially pertinent are auto-segmentation software and predictive analysis protocols to ensure device efficacy and optimal patient outcomes [17, 59, 62]. Further, and as previously mentioned, virtual and augmented reality are becoming a growing resource for both education and pre-procedural planning and are predicted to continue to progress along with related technological advancements [63].

Finally, it is important to state that none of these predicted technical and biological advancements will have met their full potential without adoption into actual clinical practice. Therefore, perhaps the most crucial next step for the field is to better integrate these technologies into medical schools, hospitals, and treatment facilities [61]. New regulatory standards and associated workflows will help to achieve this goal, such that we can effectively unite engineering advancements and clinical expertise to further revolutionize medicine in the twenty-first century.

## References

1. Su A, Al'Aref SJ (2018) History of 3D printing. In: 3D printing applications in cardiovascular medicine. Elsevier, pp 1–10
2. Wong KV, Hernandez A (2012) A review of additive manufacturing. ISRN Mech Eng 2012:1–10
3. Ventola CL (2014) Medical applications for 3D printing: current and projected uses. P T 39(10):704–711
4. Hull CW (1986) Apparatus for production of three-dimensional objects by stereolithography. US Patent No 4575330.
5. Hubs. 3D printing and additive manufacturing – a complete overview. Hubs [Online]. Available: https://www.hubs.com/guides/3d-printing/. Accessed 21 May 2021
6. Grant GT, Rybicki FJ (2017) Introduction. In: Rybicki FJ, Grant GT (eds) 3D printing in medicine: a practical guide for medical professionals. Springer, Cham, pp 1–4
7. Gross BC, Erkal JL, Lockwood SY, Chen C, Spence DM (2014) Evaluation of 3D printing and its potential impact on biotechnology and the chemical sciences. Anal Chem 86(7):3240–3253
8. Leukers B, Gülkan H, Irsen SH, Milz S, Tille C, Schieker M, Seitz H (2005) Hydroxyapatite scaffolds for bone tissue engineering made by 3D printing. J Mater Sci Mater Med 16(12):1121–1124
9. Schmauss D, Haeberle S, Hagl C, Sodian R (2015) Three-dimensional printing in cardiac surgery and interventional cardiology: a single-centre experience. Eur J Cardiothorac Surg 47(6):1044–1052
10. Wang H, Song H, Yang Y, Cao Q, Hu Y, Chen J, Guo J, Wang Y, Jia D, Cao S, Zhou Q (2020) Three-dimensional printing for cardiovascular diseases: from anatomical modeling to dynamic functionality. Biomed Eng Online 19(1):76
11. Xu C, Liang J, Yang J (2021) History of cardiovascular 3D printing. In: Yang J, Lee AP-W, Vida VL (eds) Cardiovascular 3D printing: techniques and clinical application. Springer, Singapore, pp 1–2
12. Ding P, Li L, Yang M, Yang J (2021) The methods of cardiovascular 3D printing. In: Yang J, Lee AP-W, Vida VL (eds) Cardiovascular 3D printing. Springer, Singapore, pp 3–14

13. Formlabs. SLA vs. DLP: guide to resin 3D printers. Formlabs [Online]. Available: https://formlabs.com/blog/resin-3d-printer-comparison-sla-vs-dlp/. Accessed 3 Sept 2021
14. Duan B, Wang M (2013) Selective laser sintering and its biomedical applications. In: Schmidt V, Belegratis MR (eds) Laser technology in biomimetics: basics and applications. Springer, Berlin, Heidelberg, pp 83–109
15. Kaza A, Rembalsky J, Roma N, Yellapu V, Delong W, Stawicki S (2018) Medical applications of stereolithography: an overview. Int J Acad Med 4(3):252
16. Mitsouras D, Liacouras PC (2017) 3D printing technologies. In: Rybicki FJ, Grant GT (eds) 3D printing in medicine. Springer International Publishing, Cham, pp 5–22
17. Wang DD, Qian Z, Vukicevic M, Engelhardt S, Kheradvar A, Zhang C, Little SH, Verjans J, Comaniciu D, O'Neill WW, Vannan MA (2021) 3D printing, computational modeling, and artificial intelligence for structural heart disease. JACC Cardiovasc Imaging 14(1):41–60
18. Mardis NJ (2018) Emerging technology and applications of 3D printing in the medical field. Mo Med 115(4):368–373
19. Frizziero L, Santi GM, Leon-Cardenas C, Donnici G, Liverani A, Papaleo P, Napolitano F, Pagliari C, Di Gennaro GL, Stallone S, Stilli S, Trisolino G, Zarantonello P (2021) In-house, fast FDM prototyping of a custom cutting guide for a lower-risk pediatric femoral osteotomy. Bioengineering 8(6):71
20. Saleh Q, Moscona J, Le Jemtel T (2018) Valvular heart disease. In: 3D printing applications in cardiovascular medicine. Elsevier, pp 103–139
21. Center for Devices and Radiological Health (2018) What are the radiation risks from CT? FDA [Online]. Available: https://www.fda.gov/radiation-emitting-products/medical-x-ray-imaging/what-are-radiation-risks-ct. Accessed 25 Jan 2022
22. Kutanzi KR, Lumen A, Koturbash I, Miousse IR (2016) Pediatric exposures to ionizing radiation: carcinogenic considerations. Int J Environ Res Public Health 13(11):1057
23. Gosnell J, Pietila T, Samuel BP, Kurup HKN, Haw MP, Vettukattil JJ (2016) Integration of computed tomography and three-dimensional echocardiography for hybrid three-dimensional printing in congenital heart disease. J Digit Imaging 29(6):665–669
24. Lang RM, Badano LP, Tsang W, Adams DH, Agricola E, Buck T, Faletra FF, Franke A, Hung J, Pérez de Isla L, Kamp O, Kasprzak JD, Lancellotti P, Marwick TH, McCulloch ML, Monaghan MJ, Nihoyannopoulos P, Pandian NG, Pellikka PA, Pepi M, Roberson DA, Shernan SK, Shirali GS, Sugeng L, Ten Cate FJ, Vannan MA, Zamorano JL, Zoghbi WA (2012) EAE/ASE recommendations for image acquisition and display using three-dimensional echocardiography. J Am Soc Echocardiogr 25(1):3–46
25. Corinzia L, Laumer F, Candreva A, Taramasso M, Maisano F, Buhmann JM (2020) Neural collaborative filtering for unsupervised mitral valve segmentation in echocardiography. arXiv:2008.05867
26. Montealegre-Gallegos M, Jeganathan J, Mahmood F (2017) Valvular heart disease. In: Farooqi KM (ed) Rapid prototyping in cardiac disease: 3D printing the heart. Springer International Publishing, Cham, pp 123–131
27. Tran PV (2017) A fully convolutional neural network for cardiac segmentation in short-axis MRI. arXiv:1604.00494
28. Gaasedelen E, Deakyne A, Iaizzo P (2019) Automated multiclass cardiac volume segmentation and model generation. arXiv:1909.06685
29. Foley TA, El Sabbagh A, Anavekar NS, Williamson EE, Matsumoto JM (2017) 3D-printing: applications in cardiovascular imaging. Curr Radiol Rep 5(9):43
30. Byrne N, Velasco Forte M, Tandon A, Valverde I, Hussain T (2016) A systematic review of image segmentation methodology, used in the additive manufacture of patient-specific 3D printed models of the cardiovascular system. JRSM Cardiovasc Dis 5:2048004016645467
31. Johns Hopkins School of Medicine. 3D printing & visualization services. Art Appl Med [Online]. Available: https://medicalart.johnshopkins.edu/3d-printing-advanced-3d-technologies/. Accessed 20 Dec 2021

32. Stanford Medicine. 3D printing in medicine. 3D Quant Imaging Lab [Online]. Available: https://3dqlab.stanford.edu/home/3d-prints/. Accessed 20 Dec 2021
33. Iaizzo PA (2016) The Visible Heart® project and free-access website 'Atlas of Human Cardiac Anatomy'. Europace 18(suppl_4):iv163–iv172
34. Tenhoff AC, Deakyne AJ, Iles TL, Narasimhan SL, Said SM, Griselli M, Iaizzo PA (2020) Development of an open-access library of pediatric congenital heart diseases and treatments: a tutorial on the atlas of human cardiac anatomy. American Society of Mechanical Engineers Digital Collection
35. Center for Devices and Radiological Health (2020) 3D printing of medical devices. FDA [Online]. Available: https://www.fda.gov/medical-devices/products-and-medical-procedures/3d-printing-medical-devices. Accessed 3 Sept 2021
36. ASME (2018) Assessing credibility of computational modeling through verification and validation: application to medical devices, VV 40-2018. ASME
37. Xu F, Morganti S, Zakerzadeh R, Kamensky D, Auricchio F, Reali A, Hughes TJR, Sacks MS, Hsu M-C (2018) A framework for designing patient-specific bioprosthetic heart valves using immersogeometric fluid–structure interaction analysis. Int J Numer Method Biomed Eng 34(4):e2938
38. Auricchio F, Conti M, Morganti S, Totaro P (2011) A computational tool to support pre-operative planning of stentless aortic valve implant. Med Eng Phys 33(10):1183–1192
39. Tang J, Liu Y, Zhu D, Ma Y, Lu F, Fang F, Shang X, Yang J, Wu Y, Pan X, Zhang H (2021) Valvular disease and three-dimensional printing. In: Yang J, Lee AP-W, Vida VL (eds) Cardiovascular 3D printing. Springer, Singapore, pp 53–110
40. Zhang H, Pan W, Yu S, Lee AP-W (2021) Clinical applications of cardiovascular 3D printing. In: Yang J, Lee AP-W, Vida VL (eds) Cardiovascular 3D printing. Springer, Singapore, pp 23–34
41. Shahanavaz S, Balzer D, Babaliaros V, Kim D, Dimas V, Veeram RSR, Leipsic J, Blanke P, Shirali G, Parthiban A, Gorelick J, Zahn EM (2020) Alterra adaptive prestent and SAPIEN 3 THV for congenital pulmonic valve dysfunction. JACC Cardiovasc Interv 13(21):2510–2524
42. Deakyne AJ, Iles TL, Mattson AR, Iaizzo PA (2019) Virtual prototyping: computational device placements within detailed human heart models. Appl Sci 10(1):175
43. Capelli C, Taylor AM, Migliavacca F, Bonhoeffer P, Schievano S (2010) Patient-specific reconstructed anatomies and computer simulations are fundamental for selecting medical device treatment: application to a new percutaneous pulmonary valve. Philos Trans R Soc Math Phys Eng Sci 368(1921):3027–3038
44. Capelli C, Sauvage E, Giusti G, Bosi GM, Ntsinjana H, Carminati M, Derrick G, Marek J, Khambadkone S, Taylor AM, Schievano S (2018) Patient-specific simulations for planning treatment in congenital heart disease. Interface Focus 8(1):20170021
45. Nguyen K (2017) Past developments and future directions of 3D cardiac printing: a surgeon's perspective. In: Farooqi KM (ed) Rapid prototyping in cardiac disease: 3D printing the heart. Springer, Cham, pp 183–189
46. Tenhoff AC, Aggarwal V, Ameduri R, Deakyne A, Iles TL, Said SM, Griselli M, Iaizzo PA (2021) Patient-specific three-dimensional computational heart modeling and printing to enhance clinical understandings and treatment planning: congenital recurrent pulmonary artery stenosis and transcatheter pulmonary valve replacement. American Society of Mechanical Engineers Digital Collection
47. Zhang H, Shen Y, Zhang L, Song C, Jing Z, Lu Q (2019) Preoperative evaluation of transcatheter aortic valve replacement with assistance of 3D printing technique: reanalysis of 4 death cases. J Interv Med 2(4):166–170
48. Kupfer ME, Lin W-H, Ravikumar V, Qiu K, Wang L, Gao L, Bhuiyan DB, Lenz M, Ai J, Mahutga RR, Townsend D, Zhang J, McAlpine MC, Tolkacheva EG, Ogle BM (2020) In situ expansion, differentiation, and electromechanical coupling of human cardiac muscle in a 3D bioprinted, chambered organoid. Circ Res 127(2):207–224

49. Haghiashtiani G, Qiu K, Zhingre Sanchez JD, Fuenning ZJ, Nair P, Ahlberg SE, Iaizzo PA, McAlpine MC (2020) 3D printed patient-specific aortic root models with internal sensors for minimally invasive applications. Sci Adv 6(35):eabb4641
50. Bateman MG, Durfee WK, Iles TL, Martin CM, Liao K, Erdman AG, Iaizzo PA (2020) Cardiac patient-specific three-dimensional models as surgical planning tools. Surgery 167(2):259–263
51. Juhnke B, Mattson AR, Saltzman D, Azakie A, Hoggard E, Ambrose M, Iaizzo PA, Erdman A, Fischer G (2019) Use of virtual reality for pre-surgical planning in separation of conjoined twins: a case report. Proc Inst Mech Eng H 233:1327
52. Iles TL, Holm MA, Calvin AD, Moller JH, Iaizzo PA (2020) First successful open-heart surgery utilizing cross-circulation in 1954. Ann Thorac Surg 110(1):336–341
53. Holm MA, Emfield K, Iles TL, Iaizzo PA (2021) High-resolution 3D reconstructions of human vasculatures: creation of educational tools and benchtop models for transcatheter devices. Cardiovasc Interv Ther 37:519–525
54. Anderson SE, Hill AJ, Iaizzo PA (2009) Microanatomy of human left ventricular coronary veins. Anat Rec 292(1):23–28
55. Spencer J, Fitch E, Iaizzo PA (2013) Anatomical reconstructions of the human cardiac venous system using contrast-computed tomography of perfusion-fixed specimens. J Vis Exp (74):50258
56. Christopher DR, Stephen AH, Ryan PG, Paul AI (2011) Cardiac remodeling as a consequence of atrial fibrillation: an anatomical study of perfusion-fixed human heart specimens: cardiac remodeling as a consequence of atrial fibrillation: an anatomical study of perfusion-fixed human heart specimens. J Geriatr Cardiol 8(3):141–146
57. Duan B, Hockaday LA, Kang KH, Butcher JT (2013) 3D bioprinting of heterogeneous aortic valve conduits with alginate/gelatin hydrogels. J Biomed Mater Res A 101A(5):1255–1264
58. Kucukgul C, Ozler SB, Inci I, Karakas E, Irmak S, Gozuacik D, Taralp A, Koc B (2015) 3D bioprinting of biomimetic aortic vascular constructs with self-supporting cells. Biotechnol Bioeng 112(4):811–821
59. Wang DD, Eng M, Greenbaum A, Myers E, Forbes M, Pantelic M, Song T, Nelson C, Divine G, Taylor A, Wyman J, Guerrero M, Lederman RJ, Paone G, O'Neill W (2016) Predicting LVOT obstruction after TMVR. JACC Cardiovasc Imaging 9(11):1349–1352
60. Ballard DH, Trace AP, Ali S, Hodgdon T, Zygmont ME, DeBenedectis CM, Smith SE, Richardson ML, Patel MJ, Decker SJ, Lenchik L (2018) Clinical applications of 3D printing. Acad Radiol 25(1):52–65
61. Elshazly MB, Hoosien M (2018) The future of 3D printing in cardiovascular disease. In: 3D printing applications in cardiovascular medicine. Elsevier, pp 243–253
62. Wang DD, Eng MH, Greenbaum AB, Myers E, Forbes M, Karabon P, Pantelic M, Song T, Nadig J, Guerrero M, O'Neill WW (2018) Validating a prediction modeling tool for left ventricular outflow tract (LVOT) obstruction after transcatheter mitral valve replacement (TMVR). Catheter Cardiovasc Interv 92(2):379–387
63. Sutherland J, La Russa D (2017) Virtual reality. In: Rybicki FJ, Grant GT (eds) 3D printing in medicine. Springer, Cham, pp 125–133

# Chapter 22
# Procedural Training and Education: A Multimodal and Interactive Approach


**Alex J. Deakyne, Mikayle A. Holm, Susana Arango, Tjorvi E. Perry, and Paul A. Iaizzo**

## 22.1 Introduction

Major technological advances over the last few decades have made virtual reality (VR) one of the largest growing gaming and educational markets in the United States. In 2014, the VR market revenue was $62.1 M and is projected to grow exponentially to $9.3 B in 2025 [1]. As these platforms have become more affordable and the technology more user-friendly, they are being increasingly adopted to enhance the collective experiences of customers while creating safe and effective learning environments for students. Today, the utilities of VR are broad; shoppers are now able to try on clothes in a 3D environment from the comfort of their homes, while the military is finding safer and more innovative ways to train soldiers by immersing them in large-volume and reproducible simulation environments. VR applications in healthcare aim to improve a given provider's abilities to reach patients in need and improve their cares and their experiences [2]. Current clinical applications, include VR-driven telemedicine, virtual experiential travel for the

A. J. Deakyne (✉) · M. A. Holm · P. A. Iaizzo
The Visible Heart® Laboratories, Department of Surgery, Institute for Engineering in Medicine, University of Minnesota, Minneapolis, MN, USA
e-mail: deaky007@umn.edu; iaizz001@umn.edu

S. Arango
The Visible Heart® Laboratories, Department of Surgery, Institute for Engineering in Medicine, University of Minnesota, Minneapolis, MN, USA

University of Minnesota, Division of Cardiothoracic Anesthesia, Department of Anesthesiology, Minneapolis, MN, USA

T. E. Perry
University of Minnesota, Division of Cardiothoracic Anesthesia, Department of Anesthesiology, Minneapolis, MN, USA

© The Author(s), under exclusive license to Springer Nature Switzerland AG 2023

P. A. Iaizzo et al. (eds.), *Heart Valves*, https://doi.org/10.1007/978-3-031-25541-0_22

frail, and virtual immersion options for patients with behavioral and mental health issues [3].

In general, traditional styles of teaching like PowerPoint presentations, learning management systems (LMS), and electronic text often lack formative and timely feedback [4] and also can make learning opportunities inefficient and often ineffective. In contrast, VR and mixed reality approaches are considered as a potentially highly disruptive technologies that will improve the educational experience of both the educator and student and meet the clinical practice needs of increasingly demanding environments for clinical care for patients with cardiac disease.

A multimodal approach using 3D printed and VR models of hearts and blood vessels has gained immense traction for procedural training and education over the last few years. These approaches preserve the 3D spatial information of real patient anatomies and represent them in immersive, reproducible, and easy to digest mediums. While some think that VR will replace 3D printing in developing procedural training and educational tools, we believe that the combination of the two is more than the sum of their parts. As such, VR can help augment 3D printed models to add more educational benefit by supplying a unique, immersive, perspective in a multimodal approach. Moreover, these models can serve as educational platforms for teaching precise variabilities in cardiac anatomies and physiology and medical and surgical device implantations and ultimately enhancing the care delivery for cardiac surgical and/or procedural patients. By creating a multimodal educational platform that consists of high-resolution 3D printed hearts from a large human population, VR, and interactive web/mobile environments, clinicians can study a medical device in a wide range of varied anatomical models, demonstrating how different cardiac anatomies will affect both the choice of clinically relevant implant sites and delivery pathways. In this chapter, we will overview these processes and discuss how mixed realities can be highly beneficial for procedural training and education.

## 22.2 3D Modeling of Cardiac Structures and Associated Vasculature

3D cardiac modeling has seen increased usage in the fields of medical device development and has also been deemed beneficial when used for preoperative planning and/or clinical education [5] precisely because these models retain all spatial 3D information of the original human anatomy. In addition, due to their significant cost-saving potentials, the FDA has committed significant resources into further supporting the utilities of computational modeling for medical device innovation [6].

Further, as the result of advances in medical education, presurgical planning, and the medical device industry, 3D modeling of human anatomical features has gained significant popularity in the last decade. By preserving accurate 3D spatial and relational anatomic information that is easily understood and analyzed even by the

novice clinician, 3D modeling is rapidly replacing two-dimensional (2D) representations for assessing anatomic structures [7]. Additionally, numerous investigators have used computational anatomical models and/or 3D printed models to perform computational device deployments or dissections without having to damage the original physical specimen [8]. The computational models have also fueled analyses such as statistical shape modeling and/or computational fluid dynamics [9, 10].

Nevertheless, generating 3D model requires a keen understanding of normal and pathological anatomies and their appearances employing cross-sectional imaging [11]. Specialized software such as Mimics and 3 Matic (Materialise; Leuven, Belgium) are required for model rendering and image postprocessing where in vivo or ex vivo patient imaging studies generated by MRI, CT, or 3D ultrasound are imported as DICOM (Digital Imaging and Communication in Medicine) files in which orthogonal cross sections (axial, sagittal, and coronal) can be visualized and in which any anatomy of interest can be manually or automatically isolated through a process referred to as segmentation [12]. The resulting models can be edited (wrapped, smoothed, and optimized/fixed) and then exported for 3D printing and/or online visualization (Fig. 22.1).

Once basic scans have been generated and to further enhance procedural training and education, medical or surgical devices can be computationally implanted into these models. In the Visible Heart® Laboratories (VHL) at the University of Minnesota, we have created computational images of cardiac structures and surrounding vessels and subsequently added medical devices that we can then manipulate into clinically relevant sites within the computational specimen. By understanding how these devices may ultimately "sit" within a given patient's heart or surrounding blood vessel long before they are placed in a real patient can give clinicians the confidence to safely care for patients; e.g., those undergoing complex cardiac surgery or interventional procedures. Furthermore, the abilities to computationally implant medical devices in resultant 3D printed or virtual models, as these

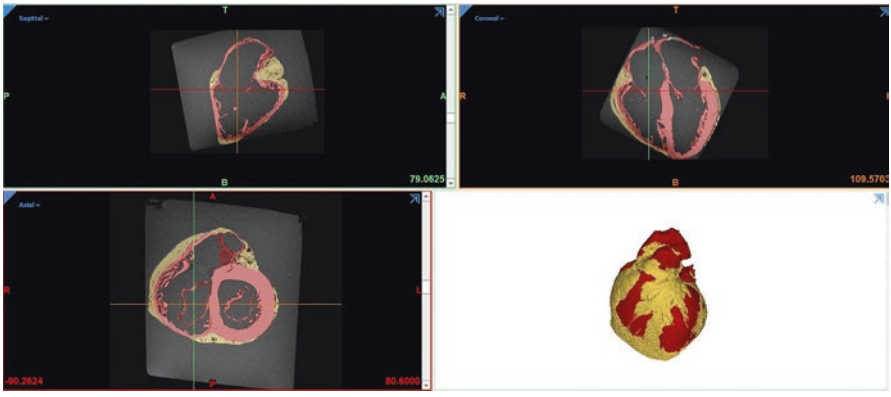

**Fig. 22.1** Heart segmentation from an ex vivo cardiac MRI. Segmentation labels superimposed onto the MRI image in the (**a**) sagittal, (**b**) axial, and (**c**) coronal view. (**d**) Volume rendering of the segmented heart. Muscle tissue can be seen in red and fat in yellow

devices are being developed toward commercialization, may replace the need for multiple deployments in preclinical animal models or in clinical trials on human patients [13]. We have already seen examples with implantable prosthetic valves in the pulmonary position and intracranial aneurysm stenting [14, 15]. Previously, our lab has performed computational deployments of a variety of cardiac devices within several unique cardiac specimen models including the Medtronic Micra™ transcatheter pacing system (TPS) (Medtronic PLC, Minneapolis, MN, USA), a leadless pacing system with an internal battery, placed into the apex or septal wall of the right ventricle of a computational human heart model [8]. Importantly, we are also able to computationally place the delivery catheter for the Micra™ TPS into the surrounding blood vessels, namely, the femoral vein and inferior vena cava as the pacing system is threaded from these blood vessels through the right atrium, past the tricuspid valve and into the right ventricle; at which point, it is imperative that the device not impede valvular or ventricular functions and/or potentially hampering appropriate blood flow through the heart (Fig. 22.2).

Computational models are also extremely useful for exposing three-dimensional dynamics of vascular structures and their anatomical and pathological variants. Within the VHL, we have develop and continue to develop a compilation of vasculature models that are being used to enhance training of medical students, residents, and fellows. In one example, we modeled the interaction and trajectory of implanted devices such as extracorporeal membrane oxygenation (ECMO) cannulas from in vivo CT (Fig. 22.3). Using ex vivo full-body CT scans, we have been able to recreate the entire vascular tree (Figs. 22.5, 22.6, and 22.7).

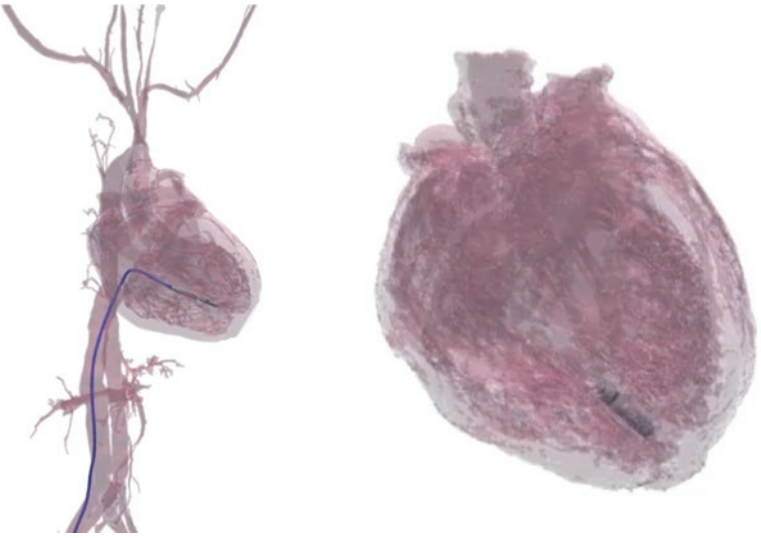

**Fig. 22.2** (Left) A 3D model showing the implant procedure for a Micra within the right ventricle of a human heart model. This depicts the delivery catheter and the vasculature of the delivery pathway. (Right) A close-up look at the Micra implanted into the right ventricular apex of the heart model

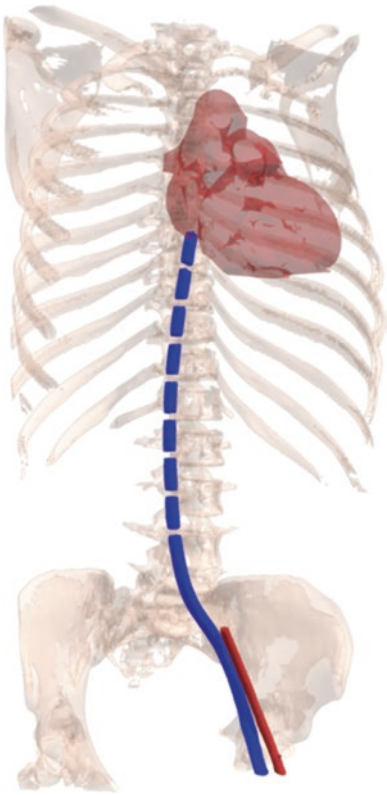

**Fig. 22.3** A 3D model depicting an arterial (red) and venous (blue) cannulas in a patient under venoarterial extracorporeal membrane oxygenation

With 3D modeling of cardiac and surrounding blood vessels and the abilities to computationally implant a variety of medical devices, we have in turn enhanced the abilities for clinicians to safely, effectively, and accurately understand a given patient's anatomy and strategize device placements well in advance of caring for a real patient in the operating or procedure rooms.

## 22.3 3D Printing of Cardiac Structures and Surrounding Blood Vessels

A number of authors in this book have discussed 3D printing of cardiac structures (see Chap. 21 Tenhoff et al.). Herein, we will focus on how 3D printed cardiac models can be utilized for procedural training and education. Specifically, we will describe how computational models can be 3D printed and paired with a modeled VR environment, so to create a unique multimodal teaching platform.

As outlined in the previous section, advances in clinical available 2D computational models of the heart and surrounding vessels enhance the abilities for clinicians to safely and effectively understand accurate patient anatomies and strategize device placement prior to actual care delivery. To further enhance one's understandings, these 2D computational models can be rendered in 3D either as a physically printed object or virtually, again allowing clinicians to gain an even deeper perspective of anatomic relationships within the heart, how medical and surgical devices can or should be oriented within the heart and/or surrounding blood vessels, as well as identifying relevant device–tissue interfaces.

There are several software packages and printers currently on the market that can be used to transform a 3D computational mesh into a 3D printed physical model. In the VHL, we have had success using Cura software from Ultimaker (Utrecht, The Netherlands) and GrabCAD from Stratasys Eden Prairie, MN, USA) to prepare computational models for printing. We operate the Ultimaker 3Extended Printer (Utrecht, The Netherlands), the Stratasys J750 Digital Anatomy Printer (Eden Prairie, MN, USA), and the Stratasys uPrint SE Plus (Eden Prairie, MN, USA) using a variety of materials including polylactic acid (PLA), a biodegradable thermoplastic material, and acrylonitrile butadiene styrene (ABS), an amorphous opaque plastic.

In another effort, we converted the computational model described in the previous section to a corresponding 3D printed model depicting how the Medtronic Micra™ transcatheter pacing system (TPS) (Medtronic PLC, Minneapolis, MN, USA) can be visualized in relation to relevant anatomic structures including the entrance to the right atrium, placement through the tricuspid valve, and ultimate fixation within the apex of the right ventricle. To further enhance perspective, we can either print the entire structure in a single color and have learners paint each structure or vary the color scheme of the printing material used via high-end printers. In both scenarios, learners can carefully study different features with high resolutions (hundreds of microns) within a model both in isolation and in relation to the surrounding structures (Fig. 22.4).

At the VHL, training tools for large bore transcatheter procedures were developed from high-resolution, full-body CT scans of human cadavers. To enhance our abilities to obtain high-resolution DICOM datasets, the vasculatures were injected with large volumes (liters) of radiopaque contrast to better visualize the complexities of the human vasculature. Once segmented, these 3D models were printed hollow so physicians can practice wiring and introducing large bore catheters into these vessels (Fig. 22.5).

As with computational models described in the previous section, 3D printing of cardiac structures, surrounding blood vessels and how medical or surgical devices interface with surrounding anatomies can enhanced the abilities for clinician with all levels of training to safely, effectively, and accurately understand a given patient's anatomy and strategize device placement(s) well in advance of actual clinical procedure.

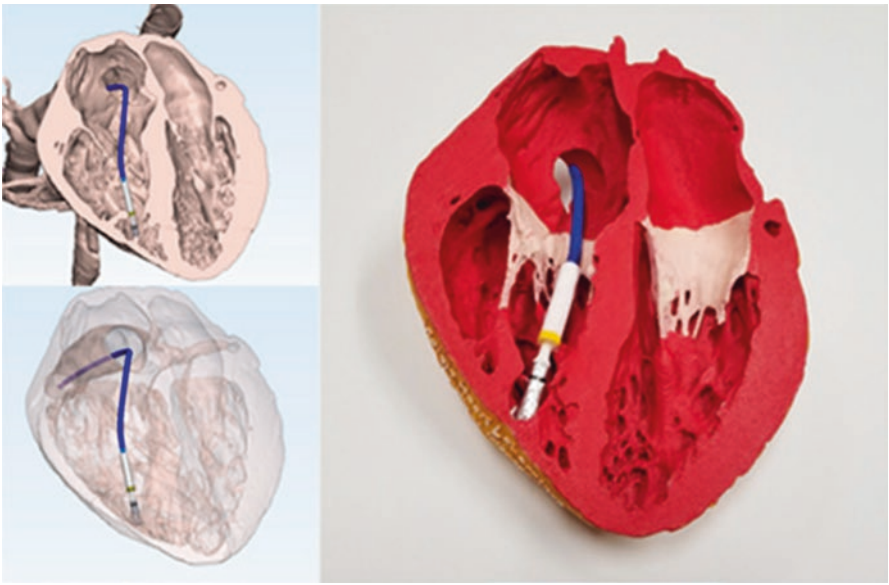

**Fig. 22.4** 3D models and 3D print of the posterior half of a human heart with a computationally placed MicraTM transcatheter pacing system (TPS) and delivery catheter. The printed heart and MicraTM TPS were hand-painted to highlight device–tissue interfaces. This image depicts the mixed reality approach of combining the computational models along with 3D printed models [4]

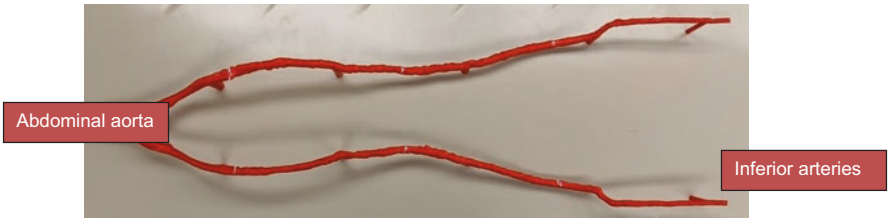


**Fig. 22.5** The arterial femoral pathway from a human cadaver donor was 3D printed in PLA and assembled for procedural training. (Figure initially printed in Holm et al. [16])

## 22.4 Virtual Reality of Cardiac Structures and Surrounding Blood Vessels

The field of VR is gaining significant traction across multiple industries including healthcare and medical education particularly as it relates to procedural training for students, residents and fellow, and physician; such is critical for expediting improved outcomes and acceptance of novel technologies. In the area of cardiovascular technologies, VR is being leveraged as an interactive and effective teaching tool to

enhance the clinician's understanding of complex cardiac structures and how medical devices may behave within the heart or surrounding blood vessels long before an actual device implantation, i.e., in a preclinical or clinical trial. The VHL research team in collaboration with our cardiology, cardiac surgery, and cardiac anesthesia colleagues have created hundreds of virtual scenes and tutorials that can be used to enhance medical education in cardiac and vascular anatomy and physiology. Again, such developed tools are aimed to better understand how medical and surgical devices may be developed and deployed and how these devices may interact with surrounding cardiovascular tissues once deployed. In the following section, we will provide examples of a few of these virtual reality scenes and how they can be leveraged toward a comprehensive mixed reality educational approach for optimizing procedural.

### *22.4.1 General Human Anatomical Education*

As previously described, an immersive VR experience allows for a more memorable, often greater understanding of the anatomical features being studied. The VHL has collected full-body CT and MR imaging from over 15 fresh human cadavers which in turn allows us to uniquely create VR scenes where users can "fly" through a computationally generated human body. Using contrast-enhanced CT scans, arteries, veins, and bones can be and were segmented and separated into individual 3D models. With the MRI scan, models of the abdominal organs including the liver, gall bladder, intestine, and kidneys can be and were created. Models can then be co-registered together into the same VR scene (Fig. 22.6). These created educational tool allows the user to drive themselves through the body to gain a better understanding of the relative distances between certain anatomical structures.

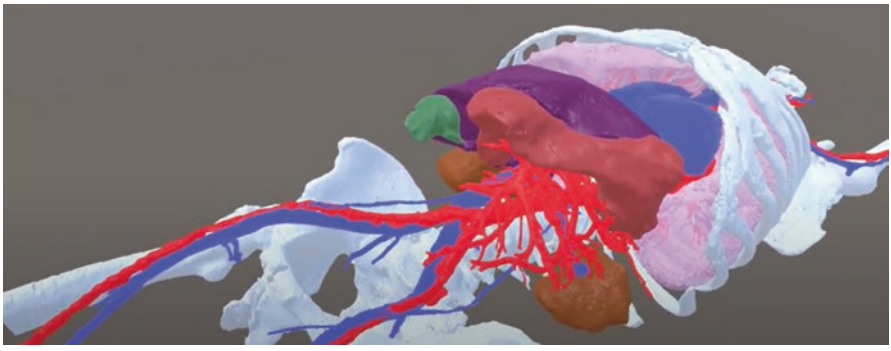

**Fig. 22.6** Anatomical structures were modeled from images of a human cadaver and merged into one VR scene so the user can "fly" through the human body

### *22.4.2 Transcatheter Aortic Valve Replacement*

Transcatheter aortic valve replacement (TAVR) is a minimally invasive procedure for replacing a diseased aortic valve using a delivery catheter with access through the femoral artery [17]. Although TAVR device technology has improved and delivery catheter profiles have decreased in size, detailed assessment of the peripheral vasculature and potential access sites remains a priority. Prior to the majority of TAVR procedures, the patient's blood vessels from the access site to the aortic annulus are scanned using high-resolution CT to look for vascular anatomy and severity of calcification or atheroma formation within the vessels [18].

If the patient is not a candidate for an iliofemoral approach, an alternative approach may be considered, including the subclavian, axillary, or carotid arteries, or gaining access to the descending aorta via the inferior vena cava. In all cases, tortuous and/or narrow blood vessels may result in prolonged procedures, vessel rupture, distal embolization of calcium or atheroma, and/or rupture of blood vessels that can result in fatal bleeding [19]. In one of the largest performed clinical trials to date, the PARTNER trial, it was cited that there was a 15% incidence vascular-related complications during TAVR procedures [20]. Although CT scanning currently remains the standard of care to assess blood vessel anatomy and pathology prior to TAVR procedures, 3D virtual rendering of the patient's vasculature has the potential to supplement or supplant this modality, i.e., to offer a more effective, efficient and more easily understood way of assessing blood vessel anatomy and pathology (Fig. 22.7).

There is increasing evidence that aberrant associated anatomies or the presence, extent, and distribution of calcification along the aortic valvular complex or "landing zone" of the TAVR prosthesis can be associated with intra- and postprocedural complications, including the following: (1) paravalvular aortic regurgitation [21, 22], (2) conduction abnormalities [23], (3) inadequate expansion and subsequent migration of the TAVR prostheses [24], or (4) occlusion of the coronary artery ostia [25, 26]. We have found utility in modeling the anatomy of potential TAVR patients to enhance the clinicians understanding of these potential complications [19]. Figures 22.8 and 22.9 describe one such example with the potential for "flying through" the patient's blood vessels from the descending aorta to the aortic valvular complex and "landing zone" of the prosthetic valve, examining anatomic variants, areas of excessive calcification, or atheromatous formation along the delivery pathway, while optimizing catheter placement and device deployment for each individual patient.

Similarly, we have developed 3D renderings and virtual scenes for various patients following device placements. Figure 22.10 employed a 10-phase CT scan of the aortic valvular complex with a TAVR device already in place. We then virtually modeled the aortic valvular complex throughout the cardiac cycle, allowing for a generated VR experience that can give the clinician remarkable insight on how a given TAVR device may or did interact with its surroundings as the heart beats and the surrounding blood vessels move.

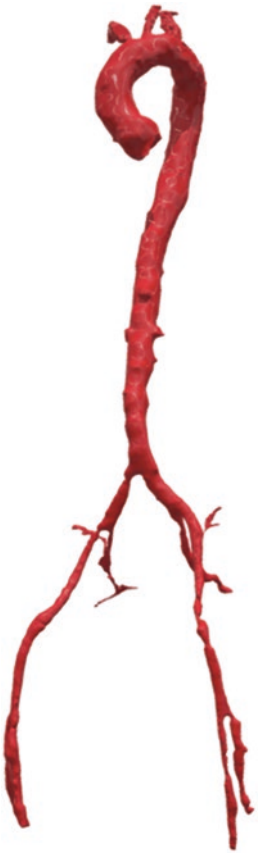

**Fig. 22.7** 3D model of the aorta and the iliac and femoral arteries

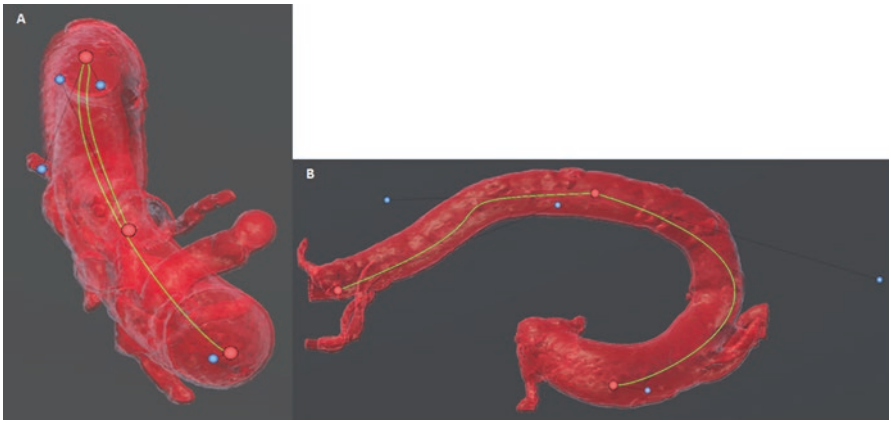


**Fig. 22.8** A 3D model of an aorta shown in the (**a**) cranial and (**b**) lateral, along with a potential pathway for the delivery catheter

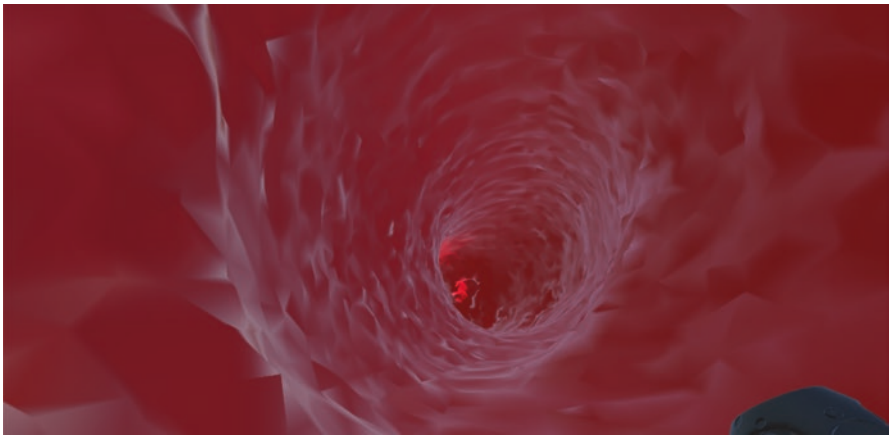

**Fig. 22.9** A VR user's view of the aorta model while navigating along the fixed spline. The VR user is currently in the abdominal aorta and moving toward the aortic arch and then the aortic root

Beyond TAVR procedures specifically, we have developed the technology to allow users to simulate any device deployment within a virtual scene by attaching any given medical device to their VR controller. In one such case, the Medtronic Micra™ transcatheter pacing system (TPS) (Medtronic PLC, Minneapolis, MN, USA) was used for this proof of principle; in other words, we are developing virtual scenes, in a cost-conscious manner [13], by which clinicians can navigate the Micra™ devices to various or multiple positions, past the tricuspid valve complex, and into the right ventricle, as misadventures through the right atrium, tricuspid annulus, and sub-tricuspid apparatus can result in significant risks for morbidity and mortality [27]. Figure 22.11 is an example of a virtual scene whereby three Micra™ devices were successfully implanted into various areas of the apex of the same right ventricle occupying at the least 1.6% and at the most 4.8% of the calculated right ventricular volumes. These virtual scenes also allow clinicians to practice extracting a Micra™ device that may have been in place for extended periods of time, resulting in peri-device scarring or thrombus formation. Future work within the VHL will focus on further developing scenes by which the Micra™ and other devices can be virtually "deployed" or removed by clinicians and medical device innovators.

While we have clearly shown proof of principle in how virtual reality can be leveraged to gain procedural insight during TAVR procedures, Micra placements, as well as other cardiac devices beyond standard imaging modalities, we are also working to enhance educational opportunities for enhanced learning of perioperative and periprocedural TEE.

As perioperative transesophageal echocardiography (TEE) has become an essential tool during the management of operative and procedural patients [28], and as an initial step toward creating an integrated, immersive, and interactive mixed reality platform in which physical and virtual models are merged, we have developed a novel virtual reality (VR) platform that allows users to slice across an infinite

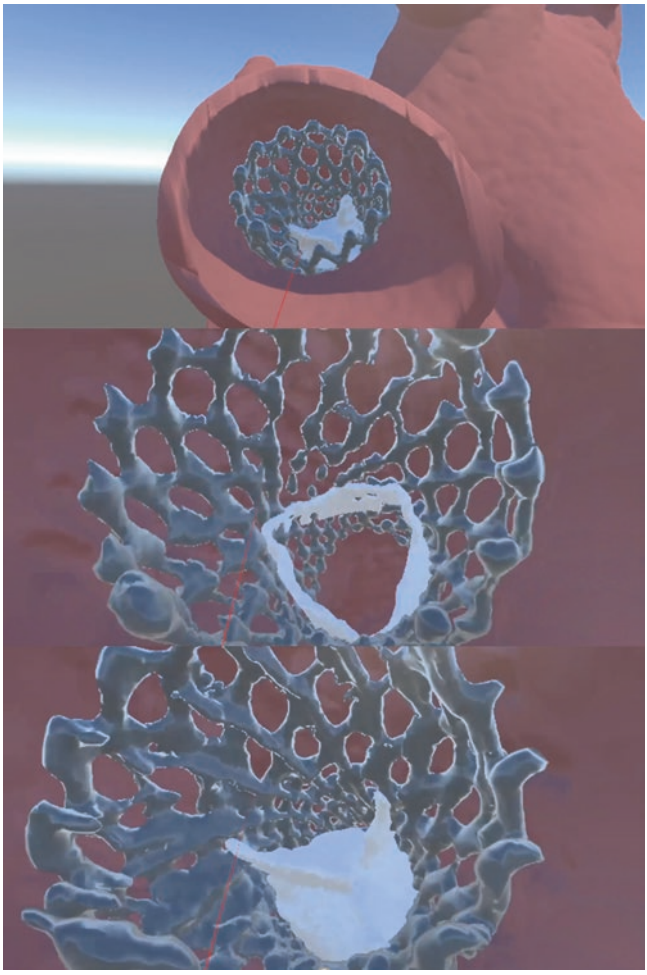

**Fig. 22.10** A user in virtual reality viewing the TAVR implant from (top) a far and up close during (middle) systole, and (bottom) diastole

number of cardiac planes on a detailed 3D models developed from end-diastolic perfusion-fixed human hearts.

## 22.5 A Multimodal Approach for Teaching Transesophageal Echocardiography (TEE)

As stated above, while we have clearly shown proof of principle in how VR and 3D printing can be leveraged to gain procedural insight during device implantation beyond standard imaging modalities, work in the VHL is ongoing to enhance educational opportunities for learning perioperative and periprocedural TEE.

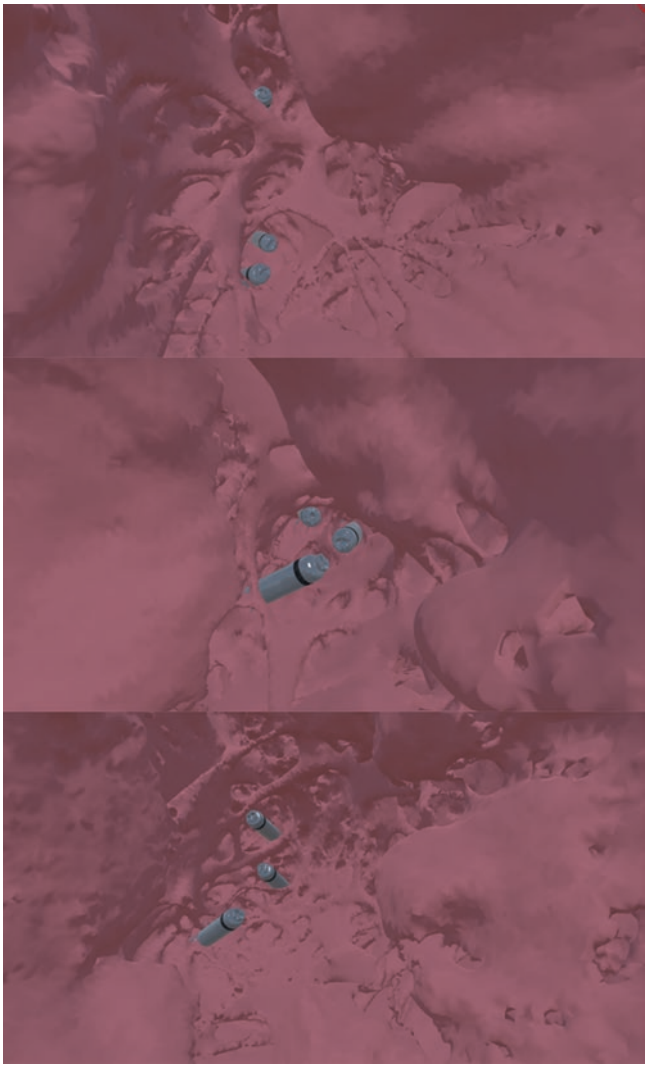

**Fig. 22.11** Shown here is a collage of three Micras computationally deployed in human heart models using VR. These devices were deployed in the right ventricle, mainly the right ventricular apex and the septal wall

To date, despite perioperative TEE being an essential tool during the management of operative and procedural patients, teaching strategies have relied mainly on digital heart models and hands-on TEE simulators, limited as flat images built from idealized human hearts with restricted visualization of intracardiac structures and associated anatomies [29]. In recent collaborative efforts between the VHL and the Division of Cardiothoracic Anesthesiology at the University of Minnesota, we have generated computational cardiac models, to mimic the American Society of

Echocardiography (ASE)-recommended intraoperative TEE views used to describe and communicate cardiac anatomy and pathophysiology during cardiac surgery. These computational models can be and have been used to generate a set of 3D printed hearts of all recommended views as well as VR scenes (see below). Thus, we aim to create an integrative, immersive, and interactive multimodal platform in which physical and virtual models are merged. As an initial step and in collaboration with the Advanced Imaging Service for Objects and Spaces (AISOS) at the University of Minnesota, we have developed a TEE teaching virtual reality application that allows visualization and navigation of both external and internal human cardiac anatomies, dynamic cutting of the heart geometry in real time, and a menu to switch between a set of predefined views recommended by the ASE. Our employed viewer feeds video directly into both the VR headset and an external display. In this way, spectators can see the same scene as the user in the headset, and in doing so, we are able to standardize the experience of multiple students and provide opportunity for immediate feedback from the instructor–proctor (Fig. 22.12).

More specifically, using the previously mentioned software (Mimics and 3 Matic), we have and continue to generate sliced human heart 3D models into planes corresponding to 10 of the 28 ASE pre-described echo views. Further, we can match two different planes to each heart and 3D print them using clear polycarbonate. Magnets have and can be inserted to hold reciprocal pieces together. These models are readily portable and currently are being used for teaching purposes in our cardiac operating rooms at the University of Minnesota. Concomitant visualizations of 2D images in TEE and the corresponding slice in the model can enhance the

**Fig. 22.12** A mid-papillary short axis view using virtual reality and a controller to slice the heart in the desired view

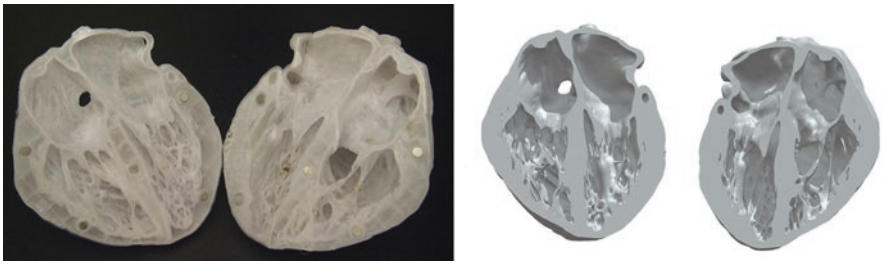

**Fig. 22.13** A 3D printed (left) and online interactive (right) model of a human heart sliced to mimic a four-chamber view

learning experience as students can appreciate detailed cardiac and associated anatomies and spatial relationships in three dimensions (Fig. 22.13).

To further increase the accessibility of this type of educational content and expand the learning environment, we uploaded the 3D renders to an online platform that can be launched remotely from any computer or mobile device allowing detailed visualization and interaction with the models (see the Atlas of Human Cardiac Anatomy: http://www.vhlab.umn.edu/atlas/). Hence, we view this as a unique opportunity to reinforce the learner contents, using VR and 3D models, as critical means to consolidate understanding and facilitate retention.

## 22.6 Conclusion

Virtual reality and 3D printing have both seen increased uses for procedural training and education within the medical field in recent years and are seeing widespread applications in medical schools across the United States and the world. Many investigators are studying the ways that these modalities can be used for enhancing educational and patient outcomes. Each poses unique characteristics of presenting the anatomical models in a new perspective while offering an immersive and engaging experience for all users. While many investigators are studying the advantages of 3D physical objects and virtual scenery separately, we contend that combining the two modalities into a "mixed reality experiences" may exponentially enhance the user experiences during procedural training and education.

## References

1. Portal S Virtual reality (VR) market revenue in the United States from 2014 to 2025. https://www.statista.com/statistics/784139/virtual-reality-market-size-in-the-us/
2. Research Brief Beyond gaming: 19 industries AR/VR Is poised to transform. https://www.cbinsights.com/research/ar-vr-industries-disrupted-beyond-gaming/

3. Workman S Mixed reality: a revolutionary breakthrough in teaching and learning. https://er.educause.edu/articles/2018/7/mixed-reality-a-revolutionary-breakthrough-in-teaching-and-learning
4. Lateef F (2010) Simulation-based learning: just like the real thing. J Emerg Trauma Shock 3(4):348–352. https://doi.org/10.4103/0974-2700.70743
5. Jurgaitis J, Paškonis M, Pivoriūnas J et al (2008) The comparison of 2-dimensional with 3-dimensional hepatic visualization in the clinical hepatic anatomy education. Medicina (Kaunas, Lithuania) 44(6)
6. Morrison TM, Pathmanathan P, Adwan M, Margerrison E (2018) Advancing regulatory science with computational modeling for medical devices at the FDA's Office of Science and Engineering Laboratories. Front Med 5. https://doi.org/10.3389/fmed.2018.00241
7. Maron MS, Olivotto I, Harrigan C et al (2011) Mitral valve abnormalities identified by cardiovascular magnetic resonance represent a primary phenotypic expression of hypertrophic cardiomyopathy. Circulation 124(1):40. https://doi.org/10.1161/CIRCULATIONAHA.110.985812
8. Deakyne AJ, Iles TL, Mattson AR, Iaizzo PA (2019) Virtual prototyping: computational device placements within detailed human heart models. Appl Sci 10(1):175. https://doi.org/10.3390/app10010175
9. Morris PD, Narracott A, von Tengg-Kobligk H et al (2016) Computational fluid dynamics modelling in cardiovascular medicine. Heart 102(1):18. https://doi.org/10.1136/heartjnl-2015-308044
10. Frangi AF, Rueckert D, Schnabel JA, Niessen WJ (2002) Automatic construction of multiple-object three-dimensional statistical shape models: application to cardiac modeling. IEEE Trans Med Imaging 21(9):1151. https://doi.org/10.1109/TMI.2002.804426
11. Yoo SJ, Thabit O, Kim EK, Ide H et al (2015) 3D printing in medicine of congenital heart diseases. 3D Print Med 2(1). https://doi.org/10.1186/s41205-016-0004-x
12. Ding P, Li L, Yang M, Yang J (2021) The methods of cardiovascular 3D printing. In: Cardiovascular 3D printing. Springer, Singapore, pp 3–14
13. P O, MD E, MD B, PA I, K W. (2016) Right ventricular anatomy can accommodate multiple Micra Transcatheter pacemakers. Pacing Clin Electrophysiol: PACE 39(4):393. https://doi.org/10.1111/pace.12804
14. Capelli C, Taylor AM, Migliavacca F, Bonhoeffer P, Schievano S (2010) Patient-specific reconstructed anatomies and computer simulations are fundamental for selecting medical device treatment: application to a new percutaneous pulmonary valve. Philos Transact A Math Phys Eng Sci 368(1921):3027. https://doi.org/10.1098/rsta.2010.0088
15. Appanaboyina S, Mut F, Löhner R, Putman C, Cebral J (2009) Simulation of intracranial aneurysm stenting: techniques and challenges. Comput Methods Appl Mech Eng 198(45–46):3567–3582. https://doi.org/10.1016/j.cma.2009.01.017
16. Holm MA, Emfield K, Iles TL, Iaizzo PA (2021) High-resolution 3D reconstructions of human vasculatures: creation of educational tools and benchtop models for transcatheter devices. Cardiovasc Interv Ther 37:519. https://doi.org/10.1007/s12928-021-00804-4
17. Latsios G, Gerckens U, Grube E (2010) Transaortic transcatheter aortic valve implantation: a novel approach for the truly "no-access option" patients. Catheter Cardiovasc Interv 75(7). https://doi.org/10.1002/ccd.22378
18. Zaman S, Gooley R, McCormick L, Harper R, Meredith IT (2015) Pre – transcatheter aortic valve implantation workup in the cardiac catheterisation laboratory. Heart Lung Circ 24(12):1162–1170. https://doi.org/10.1016/j.hlc.2015.07.018
19. Krishnaswamy A, Parashar A, Agarwal S et al (2014) Predicting vascular complications during transfemoral transcatheter aortic valve replacement using computed tomography: a novel area-based index. Catheter Cardiovasc Interv 84(5):844. https://doi.org/10.1002/ccd.25488
20. Généreux P, Webb JG, Svensson LG et al (2012) Vascular complications after transcatheter aortic valve replacement: insights from the PARTNER (Placement of AoRTic TraNscathetER Valve) trial. J Am Coll Cardiol 60(12):1043. https://doi.org/10.1016/j.jacc.2012.07.003

21. Marwan M, Achenbach S, Ensminger SM et al (2013) CT predictors of post-procedural aortic regurgitation in patients referred for transcatheter aortic valve implantation: an analysis of 105 patients. Int J Cardiovasc Imaging 29(5):1191–1198. https://doi.org/10.1007/s10554-013-0197-7
22. Zegdi R, Ciobotaru V, Noghin M et al (2008) Is it reasonable to treat all calcified stenotic aortic valves with a valved stent? Results from a human anatomic study in adults. J Am Coll Cardiol 51(5):579–584. https://doi.org/10.1016/j.jacc.2007.10.023
23. Maeno Y, Abramowitz Y, Kawamori H et al (2017) A highly predictive risk model for pacemaker implantation after TAVR. JACC Cardiovasc Imaging 10(10 Pt A):1139–1147. https://doi.org/10.1016/j.jcmg.2016.11.020
24. Kapadia SR, Schoenhagen P, Stewart W, Tuzcu EM (2010) Imaging for transcatheter valve procedures. Curr Probl Cardiol 35(5):228–276. https://doi.org/10.1016/j.cpcardiol.2010.01.002
25. Thomas M, Schymik G, Walther T et al (2010) Thirty-day results of the SAPIEN aortic Bioprosthesis European Outcome (SOURCE) Registry: a European registry of transcatheter aortic valve implantation using the Edwards SAPIEN valve. Circulation 122(1):62–69. https://doi.org/10.1161/CIRCULATIONAHA.109.907402
26. Stabile E, Sorropago G, Cioppa A et al (2010) Acute left main obstructions following TAVI. EuroIntervention 6(1):100–105. https://doi.org/10.4244/EIJV6I1A15
27. Reynolds D, Duray GZ, Omar R et al (2016) A leadless intracardiac transcatheter pacing system. N Engl J Med 374(6):533. https://doi.org/10.1056/NEJMoa1511643
28. Hahn RT, Abraham T, Adams MS et al (2013) Guidelines for performing a comprehensive transesophageal echocardiographic examination: recommendations from the American Society of Echocardiography and the Society of Cardiovascular Anesthesiologists. J Am Soc Echocardiogr 26(9):921. https://doi.org/10.1016/j.echo.2013.07.009
29. Schmauss D, Haeberle S, Hagl C, Sodian R (2015) Three-dimensional printing in cardiac surgery and interventional cardiology: a single-centre experience. Eur J Cardiothorac Surg 47(6):1044. https://doi.org/10.1093/ejcts/ezu310

# Index



© The Editor(s) (if applicable) and The Author(s), under exclusive license to Springer Nature Switzerland AG 2023

P. A. Iaizzo et al. (eds.), *Heart Valves*, https://doi.org/10.1007/978-3-031-25541-0